PHASE 2 INITIAL BOREHOLE DRILLING AND TESTING, SOUTH BRUCE

WP06: Hydraulic Testing Summary Report for SB_BH01

APM-REP-01332-0323 **July 2023**

Geofirma Engineering

NUCLEAR WASTE MANAGEMENT ORGANIZATION
SOCIÉTÉ DE GESTION DES DÉCHETS NUCLÉAIRES

Nuclear Waste Management Organization
22 St. Clair Avenue East, 4th Floor
Toronto, Ontario
M4T 2S3
Canada

Tel: 416-934-9814
Web: www.nwmo.ca

Phase 2 Initial Borehole Drilling and Testing, South Bruce

WP06: Hydraulic Testing Summary Report for SB_BH01

Revision: 0 (Final)

Prepared for:

Nuclear Waste Management Organization
22 St. Clair Avenue East. 6th Floor
Toronto, ON, M4T 2S3

Prepared by:

GEOFIRMA ENGINEERING
1 Raymond St. Suite 200, Ottawa, Ontario K1R 1A2
613.232.2525 613.232.7149 geofirma.com

APM-REP-01332-0323

Project Number: 20-211-1

Document ID: WP06 Summary Report - Hydraulic Testing for SB_BH01_R0

July 5, 2023

Title:	WP06: Hydraulic Testing Summary Report for SB_BH01	
Client:	Nuclear Waste Management Organization	
Project Number:	20-211-1	
Document ID:	WP06 Summary Report - Hydraulic Testing for SB_BH01_R0	
Revision Number:	0	Date: July 5, 2023
Prepared by:	John Avis, B.A.Sc. P.Eng., Randy Roberts, M.Sc.	
Reviewed by:	Rick Beauheim, M.Sc., Sean Sterling, M.Sc, P.Eng., P.Geo.	
Approved by:	 Sean Sterling, M.Sc, P.Eng., P.Geo. – Project Manager - Principal	

Revision Tracking Table

Revision	Revision Release Date	Description of Modifications/Edits
R0	July 5, 2023	Initial Release

TABLE OF CONTENTS

LIST OF TABLES

LIST OF FIGURES

1 INTRODUCTION

Geofirma Engineering Ltd. (Geofirma) was retained by the Nuclear Waste Management Organization (NWMO) to complete a drilling and testing program for two deep bedrock boreholes (SB_BH01 & SB_BH02) as part of the NWMO's Phase 2 Geoscientific Preliminary Field Investigations. The full scope of this deep drilling and testing program is described in the Initial Borehole Characterization Plan.

Phase 1 of NWMO's APM plan included preliminary desktop studies using available geoscientific information and a set of key geoscientific characteristics and factors that can be realistically assessed at the desktop phase of the Preliminary Assessment. The Phase 1 Preliminary Assessment of the South Bruce area identified the Cobourg Formation as the preferred host formation for a deep geological repository for used nuclear fuel. The Initial Borehole Drilling and Testing study is a key component of the Phase 2 Geoscientific Preliminary Field Investigations of the NWMO's APM plan.

The activities described in this report constitute one component of the Geofirma geoscientific investigations as part of the NWMO Phase 2 Initial Borehole Drilling and Testing Program within the South Bruce study area, near Teeswater, Ontario (Figure 1.1).

An important component of this geoscientific investigation is the acquisition of in situ estimates of rock mass hydraulic conductivity (K) and other hydrogeologic formation properties including formation pressure (P_f) and specific storage (S_s).

Specifically, this report presents the results of analyses of data collected during hydraulic testing in borehole SB_BH01 as described in Geofirma's WP06 Test Plan Testing was conducted by subcontractor HydroResolutions LLC (HR) under the direction of senior Geofirma staff.

This report describes the results of the testing and analyses associated with SB_BH01. Figure 1.2 shows the stratigraphic sequence that was encountered in the subsurface while drilling SB_BH01. The subsurface nomenclature used was based on Armstrong and Carter (2010).

1.1 Borehole SB_BH01

Borehole SB_BH01 is located approximately 3.5 km northwest of the community of Teeswater, Ontario (Figure 1.1) and was drilled vertically to a total target depth of 880.84 metres below ground surface (mBGS) through the entire sedimentary bedrock sequence down into the Precambrian bedrock. The borehole was drilled using PQ3 wireline coring equipment that produces a 123 mm nominal diameter borehole and 83 mm nominal diameter core over the period June 1, 2021 until September 18, 2021 using brine as a drilling fluid. There were extensive drilling fluid losses to the permeable Guelph formation during drilling. Borehole geophysical logging was completed over the period September 30, 2021 until October 15, 2021.

Figure 1.1 SB_BH01 Site Location.

GS elevation = 289 mASL

Standard Reference		Area of South Bruce		SB_BH01 Final Fm. Top (mBGS)	SB_BH01 Final Thickness (m)	Lithology
Devonian	Middle		Drift	0	20	n/a
Devonian	Middle	Detroit River Gp	Lucas Fm	19.6	21	dolostone
Devonian	Middle	Detroit River Gp	Amherstburg Fm	41	34	dolostone
Devonian	Lower		Bois Blanc Fm	75	26	cherty dolostone
Silurian [b]	Upper		Bass Island Fm	101	33	dolostone
Silurian [b]	Upper	Salina Fm	G Unit	134	9	argillaceous dolostone
Silurian [b]	Upper	Salina Fm	F Unit	143	43	dolomitic shale
Silurian [b]	Upper	Salina Fm	E Unit	187	23	brecciated dolostone and dolomitic shale
Silurian [b]	Upper	Salina Fm	D Unit	209	1	anhydritic dolostone
Silurian [b]	Upper	Salina Fm	C Unit	210	14	dolomitic shale and shale
Silurian [b]	Upper	Salina Fm	B Unit	225	6	argillaceous dolostone
Silurian [b]	Upper	Salina Fm	B Unit-Equivalent	231	20	salt
Silurian [b]	Upper	Salina Fm	B Unit-Evaporite	251	3	anhydrite
Silurian [b]	Upper	Salina Fm	A2 Unit-Carbonate	254	20	dolostone
Silurian [b]	Upper	Salina Fm	A2 Unit-Evaporite	274	2	anhydritic dolostone
Silurian [b]	Upper	Salina Fm	A1 Unit-Carbonate	276	15	argillaceous dolostone
Silurian [b]	Upper	Salina Fm	A1 Unit-Evaporate	291	0.2	anhydritic dolostone
Silurian [b]	Upper	Salina Fm	A0 Unit [c]	--	-- [d]	bituminous dolostone
Silurian [b]	Lower		Guelph Fm	291	49	dolostone
Silurian [b]	Lower		Goat Island Fm	340	45	dolostone
Silurian [b]	Lower		Gasport Fm	385	6	dolostone and dolomitic dolostone
Silurian [b]	Lower		Lions Head Fm	391	3	dolostone and dolomitic dolostone
Silurian [b]	Lower		Fossil Hill Fm	395	1	dolostone and dolomitic dolostone
Silurian [b]	Lower		Cabot Head Fm	396	20	shale
Silurian [b]	Lower		Manitoulin Fm	416	9	cherty dolostone and minor shale
Ordovician [a]	Upper		Queenston Fm	424	85	red shale
Ordovician [a]	Upper		Georgian Bay Fm	509	87	grey shale
Ordovician [a]	Upper		Blue Mountain Fm	596	49	dark grey shale
Ordovician [a]	Upper	Trenton Gp	Cobourg Fm Collingwood Mb)	645	8	black calcareous shale
Ordovician [a]	Upper	Trenton Gp	Cobourg Fm [1]	653	40	argillaceous limestone
Ordovician [a]	Upper	Trenton Gp	Sherman Fall Fm [2]	693	45	argillaceous limestone
Ordovician [a]	Upper	Trenton Gp	Kirkfield Fm [3]	738	43	argillaceous limestone
Ordovician [a]	Upper	Black River Gp	Coboconk Fm [3]	781	21	bioturnated limestone
Ordovician [a]	Upper	Black River Gp	Gull River Fm	802	53	lithographic limestone
Ordovician [a]	Upper	Black River Gp	Shadow Lake Fm	855	5	siltstone and sandstone
Cambrian			Cambrian (Unsubdivided)	--	-- [d]	sandstone
Precambrian			Precambrian Basement	860		gneiss

Notes:

a - Strata traditionally referred to as Middle Ordovician (i.e., Black River and Trenton groups; Armstrong and Carter, 2006) are now considered Part of the Upper Ordovician.
b - The formal term Middle Silurian (e.g., Armstrong and Carter, 2006) has been abandoned so all strata have been re-assigned to either the Lower or Upper Silurian.
c - A0 Unit (Salina Formation) is recognized based on site characterization activities at the Bruce nuclear site (Intera, 2011).
d - Unit/Formation is not present.

Surface Nomenclature Equivalent (approx.): 1 - Lindsay Fm; 2 - Verulam Fm; 3 - Bobcaygeon Fm

------------ Unconformity

Figure 1.2 Generalized Stratigraphic Bedrock Sequence in South Bruce Area (after Armstrong and Carter, 2010).

1.2 Hydraulic Testing Activities

Straddle-packer hydraulic testing of South Bruce borehole SB_BH01 provided the data required to determine in situ values of hydrogeologic properties. A custom test tool and support trailer with a data-acquisition system was developed to address the unique requirements of low-permeability testing in deep boreholes. The test equipment was designed and constructed by HR staff and drew upon years of experience in testing of low-permeability strata at multiple locations around the globe.

The key components of the test tool are: two inflatable packers to isolate a test interval within a borehole; a downhole shut-in valve that connects or isolates the test interval from the tubing on which the test tool is suspended in the hole; a hydraulic piston that can be extended or retracted to cause a pressure increase or decrease in the test interval; and pressure transducers that measure the pressure in the test interval, in the bottom of the hole below the lower packer, in the tubing string above the test tool, and in the annulus between the tubing and borehole wall above the upper packer.

SB_BH01 testing was carried out between November 7, 2021, and May 12, 2022, in fifteen 30.05-m intervals and five 5.03-m intervals. These tests were performed under control of WP06 Test Plan . Preliminary analyses of these tests indicated relatively low-permeability formations with estimated average hydraulic conductivities of between 10^{-14} and 10^{-13} m/s throughout the Ordovician formations with higher permeabilities found in several Silurian aged formations. Additionally, formation hydraulic pressures in the Ordovician and Precambrian were estimated at values consistent with under-pressured conditions.

Subsequently, a multilevel monitoring system (Westbay MP55) was installed in SB_BH01 and a long-term pressure measurement program undertaken.

1.3 Reported Analyses

This report summarizes the analyses of straddle-packer hydraulic testing performed in borehole SB_BH01. This testing included twelve pulse tests and three slug tests in the 30.05-m intervals and four pulse tests and one slug test in the 5.03-m intervals.

Transient pressure data collected during straddle-packer hydraulic testing were analyzed using version 3.00T of the nSIGHTS (**n**-dimensional **S**tatistical **I**nverse **G**raphical **H**ydraulic **T**est **S**imulator) well-test-analysis software, a numerical well-test analysis code written in C++ and described in detail in the nSIGHTS User Manual (Geofirma and INTERA, 2011).

2 EQUIPMENT

Low-permeability testing is subject to non-ideal testing conditions that can have significant impact on testing results and suitability of results for analysis. The uncertainty associated with these conditions was minimized through effective equipment design for the SB_BH01 testing.

The majority of tests performed in the SB_BH01 borehole were pulse tests. The pressure response observed during a pulse test is directly proportional to the wellbore storage coefficient of the test interval. The wellbore storage coefficient has two components: the volume of fluid contained within the test zone (V_{tz}) and the compressibility of all the materials within or in contact with the test zone (C_{tz}). V_{tz} includes the volume of fluid between the packers, within any tubing or equipment components below the shut-in valve, and within the feedthrough line connected to the test-zone transducer. C_{tz} is a composite compressibility that includes contributions from the test equipment, the borehole fluid, and the geomechanical response of the borehole wall. To minimize the time required to complete a pulse test, the SB_BH01 equipment was carefully designed and selected to minimize both V_{tz} and C_{tz}. During the SB_BH01 borehole testing, V_{tz} was approximately 0.44 m^3 for 30.05-m test intervals and approximately 0.085 m^3 for 5.03-m test intervals. C_{tz} was minimized through use of extremely stiff packers with high inflation pressures and strong interconnecting components. Most tool feedthroughs and connections were custom-machined stainless-steel components.

During pulse tests in low-permeability formations, variations in packer pressures can cause perceptible changes in test-zone pressure that can mask the actual formation response. To minimize variations in packer pressures, a pressure maintenance system (PMS, see Section 2.3) was hydraulically connected to the packers during testing. The PMS was hydraulically connected to the shut-in valve and the pulse piston as well.

Another important equipment design feature was to provide remote access to the test data in real time. This allowed for off-site supervision of testing and for continuous monitoring of the test response. Remote access also allowed for near real-time preliminary test analyses.

The testing equipment consisted of downhole and surface components. The downhole equipment was connected to surface with four stainless steel hydraulic lines (packer inflate/deflate, piston extend, piston retract, shut-in valve close) and an umbilical cable with transducer power and communication lines. The hydraulic lines and umbilical cable were clamped to the outside of a 2-3/8 inch tubing string that provided the overall mechanical connection between the service rig at surface and the downhole tool.

2.1 Mobile Integrated Aquifer Testing & Analysis (MIATA) Platform

The MIATA platform is a testing system developed by HR and provided capabilities for conducting the SB_BH01 hydraulic tests through a wide range of weather conditions. The MIATA platform provided a controlled environment from which personnel conducted the on-site operations required to successfully execute the hydraulic testing program. The MIATA platform protected all above-ground instrumentation and equipment from exposure to the weather and animals.

The MIATA platform was designed and developed to accommodate both low-permeability and conventional hydraulic testing activities. The operation of the hydraulic test tool (HTT) for low-permeability hydraulic testing applications was one of its core capabilities. The MIATA platform design included:

- Internal hydraulic line control through a pressure manifold;
- Pressure maintenance system to minimize temperature-dependent pressure fluctuations in the packers and downhole hydraulic lines;
- Custom data acquisition and control system (DACS).

Figure 2.1 and Figure 2.2 show the exterior and interior of the MIATA platform, respectively.

Figure 2.1 MIATA platform (white trailer) at the SB_BH01 testing site.

Figure 2.2 Interior of MIATA platform.

2.2 Data Acquisition and Control System (DACS)

The DACS allowed for the collection of data associated with the hydraulic testing and for secure off-site remote access via the internet. This capability reduced the number of on-site personnel required by allowing real-time analysis of the hydraulic tests to be conducted remotely. This also allowed designated parties real-time access to the data and the ability to provide input to the hydraulic testing process as it took place.

The DACS consisted of a remote terminal unit (RTU) connected via ethernet to a field laptop running a real-time monitoring and control system (RTMCS). The RTU received digital and analog measurements from the sensors, converted the analog measurements to engineering units, and recorded the measurements with date-time timestamps to an ASCII file in internal memory using a time interval set by the operator. A file server then automatically transferred the data to the field laptop. If the connection to the field laptop was lost, the RTU continued to record the data until a connection was re-established, at which time it transferred all the buffered data to the field laptop where it was stored in a OneDrive directory accessible by remote staff. The RTMCS provided graphic and numeric read outs of the measurements and allowed the operator to set the recording interval. The RTMCS also maintained an independent database of the measurements, read directly from the RTU, and recorded with a 10-second interval.

2.3 Pressure Maintenance System

The pressure maintenance system (PMS) was a critical component in successfully conducting high quality hydraulic tests in very low-permeability systems. Diurnal temperature changes on the surface cause the expansion/contraction of fluid in the packer inflation lines. In low-permeability intervals, even small variations in packer pressure directly affect the pressure response in the test zone. The PMS virtually eliminated the pressure fluctuations, resulting in a much cleaner pressure response in the test zone.

The PMS had three principal components:

- A pressurised nitrogen source (bottle) with pressure regulator,
- An Alicat pressure controller, and
- A high-pressure hydraulic accumulator containing pressurised nitrogen in a bladder over packer-inflation fluid.

The Alicat pressure controller is connected to the nitrogen bottle and to the accumulator (see schematic diagram in Figure 2.3). The desired packer-inflation pressure ("set" point) is entered into the controller, which has an integral pressure sensor. The controller then adds nitrogen to the accumulator if the pressure drops below the set point or vents nitrogen from the accumulator if the pressure rises above the set point.

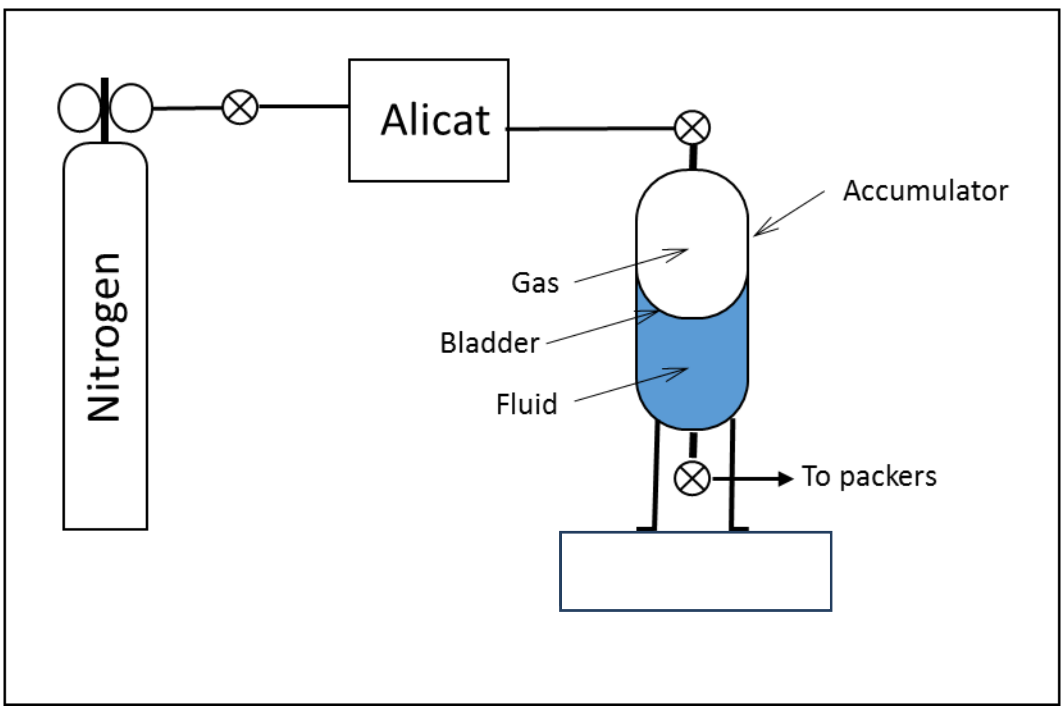

Figure 2.3 Schematic of Packer Pressure Maintenance System.

2.4 Hydraulic Test Tool (HTT)

The straddle-packer HTT (Figure 2.4) consisted of two inflatable packers, a downhole shut-in valve (DHSIV), a piston-pulse generator (PPG), a sensor or (Gauge) carrier, a perforated section, and miscellaneous subs and pass-throughs to connect the various pieces and minimize the fluid volume in the test zone.

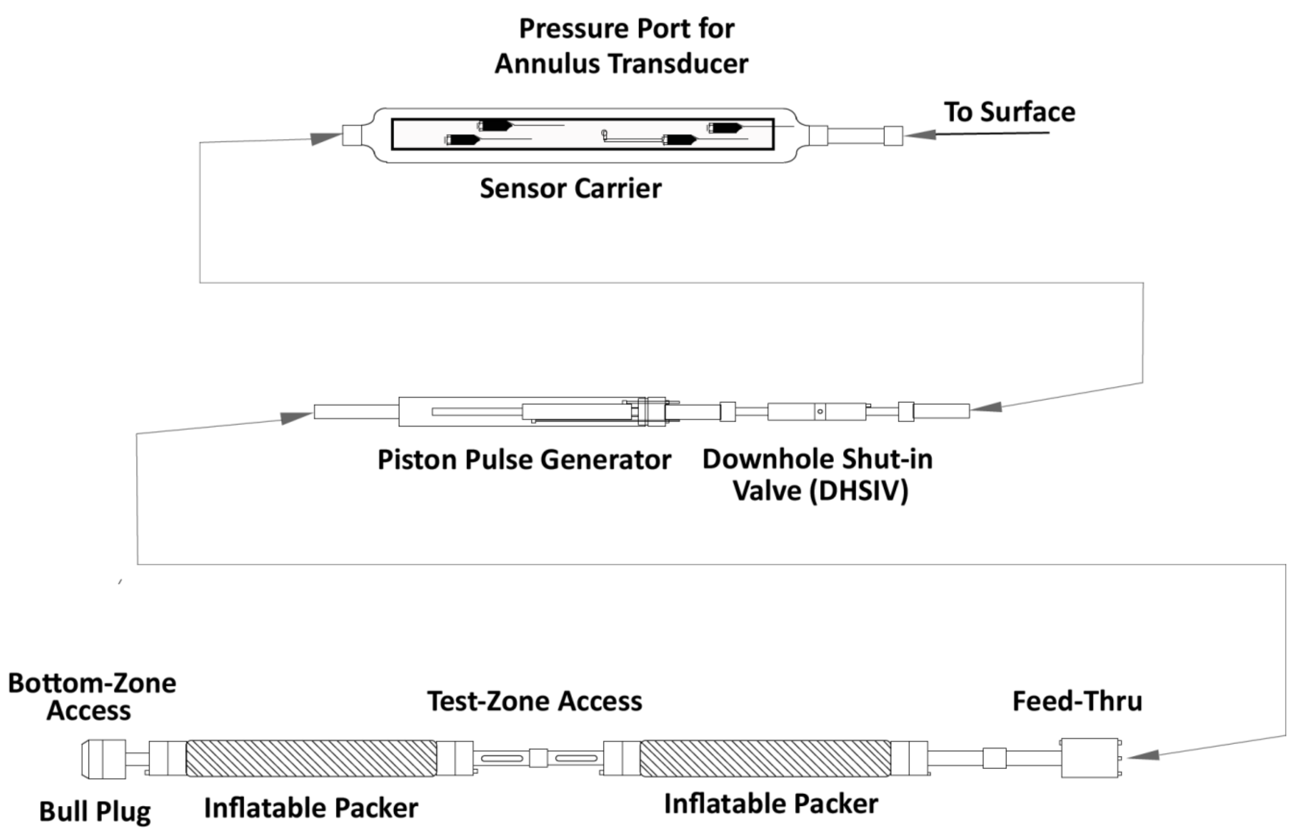

Figure 2.4 General Hydraulic Test Tool Schematic.

2.4.1 Packers

Baski 4.1-inch (104 mm) external-inflate sliding-end Fracker packers (Figure 2.5) were used in the HTT for testing in the PQ (123 mm) borehole. The packers had an uninflated diameter of 104 mm and an element length of 1.14 m, which provided a seal length of approximately 1.0 m in a 123-mm-diameter hole. The packers were capable of withstanding differential pressures of up to 20.7 MPa (3000 psi). The packers and packer-inflation line were filled with non-toxic antifreeze with a density less than 1 gm/cm^3 and inflated using a single ¼-inch stainless steel line by pressurizing a fluid reservoir at the surface with compressed nitrogen to 5 to 15 MPa (725 to 2175 psi), depending upon depth and formation properties. Actual packer inflation pressure depended upon interval depth. The packers were placed on the pressure maintenance system (PMS) once inflated to the desired initial pressure. The packers were oriented so that their fixed ends were up and their sliding ends were down, to avoid putting inflation lines in tension and so that the packers didn't compress and expand during HTT removal.

Some element of abrasion protection for the packers was provided by the largest diameter (115 mm) components in the system, which were the bull plug below the bottom packer and the feedthrough above the top packer.

Figure 2.5 Baski Fracker Packer.

2.4.2 Downhole Shut-In Valve

A downhole shut-in valve (DHSIV) (Figure 2.6) was used to control the connection between the interior of the tubing string above the HTT and the test zone between the inflatable packers. The DHSIV was manufactured by Inflatable Packers International Pty. Ltd. (IPI) of Australia, and used a piston-actuated ball valve within a stainless steel housing. The valve was set up in a normally open position and hydraulic pressure was applied to push an annular piston down, rotating the ball 90° to close the valve. A spring pushed the piston up, opening the valve, when the hydraulic pressure was relieved. The ball had a 1.27-cm-diameter opening and caused no displacement in the test interval when it was actuated. A single ¼ inch stainless steel line was used for DHSIV actuation. As for the packers, a lighter than water non-toxic antifreeze (plumber's antifreeze) was used as the hydraulic fluid for operation of the DHSIV.

Figure 2.6 Downhole Shut-In Valve (DHSIV).

2.4.3 Sensor Carrier

The transducers (Section 2.4.6) used to monitor pressures were mounted in a sensor carrier that was located at the top of the HTT and enclosed and protected the transducers in the borehole.

2.4.4 Piston Pulse Generators

For pulse-testing applications, a pressure pulse was created by displacing a known volume of fluid in the test zone using a hydraulically actuated piston (Figure 2.7). Four versions of the PPG were available with displacement volumes of 15, 30, 60, and 100 cm^3 so that several hundred kPa pulses could be produced in test intervals with different volumes. For the SB_BH01 pulse tests, the 15 cm^3 piston was used in all the 5.03-m intervals and the 100 cm^3 piston was used in all the 30.05-m intervals. The hydraulically actuated pistons were located inside a custom housing that resided above the top packer (but was hydraulically connected to the test zone). The PPG was extended/retracted using two ¼ inch stainless steel hydraulic lines.

Figure 2.7 Hydraulic Pulse Generating Piston.

2.4.5 Test Interval

Two sections of the tool string between the straddle packers allowed flow from the straddled test zone into the tool string. Two perforated 1-ft (0.3048 m) long pup joints of 2-inch NUE stainless steel pipe were used for this purpose. The pup joints (Figure 2.8) had a total of 10,000 mm^2 (15 in^2) open area available to flow into the HTT.

In addition to the perforated sections, two nominal 10m tubing joints and 6 pup joints were used to create the 30.05 m test zone interval. The 5.03 m test zone interval was created with 2 pup joints.

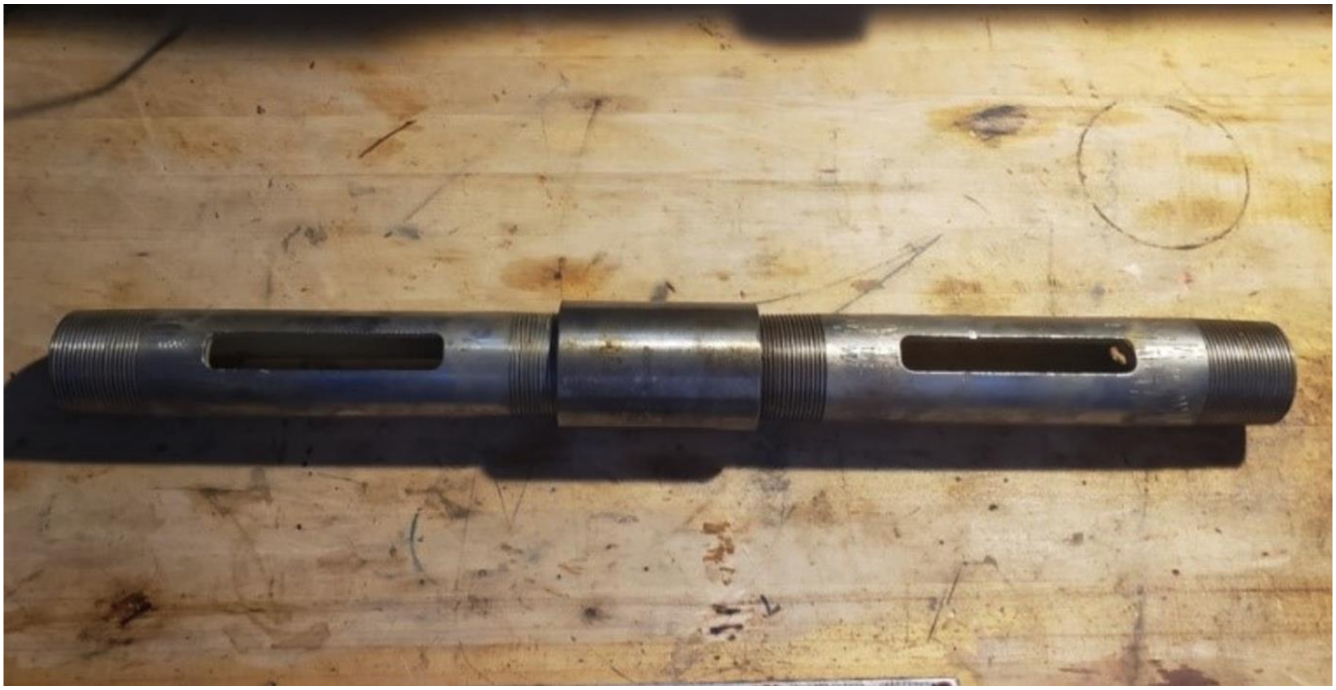

Figure 2.8 Perforated Pup Joints.

2.4.6 Pressure Transducers

For both the 30.05-m and 5.03-m straddle-packer tool configuration, four Keller PAA-33X 30 MPa (300 bar) pressure transducers were used to monitor pressure in the zone below the bottom packer (BZ), the zone in between the packers (TZ), the zone above the top packer between the tubing and borehole wall above the upper packer (Annulus), and inside the tubing string (Tubing). The transducers were housed in a sensor carrier (described above) positioned above the shut-in valve. The transducers had internal electronics that produce temperature-compensated floating point values that were transmitted as text to the data acquisition and control system (DACS) via RS485 Modbus serial data link. The Keller transducers were factory calibrated by Keller, Inc., in May 2020. Transducer calibration times (1 year) were exceeded during SB_BH01 testing. A post-calibration at the conclusion of testing confirmed that all transducers remained in calibration during the SB_BH01 testing campaign (Table 2.1).

The packer pressures, shut-in valve pressure, and piston pressures were monitored with Omegadyne pressure transducers with an operating range of 0-3000 psia (~0-20.7 MPaa). The Omegadyne transducers had a 4-20 mA output which was monitored by the DACS and converted to pressure in engineering units (psi). Hydraulic pressures are not quality-affecting data; the primary purpose of monitoring pressures is to verify that the packers have inflated and to keep their pressure constant.

2.4.7 Temperature Transducers

HOBO temperature logging transducers were installed in the test zone and bottom zone by taping the transducers to the tool below the top and bottom packers. These transducers had internal data logging and thus data were not available in real-time. At completion of the 30 m testing program, both transducers had failed while down hole. New transducers were acquired prior to the 5 m testing program and data from these transducer are used to justify isothermal simulations (Section 4.6)

2.4.8 Tubing String

The test tool was raised and lowered in the borehole using a tubing string comprised of nominally 28 to 32 ft (8.5 to 9.8 m) long joints of 2-3/8" diameter EUE tubing, rated for pressures in excess of 75 MPa. The 2-3/8" EUE tubing string threaded directly into the top of the sensor carrier. Shorter lengths of tubing (pup joints) were used for adjustment of the tool depth, allowing the open end of the tubing to be a reasonable length above the rig deck (nominally 1 m). All pup joints were measured and included in the recorded tubing tally.

2.4.9 Barometer

Barometric pressure was monitored during all hydraulic tests using an In-Situ BaroTroll with a useable pressure range of 16.5 psi (113.7 kPa). The BaroTroll has internal electronics that produce temperature-compensated floating point values that are transmitted to the DACS via RS485 Modbus.

2.5 Summary of Measurement and Test Equipment

Measurement and test equipment (M&TE) requiring calibration, and calibration status are listed in Table 2.1. With the exception of the Alicat and BaroTroll transducers, calibration dates listed in the table for are for the post-calibration conducted at the completion of SB_BH01 testing.

Table 2.1 Measurement and Test Equipment Calibration Summary.

ID	Description	Serial #	Calibration Date	Calibration Renewal Date
Keller-1	TZ transducer	1096425	26 May 2022	26 May 2023
Keller-2	BZ transducer	1096424	26 May 2022	26 May 2023
Keller-3	Annulus transducer	1096427	26 May 2022	26 May 2023
Keller-4	Tubing transducer	1096426	26 May 2022	26 May 2023
Keller-5	Backup transducer	1096428	26 May 2022	26 May 2023
Alicat-1	PMS pressure controller	293473	29 Sep 2021	n/a
Alicat-2	Backup PMS pressure controller	293474	29 Sep 2021	n/a
In-Situ BaroTroll	Barometer	471449	12 Jul 2020	n/a
HOBO-1	TZ temperature	21281229	2 Jun 2022	2 Jun 2023
HOBO-2	BZ temperature	21281231	2 Jun 2022	2 Jun 2023
Omegadyne-1	Packer inflation pressure transducer	430994	31 May 2022	31 May 2023
Omegadyne-2	DHSIV pressure transducer	432809	31 May 2022	31 May 2023
Omegadyne-3	Piston extend pressure transducer	432801	31 May 2022	31 May 2023
Omegadyne-4	Piston retract pressure transducer	430979	31 May 2022	31 May 2023

The as-built 30.05-m and 5.03-m test tool assembly schematics are shown in Figure 2.9 and Figure 2.10.

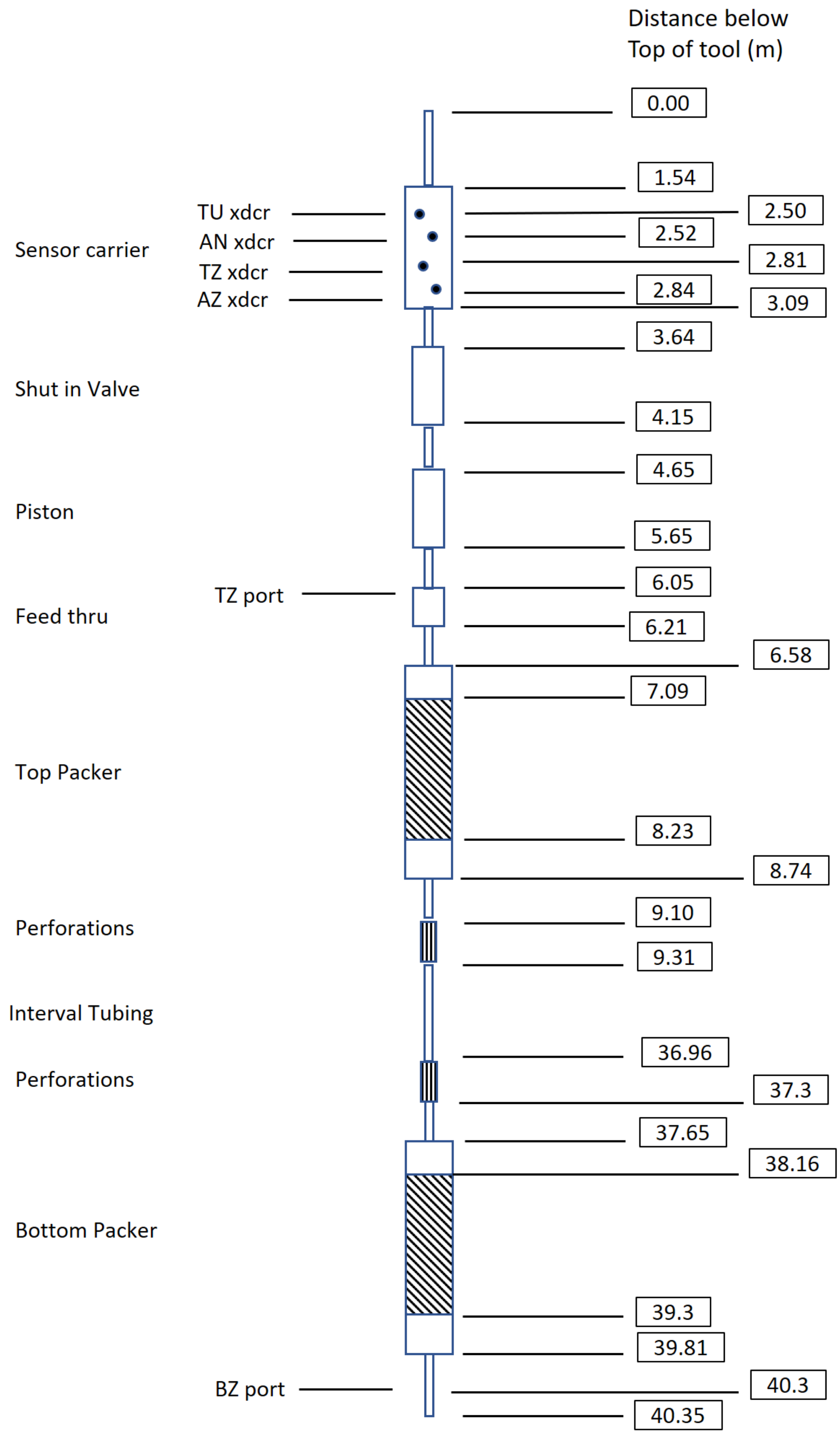

Figure 2.9 As-built 30.05-m test tool with measurements.

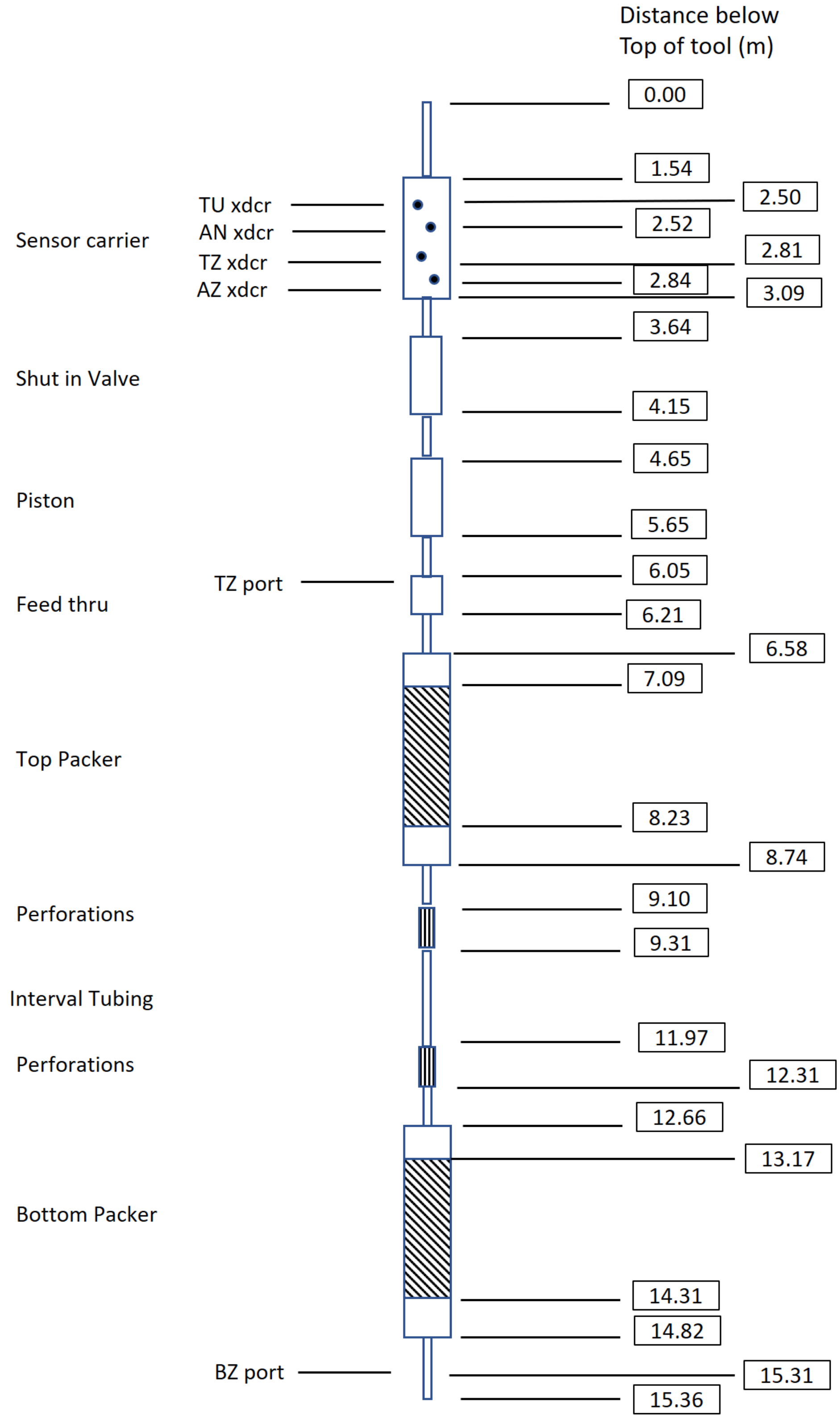

Figure 2.10 As-built 5.03-m test tool with measurements.

3 TESTING METHODOLOGY

3.1 Tool Assembly

The HTT was too long to be completely assembled at surface and then lowered in the hole. Consequently, the tool was assembled in sections (top of tool to upper packer, interval joints, lower packer and below) on surface with the individual sections assembled over the borehole. Hydraulic lines and fittings were pressure tested and “snooped” as the tool was assembled. “Snooping” involves squirting soapy water over the connection and visually monitoring for bubbles.

3.2 HTT Installation and Leak Testing

The HTT was lowered into the well on 2-3/8 inch tubing with the shut-in valve open to its desired position with respect to the first interval to be tested. Tubing joints were prepared with PTFE thread sealant and assembled with pipe wrenches to ensure a leak proof seal. For subsequent intervals, the tool was moved down to the specified interval position.

Leak testing in the surface casing was performed before the test tool was lowered to formation depths. The tool was typically lowered to a depth of 40 metres below the static water level in the BH. Packers were inflated with the DHSIV open and the pulse piston in retracted position. After inflation, the DHSIV was closed and the pressure monitored for fluctuations that indicate fluid leakage into the TZ. The pulse piston was extended producing a pulse , and the response monitored for several hours. The leak tests were analyzed in nSIGHTS to ensure the hydraulic conductivity met the criteria of less than 10^{-13} m/s. Leak testing was also performed after each tool reconfiguration or repair during testing. All accepted leak tests were significantly tighter than the acceptance criteria, with hydraulic conductivities down to 10^{-15} m/s. Results for initial leak testing on the 30 m tool configuration are shown in Figure 3.1.

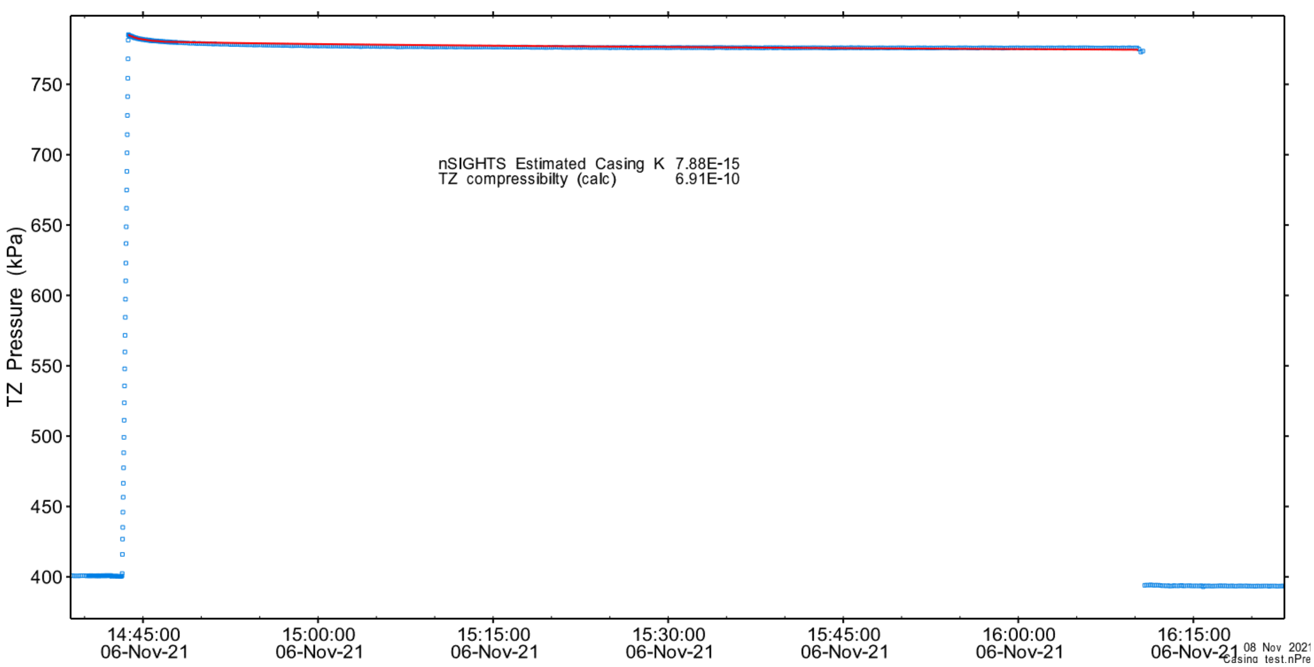

Figure 3.1 Analysis of leak test of 30.05 m HTT system.

Based on the target depth and tool measurements, the number of full joints of tubing needed for the HTT installation was calculated. Additional tubing joints and/or pup joints were added as needed to position the HTT precisely. In selecting and positioning pup joints, allowance was made for handling requirements at the surface. All tubing tallies and depth calculations were verified by a second individual and recorded before testing of an interval began. Tubing and pup joint calculations were recorded in the DQCW tubing tally sheet for each test.

Communication with the downhole pressure transducers was verified after every 10 joints (approximately 100 m) of tubing was installed.

Once the HTT was positioned at the desired depth, all transducers were connected to the DACS and data acquisition was initiated. The water levels in the annulus and the tubing string were measured at this time. The heights of the water columns in the tubing and annulus above the tubing and annulus transducer ports, respectively, combined with coincident pressure measurements allowed for two calculations of the effective water density, serving as a cross-check. All data relevant to these calculations and the calculation results were recorded in the DQCW. If calculated densities were significantly different, water level measurements were rechecked until reasonable agreement was established.

After all planned 30-m test intervals were completed, the HTT was tripped out of the borehole and a final leak test performed prior to reconfiguring the HTT for the 5-m testing.

3.3 Packer Inflation

Minimizing test-zone compressibility (C_{tz}) is imperative to maximize pulse test pressure response in low-permeability intervals. The most significant factor in test-zone compressibility is packer inflation pressure. Packers were inflated to the maximum pressure possible without impacting formation integrity and consistent with operational constraints. A geo-mechanical analysis of formation breakdown pressures (Figure 3.2) calculated maximum packer inflation system pressures at surface as a function of test interval depth. Formation breakdown pressure is an estimate of the radial pressure at which fracturing of the adjacent formation may occur. Combining the maximum calculated pressure with an operating pressure range (minimum required to inflate packers and maximum safe operating pressure of MIATA components) yielded a linearly varying range of maximum packer inflation from 6 MPa at 200 mBGS to 15 MPa below 560 mBGS.

Excessive N_2 consumption by the Alicat controller during testing required a reduction of maximum pressure to 11.7 MPa (1700 psi) which was used for all tests deeper than 430 mBGS.

Packers were inflated to the desired pressures and PMS settings were recorded. The shut-in valve was maintained in an open position while the packers were inflated to avoid pressure squeeze in the test interval.

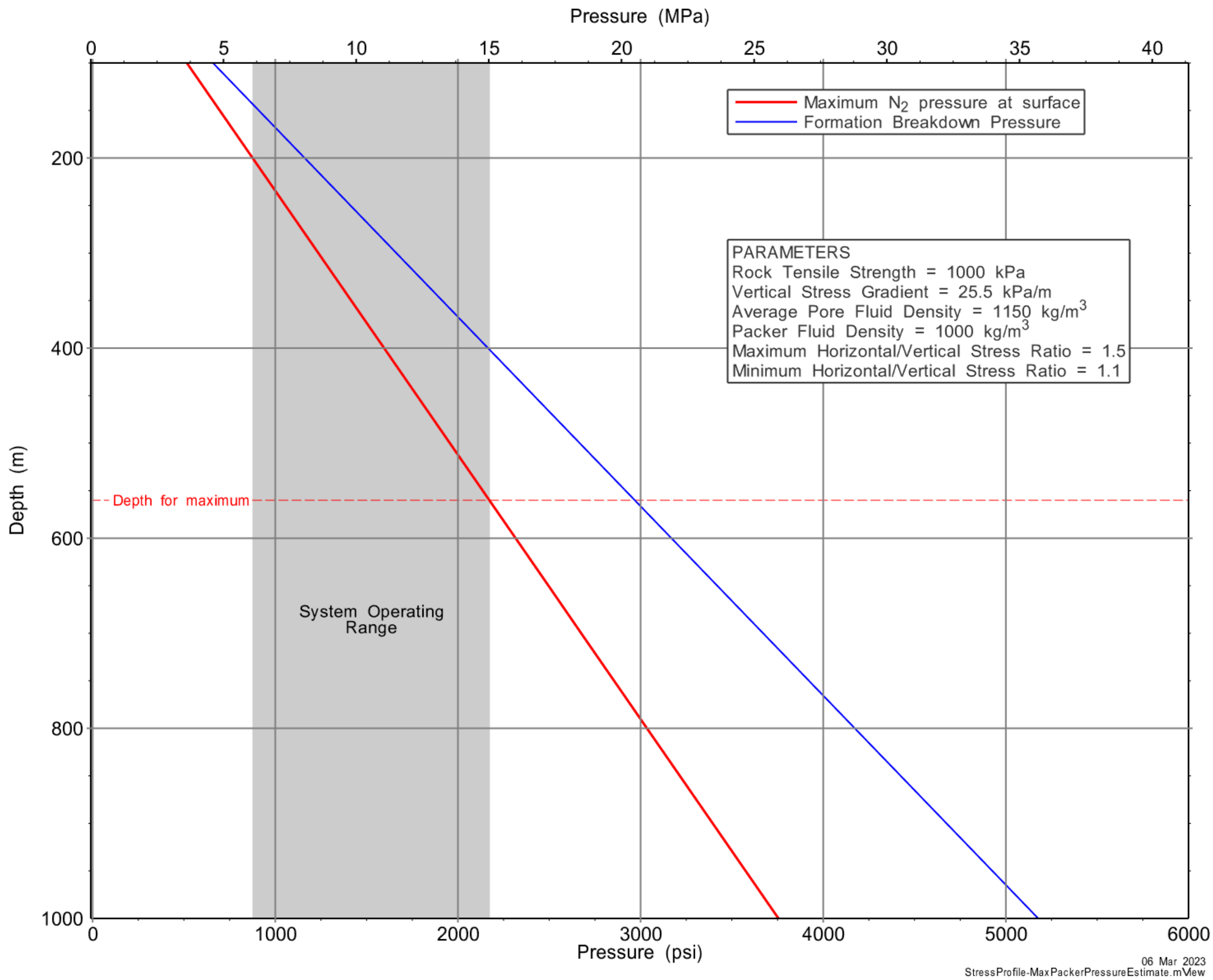

Figure 3.2 Packer Inflation Pressure Ranges

3.4 System Stabilization

Hydraulic pressures were reviewed to ensure the pulse piston position was "retracted" for testing to begin with a pulse injection.

After the pulse piston position was confirmed, the DHSIV was closed. Piston position and DHSIV closing time were recorded. The pressure in the now isolated test zone then began to change relative to the annulus pressure and the tubing pressure, as the test-zone pressure equilibrated with the far-field static pressure of the interval being tested. The bottom hole pressure typically showed a pressure increase during packer inflation due to "packer squeeze," and then either increased or decreased depending on the natural formation pressure in the interval isolated below the bottom packer. Tubing string pressure remained constant apart from minor effects due to the atmospheric pressure changes once the DHSIV was closed.

Initially, the tubing pressure and annulus pressure were similar. Prior to initiating a slug test, enough water was removed from the tubing to lower the tubing pressure by approximately 150 to 350 kPa.

The system was then typically left to stabilize/equilibrate overnight. The stabilization period was sometimes shortened if relatively stable pressure conditions were obtained rapidly, as was the case in higher permeability test intervals. Note that equilibration did not necessarily mean a constant TZ pressure, as under-pressured or over-pressured formations and/or borehole history sometimes caused TZ pressure to rise and fall, and several hours of equilibration would not compensate for the effects of weeks of pre-test borehole history.

3.5 Slug Testing

After equilibration, the DHSIV was opened in certain intervals to initiate a slug withdrawal and the event was recorded. Slug tests were performed in four SB_BH01 intervals: HT02_30 (Salina B); HT03_30 (Guelph); HT04_30 (Gasport/Lions Head/Fossil Hill); and HT01_05 (Salina A2 Evaporite).

3.6 Pulse Testing

After equilibration, pulse-injection tests were initiated in certain intervals by extending the piston. The pulse pressure differential (TZ pressure immediately before and after pulse initiation) was used along with the test-zone volume and pulse-piston displacement volume to calculate the test-zone compressibility (C_{tz}). Test-specific C_{tz} is an essential parameter for accurate simulation of pulse tests. C_{tz} integrates the essential components of the combined test tool, test zone and formation mechanical response. When combined with the actual test zone fluid volume, it forms the boundary condition term for pulse tests. It is not possible to accurately estimate C_{tz} without either a PPG or accurate measurements of tubing string fluid level changes in response to the DHSIV open/close sequences. Test-specific variables such as packer construction details, packer inflation pressure, formation rock compressibility, and test zone fluid compressibility preclude using estimated or generic values. Uncertainty in formation hydraulic parameter estimates is not quantifiable unless actual test-specific C_{tz} data are used.

At completion of the PI tests, the pulse piston was retracted to initiate a brief PW. This allowed verification that the same magnitude pulse was created by piston retraction as was created by piston extension at the start of the test. This confirmed that C_{tz} was constant over the test duration.

3.7 Test Termination

After a test was terminated, the DHSIV was opened, the packers were deflated, data acquisition terminated, and the raw test data file was produced. The file (CSV format) contained date/time stamps and pressure responses for all real-time transducers. The file was imported into nSIGHTS to produce a set of reference plots to be included with the DQC workbook.

3.8 Real-Time Analysis

The nSIGHTS well-test-analysis software (Section 4) was used to provide preliminary estimates of formation properties as testing progressed. Test-zone pressure histories were constructed for each testing sequence using the relevant data starting from drilling intercept to the start of the current sequence and were included in the analyses.

The measured test response for the equilibration/stabilization period during a testing sequence formed an additional pre-test history sequence. As a test progressed, measured TZ pressures were used to update the test sequence and the analysis continued. A final optimization with all the test data was performed immediately following test termination. These preliminary test analyses were recorded in the DQCW describing test results. All real-time analysis results are superseded by analyses presented in this report.

4 ANALYSIS APPROACH

A discussion of the conceptual flow models, descriptions of the types of hydraulic tests performed, definitions of the various fitting parameters, a discussion on borehole pressure history, and an overview of the analysis process, including the uncertainty calculations, are given below.

4.1 Conceptual Model

The term *conceptual model* in this report refers to the mathematical description of the hydrogeologic system. Selecting a conceptual model is the first step in the overall analysis process. The choice of conceptual model, along with the type of hydraulic test(s) performed, determines which parameters will be estimated, i.e., which parameters will be fitting parameters in the analysis process.

In a near horizontally layered sedimentary sequence, like that tested in borehole SB_BH01, where the borehole is drilled approximately perpendicular to the layers, the simplest conceptual model that is generally invoked in well-test analysis is described as an infinite-acting, radial-flow system with wellbore storage and skin. *Infinite-acting* means that the hydraulic parameters controlling the test response, such as transmissivity (T) and storativity (S), are constant within the region affected by the test and the test is not affected by external boundary conditions. The term radial indicates horizontal convergent flow toward and/or away from the test zone (depending on the gradient induced during a test). Note that all flow is assumed to be horizontal within the tested layer, i.e., flow with no vertical component. A further assumption made in the conceptual model is that the hydraulic properties of the tested interval do not vary vertically. This assumption may not hold true when multiple formations are included in the test interval.

Wellbore storage is that property of the testing system whereby some portion of the fluid injected/withdrawn during a hydraulic test is taken up by / derived from the test zone (shut-in valve is closed) or the tubing (shut-in valve is open) rather than the formation. During the wellbore-storage dominated period of a test, the formation properties of interest have little effect on the observed pressure response, meaning the formation properties are masked to some extent. The wellbore-storage dominated period of a test is that period in a test where the total system compressibility acts to mask the formation pressure response by absorbing/producing fluid unrelated to fluid movement in/out of the formation. Ideally, a test will proceed long enough such that the formation-flow component dominates the wellbore-storage component and the formation properties can be reliably estimated. The adequacy of the SB_BH01 test durations was determined by real-time analysis.

An area of altered hydraulic conductivity surrounding the wellbore that results from drilling activities (e.g., mud infiltration, stress relief, etc.) is termed a skin. A positive skin is a zone in which K has been decreased relative to the unaltered formation K. A negative skin is a zone in which K near the wellbore has been enhanced. Skin was included in all SB_BH01 simulations and was implemented using nSIGHTS' radially varying hydraulic conductivity functionality in which hydraulic conductivity changes logarithmically as a function of distance. A fixed radius point was placed at the wellbore with hydraulic conductivity optimized to represent initial skin conductivity. An adjustable radius point was placed to define the skin thickness and the optimized formation hydraulic conductivity. Formation hydraulic conductivity was constant beyond this adjustable radius point.

4.2 Parameters

Hydraulic conductivity (K) [L/T] is a constant of proportionality that was empirically derived by Darcy (1856) expressing the ratio of fluid flux to gradient within a porous medium. Darcy's empirical relationship is generally referred to as Darcy's Law, and can be written as follows:

$$Q = -K \frac{dh}{dl} A$$ **Equation 4-1**

where:

Q	=	flow rate	$[L^3/T]$
dh/dl	=	hydraulic gradient	[ ]
A	=	flow area	$[L^2]$

The specific storage (Ss) [1/L] of a saturated geologic unit describes the amount of fluid released as a function of both the rock and fluid compressibility per unit decline in hydraulic head per unit volume of rock, and is given as:

$$S_s = \rho g(\alpha + n\beta)$$ **Equation 4-2**

where:

ρ	=	fluid density	$[M/L^3]$
g	=	gravity	$[L/T^2]$
α	=	rock compressibility	$[LT^2/M]$
n	=	porosity	[ ]
β	=	fluid compressibility	$[LT^2/M]$

Well-test analysis does not provide estimates of K and Ss, but of their products when multiplied by the test-interval length, transmissivity (T) $[L^2/T]$ and storativity (S) [-]. For the analyses presented in this report, K and Ss were calculated by assuming that all test intervals were vertically homogeneous and simply dividing the inferred values of T and S by the test-interval length. The validity of this assumption undoubtedly varies from test interval to test interval; when a test interval is wholly contained within a single formation, vertical homogeneity may be a reasonable assumption. But when a test interval spans portions of several formations, the assumption is less defensible. In such a case, other information must be used to try to infer what portion of the total T (or S) is contributed by the K (or Ss) and thickness of each formation in the test interval.

Static formation pressure (P_f) $[M/LT^2]$ is the undisturbed fluid pressure within a formation prior to drilling and testing. "Raw", or uncorrected, formation pressures are those measured by the transducer, which is located some distance above the centre of the test zone. These "raw" numbers are used in the individual test analyses presented below. The raw values are subsequently corrected to represent the pressure in the centre of the test interval. Borehole fluid density estimates and measured transducer locations are used in calculating corrections. The corrected values are presented in the test summary tables and the borehole summary tables (Section 0).

The observed pressure change (*ΔPressure*) in the isolated test zone for a given amount of fluid (*ΔVolume*) that enters/leaves the test zone is controlled by the test-zone compressibility (C_{tz}), defined as follows:

$$C_{tz} = \frac{1}{TotalVolume} \frac{\Delta Volume}{\Delta Pressure}$$ **Equation 4-3**

where: *Total Volume* = total volume of fluid within the isolated test zone

The skin factor (s) [ ] is a dimensionless parameter that indicates the relative degree to which skin hydraulic conductivity (K_s) near the borehole differs from the undisturbed formation hydraulic conductivity (K_f) at some distance away from the borehole. The skin factor is defined by Hawkins (1956) as:

$$s = \left(\frac{K_f}{K_s} - 1 \right) \times \ln \left(\frac{(r_w + t_s)}{r_w} \right)$$ **Equation 4-4**

where:

r_w = nominal well radius [L]
t_s = skin thickness [L]

In the case where the value of K_s is changing logarithmically with distance from the borehole wall to the value of K_f, the value of K_s used in Equation 4-4 is the log average of K_s at the borehole wall (which is the value fitted by nSIGHTS) and K_f.

4.3 Tests

A pulse injection (PI) or pulse withdrawal (PW) test is an instantaneous (within the limitations of the equipment) pressure increase or decrease induced in the test zone that is subsequently allowed to dissipate back toward static pressure conditions. The rate of pressure decay is used to infer the hydraulic properties of the tested geologic unit. During a pulse test, the test zone is shut-in, i.e., it is isolated from the fluid column in the tubing by closing the shut-in valve. Pulse tests are most suitable for testing formations with hydraulic conductivities less than 1E-10 m/s, and were performed in the majority of the test intervals.

Compressibility of the SB_BH01 test zones was calculated for each pulse test. All SB_BH01 pulse tests were initiated by rapidly extending the downhole pulse piston of known volume. The C_{tz} was then calculated from Equation 4-3 by measuring the initial pressure change, given that the test-zone fluid volume was known. (Note that the test-zone fluid volume comprises the fluid in the borehole between the two packers as well as all fluid contained within the test tool below the shut-in valve.) Note that hydraulic parameters such as K cannot be estimated accurately from pulse responses without knowing C_{tz}. All pulse tests performed in SB_BH01 used an initial PI, followed by a PW at the end of the test to confirm C_{tz}.

Slug withdrawal (SW) tests are similar to pulse tests, but the shut-in valve remains open during a slug test and fluid flowing out of the formation results in changing water levels within the tubing. Slug tests were initiated by removing water from the tubing to a desired level while the shut-in valve was closed, and then rapidly opening the shut-in valve. Analogous to C_{tz} in a pulse test, the tubing radius and fluid density controlled the observed pressure change for a given amount of fluid that entered/left the tested formation. The tubing string radius must be known to estimate K from a slug-test response.

4.4 Formation Specific Storage - Skin Conductivity - Skin Thickness

Simultaneously estimating Ss, skin K (K_s), and skin thickness (t_s) values from analysis of single-well data (i.e., no cross-hole response) is complicated by the high degree of correlation among these fitting parameters in the regression process. Figure 4.1 shows 1345 estimates of these three parameters obtained from perturbation analysis (Section 4.6) of an example pulse test conducted in a low-permeability sedimentary formation. Note that each of the 1345 solution sets produced effectively equivalent matches (small change in the fit value) to the measured response. The values of K_s and t_s can be simultaneously increased/decreased over a range that results in approximately the same skin factor, s (Equation 4-4).

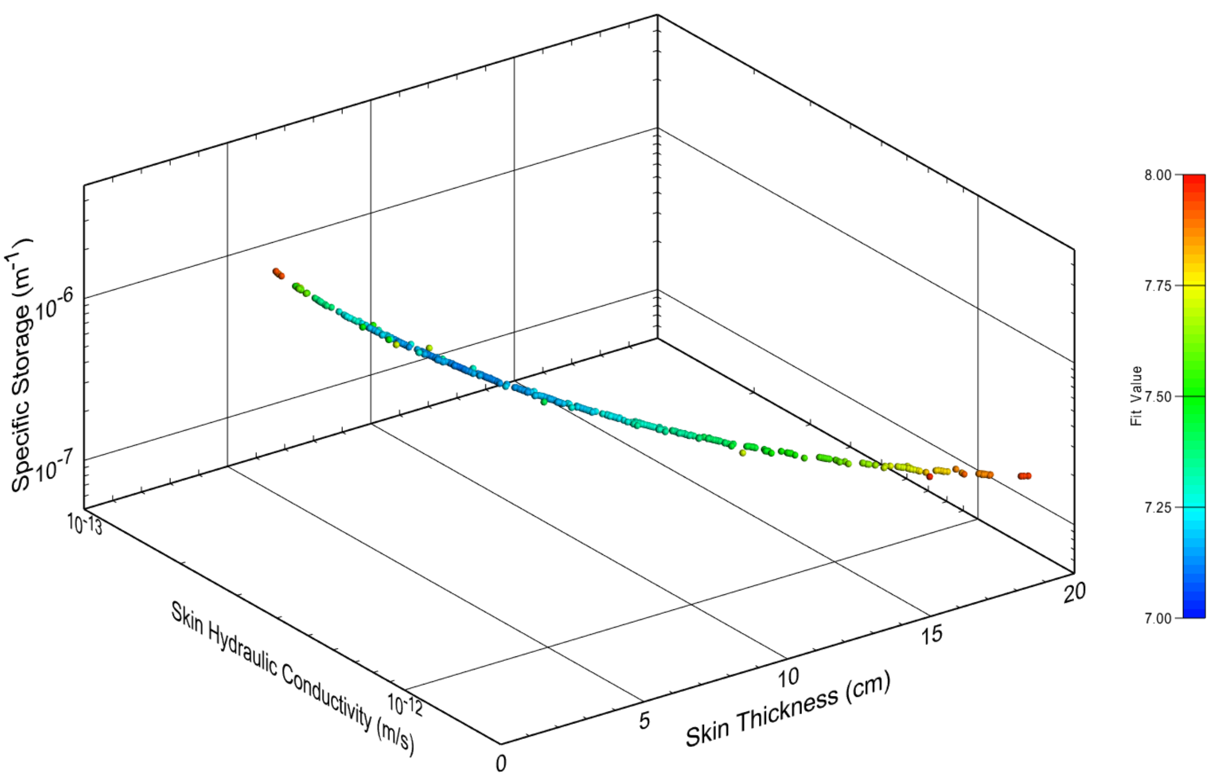

Figure 4.1 An X-Y-Z scatter plot showing the correlation among skin thickness, skin hydraulic conductivity, and specific storage that can occur in a single-well test.

In addition, Ss and s affect the match to a single-well pressure response in much the same way, so they can be simultaneously changed to produce a series of equivalent matches. Figure 4.2 shows simulated pulse-test responses assuming equilibrium initial conditions plotted on a log-log scale as a normalized pressure response and its derivative; a standard well-test diagnostic plot known as a Ramey B plot

(Ramey et al., 1975). Various parameter possibilities are simulated to illustrate the difficulty in distinguishing among variations in Ss and s.

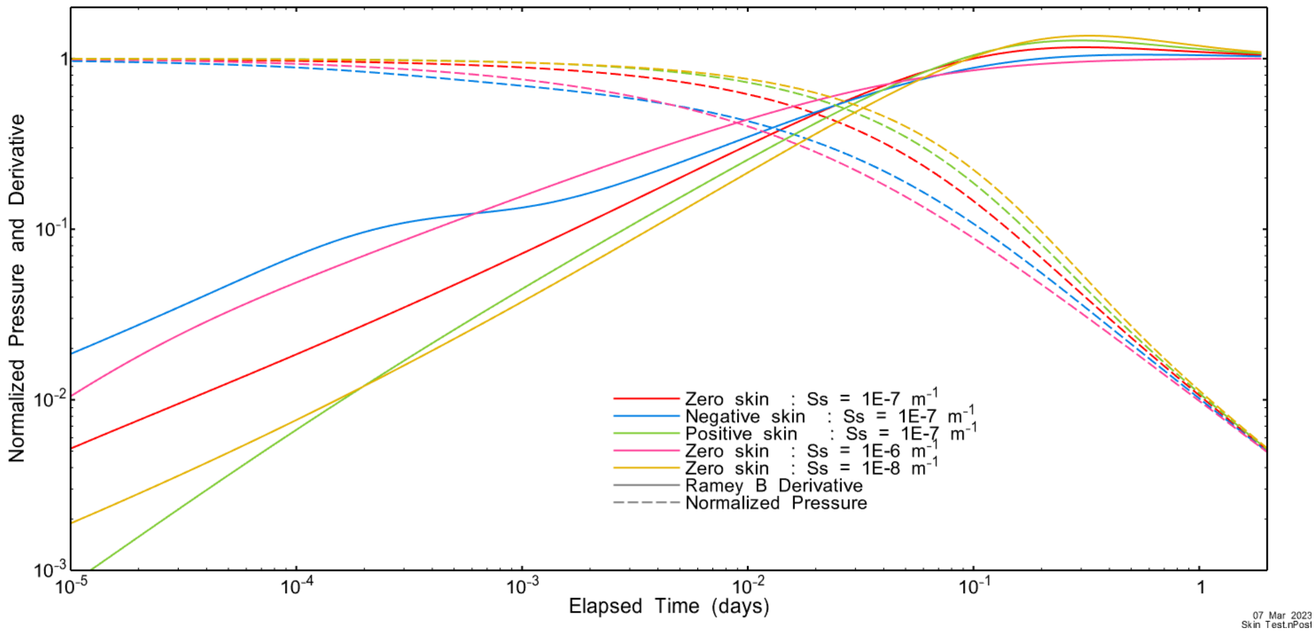

Figure 4.2 Ramey B diagnostic plots showing various combinations of skin factors and formation specific storage.

The baseline example shown in red in Figure 4.2 shows simulated responses when the hydraulic properties around the wellbore have not been altered – a condition known as a "zero" skin. Note that Ss for the baseline case is 1E-7 m^{-1} and the formation K (K_f) for all examples is constant. When the drilling process results in increased K_s over some distance t_s near the wellbore relative to the unaltered formation K_f, the condition is known as a "negative" skin, plotted as a blue line in Figure 4.2. Notice that the negative skin produces a distinctive downward inflection in that part of the Ramey B derivative that appears as an upward-sloping straight line when no skin is present (timing and magnitude of this inflection depend on the contrast between skin and formation properties). This inflection is observed in most of the DGR pulse responses. A decrease in K_s over some distance t_s around the wellbore is known as a "positive" skin, plotted in green in Figure 4.2. Unlike the negative skin, a positive skin causes no distinct inflection in the Ramey B derivative; it simply changes the slope of the derivative (the pulse recovery is slowed), effectively translating it to the right on the graph relative to the zero-skin case. Shown in magenta and gold are two zero-skin examples where Ss has been increased to 1E-6 m^{-1} and decreased to 1E-8 m^{-1}, respectively. As with the positive-skin case, simply changing the value of Ss does not result in a notable inflection in the derivative, it primarily changes the position of the derivative with respect to the baseline case. Figure 4.1 shows that changing K_s or Ss can result in similar responses, and consequently, estimates for each of these parameters can be paired in non-unique combinations to achieve similar matches to field data. In the case where the initial conditions at the start of a pulse are transient rather than in equilibrium (i.e., pressure is still responding to borehole history), the early-time derivative response may be altered from what is shown in Figure 4.2. Under these conditions, an inflection in the early-time derivative reflects the presence of a skin, but not whether it is positive or negative. Also note that any small transient changes in test-tool position or packer shape at the start of a pulse or slug test can affect the pressure response in such a way that these nonformation responses resemble a skin effect. The approach used in these analyses for estimating Ss is discussed below in Section 4.7.

4.5 Pre-Test Borehole History

Each nSIGHTS simulation description includes a detailed specification of the sequence of borehole boundary conditions from the point at which the borehole perturbs the in situ, or formation, pressure. The sequence of pressures experienced by a test interval during the period between interception of the interval by drilling and the start of testing is denoted the "pressure history".

Pressure histories were included in the analyses performed for each test interval as specified-pressure boundary conditions in the test zone. Part of the pressure history consisted of the calculated pressure (not measured by transducer) at the centre of each test interval from the approximate time of drilling intercept to the time that the pressure at that interval was measured by a pressure transducer.

Fluid densities recorded during drilling and logging were nominally 1100 g/L with some measurements as low as 1086 g/L. There were considerable drilling fluid losses after drilling through and below permeable Silurian formations, primarily the Guelph. Subsequent to completion of drilling, borehole fluid equilibration occurred as lower density formation fluids from intervals above the Guelph replaced the higher-density drilling fluids that migrated into the Guelph. It is assumed that borehole pressures would remain relatively constant as Guelph formation pressures dictated overall borehole response. Accordingly, the borehole pressure history prior to testing was fixed at the first measured pressure at the start of the first test (HT01_30). Testing was halted after HT13_30 to remove accumulated fines and borehole debris from the borehole. This process required extensive flushing of the borehole with 1100 mg/L brine. This fluid remained in the borehole for the duration of BH01 testing.

Subsequent to the start of straddle-packer testing in a given interval, pressure histories are extracted from measured pressures in the annulus and bottom zones of previous tests. As an illustrative example, the borehole history for the 30.05-m test conducted in the Upper Cobourg (HT11_30, 646 to 676 mBGS) is shown in Figure 4.3. The constant pressure from drilling intercept until start of HT testing reflects the TZ pressure measured at the beginning of HT01_30. Tests conducted above the permeable Guelph Formation did not result in significant BZ pressure changes. However, subsequent tests on lower intervals all showed an under-pressured response in the BZ which is included in the borehole history. Measured BZ pressures were adjusted to the center of the test interval using the average borehole fluid density. Figure 4.4 shows the history for test HT14_30 which incorporates the borehole cleaning period as a constant pressure equal to the initial on-depth pressure for the HT14_30 test.

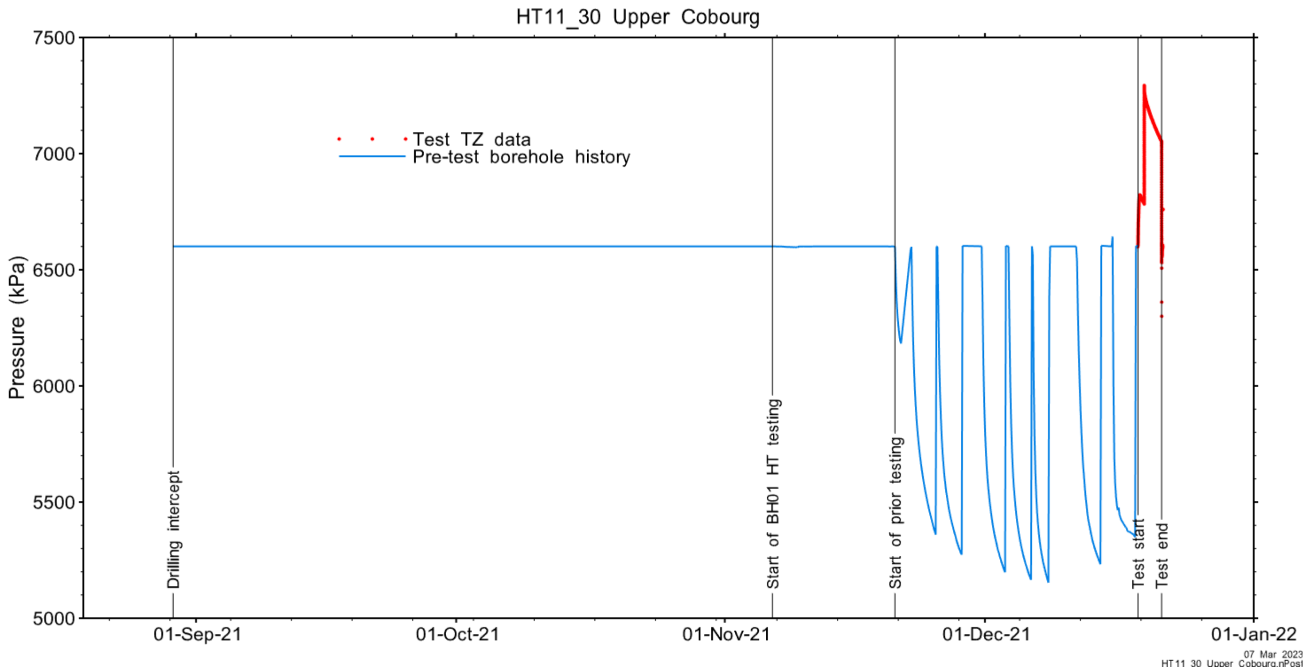

Figure 4.3 Pre-test borehole history for test HT11_30.

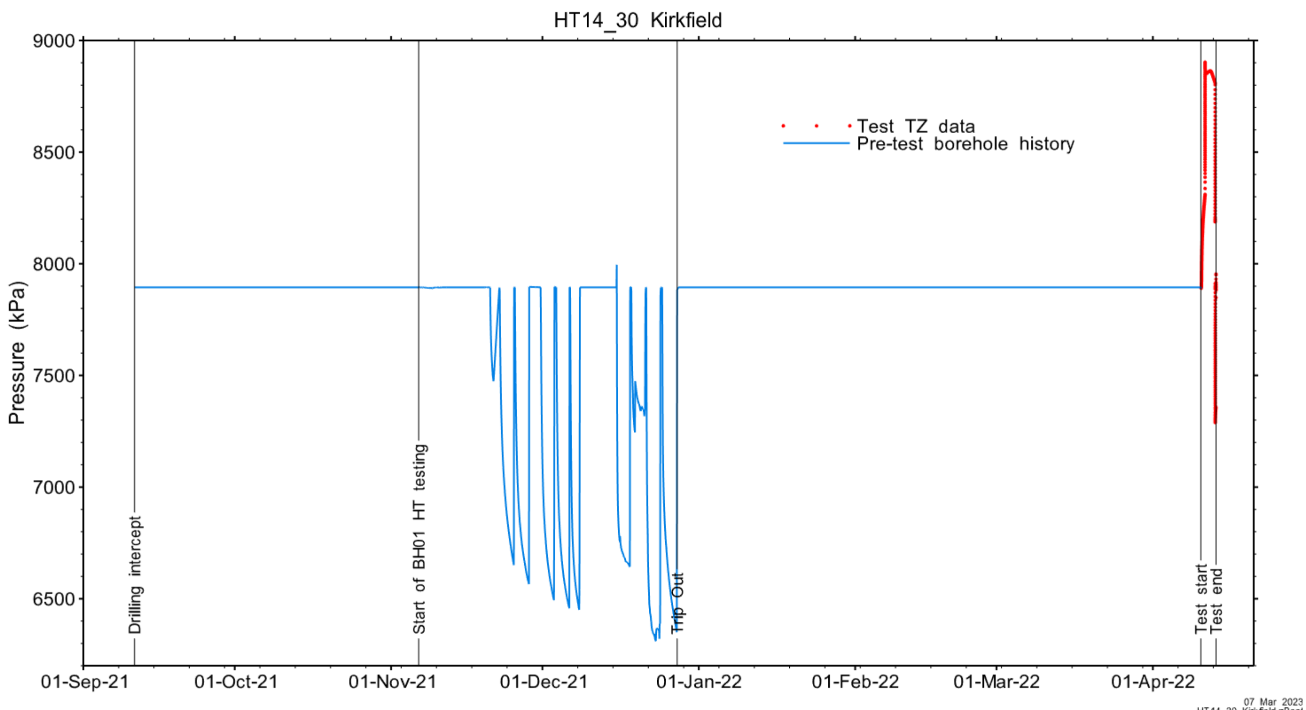

Figure 4.4 Pre-test borehole history for test HT14_30.

4.6 Test Zone Thermal Effects

Temperature changes in the shut-in test zone during pulse tests will cause thermal expansion or contraction of the borehole fluid, leading to pressure changes which complicate the analyses. Although nSIGHTS has the capability of including thermal effects in analyses, this leads to additional uncertainties in analysis results. Test zone temperatures for the four 5 m pulse tests in BH01 (Figure 4.5) showed no evidence of thermal effects. All analyses were conducted as isothermal.

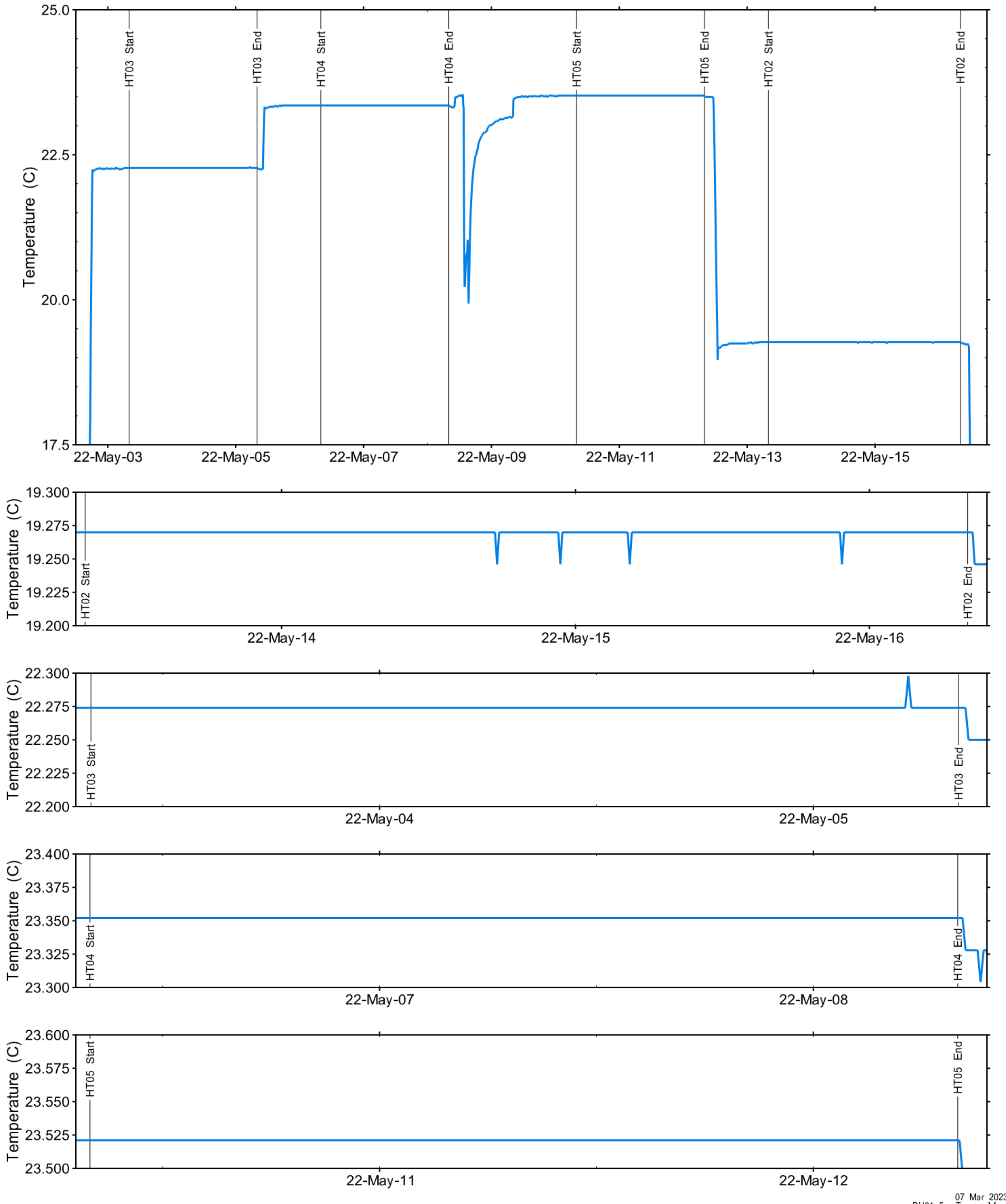

Figure 4.5 Test zone temperature during 5 m pulse tests in BH01.

4.7 Uncertainty Analysis

All tests analyzed in this report assumed the skin conceptual model described in Section 4.1, which requires five fitting parameters: K_f, P_f, K_s, t_s, and Ss. Preliminary analyses obtained a single set of optimized baseline fitting-parameter values. These were used to determine limiting ranges, or domains, for each optimized parameter. Perturbation analyses were then performed to obtain the final best-fit parameter values and the corresponding uncertainty ranges.

For these analyses, 10,000 simulations were performed using randomized starting parameter estimates uniformly distributed over the potential parameter domain. Simulations which converged on an optimized solution (typically the vast majority of the 10,000 perturbations) were retained for further analyses. Initial and converged parameter estimates for selected parameters in the HT11_30 test analyses are shown in Figure 4.6 through Figure 4.9. Each figure shows data for three parameter domains – K_f is shown on all figures.

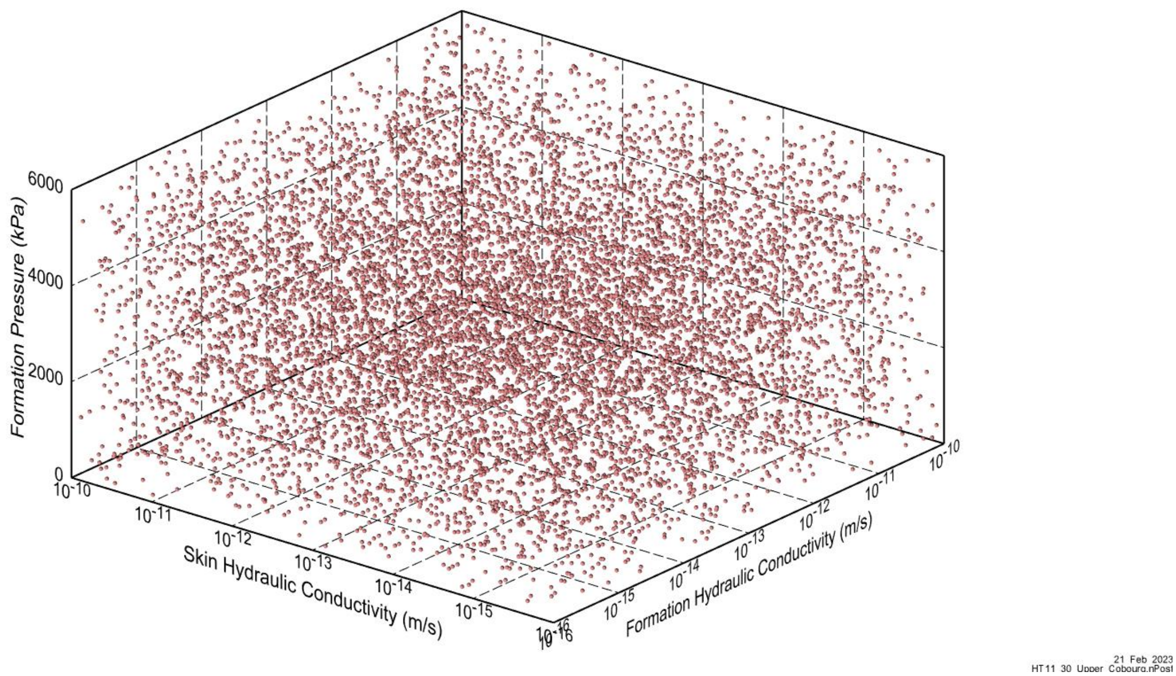

Figure 4.6 Initial parameter estimates for K_f, K_s, and P_f (HT11_30).

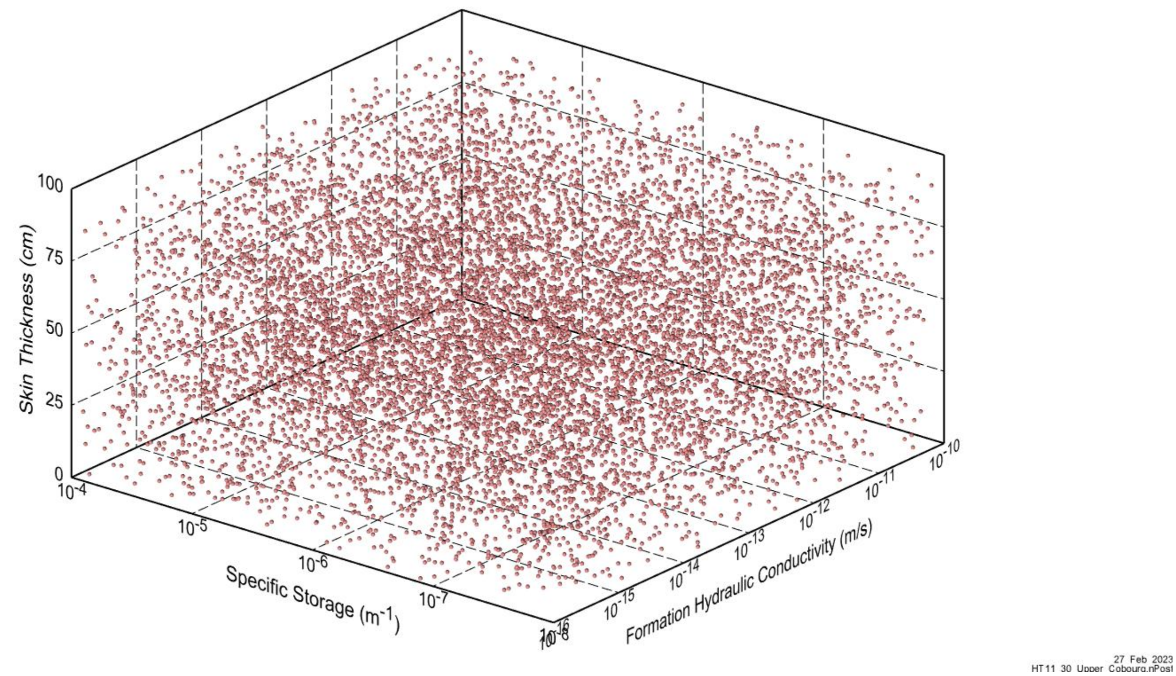

Figure 4.7 Initial parameter estimates for K_f, Ss, and t_s (HT11_30).

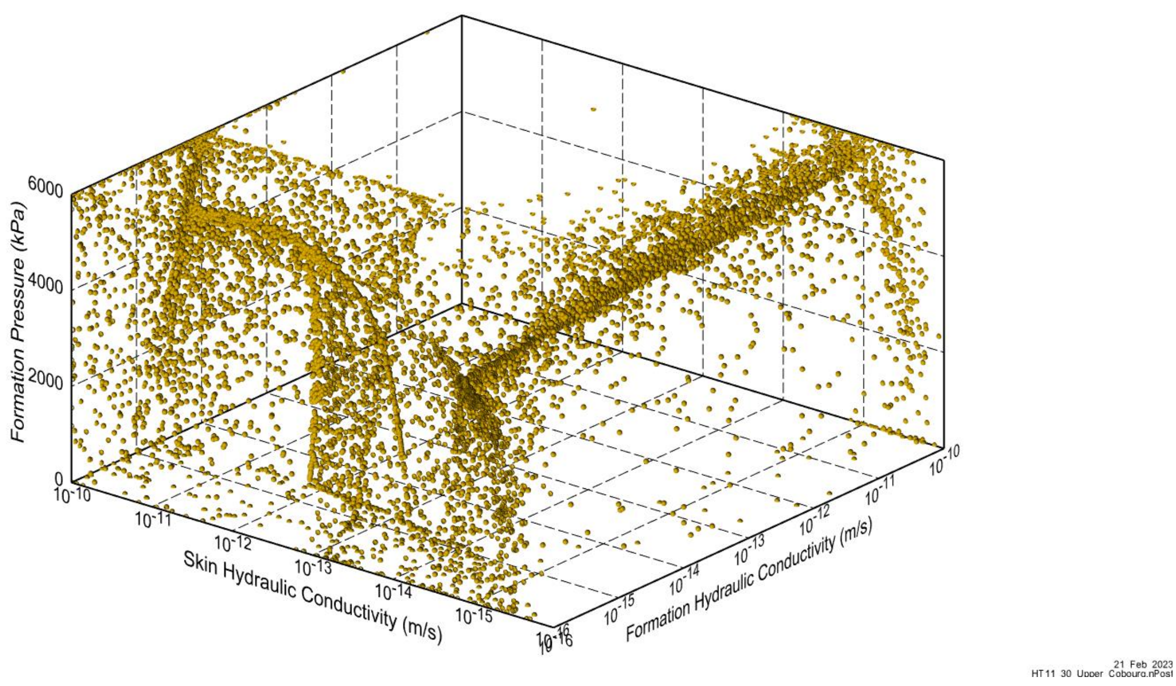

Figure 4.8 Converged parameter estimates for K_f, K_s, and P_f parameters (HT11_30).

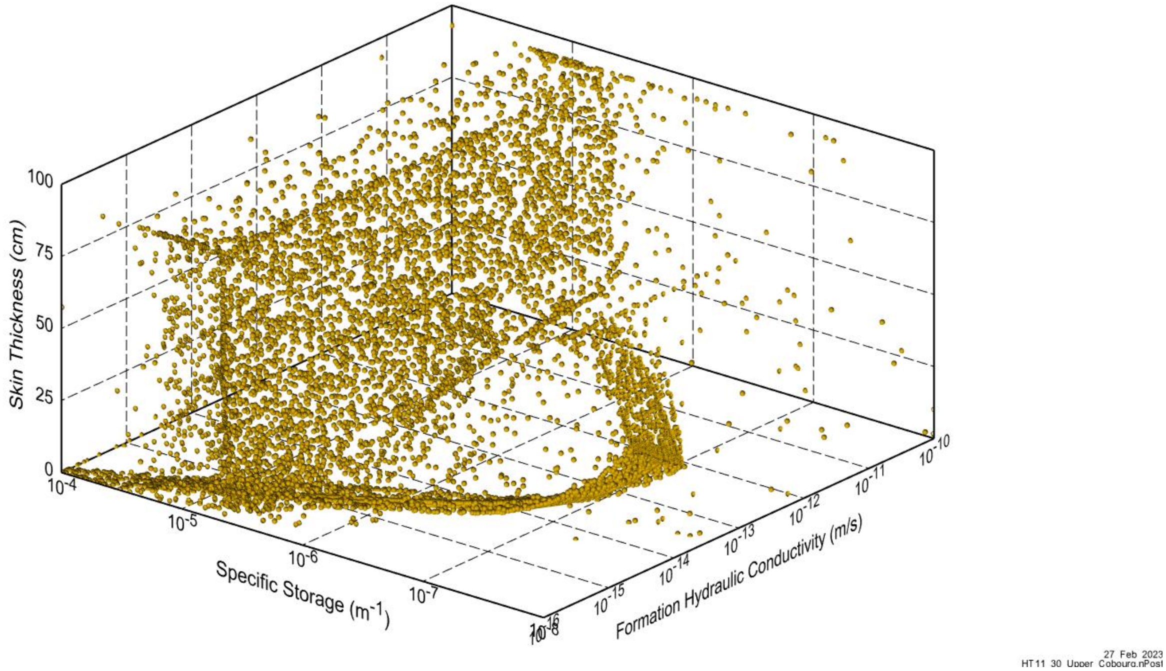

Figure 4.9 Converged parameter estimates for K_f, Ss, and t_s (HT11_30).

Goodness-of-fit is determined by the fit value, which is the sum-of-squared errors (SSE) between the simulated response and the TZ pressure data. Fit-values were normalized to the minimum (or best fit) value and the cumulative distribution function (CDF) calculated. The structure of the CDF was then examined and a “fit-discriminant” value determined. Generally, the fit discriminant was set at the first value where the CDF shape changes or inflects. A secondary criterion was to ensure that all selected fits closely matched the TZ field data. All fits with fit-values less than the discriminant were accepted as being representative of the formation response. This approach limits the fits to those within the apparent global minimum of the five-dimensional parameter space. Typically, at least several hundred perturbations were accepted for each test. Figure 4.10 shows the normalized fit CDF and the fit discriminant for the HT11_30 test.

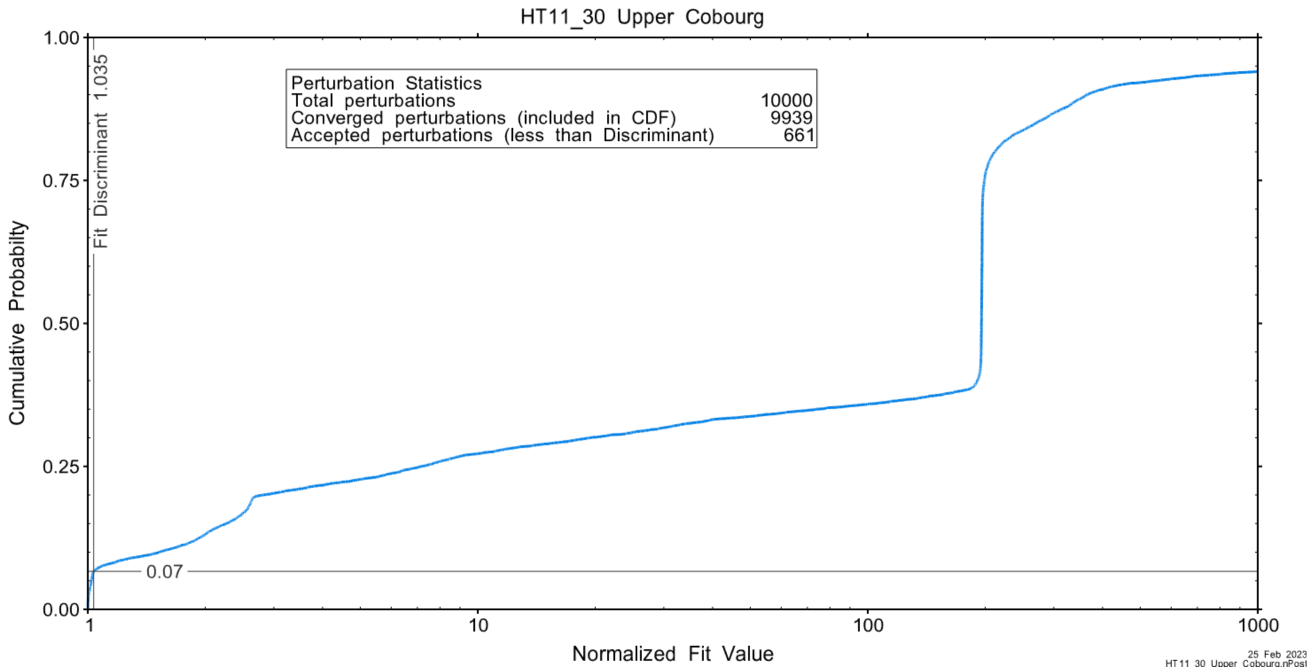

Figure 4.10 Normalized fit CDF (HT11_30).

Examination of individual fit distributions (Figure 4.11) provides confirmation that local minima are not included.

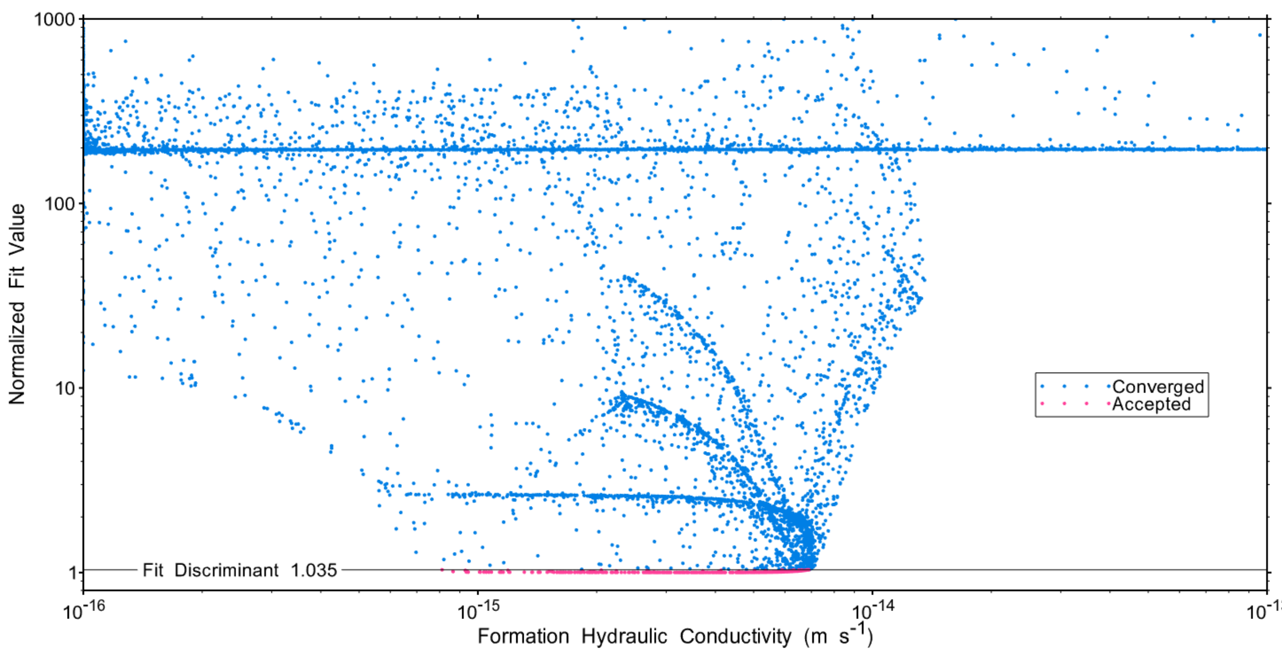

Figure 4.11 Fit distribution for K_f (HT11_30).

The parameter estimates and fit values for the 661 perturbations that met the fit-discriminant value are shown in Figure 4.12 and Figure 4.13.

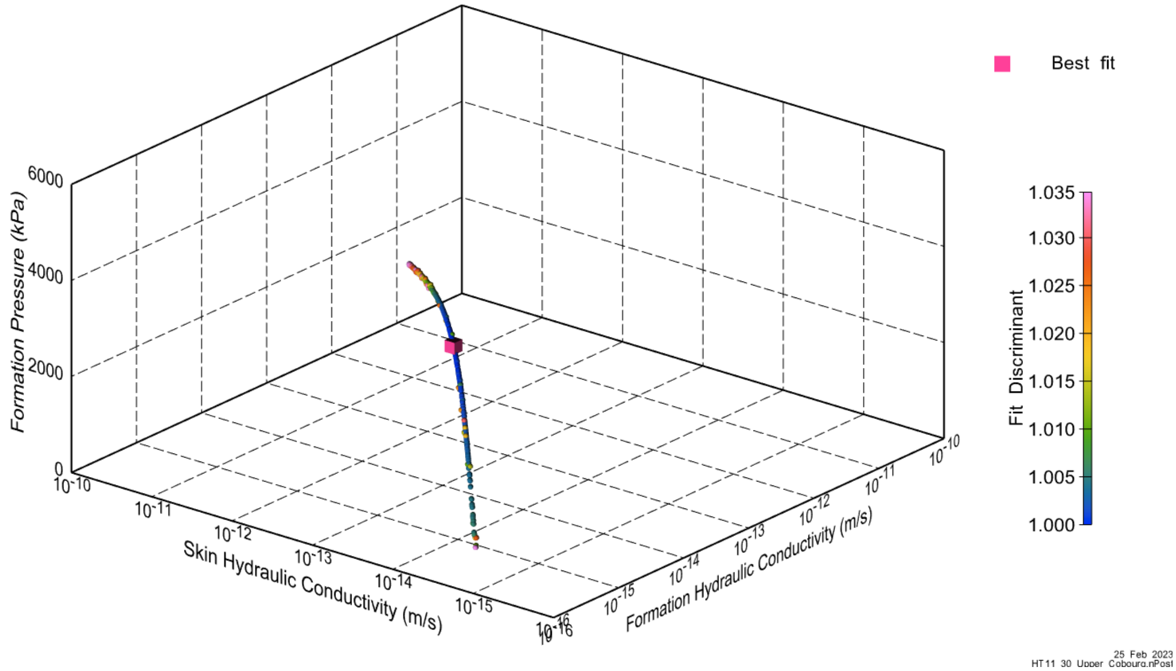

Figure 4.12 Accepted estimates for K_f, K_s, and P_f with fit values and best-fit (HT11_30).

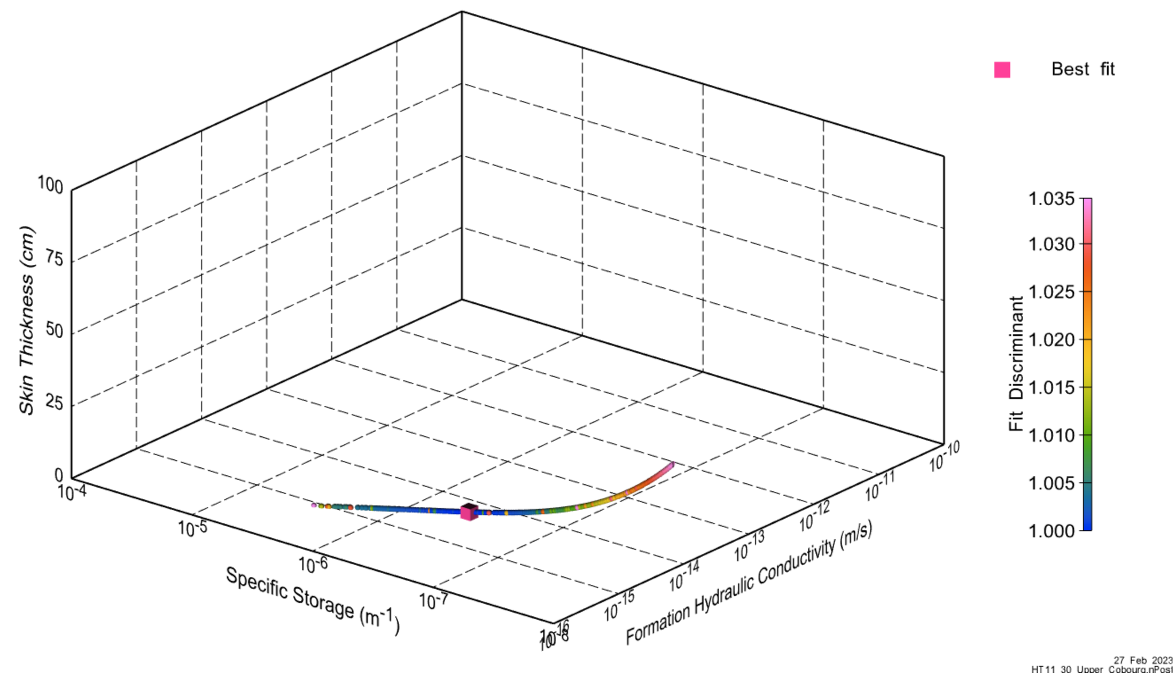

Figure 4.13 Accepted estimates for K_f, Ss, and t_s with fit values and best-fit (HT11_30).

CDFs were constructed for each of the estimated parameters from the accepted perturbations to determine parameter uncertainty. The parameter CDF for K_f is constructed for all accepted values below the fit-discriminant line in Figure 4.11, and is shown in Figure 4.14.

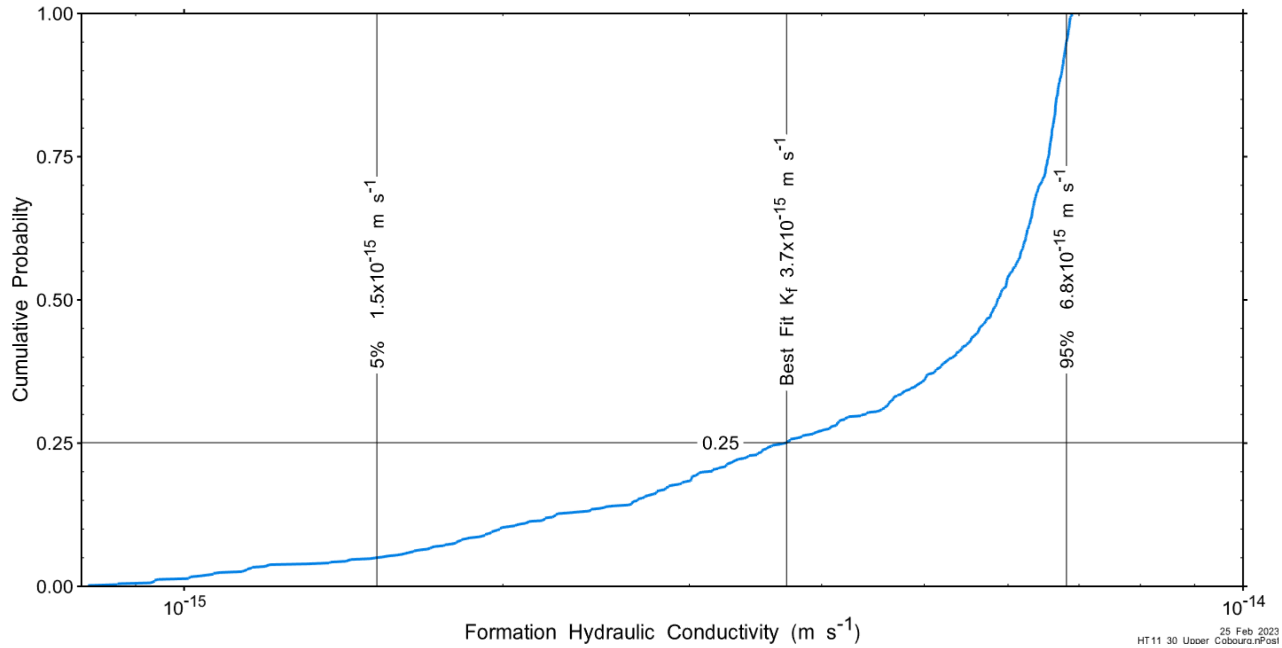

Figure 4.14 Cumulative distribution of accepted formation hydraulic conductivity (HT11_30).

Simulated results for all perturbations where all accepted parameter values were within the 5% to 95% range are shown in Figure 4.15. Note that the blue line shows results for all 592 perturbations with all parameters in the 5% to 95% range.

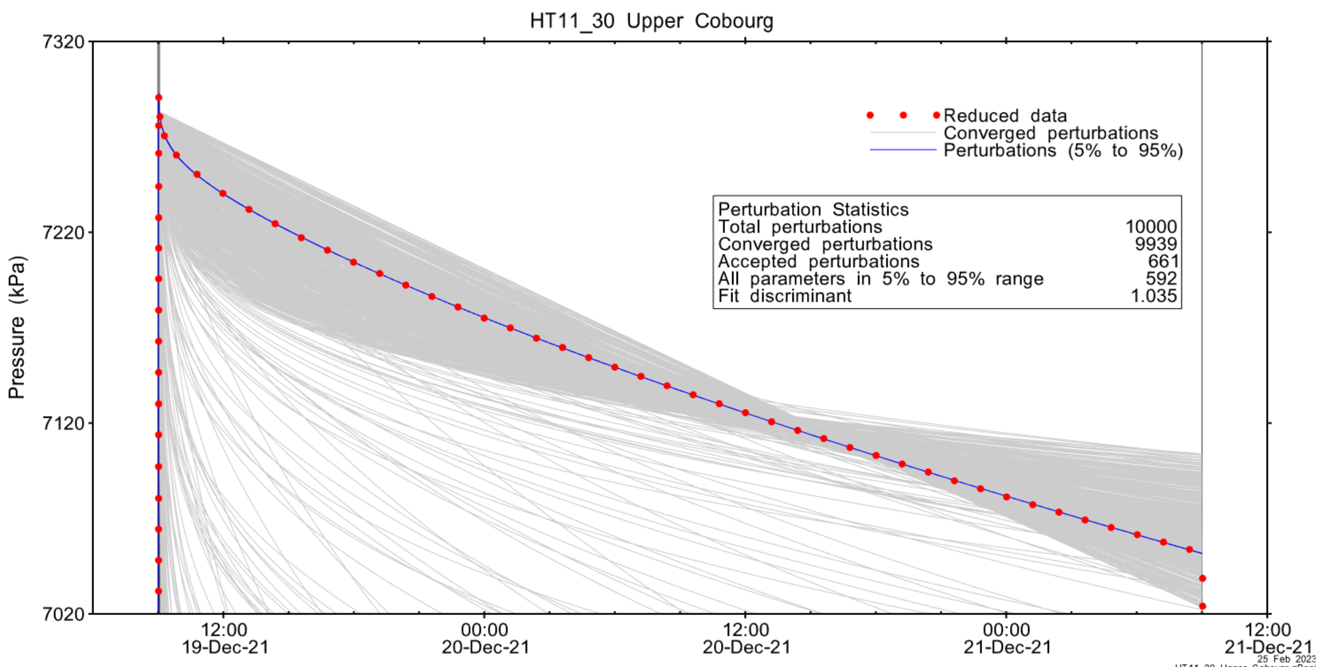

Figure 4.15 Horsetail plot showing perturbation results.

Ramey B processed results (Figure 4.16) illustrate the uncertainty range in processed derivatives.

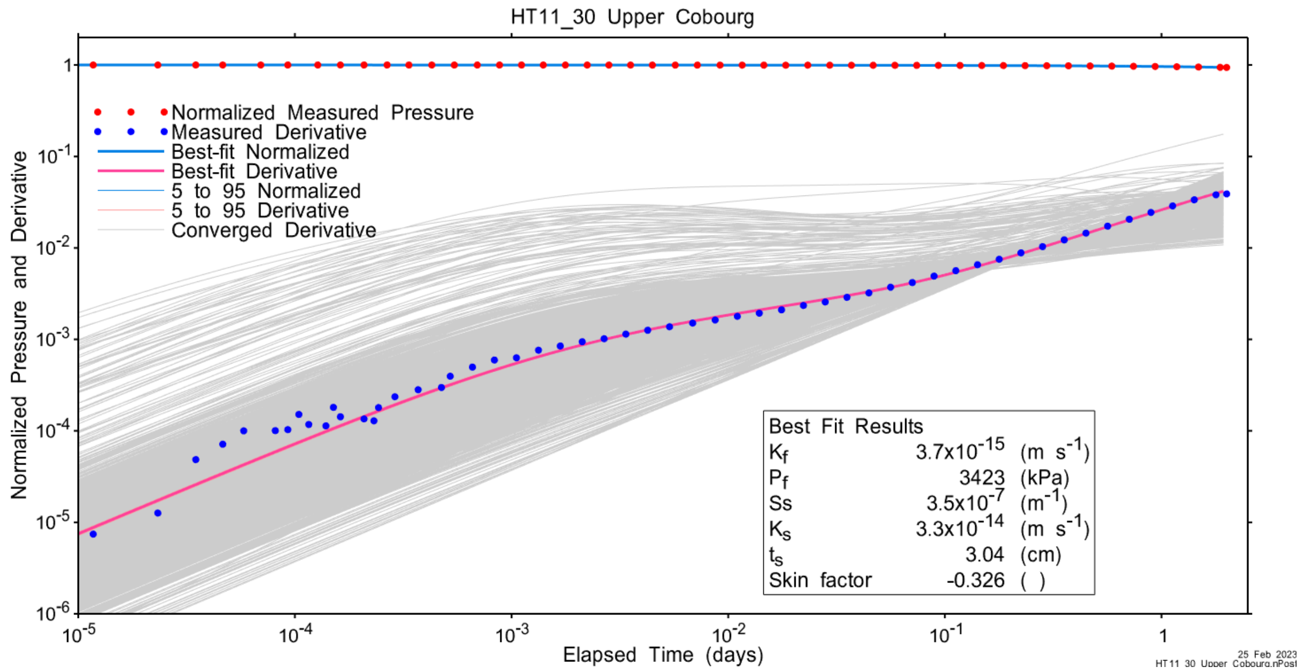

Figure 4.16 Ramey B processed horsetail plot showing perturbation results (HT11_30).

As a final analysis, fitted parameter correlations are calculated for all accepted optimizations (Table 4.1).

Table 4.1 Pearson cross-correlations of 5% to 95% parameters (HT11_30).

	$Log(K_f)$	P_f	Log(Ss)	$Log(K_s)$	t_s	s
$Log(K_f)$	1.000	0.999	-0.938	0.977	0.785	-0.876
P_f	0.999	1.000	-0.921	0.965	0.759	-0.853
Log(Ss)	-0.938	-0.921	1.000	-0.990	-0.947	0.989
$Log(K_s)$	0.977	0.965	-0.990	1.000	0.892	-0.958
t_s	0.785	0.759	-0.947	0.892	1.000	-0.982
s	-0.876	-0.853	0.989	-0.958	-0.982	1.000

5 TEST INTERVALS

Test intervals were selected by Geofirma in consultation with NWMO staff. In general, individual formations were targeted, with most testing focussed on the Ordovician-age formations. The shorter 5-m tests were assigned to relatively thin formations. Within individual formations, test intervals were adjusted vertically to ensure packer seats were located in zones with minimal borehole diameter changes as indicated by caliper logs. Borehole geophysical logs, core photos and core logging data were also reviewed during the interval selection process. Intervals were selected based on nominal 30-m and 5-m interval lengths. These have been corrected to the actual 30.05-m and 5.03-m test interval lengths resulting from selection of available tubing and pup joints during testing. Test durations were specified as 2 days for all tests above the Queenston Formation shale, and 3 days for Queenston Formation shale and deeper tests. This provided longer test response times for the lower permeability Ordovician formations.

The Cobourg Formation and Collingwood Member were targeted with three tests: two 30-m intervals which overlapped to give complete coverage of the Cobourg (HT11_30 and HT12_30), and a single 5-m test for the Collingwood Member (HT02_05). However, formation tops were subsequently revised and the Collingwood Member top adjusted downward by approximately 8 m, resulting in the 5-m "Collingwood" test covering the lower 4.5 m of the Blue Mountain Formation and only the upper 0.5 m of the Collingwood Member. The test did, however, include a zone with significant caliper changes which provided a secondary rationale for selecting the HT02_05 interval. Similarly, the 30-m test designed to cover the top 30 m of the Cobourg Formation (HT11_30) ended up including 6.65 m of the Collingwood as well.

Table 5.1 and Figure 5.1 summarize the selected test intervals. The third panel of the figure presents caliper data and the mean caliper values for each test interval. Mean caliper values were used as the well radius in nSIGHTS analyses. Logged core features are presented in the fourth panel of the figure.

Table 5.1 SB_BH01 hydraulic testing intervals.

Test ID	Top (mBGS)	Bottom (mBGS)	Formation	Caliper Mean Diameter (cm)	Specified Packer Pressure (psi)
30-m Tests					
HT01_30	151.50	181.55	Salina F	13.27	750
HT02_30	224.00	254.05	Salina B	13.29	975
HT03_30	291.60	321.65	Guelph	13.41	1200
HT04_30	361.40	391.45	Gasport/Lions Head/Fossil Hill	13.26	1450
HT05_30	395.50	425.55	Cabot Head/Manitoulin	13.88	1575
HT06_30	428.50	458.55	Queenston – Upper	14.19	1700
HT07_30	463.00	493.05	Queenston – Lower	13.54	1700
HT08_30	509.00	539.05	Georgian Bay – Upper	12.86	1700
HT09_30	559.00	589.05	Georgian Bay – Lower	12.91	1700
HT10_30	602.20	632.25	Blue Mountain	14.38	1700
HT11_30	646.00	676.05	Collingwood/Cobourg	13.72	1700
HT12_30	661.40	691.45	Cobourg	13.85	1700
HT13_30	706.75	736.80	Sherman Fall	13.72	1700
HT14_30	750.75	780.80	Kirkfield	13.35	1700
HT15_30	815.00	845.05	Gull River	12.57	1700
5-m Tests					
HT01_05	269.70	274.73	Lower A2 Carbonate	12.70	1150
HT02_05	640.20	645.23	Blue Mountain/Collingwood	13.79	1700
HT03_05	788.00	793.03	Coboconk	12.68	1700
HT04_05	855.50	860.53	Shadow Lake	12.63	1700
HT05_05	864.00	869.03	Precambrian	12.39	1700

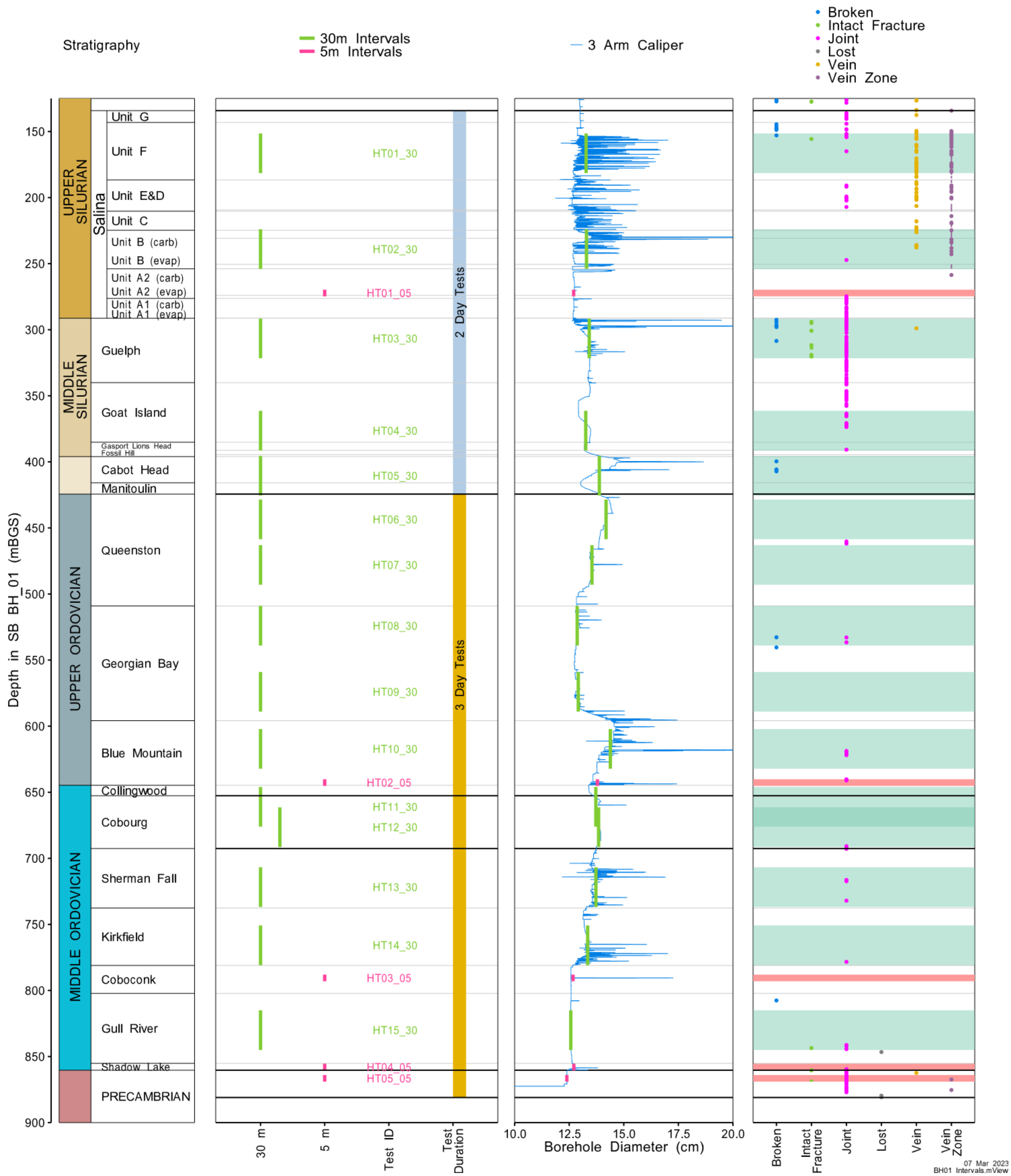

Figure 5.1 SB_BH01 hydraulic testing test intervals.

6 INDIVIDUAL TEST ANALYSES

All analyses follow a common structure:

1. Test Data Summary – a table describing timing and duration of test events and a figure displaying pressures for all downhole pressure transducers over the period of active testing.

2. Test Analyses – tables showing test-specific nSIGHTS input parameters and ranges for optimized fitting parameters. Figures are presented showing: a) the single-best fit result, b) the borehole history, c) the Ramey B plot for the best fit, and d) the normalized Jacobian parameter sensitivity plot.

3. Uncertainly Analyses – figures include: a) the CDF of normalized fit values annotated with the selected fit discriminant, b) cross plots (K_f vs P_f, K_f vs Ss, P_f vs Ss, and K_s vs t_s) showing initial parameter estimates, converged simulations and simulations meeting fit-discriminant criteria, c) parameter CDFs for all simulations meeting fit-discriminant criteria, d) horsetail Cartesian and Ramey B plots showing converged and accepted simulations, e) tables summarizing parameter ranges (best fit, 5%, median, and 95%) and fitted parameter correlations.

4. Additional Figures – includes: a) hydraulic system pressures and weather data (barometric pressure, surface temperature), and b) structure of normalized fit values for each fitted parameter.

Individual test analyses are presented in Appendix A.1 through A.20.

7 ANALYSES SUMMARY

Results from analyses documented in Section 6 are presented in summary form by test interval.

7.1 Summary Tables

CDFs of all accepted perturbations for each parameter represent the range of values for which analyses are visually indistinguishable on a Cartesian plot. The "Best Fit", 5%, Median (50%), and 95% CDF values are extracted for each parameter to indicate the possible range of parameter values. The "Best Fit" value represents the minimum SSE for all accepted perturbations but should not be considered as the most representative value, as occasionally the Best Fit falls outside the 5% and 95% confidence interval range. The Median value should be used as the representative single value for each parameter where necessary.

Table 7.1 through Table 7.6 provide the Best Fit, 5%, Median (50%), and 95% CDF values for each fitting parameter and for the calculated skin factor. Formation pressures (Table 7.2) are adjusted to the interval midpoint. A final table shows simulation input parameters (Table 7.7).

Table 7.1 BH01 Summary of Formation Hydraulic Conductivity Estimates.

Formation Hydraulic Conductivity (m/s)					
Test ID	**Formation**	**Best Fit**	**5%**	**Median**	**95%**
HT01_30	Salina F	2.9E-13	2.8E-13	2.9E-13	2.9E-13
HT02_30	Salina B	3.1E-09	3.1E-09	3.2E-09	3.4E-09
HT03_30	Guelph	7.9E-01	1.2E-05	1.1E-02	8.7E-01
HT04_30	Gasport/Lions Head/Fossil Hill	3.3E-09	3.0E-09	3.1E-09	3.4E-09
HT05_30	Cabot Head/Manitoulin	5.9E-14	2.6E-14	6.0E-14	1.0E-13
HT06_30	Queenston – Upper	3.9E-15	1.5E-15	1.5E-14	3.3E-14
HT07_30	Queenston – Lower	1.5E-15	1.1E-15	5.0E-15	1.7E-14
HT08_30	Georgian Bay – Upper	2.4E-14	1.1E-14	2.6E-14	7.8E-14
HT09_30	Georgian Bay – Lower	3.0E-14	9.0E-15	2.8E-14	3.9E-14
HT10_30	Blue Mountain/Collingwood	8.7E-15	3.5E-15	1.6E-14	4.6E-14
HT11_30	Cobourg - Upper	3.7E-15	1.5E-15	5.9E-15	6.8E-15
HT12_30	Cobourg – Lower	2.5E-15	2.1E-15	3.1E-15	5.6E-15
HT13_30	Sherman Fall	7.4E-15	6.3E-15	7.2E-15	1.0E-14
HT14_30	Kirkfield	1.3E-16	4.1E-16	2.5E-15	6.2E-15
HT15_30	Gull River	9.0E-12	7.6E-12	9.0E-12	9.5E-12
HT01_05	Lower A2 Carbonate	2.5E-05	2.4E-05	2.5E-05	2.5E-05
HT02_05	Blue Mountain/Collingwood	1.9E-13	2.0E-13	8.4E-13	1.1E-12
HT03_05	Coboconk	2.3E-13	1.8E-13	6.0E-13	9.3E-13
HT04_05	Shadow Lake	4.9E-14	1.8E-14	5.0E-14	6.9E-14
HT05_05	Precambrian	3.9E-13	3.1E-13	3.9E-13	4.2E-13

Table 7.2 BH01 Summary of Formation Pressure Estimates (Adjusted to Interval Midpoint).

Formation Pressure (kPa)					
Test ID	**Formation**	**Best Fit**	**5%**	**Median**	**95%**
HT01_30	Salina F	578	545	575	586
HT02_30	Salina B	2478	2476	2478	2481
HT03_30	Guelph	3183	3183	3183	3183
HT04_30	Gasport/Lions Head/Fossil Hill	3918	3917	3919	3919
HT05_30	Cabot Head/Manitoulin	4508	4446	4509	4524
HT06_30	Queenston – Upper	4183	4010	4452	4578
HT07_30	Queenston – Lower	816	289	2108	3409
HT08_30	Georgian Bay – Upper	5004	4823	5020	5169
HT09_30	Georgian Bay – Lower	4066	2222	3966	4327
HT10_30	Blue Mountain/Collingwood	290	209	2373	4771
HT11_30	Cobourg - Upper	3631	1623	4493	4749
HT12_30	Cobourg – Lower	209	209	1905	4414
HT13_30	Sherman Fall	684	209	609	2398
HT14_30	Kirkfield	4774	4223	5611	7683
HT15_30	Gull River	5261	5025	5261	5302
HT01_05	Lower A2 Carbonate	2838	2838	2838	2838
HT02_05	Blue Mountain/Collingwood	6514	6519	6602	6612
HT03_05	Coboconk	8614	8482	8512	8651
HT04_05	Shadow Lake	8872	8787	8882	8958
HT05_05	Precambrian	7223	7015	7223	7278

Table 7.3 BH01 Summary of Specific Storage Estimates.

Specific Storage (m^{-1})					
Test ID	**Formation**	**Best Fit**	**5%**	**Median**	**95%**
HT01_30	Salina F	1.9E-08	1.0E-08	2.3E-08	8.8E-08
HT02_30	Salina B	9.0E-05	1.1E-08	5.8E-08	3.0E-06
HT03_30	Guelph	5.3E-08	1.0E-08	2.8E-07	6.7E-05
HT04_30	Gasport/Lions Head/Fossil Hill	5.7E-07	1.0E-08	4.6E-07	7.8E-06
HT05_30	Cabot Head/Manitoulin	7.2E-07	3.5E-08	6.8E-07	2.4E-06
HT06_30	Queenston – Upper	6.5E-06	5.6E-08	1.1E-06	1.8E-05
HT07_30	Queenston – Lower	2.0E-05	9.0E-07	5.0E-06	3.0E-05
HT08_30	Georgian Bay – Upper	5.5E-06	3.3E-07	4.8E-06	1.4E-05
HT09_30	Georgian Bay – Lower	2.7E-07	1.2E-08	3.9E-07	3.0E-06
HT10_30	Blue Mountain/Collingwood	7.9E-07	1.0E-08	8.8E-08	1.7E-05
HT11_30	Cobourg - Upper	3.5E-07	1.2E-08	7.2E-08	1.4E-06
HT12_30	Cobourg – Lower	1.0E-08	1.0E-08	1.7E-08	2.6E-07
HT13_30	Sherman Fall	1.0E-08	1.0E-08	1.4E-08	7.0E-08
HT14_30	Kirkfield	3.0E-05	1.9E-08	2.4E-07	8.1E-06
HT15_30	Gull River	2.3E-07	2.5E-08	2.4E-07	1.3E-05
HT01_05	Lower A2 Carbonate	6.7E-08	6.2E-08	6.6E-08	7.2E-08
HT02_05	Blue Mountain/Collingwood	1.0E-04	9.0E-07	5.8E-06	1.0E-04
HT03_05	Coboconk	6.0E-05	4.8E-06	1.5E-05	8.3E-05
HT04_05	Shadow Lake	1.0E-08	1.0E-08	1.1E-08	7.4E-08
HT05_05	Precambrian	3.5E-07	3.3E-07	3.5E-07	3.8E-07

Table 7.4 BH01 Summary of Skin Hydraulic Conductivity Estimates.

Skin Hydraulic Conductivity (m/s)					
Test ID	**Formation**	**Best Fit**	**5%**	**Median**	**95%**
HT01_30	Salina F	2.8E-12	2.0E-12	2.7E-12	3.1E-12
HT02_30	Salina B	4.8E-10	7.8E-10	2.5E-09	2.7E-09
HT03_30	Guelph	1.2E-04	1.1E-06	5.7E-05	5.4E-04
HT04_30	Gasport/Lions Head/Fossil Hill	2.5E-09	1.2E-09	2.4E-09	8.9E-09
HT05_30	Cabot Head/Manitoulin	1.1E-13	3.5E-14	1.3E-13	3.1E-13
HT06_30	Queenston – Upper	6.5E-15	2.4E-15	3.1E-14	1.6E-13
HT07_30	Queenston – Lower	1.8E-15	2.4E-15	1.0E-14	2.4E-13
HT08_30	Georgian Bay – Upper	3.6E-14	1.5E-14	5.2E-14	1.8E-13
HT09_30	Georgian Bay – Lower	5.9E-14	1.2E-14	5.8E-14	1.7E-13
HT10_30	Blue Mountain/Collingwood	6.5E-14	1.9E-14	5.3E-13	1.7E-11
HT11_30	Cobourg - Upper	3.3E-14	1.0E-14	9.1E-14	1.8E-13
HT12_30	Cobourg – Lower	3.0E-13	4.3E-14	2.4E-13	6.4E-13
HT13_30	Sherman Fall	1.9E-13	3.2E-14	1.4E-13	8.3E-13
HT14_30	Kirkfield	7.1E-16	1.7E-15	1.9E-14	6.3E-14
HT15_30	Gull River	1.2E-11	2.6E-12	1.2E-11	1.5E-11
HT01_05	Lower A2 Carbonate	1.5E-06	3.8E-06	5.9E-06	6.3E-06
HT02_05	Blue Mountain/Collingwood	3.5E-14	3.6E-14	2.6E-13	6.8E-13
HT03_05	Coboconk	7.4E-14	5.6E-14	2.4E-13	4.9E-13
HT04_05	Shadow Lake	4.2E-13	2.5E-13	4.1E-13	4.4E-13
HT05_05	Precambrian	1.7E-12	1.5E-12	1.7E-12	1.8E-12

Table 7.5 BH01 Summary of Skin Thickness Estimates.

Skin Thickness (cm)					
Test ID	**Formation**	**Best Fit**	**5%**	**Median**	**95%**
HT01_30	Salina F	56.36	23.86	50.65	78.58
HT02_30	Salina B	4.12	5.15	374.57	966.69
HT03_30	Guelph	8.11	2.70	300.41	992.92
HT04_30	Gasport/Lions Head/Fossil Hill	993.30	2.49	400.59	984.19
HT05_30	Cabot Head/Manitoulin	1.30	0.38	1.52	23.02
HT06_30	Queenston – Upper	0.78	0.50	3.03	23.13
HT07_30	Queenston – Lower	0.06	0.04	0.41	3.08
HT08_30	Georgian Bay – Upper	0.22	0.09	0.41	9.63
HT09_30	Georgian Bay – Lower	6.03	0.23	4.36	42.84
HT10_30	Blue Mountain/Collingwood	2.21	0.11	13.25	50.74
HT11_30	Cobourg - Upper	3.04	0.84	10.61	32.15
HT12_30	Cobourg – Lower	37.91	3.98	26.05	37.48
HT13_30	Sherman Fall	20.08	4.72	16.03	21.66
HT14_30	Kirkfield	0.02	0.08	3.68	22.65
HT15_30	Gull River	170.60	1.22	176.14	326.69
HT01_05	Lower A2 Carbonate	5.95	140.35	4517.62	9514.19
HT02_05	Blue Mountain/Collingwood	0.23	0.24	2.44	10.65
HT03_05	Coboconk	0.50	0.37	1.76	4.54
HT04_05	Shadow Lake	203.87	73.40	190.57	228.25
HT05_05	Precambrian	95.16	94.47	95.18	98.46

Table 7.6 BH01 Summary of Calculated Skin Factor.

Skin Factor ( )					
Test ID	**Formation**	**Best Fit**	**5%**	**Median**	**95%**
HT01_30	Salina F	-2.017	-2.309	-1.925	-1.311
HT02_30	Salina B	2.594	0.627	1.235	2.348
HT03_30	Guelph	5413	9.411	655	6416
HT04_30	Gasport/Lions Head/Fossil Hill	1.777	-0.703	1.222	2.548
HT05_30	Cabot Head/Manitoulin	-0.081	-0.997	-0.097	-0.010
HT06_30	Queenston – Upper	-0.043	-1.165	-0.188	-0.027
HT07_30	Queenston – Lower	-0.001	-0.146	-0.015	-0.002
HT08_30	Georgian Bay – Upper	-0.012	-0.511	-0.020	-0.002
HT09_30	Georgian Bay – Lower	-0.317	-1.586	-0.213	-0.007
HT10_30	Blue Mountain/Collingwood	-0.232	-2.064	-0.998	-0.008
HT11_30	Cobourg - Upper	-0.326	-1.673	-0.875	-0.098
HT12_30	Cobourg – Lower	-1.853	-1.846	-1.535	-0.422
HT13_30	Sherman Fall	-1.315	-1.400	-1.104	-0.438
HT14_30	Kirkfield	-0.002	-1.378	-0.363	-0.009
HT15_30	Gull River	-0.853	-1.639	-0.853	0.428
HT01_05	Lower A2 Carbonate	10.180	17.010	21.039	22.143
HT02_05	Blue Mountain/Collingwood	0.146	0.156	0.616	0.746
HT03_05	Coboconk	0.161	0.124	0.382	0.502
HT04_05	Shadow Lake	-3.098	-3.363	-3.028	-2.113
HT05_05	Precambrian	-2.144	-2.234	-2.145	-2.127

Table 7.7 BH01 Summary of Simulation Input Parameters

Simulation Input Parameters				
Test ID	**Formation**	**Test Zone Compressibility (Pa^{-1})**	**Test Zone Radius (cm)**	**Test Zone Fluid Density (g/L)**
HT01_30	Salina F	5.17E-10	6.64	1036
HT02_30	Salina B	n/a - slug test	6.65	1044
HT03_30	Guelph	n/a - slug test	6.71	1052
HT04_30	Gasport/Lions Head/Fossil	n/a - slug test	6.63	1048
HT05_30	Cabot Head/Manitoulin	4.42E-10	6.94	1050
HT06_30	Queenston – Upper	4.76E-10	7.10	1051
HT07_30	Queenston – Lower	4.66E-10	6.77	1050
HT08_30	Georgian Bay – Upper	4.76E-10	6.43	1050
HT09_30	Georgian Bay – Lower	4.75E-10	6.46	1050
HT10_30	Blue Mountain/Collingwood	6.40E-10	7.19	1047
HT11_30	Cobourg - Upper	4.54E-10	6.86	1046
HT12_30	Cobourg – Lower	4.70E-10	6.92	1046
HT13_30	Sherman Fall	4.54E-10	6.86	1047
HT14_30	Kirkfield	4.12E-10	6.67	1092
HT15_30	Gull River	4.43E-10	6.29	1092
HT01_05	Lower A2 Carbonate	n/a - slug test	6.35	1092
HT02_05	Blue Mountain/Collingwood	6.87E-10	6.90	1096
HT03_05	Coboconk	4.23E-10	6.34	1084
HT04_05	Shadow Lake	3.82E-10	6.36	1085
HT05_05	Precambrian	3.93E-10	6.20	1086

7.2 Summary Figures

Figure 7.1 and Figure 7.2 show the Best Fit, 5%, Median, and 95% CDF values for each fitting parameter and for the calculated skin factor plotted against the stratigraphy. Formation pressures (Figure 7.1) are adjusted to the interval midpoint. The Silurian strata are generally normally pressured, whereas the majority of the Ordovician strata show significant under-pressures. Test-specific simulation input parameters are presented in Figure 7.3.

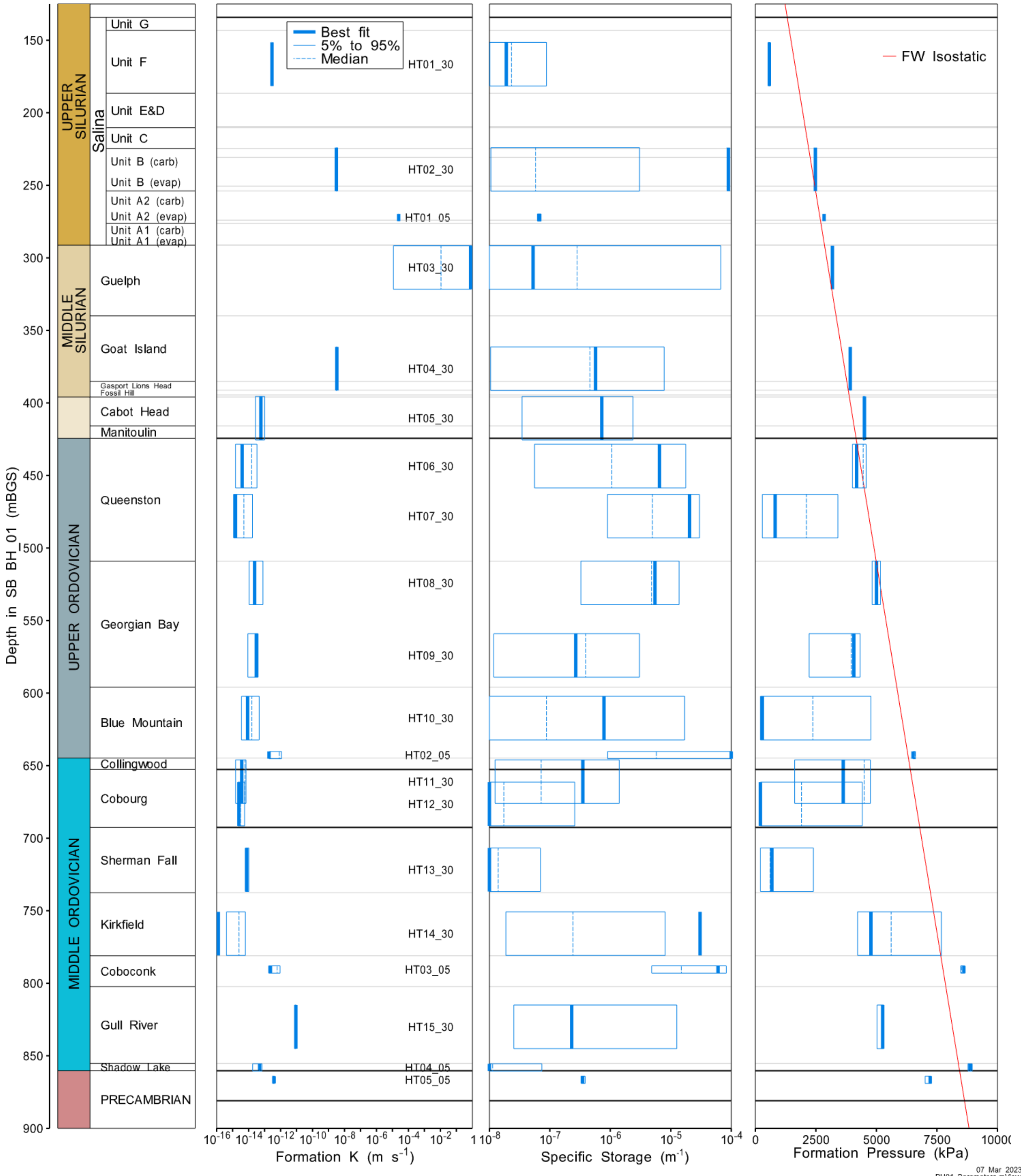

Figure 7.1 Formation Hydraulic Conductivity, Specific Storage and Adjusted Formation Pressure.

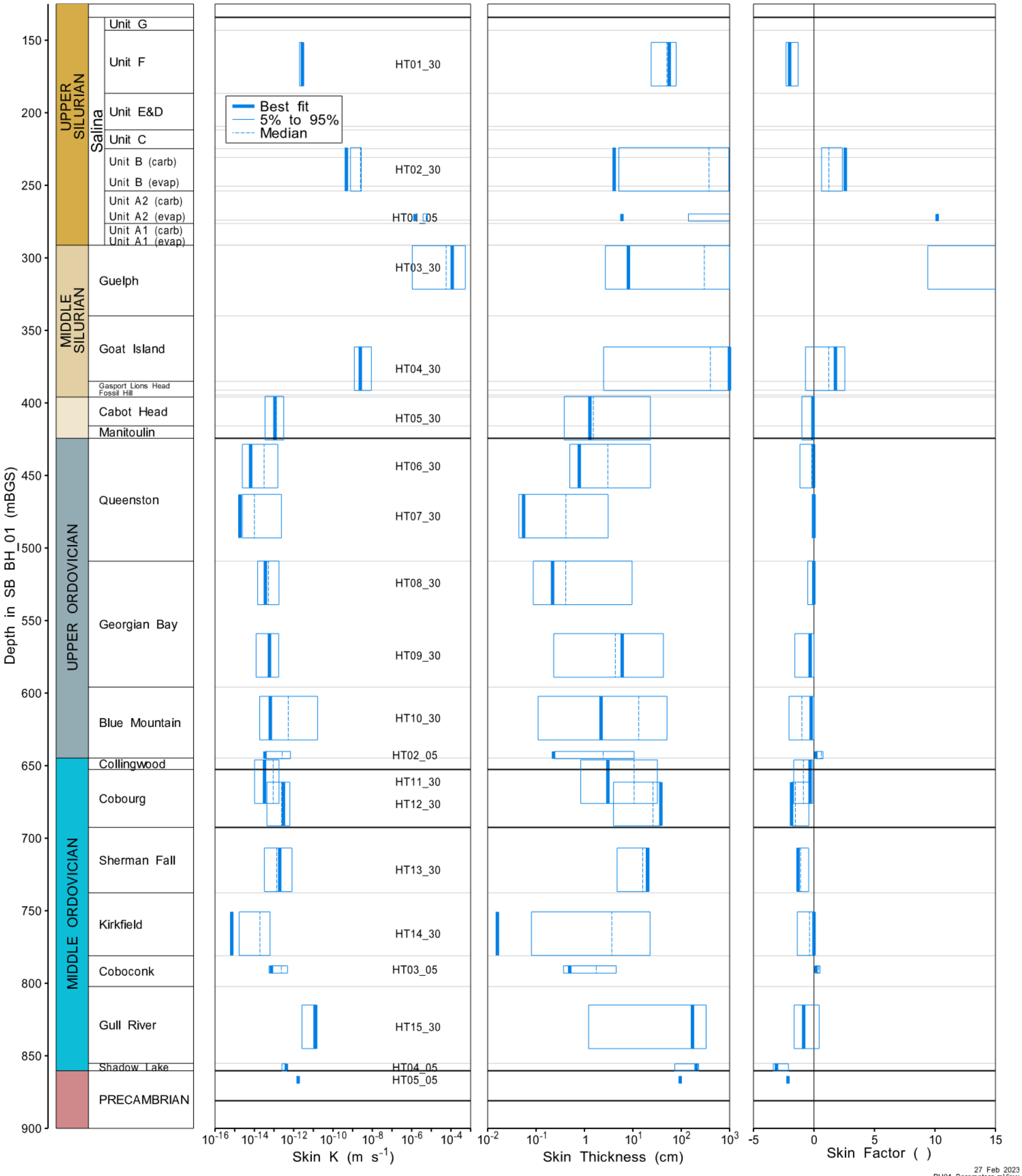

Figure 7.2 Skin Hydraulic Conductivity, Skin Thickness and Skin Factor.

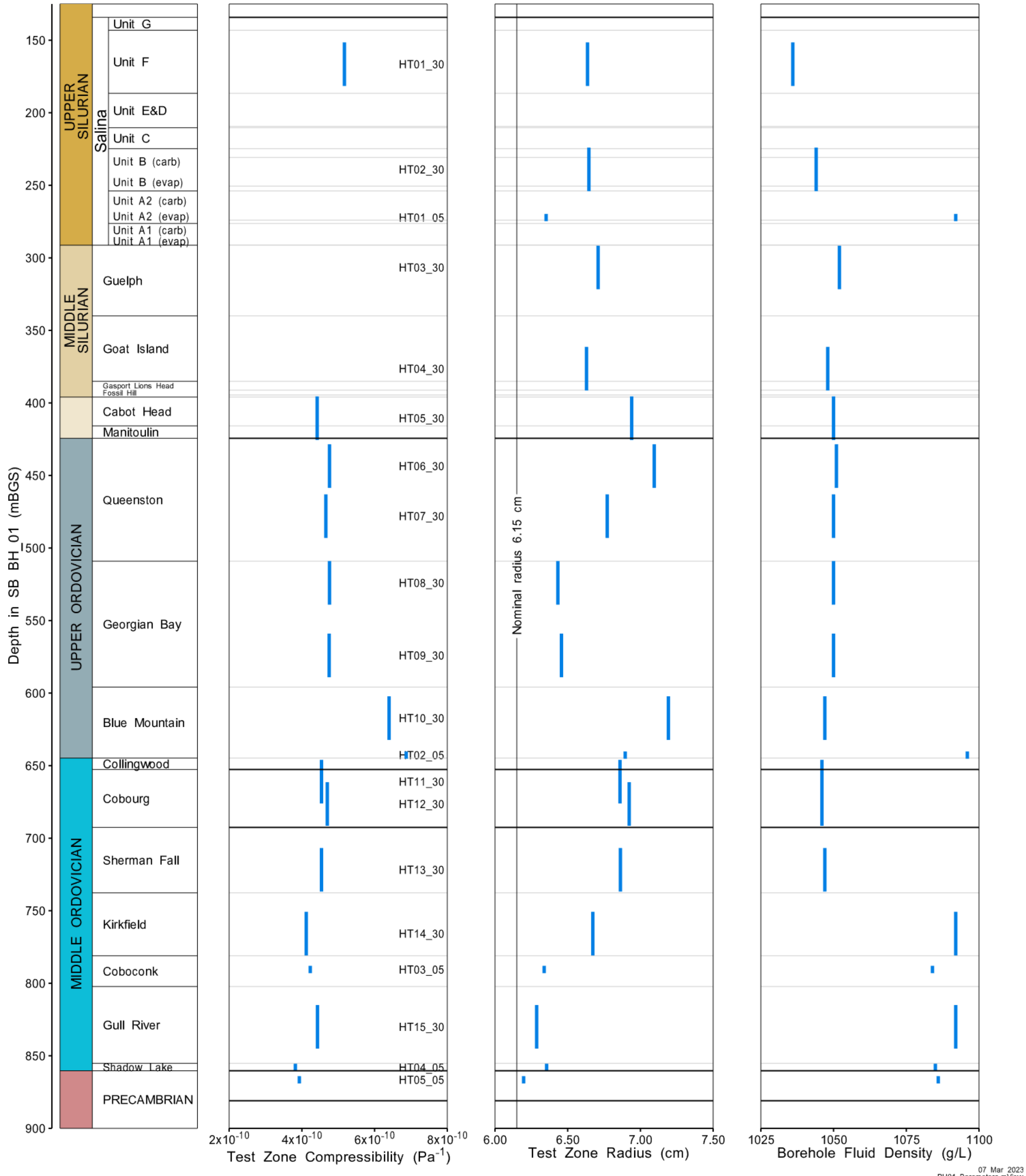

Figure 7.3 Simulation Parameters: Test Zone Compressibility, Test Zone Radius, Borehole Fluid Density.

8 REFERENCES

Armstrong, D.K., and T.R. Carter, 2010. The Subsurface Paleozoic Stratigraphy of Southern Ontario. Ontario Geological Survey – Special Volume 7; 301p.

Avis, J.D., R.L.Beauheim, D. Chace, and R. Roberts, 2021. Phase 2 Initial Borehole Drilling and Testing, South Bruce, Geofirma Engineering Ltd. Ottawa, ON

Geofirma Engineering Ltd. and INTERA Inc. 2011. nSIGHTS Version 2.50 User Manual. INTERA Inc., Austin, TX, USA.

APPENDIX A

INDIVIDUAL TEST ANALYSES

A.1 HT01_30 Salina F

The SB_BH01 interval from 151.50 to 181.55 mBGS tested in HT01_30 includes the majority of Unit F of the Salina Group. A single PI test with a duration of 1 day was conducted.

A.1.1 Test Data Summary

Table 0.1 and Figure 0.1 provide a summary of test events and a plot of pressures measured while testing, respectively.

Table 0.1 HT01_30 Summary of Test Events

Event	Start Date & Time	Duration (days)	TZ Pressure (kPa)
Drilling intercept	21-07-17 00:15	113.54	1548
Shut-in	21-11-07 13:08	0.79	1548
Pulse injection	21-11-08 08:01	0.98	1793
Test end	21-11-09 07:39		1290

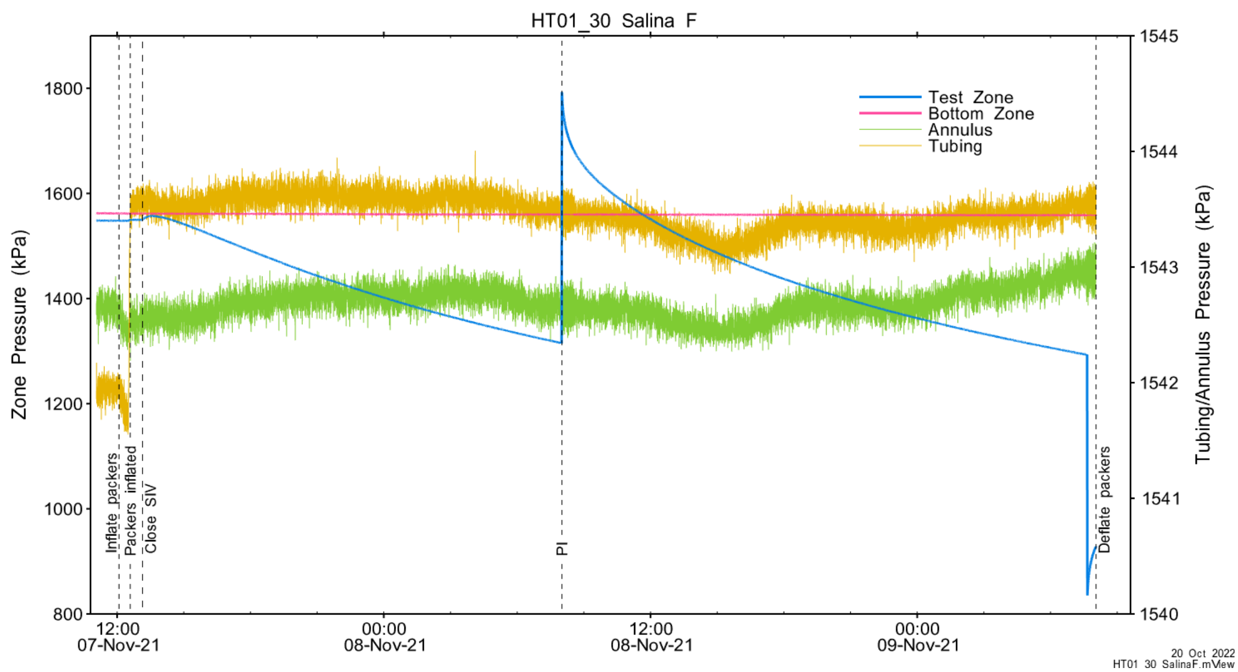

Figure 0.1 HT01_30 test events and pressures.

A.1.2 Test Analyses

Table 0.2 is a summary of test-specific input parameters used in the analyses, while Table 0.3 presents the optimized parameters and allowed ranges.

Table 0.2 nSIGHTS Input Parameters.

Parameter	Value	Units
Test zone radius	6.636	cm
Test zone compressibility	5.17E-10	1/Pa
Test zone fluid density	1036	g/L
Test zone length	30.05	m

Table 0.3 nSIGHTS Parameter Optimization Ranges.

Parameter	Minimum	Maximum	Units	Type
Formation hydraulic conductivity (K_f)	1E-15	1E-08	m/s	log
Formation pressure (P_f)	0	2000	kPa	linear
Specific storage (Ss)	1E-08	1E-04	1/m	log
Skin hydraulic conductivity (K_s)	1E-15	1E-08	m/s	log
Skin thickness (t_s)	0.1	10000	mm	linear

Figure 0.2 shows the measured test zone pressure record (with reduced data density for clarity) used in the analysis along with the best-fit simulation and parameter values. Figure 0.3 presents the pre-test history, and Figure 0.4 shows the Ramey B normalized best-fit pressure and pressure derivatives.

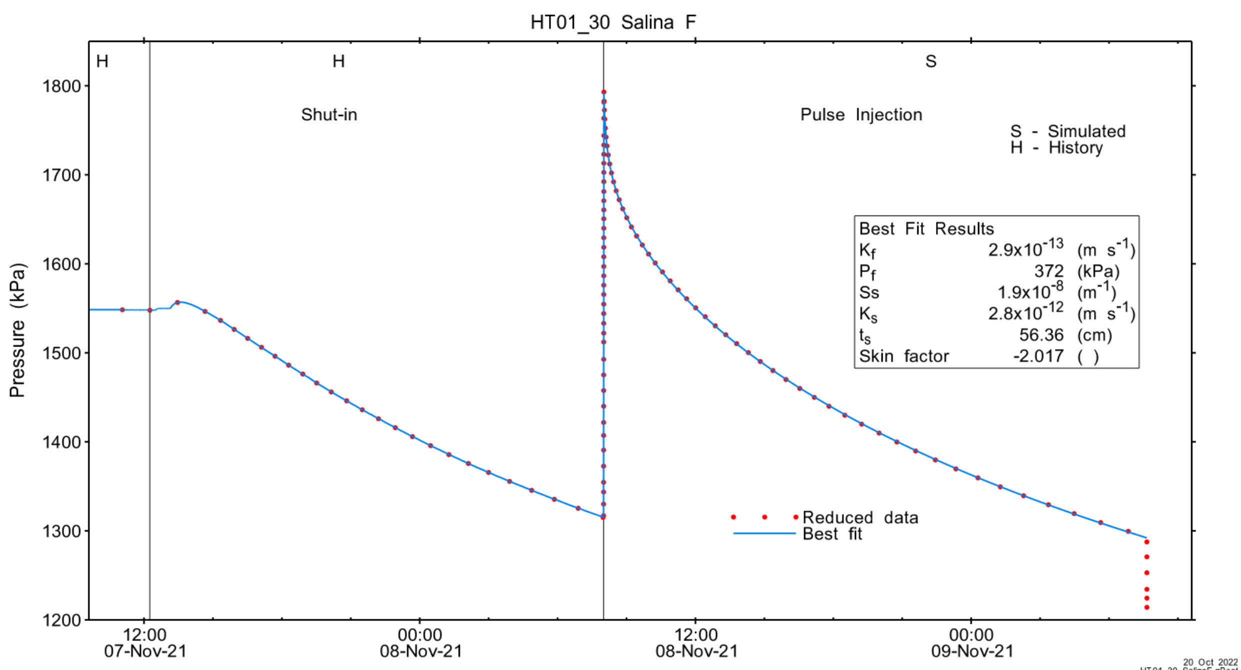

Figure 0.2 Annotated testing sequence showing best-fit simulation and parameter estimates.

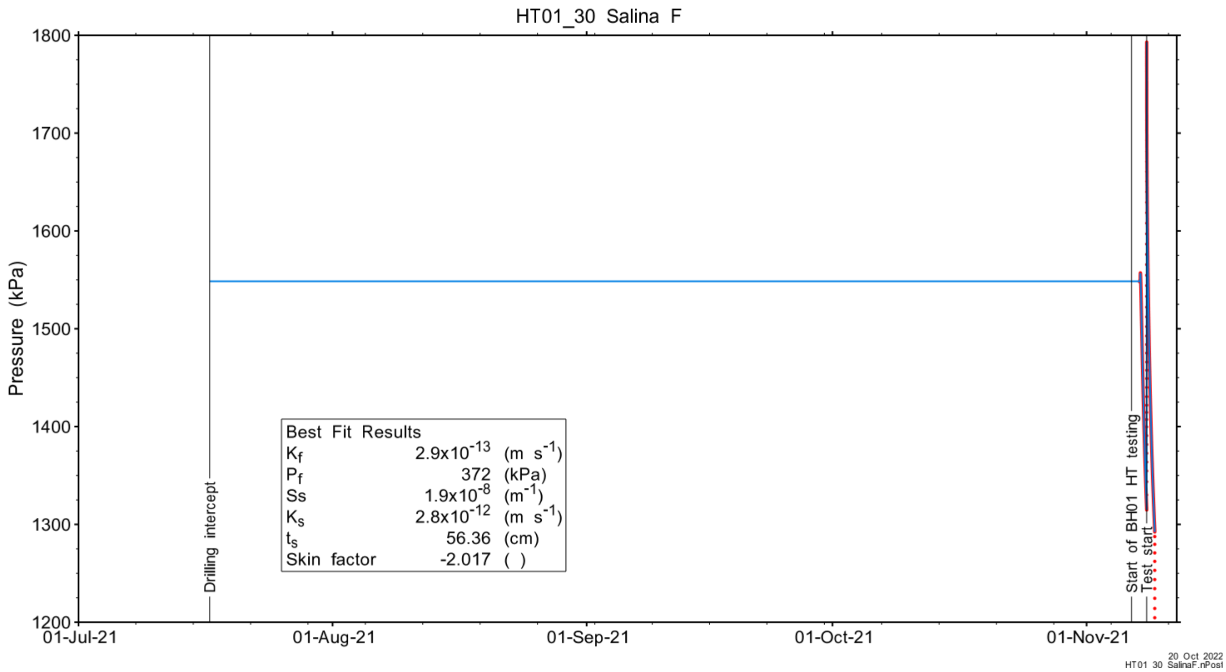

Figure 0.3 Annotated HT01_30 testing sequence showing pre-test history, best-fit simulation and parameter estimates.

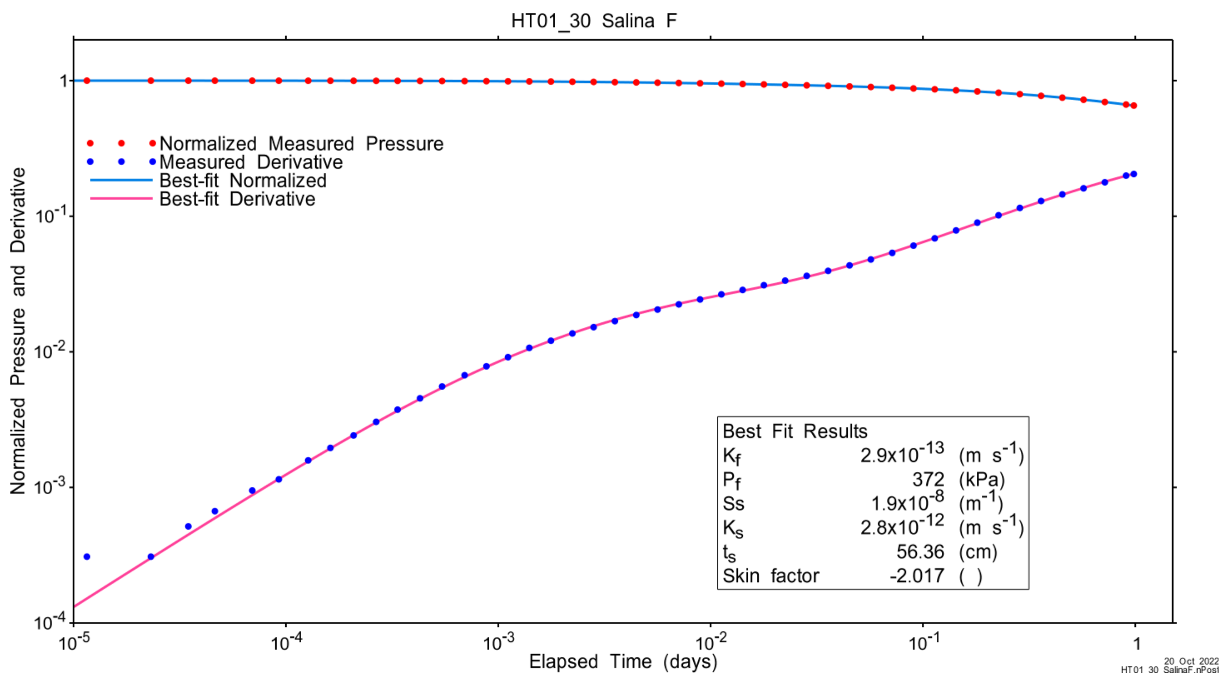

Figure 0.4 Log-log plot showing PI Ramey B normalized pressure and derivative response for best-fit simulation.

Figure 0.5 shows the normalized parameter sensitivity response for the best fit. Skin-related parameters are most sensitive during the early-time response. Sensitivity for K_f, P_f and Ss continues to rise – additional test time might have improved the estimates.

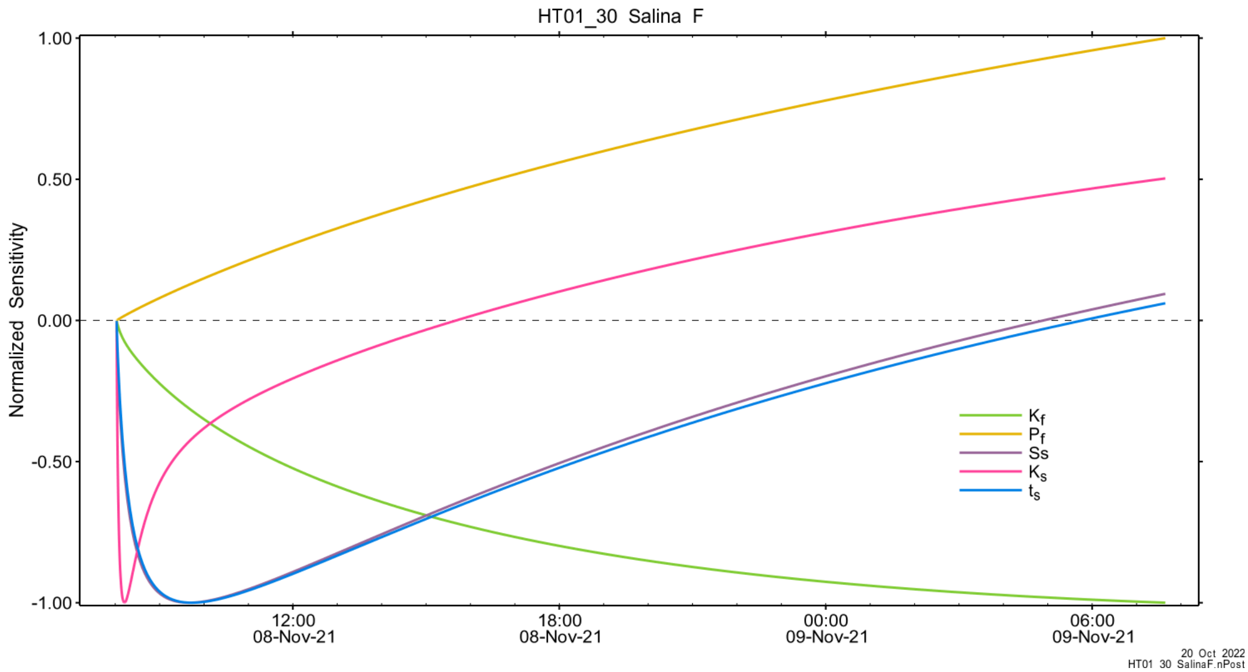

Figure 0.5 Normalized Jacobian for best-fit PI simulation.

A.1.3 Uncertainty Analyses

The CDF of normalized fit values for all converged simulations and the selected fit discriminant are shown in Figure 0.6.

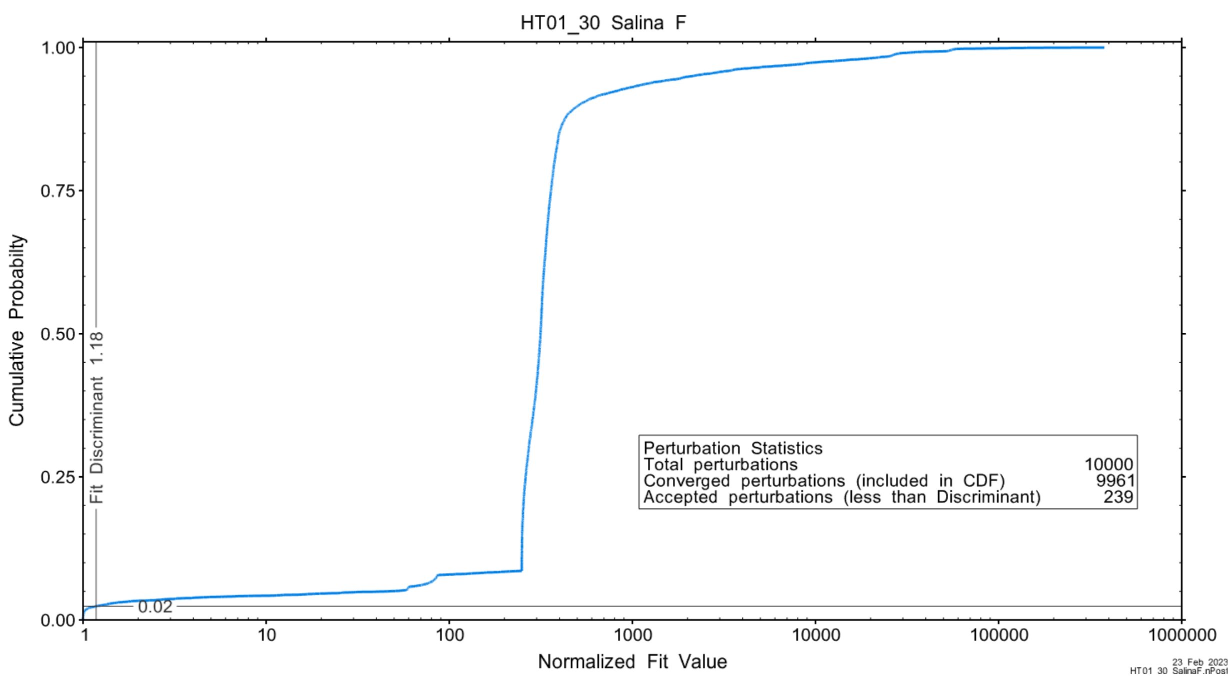

Figure 0.6 Fit value cumulative distribution function.

Summary cross parameter scatter plots for selected formation and skin parameters are given in Figure 0.7 and Figure 0.8. The light pink dots on the figures are the initial parameter estimates, with red dots overlaying those initial parameter values that resulted in accepted optimization results. The grey dots are converged optimizations which did not meet the fit discriminant. Larger varying color symbols represent the fit value of accepted optimizations, with the blue values representing the best fit.

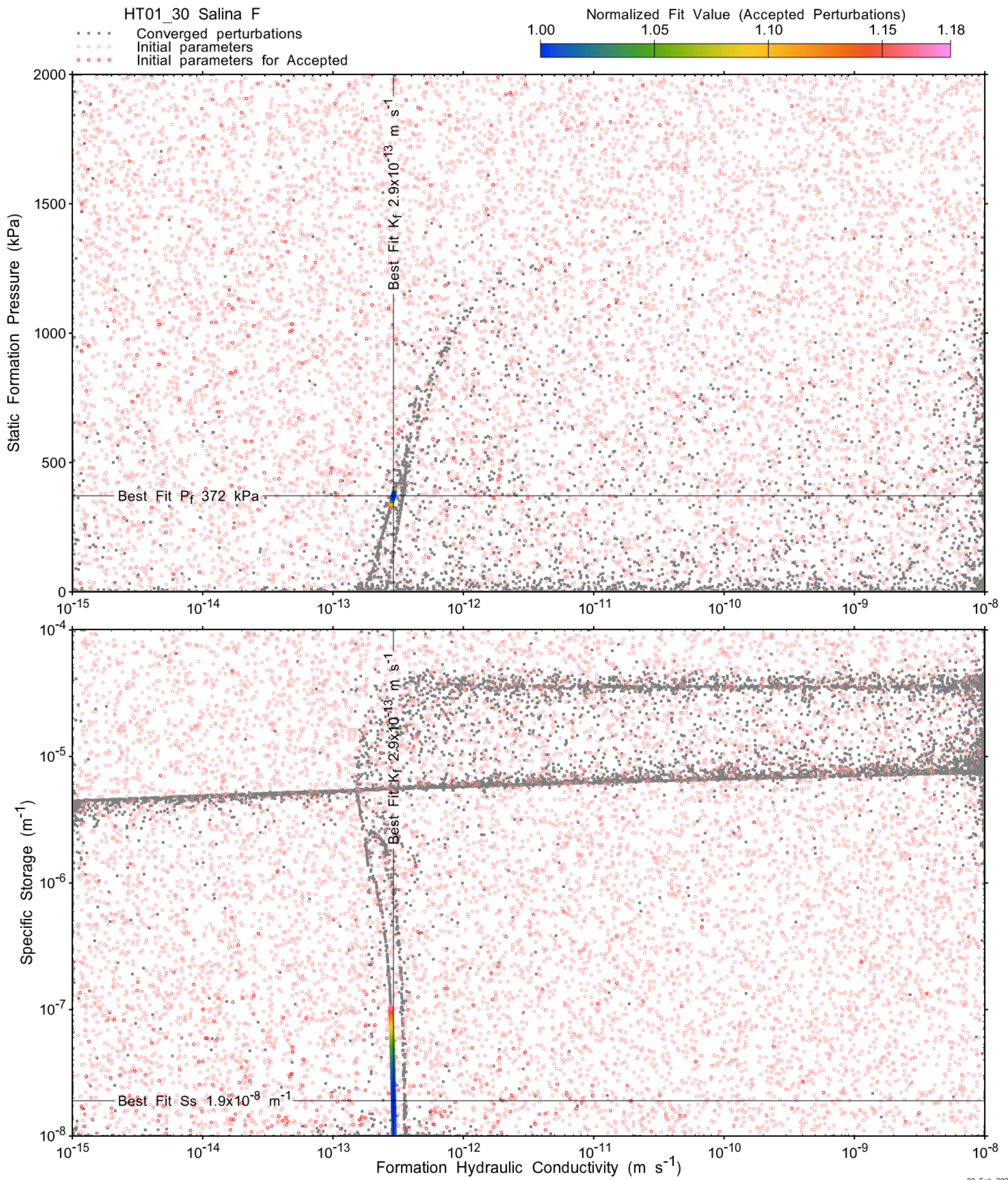

Figure 0.7 XY-scatter plot showing estimates of formation hydraulic conductivity (K_f) vs static formation pressure (P_f) (top panel) and specific storage (Ss) (bottom panel).

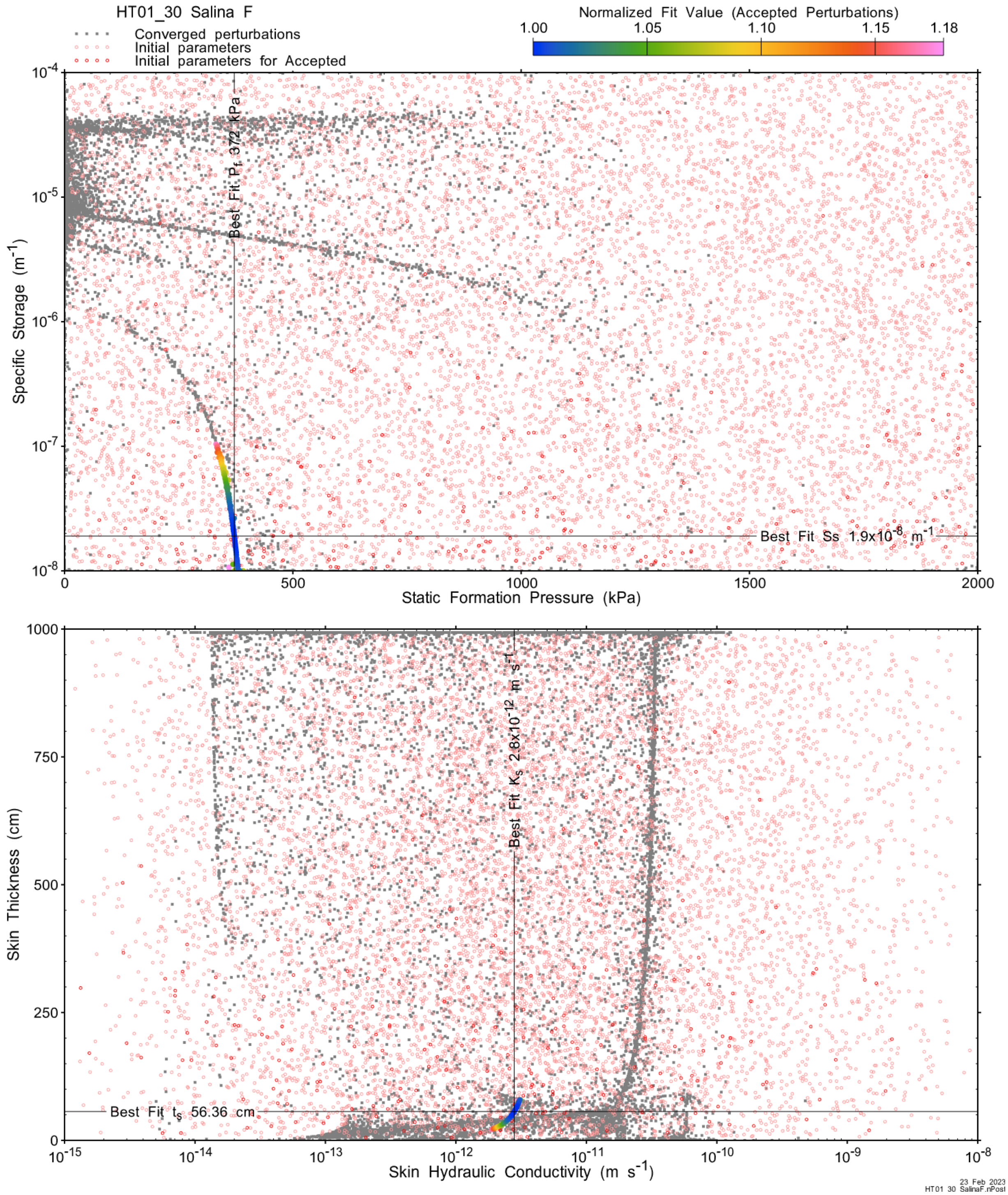

Figure 0.8 XY-scatter plot showing estimates of static formation pressure (P_f) vs specific storage (Ss) (top panel) and skin hydraulic conductivity (K_s) vs skin thickness (t_s) (bottom panel).

Confidence limits and median values are determined from the CDF of accepted optimization results (i.e. the varying color values in the above figures), with best fit value, 5% and 95% confidence indicated on Figure 0.9 and Figure 0.10.

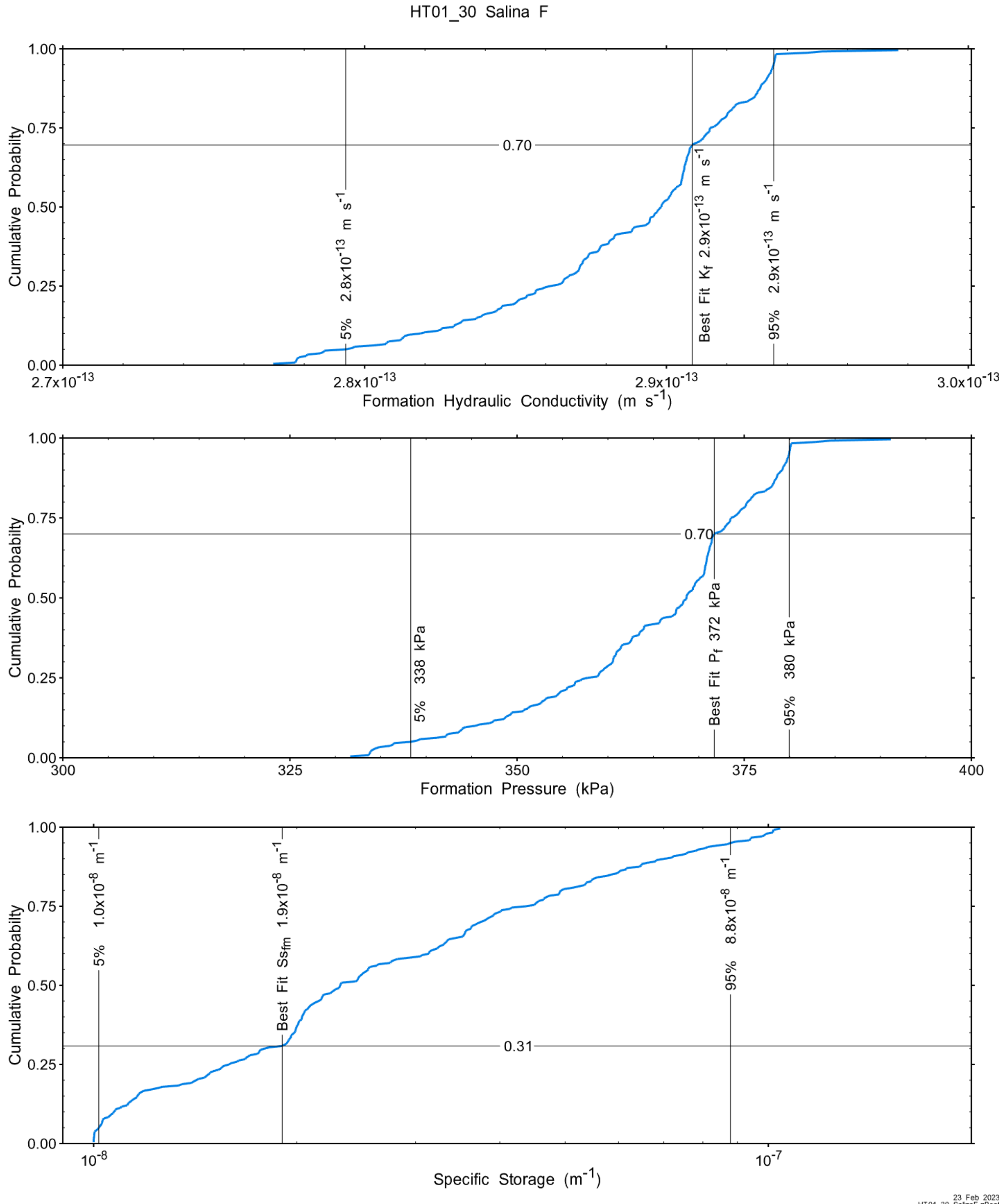

Figure 0.9 Cumulative distribution functions and parameter limits for formation hydraulic conductivity (K_f) (top panel), static formation pressure (P_f) (middle panel) and specific storage (Ss) (bottom panel).

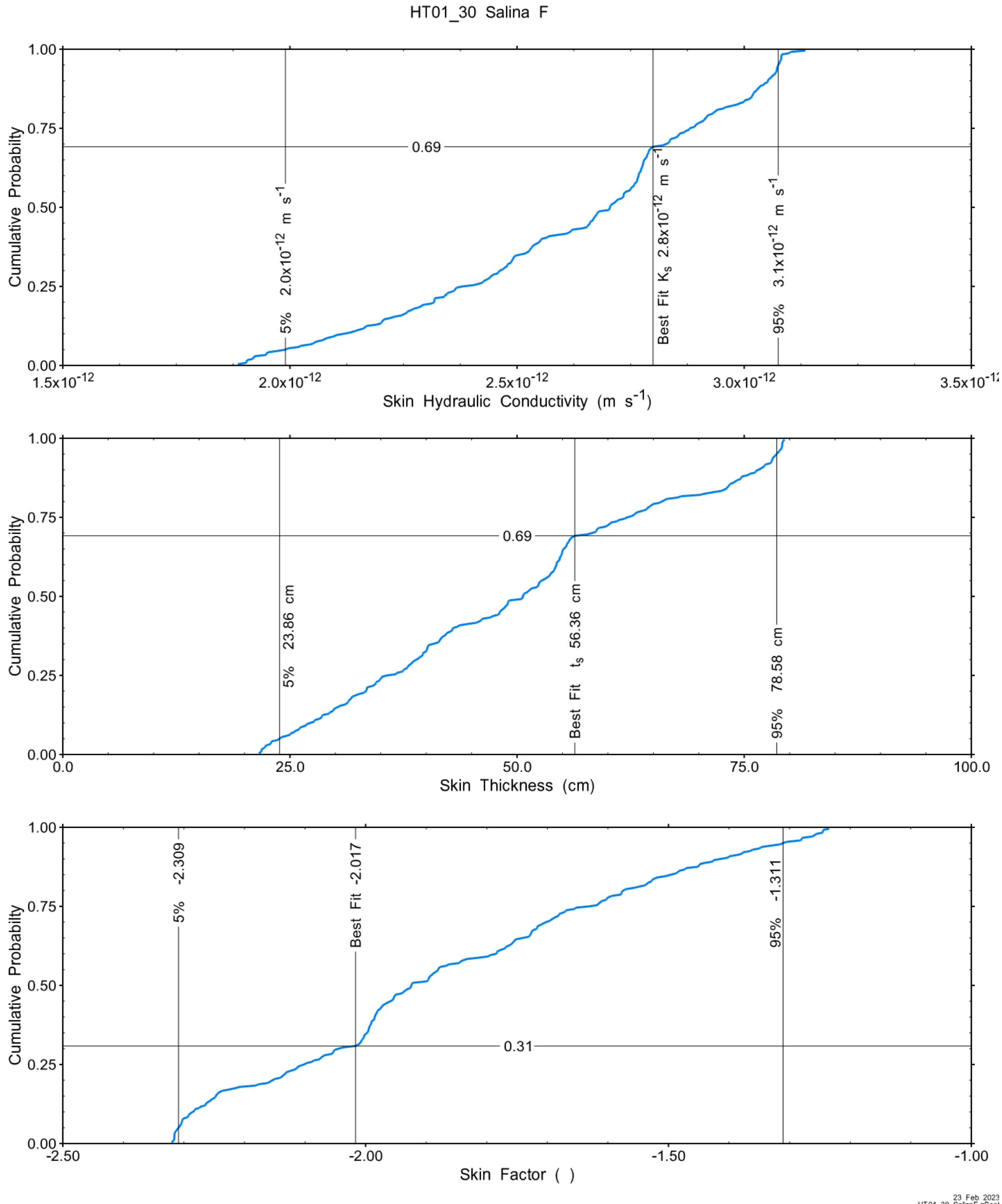

Figure 0.10 Cumulative distribution functions and parameter limits for skin hydraulic conductivity (K_s) (top panel), skin thickness (t_s) (middle panel) and skin factor (s) (bottom panel).

A summary of perturbation results is presented in Figure 0.11, with Ramey-processed perturbations in Figure 0.12. Those perturbations (214 of 10,000) with all parameters within the 5% and 95% range present a good fit to the measured test zone data.

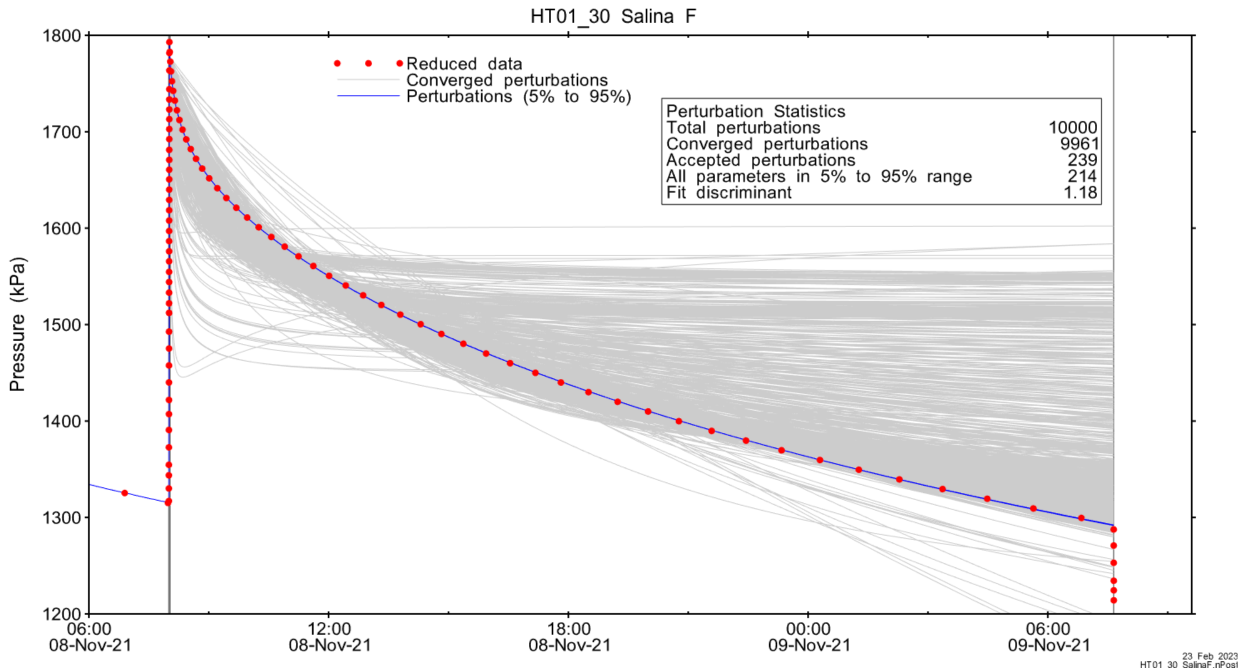

Figure 0.11 Perturbation results – all converged, accepted, and within 5% to 95% for all parameters.

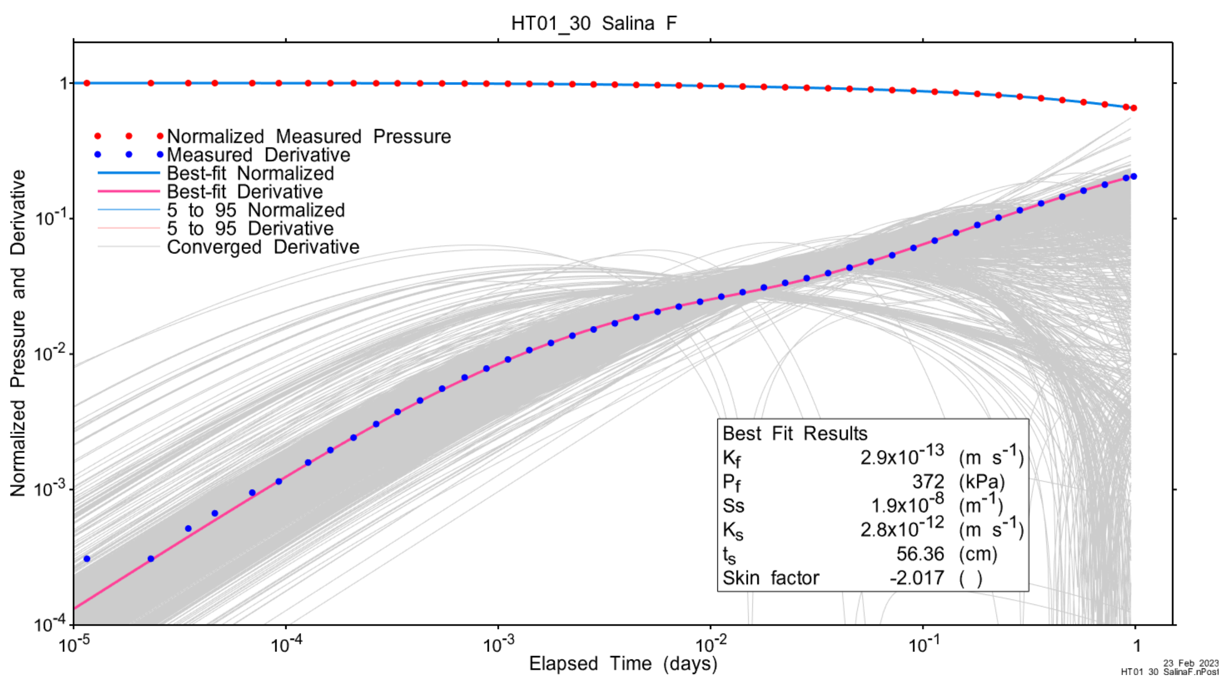

Figure 0.12 Log-log plot showing PI Ramey B normalized pressure and derivative response for all converged optimizations and those within 5% to 95% for all parameters.

A summary of best-fit parameter estimates and ranges is given in Table 0.4.

Table 0.4 Summary of the HT01_30 parameter estimates.

Parameter	Best Fit	5%	Median	95%
K_f (m/s)	2.9E-13	2.8E-13	2.9E-13	2.9E-13
P_f (kPa)	372	338	369	380
Ss (1/m)	1.9E-08	1.0E-08	2.3E-08	8.8E-08
K_s (m/s)	2.8E-12	2.0E-12	2.7E-12	3.1E-12
t_s (cm)	56.36	23.86	50.65	78.58
s (-)	-2.017	-2.309	-1.925	-1.311

Parameter correlations for perturbations with all parameters within the 5% to 95% limits are given in Table 0.5.

Table 0.5 Pearson cross-correlations of 5% to 95% parameters

	Log(K_f)	P_f	Log(Ss)	Log(K_s)	t_s	s
Log(K_f)	1.000	1.000	-0.969	0.986	0.932	-0.968
P_f	1.000	1.000	-0.974	0.989	0.940	-0.973
Log(Ss)	-0.969	-0.974	1.000	-0.994	-0.989	1.000
Log(K_s)	0.986	0.989	-0.994	1.000	0.968	-0.993
t_s	0.932	0.940	-0.989	0.968	1.000	-0.990
s	-0.968	-0.973	1.000	-0.993	-0.990	1.000

A.1.4 Additional Figures

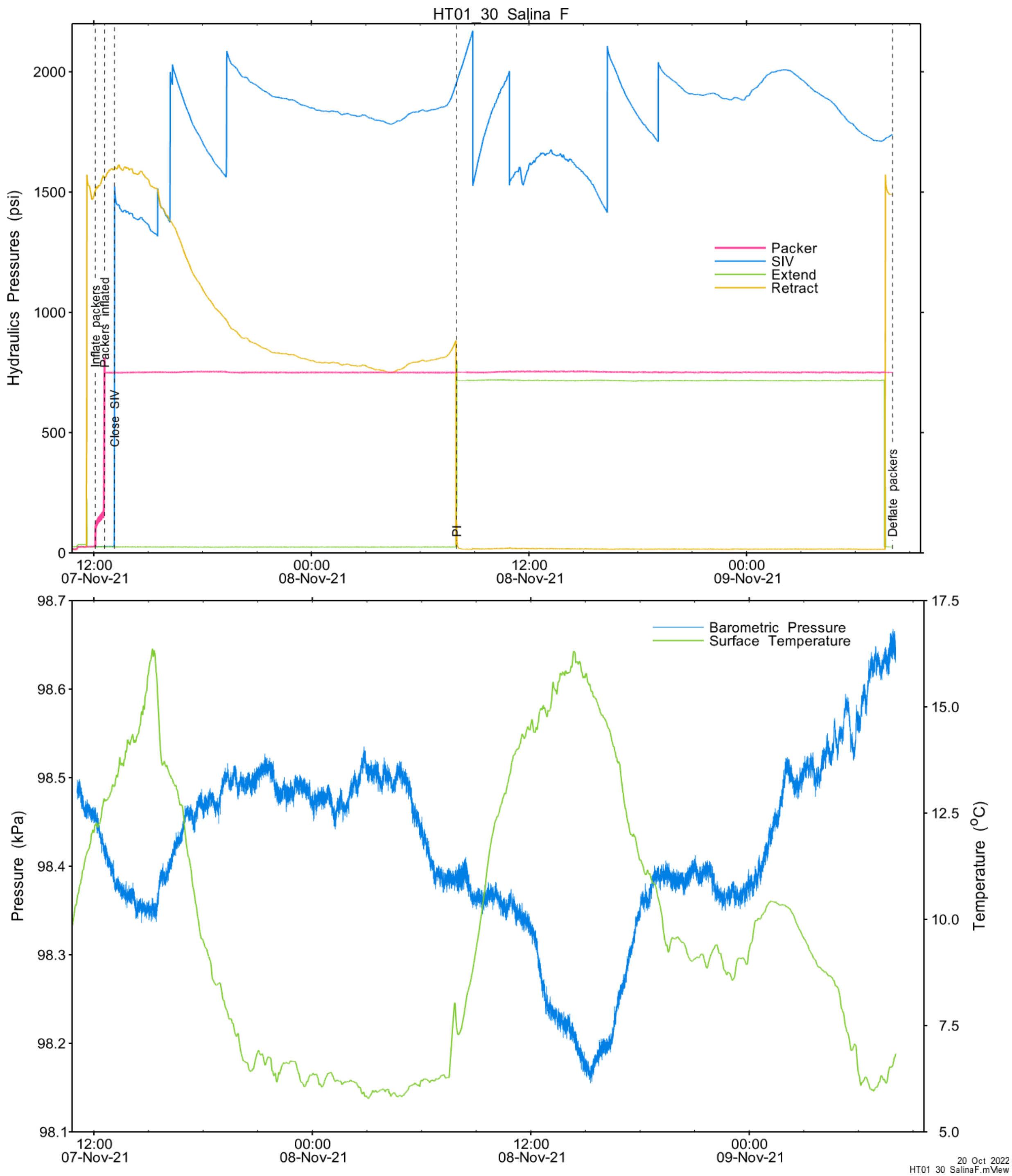

Figure 0.13 Hydraulics pressures and surface temperature/barometric pressure.

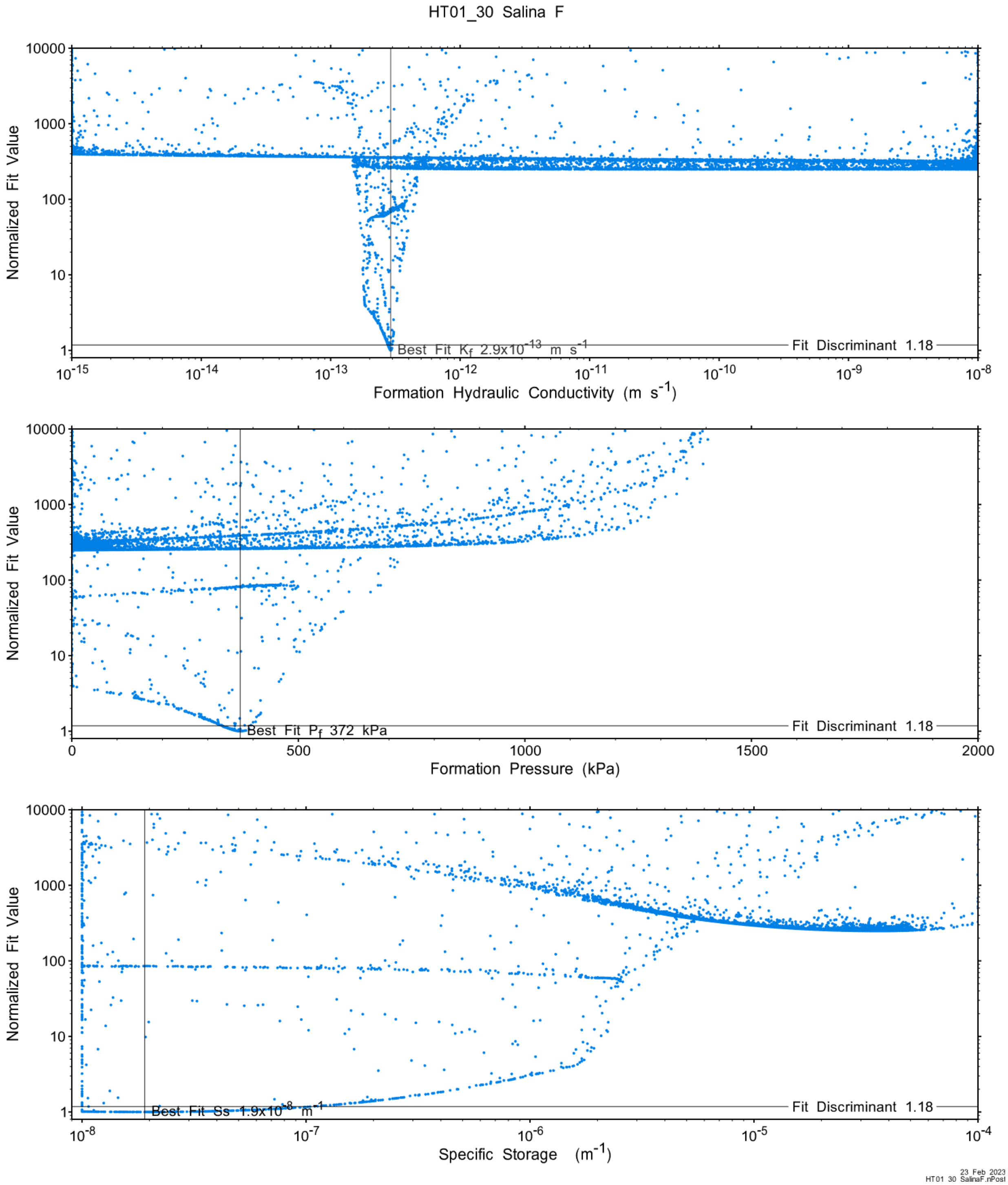

Figure 0.14 XY-scatter plot showing the formation parameter space normalized fit values.

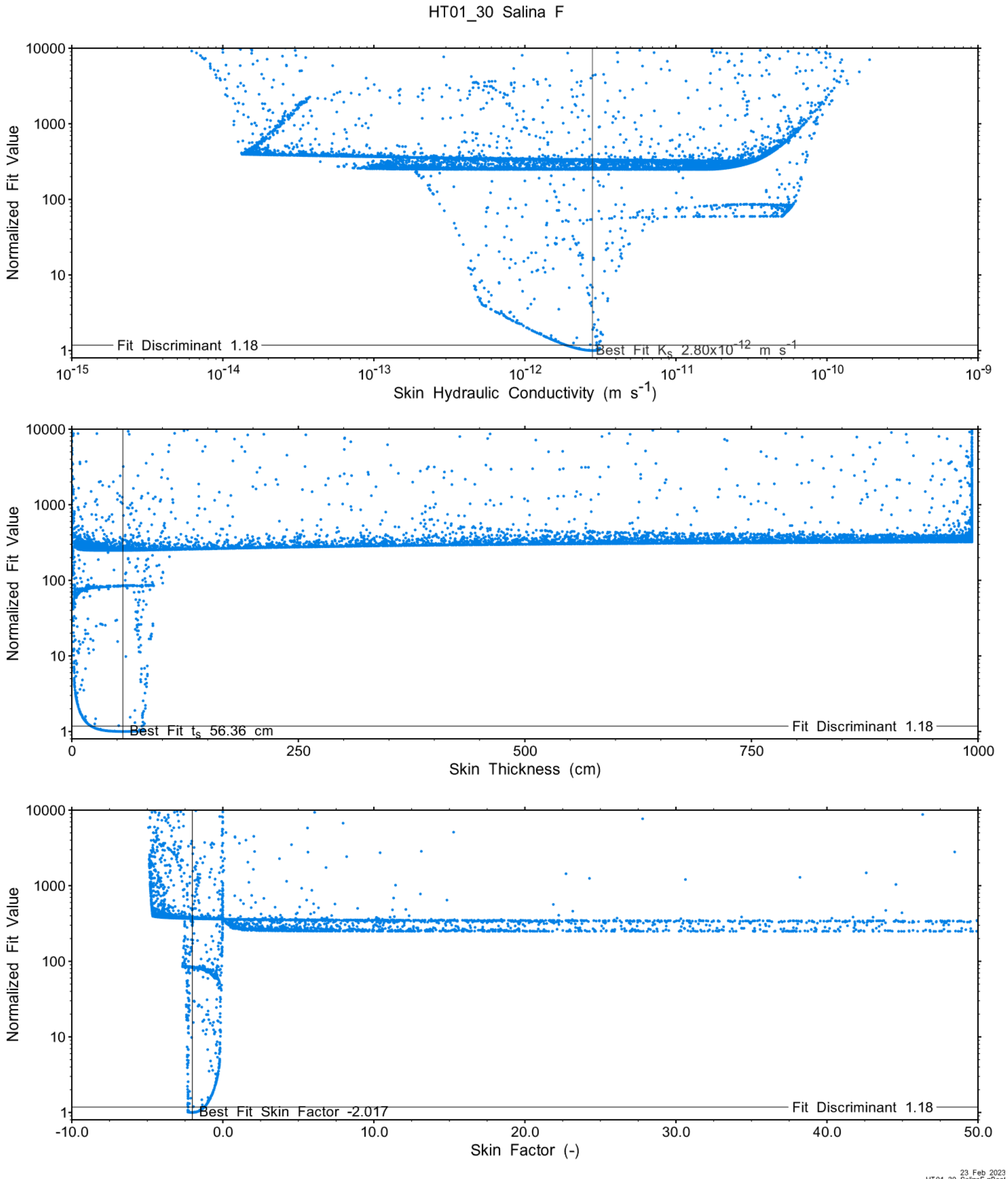

Figure 0.15 XY-scatter plot showing the skin parameter space normalized fit values.

A.2 HT02_30 Salina B

The SB_BH01 interval from 224.00 to 254.05 mBGS tested in HT02_30 includes the majority of the carbonate and evaporite sections of Unit B of the Salina Group. A PI test was conducted initially but responded extremely quickly. An SW was subsequently conducted. Data communication issues limited the slug response to 0.34 days which, given the apparent high conductivity, provided sufficient data for analyses.

A.2.1 Test Data Summary

Table 0.6 and Figure 0.16 provide a summary of test events and a plot of pressures measured while testing, respectively.

Table 0.6 HT02_30 Summary of Test Events.

Event	Start Date & Time	Duration (days)	TZ Pressure (kPa)
Drilling intercept	21-07-19 20:42	112.78	2294
Shut-in	21-11-09 15:20	0.68	2294
Pulse injection	21-11-10 07:45	0.37	2405
Slug withdrawal	21-11-10 16:38	0.34	1967
Test end	21-11-11 00:47		2162

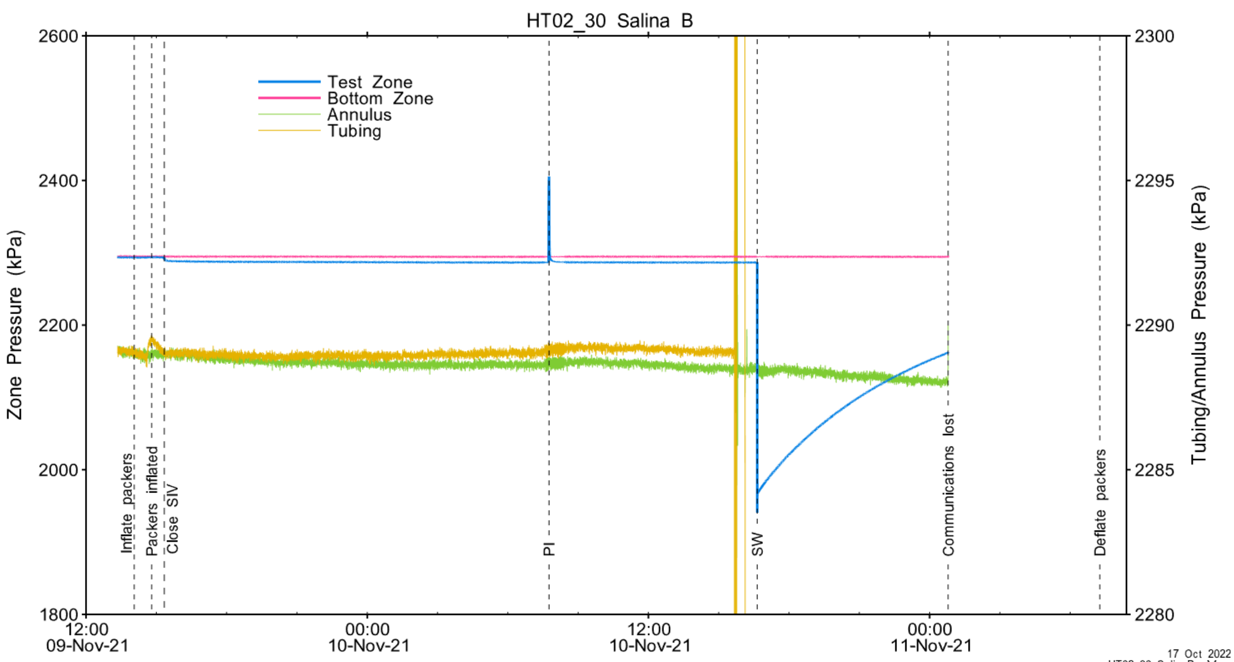

Figure 0.16 HT02_30 test events and pressures.

A.2.2 Test Analyses

Table 0.7 is a summary of test-specific input parameters used in the analyses, while Table 0.8 presents the optimized parameters and allowed ranges.

Table 0.7 nSIGHTS Input Parameters.

Parameter	Value	Units
Test zone radius	6.645	cm
Tubing string radius	2.54	cm
Test zone fluid density	1044	g/L
Test zone length	30.05	m

Table 0.8 nSIGHTS Parameter Optimization Ranges.

Parameter	Minimum	Maximum	Units	Type
Formation hydraulic conductivity (K_f)	1E-12	1E-07	m/s	log
Formation pressure (P_f)	1500	3000	kPa	linear
Specific storage (Ss)	1E-08	1E-04	1/m	log
Skin hydraulic conductivity (K_s)	1E-12	1E-07	m/s	log
Skin thickness (t_s)	0.1	10000	mm	linear

Figure 0.17 shows the measured test zone pressure record (with reduced data density for clarity) used in the analysis along with the best-fit simulation and parameter values. Figure 0.18 presents the pre-test history, and Figure 0.19 shows the Ramey B normalized best-fit pressure and pressure derivatives.

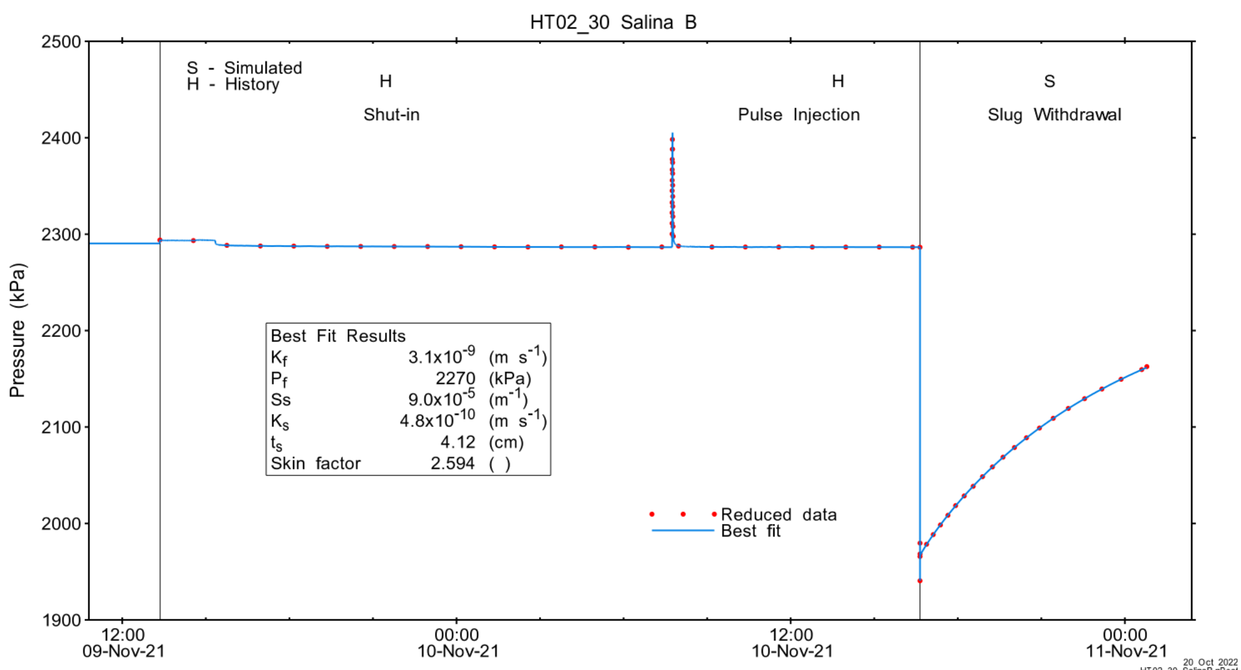

Figure 0.17 Annotated testing sequence showing best-fit simulation and parameter estimates.

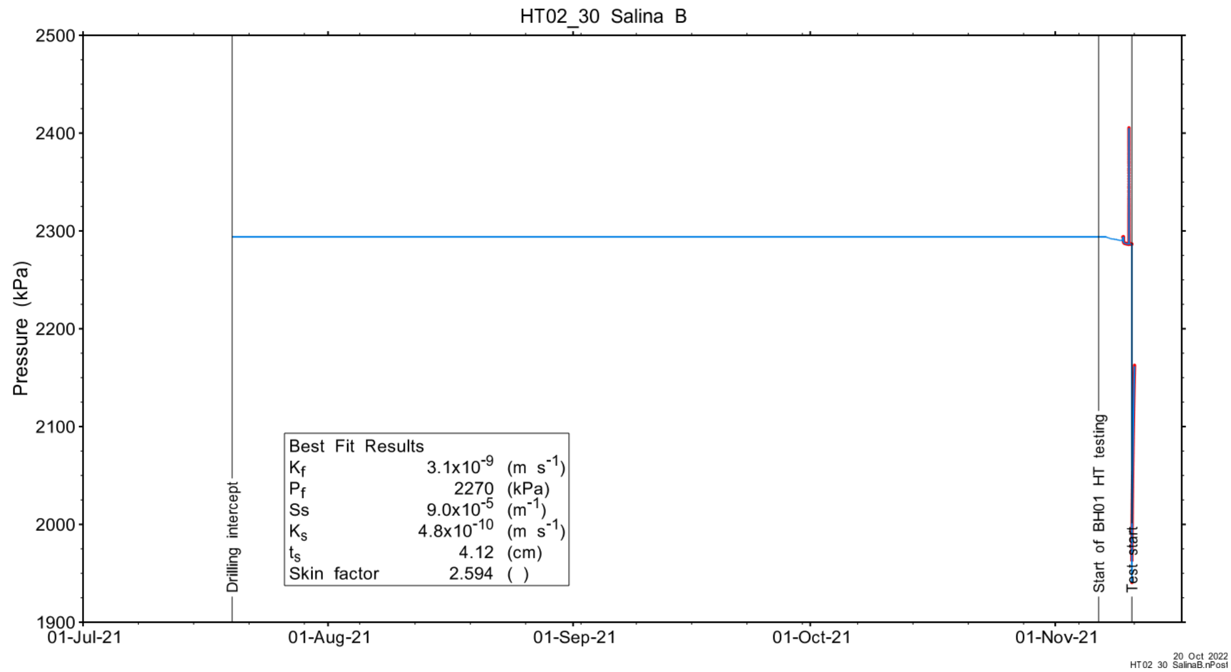

Figure 0.18 Annotated HT02_30 testing sequence showing pre-test history, best-fit simulation and parameter estimates.

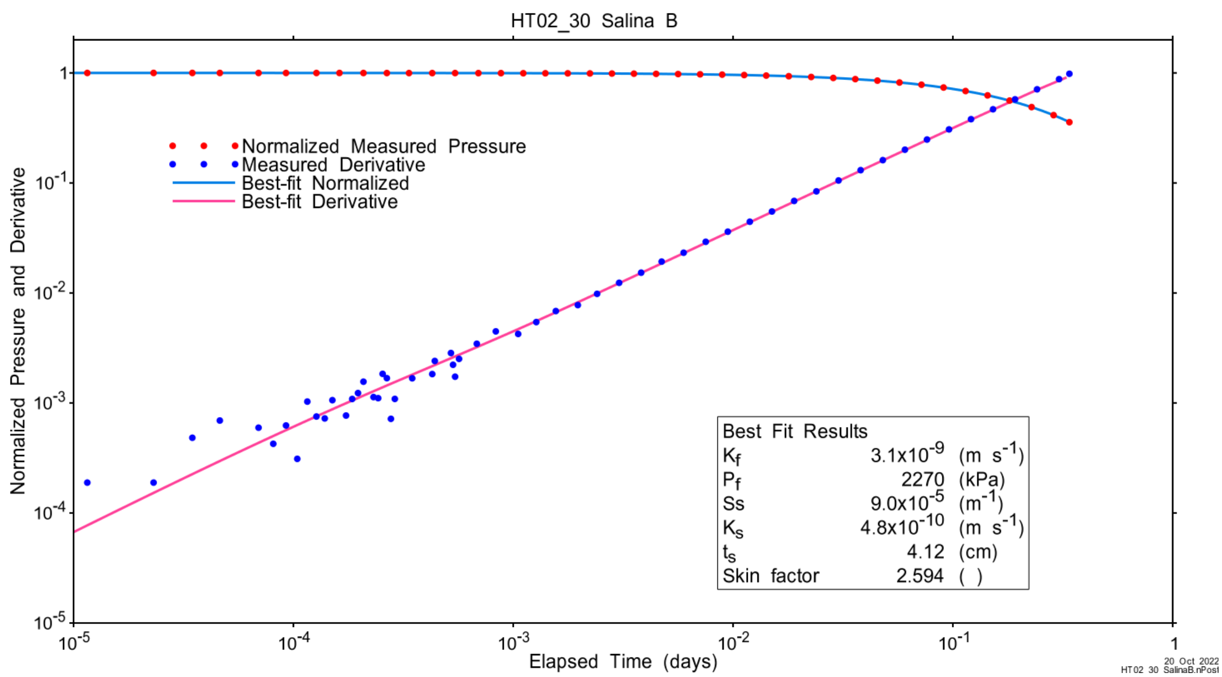

Figure 0.19 Log-log plot showing SW Ramey B normalized pressure and derivative response for best-fit simulation.

Figure 0.20 shows the normalized parameter sensitivity response for the best fit. Skin-related parameters are most sensitive during the early-time response. Sensitivity to all parameters except P_f had reached maximum values – solution would not likely have been improved with additional testing time.

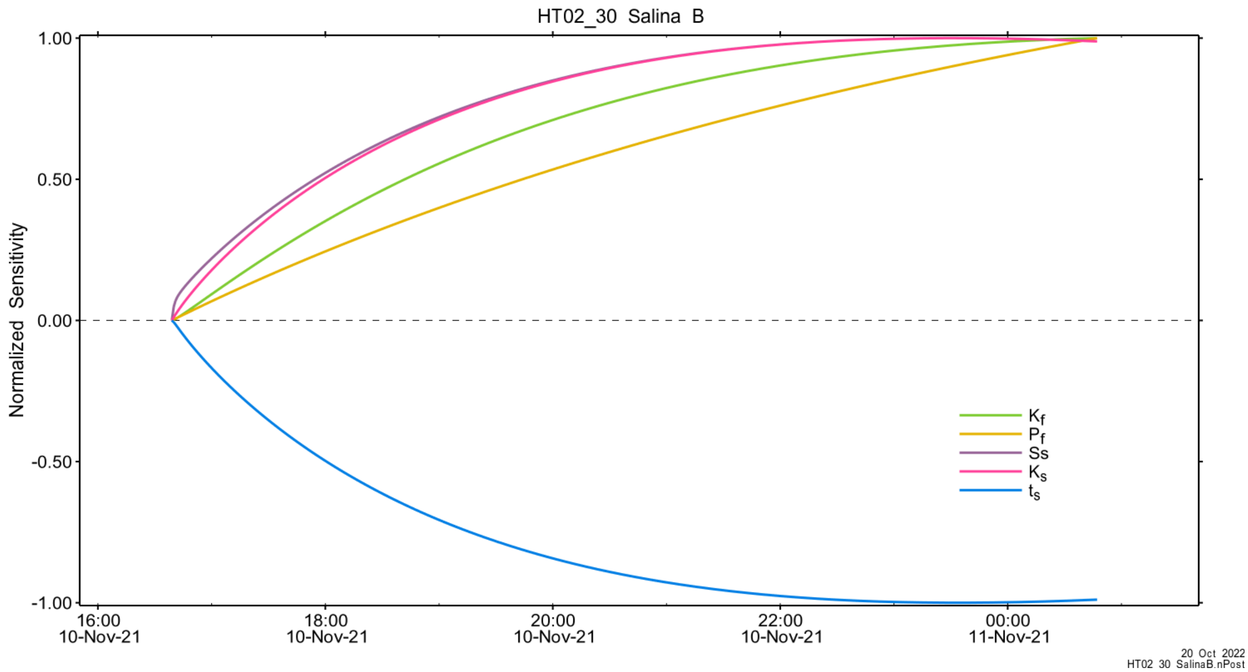

Figure 0.20 Normalized Jacobian for best-fit SW simulation.

A.2.3 Uncertainty Analyses

The CDF of normalized fit values for all converged simulations and the selected fit discriminant are shown in Figure 0.21.

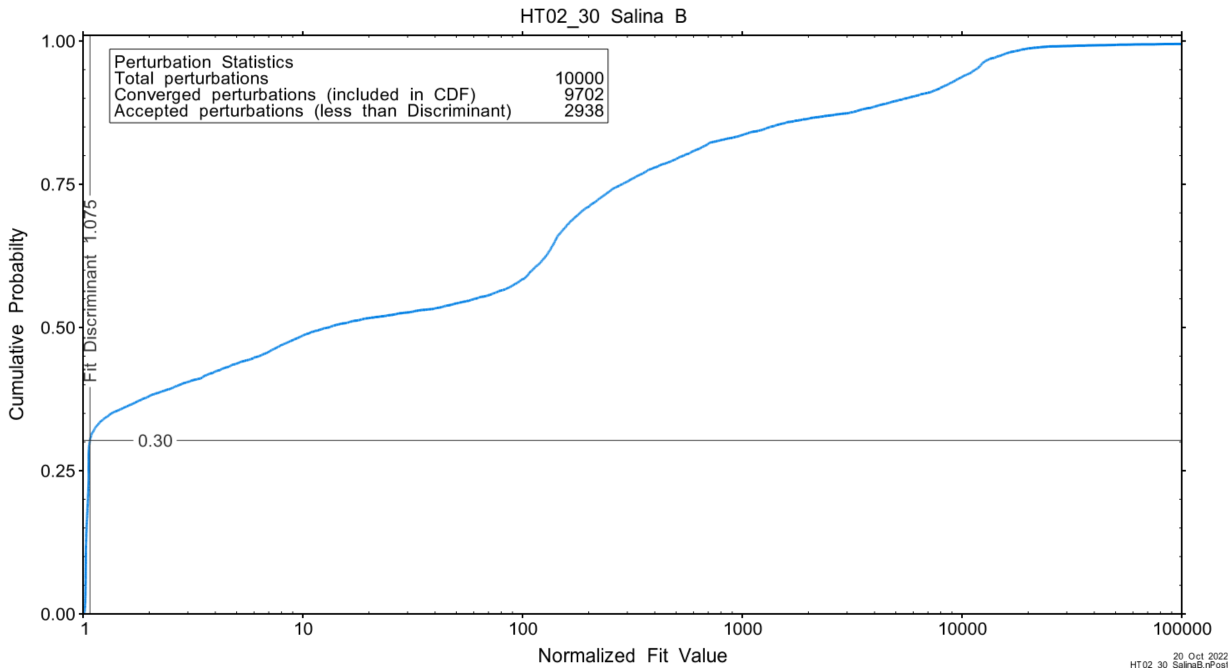

Figure 0.21 Fit value cumulative distribution function.

Summary cross parameter scatter plots for selected formation and skin parameters are given in Figure 0.22 and Figure 0.23. The light pink dots on the figures are the initial parameter estimates, with red dots overlaying those initial parameter values that resulted in accepted optimization results. The grey dots are converged optimizations which did not meet the fit discriminant. Larger varying color symbols represent the fit value of accepted optimizations, with the blue values representing the best fit.

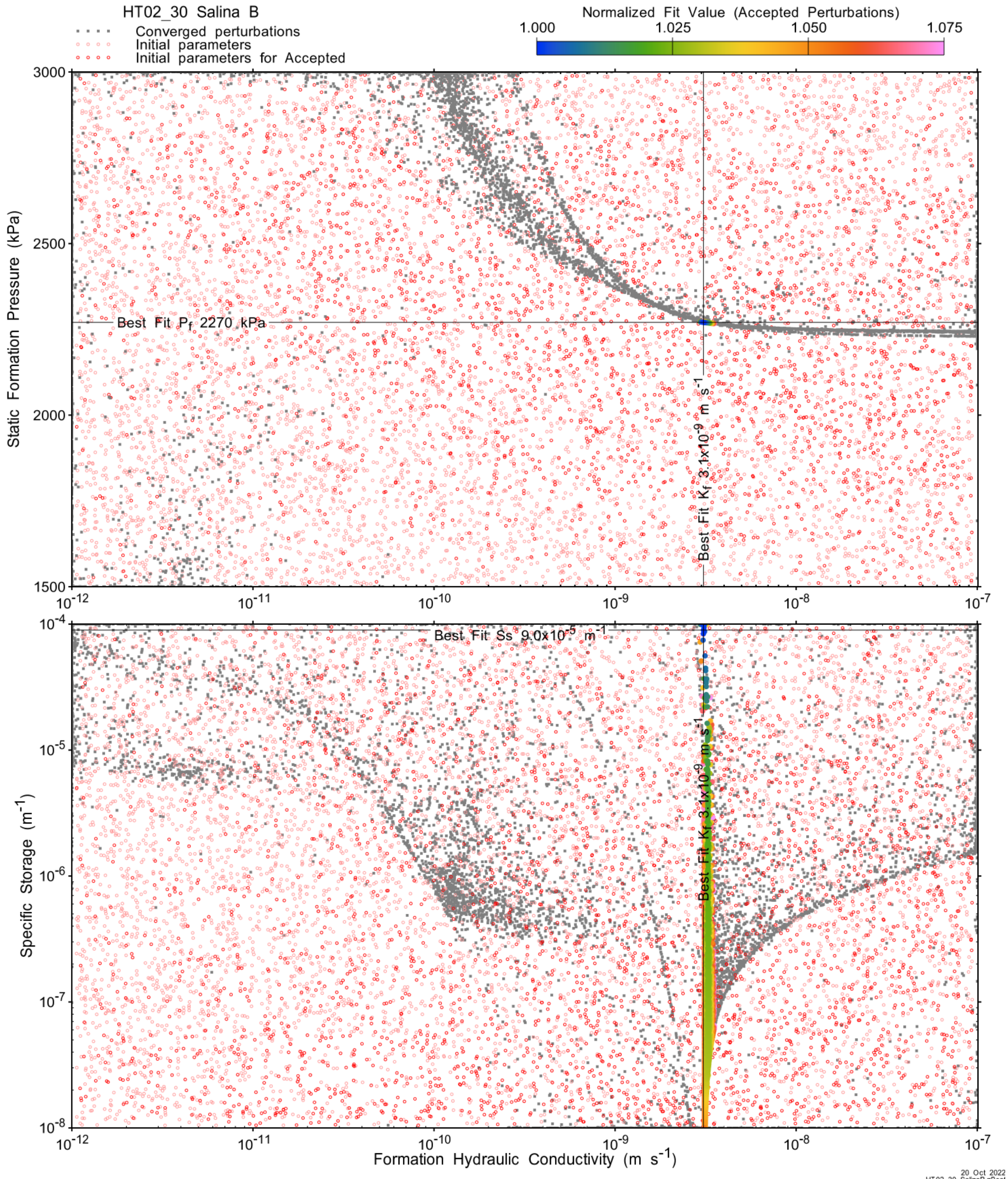

Figure 0.22 XY-scatter plot showing estimates of formation hydraulic conductivity (K_f) vs static formation pressure (P_f) (top panel) and specific storage (Ss) (bottom panel).

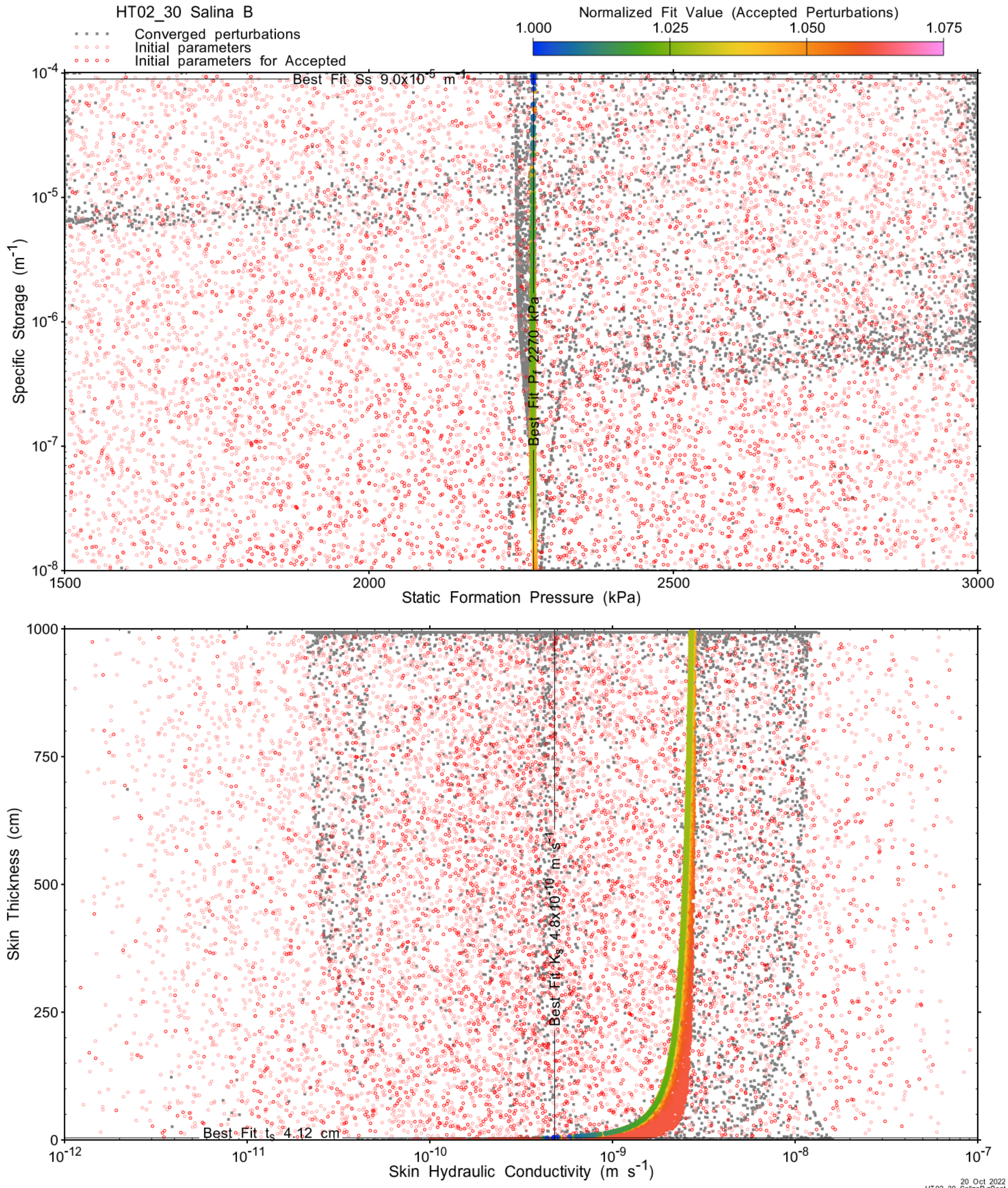

Figure 0.23 XY-scatter plot showing estimates of static formation pressure (P_f) vs specific storage (Ss) (top panel) and skin hydraulic conductivity (K_s) vs skin thickness (t_s) (bottom panel).

Confidence limits and median values are determined from the CDF of accepted optimization results (i.e. the varying color values in the above figures), with best fit value, 5% and 95% confidence indicated on Figure 0.24 and Figure 0.25.

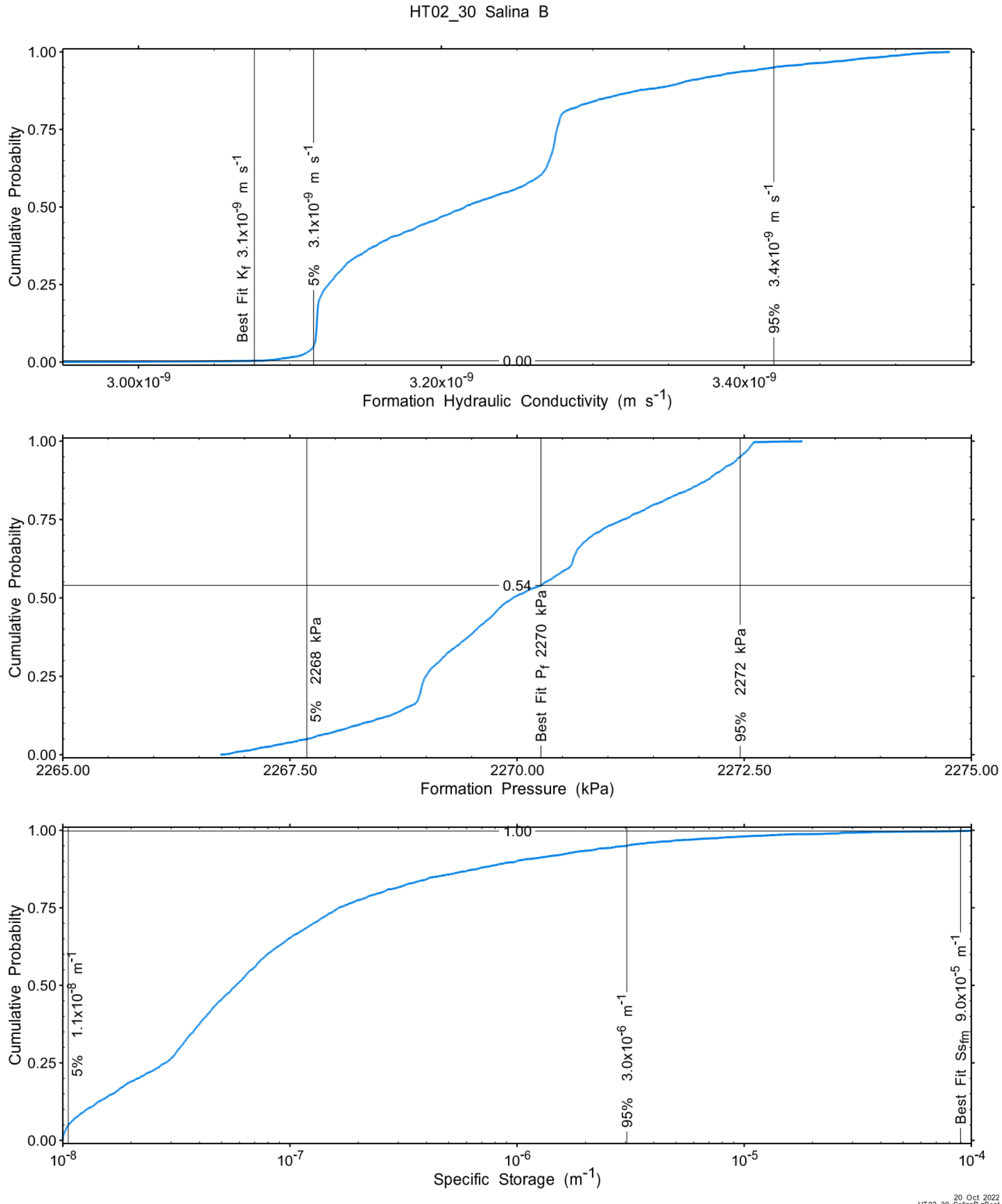

Figure 0.24 Cumulative distribution functions and parameter limits for formation hydraulic conductivity (K_f) (top panel), static formation pressure (P_f) (middle panel) and specific storage (Ss) (bottom panel).

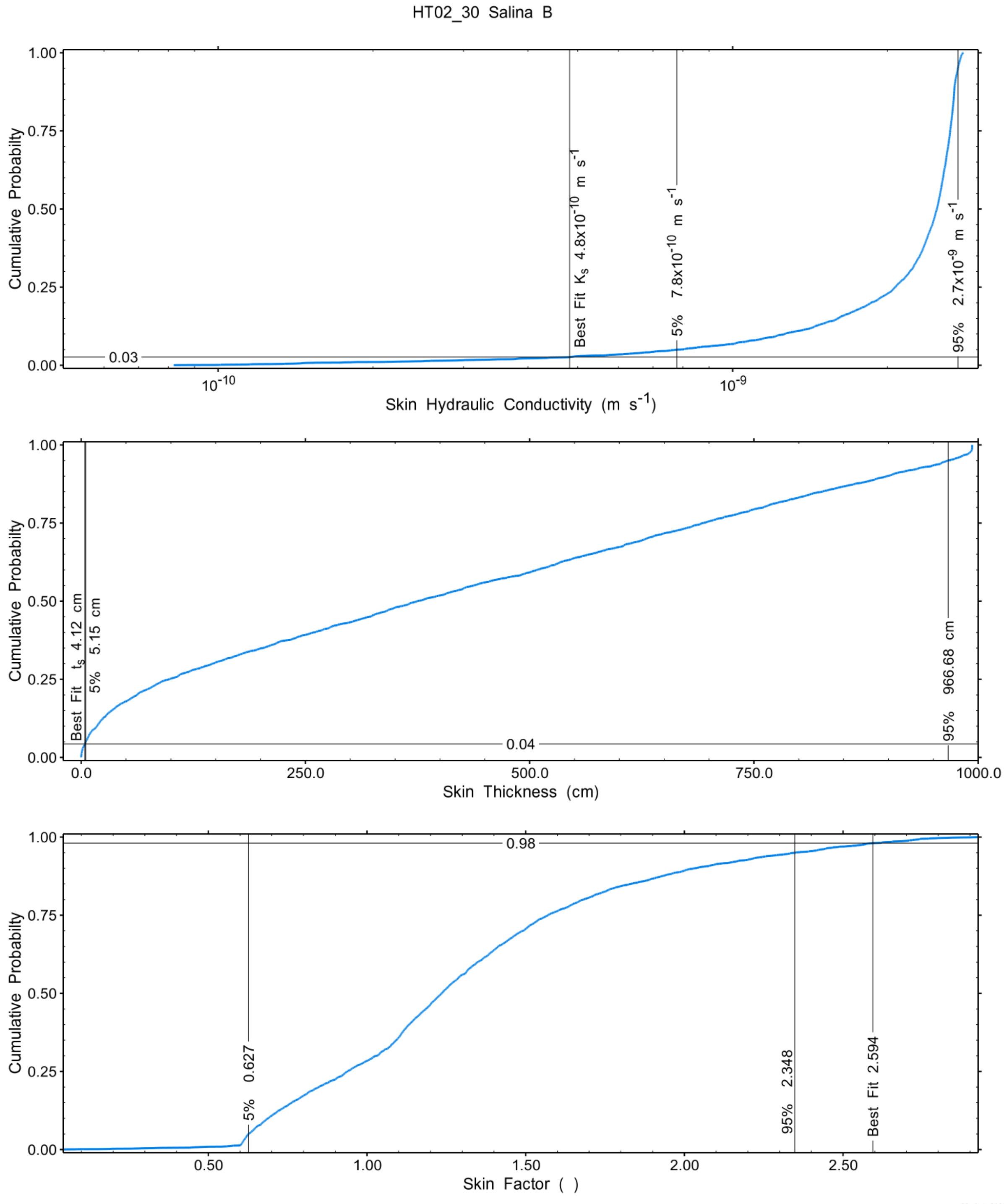

Figure 0.25 Cumulative distribution functions and parameter limits for skin hydraulic conductivity (K_s) (top panel), skin thickness (t_s) (middle panel) and skin factor (s) (bottom panel).

A summary of perturbation results is presented in Figure 0.26, with Ramey-processed perturbations in Figure 0.27. Those perturbations (2066 of 10,000) with all parameters within the 5% and 95% range present a good fit to the measured test zone data.

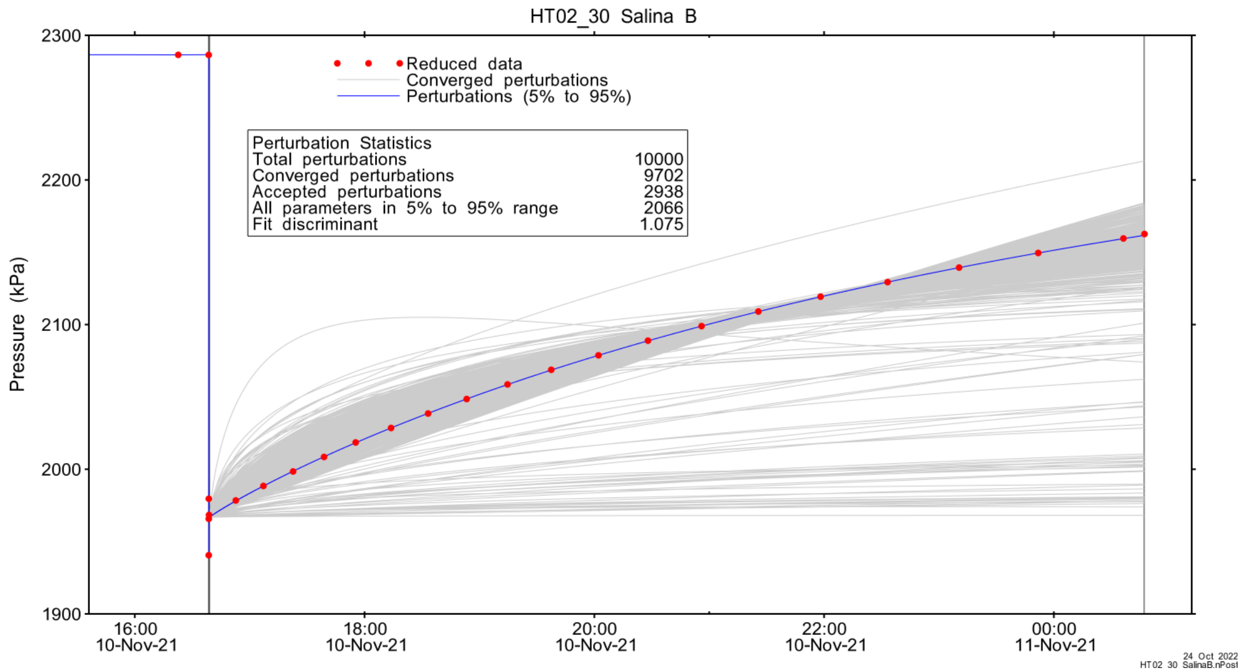

Figure 0.26 Perturbation results – all converged, accepted, and within 5% to 95% for all parameters.

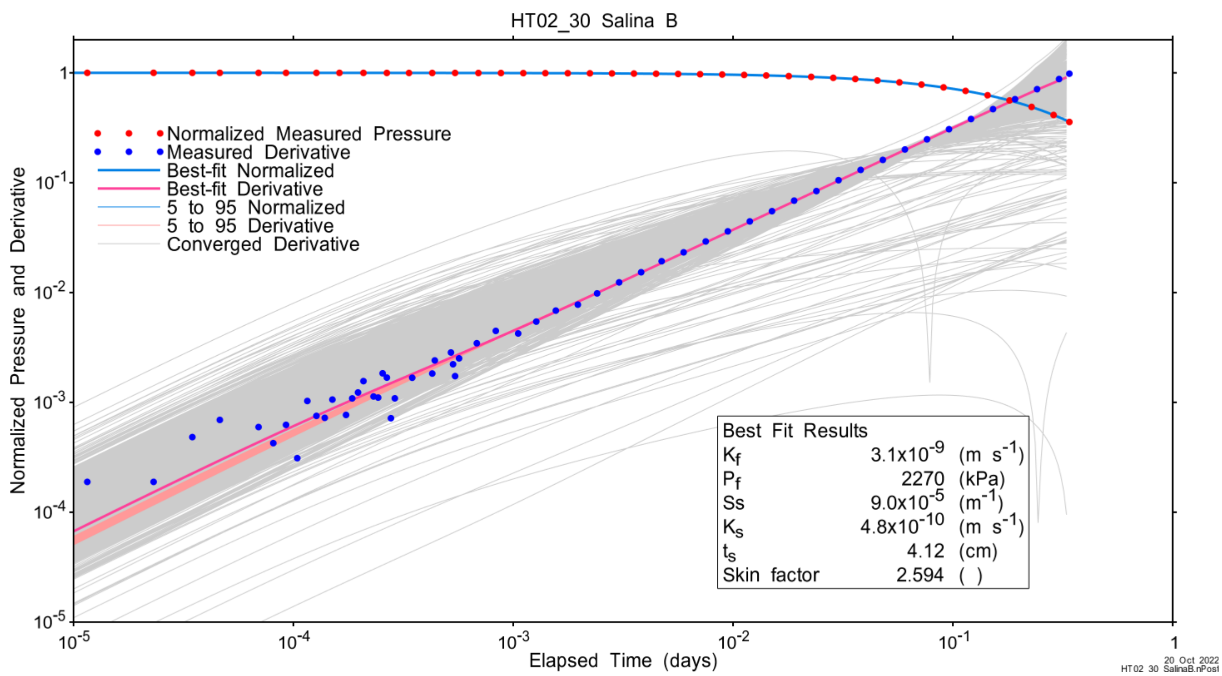

Figure 0.27 Log-log plot showing SW Ramey B normalized pressure and derivative response for all converged optimizations and those within 5% to 95% for all parameters.

A summary of best-fit parameter estimates and ranges is given in Table 0.9.

Table 0.9 Summary of the HT02_30 parameter estimates.

Parameter	Best Fit	5%	Median	95%
K_f (m/s)	3.1E-09	3.1E-09	3.2E-09	3.4E-09
P_f (kPa)	2270	2268	2270	2272
Ss (1/m)	9.0E-05	1.1E-08	5.8E-08	3.0E-06
K_s (m/s)	4.8E-10	7.8E-10	2.5E-09	2.7E-09
t_s (cm)	4.12	5.15	374.57	966.69
s (-)	2.594	0.627	1.235	2.348

Parameter correlations for all perturbations with all parameters within the 5% to 95% limits are given in Table 0.10.

Table 0.10 Pearson cross-correlations of 5% to 95% parameters

	Log(K_f)	P_f	Log(Ss)	Log(K_s)	t_s	s
Log(K_f)	1.000	-0.908	0.366	0.238	0.426	0.488
P_f	-0.908	1.000	-0.654	0.056	-0.119	-0.747
Log(Ss)	0.366	-0.654	1.000	-0.644	-0.511	0.988
Log(K_s)	0.238	0.056	-0.644	1.000	0.757	-0.601
t_s	0.426	-0.119	-0.511	0.757	1.000	-0.436
s	0.488	-0.747	0.988	-0.601	-0.436	1.000

A.2.4 Additional Figures

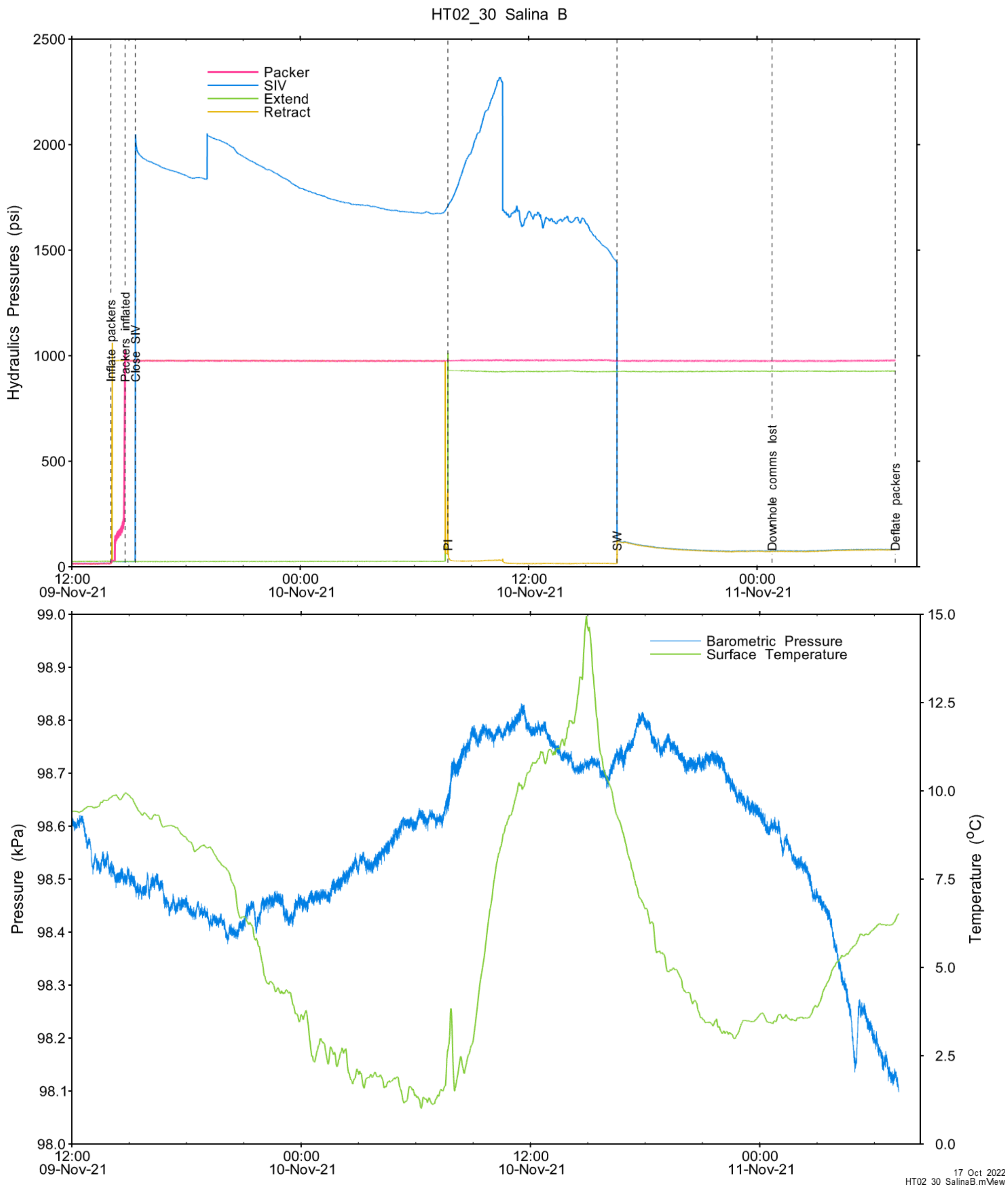

Figure 0.28 Hydraulics pressures and surface temperature/barometric pressure.

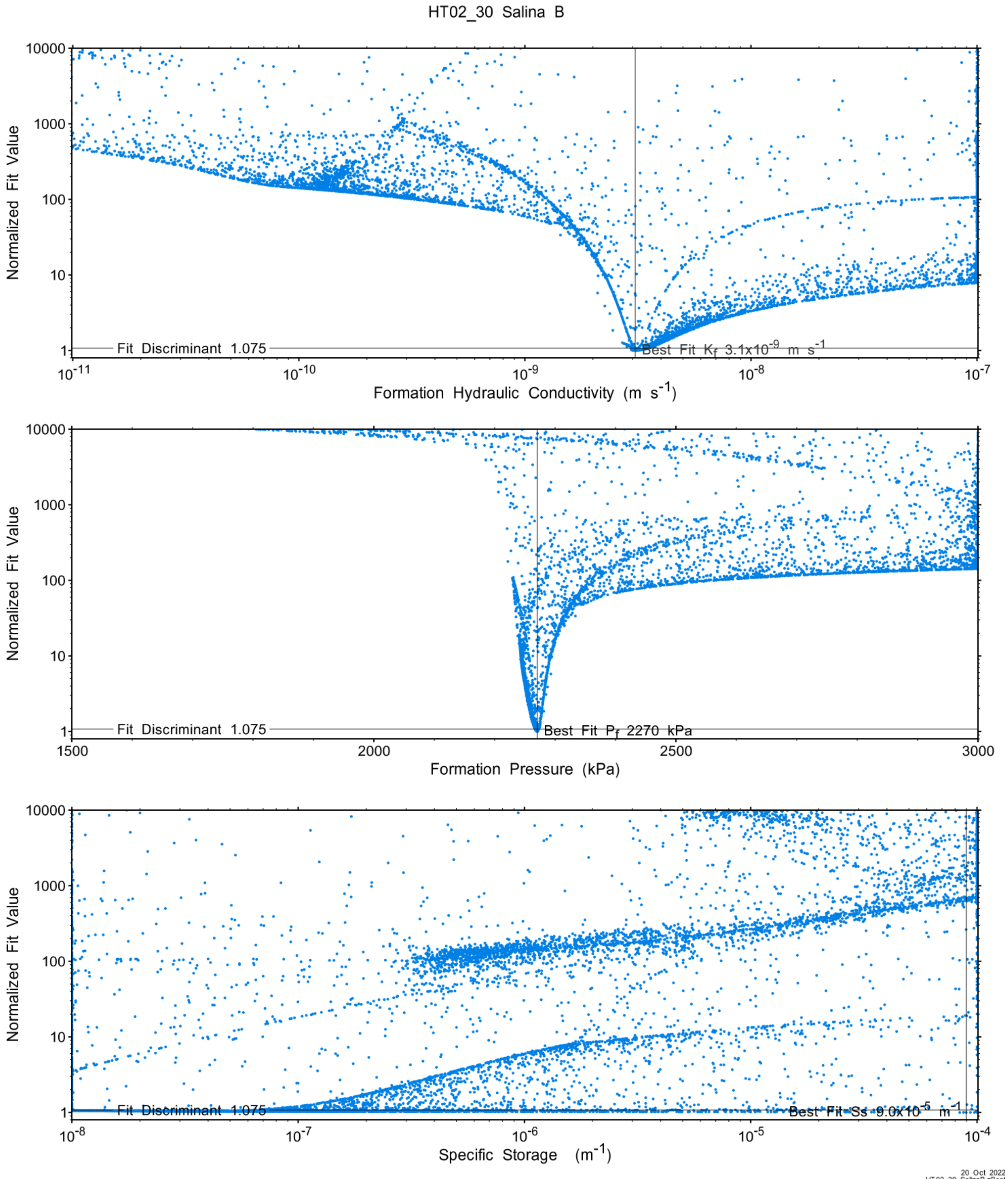

Figure 0.29 XY-scatter plot showing the formation parameter space normalized fit values.

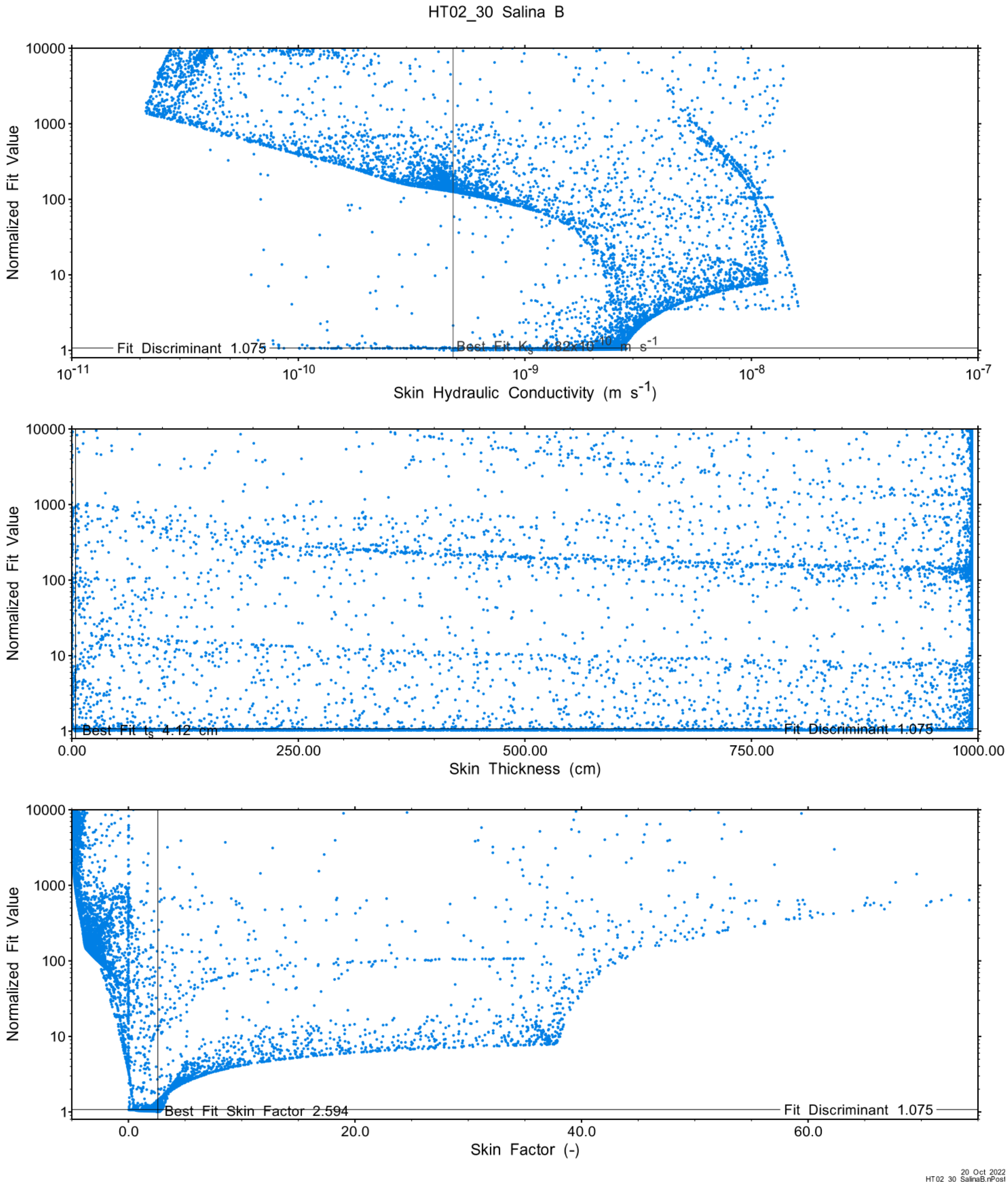

Figure 0.30 XY-scatter plot showing the skin parameter space normalized fit values.

A.3 HT03_30 Guelph

The SB_BH01 interval from 291.60 to 321.65 mBGS tested in HT03_30 includes the upper 30 m of the approximately 50-m-thick Guelph Formation. At this location, the Guelph is a pinnacle reef with extremely high hydraulic conductivity. A single SW test recovered completely in less than 10 minutes.

A.3.1 Test Data Summary

Table 0.11 and Figure 0.31 provide a summary of test events and a plot of pressures measured while testing, respectively.

Table 0.11 HT03_30 Summary of Test Events.

Event	Start Date & Time	Duration (days)	TZ Pressure (kPa)
Drilling intercept	21-07-31 04:30	111.50	2973
Shut-in	21-11-19 16:34	0.61	2973
Slug withdrawal	21-11-20 07:09	0.01	2952
Test end	21-11-20 07:19		2973

Note that the test was terminated early based on the fast response. Data was collected for a period after until NWMO concurrence of early termination was received.

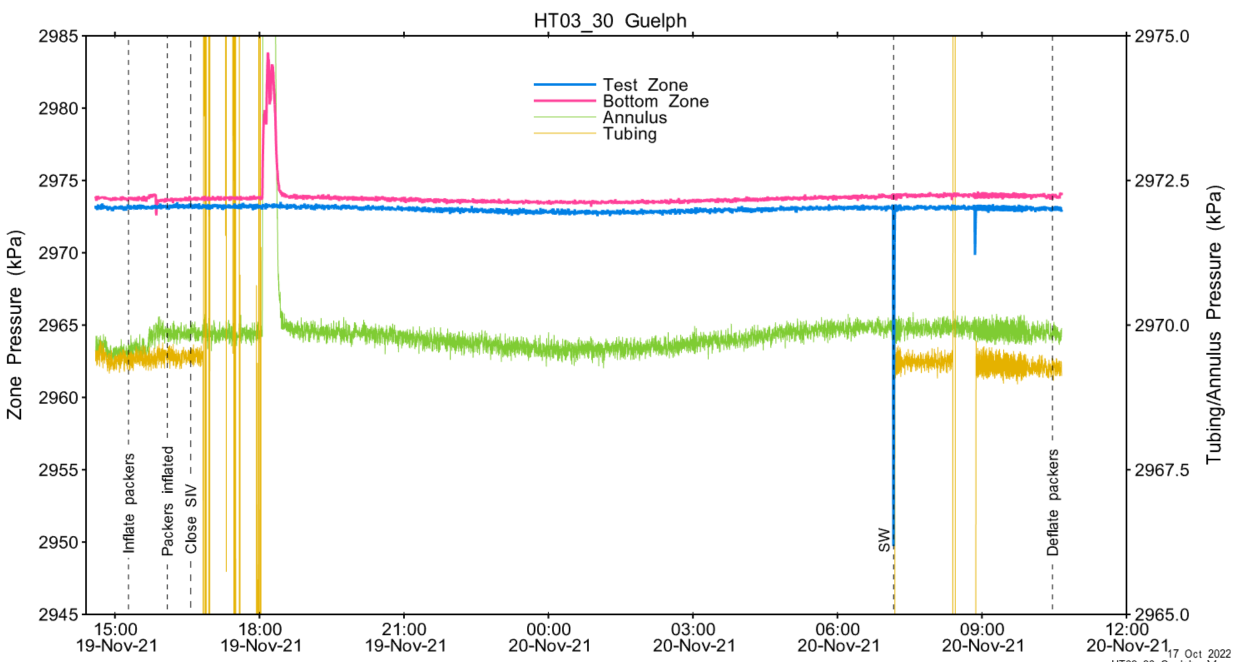

Figure 0.31 HT03_30 test events and pressures.

A.3.2 Test Analyses

Table 0.12 is a summary of test-specific input parameters used in the analyses, while Table 0.13 presents the optimized parameters and allowed ranges.

Table 0.12 nSIGHTS Input Parameters.

Parameter	Value	Units
Test zone radius	6.705	cm
Tubing string radius	2.54	cm
Test zone fluid density	1052	g/L
Test zone length	30.05	m

Table 0.13 nSIGHTS Parameter Optimization Ranges.

Parameter	Minimum	Maximum	Units	Type
Formation hydraulic conductivity (K_f)	1E-08	1E+00	m/s	log
Formation pressure (P_f)	2950	2975	kPa	linear
Specific storage (Ss)	1E-08	1E-04	1/m	log
Skin hydraulic conductivity (K_s)	1E-08	1E+00	m/s	log
Skin thickness (t_s)	0.1	10000	mm	linear

Figure 0.32 shows the measured test zone pressure record (with reduced data density for clarity) used in the analysis along with the best-fit simulation and parameter values. Figure 0.33 presents the pre-test history, and Figure 0.34 shows the Ramey B normalized best-fit pressure and pressure derivatives.

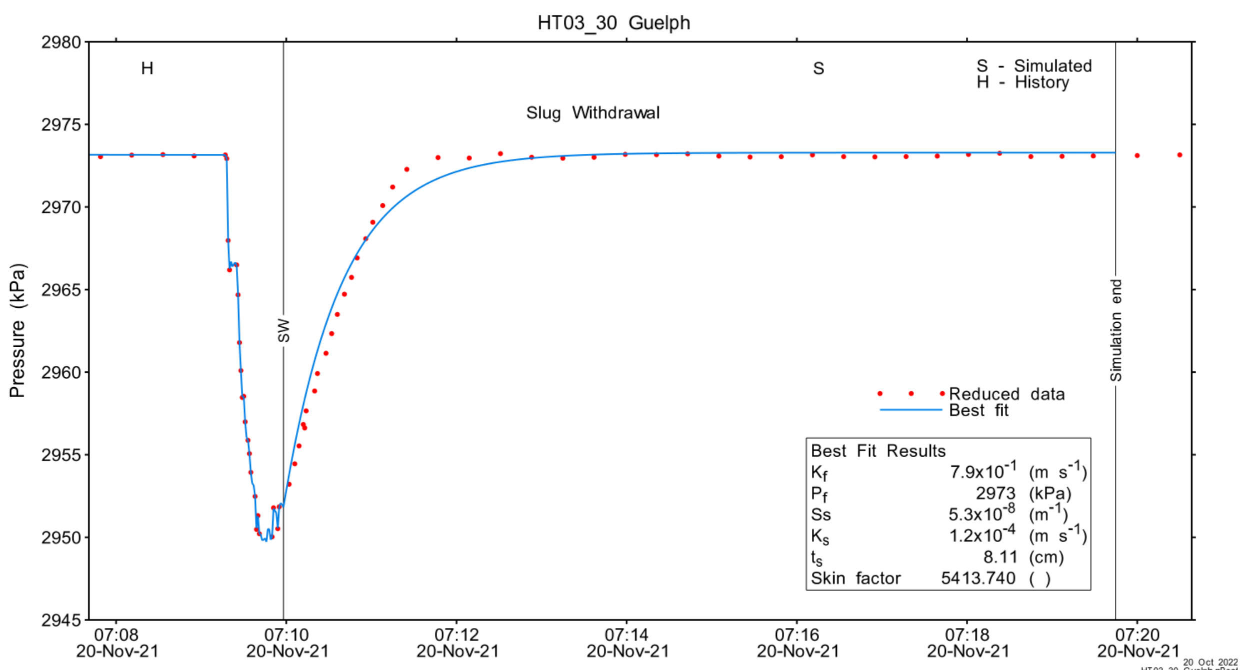

Figure 0.32 Annotated testing sequence showing best-fit simulation and parameter estimates.

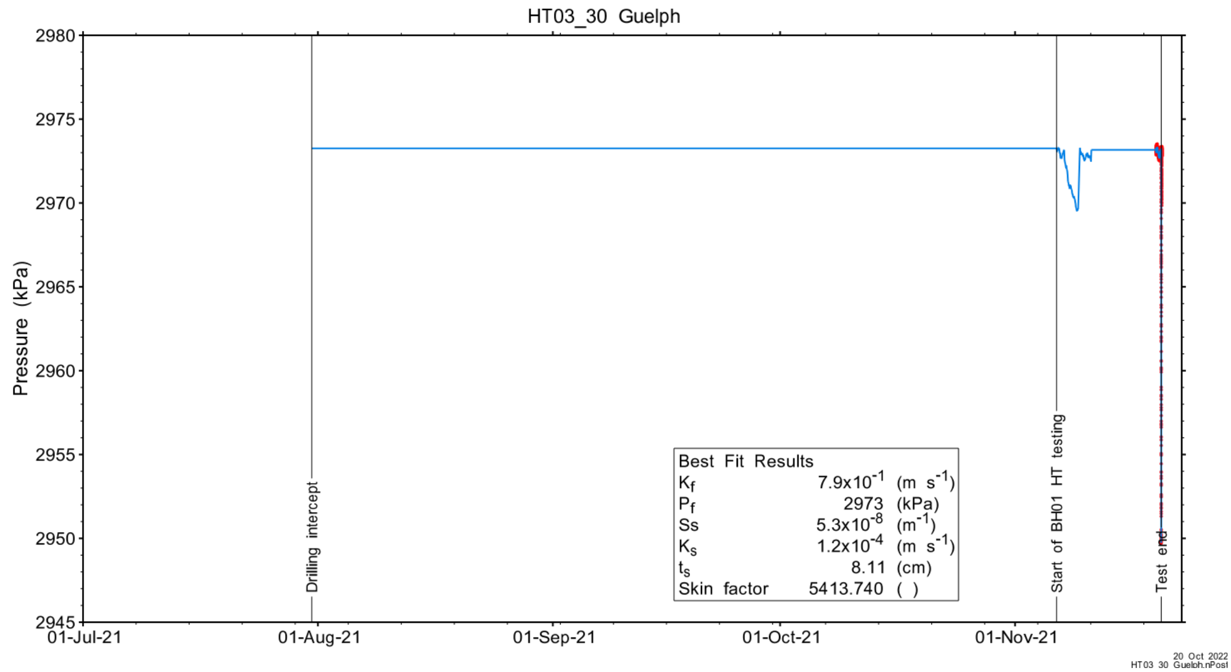

Figure 0.33 Annotated HT03_30 testing sequence showing pre-test history, best-fit simulation and parameter estimates.

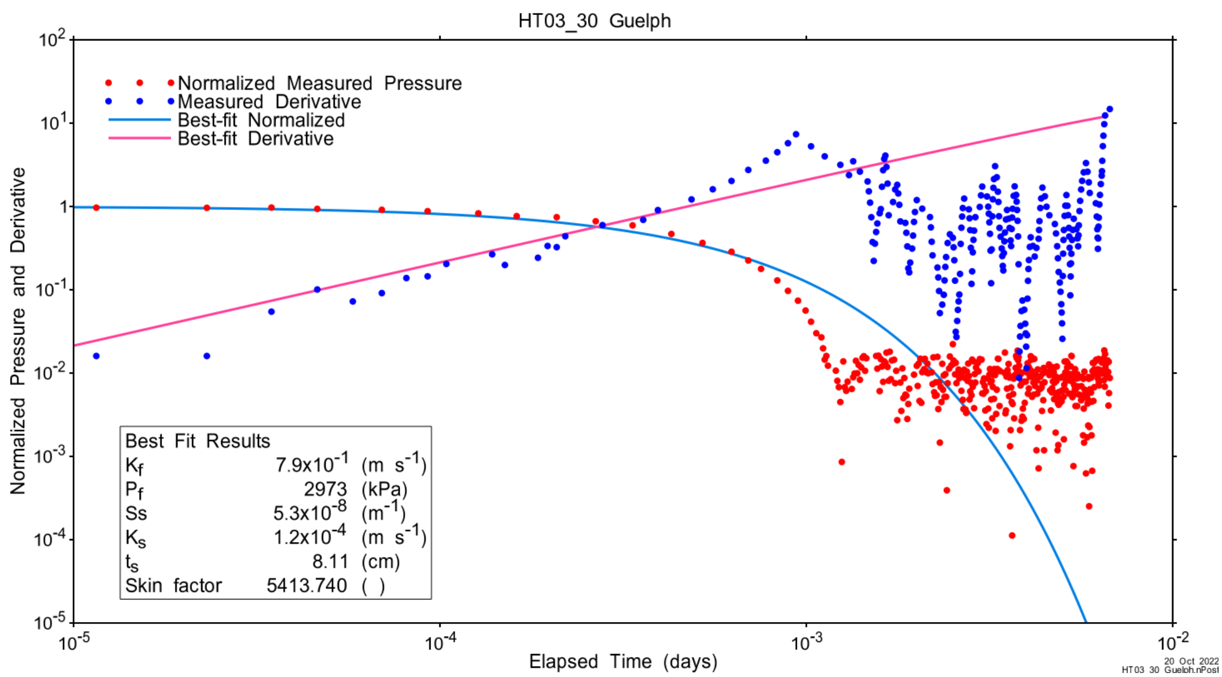

Figure 0.34 Log-log plot showing SW Ramey B normalized pressure and derivative response for best-fit simulation.

Figure 0.35 shows the normalized parameter sensitivity response for the best fit. Sensitivity to all parameters except Ss had reached maximum values. The variability in sensitivity to Ss reflects the general insensitivity of the simulation to that parameter.

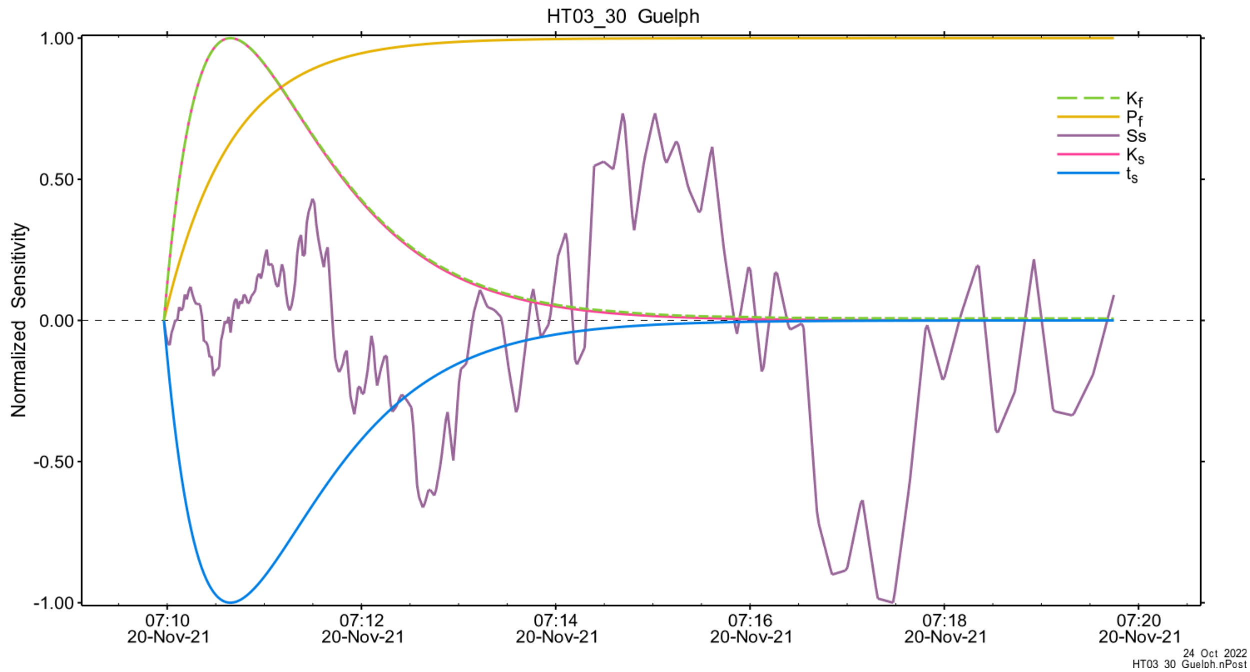

Figure 0.35 Normalized Jacobian for best-fit SW simulation.

A.3.3 Uncertainty Analyses

The CDF of normalized fit values for all converged simulations and the selected fit discriminant are shown in Figure 0.36.

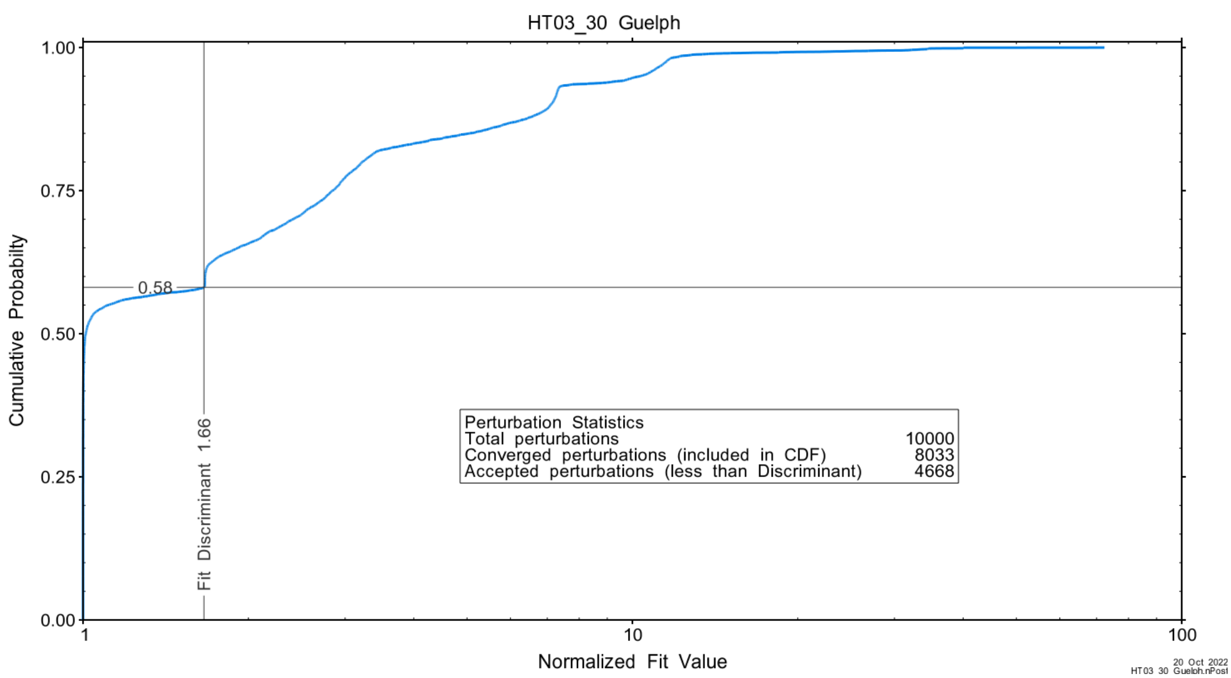

Figure 0.36 Fit value cumulative distribution function.

Summary cross parameter scatter plots for selected formation and skin parameters are given in Figure 0.37 and Figure 0.38. The light pink dots on the figures are the initial parameter estimates, with red dots overlaying those initial parameter values that resulted in accepted optimization results. The grey dots are converged optimizations which did not meet the fit discriminant. Larger varying color symbols represent the fit value of accepted optimizations, with the blue values representing the best fit.

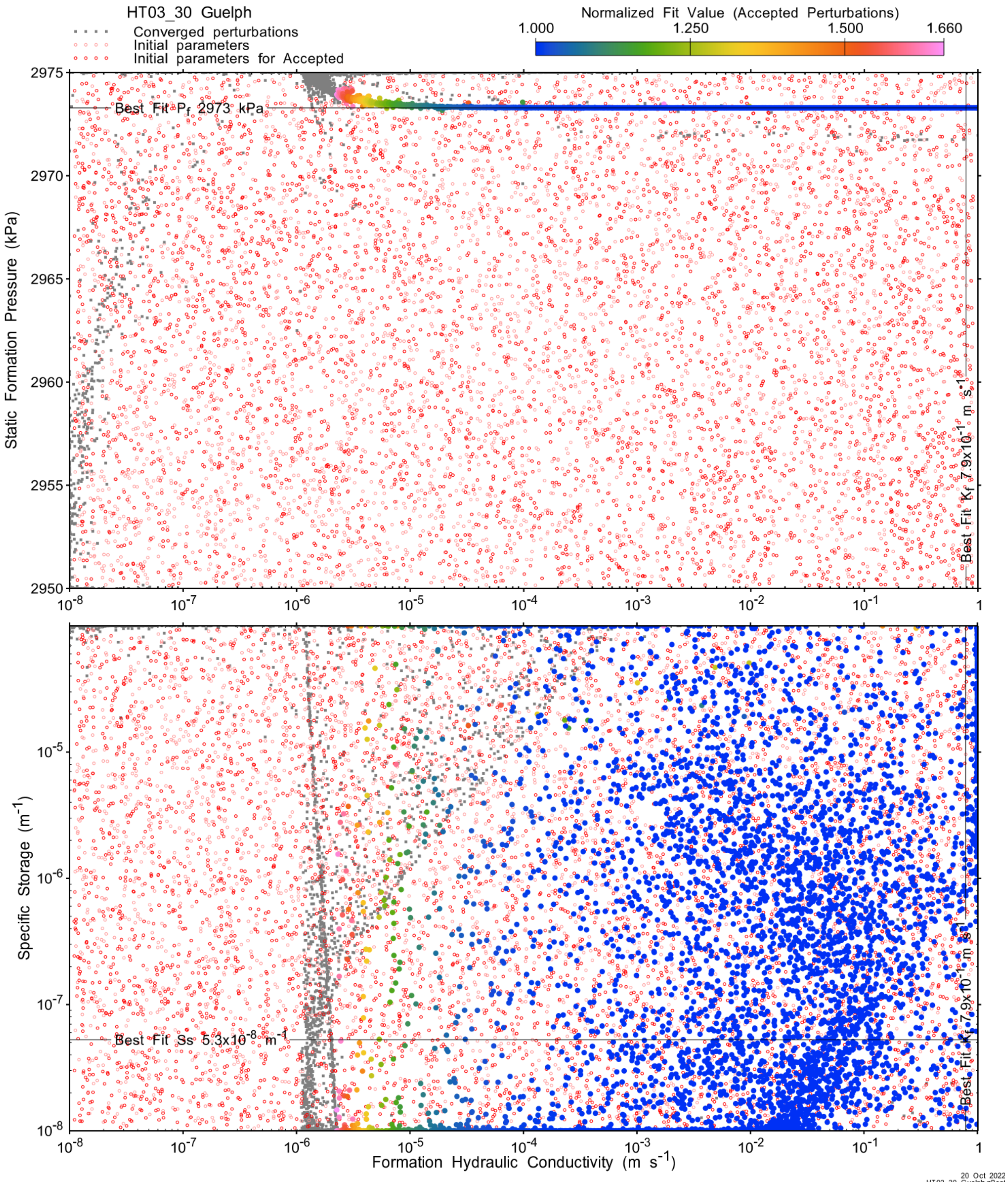

Figure 0.37 XY-scatter plot showing estimates of formation hydraulic conductivity (K_f) vs static formation pressure (P_f) (top panel) and specific storage (Ss) (bottom panel).

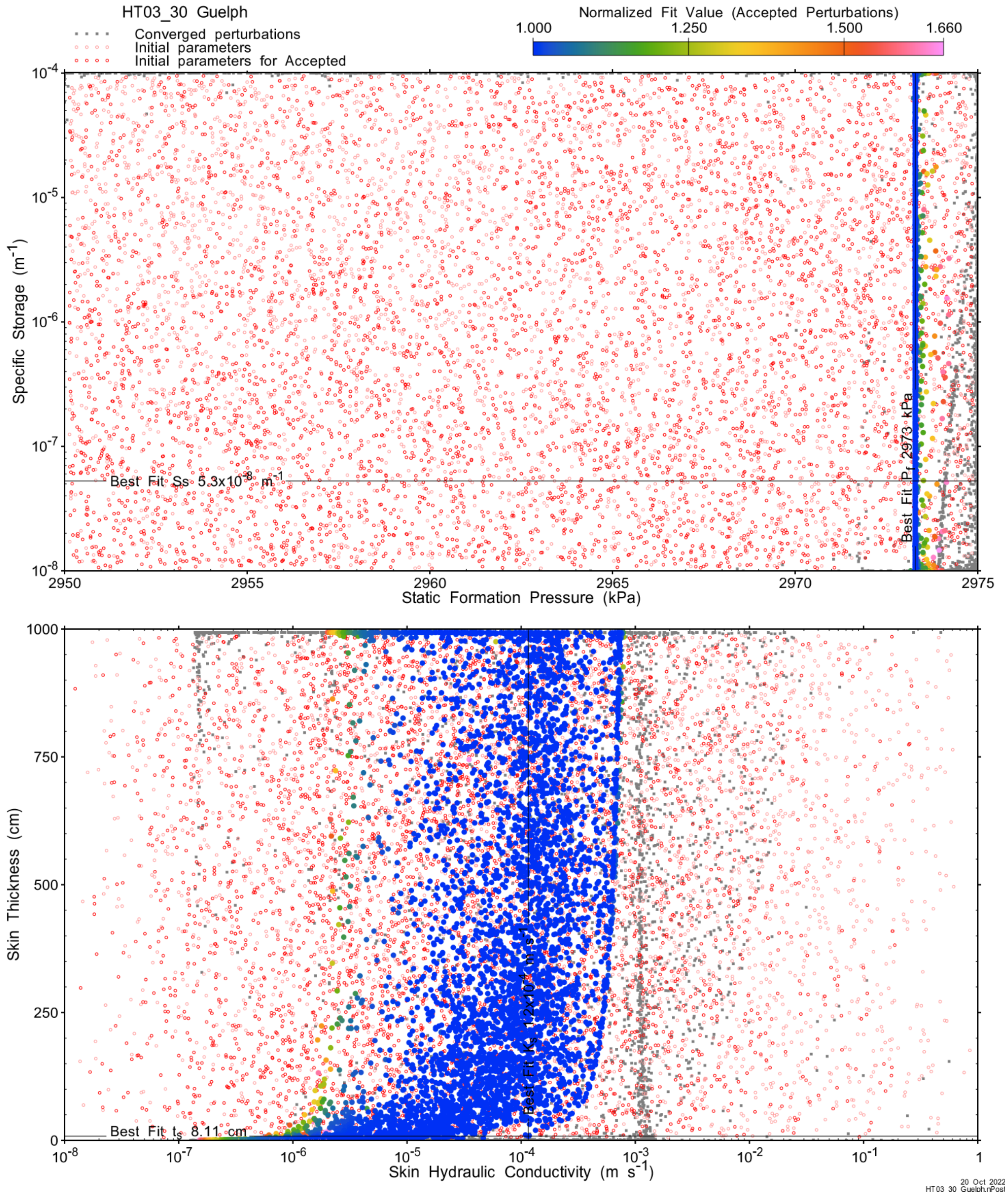

Figure 0.38 XY-scatter plot showing estimates of static formation pressure (P_f) vs specific storage (Ss) (top panel) and skin hydraulic conductivity (K_s) vs skin thickness (t_s) (bottom panel).

Confidence limits and median values are determined from the CDF of accepted optimization results (i.e. the varying color values in the above figures), with best fit value, 5% and 95% confidence indicated on Figure 0.39 and Figure 0.40.

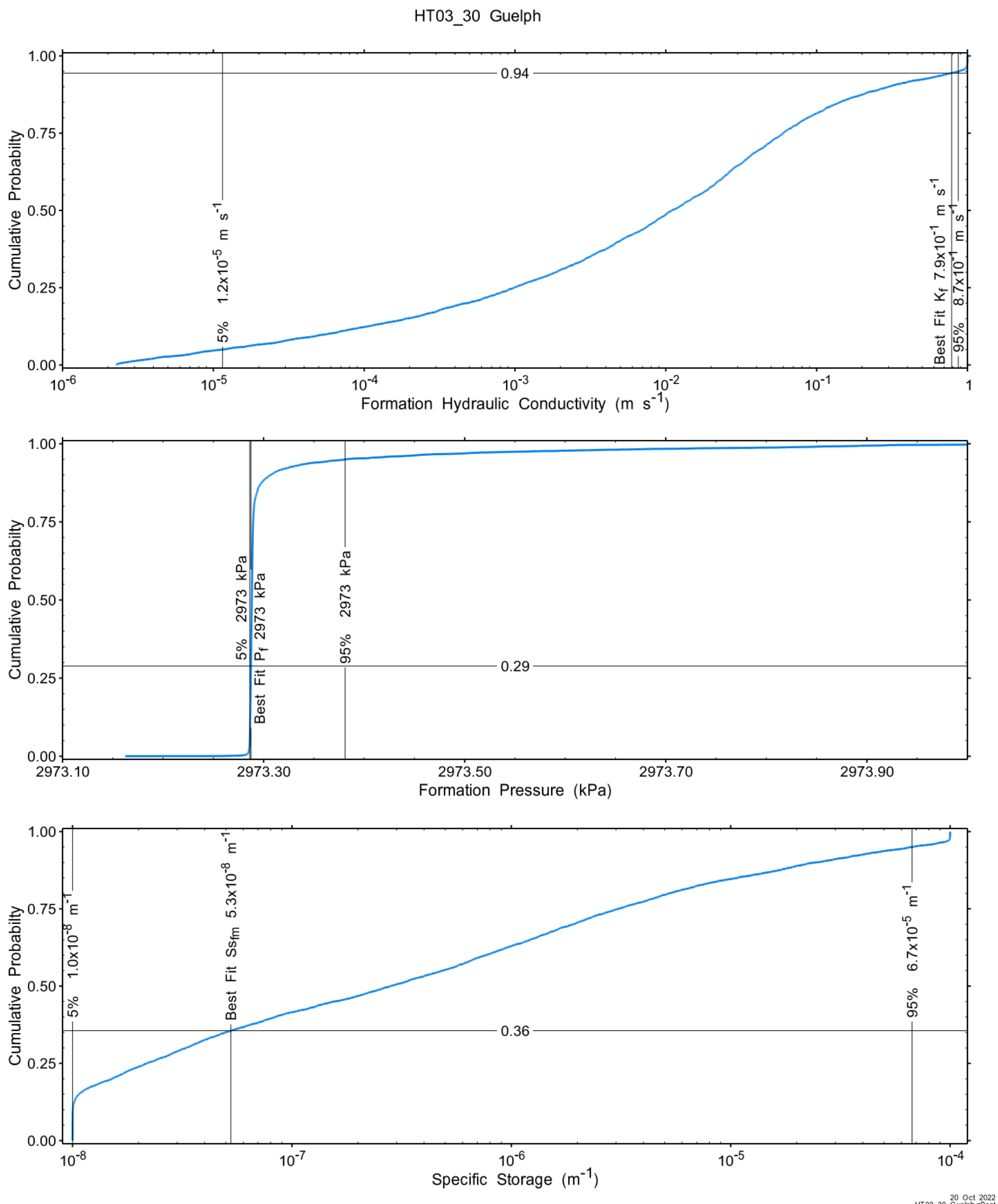

Figure 0.39 Cumulative distribution functions and parameter limits for formation hydraulic conductivity (K_f) (top panel), static formation pressure (P_f) (middle panel) and specific storage (Ss) (bottom panel).

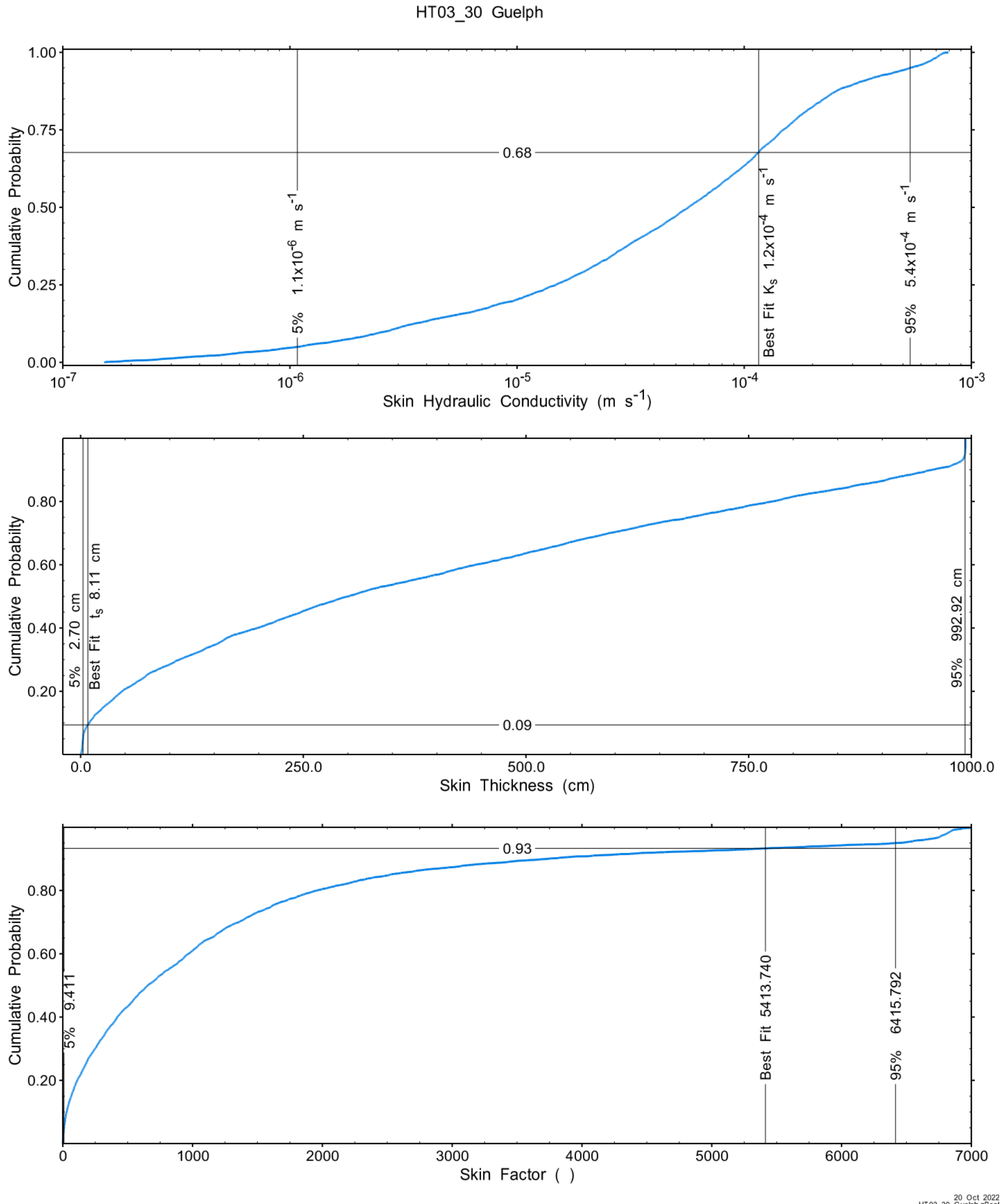

Figure 0.40 Cumulative distribution functions and parameter limits for skin hydraulic conductivity (K_s) (top panel), skin thickness (t_s) (middle panel) and skin factor (s) (bottom panel).

A summary of perturbation results is presented in Figure 0.41, with Ramey-processed perturbations in Figure 0.42. Those perturbations (3314 of 10,000) with all parameters within the 5% and 95% range present the best fit to the measured test zone data. Note that simulated test responses are, in general, a poor fit to the test data. This is likely due to the extremely high conductivity response includeing factors, particularly inertial effects, that are not consistent with the nSIGHTS conceptual model. Formation pressure estimates are accurate, but formation and skin hydraulic conductivity estimates are more uncertain. Given the limited domain of the assumed reef structure, this is likely not a significant uncertainty.

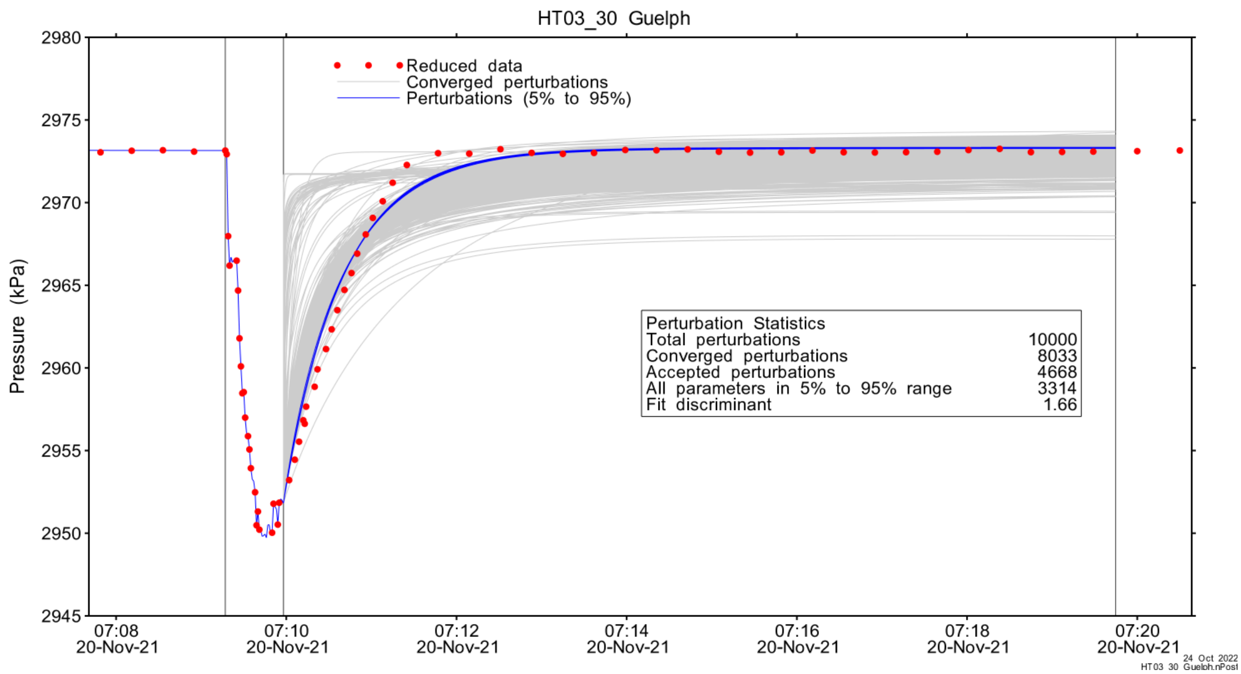

Figure 0.41 Perturbation results – all converged, accepted, and within 5% to 95% for all parameters.

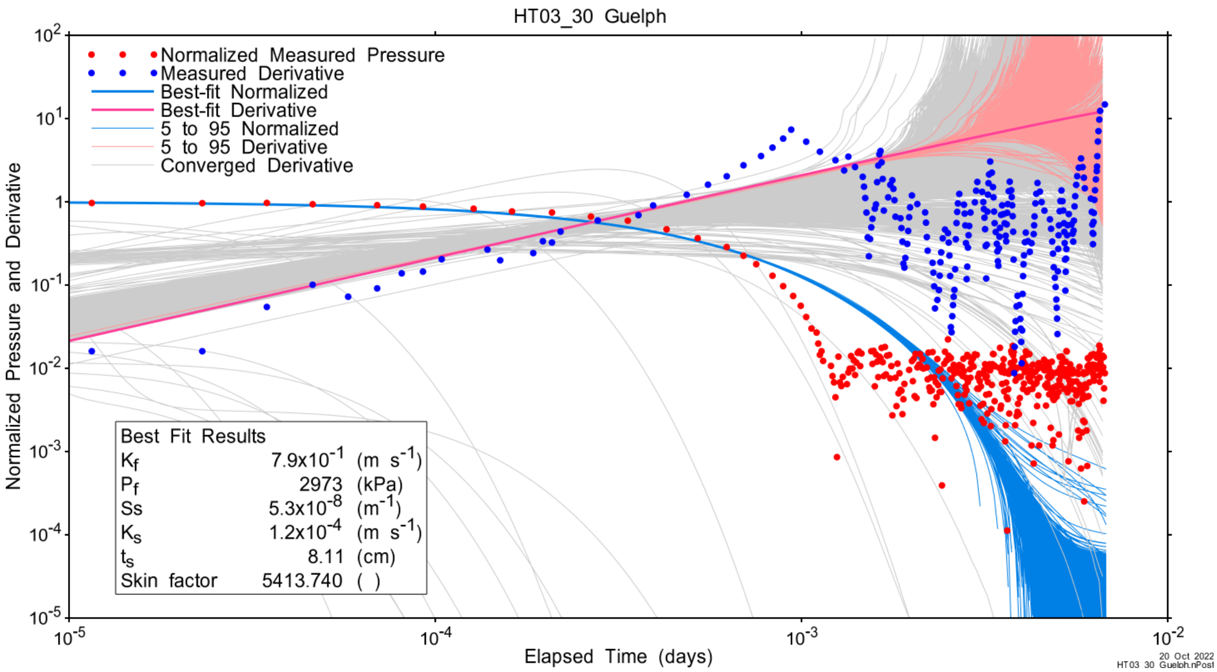

Figure 0.42 Log-log plot showing SW Ramey B normalized pressure and derivative response for all converged optimizations and those within 5% to 95% for all parameters.

A summary of best-fit parameter estimates and ranges is given in Table 0.14.

Table 0.14 Summary of the HT03_30 parameter estimates.

Parameter	Best Fit	5%	Median	95%
K_f (m/s)	7.9E-01	1.2E-05	1.1E-02	8.7E-01
P_f (kPa)	2973	2973	2973	2973
Ss (1/m)	5.3E-08	1.0E-08	2.8E-07	6.7E-05
K_s (m/s)	1.2E-04	1.1E-06	5.7E-05	5.4E-04
t_s (cm)	8.11	2.70	300.41	992.92
s (-)	5413.740	9.411	655.445	6415.790

Parameter correlations for all perturbations with all parameters within the 5% to 95% limits are given in Table 0.15.

Table 0.15 Pearson cross-correlations of 5% to 95% parameters

	Log(K_f)	P_f	Log(Ss)	Log(K_s)	t_s	s
Log(K_f)	1.000	-0.441	0.100	0.931	0.165	0.844
P_f	-0.441	1.000	-0.042	-0.391	-0.053	-0.182
Log(Ss)	0.100	-0.042	1.000	0.027	-0.203	0.112
Log(K_s)	0.931	-0.391	0.027	1.000	0.421	0.780
t_s	0.165	-0.053	-0.203	0.421	1.000	0.114
s	0.844	-0.182	0.112	0.780	0.114	1.000

A.3.4 Additional Figures

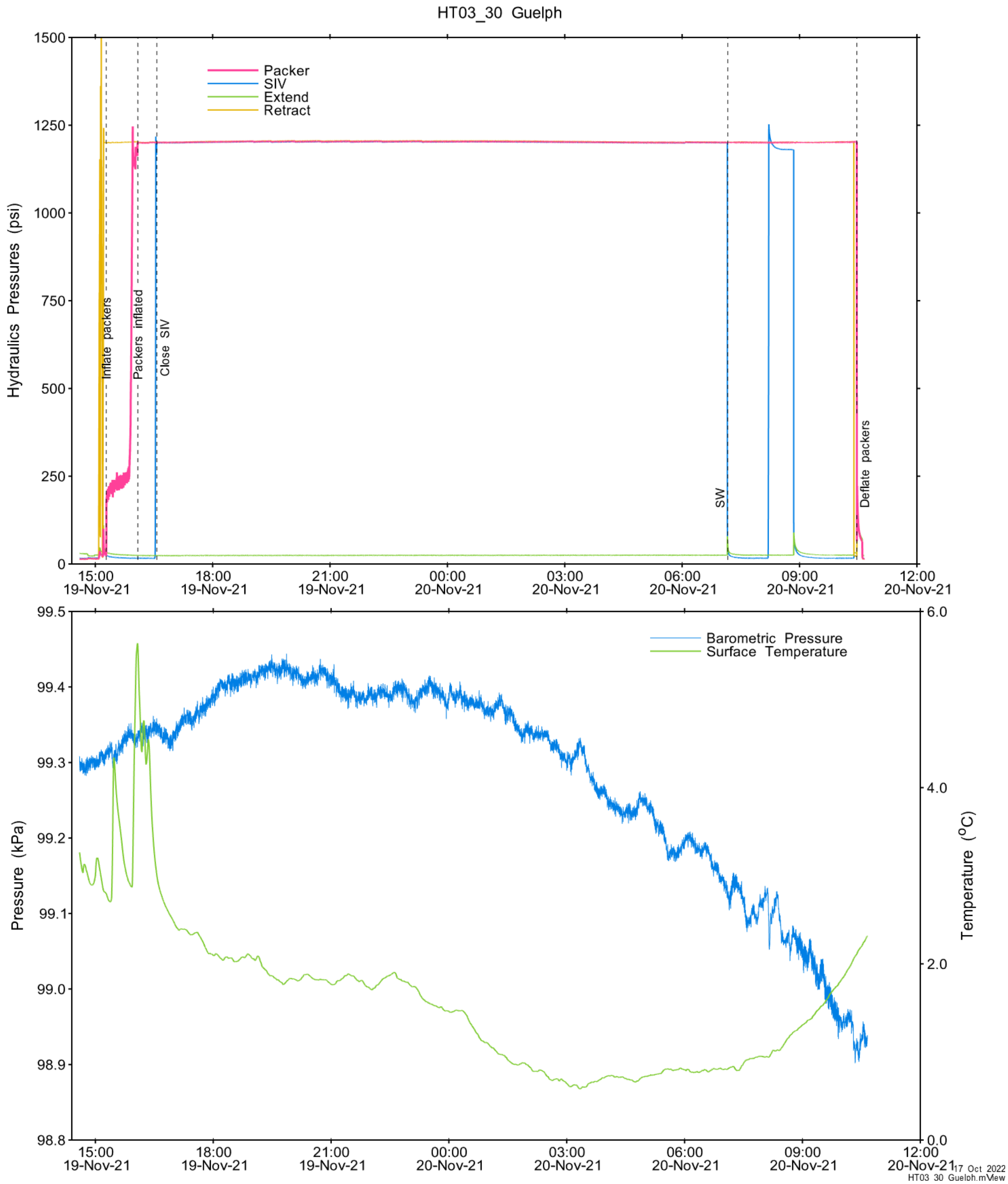

Figure 0.43 Hydraulics pressures and surface temperature/barometric pressure.

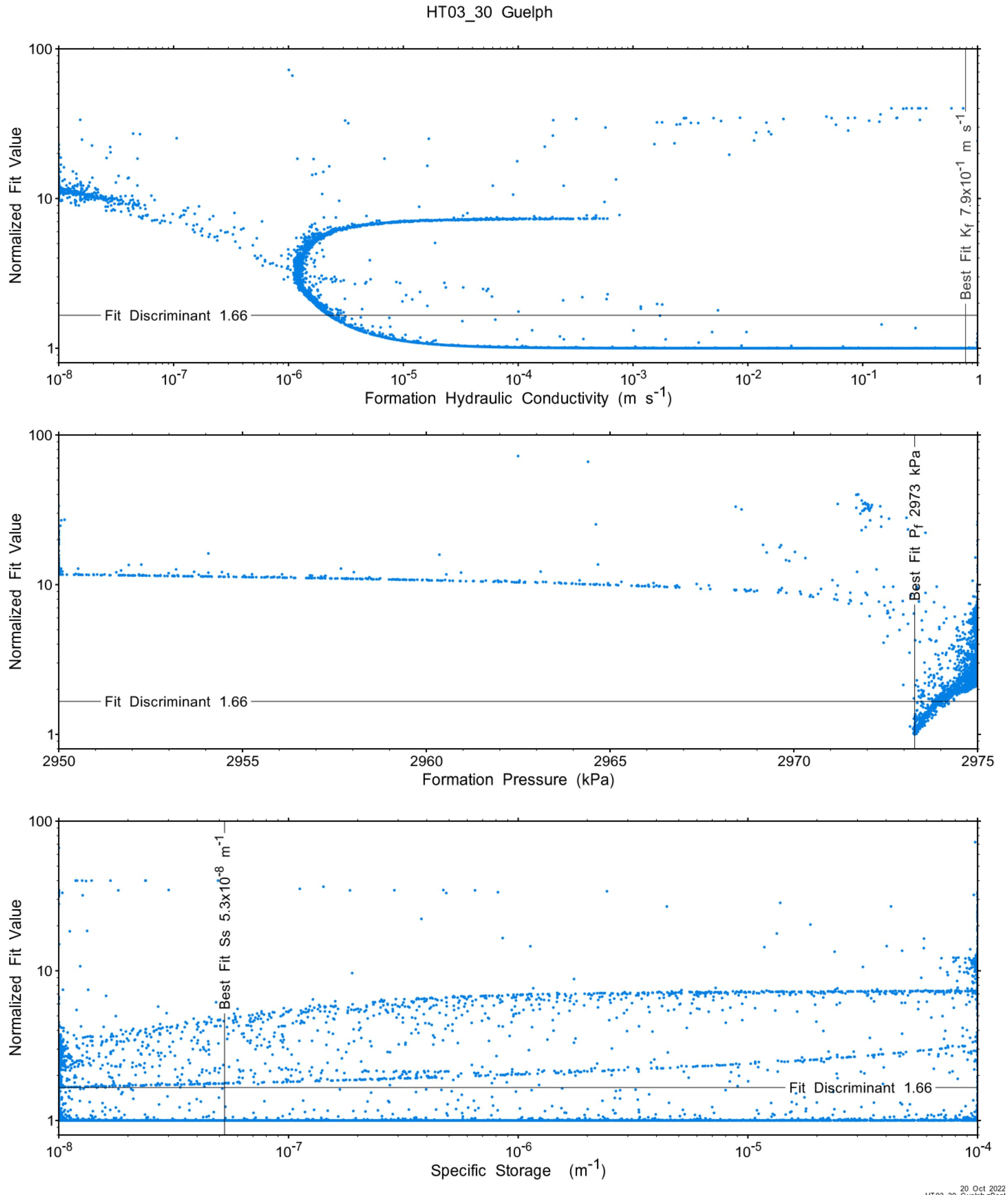

Figure 0.44 XY-scatter plot showing the formation parameter space normalized fit values.

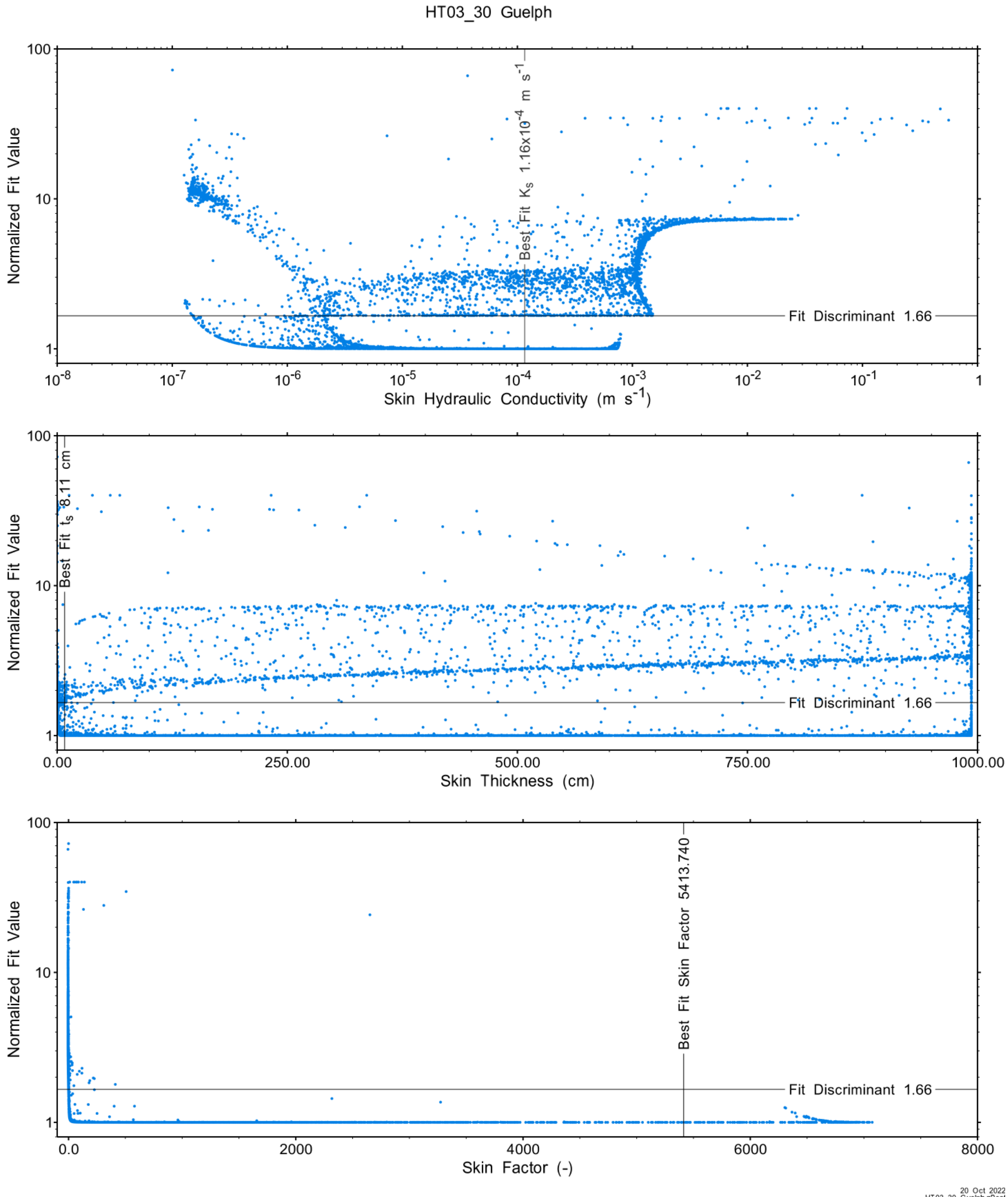

Figure 0.45 XY-scatter plot showing the skin parameter space normalized fit values.

A.4 HT04_30 Gasport

The SB_BH01 interval from 361.40 to 391.45 mBGS tested in HT04_30 includes the Gasport, Lions Head, and Fossil Hill Formations. An initial PI test responded very rapidly (recovery under 10 minutes). This was followed by a confirmatory PW which also recovered quickly. A single SW test was then conducted.

A.4.1 Test Data Summary

Table 0.16 and Figure 0.46 provide a summary of test events and a plot of pressures measured while testing, respectively.

Table 0.16 HT04_30 Summary of Test Events.

Event	Start Date & Time	Duration (days)	TZ Pressure (kPa)
Drilling intercept	21-08-05 02:06	107.57	3683
Shut-in	21-11-20 15:42	0.79	3690
Pulse injection	21-11-21 07:57	0.04	3793
Pulse withdrawal	21-11-21 08:54	0.06	3596
Slug withdrawal	21-11-21 10:25	0.90	3378
Test end	21-11-22 08:00		3680

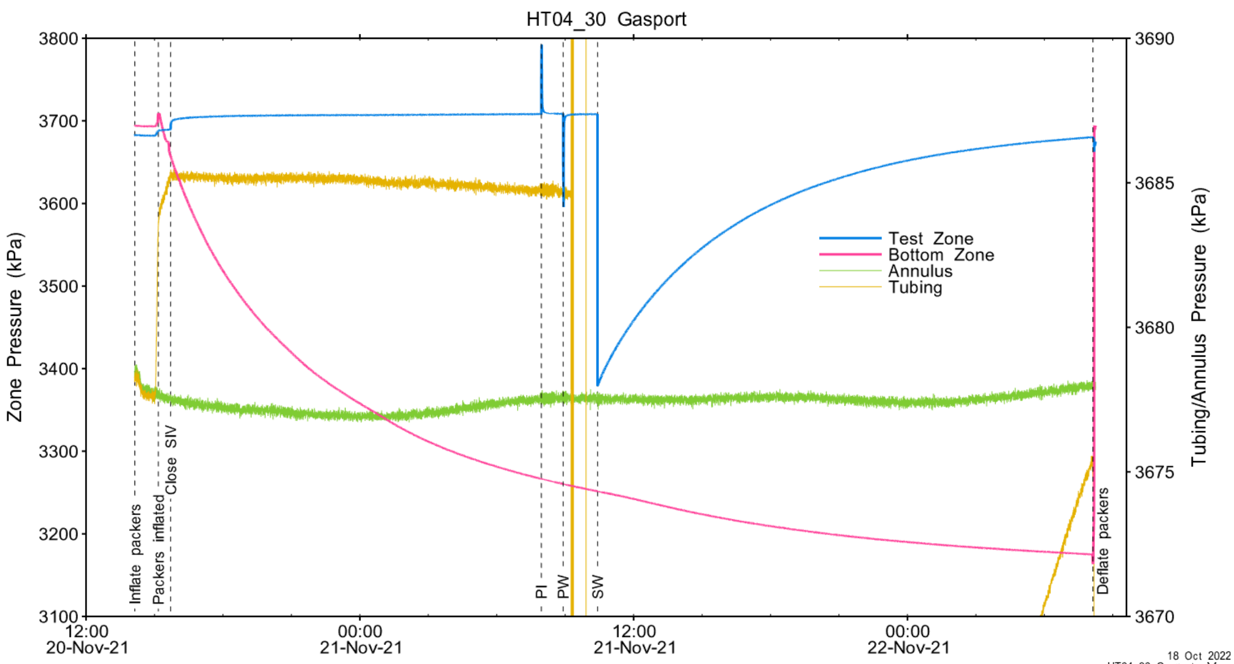

Figure 0.46 HT04_30 test events and pressures.

A.4.2 Test Analyses

Table 0.17 is a summary of test-specific input parameters used in the analyses, while Table 0.18 presents the optimized parameters and allowed ranges.

Table 0.17 nSIGHTS Input Parameters.

Parameter	Value	Units
Test zone radius	6.645	cm
Tubing string radius	2.54	cm
Test zone fluid density	1048	g/L
Test zone length	30.05	m

Table 0.18 nSIGHTS Parameter Optimization Ranges.

Parameter	Minimum	Maximum	Units	Type
Formation hydraulic conductivity (K_f)	1E-11	1E-06	m/s	log
Formation pressure (P_f)	3300	4000	kPa	linear
Specific storage (Ss)	1E-08	1E-04	1/m	log
Skin hydraulic conductivity (K_s)	1E-11	1E-06	m/s	log
Skin thickness (t_s)	0.1	10000	mm	linear

Figure 0.47 shows the measured test zone pressure record (with reduced data density for clarity) used in the analysis along with the best-fit simulation and parameter values. Figure 0.48 presents the pre-test history, and Figure 0.49 shows the Ramey B normalized best-fit pressure and pressure derivatives.

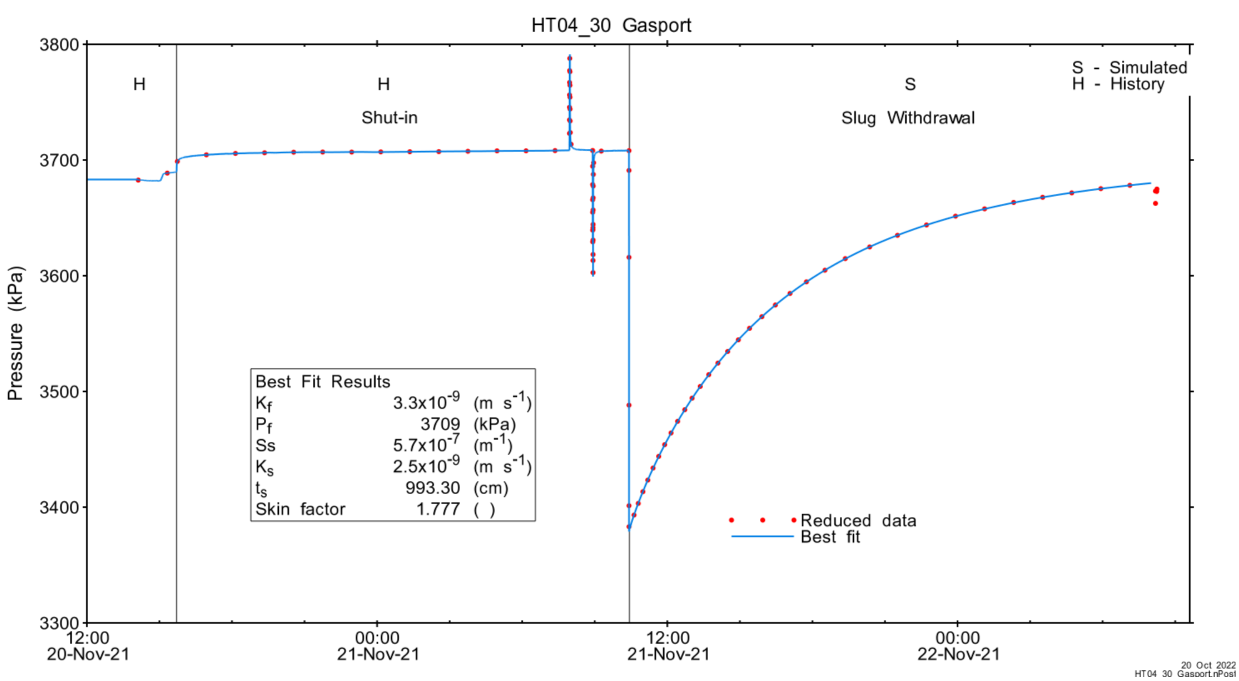

Figure 0.47 Annotated testing sequence showing best-fit simulation and parameter estimates.

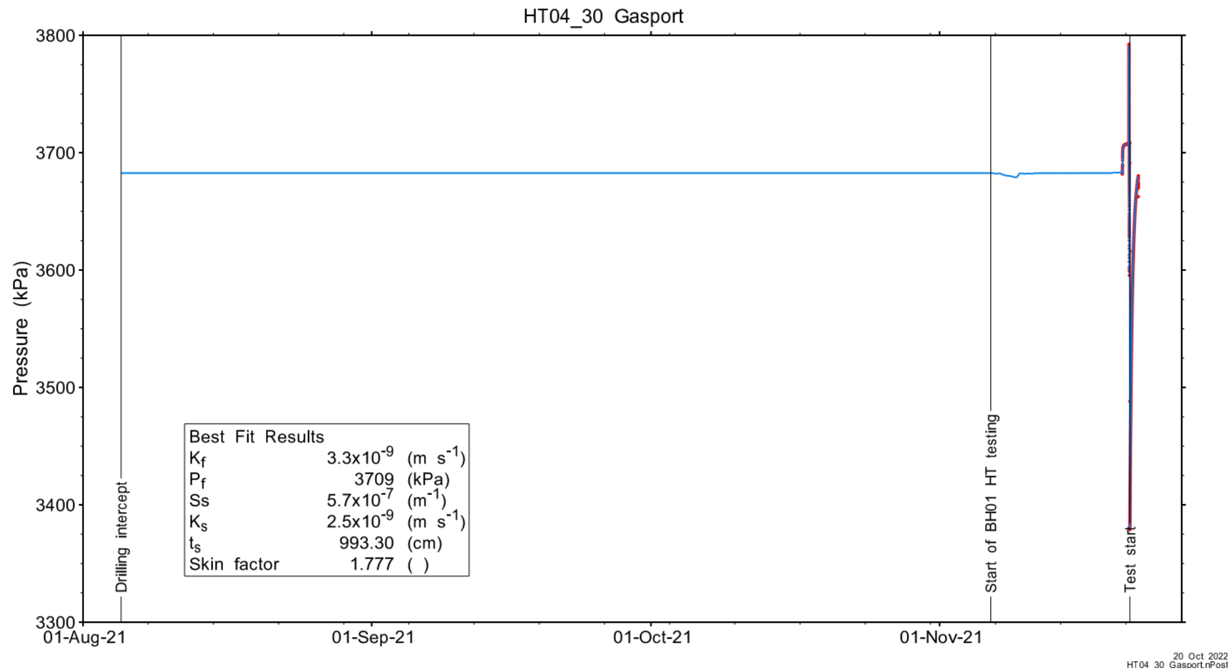

Figure 0.48 Annotated HT04_30 testing sequence showing pre-test history, best-fit simulation and parameter estimates.

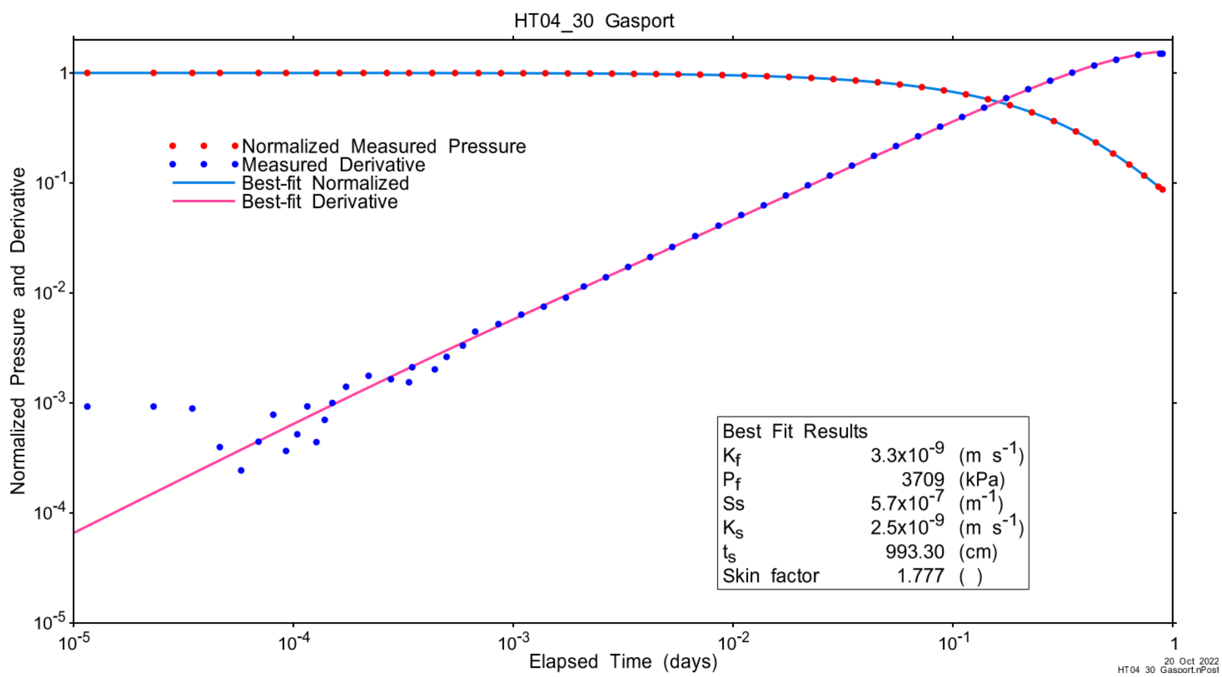

Figure 0.49 Log-log plot showing Ramey B normalized pressure and derivative response for best-fit simulation.

Figure 0.50 shows the normalized parameter sensitivity response for the best fit. Skin-related parameters are most sensitive during the early-time response.

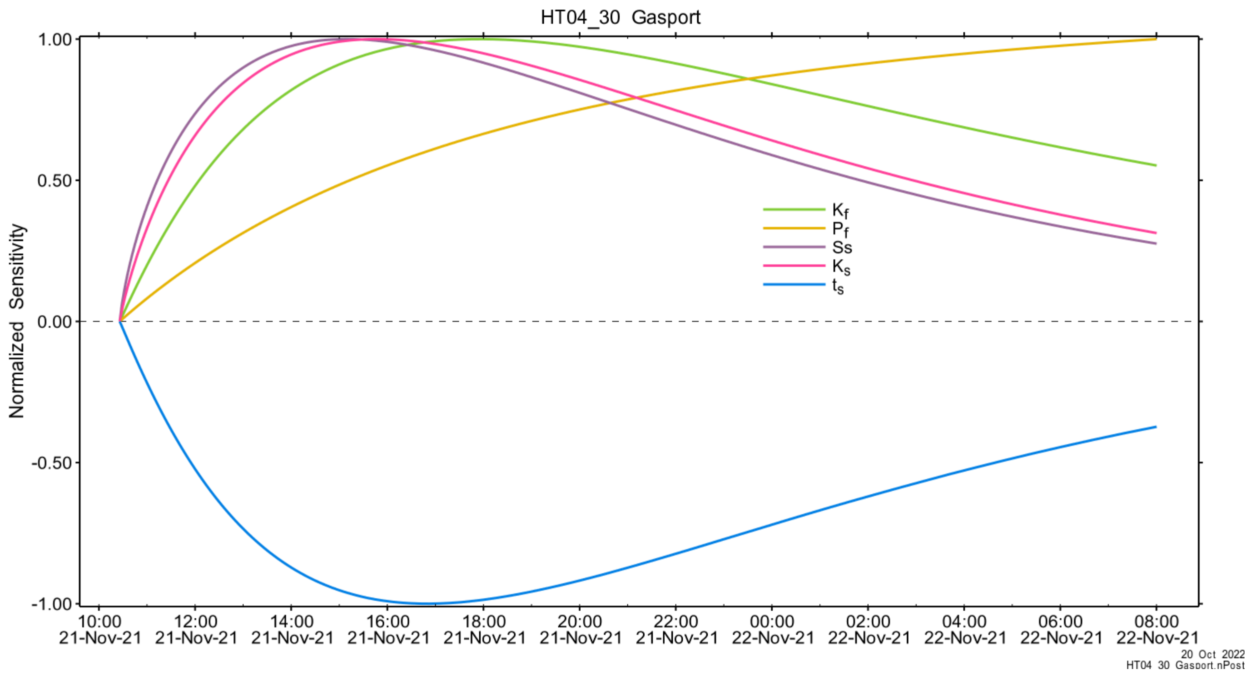

Figure 0.50 Normalized Jacobian for best-fit simulation.

A.4.3 Uncertainty Analyses

The CDF of normalized fit values for all converged simulations and the selected fit discriminant are shown in Figure 0.51.

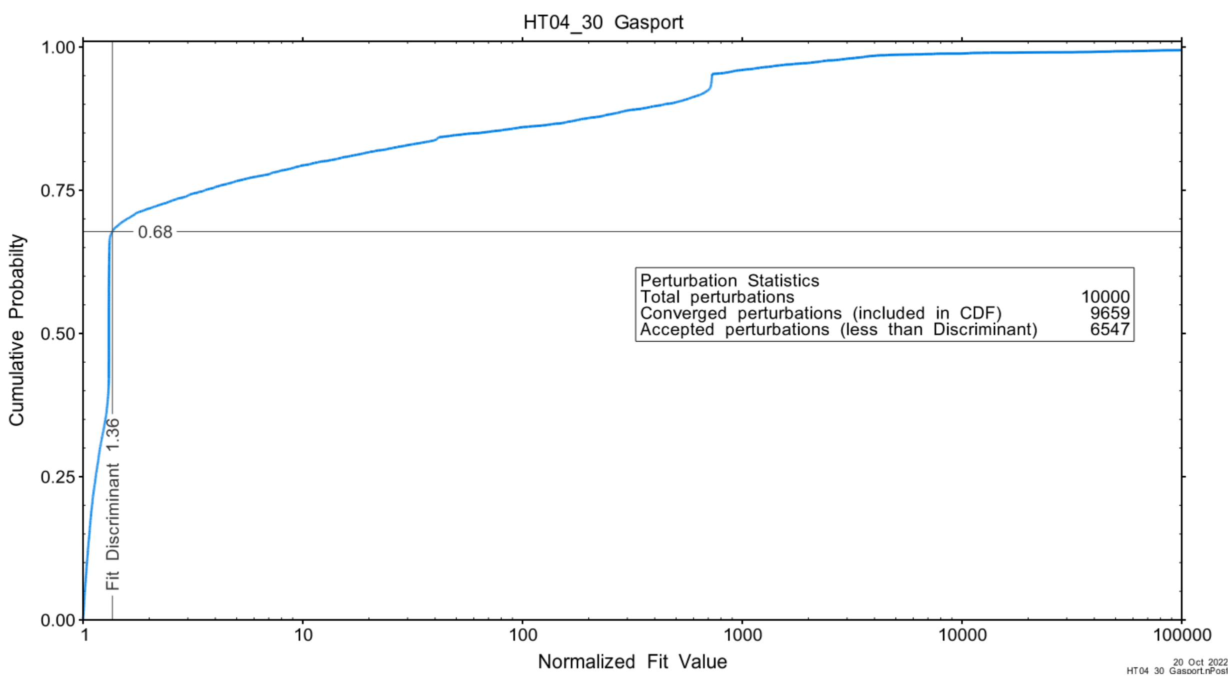

Figure 0.51 Fit value cumulative distribution function.

Summary cross parameter scatter plots for selected formation and skin parameters are given in Figure 0.52 and Figure 0.53. The light pink dots on the figures are the initial parameter estimates, with red dots overlaying those initial parameter values that resulted in accepted optimization results. The grey dots are converged optimizations which did not meet the fit discriminant. Larger varying color symbols represent the fit value of accepted optimizations, with the blue values representing the best fit.

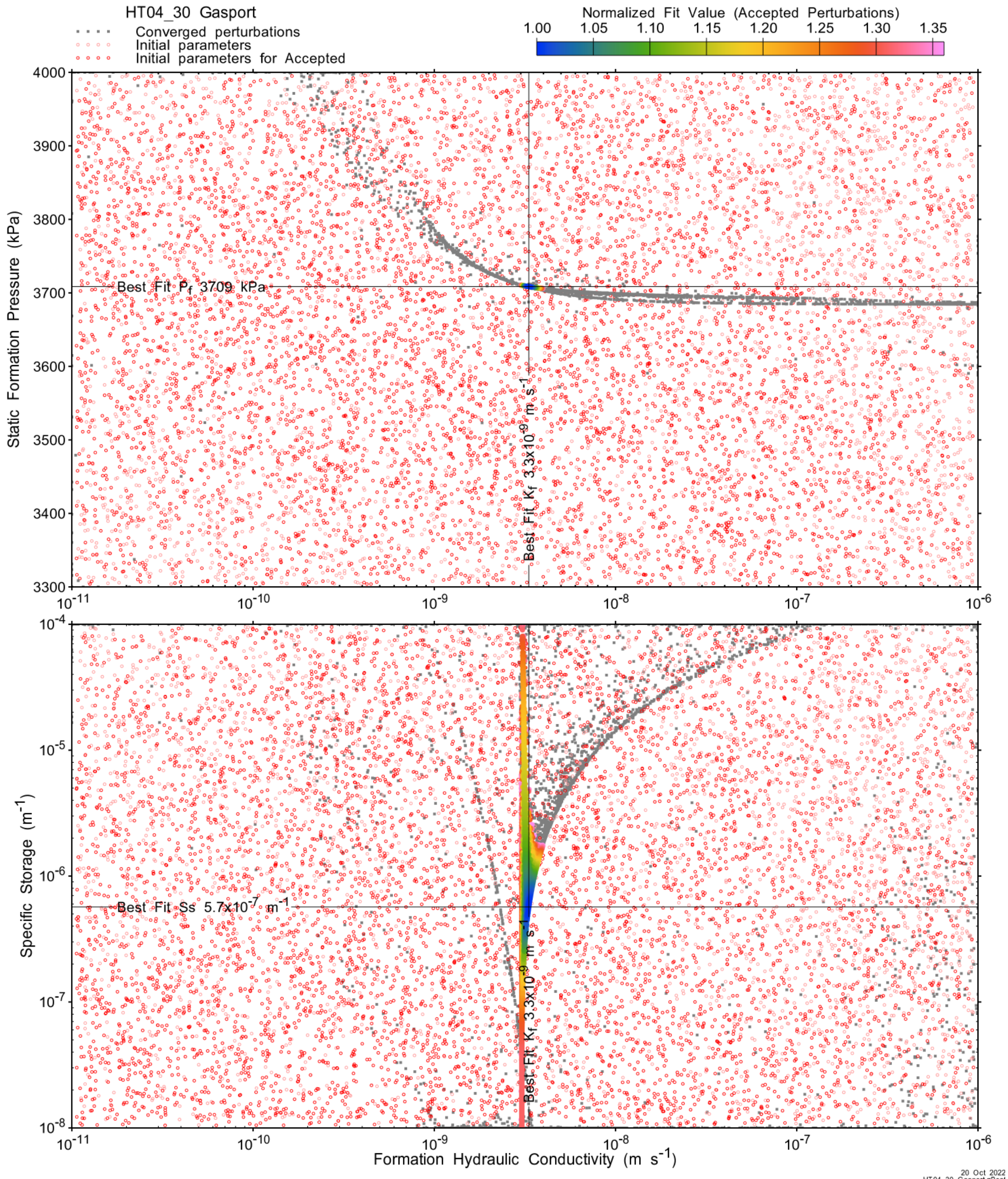

Figure 0.52 XY-scatter plot showing estimates of formation hydraulic conductivity (K_f) vs static formation pressure (P_f) (top panel) and specific storage (Ss) (bottom panel).

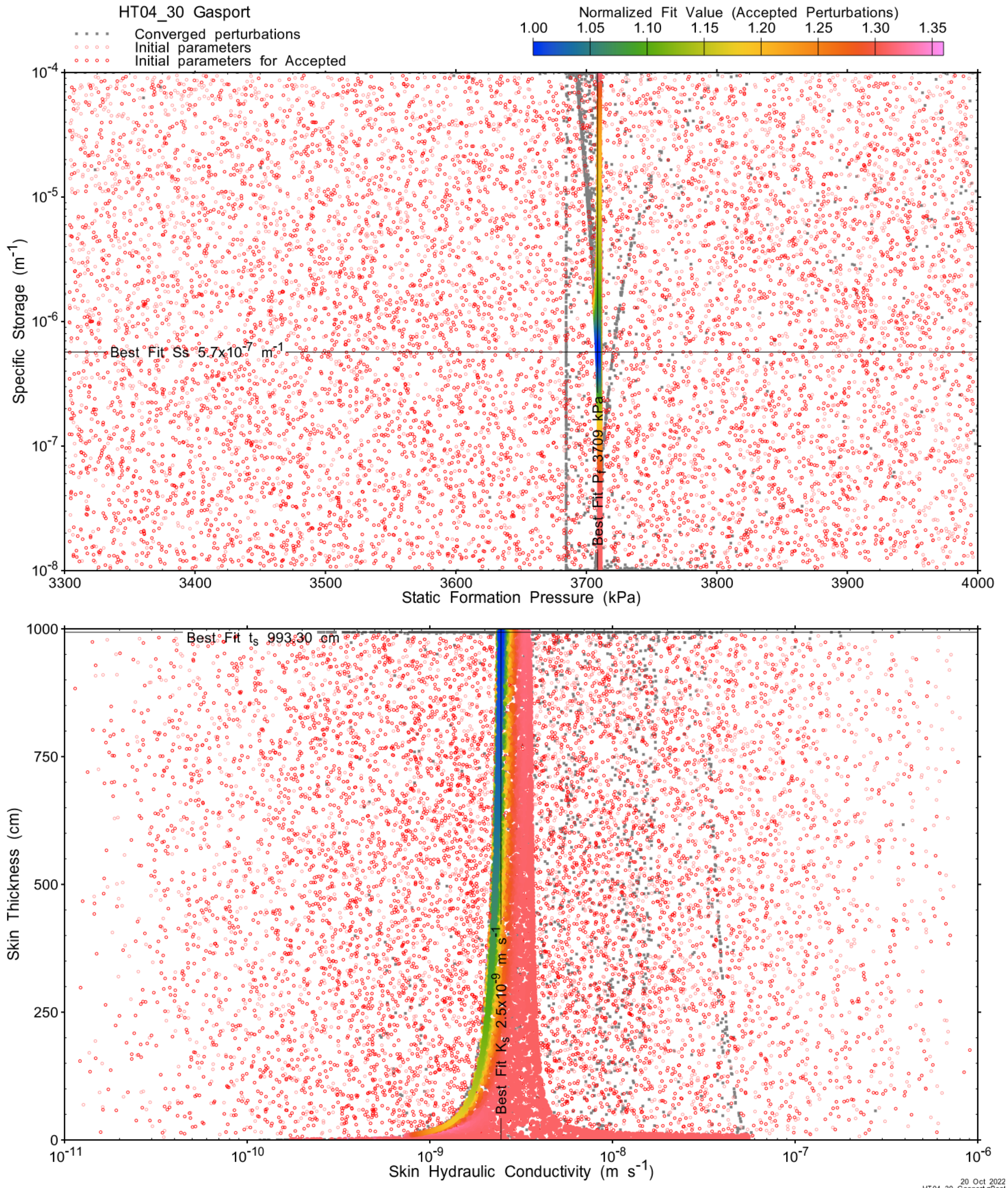

Figure 0.53 XY-scatter plot showing estimates of static formation pressure (P_f) vs specific storage (Ss) (top panel) and skin hydraulic conductivity (K_s) vs skin thickness (t_s) (bottom panel).

Confidence limits and median values are determined from the CDF of accepted optimization results (i.e. the varying color values in the above figures), with best fit value, 5% and 95% confidence indicated on Figure 0.54 and Figure 0.55.

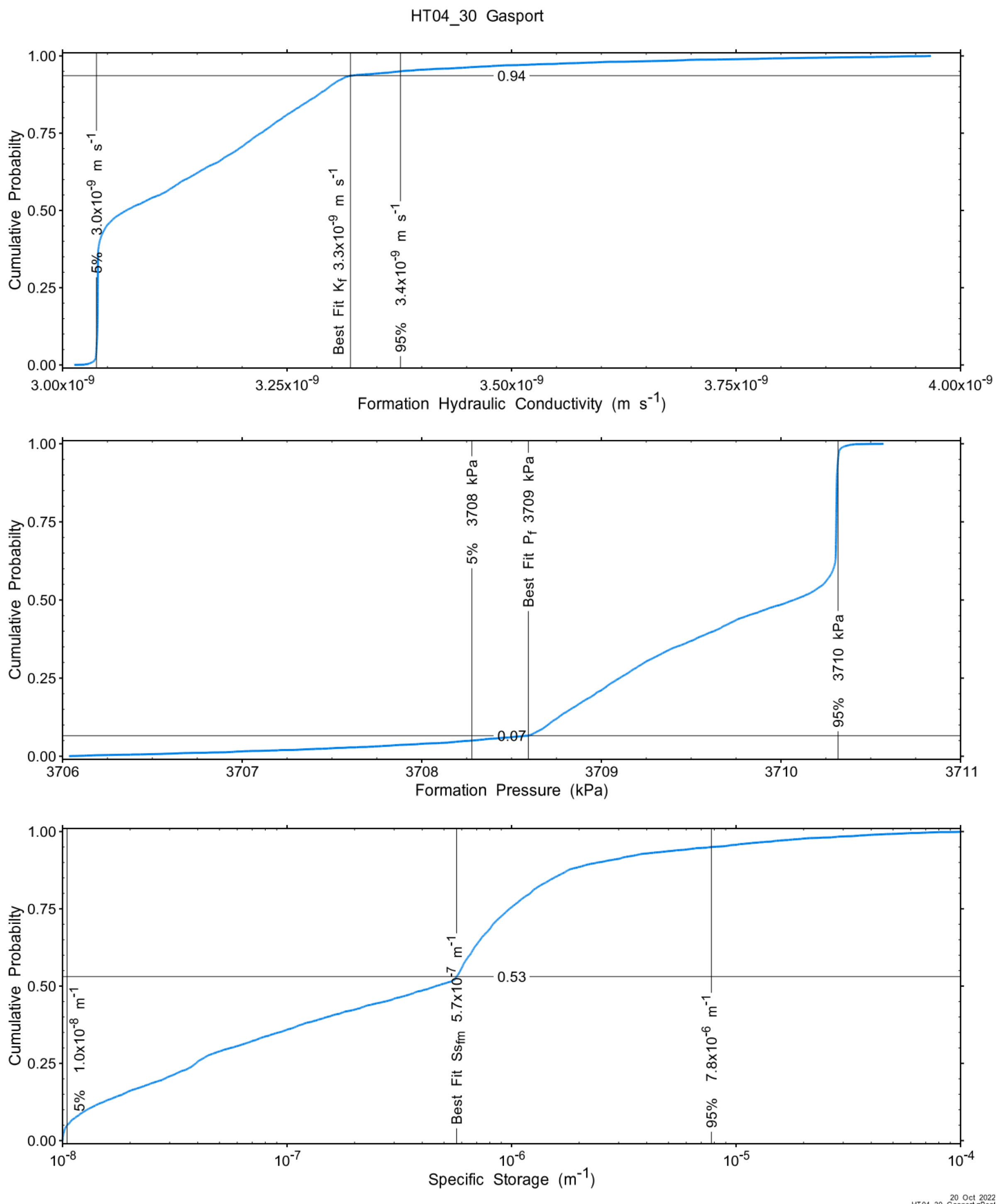

Figure 0.54 Cumulative distribution functions and parameter limits for formation hydraulic conductivity (K_f) (top panel), static formation pressure (P_f) (middle panel) and specific storage (Ss) (bottom panel).

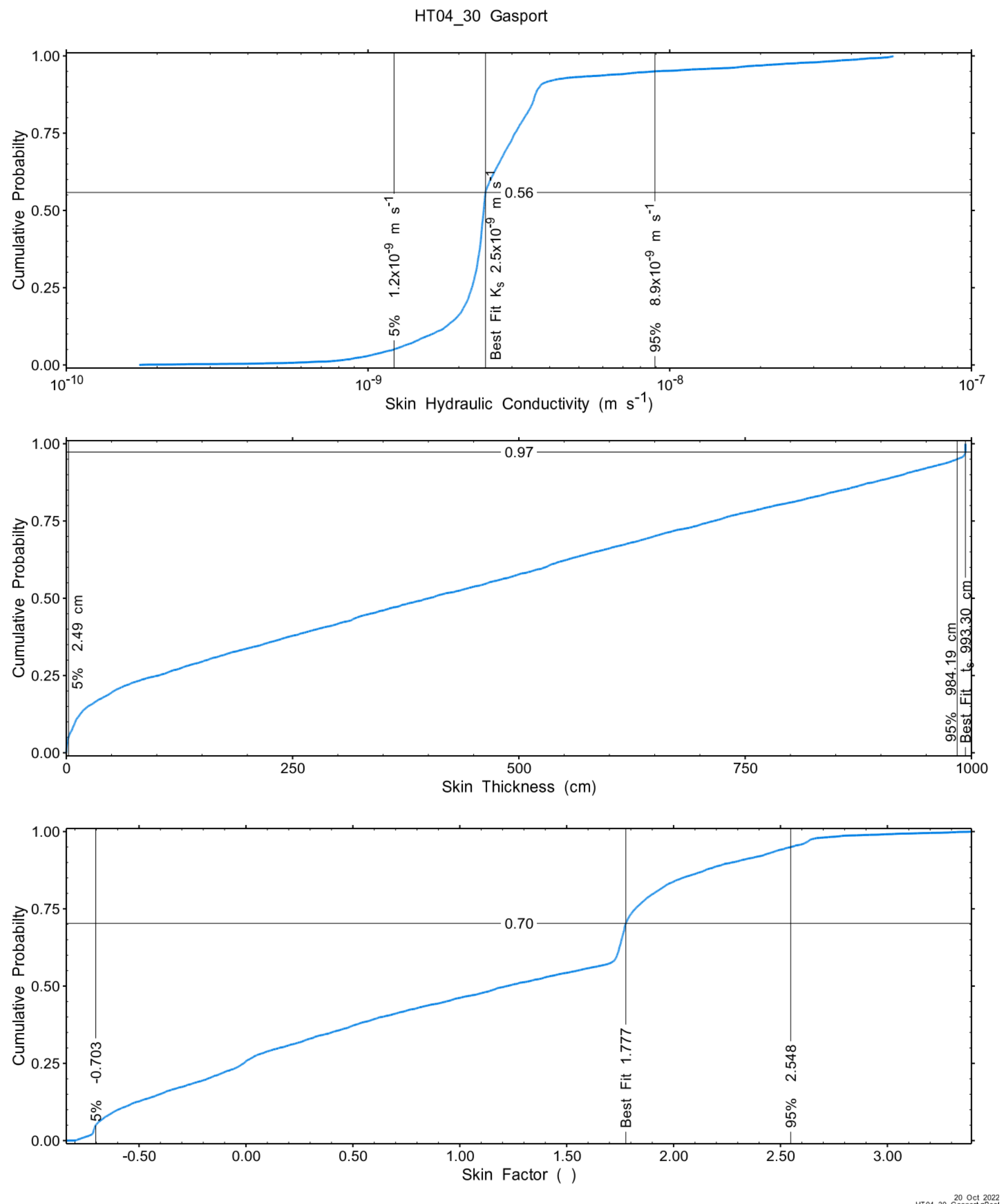

Figure 0.55 Cumulative distribution functions and parameter limits for skin hydraulic conductivity (K_s) (top panel), skin thickness (t_s) (middle panel) and skin factor (s) (bottom panel).

A summary of perturbation results is presented in Figure 0.56, with Ramey-processed perturbations in Figure 0.57. Those perturbations (4634 of 10,000) with all parameters within the 5% and 95% range present a good fit to the measured test zone data.

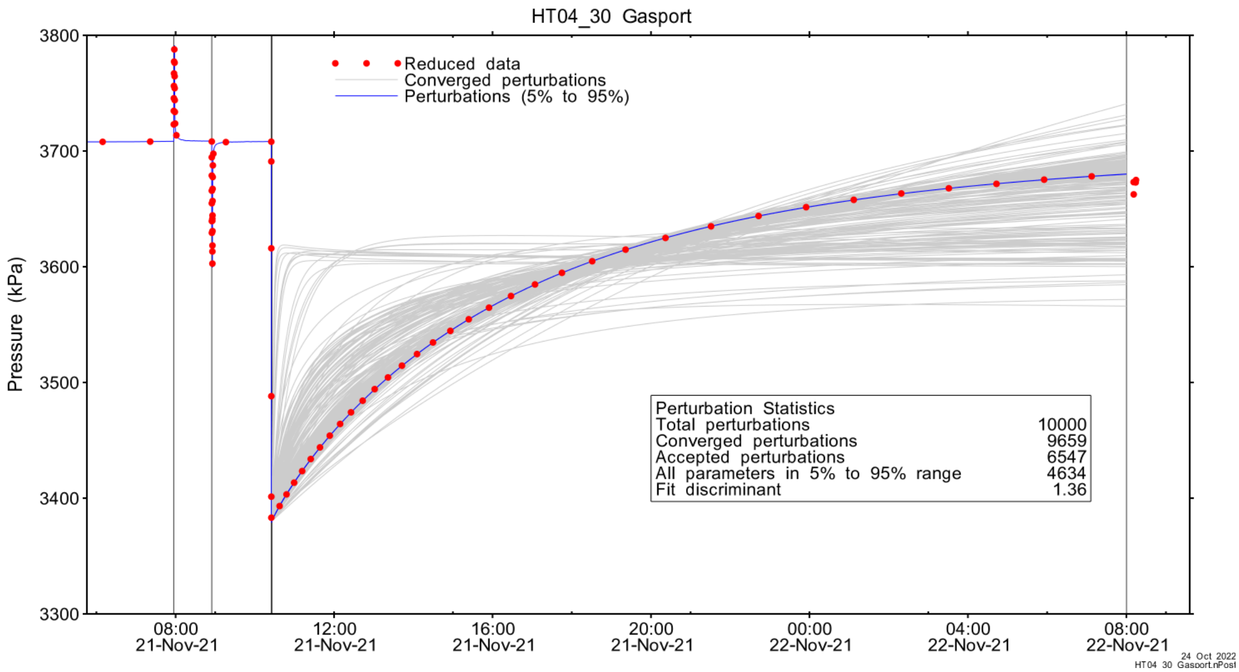

Figure 0.56 Perturbation results – all converged, accepted, and within 5% to 95% for all parameters.

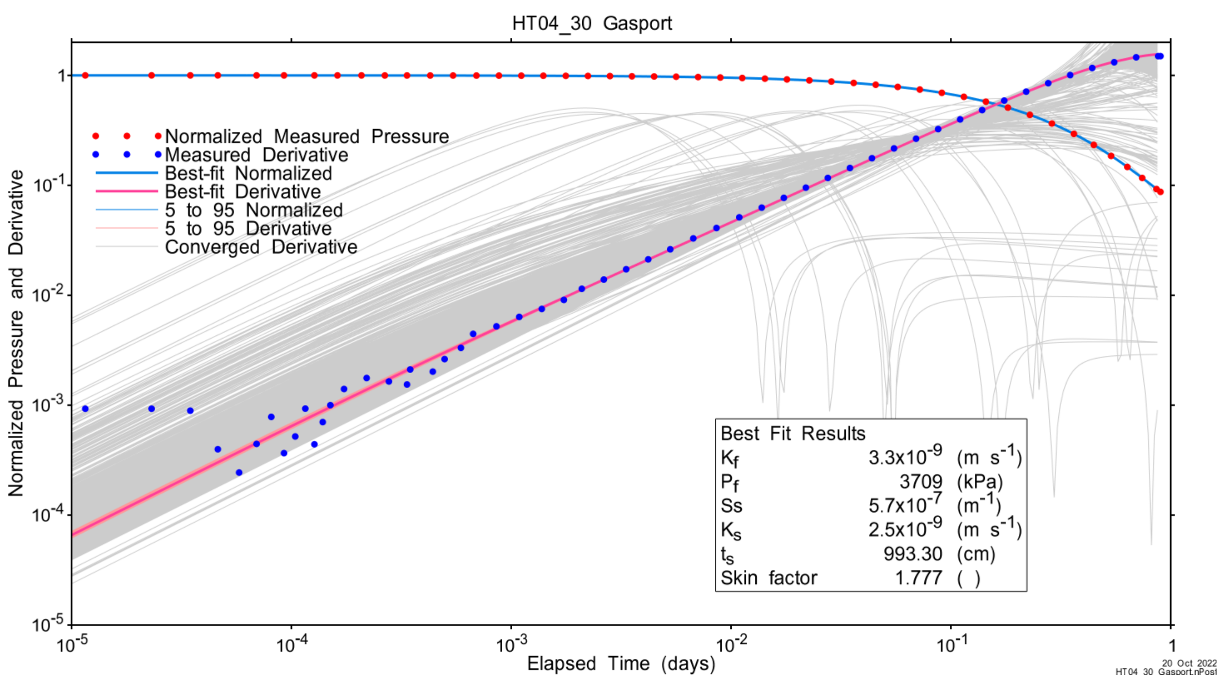

Figure 0.57 Log-log plot showing Ramey B normalized pressure and derivative response for all converged optimizations and those within 5% to 95% for all parameters.

A summary of best-fit parameter estimates and ranges is given in Table 0.19.

Table 0.19 Summary of the HT04_30 parameter estimates.

Parameter	Best Fit	5%	Median	95%
K_f (m/s)	3.3E-09	3.0E-09	3.1E-09	3.4E-09
P_f (kPa)	3709	3708	3710	3710
Ss (1/m)	5.7E-07	1.0E-08	4.6E-07	7.8E-06
K_s (m/s)	2.5E-09	1.2E-09	2.4E-09	8.9E-09
t_s (cm)	993.30	2.49	400.59	984.19
s (-)	1.777	-0.703	1.222	2.548

Parameter correlations for all perturbations with all parameters within the 5% to 95% limits are given in Table 0.20.

Table 0.20 Pearson cross-correlations of 5% to 95% parameters

	Log(K_f)	P_f	Log(Ss)	Log(K_s)	t_s	s
Log(K_f)	1.000	-0.999	0.705	-0.473	0.442	0.808
P_f	-0.999	1.000	-0.725	0.491	-0.424	-0.824
Log(Ss)	0.705	-0.725	1.000	-0.879	-0.025	0.986
Log(K_s)	-0.473	0.491	-0.879	1.000	0.102	-0.836
t_s	0.442	-0.424	-0.025	0.102	1.000	0.093
s	0.808	-0.824	0.986	-0.836	0.093	1.000

A.4.4 Additional Figures

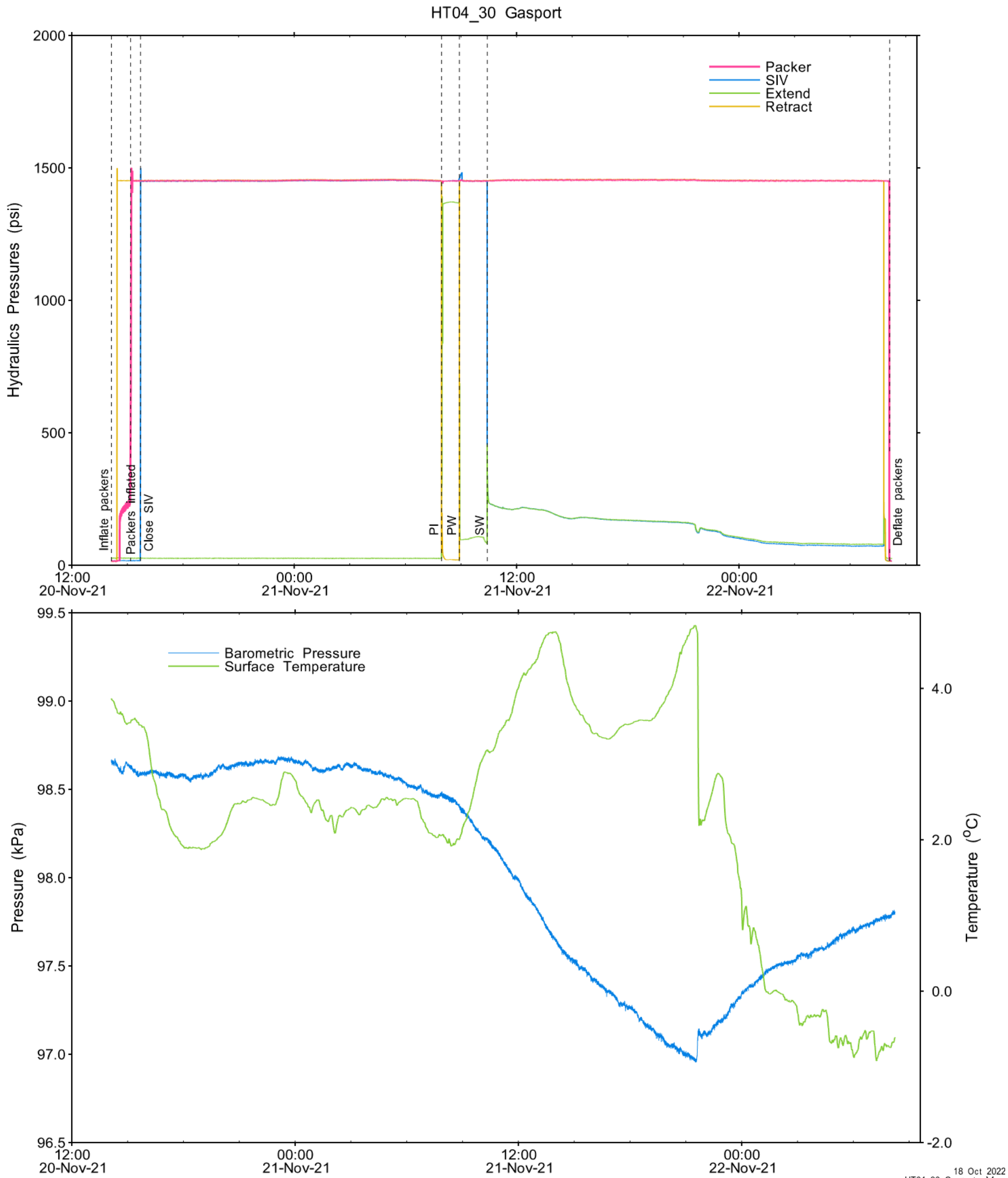

Figure 0.58 Hydraulics pressures and surface temperature/barometric pressure.

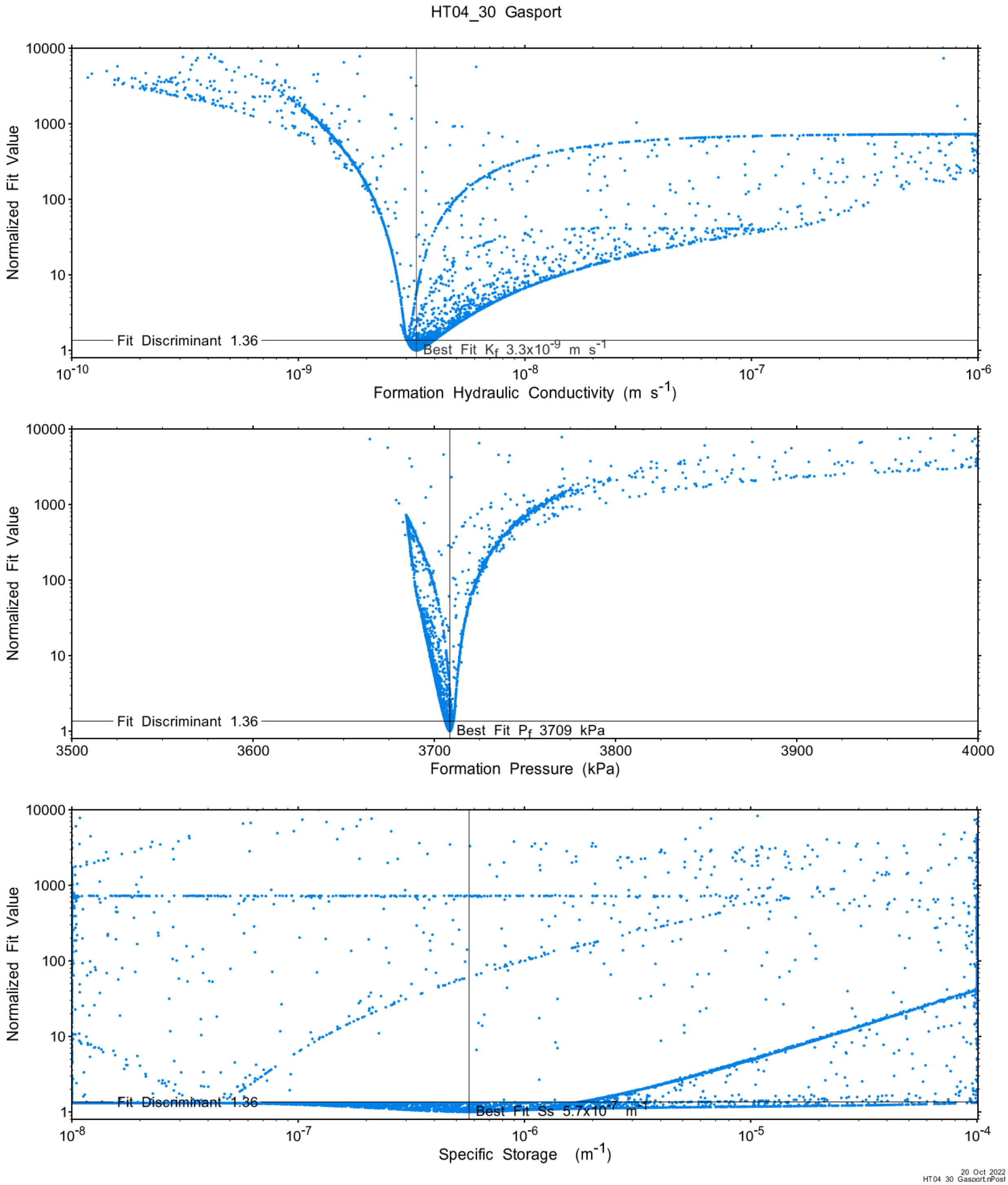

Figure 0.59 XY-scatter plot showing the formation parameter space normalized fit values.

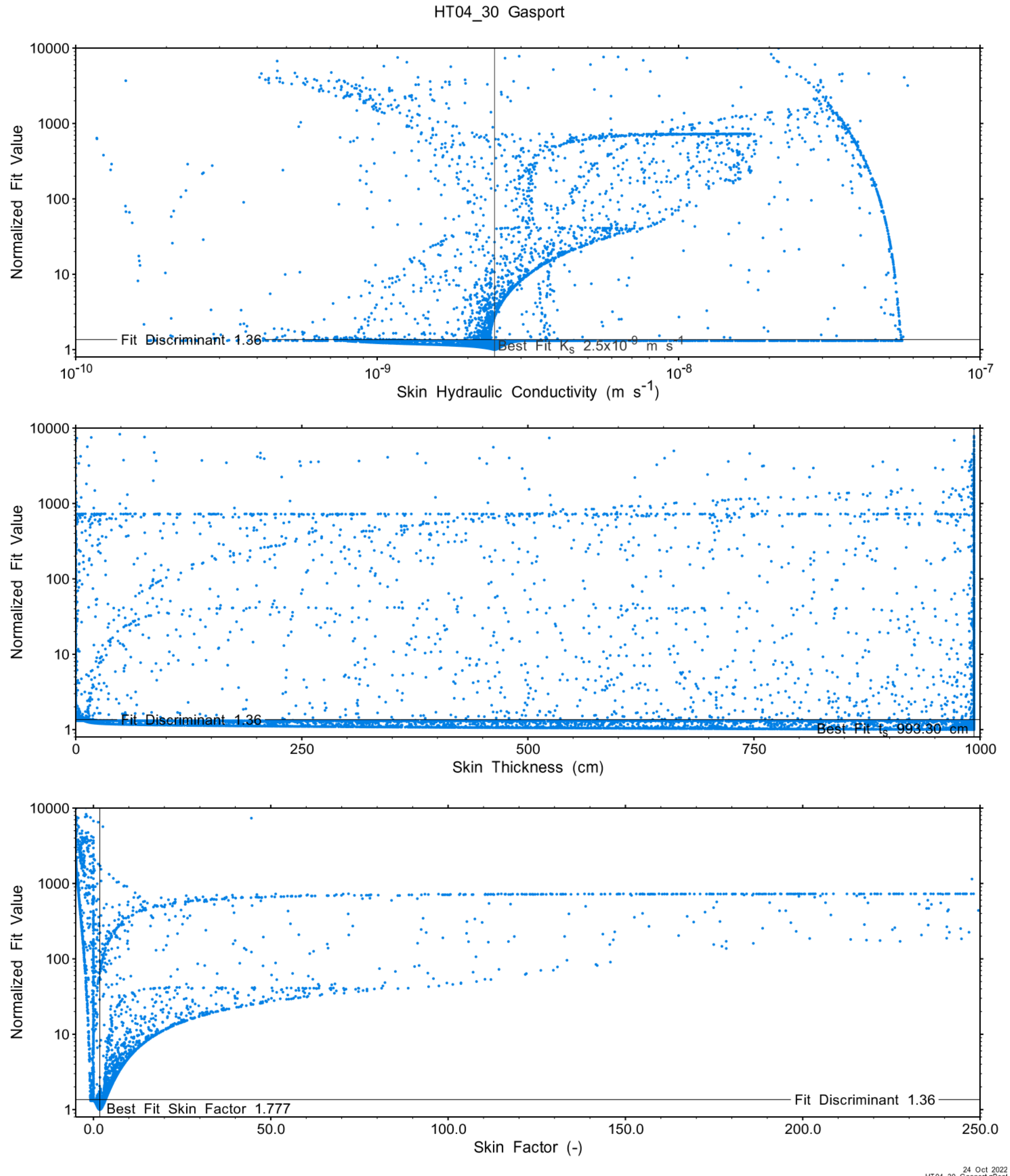

Figure 0.60 XY-scatter plot showing the skin parameter space normalized fit values.

A.5 HT05_30 Cabot Head – Manitoulin

The SB_BH01 interval from 395.50 to 425.55 mBGS tested in HT05_30 includes the entirety of the Cabot Head and Manitoulin Formations plus the upper 1 m of the Queenston shale. A single PI test with a duration of 2 days was conducted.

A.5.1 Test Data Summary

Table 0.21 and Figure 0.61 provide a summary of test events and a plot of pressures measured while testing, respectively.

Table 0.21 HT05_30 Summary of Test Events

Event	Start Date & Time	Duration (days)	TZ Pressure (kPa)
Drilling intercept	21-08-09 08:00	103.28	4040
Prior testing	21-11-20 14:45	1.94	variable
Shut-in	21-11-22 13:15	0.81	4046
Pulse injection	21-11-22 08:40	1.97	4557
Test end	21-11-25 08:02		4297

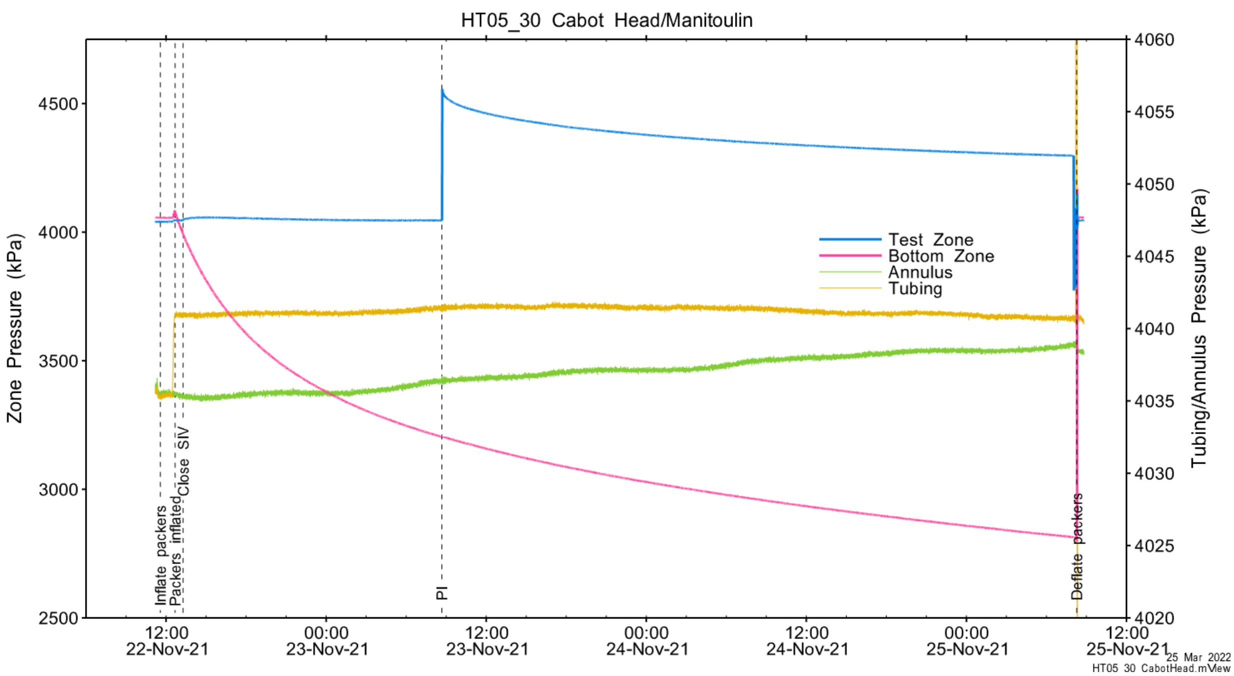

Figure 0.61 HT05_30 test events and pressures.

A.5.2 Test Analyses

Table 0.22 is a summary of test-specific input parameters used in the analyses, while Table 0.23 presents the optimized parameters and allowed ranges.

Table 0.22 nSIGHTS Input Parameters.

Parameter	Value	Units
Test zone radius	6.940	cm
Test zone compressibility	4.42E-10	1/Pa
Test zone fluid density	1050	g/L
Test zone length	30.05	m

Table 0.23 nSIGHTS Parameter Optimization Ranges.

Parameter	Minimum	Maximum	Units	Type
Formation hydraulic conductivity (K_f)	1E-15	1E-12	m/s	log
Formation pressure (P_f)	3500	5000	kPa	linear
Specific storage (Ss)	1E-08	1E-04	1/m	log
Skin hydraulic conductivity (K_s)	1E-15	1E-12	m/s	log
Skin thickness (t_s)	0.1	930	mm	linear

Figure 0.62 shows the measured test zone pressure record (with reduced data density for clarity) used in the analysis along with the best-fit simulation and parameter values. Figure 0.63 presents the pre-test history, and Figure 0.64 shows the Ramey B normalized best-fit pressure and pressure derivatives.

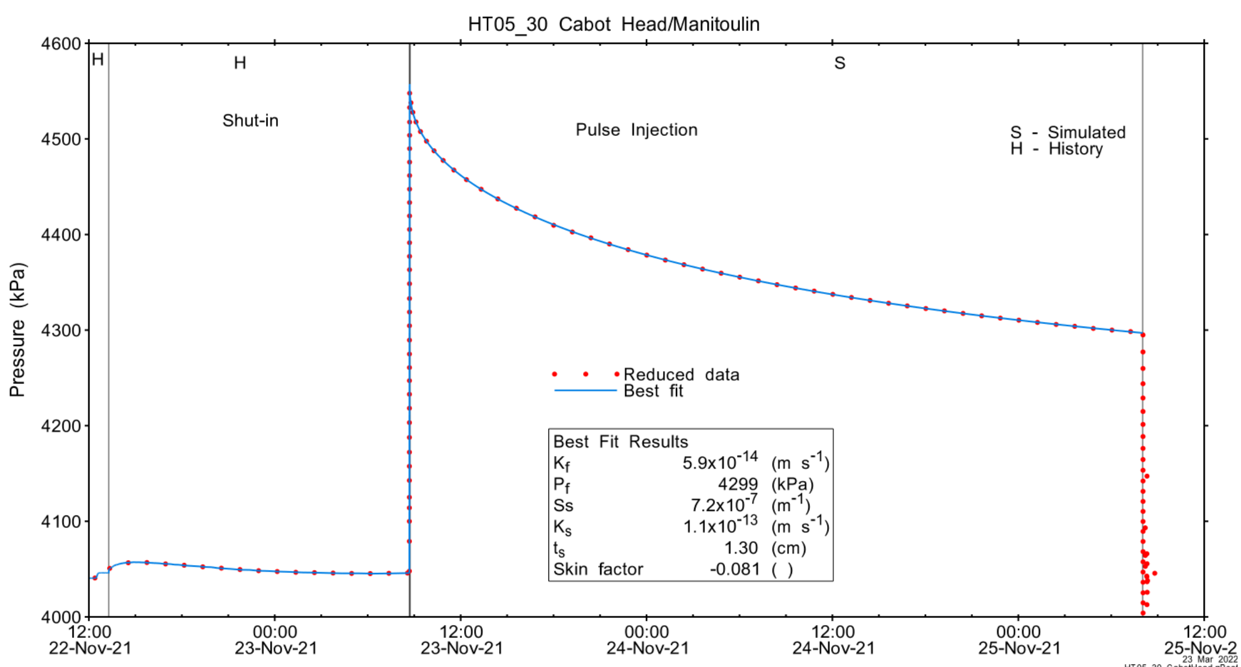

Figure 0.62 Annotated testing sequence showing best-fit simulation and parameter estimates.

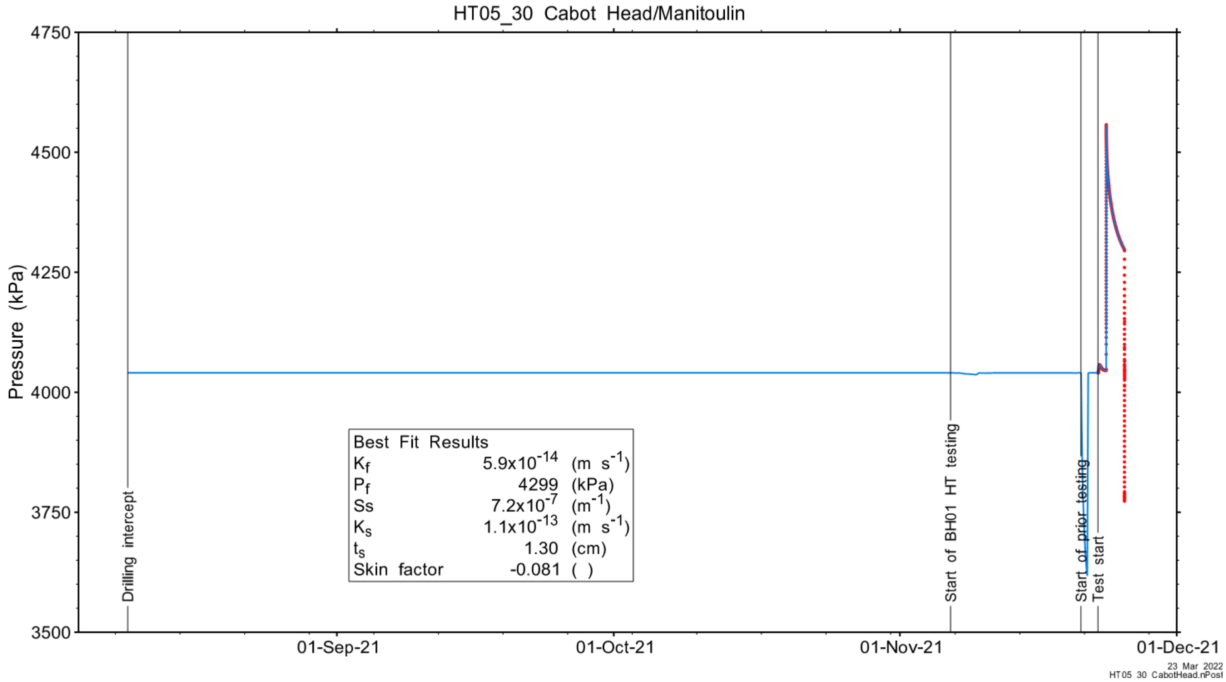

Figure 0.63 Annotated HT05_30 testing sequence showing pre-test history, best-fit simulation and parameter estimates.

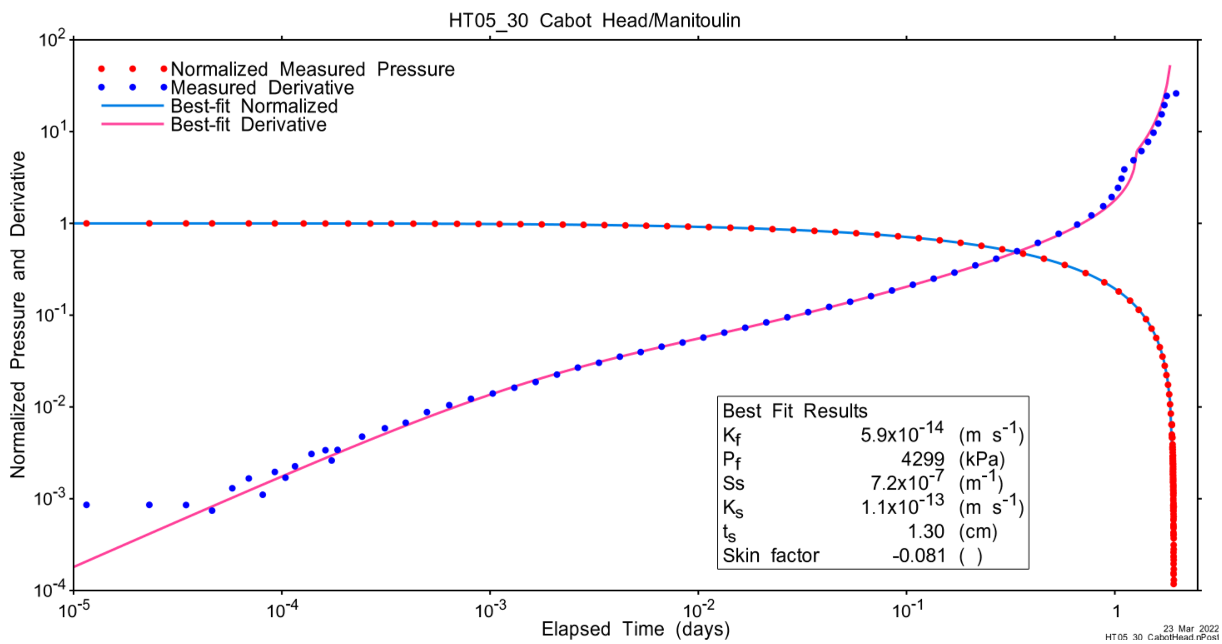

Figure 0.64 Log-log plot showing Ramey B normalized pressure and derivative response for best-fit simulation.

Figure 0.65 shows the normalized parameter sensitivity response for the best fit. Skin-related parameters are most sensitive during the early-time response. K_f response is nearly flat at the test end, indicating that the estimate would not have been significantly improved by increased test duration. Sensitivity to P_f is continuing to rise – additional test duration may have improved the estimate.

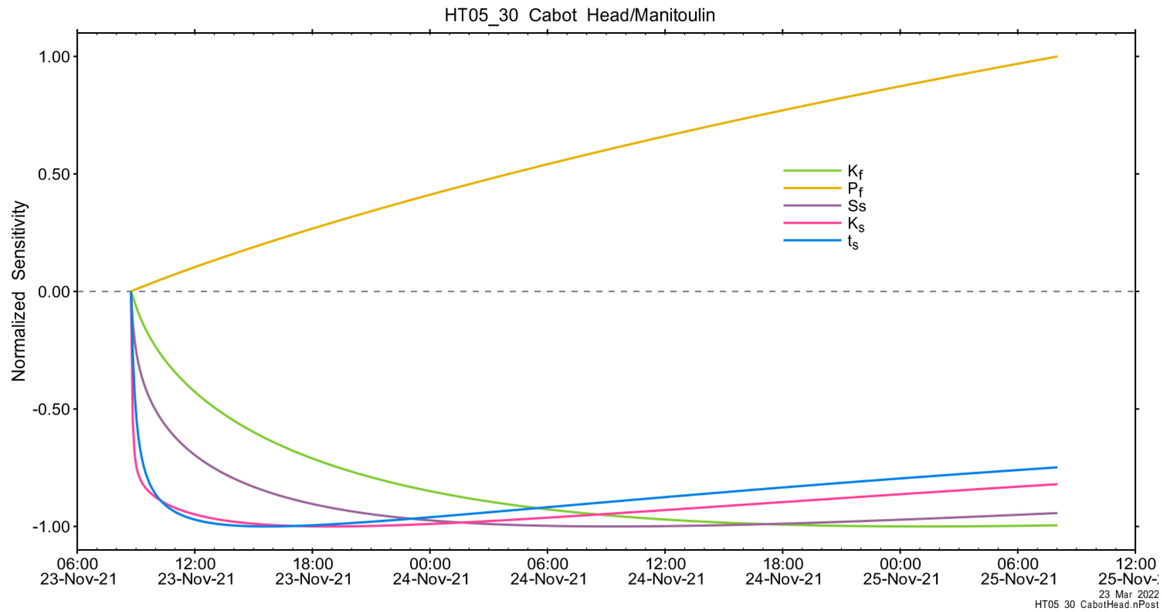

Figure 0.65 Normalized Jacobian for best-fit simulation.

A.5.3 Uncertainty Analyses

The CDF of normalized fit values for all converged simulations and the selected fit discriminant are shown in Figure 0.66.

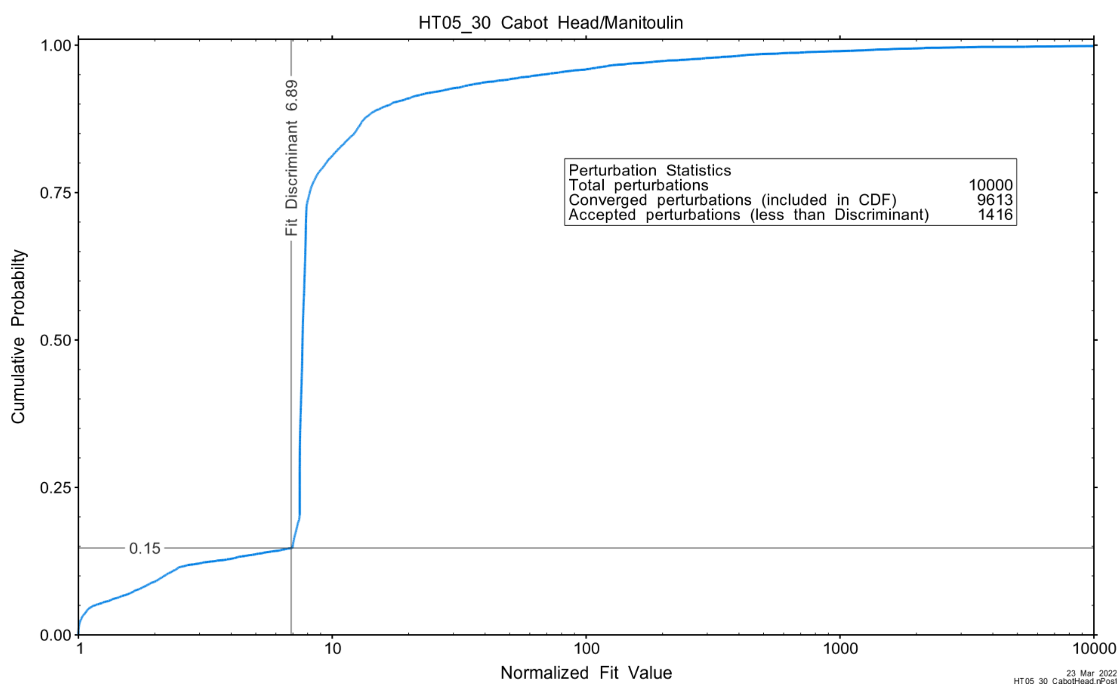

Figure 0.66 Fit value cumulative distribution function.

Summary cross parameter scatter plots for selected formation and skin parameters are given in Figure 0.67 and Figure 0.68. The light pink dots on the figures are the initial parameter estimates, with red dots overlaying those initial parameter values that resulted in accepted optimization results. The grey dots are converged optimizations which did not meet the fit discriminant. Larger varying color symbols represent the fit value of accepted optimizations, with the blue values representing the best fit.

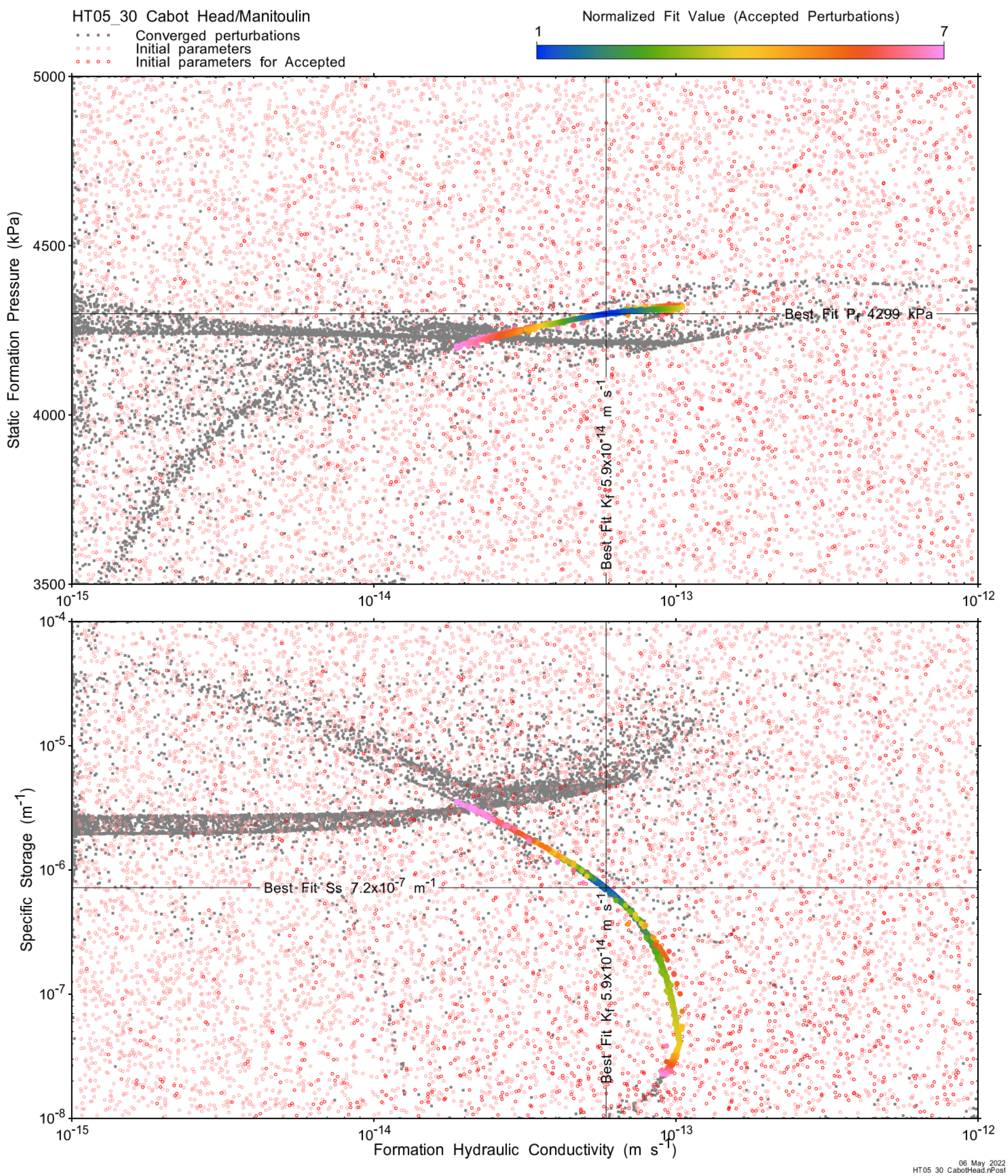

Figure 0.67 XY-scatter plot showing estimates of formation hydraulic conductivity (K_f) vs static formation pressure (P_f) (top panel) and specific storage (Ss) (bottom panel).

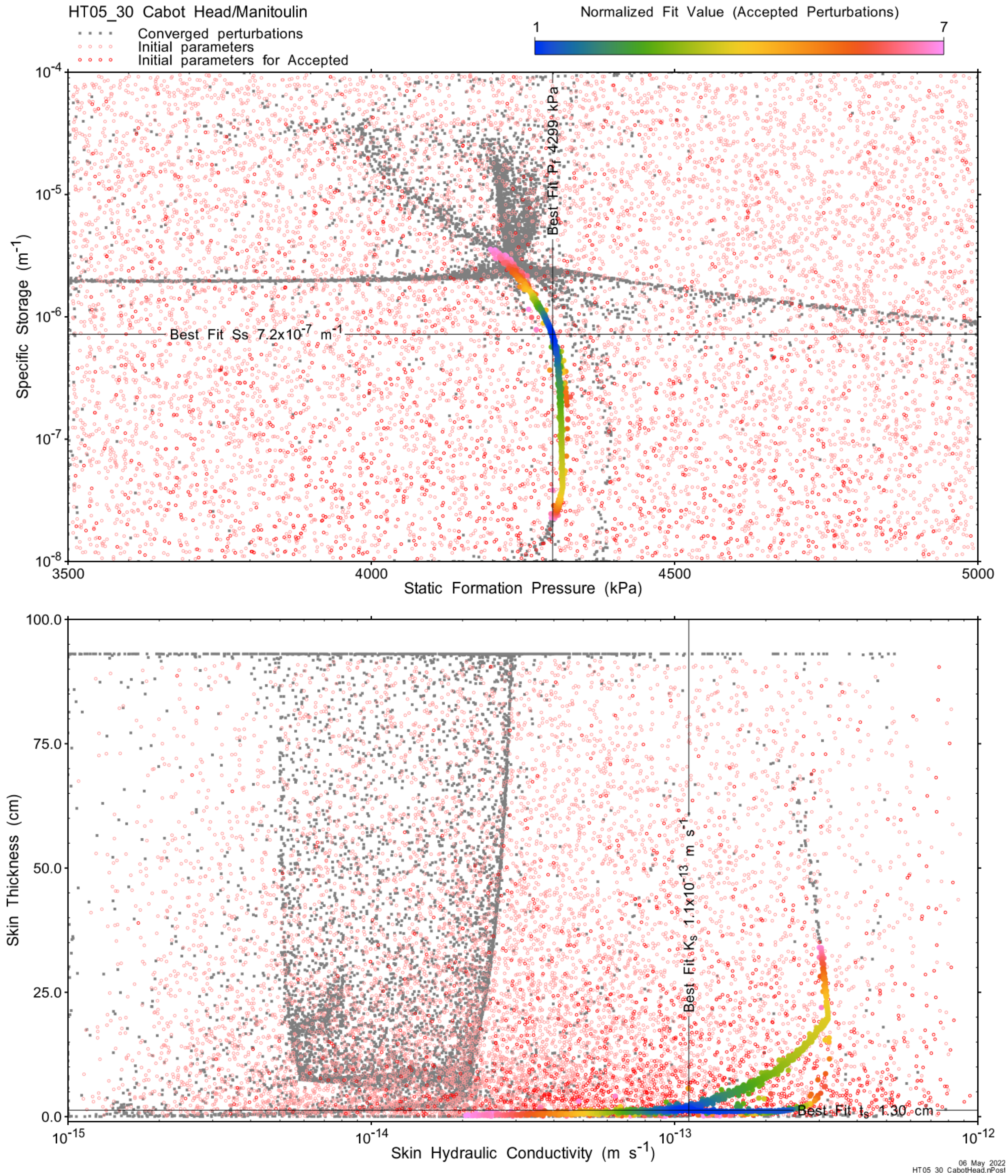

Figure 0.68 XY-scatter plot showing estimates of static formation pressure (P_f) vs specific storage (Ss) (top panel) and skin hydraulic conductivity (K_s) vs skin thickness (t_s) (bottom panel).

Confidence limits and median values are determined from the CDF of accepted optimization results (i.e. the varying color values in the above figures), with best fit value, 5% and 95% confidence indicated on Figure 0.69 and Figure 0.70.

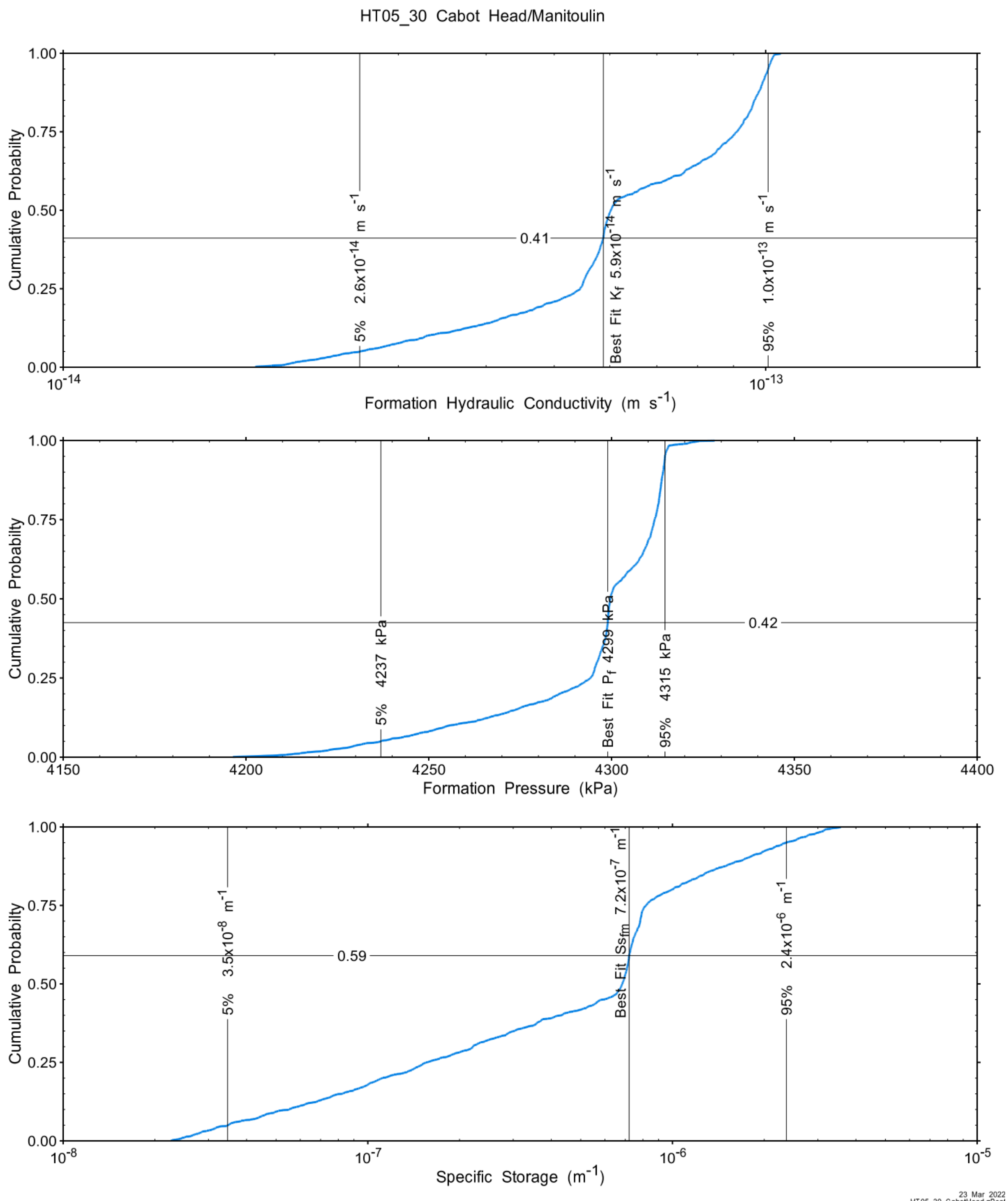

Figure 0.69 Cumulative distribution functions and parameter limits for formation hydraulic conductivity (K_f) (top panel), static formation pressure (P_f) (middle panel) and specific storage (Ss) (bottom panel).

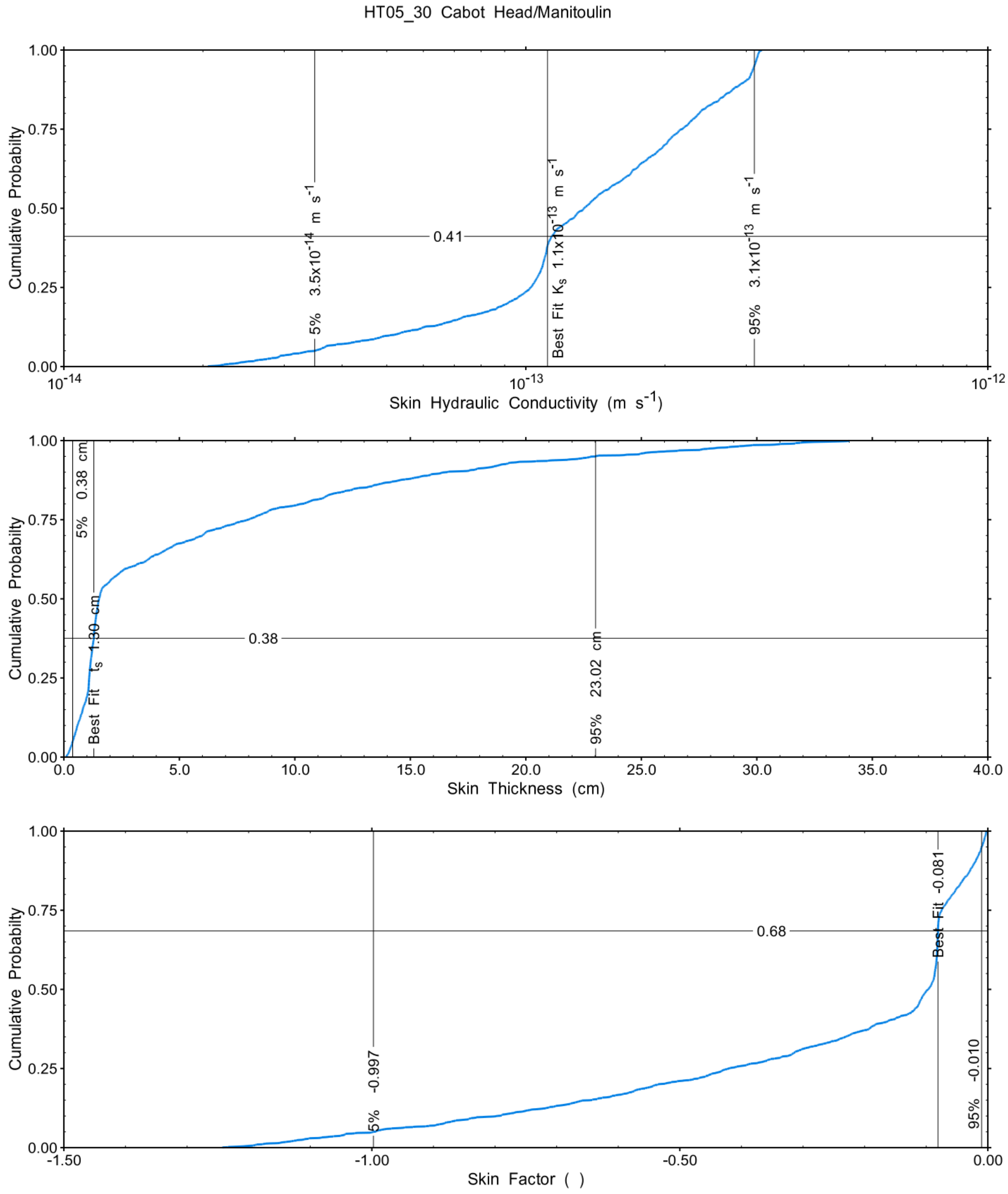

Figure 0.70 Cumulative distribution functions and parameter limits for skin hydraulic conductivity (K_s) (top panel), skin thickness (t_s) (middle panel) and skin factor (s) (bottom panel).

A summary of perturbation results is presented in Figure 0.71, with Ramey-processed perturbations in Figure 0.72. Those perturbations (1139 of 10,000) with all parameters within the 5% and 95% range present a very good fit to the measured test zone data.

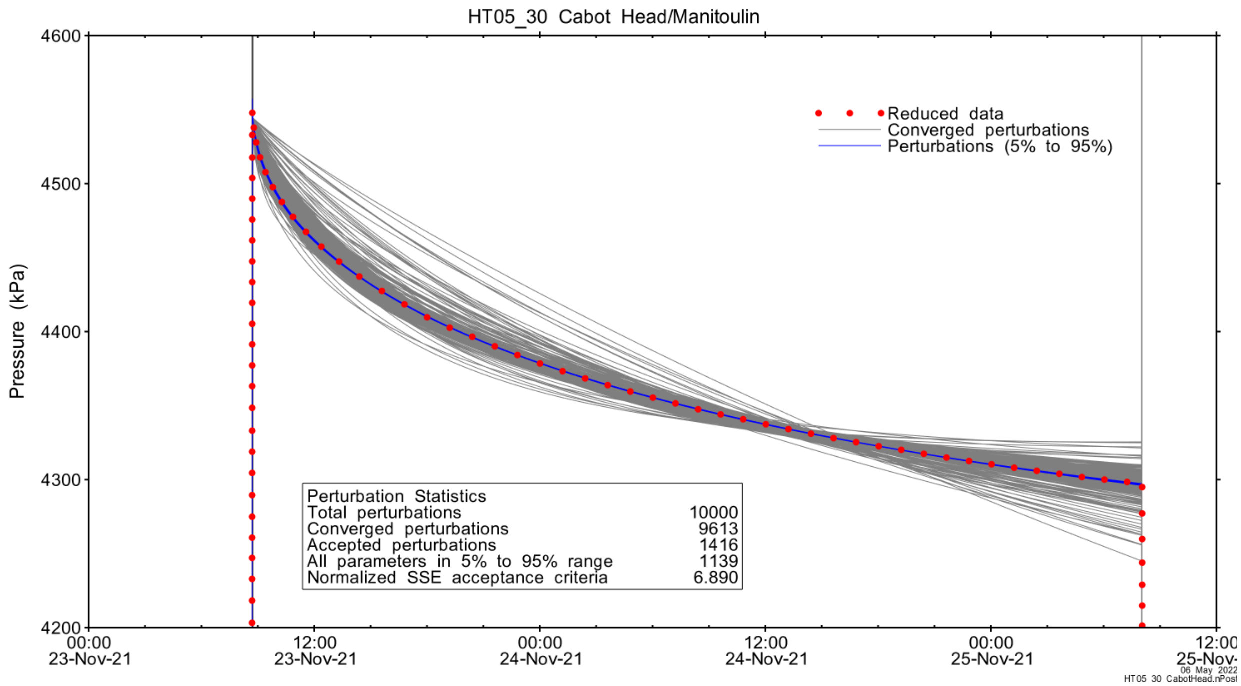

Figure 0.71 Perturbation results – all converged, accepted, and within 5% to 95% for all parameters.

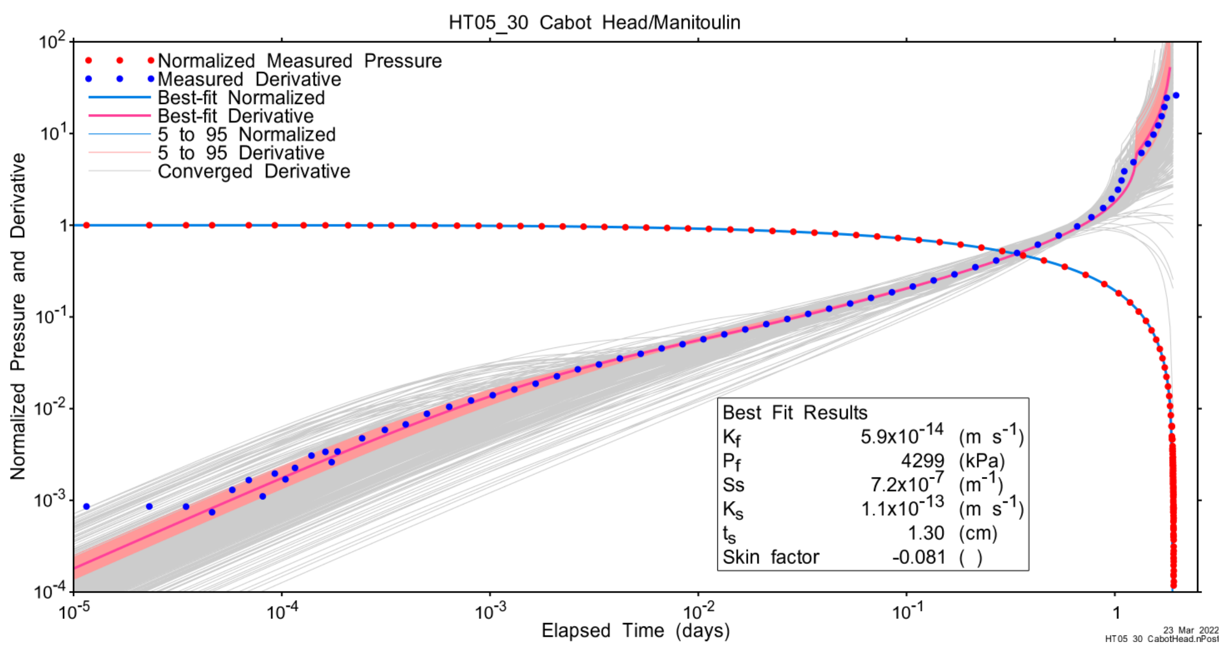

Figure 0.72 Log-log plot showing Ramey B normalized pressure and derivative response for all converged optimizations and those within 5% to 95% for all parameters.

A summary of best-fit parameter estimates and ranges is given in Table 0.24.

Table 0.24 Summary of the HT05_30 parameter estimates.

Parameter	Best Fit	5%	Median	95%
K_f (m/s)	5.9E-14	2.6E-14	6.0E-14	1.0E-13
P_f (kPa)	4299	4237	4300	4315
Ss (1/m)	7.2E-07	3.5E-08	6.8E-07	2.4E-06
K_s (m/s)	1.1E-13	3.5E-14	1.3E-13	3.1E-13
t_s (cm)	1.30	0.38	1.52	23.02
s (-)	-0.081	-0.997	-0.097	-0.010

Parameter correlations for all perturbations with all parameters within the 5% to 95% limits are given in Table 0.25.

Table 0.25 Pearson cross-correlations of 5% to 95% parameters

	Log(K_f)	P_f	Log(Ss)	Log(K_s)	t_s	s
Log(K_f)	1.000	0.950	-0.946	0.794	0.814	-0.833
P_f	0.950	1.000	-0.810	0.744	0.619	-0.648
Log(Ss)	-0.946	-0.810	1.000	-0.788	-0.957	0.965
Log(K_s)	0.794	0.744	-0.788	1.000	0.700	-0.759
t_s	0.814	0.619	-0.957	0.700	1.000	-0.995
s	-0.833	-0.648	0.965	-0.759	-0.995	1.000

A.5.4 Additional Figures

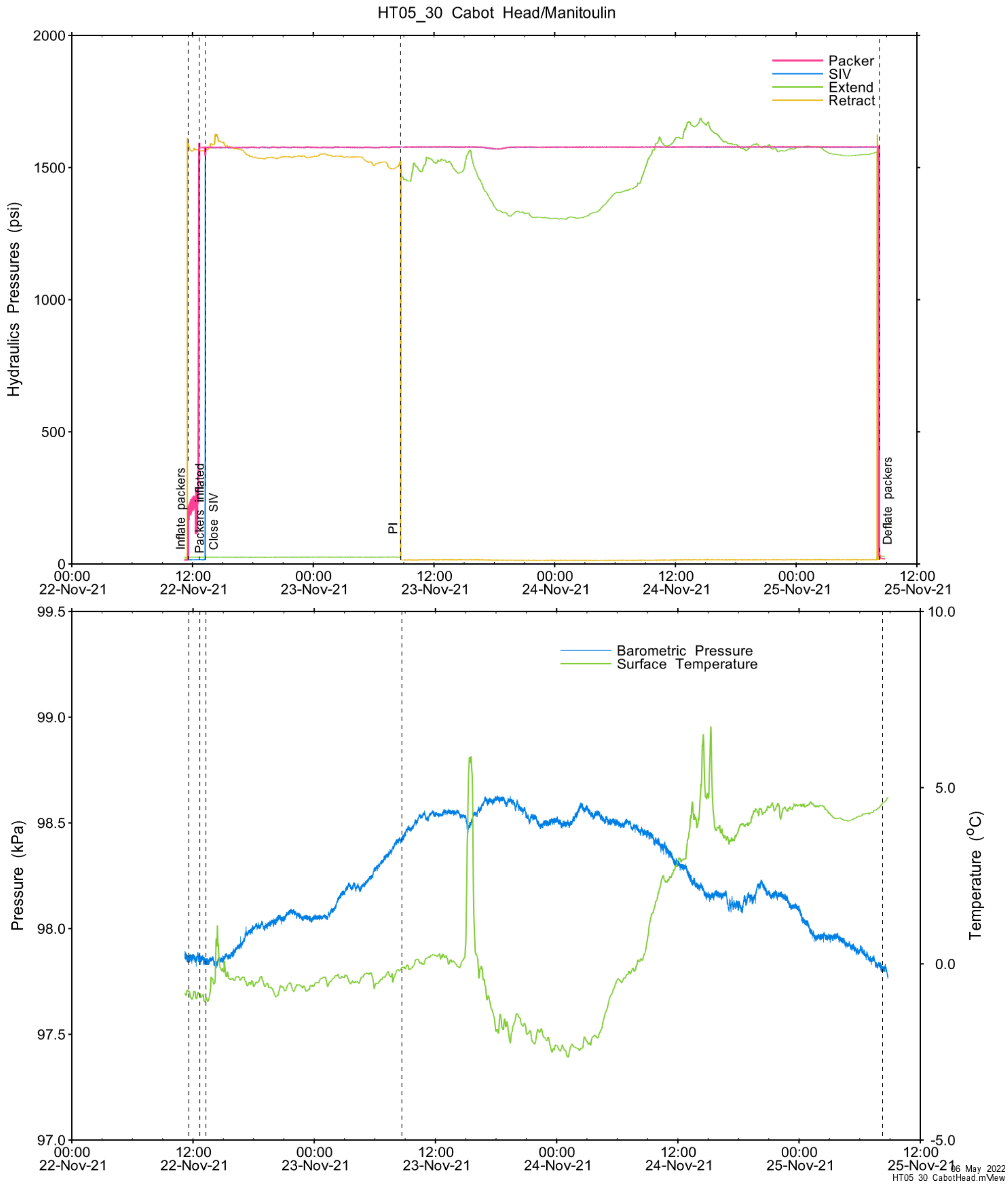

Figure 0.73 Hydraulics pressures and surface temperature/barometric pressure.

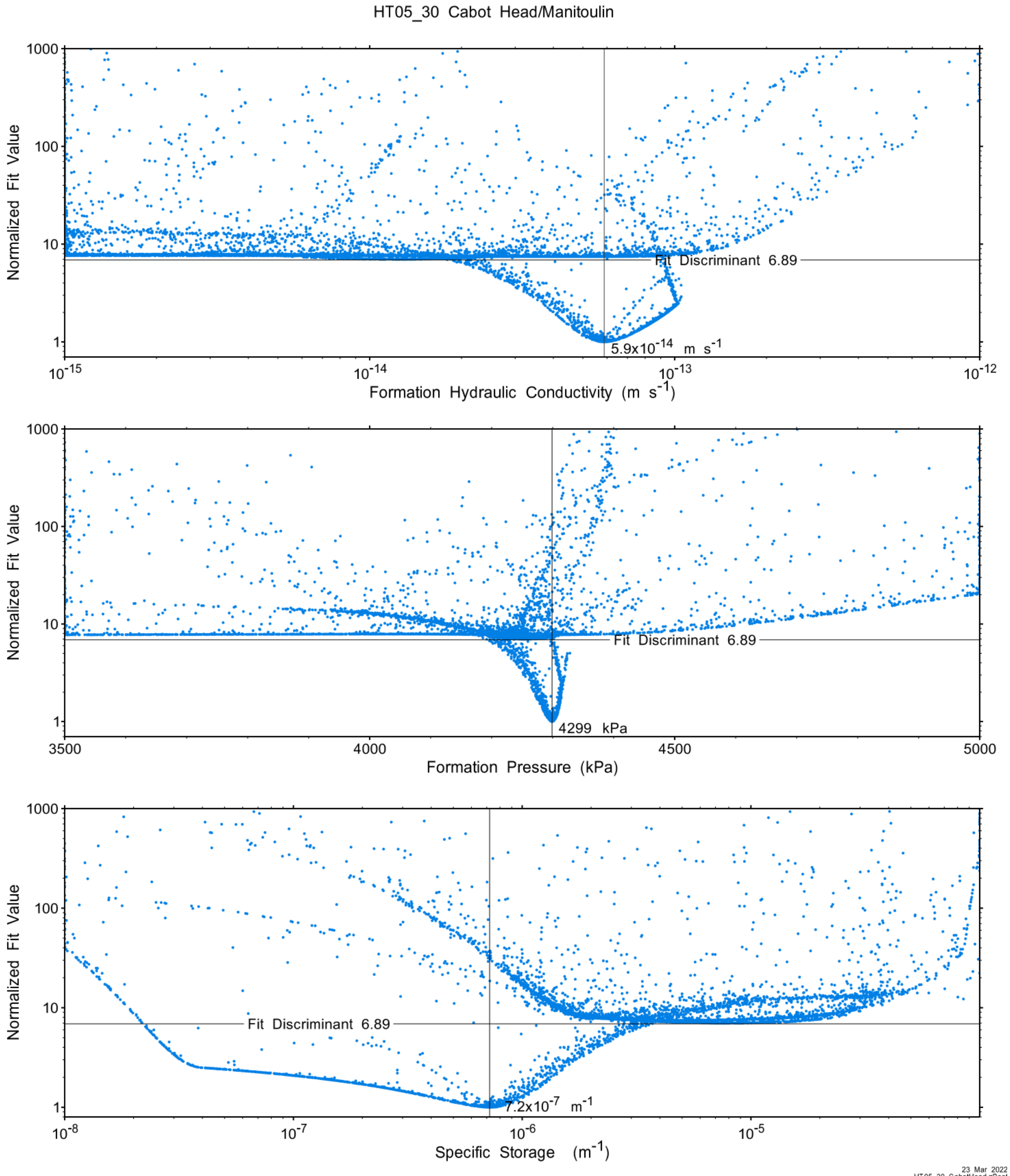

Figure 0.74 XY-scatter plot showing the formation parameter space normalized fit values.

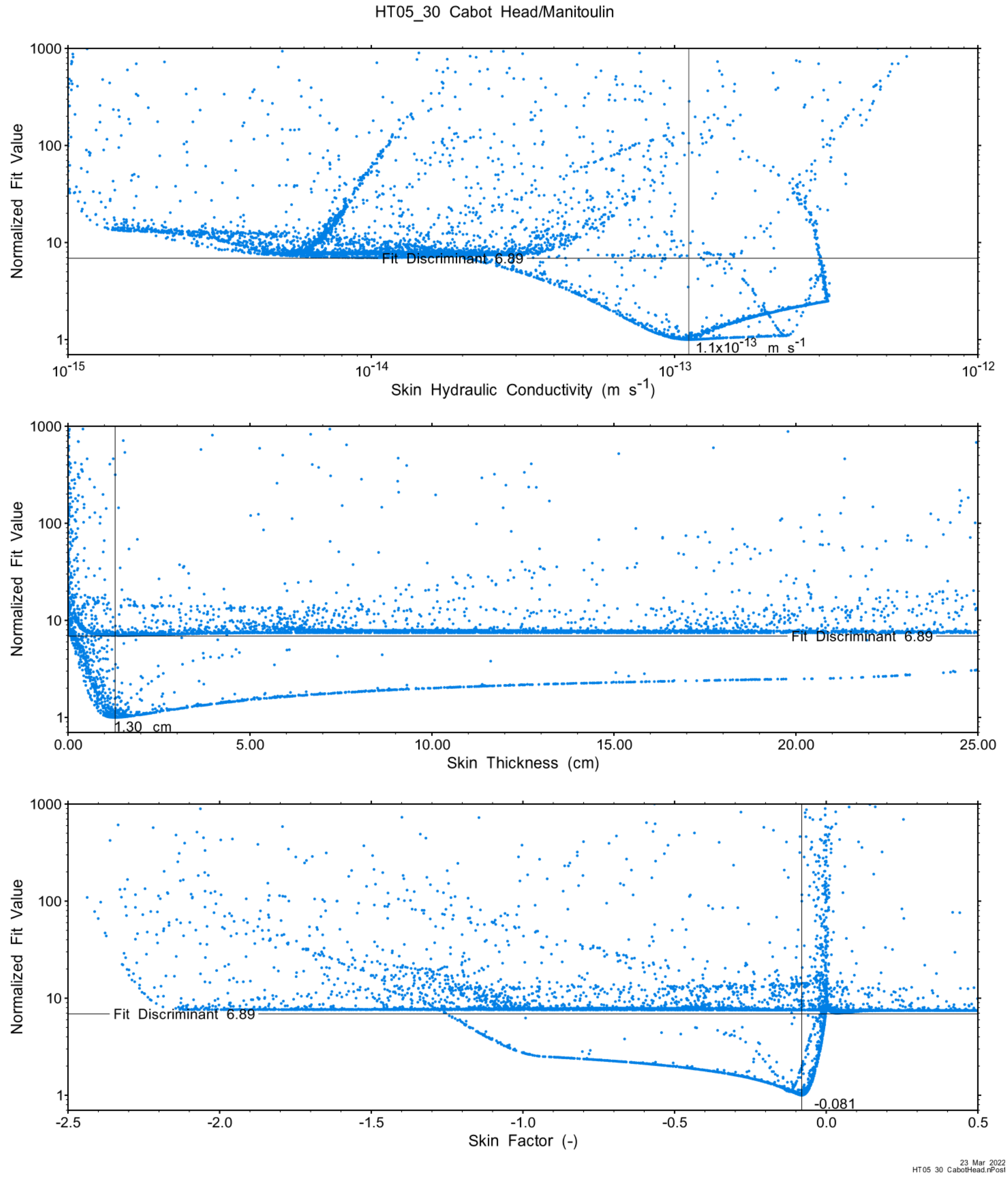

Figure 0.75 XY-scatter plot showing the skin parameter space normalized fit values.

A.6 HT06_30 Upper Queenston

The SB_BH01 interval from 428.50 to 458.55 mBGS tested in HT06_30 was contained entirely in the upper portion of the Queenston Formation. A single PI test with a duration of 2 days was conducted.

A.6.1 Test Data Summary

Table 0.26 and Figure 0.76 provide a summary of test events and a plot of pressures measured while testing, respectively.

Table 0.26 HT06_30 Summary of Test Events.

Event	Start Date & Time	Duration (days)	TZ Pressure (kPa)
Drilling intercept	21-08-10 14:20	101.02	4386
Prior testing	21-11-20 14:45	4.96	variable
Shut-in	21-11-25 13:50	0.75	4388
Pulse injection	21-11-26 07:50	2.02	4780
Test end	21-11-28 08:21		4531

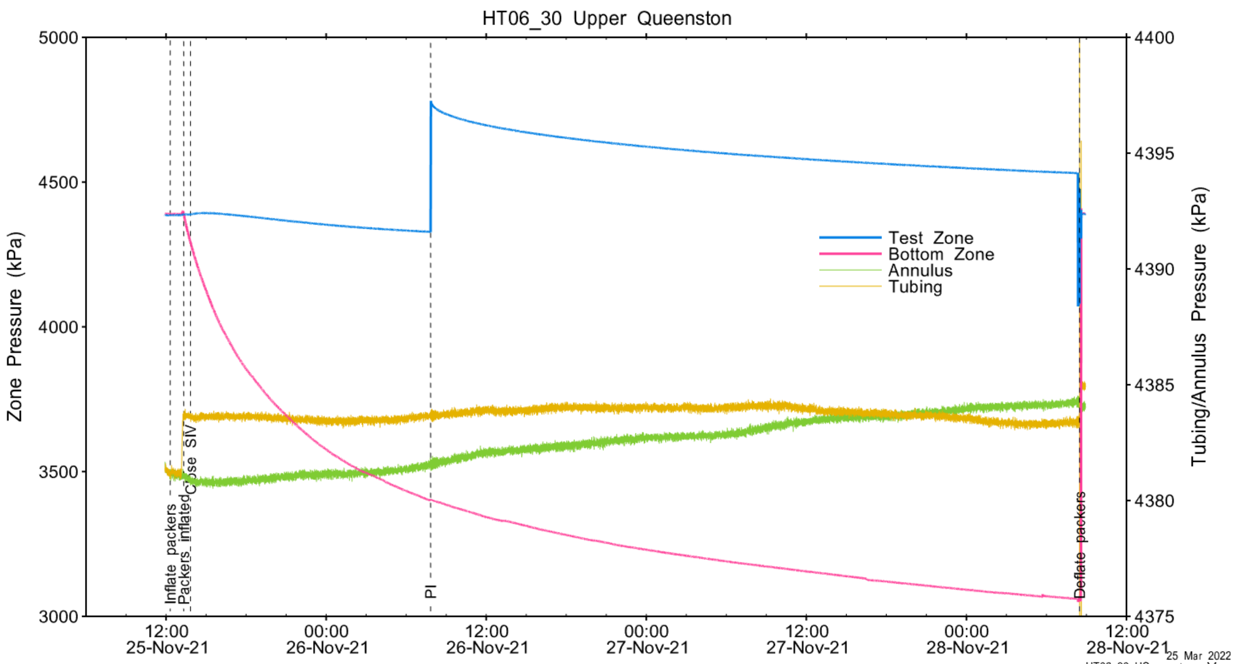

Figure 0.76 HT06_30 test events and pressures.

A.6.2 Test Analyses

Table 0.27 is a summary of test-specific input parameters used in the analyses, while Table 0.28 presents the optimized parameters and allowed ranges.

Table 0.27 nSIGHTS Input Parameters.

Parameter	Value	Units
Test zone radius	7.10	cm
Test zone compressibility	4.76E-10	1/Pa
Test zone fluid density	1051	g/L
Test zone length	30.05	m

Table 0.28 nSIGHTS Optimized Parameters.

Parameter	Minimum	Maximum	Units	Type
Formation hydraulic conductivity (K_f)	1E-15	1E-12	m/s	log
Formation pressure (P_f)	3000	5000	kPa	linear
Specific storage (Ss)	1E-08	1E-04	1/m	log
Skin hydraulic conductivity (K_s)	1E-15	1E-12	m/s	log
Skin thickness (t_s)	0.1	929	mm	linear

Figure 0.77 shows the measured test zone pressure record (with reduced data density for clarity) used in the analysis along with the best-fit simulation and parameter values. Figure 0.78 presents the pre-test history, and Figure 0.79 shows the Ramey B normalized best-fit pressure and pressure derivatives.

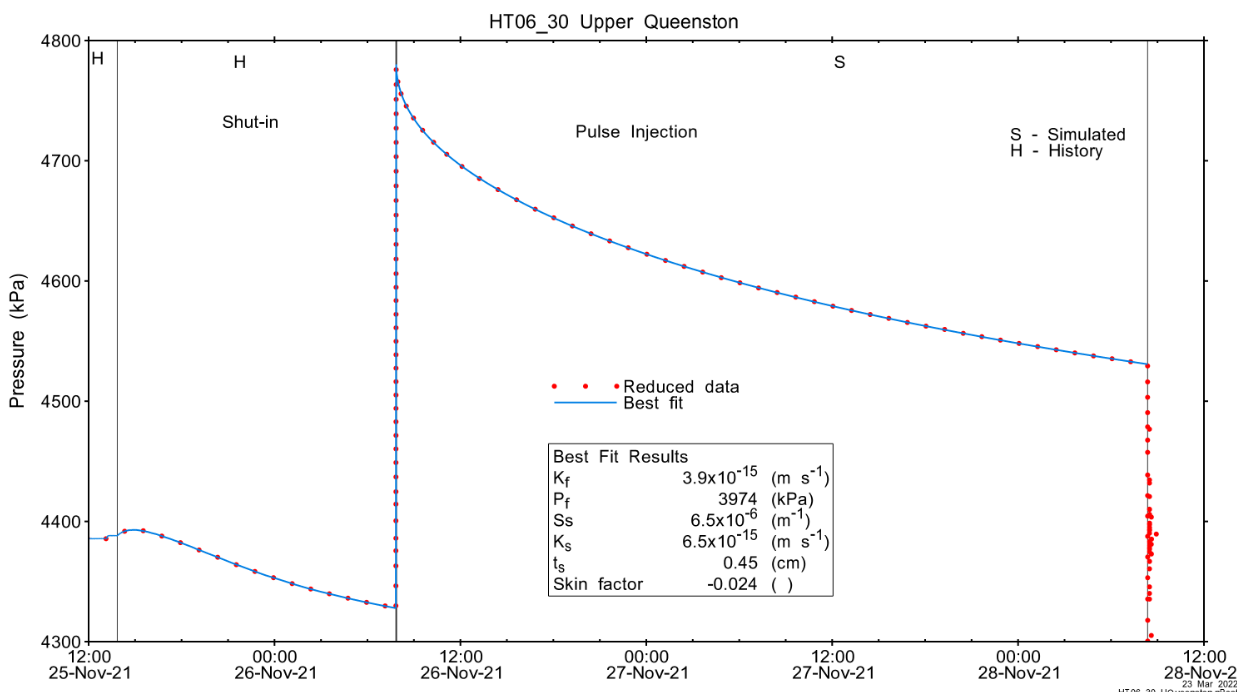

Figure 0.77 Annotated testing sequence showing best-fit simulation and parameter estimates.

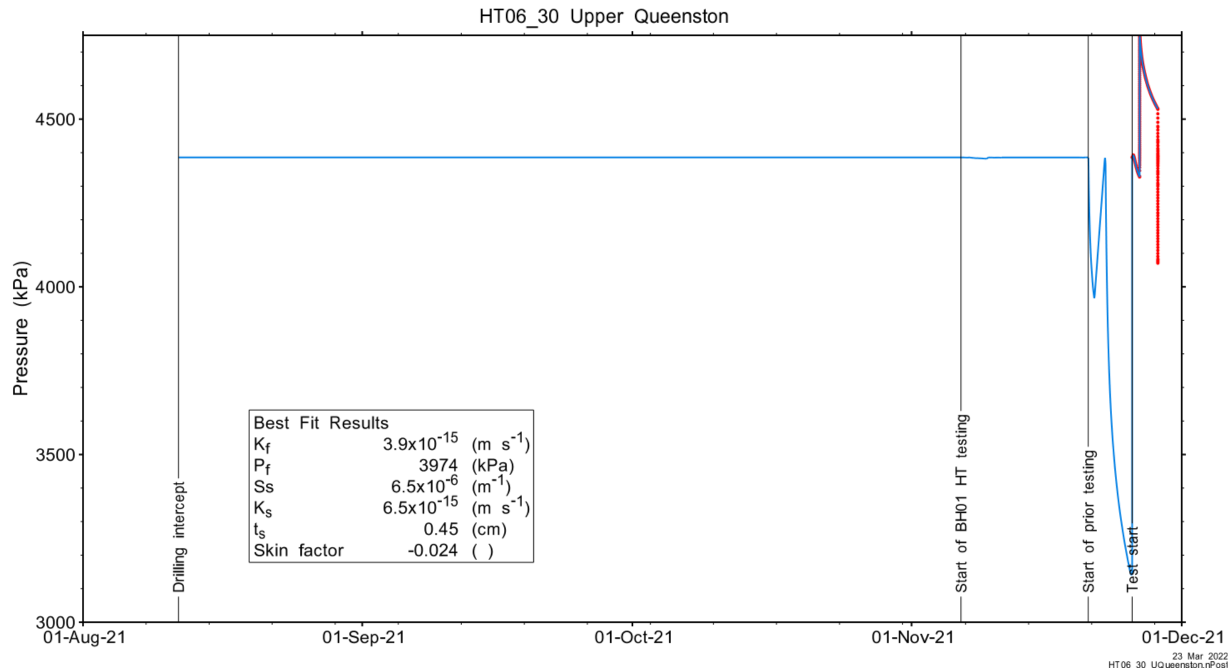

Figure 0.78 Annotated HT06_30 testing sequence showing pre-test history, best-fit simulation and parameter estimates.

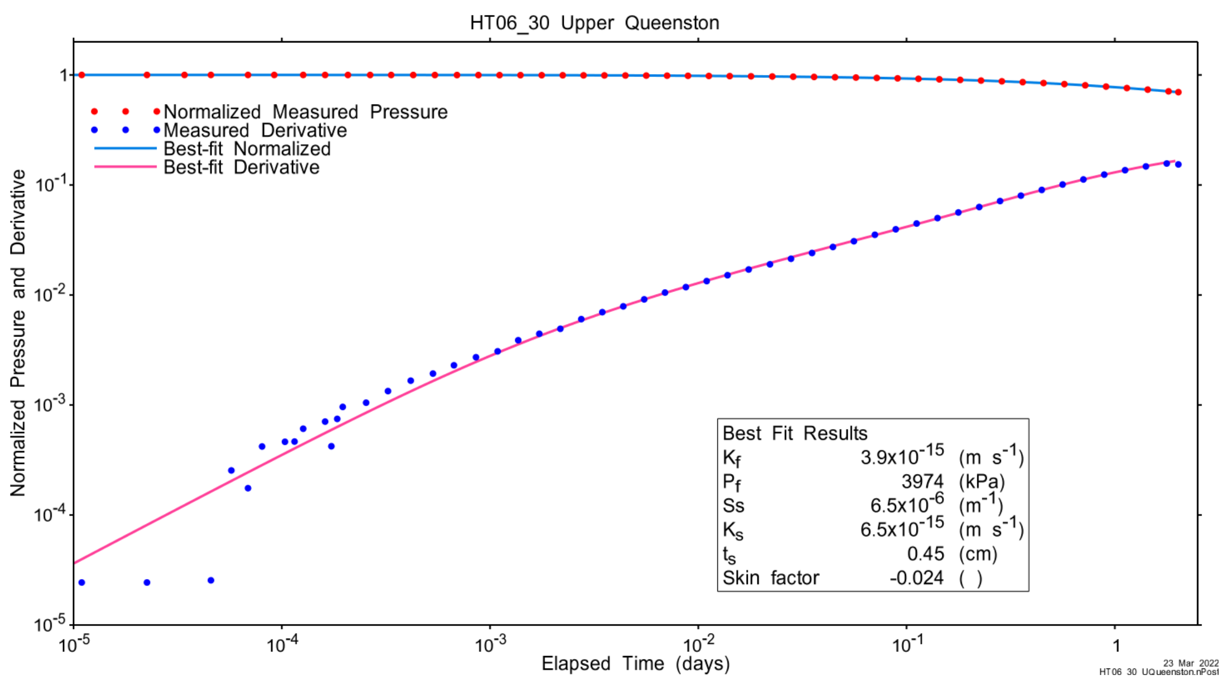

Figure 0.79 Log-log plot showing Ramey B normalized pressure and derivative response for best-fit simulation.

Figure 0.80 shows the normalized parameter sensitivity response for the best fit. Skin-related parameters are most sensitive during the early-time response. Sensitivity to K_f, and P_f, and Ss is continuing to rise – additional test duration may have improved the estimates.

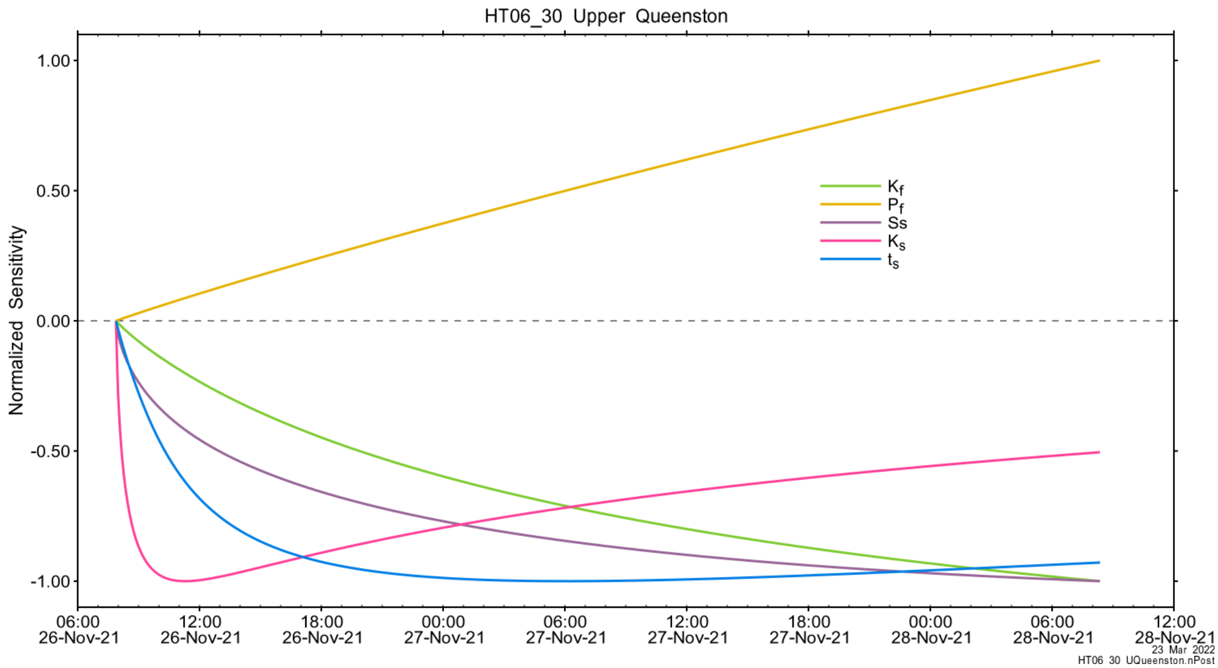

Figure 0.80 Normalized Jacobian for best-fit simulation.

A.6.3 Uncertainty Analyses

The CDF of normalized fit values for all converged simulations and the selected fit discriminant are shown in Figure 0.81.

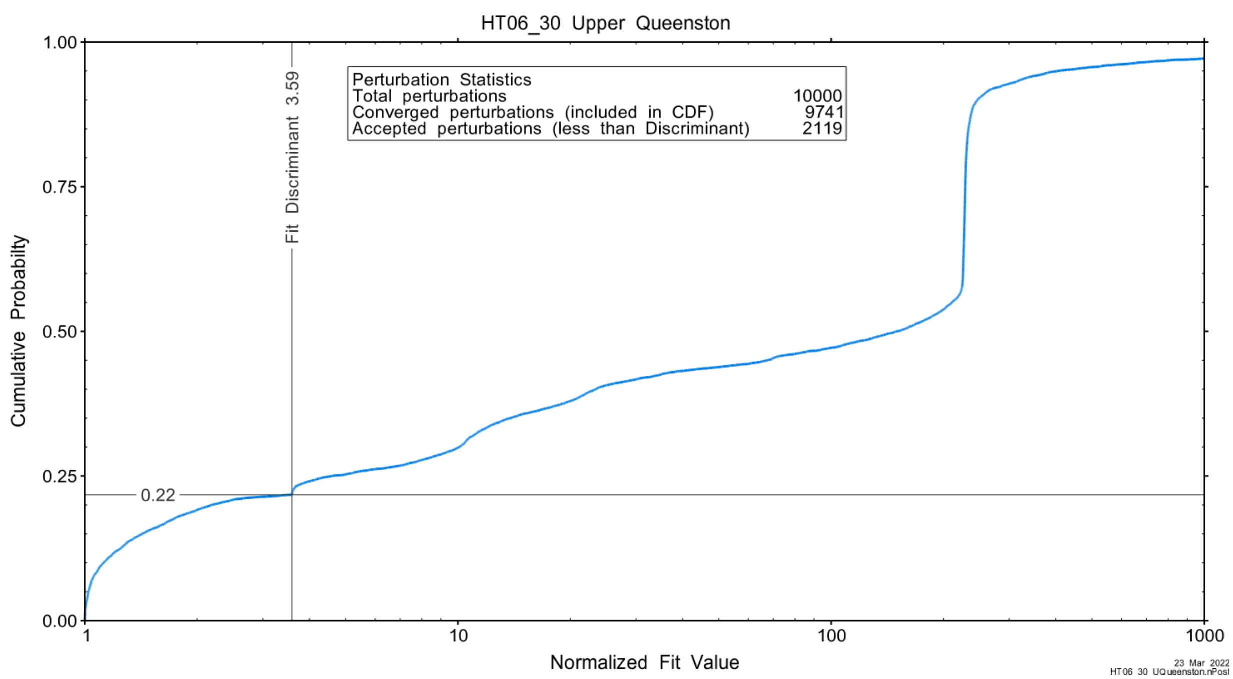

Figure 0.81 Fit value cumulative distribution function.

Summary cross parameter scatter plots for selected formation and skin parameters are given in Figure 0.82 and Figure 0.83. The light pink dots on the figures are the initial parameter estimates, with red dots overlaying those initial parameter values that resulted in accepted optimization results. The grey dots are converged optimizations which did not meet the fit discriminant. Larger varying color symbols represent the fit value of accepted optimizations, with the blue values representing the best fit.

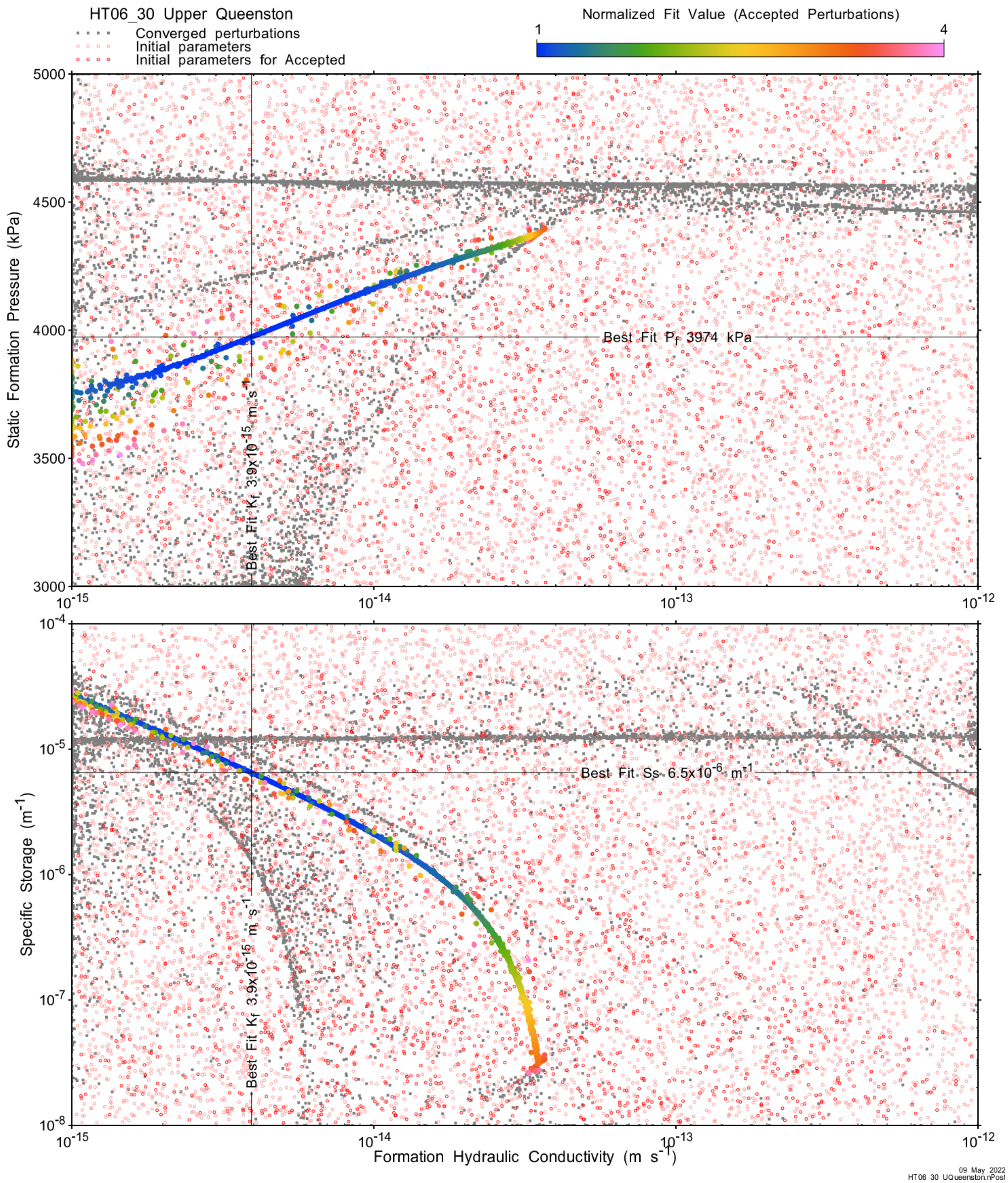

Figure 0.82 XY-scatter plot showing estimates of formation hydraulic conductivity (K_f) vs static formation pressure (P_f) (top panel) and specific storage (Ss) (bottom panel).

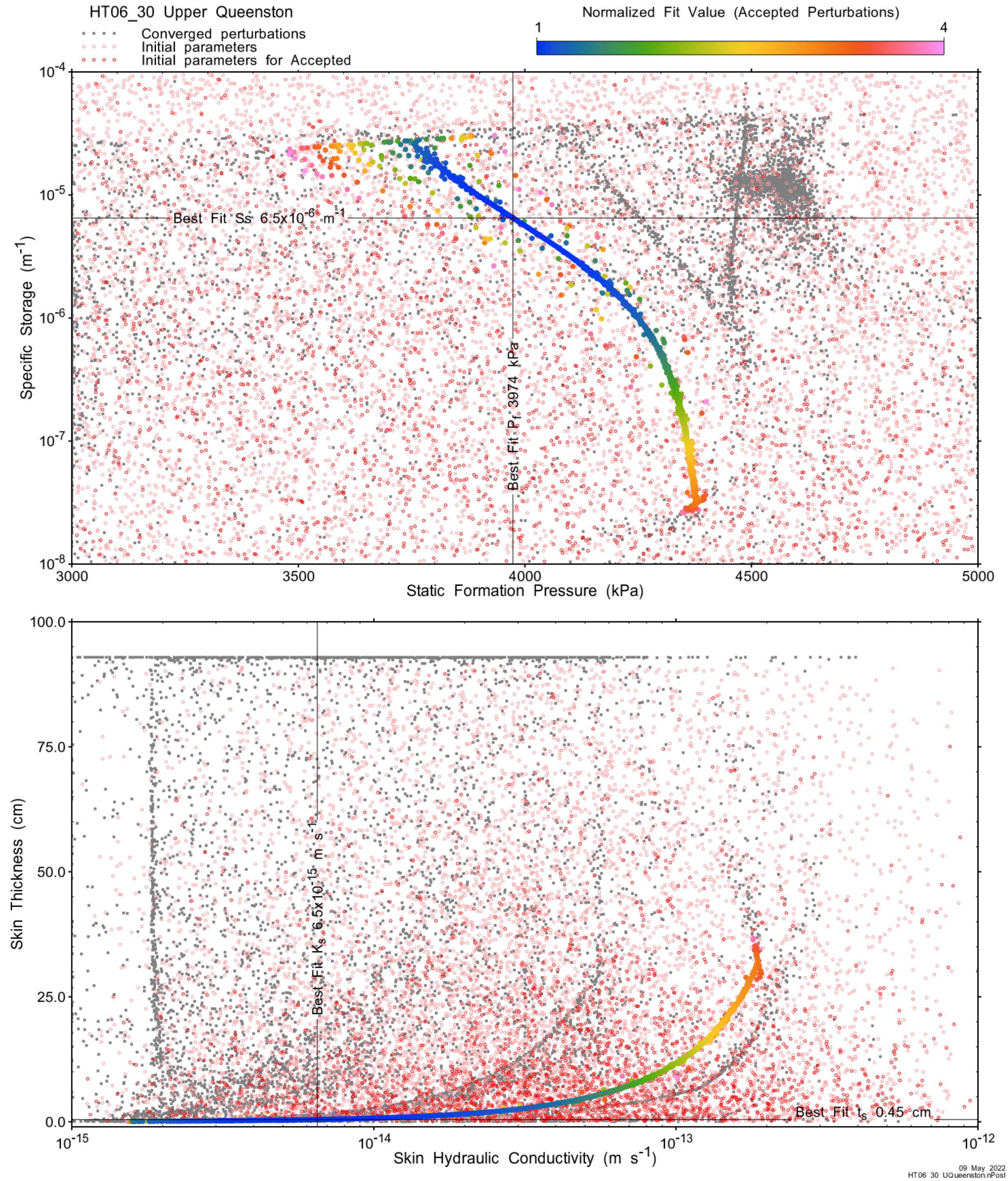

Figure 0.83 XY-scatter plot showing estimates of static formation pressure (P_f) vs specific storage (Ss) (top panel) and skin hydraulic conductivity (K_s) vs skin thickness (t_s) (bottom panel).

Confidence limits and median values are determined from the CDF of accepted optimization results (i.e. the varying color values in the above figures), with best fit value, 5% and 95% confidence indicated on Figure 0.84 and Figure 0.85.

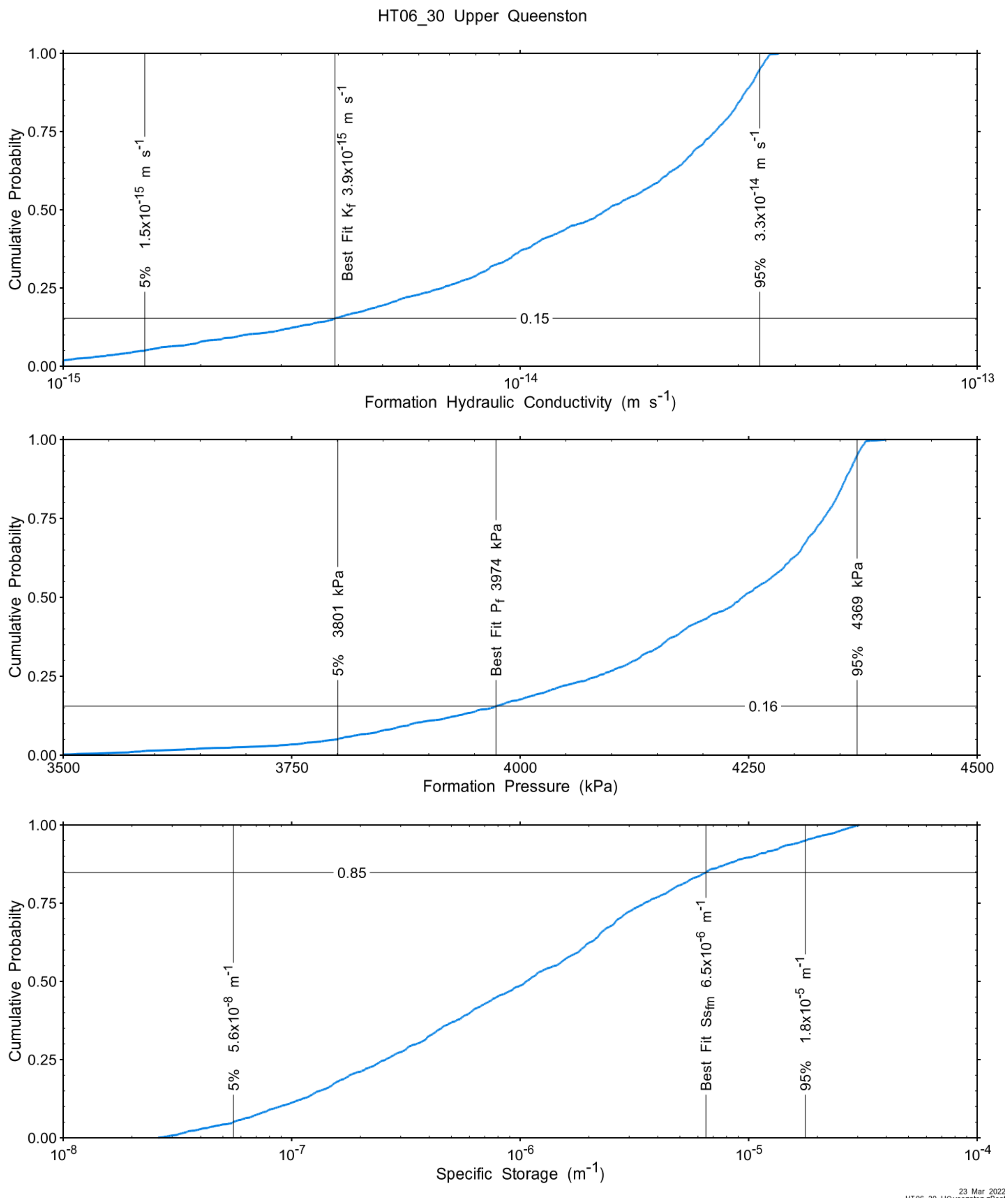

Figure 0.84 Cumulative distribution functions and parameter limits for formation hydraulic conductivity (K_f) (top panel), static formation pressure (P_f) (middle panel) and specific storage (Ss) (bottom panel).

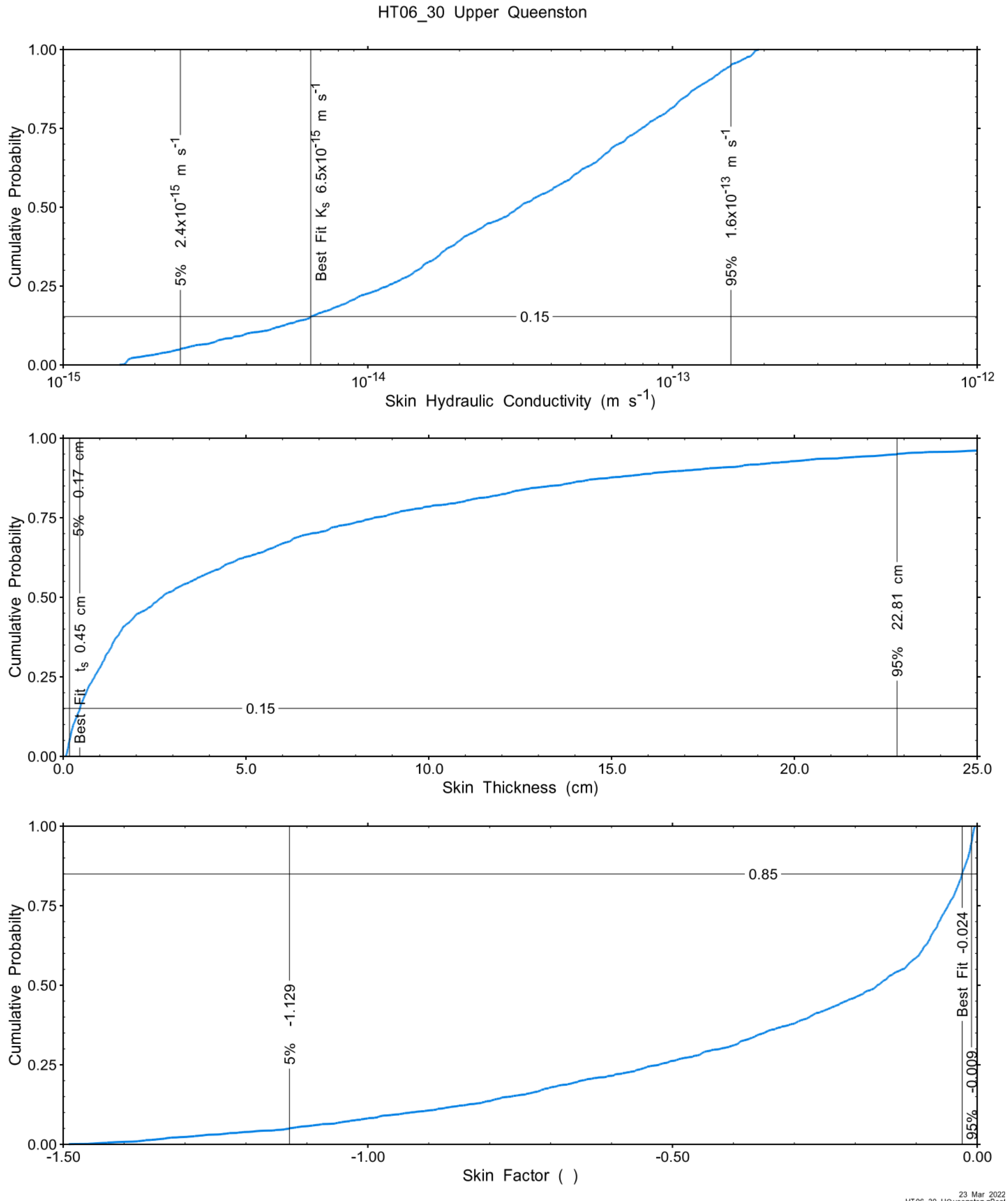

Figure 0.85 Cumulative distribution functions and parameter limits for skin hydraulic conductivity (K_s) (top panel), skin thickness (t_s) (middle panel) and skin factor (s) (bottom panel).

A summary of perturbation results is presented in Figure 0.86, with Ramey-processed perturbations in Figure 0.87. Those perturbations (1851 of 10,000) with all parameters within the 5% and 95% range present a very good fit to the measured test zone data.

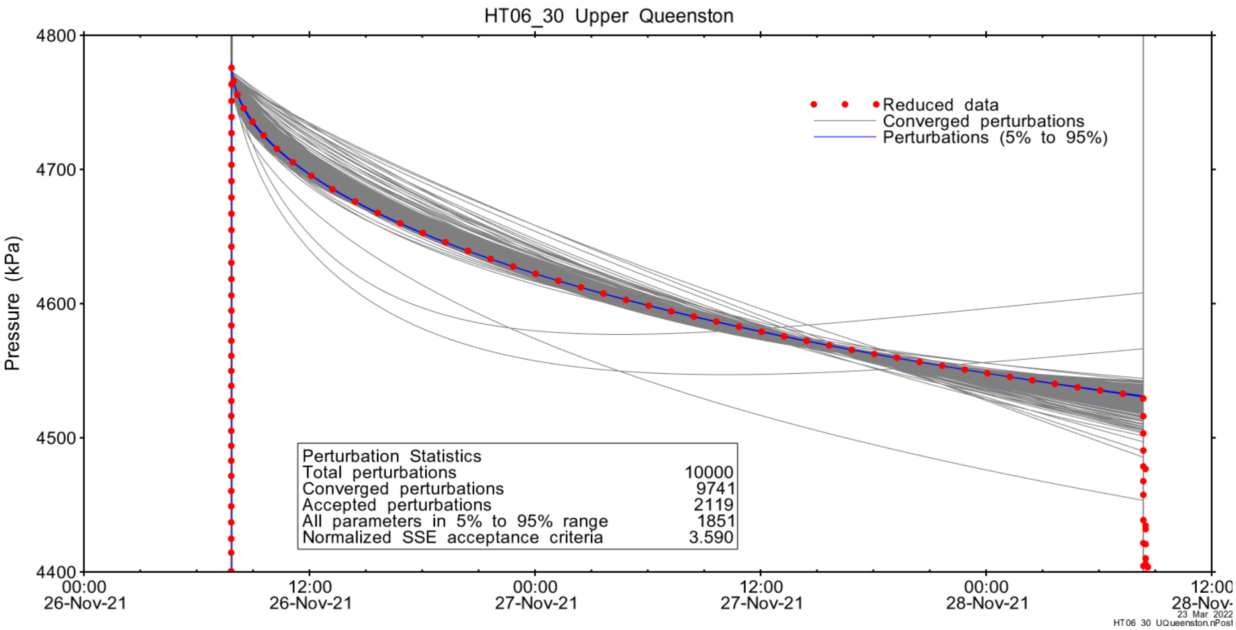

Figure 0.86 Perturbation results – all converged, accepted, and within 5% to 95% for all parameters.

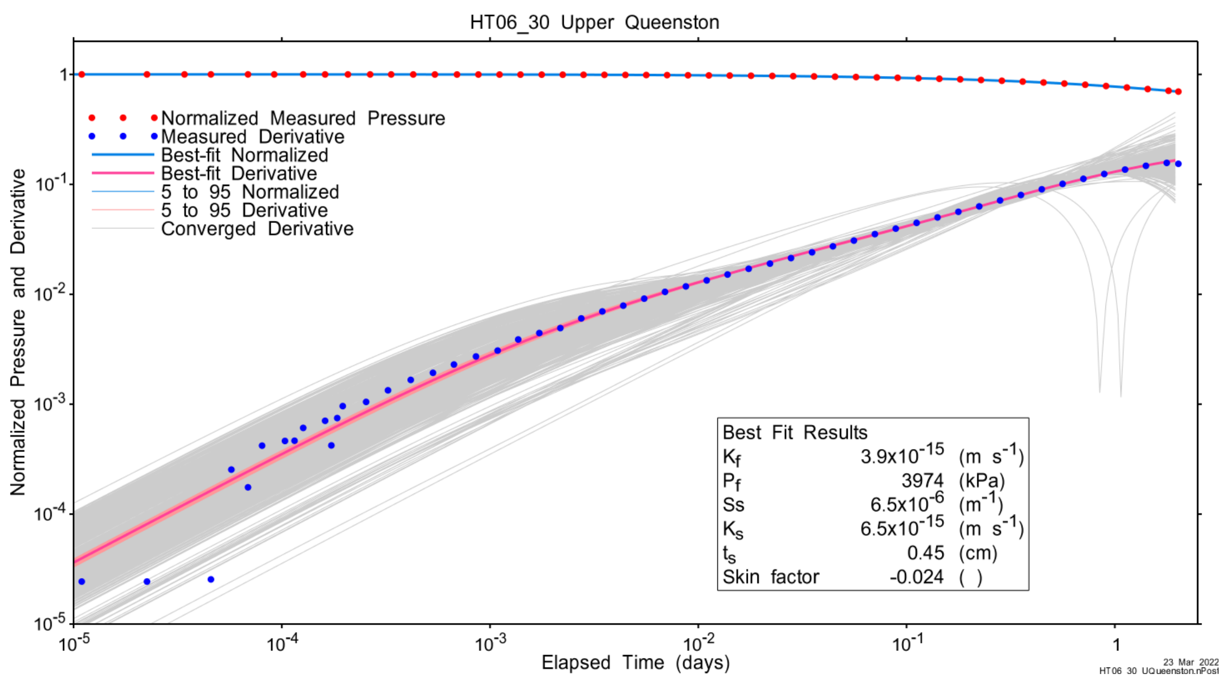

Figure 0.87 Log-log plot showing Ramey B normalized pressure and derivative response for all converged optimizations and those within 5% to 95% for all parameters.

A summary of best-fit parameter estimates and ranges is given in Table 0.29.

Table 0.29 Summary of the HT06_30 parameter estimates.

Parameter	Best Fit	5%	Median	95%
K_f (m/s)	3.9E-15	1.5E-15	1.5E-14	3.3E-14
P_f (kPa)	3974	3801	4243	4369
Ss (1/m)	6.5E-06	5.6E-08	1.1E-06	1.8E-05
K_s (m/s)	6.5E-15	2.4E-15	3.1E-14	1.6E-13
t_s (cm)	0.45	0.17	2.71	22.81
s (-)	-0.024	-1.129	-0.164	-0.009

Parameter correlations for all perturbations with all parameters within the 5% to 95% limits are given in Table 0.30.

Table 0.30 Pearson cross-correlations of 5% to 95% parameters

	Log(K_f)	P_f	Log(Ss)	Log(K_s)	t_s	s
Log(K_f)	1.000	0.994	-0.961	0.989	0.769	-0.805
P_f	0.994	1.000	-0.942	0.976	0.738	-0.774
Log(Ss)	-0.961	-0.942	1.000	-0.991	-0.913	0.937
Log(K_s)	0.989	0.976	-0.991	1.000	0.853	-0.883
t_s	0.769	0.738	-0.913	0.853	1.000	-0.996
s	-0.805	-0.774	0.937	-0.883	-0.996	1.000

A.6.4 Additional Figures

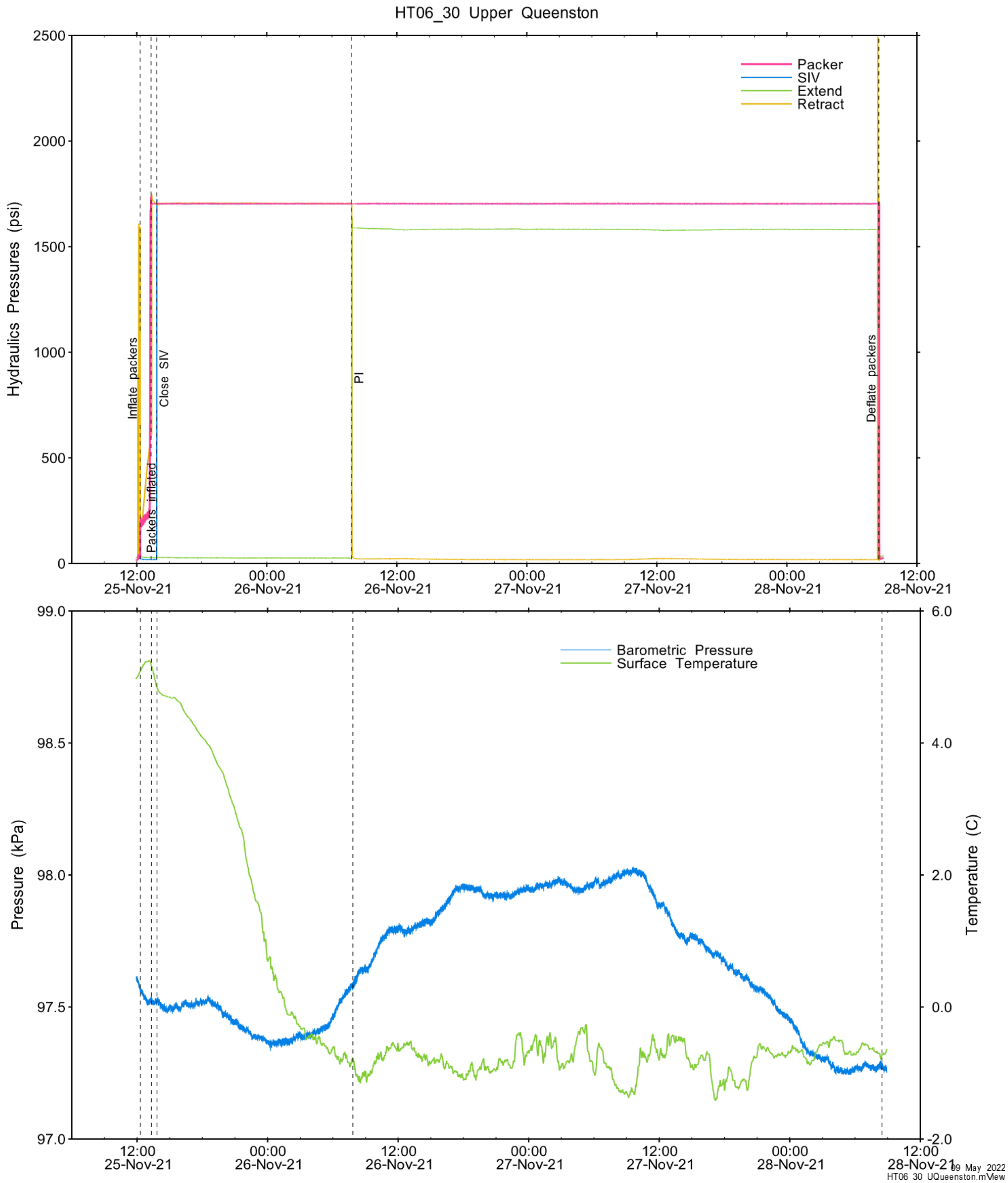

Figure 0.88 Hydraulics pressures and surface temperature/barometric pressure.

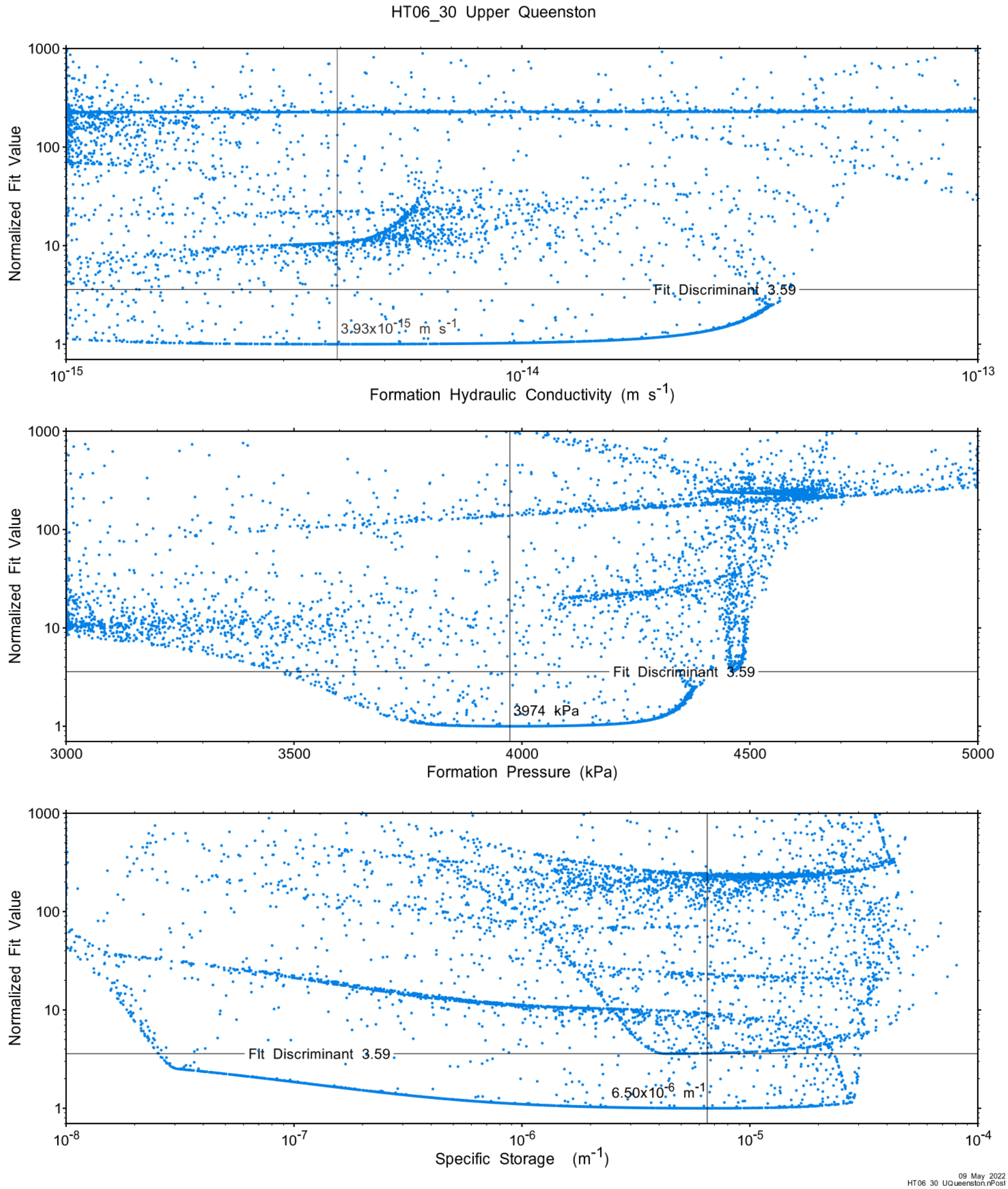

Figure 0.89 XY-scatter plot showing the formation parameter space normalized fit values.

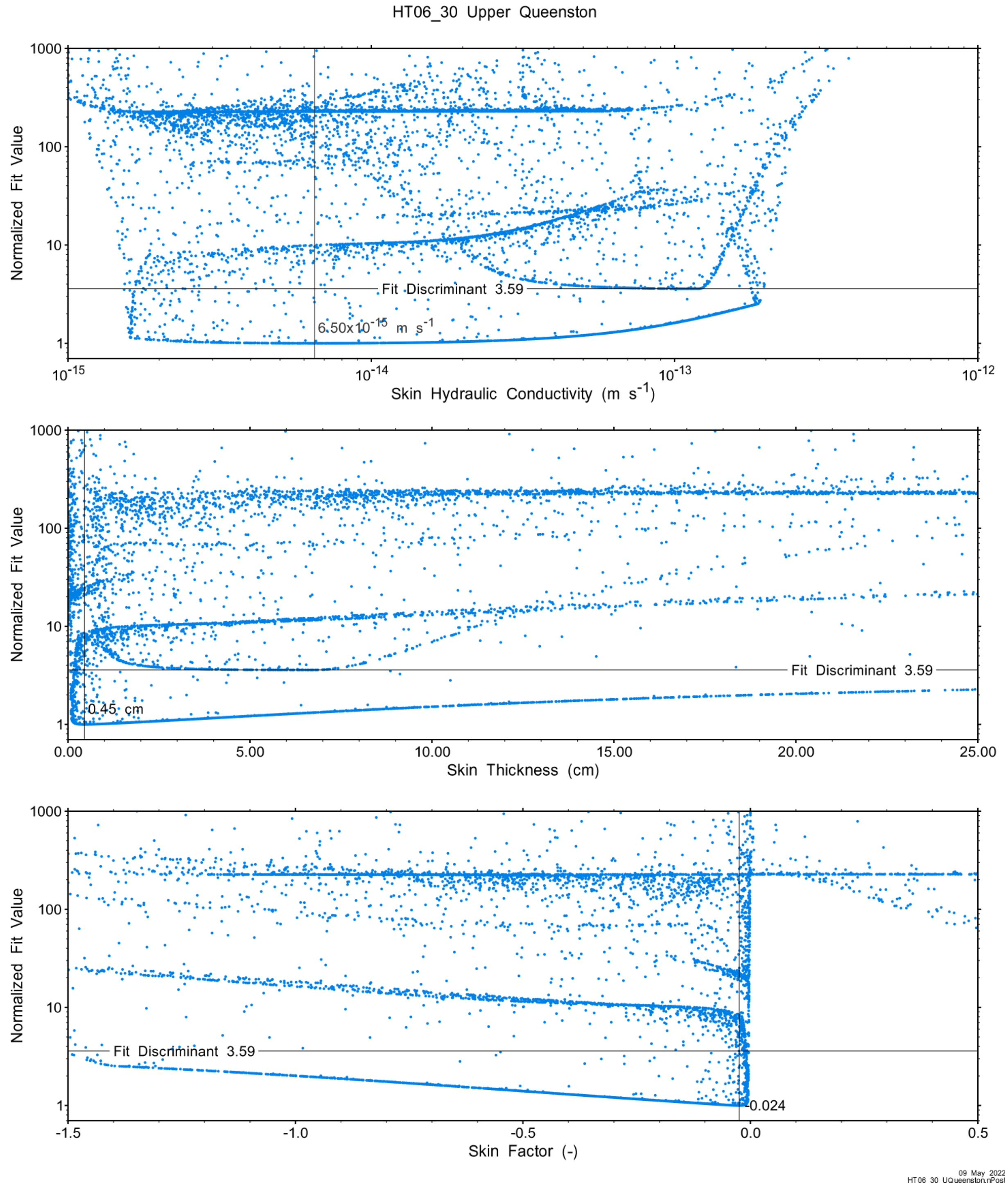

Figure 0.90 XY-scatter plot showing the skin parameter space normalized fit values.

A.7 HT07_30 Lower Queenston

The SB_BH01 interval from 463.00 to 493.05 mBGS tested in HT07_30 was contained entirely within the lower portion of the Queenston Formation. A single PI test with a duration of 2 days was conducted.

A.7.1 Test Data Summary

Table 0.31 and Figure 0.91 provide a summary of test events and a plot of pressures measured while testing, respectively.

Table 0.31 HT07_30 Summary of Test Events.

Event	Start Date & Time	Duration (days)	TZ Pressure (kPa)
Drilling intercept	21-08-13 02:00	99.53	4738
Prior testing	21-11-20 14:45	10.08	variable
Shut-in	21-11-30 16:44	0.68	4740
Pulse injection	21-12-01 09:11	1.94	5201
Test end	21-12-03 07:45		4847

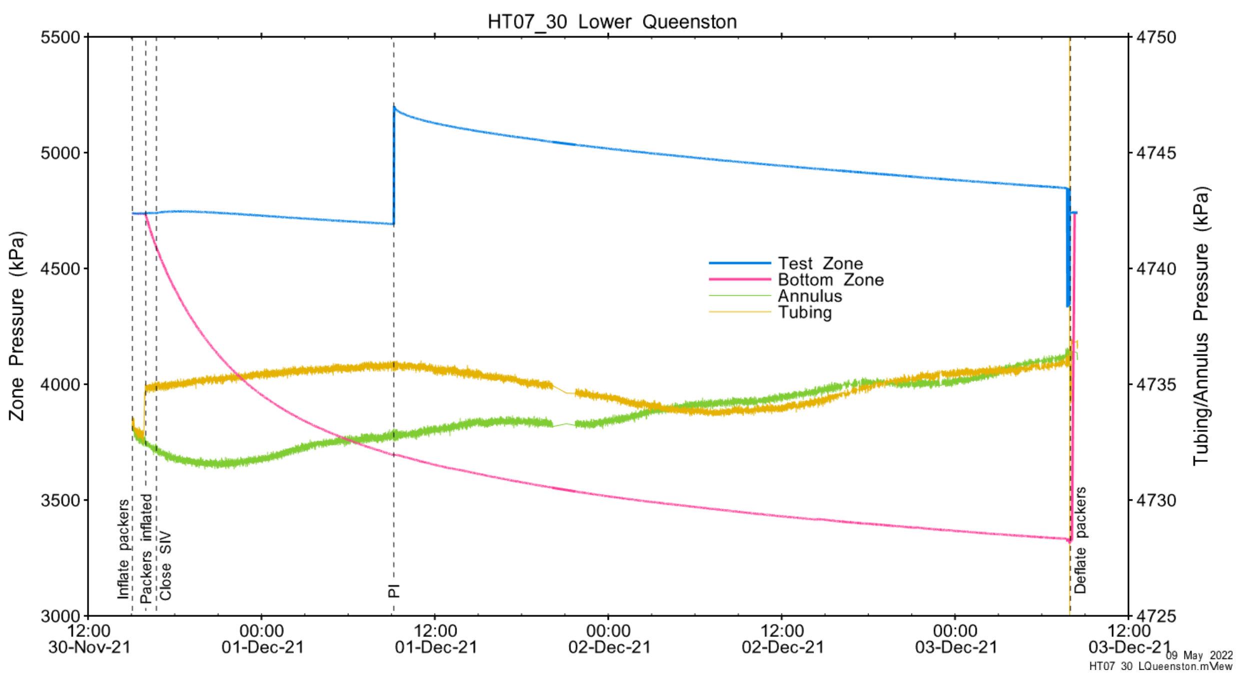

Figure 0.91 HT07_30 test events and pressures.

A.7.2 Test Analyses

Table 0.32 is a summary of test-specific input parameters used in the analyses, while Table 0.33 presents the optimized parameters and allowed ranges.

Table 0.32 nSIGHTS Input Parameters.

Parameter	Value	Units
Test zone radius	6.77	cm
Test zone compressibility	4.65E-10	1/Pa
Test zone fluid density	1050	g/L
Test zone length	30.05	m

Table 0.33 nSIGHTS Parameter Optimization Ranges.

Parameter	Minimum	Maximum	Units	Type
Formation hydraulic conductivity (K_f)	1E-16	1E-12	m/s	log
Formation pressure (P_f)	0	4000	kPa	linear
Specific storage (Ss)	1E-08	1E-04	1/m	log
Skin hydraulic conductivity (K_s)	1E-16	1E-10	m/s	log
Skin thickness (t_s)	0.1	932	mm	linear

Figure 0.92 shows the measured test zone pressure record (with reduced data density for clarity) used in the analysis along with the best-fit simulation and parameter values. Figure 0.93 presents the pre-test history, and Figure 0.94 shows the Ramey B normalized best-fit pressure and pressure derivatives.

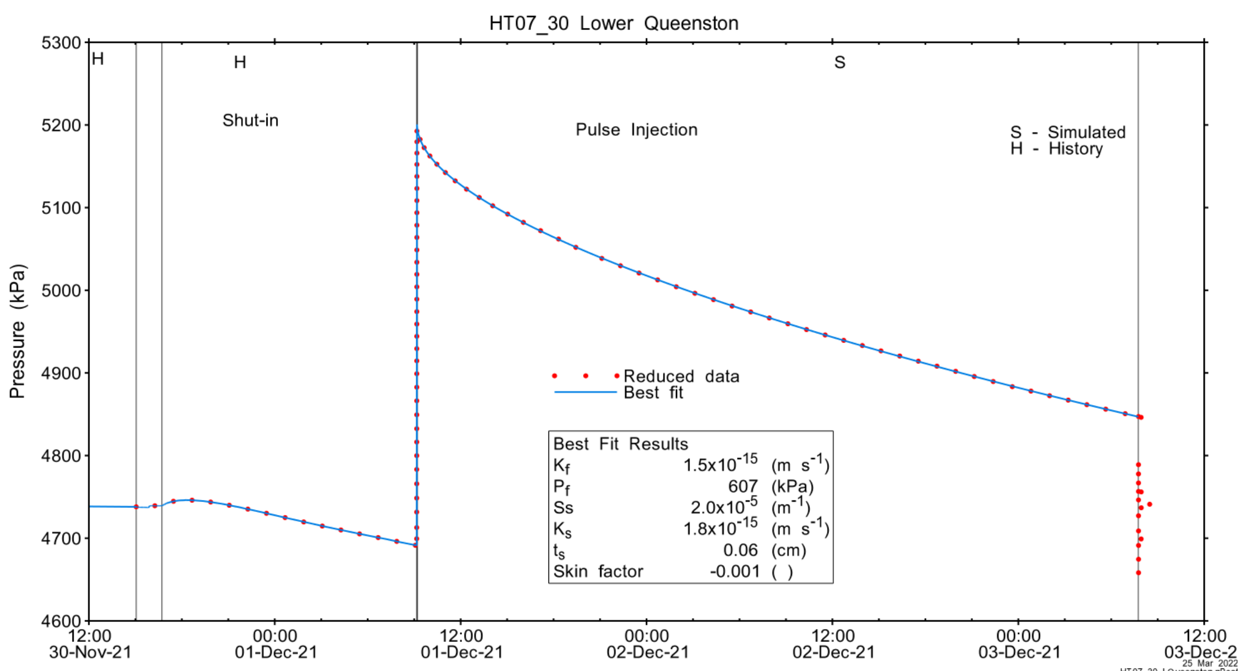

Figure 0.92 Annotated testing sequence showing best-fit simulation and parameter estimates.

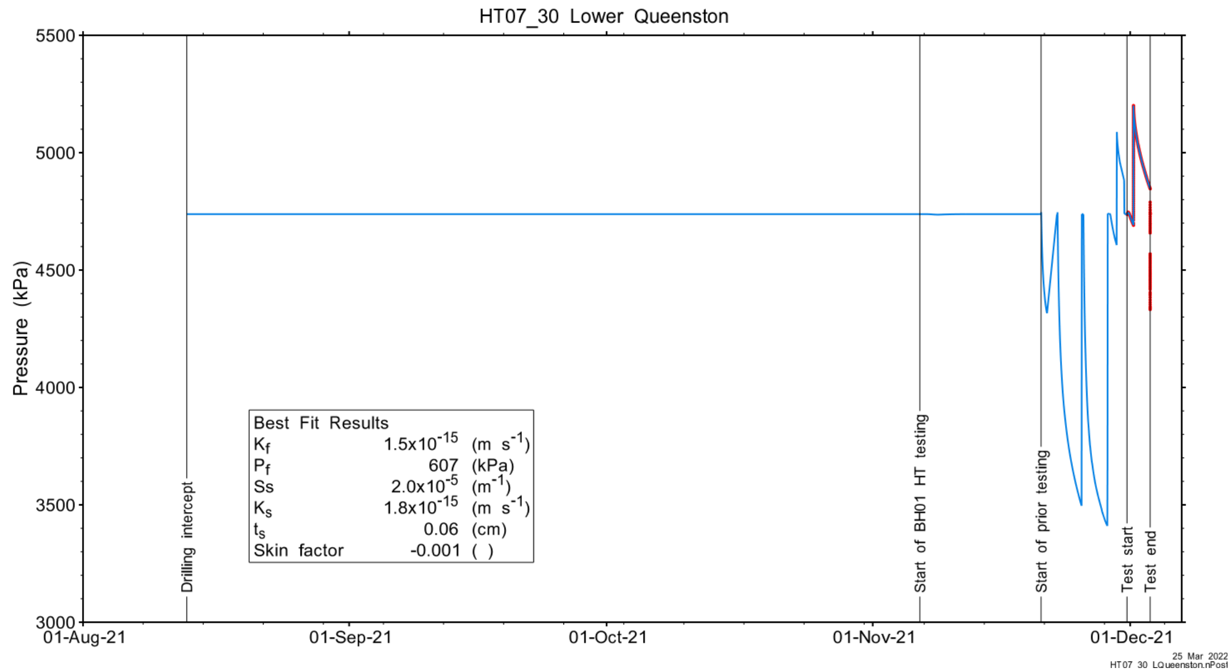

Figure 0.93 Annotated HT07_30 testing sequence showing pre-test history, best-fit simulation and parameter estimates.

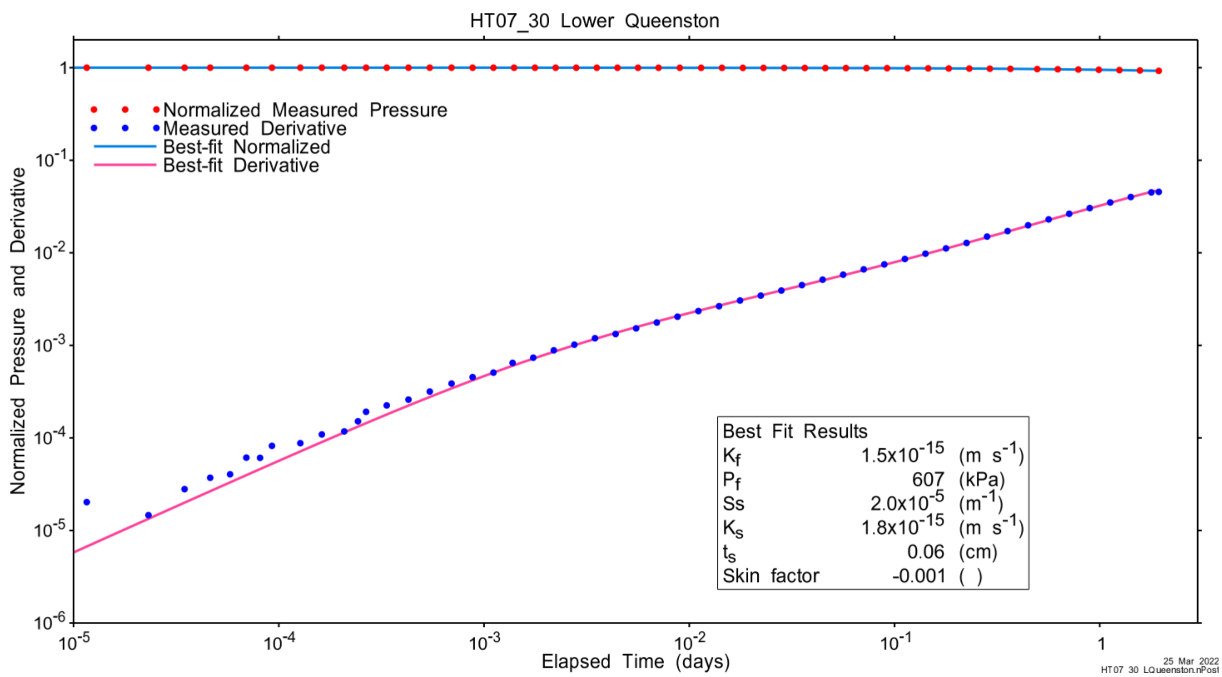

Figure 0.94 Log-log plot showing Ramey B normalized pressure and derivative response for best-fit simulation.

Figure 0.95 shows the normalized parameter sensitivity response for the best fit. Skin-related parameters are most sensitive during the early-time response. Sensitivity to K_f, P_f, and Ss is continuing to increase – additional test duration may have improved the estimates.

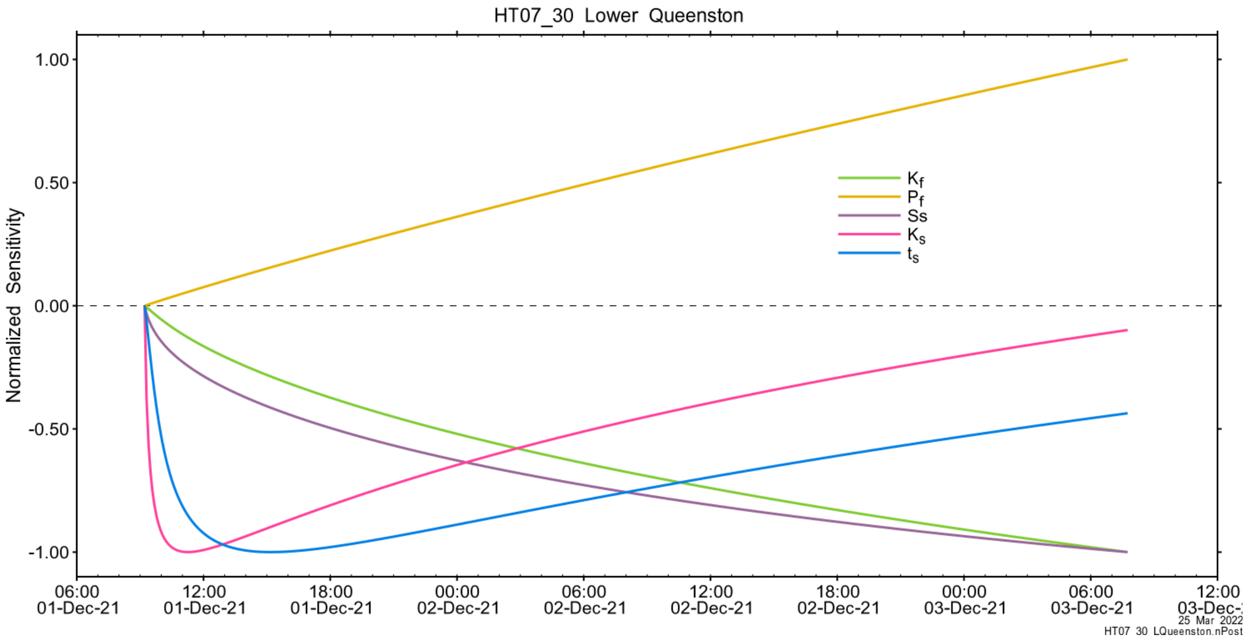

Figure 0.95 Normalized Jacobian for best-fit simulation.

A.7.3 Uncertainty Analyses

The CDF of normalized fit values for all converged simulations and the selected fit discriminant are shown in Figure 0.96.

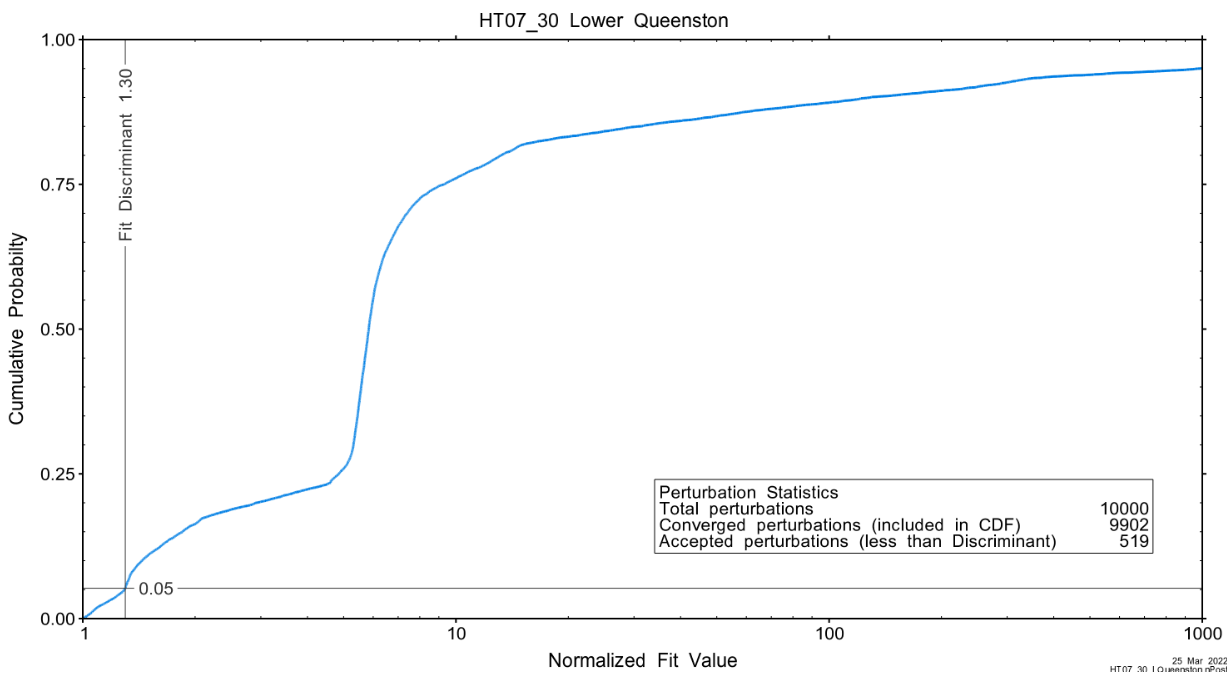

Figure 0.96 Fit value cumulative distribution function.

Summary cross parameter scatter plots for selected formation and skin parameters are given in Figure 0.97 and Figure 0.98. The light pink dots on the figures are the initial parameter estimates, with red dots overlaying those initial parameter values that resulted in accepted optimization results. The grey dots are converged optimizations which did not meet the fit discriminant. Larger varying color symbols represent the fit value of accepted optimizations, with the blue values representing the best fit.

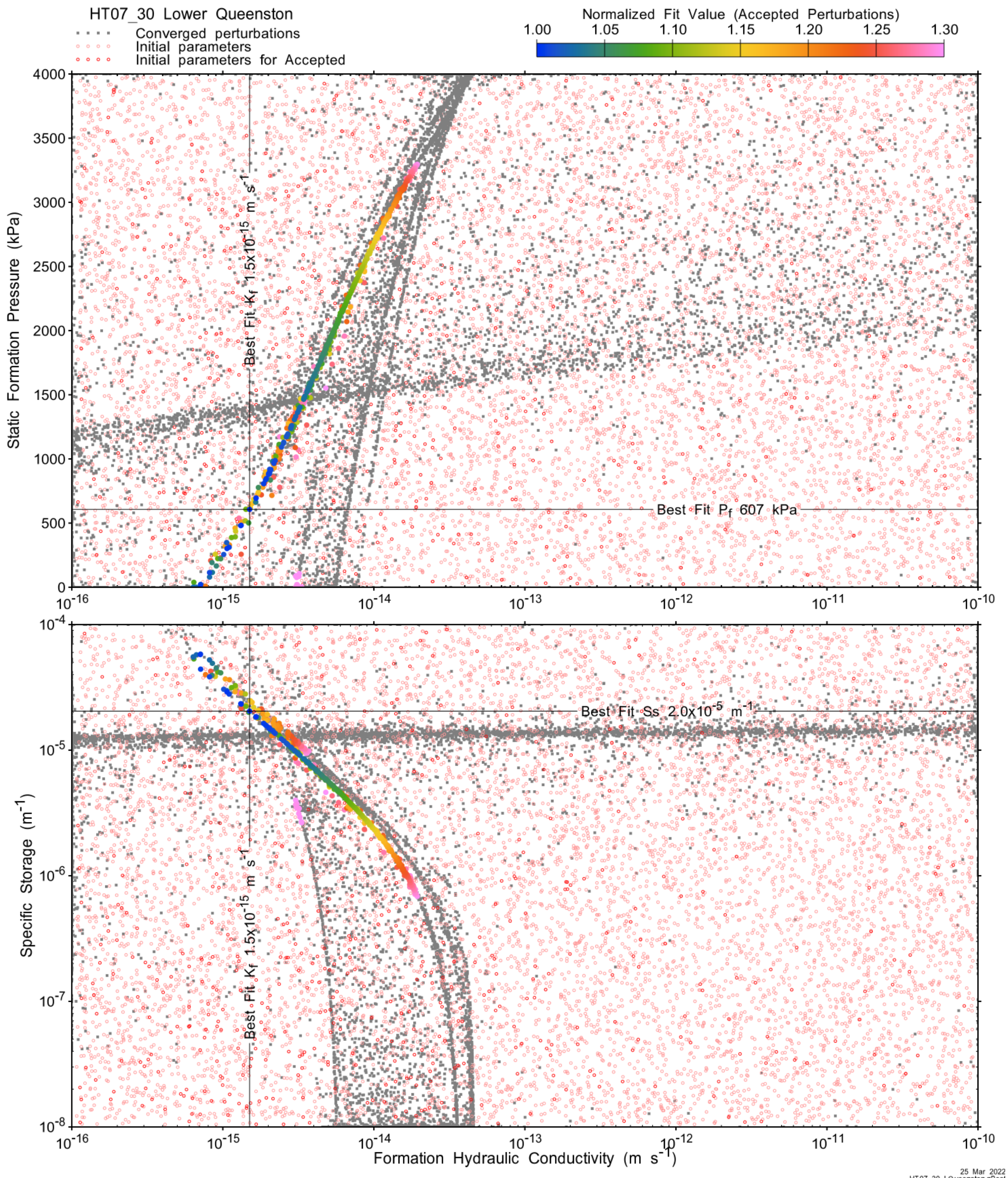

Figure 0.97 XY-scatter plot showing estimates of formation hydraulic conductivity (K_f) vs static formation pressure (P_f) (top panel) and specific storage (Ss) (bottom panel).

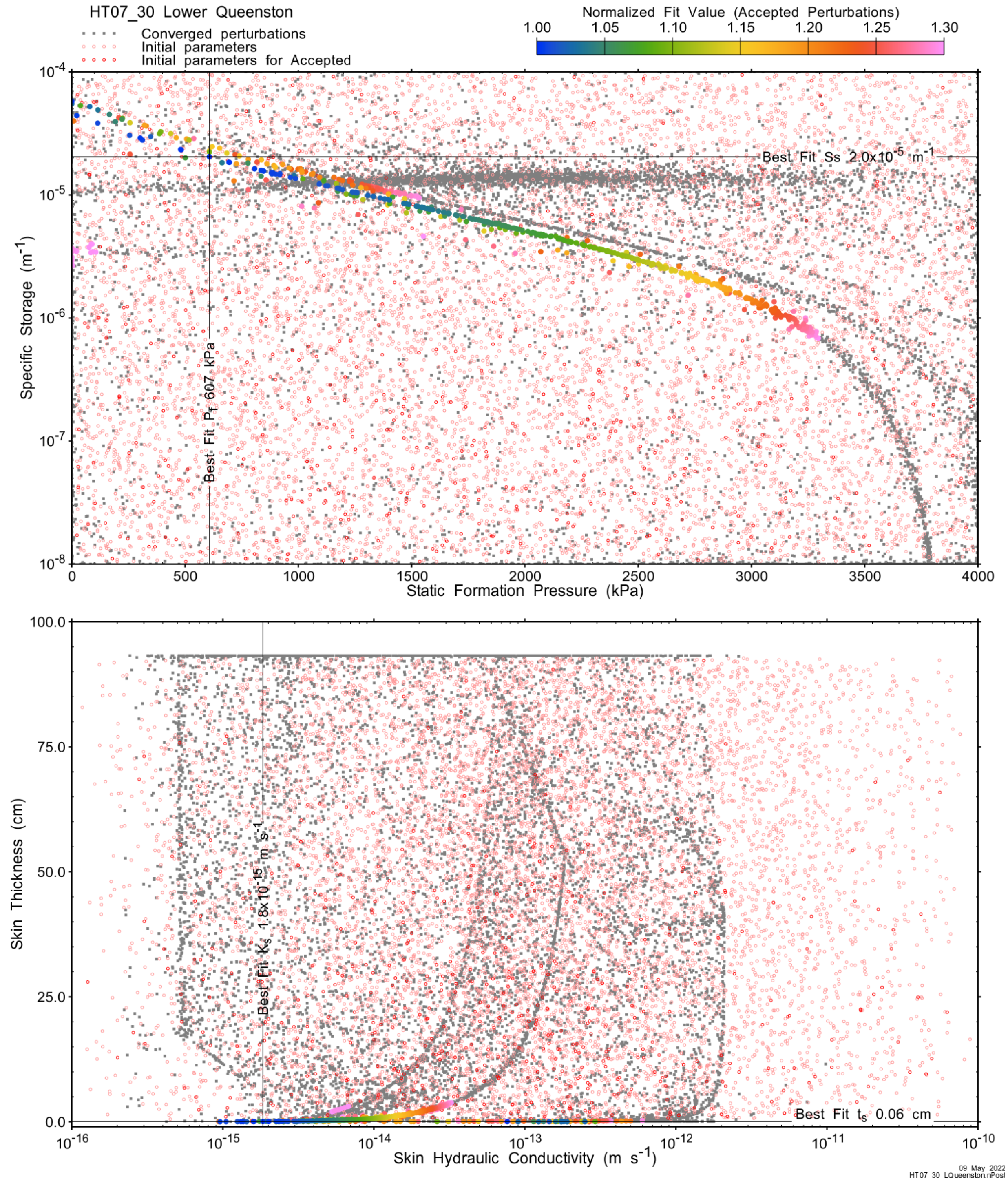

Figure 0.98 XY-scatter plot showing estimates of static formation pressure (P_f) vs specific storage (Ss) (top panel) and skin hydraulic conductivity (K_s) vs skin thickness (t_s) (bottom panel).

Confidence limits and median values are determined from the CDF of accepted optimization results (i.e. the varying color values in the above figures), with best fit value, 5% and 95% confidence indicated on Figure 0.99 and Figure 0.100.

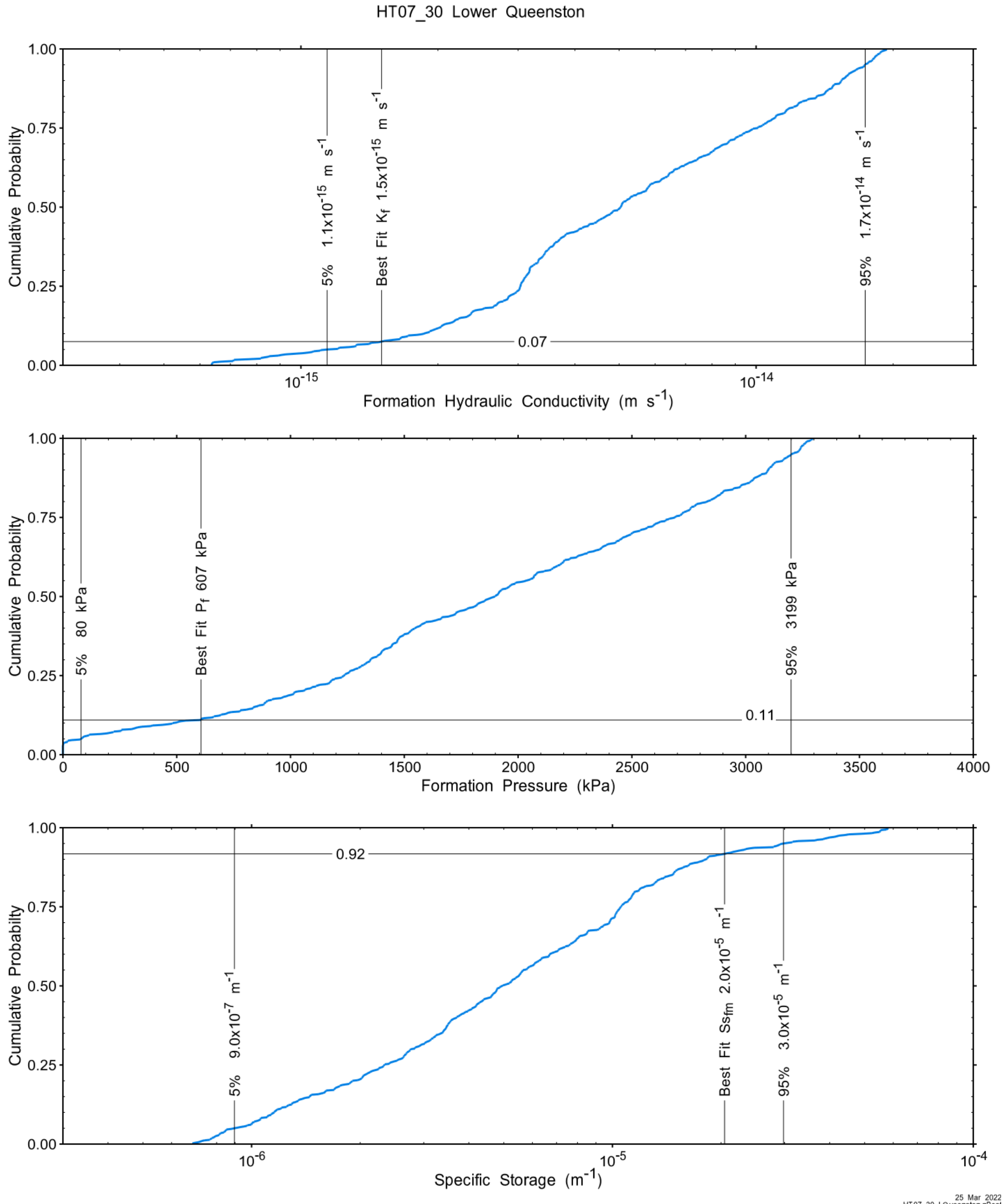

Figure 0.99 Cumulative distribution functions and parameter limits for formation hydraulic conductivity (K_f) (top panel), static formation pressure (P_f) (middle panel) and specific storage (Ss) (bottom panel).

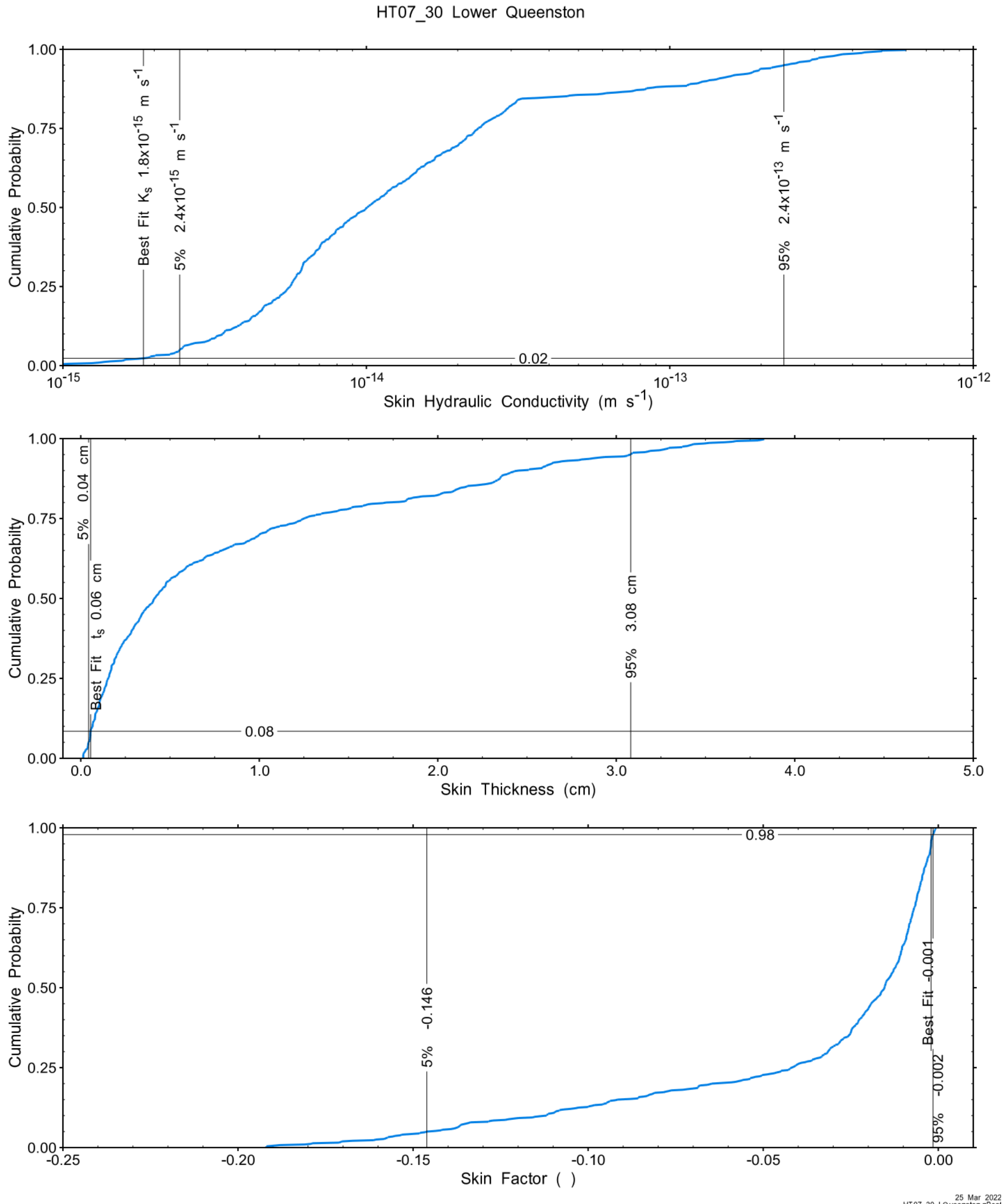

Figure 0.100 Cumulative distribution functions and parameter limits for skin hydraulic conductivity (K_s) (top panel), skin thickness (t_s) (middle panel) and skin factor (s) (bottom panel).

A summary of perturbation results is presented in Figure 0.101, with Ramey processed perturbations in Figure 0.102. Those perturbations (404 of 10,000) with all parameters within the 5% and 95% range present a very good fit to the measured test zone data.

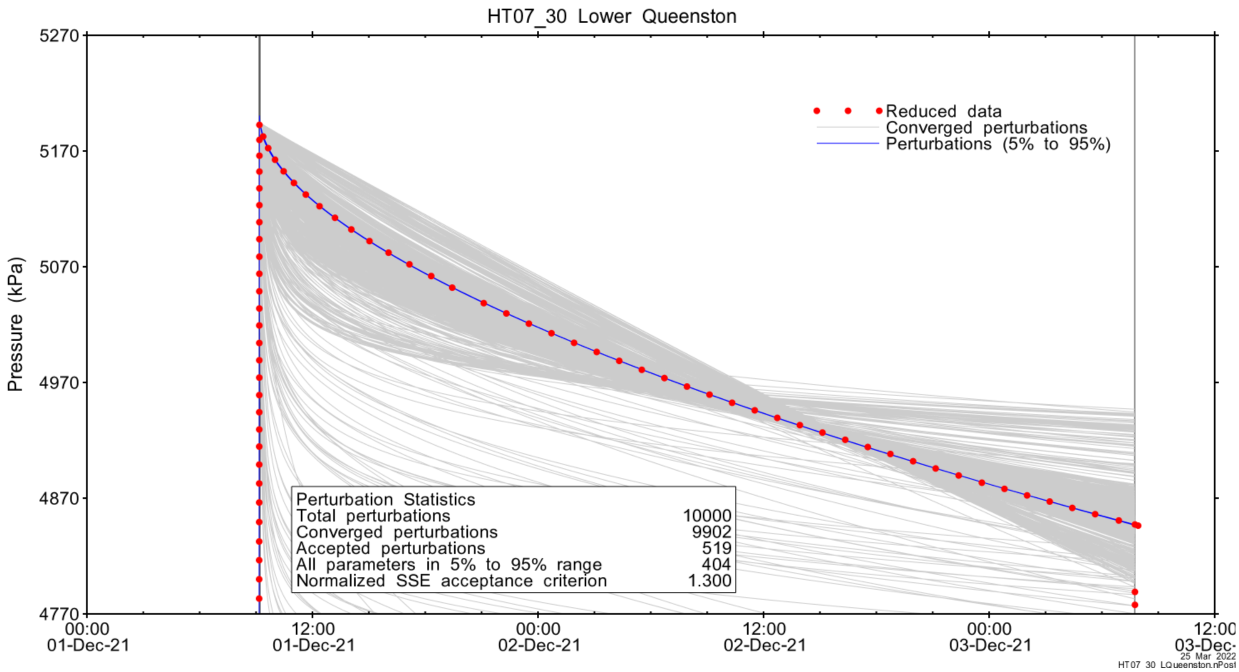

Figure 0.101 Perturbation results – all converged, accepted, and within 5% to 95% for all parameters.

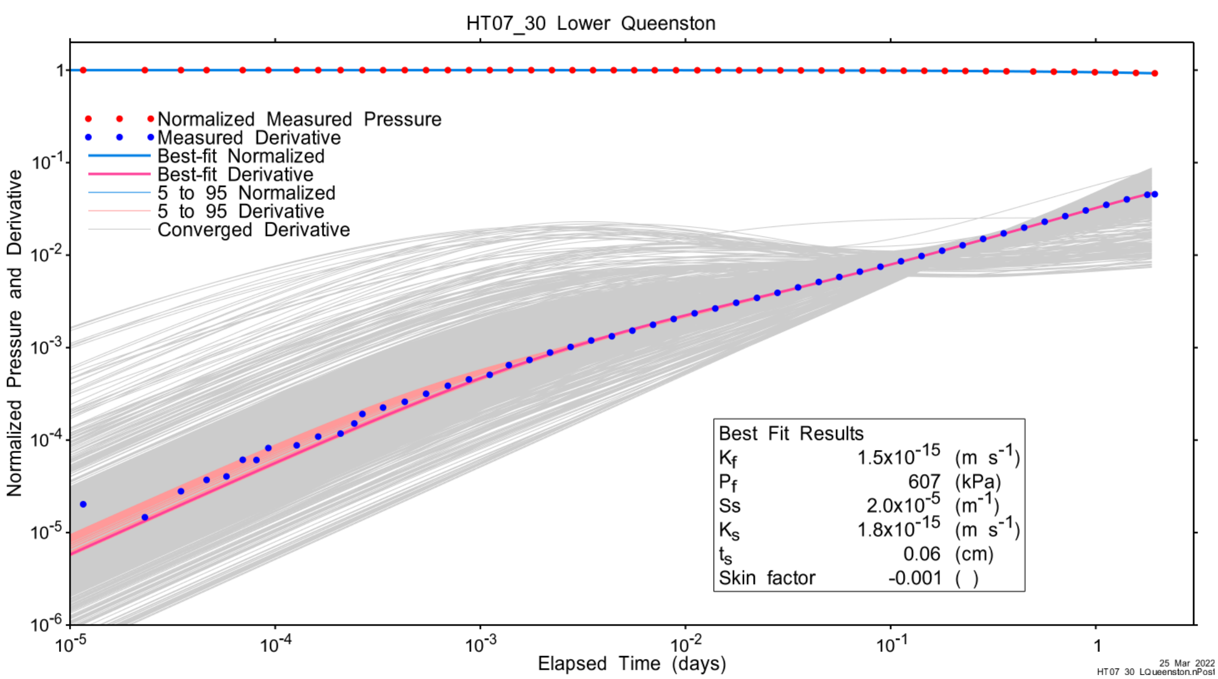

Figure 0.102 Log-log plot showing Ramey B normalized pressure and derivative response for all converged optimizations and those within 5% to 95% for all parameters.

A summary of best-fit parameter estimates and ranges is given in Table 0.34.

Table 0.34 Summary of the HT07_30 parameter estimates.

Parameter	Best Fit	5%	Median	95%
K_f (m/s)	1.5E-15	1.1E-15	5.0E-15	1.7E-14
P_f (kPa)	607	80	1899	3199
Ss (1/m)	2.0E-05	9.0E-07	5.0E-06	3.0E-05
K_s (m/s)	1.8E-15	2.4E-15	1.0E-14	2.4E-13
t_s (cm)	0.06	0.04	0.41	3.08
s (-)	-0.001	-0.146	-0.015	-0.002

Parameter correlations for all perturbations with all parameters within the 5% to 95% limits are given in Table 0.35

Table 0.35 Pearson cross-correlations of 5% to 95% parameters

	Log(K_f)	P_f	Log(Ss)	Log(K_s)	t_s	s
Log(K_f)	1.000	0.978	-0.986	0.159	0.827	-0.699
P_f	0.978	1.000	-0.934	0.172	0.732	-0.585
Log(Ss)	-0.986	-0.934	1.000	-0.118	-0.895	0.783
Log(K_s)	0.159	0.172	-0.118	1.000	0.246	-0.363
t_s	0.827	0.732	-0.895	0.246	1.000	-0.969
s	-0.699	-0.585	0.783	-0.363	-0.969	1.000

A.7.4 Additional Figures

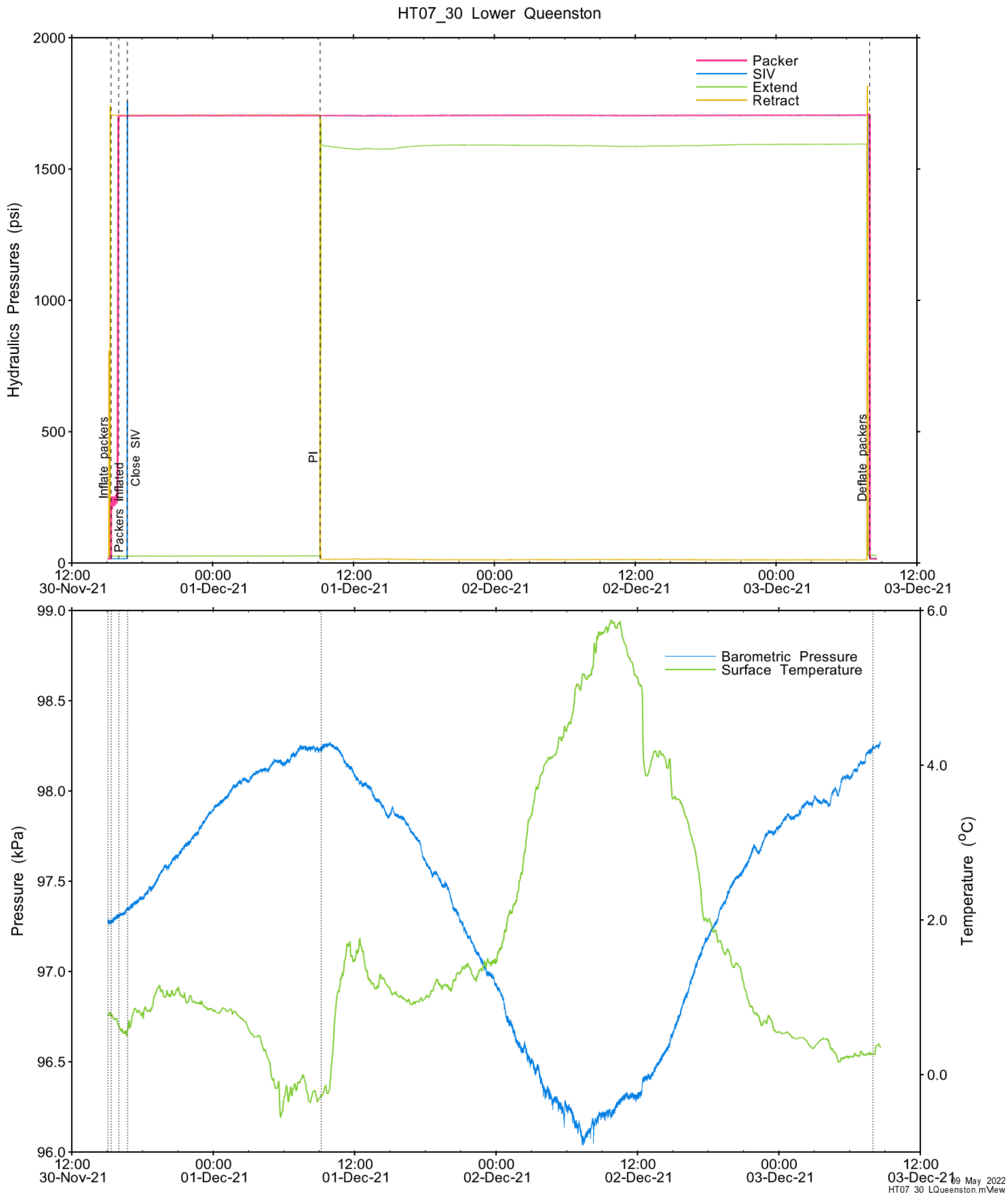

Figure 0.103 Hydraulics pressures and surface temperature/barometric pressure.

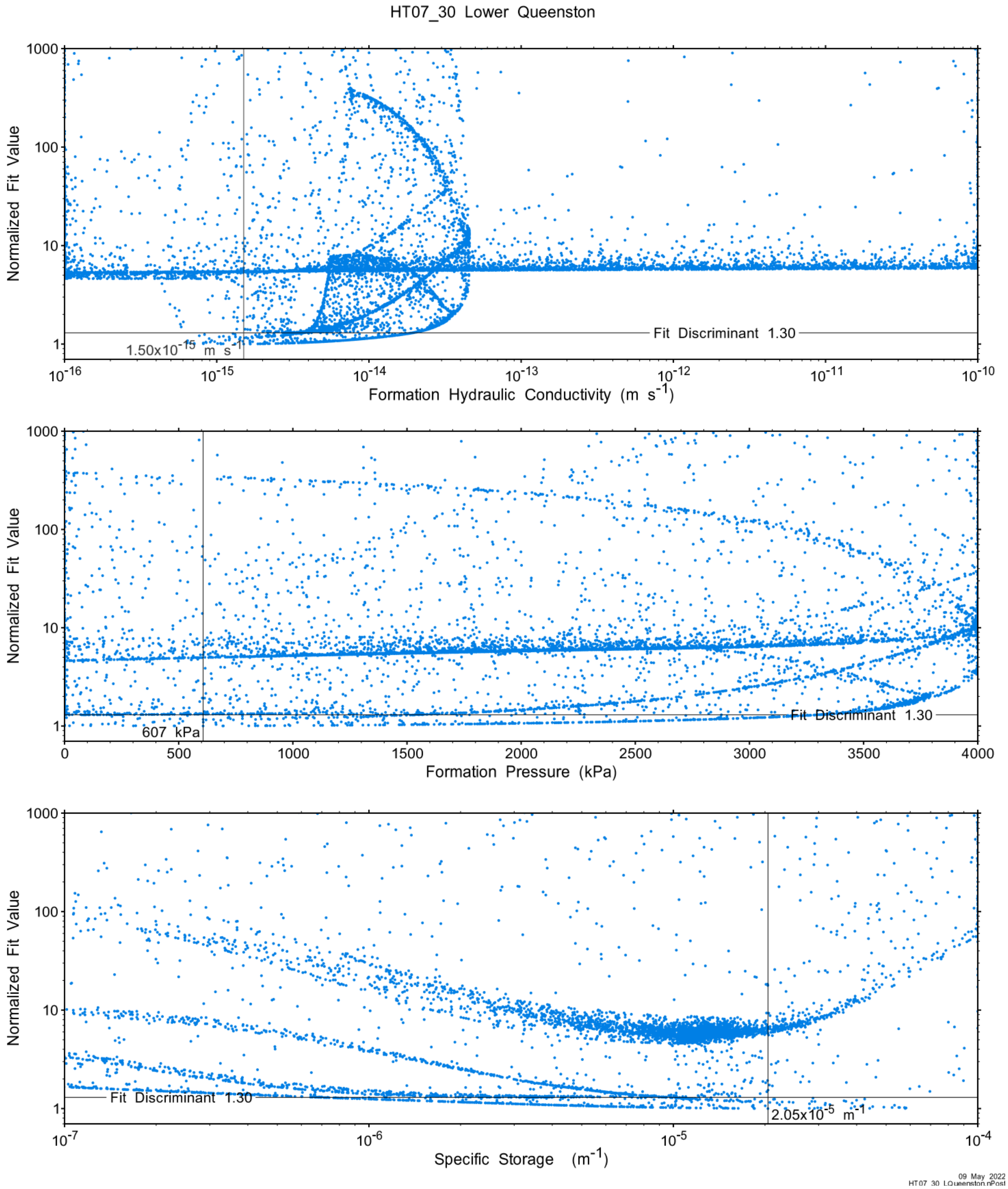

Figure 0.104 XY-scatter plot showing the formation parameter space normalized fit values.

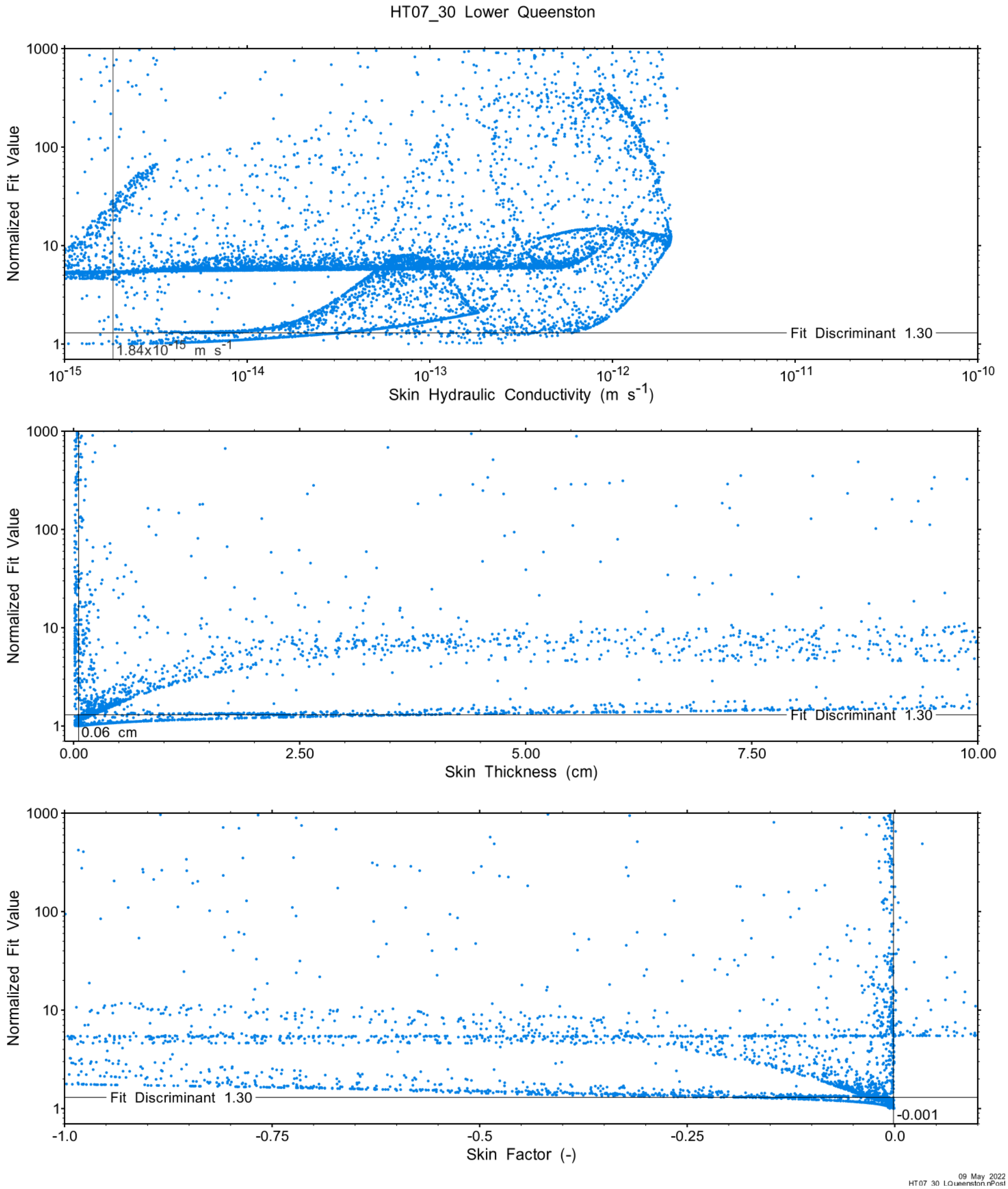

Figure 0.105 XY-scatter plot showing the skin parameter space normalized fit values.

A.8 HT08_30 Upper Georgian Bay

The SB_BH01 interval from 509.00 to 539.05 mBGS tested in HT08_30 was contained entirely within the upper portion of the Georgian Bay Formation. A single PI test with a duration of 2 days was conducted.

A.8.1 Test Data Summary

Table 0.36 and Figure 0.106 provide a summary of test events and a plot of pressures measured while testing, respectively.

Table 0.36 HT08_30 Summary of Test Events.

Event	Start Date & Time	Duration (days)	TZ Pressure (kPa)
Drilling intercept	21-08-15 10:30	97.18	5207
Prior testing	21-11-20 14:45	20.96	variable
Shut-in	21-12-03 18:28	0.58	4740
Pulse injection	21-12-04 08:22	2.00	5621
Test end	21-12-06 08:15		5126

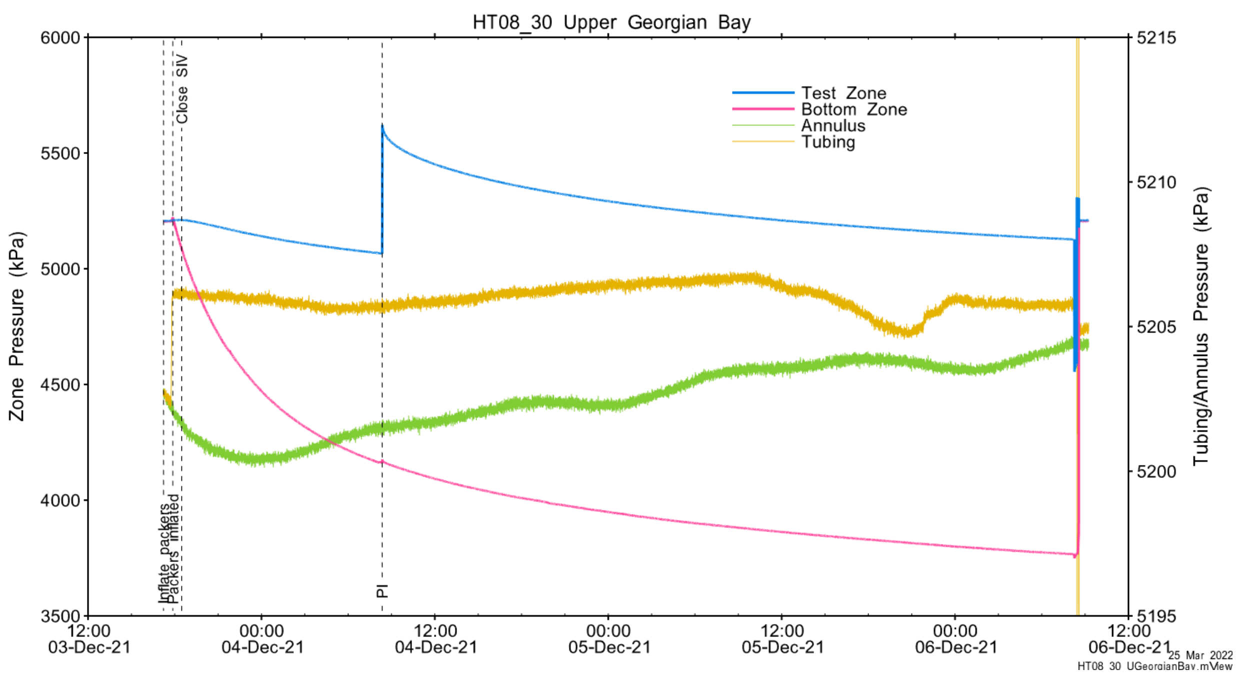

Figure 0.106 HT08_30 test events and pressures.

A.8.2 Test Analyses

Table 0.37 is a summary of test specific input parameters used in the analyses, while Table 0.38 presents the optimized parameters and allowed ranges.

Table 0.37 nSIGHTS Input Parameters

Parameter	Value	Units
Test zone radius	6.43	cm
Test zone compressibility	4.75E-10	1/Pa
Test zone fluid density	1050	g/L
Test zone length	30.05	m

Table 0.38 nSIGHTS Parameter Optimization Ranges

Parameter	Minimum	Maximum	Units	Type
Formation hydraulic conductivity (K_f)	1E-15	1E-12	m/s	log
Formation pressure (P_f)	3000	6000	kPa	linear
Specific storage (Ss)	1E-08	1E-04	1/m	log
Skin hydraulic conductivity (K_s)	1E-15	1E-12	m/s	log
Skin thickness (t_s)	0.1	936	mm	linear

Figure 0.107 shows the measured test zone pressure record (with reduced data density for clarity) used in the analysis along with the best-fit simulation and parameter values. Figure 0.108 presents the pre-test history, and Figure 0.109 shows the Ramey B normalized best-fit pressure and pressure derivatives.

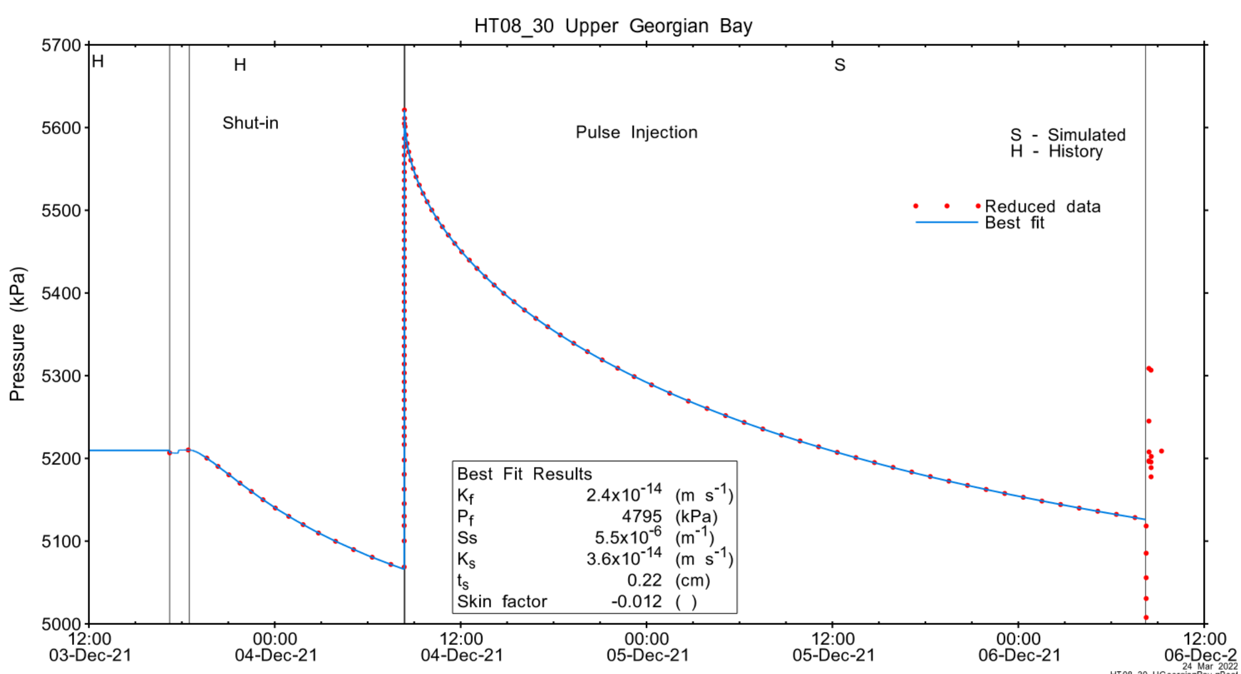

Figure 0.107 Annotated testing sequence showing best-fit simulation and parameter estimates.

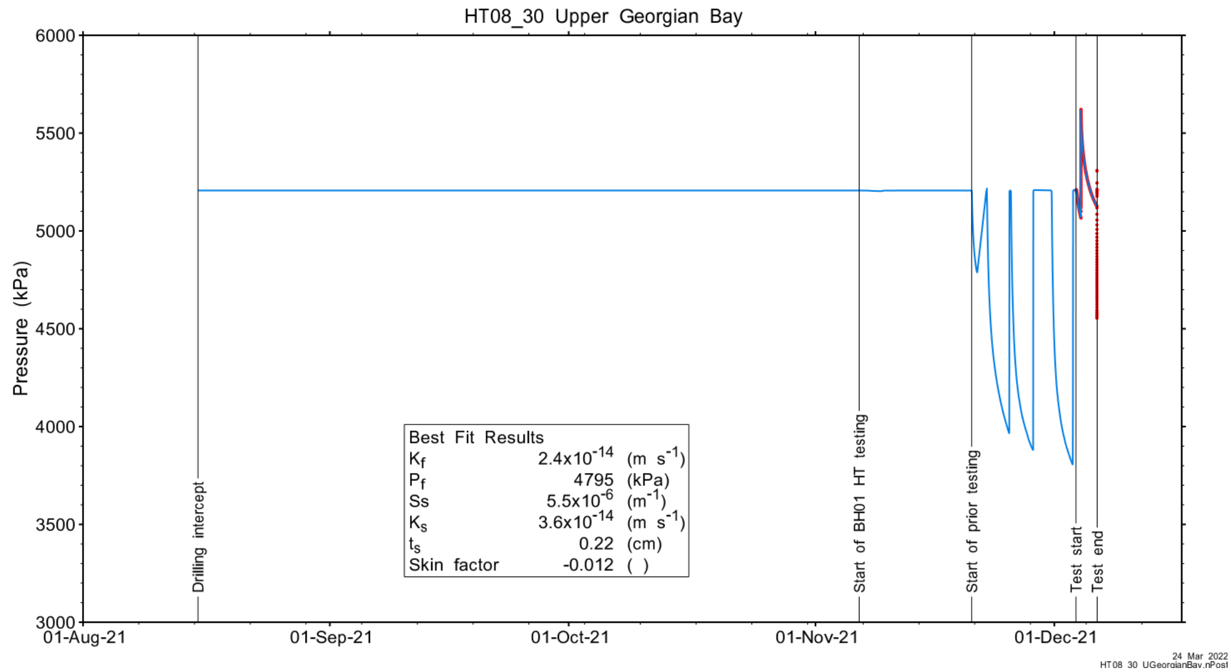

Figure 0.108 Annotated HT08_30 testing sequence showing pre-test history, best-fit simulation and parameter estimates.

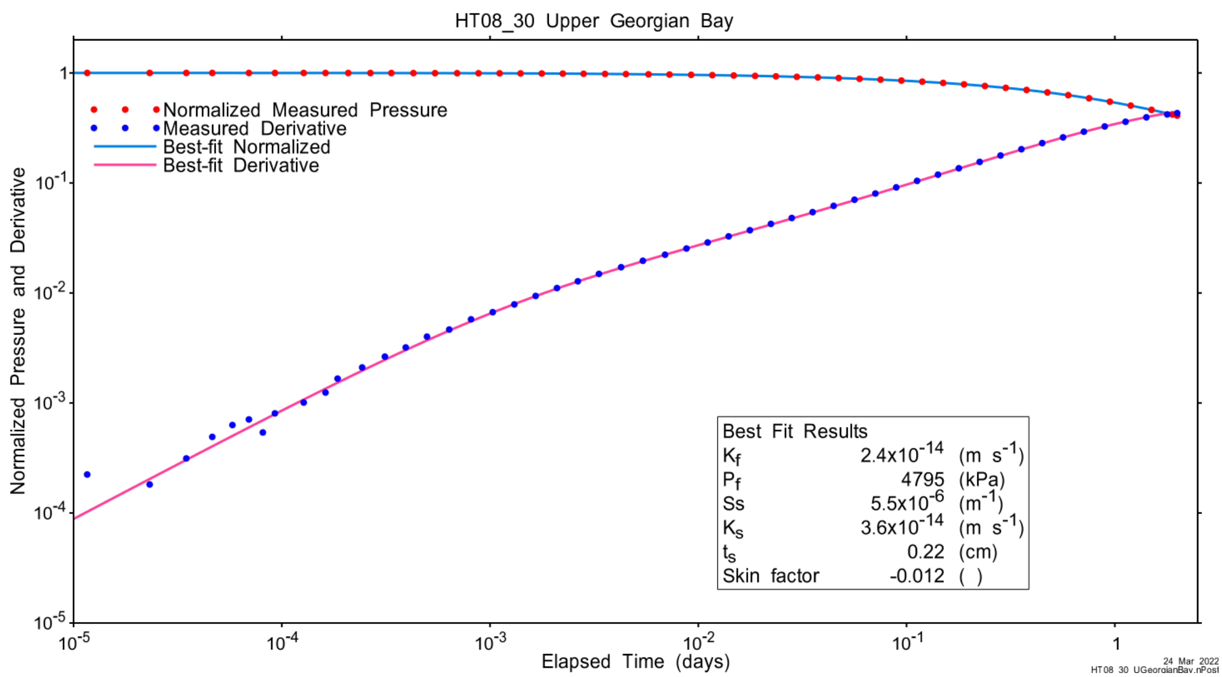

Figure 0.109 Log-log plot showing Ramey B normalized pressure and derivative response for best-fit simulation.

Figure 0.110 shows the normalized parameter sensitivity response for the best fit. Skin-related parameters are most sensitive during the early-time response. K_f response is nearly flat at the test end, indicating that the estimate would not be significantly improved by increased test duration. P_f is continuing to rise – additional test duration may have improved the fit.

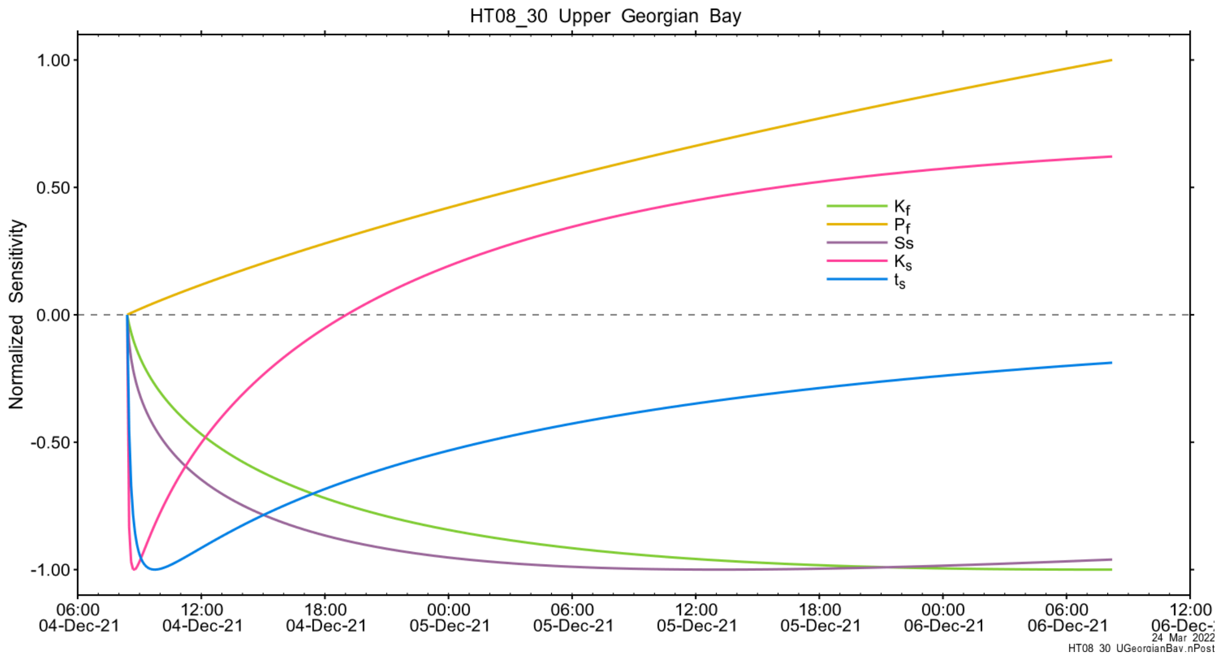

Figure 0.110 Normalized Jacobian for best-fit simulation.

A.8.3 Uncertainty Analyses

The CDF of normalized fit values for all converged simulations and the selected fit discriminant are shown in Figure 0.111.

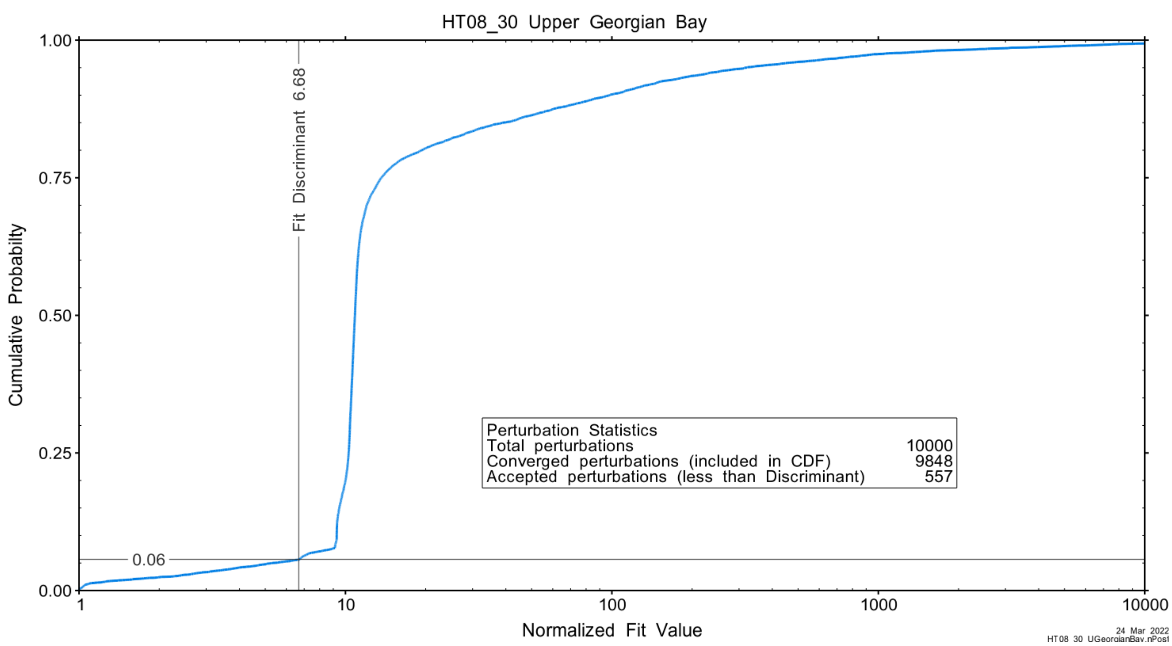

Figure 0.111 Fit value cumulative distribution function.

Summary cross parameter scatter plots for selected formation and skin parameters are given in Figure 0.112 and Figure 0.113. The light pink dots on the figures are the initial parameter estimates, with red dots overlaying those initial parameter values that resulted in accepted optimization results. The grey dots are converged optimizations which did not meet the fit discriminant. Larger varying color symbols represent the fit value of accepted optimizations, with the blue values representing the best fit.

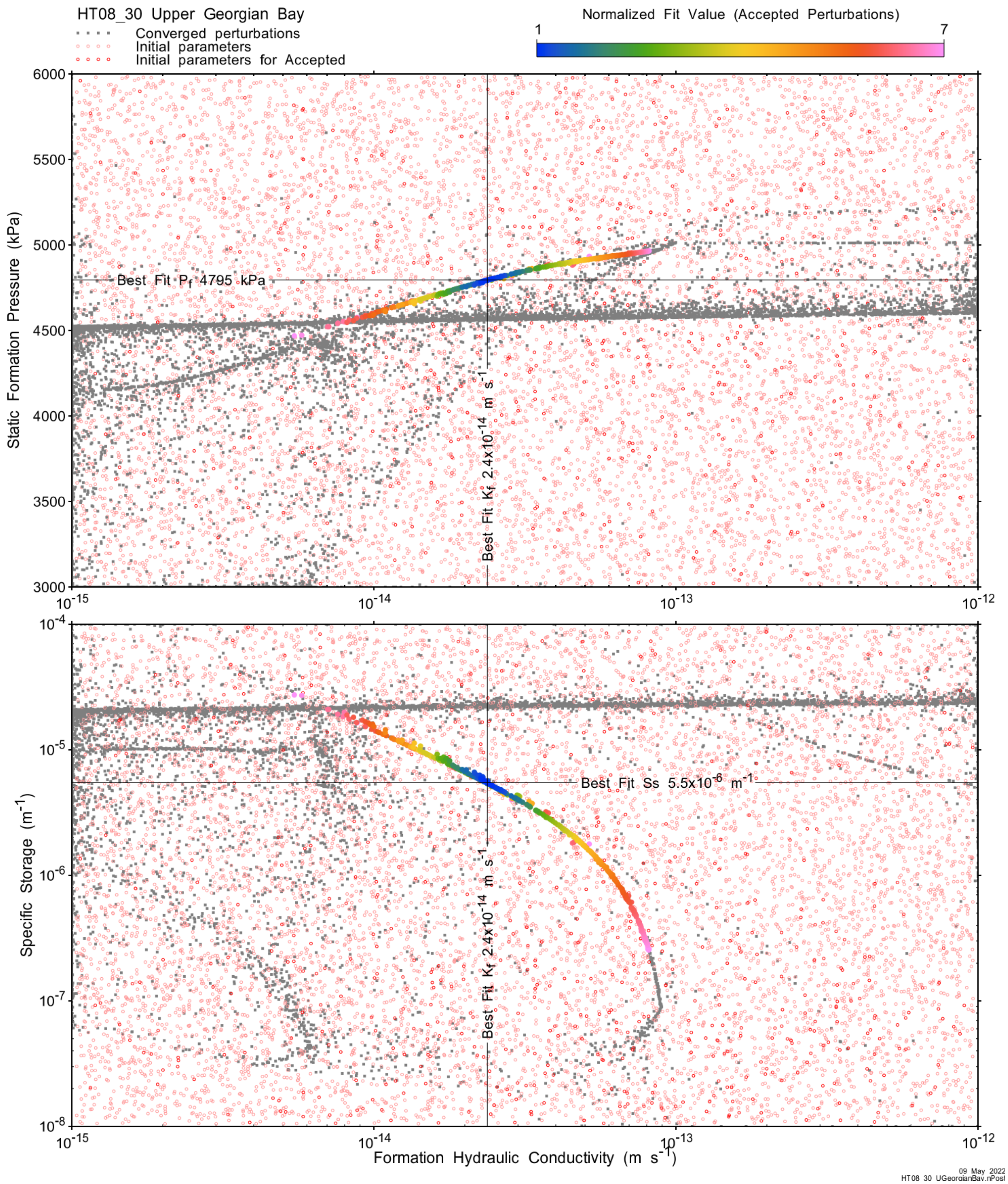

Figure 0.112 XY-scatter plot showing estimates of formation hydraulic conductivity (K_f) vs static formation pressure (P_f) (top panel) and specific storage (Ss) (bottom panel).

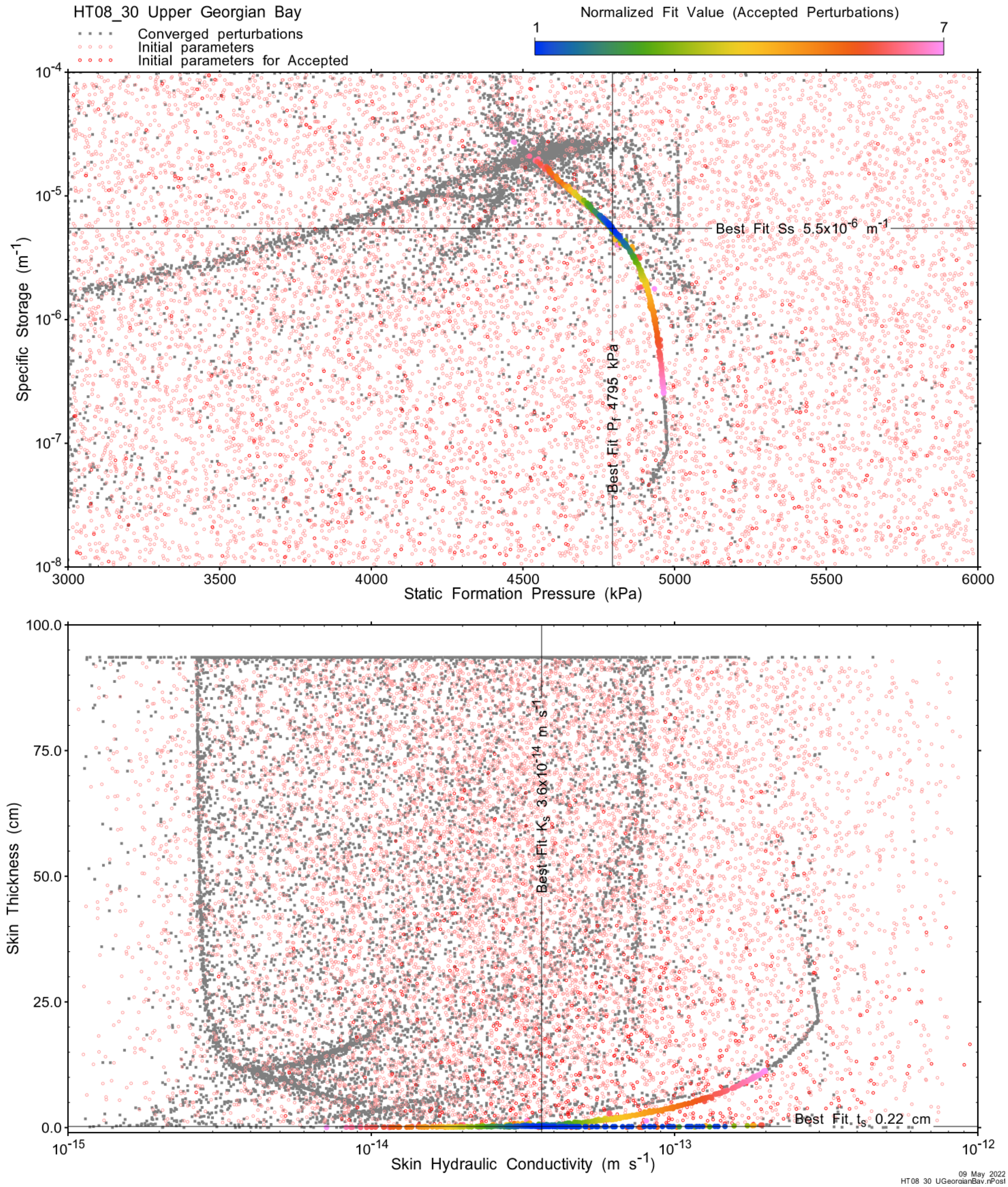

Figure 0.113 XY-scatter plot showing estimates of static formation pressure (P_f) vs specific storage (Ss) (top panel) and skin hydraulic conductivity (K_s) vs skin thickness (t_s) (bottom panel).

Confidence limits and median values are determined from the CDF of accepted optimization results (i.e. the varying color values in the above figures), with best fit value, 5% and 95% confidence indicated on Figure 0.114 and Figure 0.115.

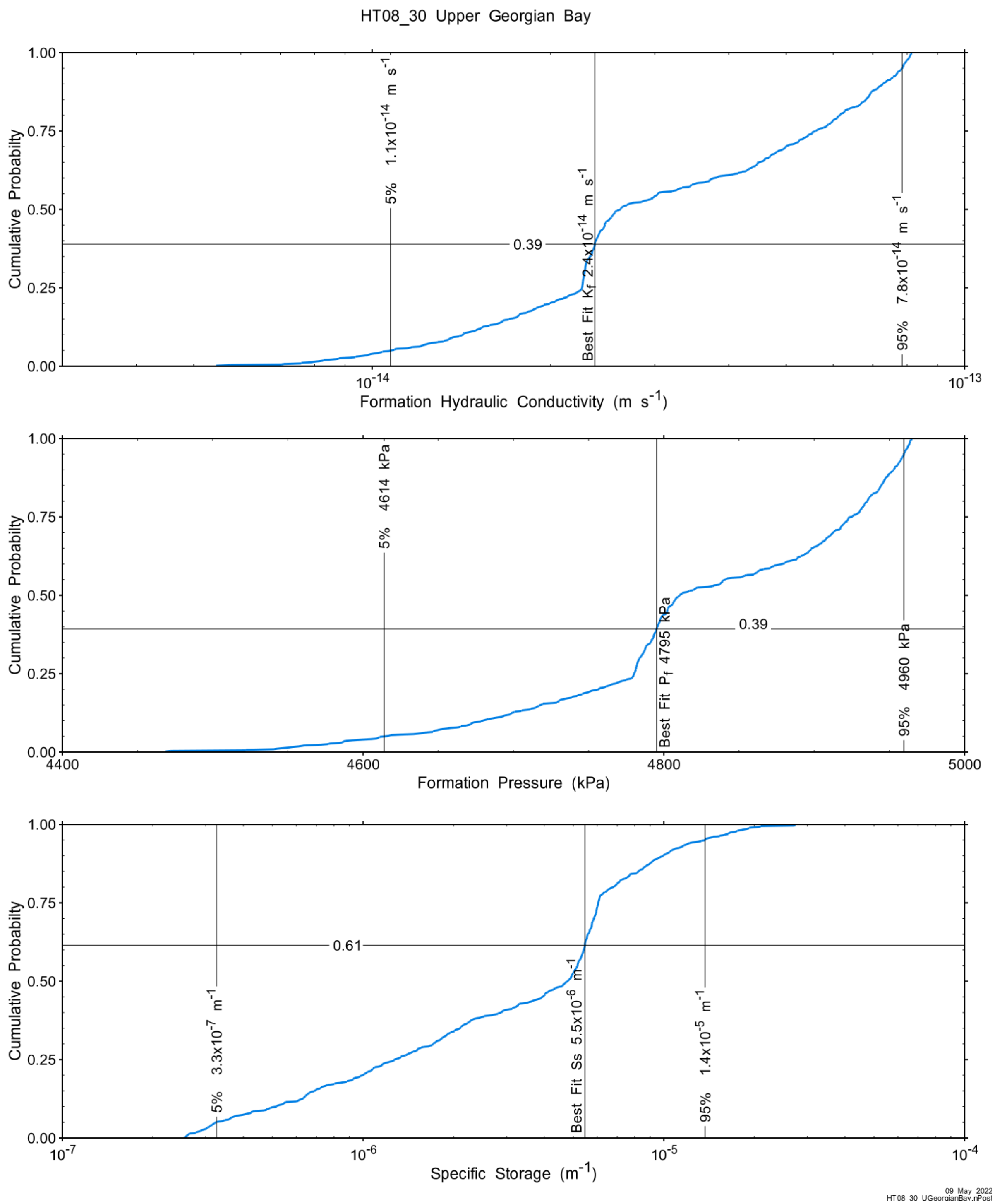

Figure 0.114 Cumulative distribution functions and parameter limits for formation hydraulic conductivity (K_f) (top panel), static formation pressure (P_f) (middle panel) and specific storage (Ss) (bottom panel).

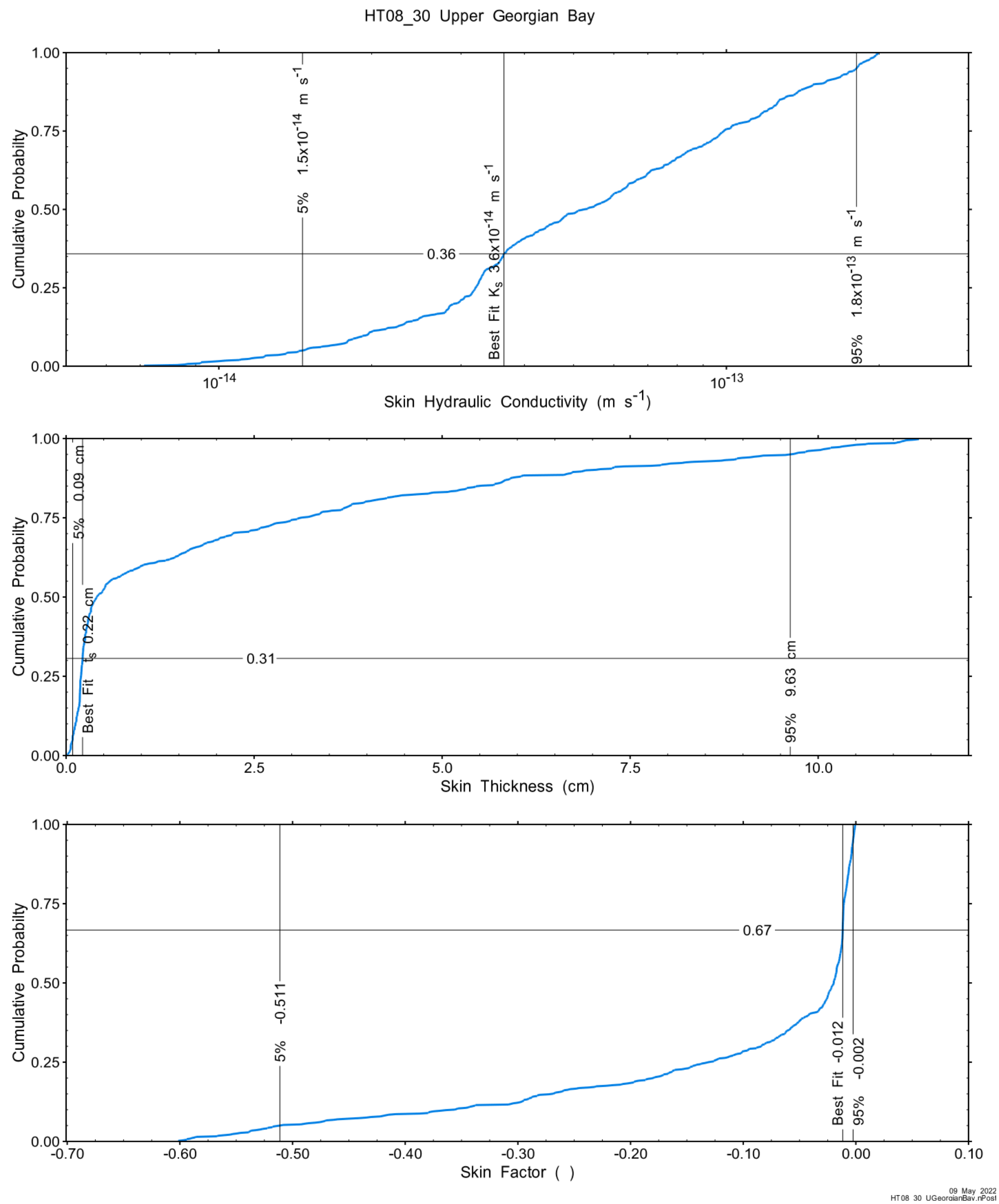

Figure 0.115 Cumulative distribution functions and parameter limits for skin hydraulic conductivity (K_s) (top panel), skin thickness (t_s) (middle panel) and skin factor (s) (bottom panel).

A summary of perturbation results is presented in Figure 0.116, with Ramey processed perturbations in Figure 0.117. Those perturbations (478 of 10,000) with all parameters within the 5% and 95% range present a very good fit to the measured test zone data.

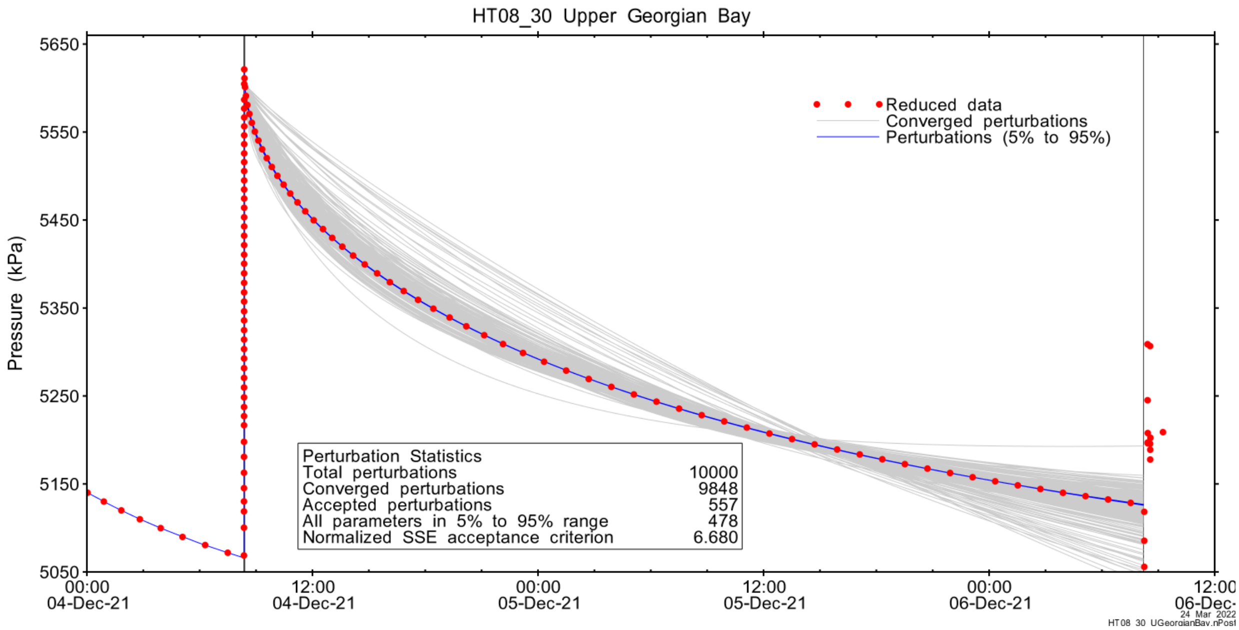

Figure 0.116 Perturbation results – all converged, accepted, and within 5% to 95% for all parameters.

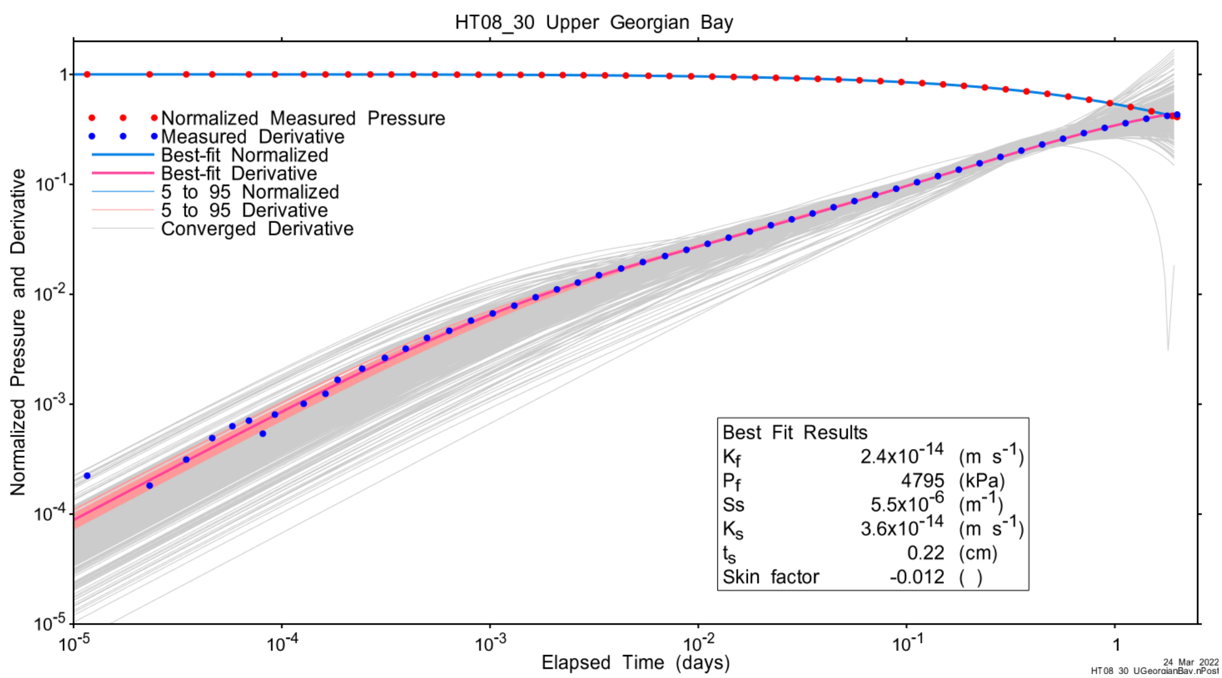

Figure 0.117 Log-log plot showing Ramey B normalized pressure and derivative response for all converged optimizations and those within 5% to 95% for all parameters.

A summary of best-fit parameter estimates and ranges is given in Table 0.39.

Table 0.39 Summary of the HT08_30 parameter estimates.

Parameter	Best Fit	5%	Median	95%
K_f (m/s)	2.4E-14	1.1E-14	2.6E-14	7.8E-14
P_f (kPa)	4795	4614	4811	4960
Ss (1/m)	5.5E-06	3.3E-07	4.8E-06	1.4E-05
K_s (m/s)	3.6E-14	1.5E-14	5.2E-14	1.8E-13
t_s (cm)	0.22	0.09	0.41	9.63
s (-)	-0.012	-0.511	-0.020	-0.002

Parameter correlations for all perturbations with all parameters within the 5% to 95% limits are given in Table 0.40.

Table 0.40 Pearson cross-correlations of 5% to 95% parameters

	Log(K_f)	P_f	Log(Ss)	Log(K_s)	t_s	s
Log(K_f)	1.000	0.991	-0.980	0.791	0.873	-0.827
P_f	0.991	1.000	-0.948	0.764	0.808	-0.759
Log(Ss)	-0.980	-0.948	1.000	-0.791	-0.951	0.919
Log(K_s)	0.791	0.764	-0.791	1.000	0.753	-0.761
t_s	0.873	0.808	-0.951	0.753	1.000	-0.993
s	-0.827	-0.759	0.919	-0.761	-0.993	1.000

A.8.4 Additional Figures

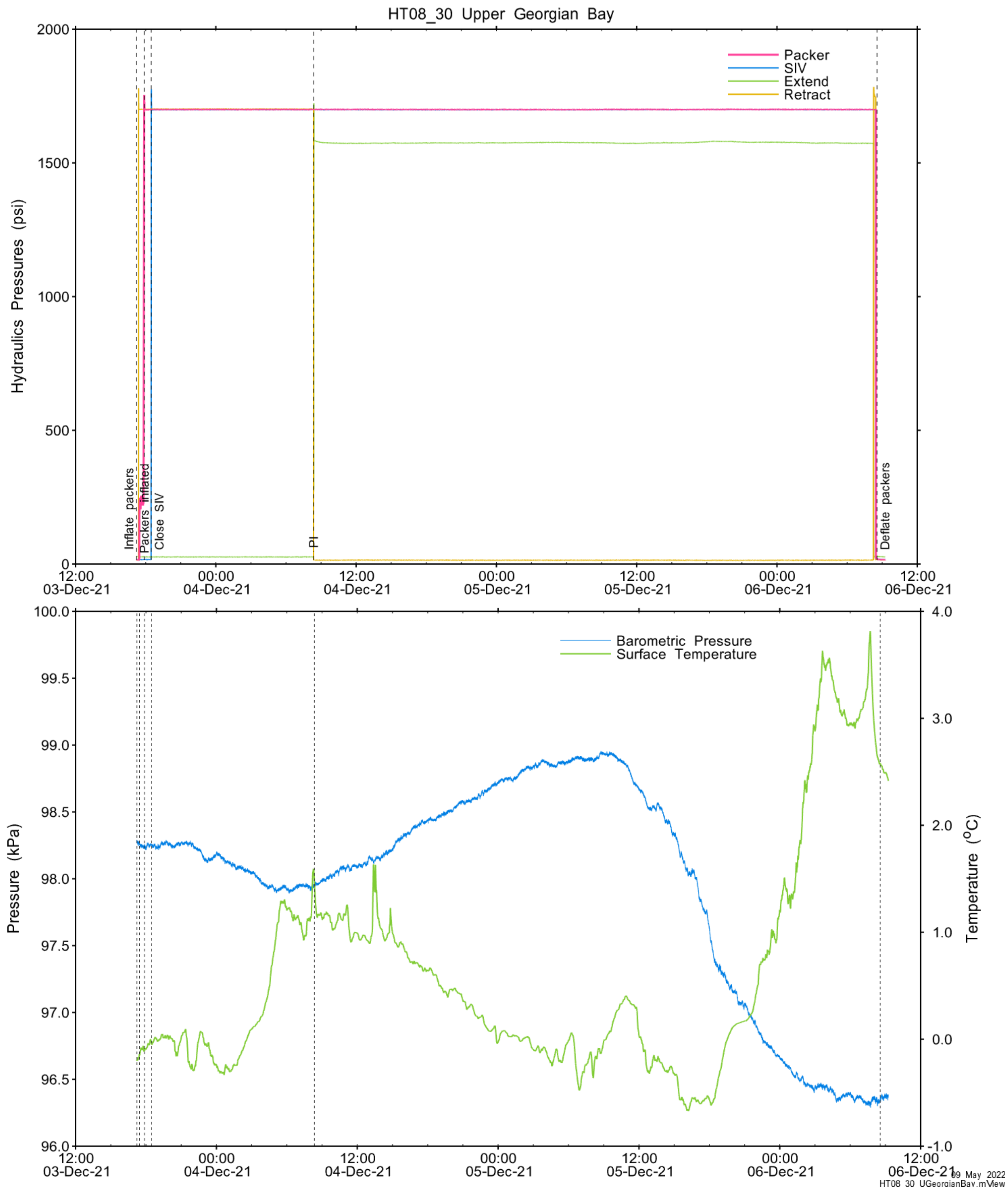

Figure 0.118 Hydraulic pressures and surface temperature/barometric pressure.

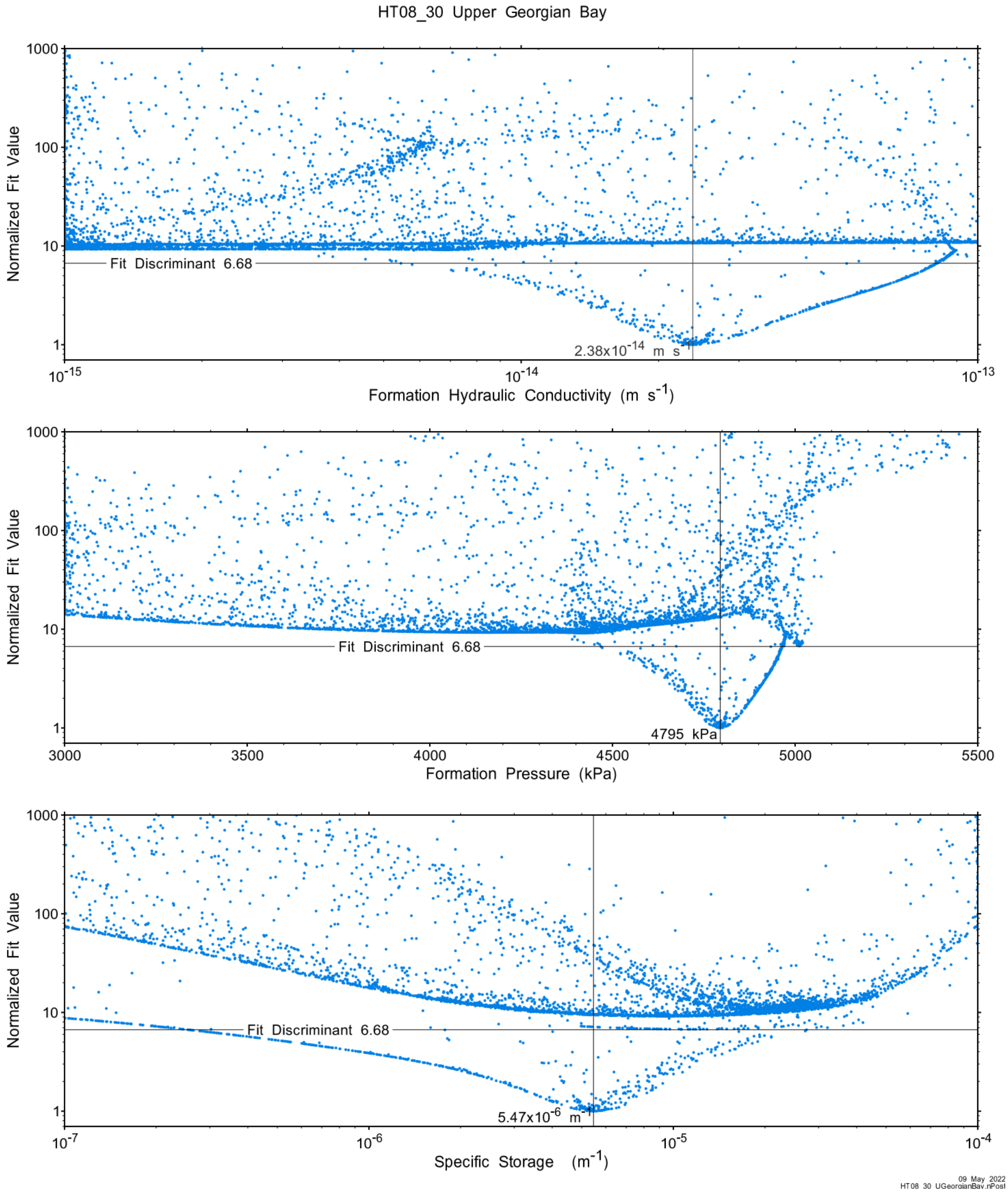

Figure 0.119 XY-scatter plot showing the formation parameter space normalized fit values.

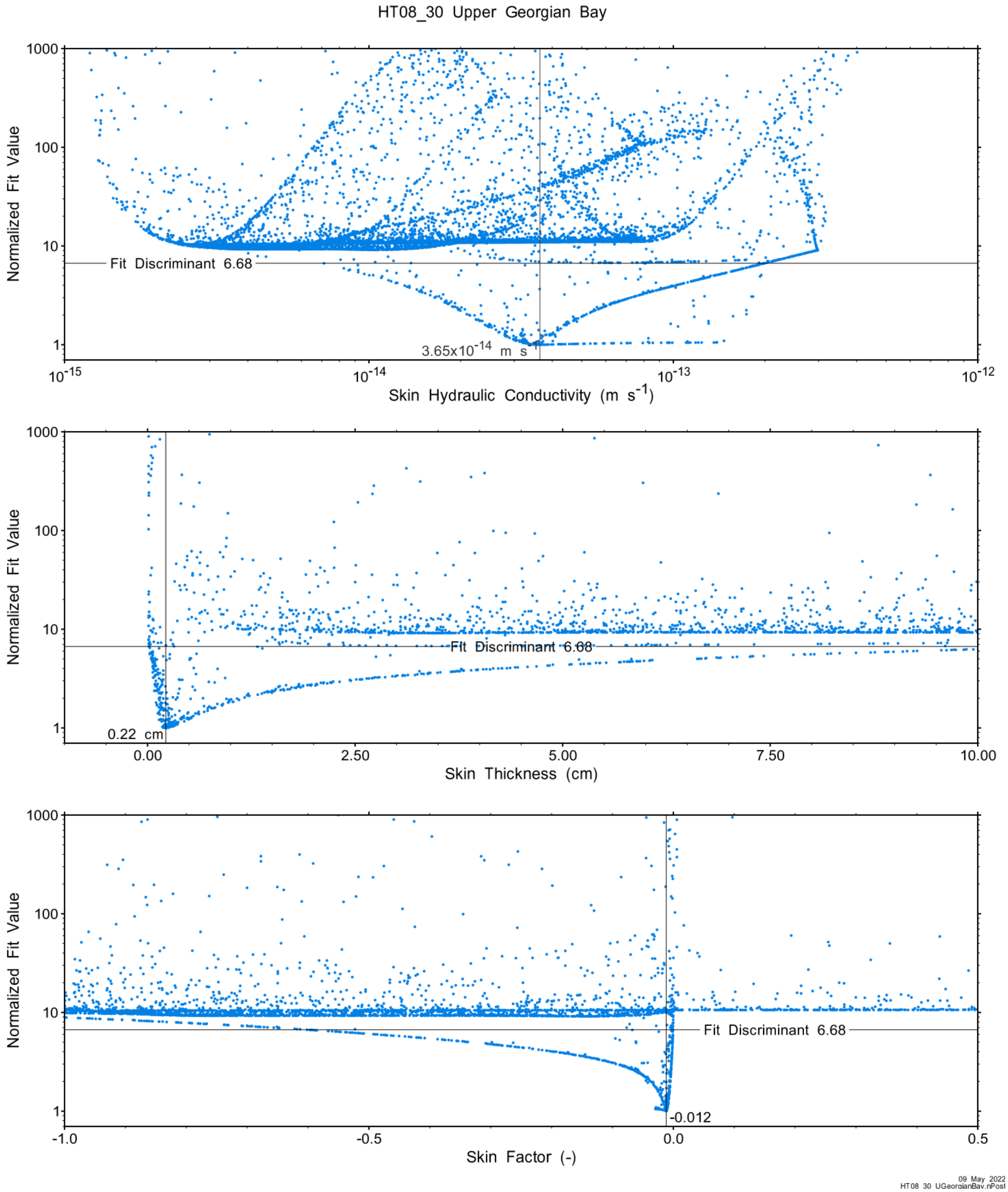

Figure 0.120 XY-scatter plot showing the skin parameter space normalized fit values.

A.9 HT09_30 Lower Georgian Bay

The SB_BH01 interval from 559.00 to 589.05 mBGS tested in HT09_30 was contained entirely within the lower portion of the Georgian Bay Formation. A single PI test with a duration of 2 days was conducted.

A.9.1 Test Data Summary

Table 0.41 and Figure 0.121 provide a summary of test events and a plot of pressures measured while testing, respectively.

Table 0.41 HT09_30 Summary of Test Events.

Event	Start Date & Time	Duration (days)	TZ Pressure (kPa)
Drilling intercept	21-08-19 08:20	93.27	5712
Prior testing	21-11-20 14:45	20.96	variable
Shut-in	21-12-11 13:52	0.80	6199
Pulse injection	21-12-12 09:01	2.01	6206
Test end	21-12-14 09:20		5727

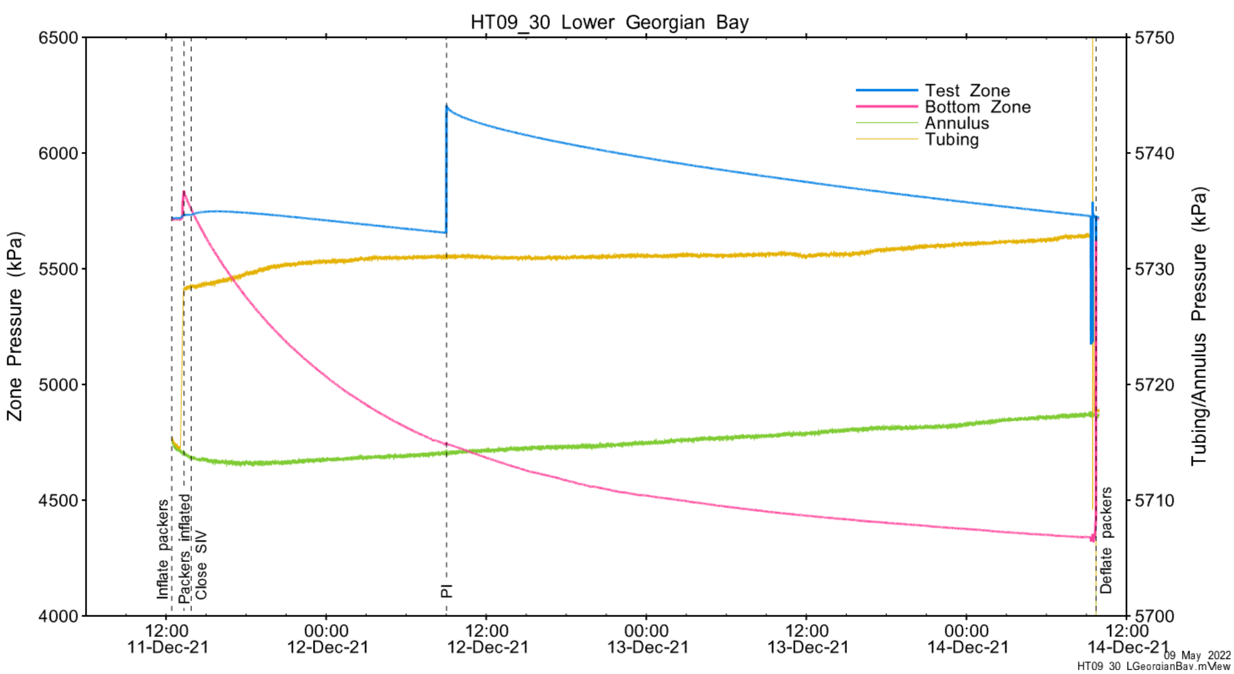

Figure 0.121 HT09_30 test events and pressures.

A.9.2 Test Analyses

Table 0.42 is a summary of test-specific input parameters used in the analyses, while Table 0.43 presents the optimized parameters and allowed ranges.

Table 0.42 nSIGHTS Input Parameters.

Parameter	Value	Units
Test zone radius	6.46	cm
Test zone compressibility	4.75E-10	1/Pa
Test zone fluid density	1050	g/L
Test zone length	30.05	m

Table 0.43 nSIGHTS Parameter Optimization Ranges.

Parameter	Minimum	Maximum	Units	Type
Formation hydraulic conductivity (K_f)	1E-15	1E-10	m/s	log
Formation pressure (P_f)	100	5000	kPa	linear
Specific storage (Ss)	1E-08	1E-04	1/m	log
Skin hydraulic conductivity (K_s)	1E-15	1E-10	m/s	log
Skin thickness (t_s)	0.1	935	mm	linear

Figure 0.122 shows the measured test zone pressure record (with reduced data density for clarity) used in the analysis along with the best-fit simulation and parameter values. Figure 0.123 presents the pre-test history, and Figure 0.124 shows the Ramey B normalized best-fit pressure and pressure derivatives.

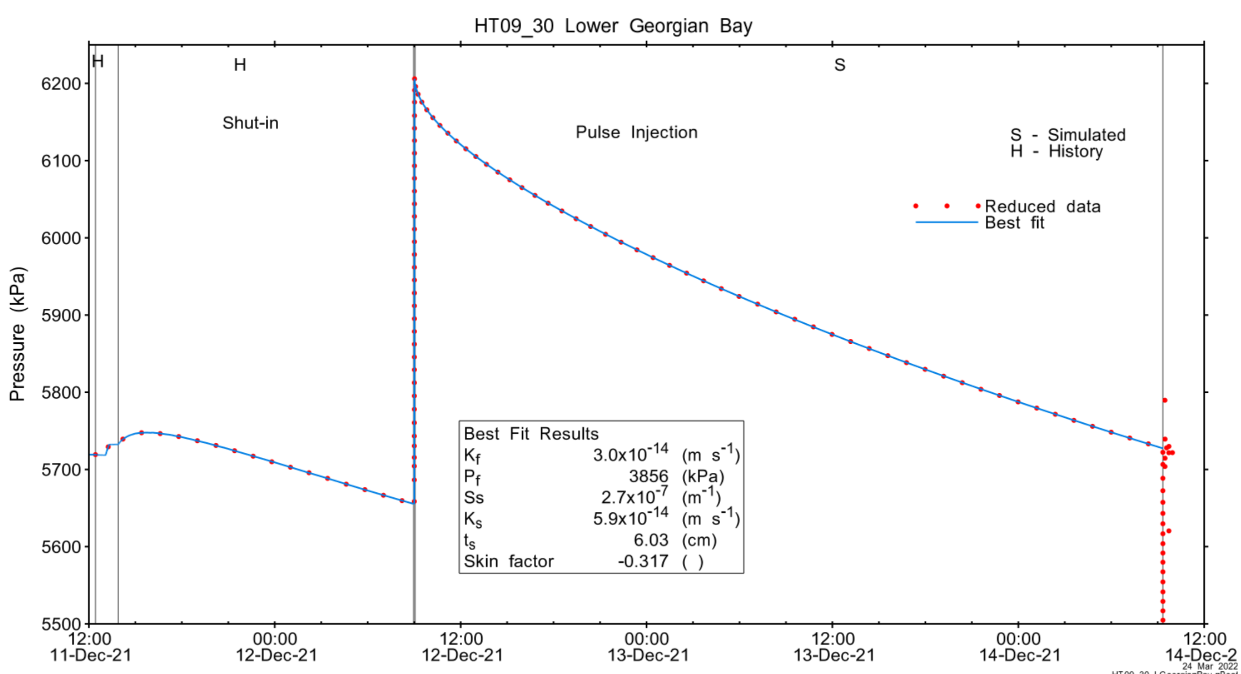

Figure 0.122 Annotated testing sequence showing best-fit simulation and parameter estimates.

GEOFIRMA ENGINEERING

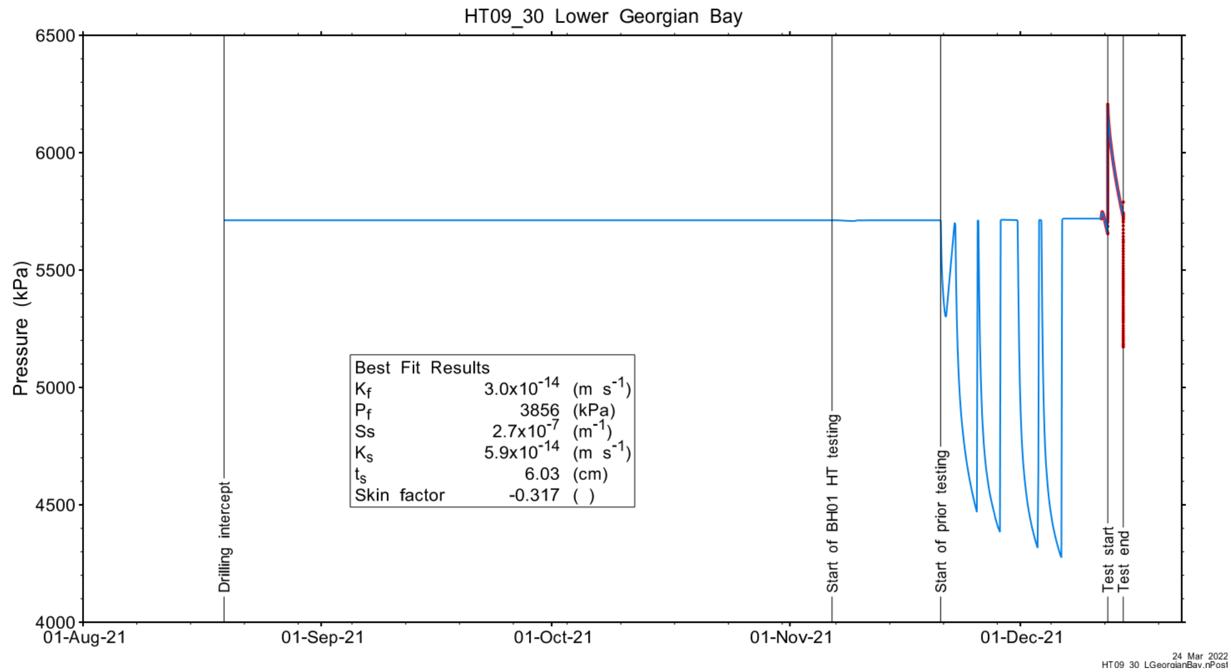

Figure 0.123 Annotated HT09_30 testing sequence showing pre-test history, best-fit simulation and parameter estimates.

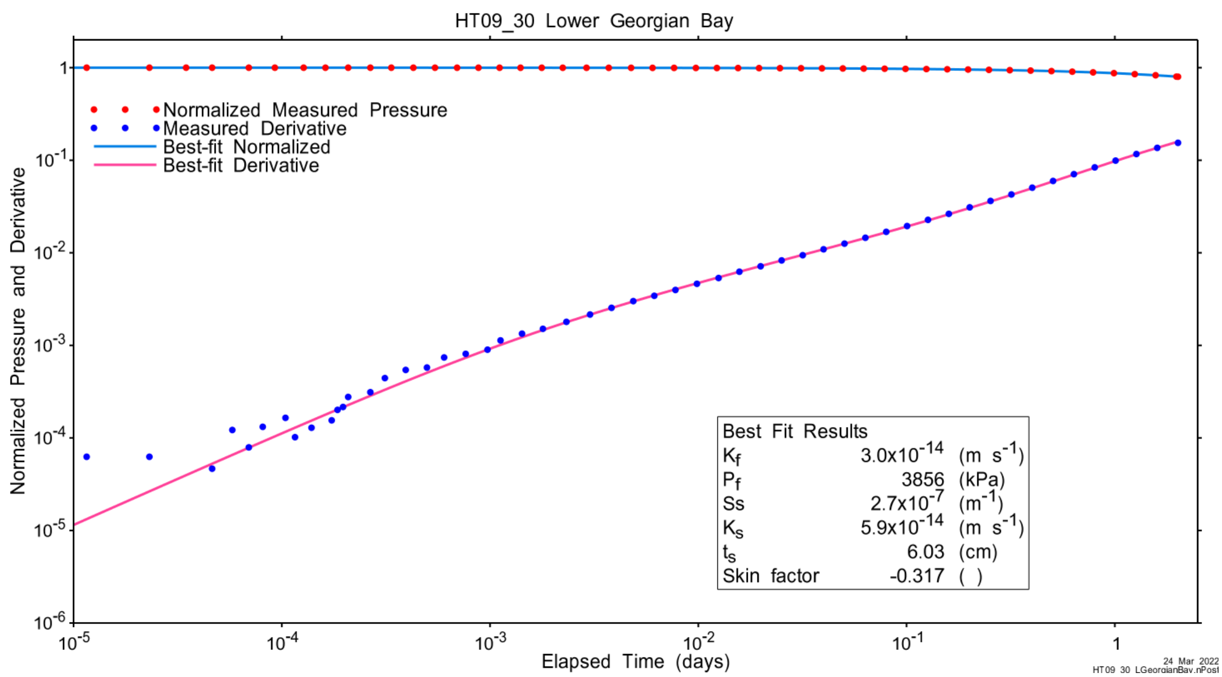

Figure 0.124 Log-log plot showing Ramey B normalized pressure and derivative response for best-fit simulation.

Figure 0.125 shows the normalized parameter sensitivity response for the best fit. Skin-related parameters are most sensitive during the early-time response. K_f and P_f are decreasing and increasing respectively at the end of the test, indicating that additional test duration may have improved the fit.

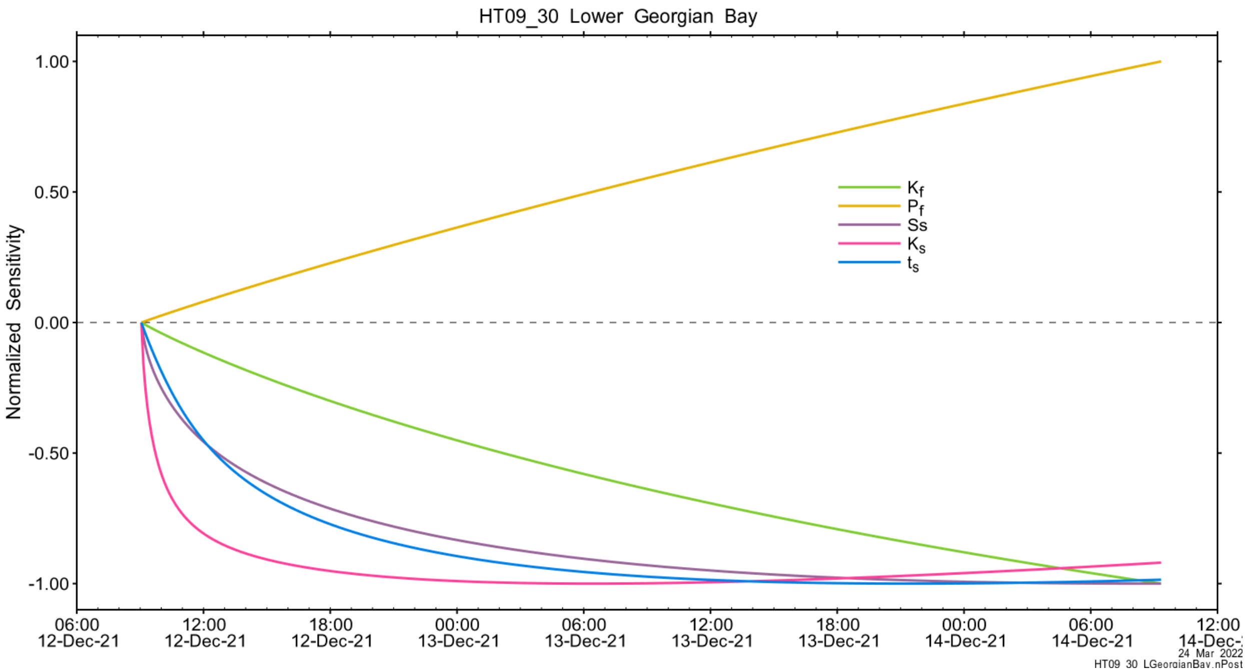

Figure 0.125 Normalized Jacobian for best-fit simulation.

A.9.3 Uncertainty Analyses

The CDF of normalized fit values for all converged simulations and the selected fit discriminant are shown in Figure 0.126.

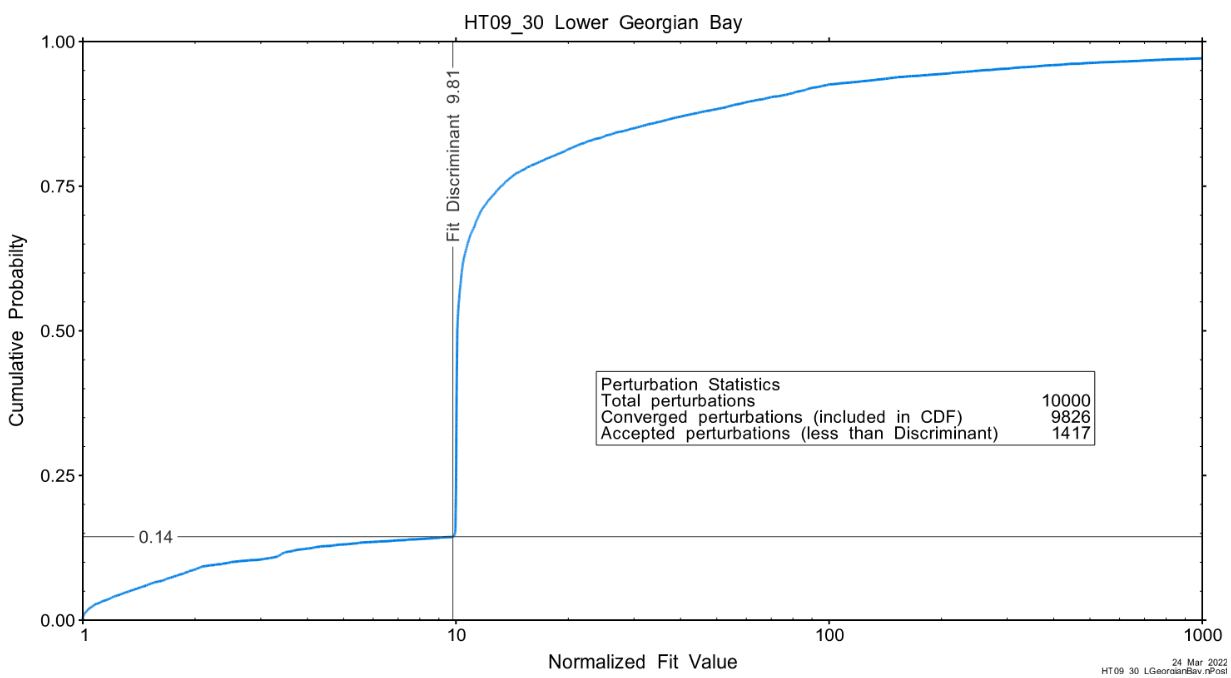

Figure 0.126 Fit value cumulative distribution function.

Summary cross parameter scatter plots for selected formation and skin parameters are given in Figure 0.127 and Figure 0.128. The light pink dots on the figures are the initial parameter estimates, with red dots overlaying those initial parameter values that resulted in accepted optimization results. The grey dots are converged optimizations which did not meet the fit discriminant. Larger varying color symbols represent the fit value of accepted optimizations, with the blue values representing the best fit.

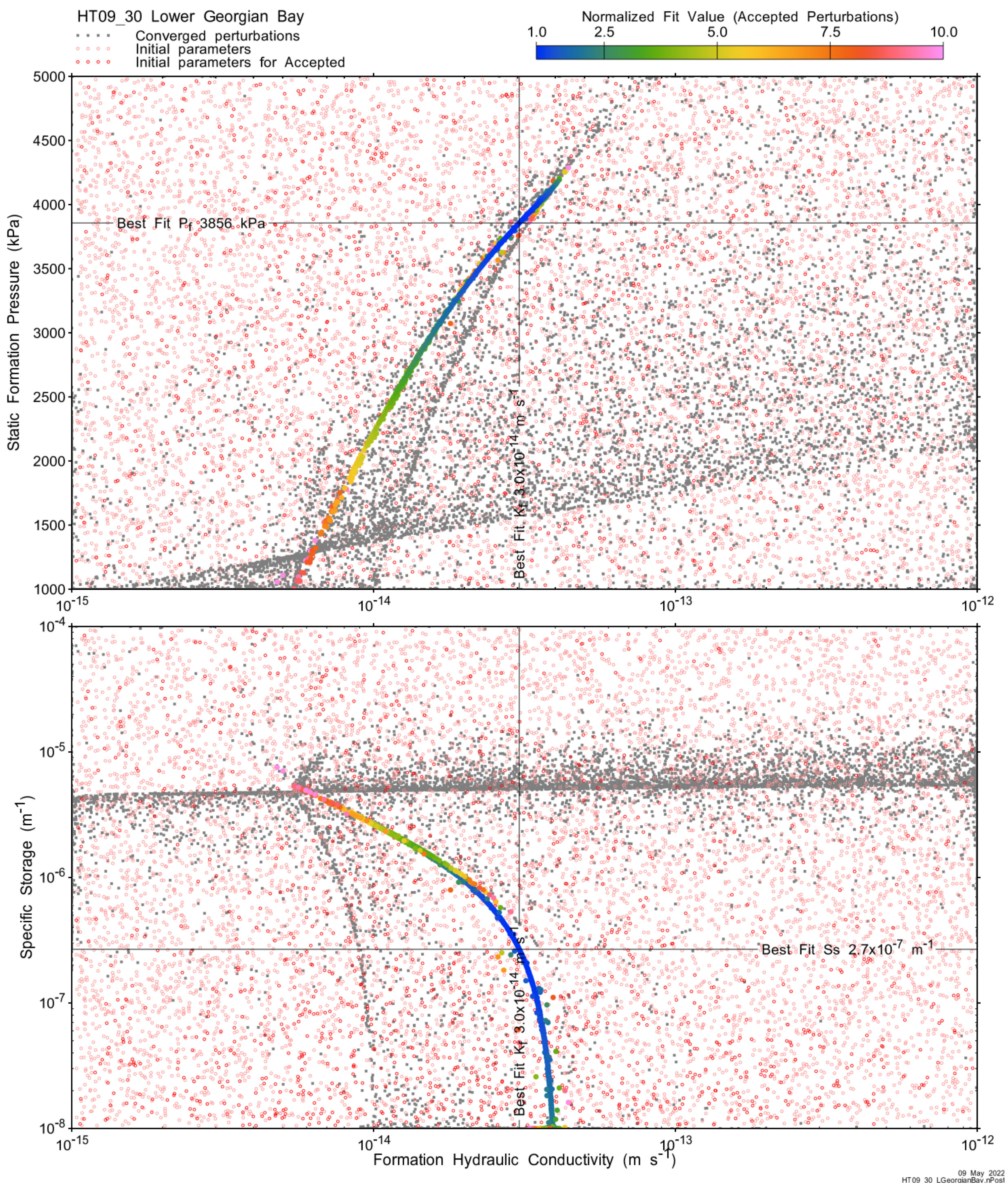

Figure 0.127 XY-scatter plot showing estimates of formation hydraulic conductivity (K_f) vs static formation pressure (P_f) (top panel) and specific storage (Ss) (bottom panel).

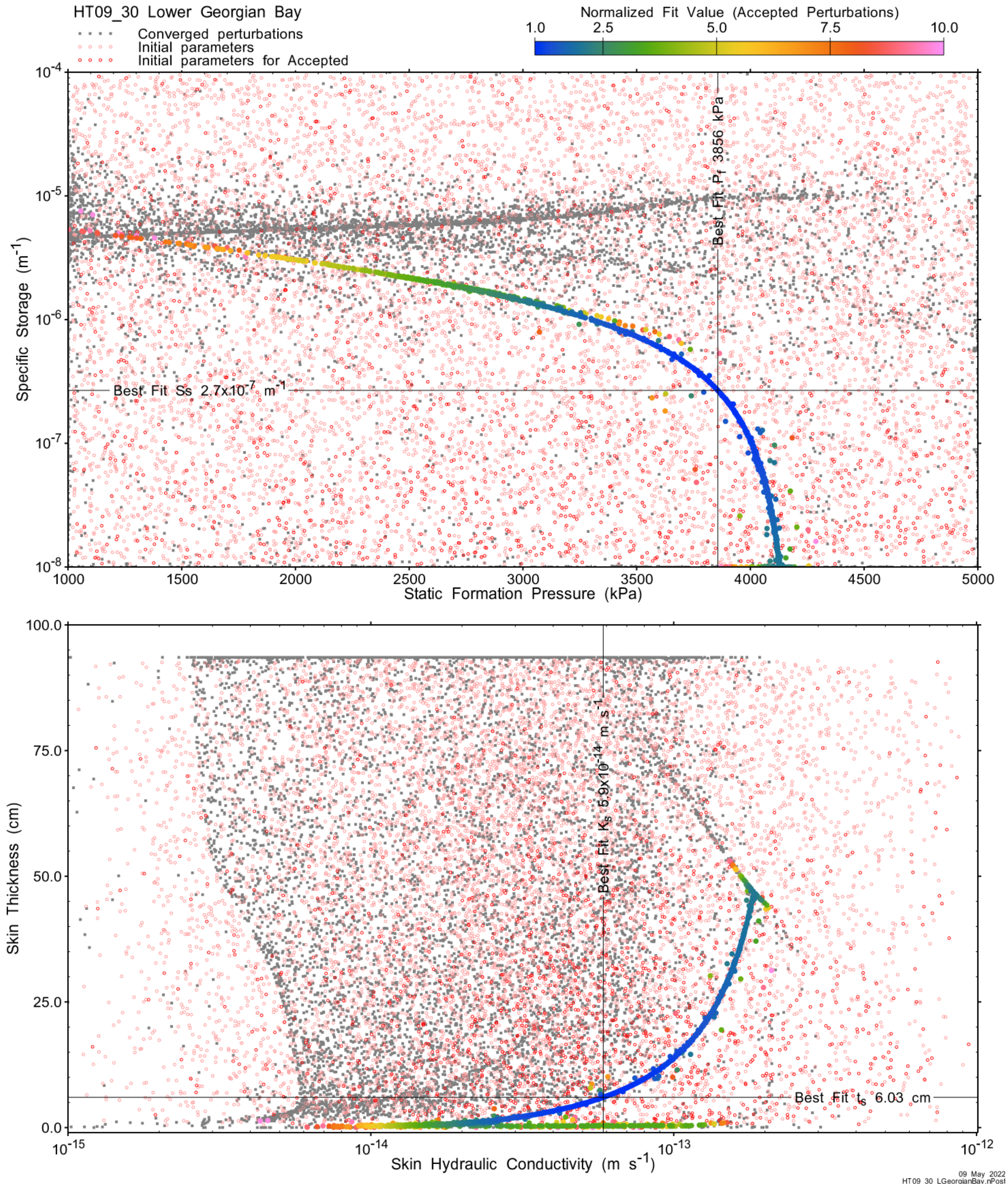

Figure 0.128 XY-scatter plot showing estimates of static formation pressure (P_f) vs specific storage (Ss) (top panel) and skin hydraulic conductivity (K_s) vs skin thickness (t_s) (bottom panel).

Confidence limits and median values are determined from the CDF of accepted optimization results (i.e. the varying color values in the above figures), with best fit value, 5% and 95% confidence indicated on Figure 0.129 and Figure 0.130.

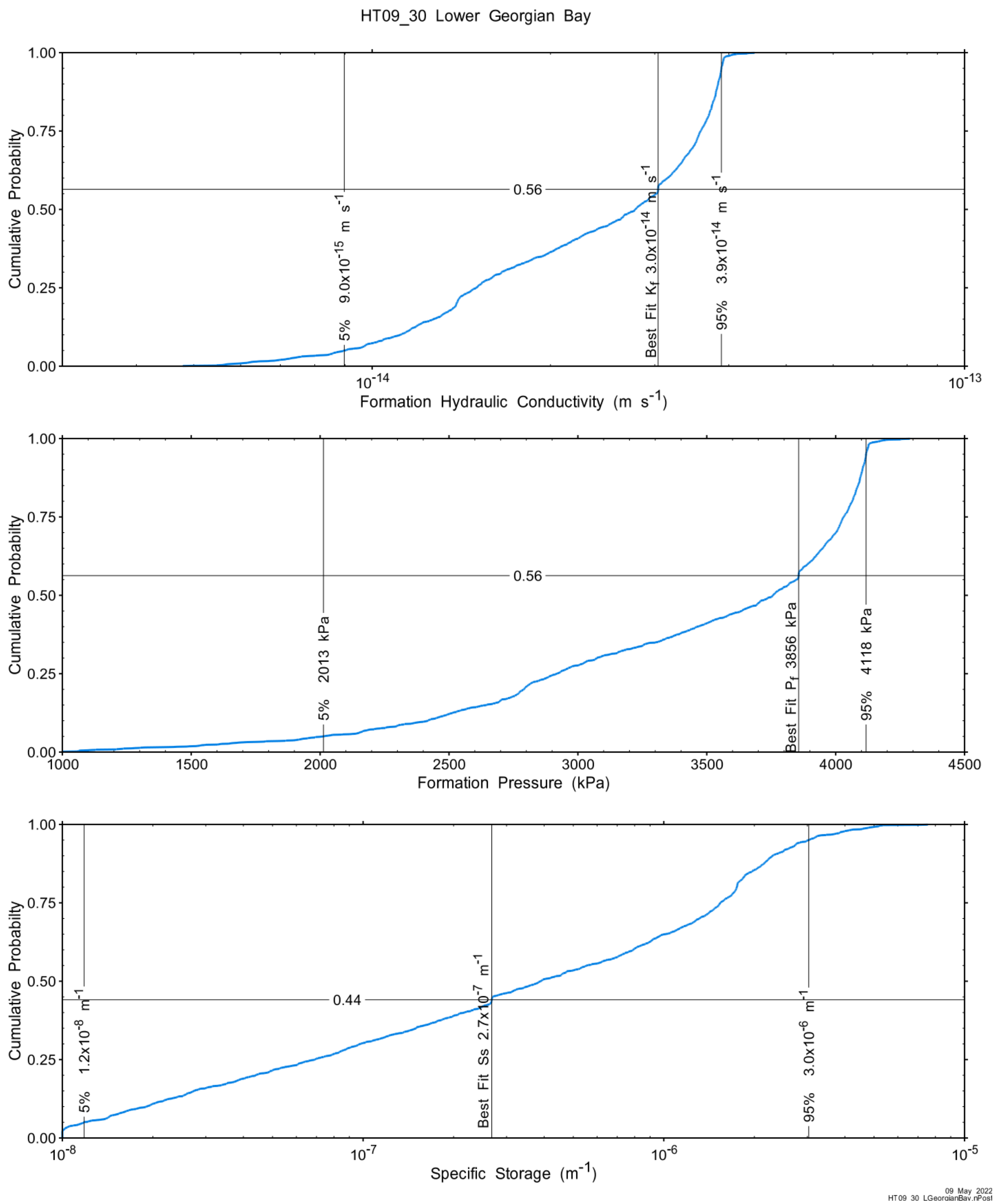

Figure 0.129 Cumulative distribution functions and parameter limits for formation hydraulic conductivity (K_f) (top panel), static formation pressure (P_f) (middle panel) and specific storage (Ss) (bottom panel).

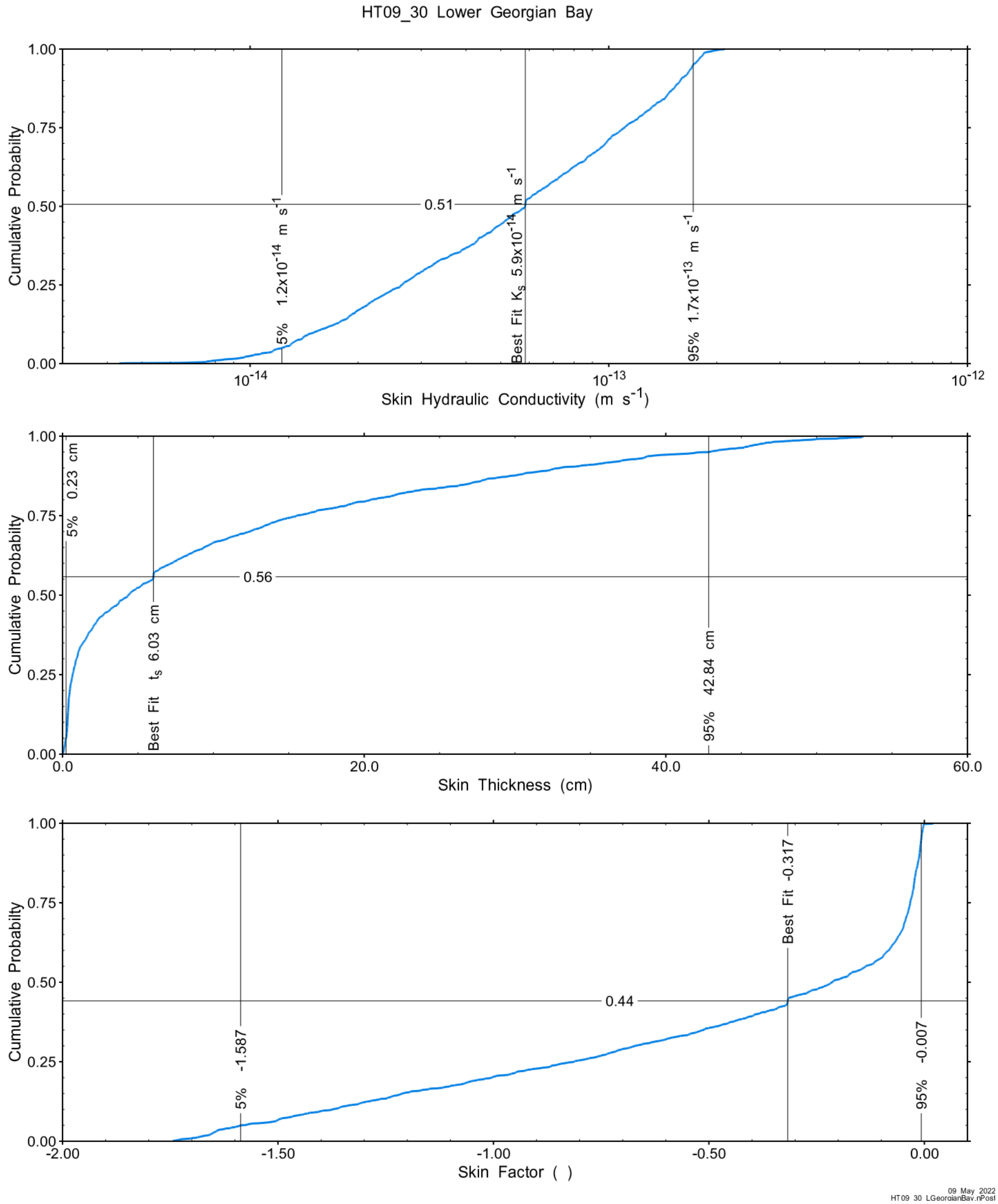

Figure 0.130 Cumulative distribution functions and parameter limits for skin hydraulic conductivity (K_s) (top panel), skin thickness (t_s) (middle panel) and skin factor (s) (bottom panel).

A summary of perturbation results is presented in Figure 0.131, with Ramey processed perturbations in Figure 0.132. Those perturbations (1197 of 10,000) with all parameters within the 5% and 95% range present a very good fit to the measured test zone data.

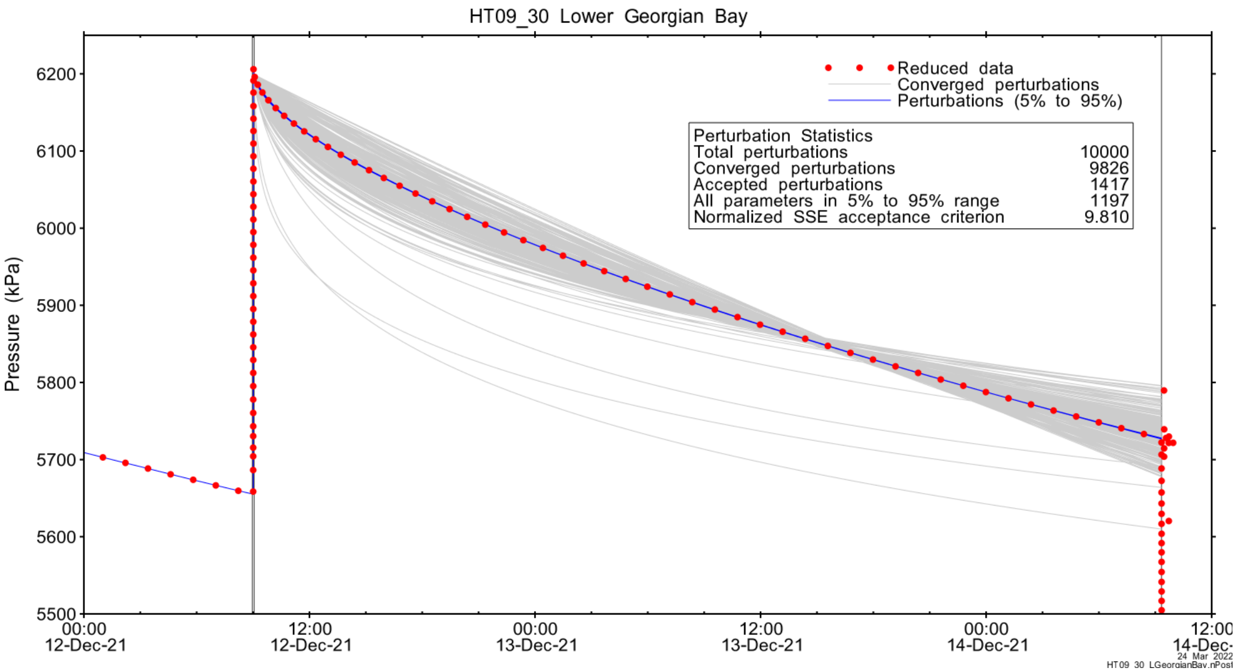

Figure 0.131 Perturbation results – all converged, accepted, and within 5% to 95% for all parameters.

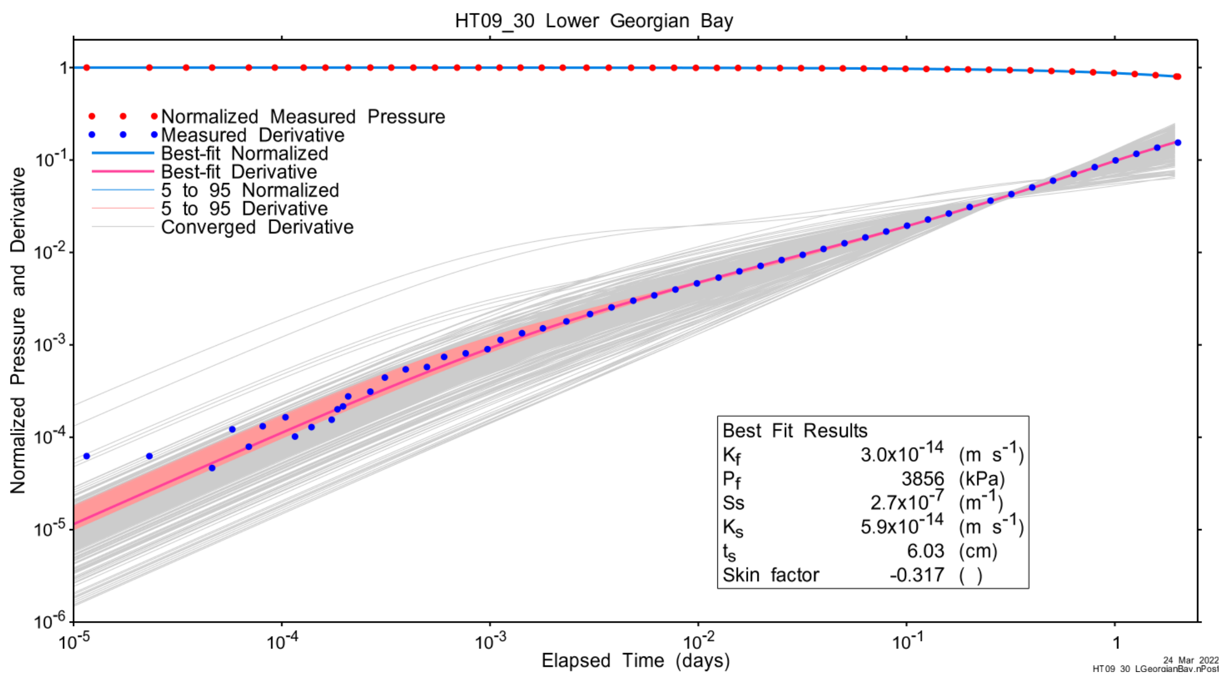

Figure 0.132 Log-log plot showing Ramey B normalized pressure and derivative response for all converged optimizations and those within 5% to 95% for all parameters.

A summary of best-fit parameter estimates and ranges is given in Table 0.44.

Table 0.44 Summary of the HT09_30 parameter estimates.

Parameter	Best Fit	5%	Median	95%
K_f (m/s)	3.0E-14	9.0E-15	2.8E-14	3.9E-14
P_f (kPa)	3856	2013	3757	4118
Ss (1/m)	2.7E-07	1.2E-08	3.9E-07	3.0E-06
K_s (m/s)	5.9E-14	1.2E-14	5.8E-14	1.7E-13
t_s (cm)	6.03	0.23	4.36	42.84
s (-)	-0.317	-1.587	-0.214	-0.007

Parameter correlations for all perturbations with all parameters within the 5% to 95% limits are given in Table 0.45.

Table 0.45 Pearson cross-correlations of 5% to 95% parameters

	Log(K_f)	P_f	Log(Ss)	Log(K_s)	t_s	s
Log(K_f)	1.000	0.997	-0.925	0.812	0.758	-0.807
P_f	0.997	1.000	-0.897	0.785	0.720	-0.767
Log(Ss)	-0.925	-0.897	1.000	-0.869	-0.944	0.970
Log(K_s)	0.812	0.785	-0.869	1.000	0.805	-0.848
t_s	0.758	0.720	-0.944	0.805	1.000	-0.990
s	-0.807	-0.767	0.970	-0.848	-0.990	1.000

A.9.4 Additional Figures

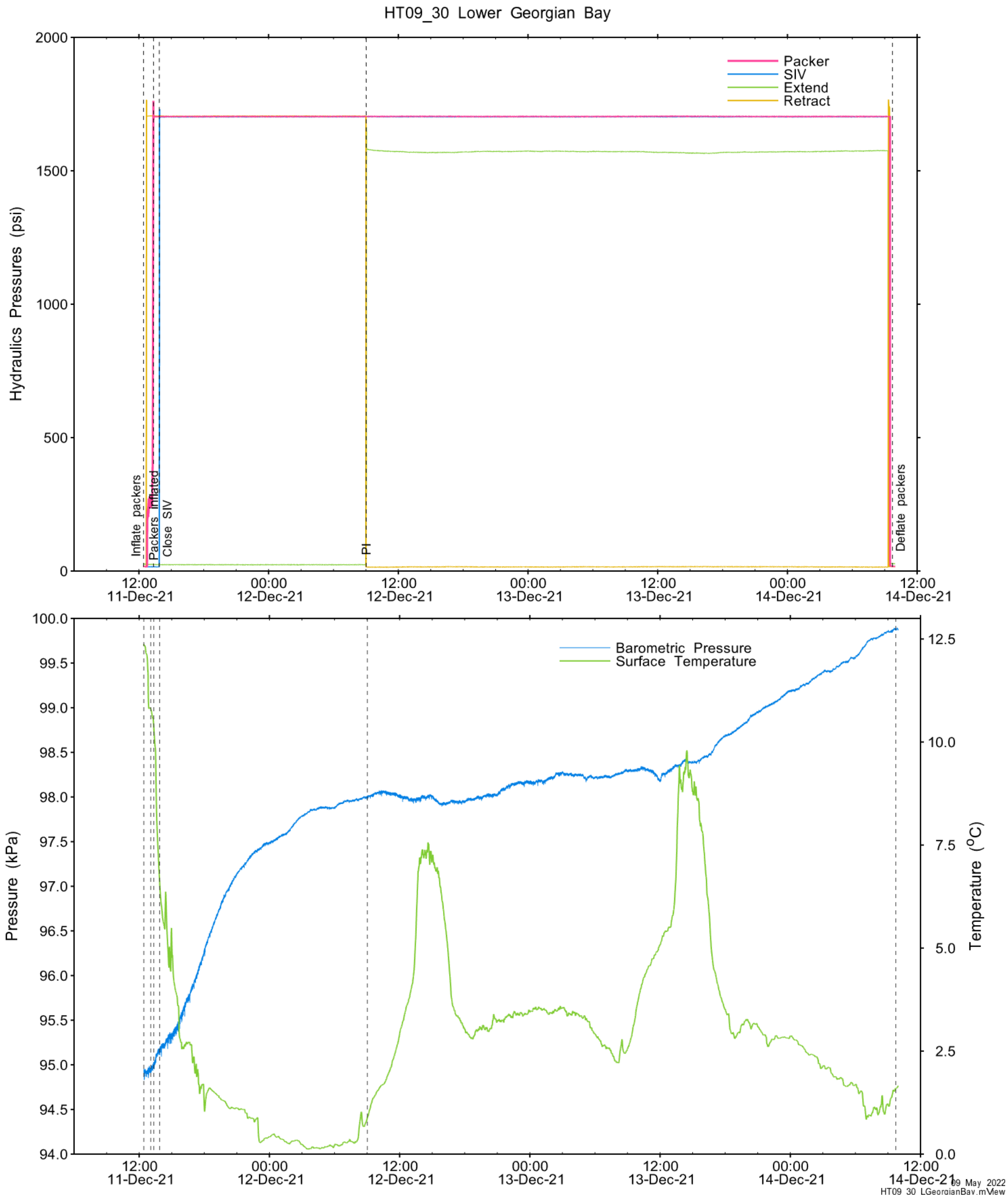

Figure 0.133 Hydraulics pressures and surface temperature/barometric pressure.

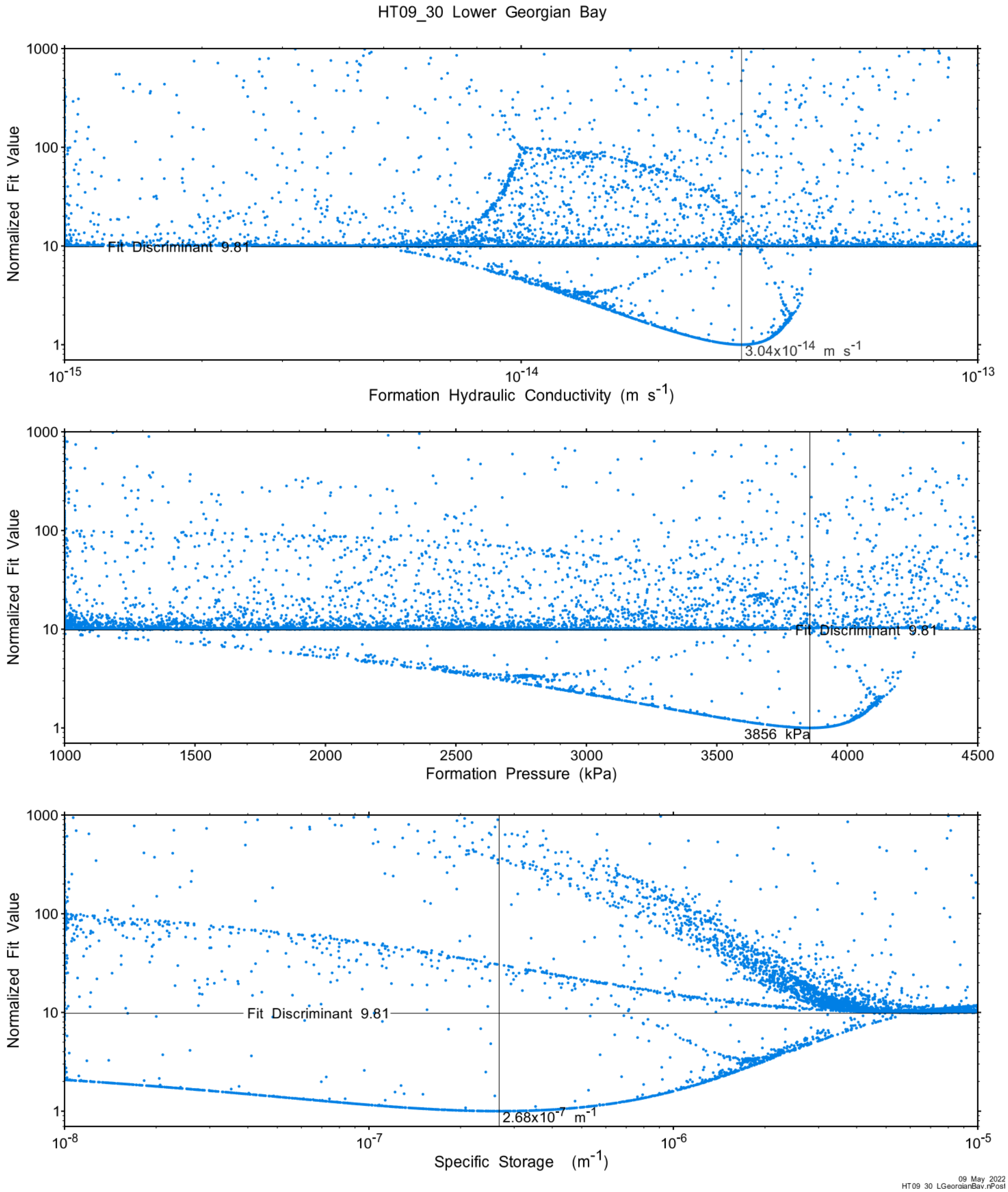

Figure 0.134 XY-scatter plot showing the formation parameter space normalized fit values.

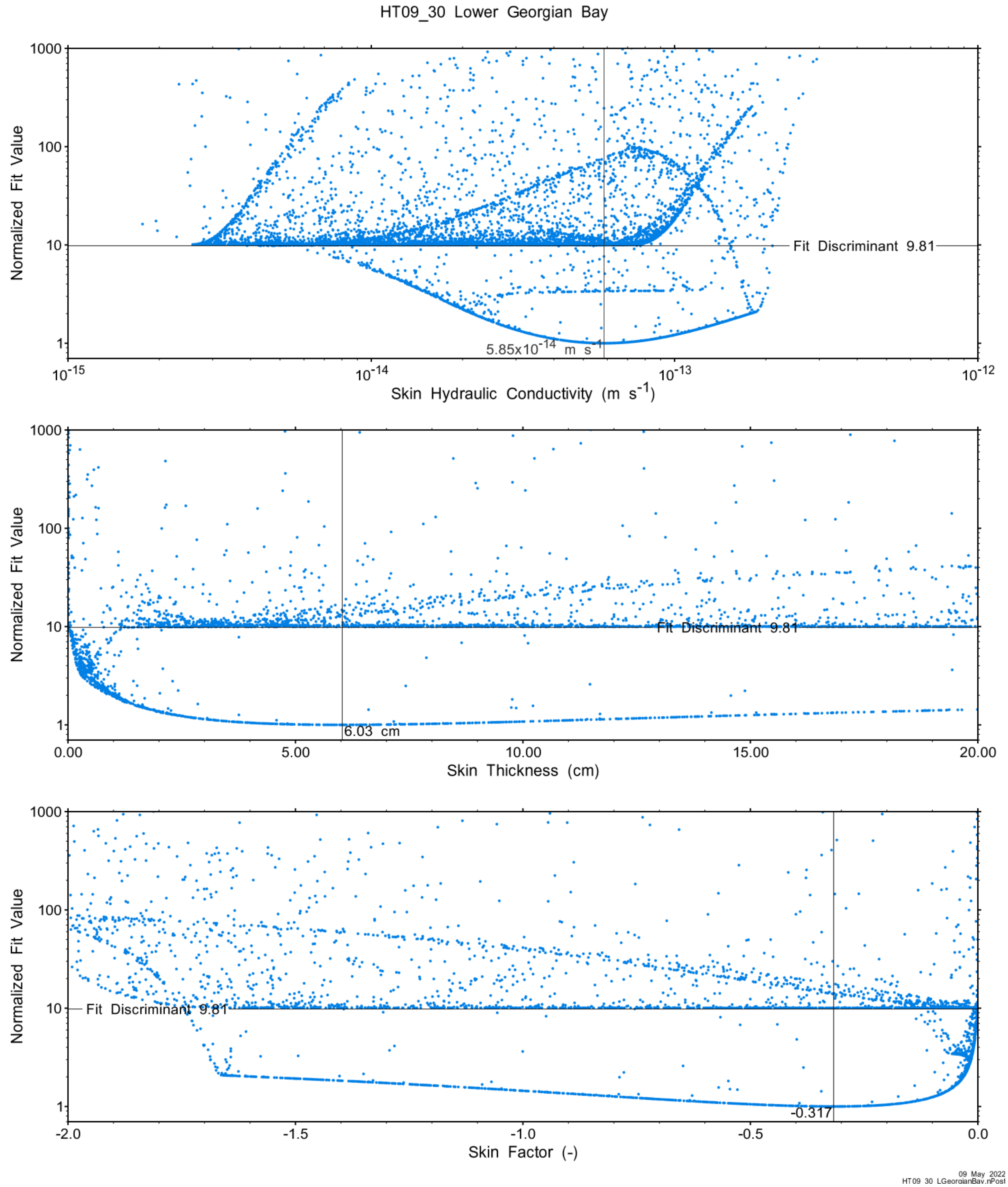

Figure 0.135 XY-scatter plot showing the skin parameter space normalized fit values.

A.10 HT10_30 Blue Mountain

The SB_BH01 interval from 602.20 to 632.25 mBGS tested in HT10_30 includes the majority of the Blue Mountain Formation. An initial PI test showed signs of anomalous behaviour (an inflection in the TZ pressure response) which would have precluded an analysis based on the assumed conceptual model. Subsequent investigations determined there was a void present in the Blue Mountain Formation which may have partially collapsed during the test. Shards of friable shale were found on top of the test tool when it was removed from the borehole. Because of the anomalous response, the PI test was divided into two components for analyses: a) prior to the inflection, the TZ response was specified as borehole history, and b) subsequent to the inflection, a pulse response was assumed. The confirmatory PW at the end of testing was also included in the simulation to provide sensitivity to skin parameters which were insensitive to the portion of the PI test simulated. A combined fit function that incorporated the responses from the PI and PW was used in the optimization.

A.10.1 Test Data Summary

Table 0.46 and Figure 0.136 provide a summary of test events and a plot of pressures measured while testing, respectively.

Table 0.46 HT10_30 Summary of Test Events.

Event	Start Date & Time	Duration (days)	TZ Pressure (kPa)
Drilling intercept	21-08-05 02:06	86.20	6155
Prior testing	21-11-20 14:45	25.13	
Shut-in	21-12-15 17:51	0.63	6154
Pulse injection	21-12-16 09:01	1.39	6416
Pulse injection (analyzed)	21-12-17 18:20	0.60	6211
Pulse withdrawal	21-12-18 08:43	0.01	5798
Test end	21-12-18 08:57		5812

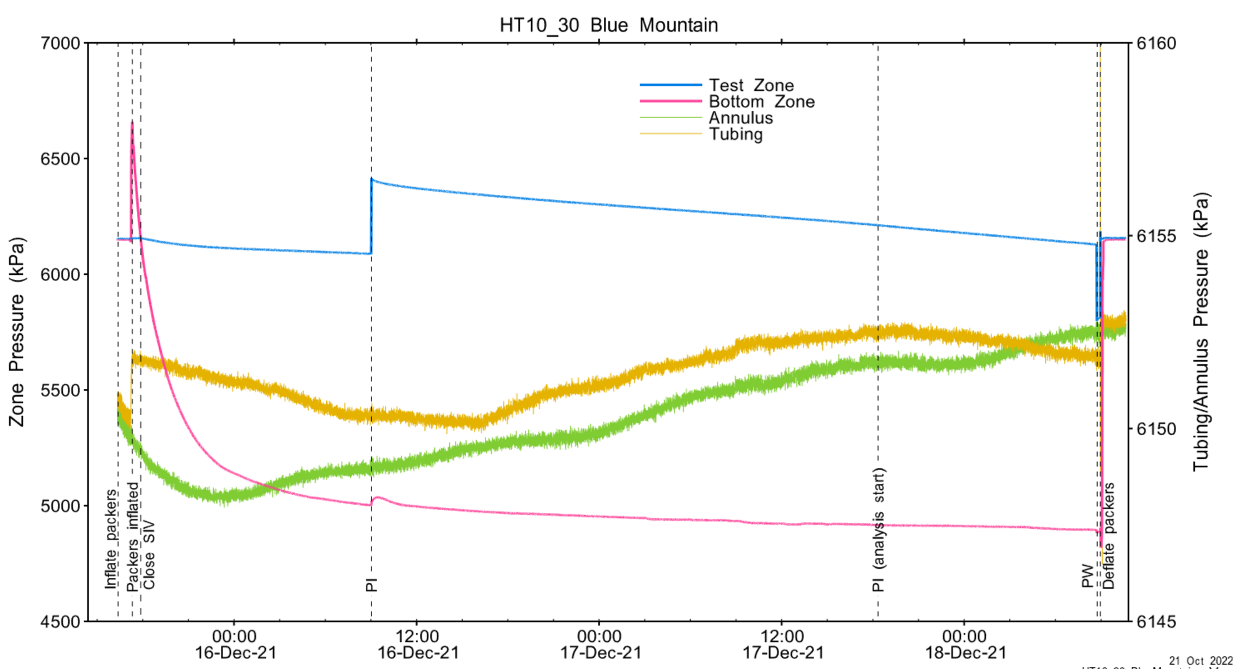

Figure 0.136 HT10_30 test events and pressures.

A.10.2 Test Analyses

Table 0.47 is a summary of test-specific input parameters used in the analyses, while Table 0.48 presents the optimized parameters and allowed ranges.

Table 0.47 nSIGHTS Input Parameters.

Parameter	Value	Units
Test zone radius	7.19	cm
Test zone compressibility	6.36E-10	1/Pa
Test zone fluid density	1047	g/L
Test zone length	30.05	m

Table 0.48 nSIGHTS Parameter Optimization Ranges.

Parameter	Minimum	Maximum	Units	Type
Formation hydraulic conductivity (K_f)	1E-15	1E-08	m/s	log
Formation pressure (P_f)	0	8000	kPa	linear
Specific storage (Ss)	1E-08	1E-04	1/m	log
Skin hydraulic conductivity (K_s)	1E-15	1E-08	m/s	log
Skin thickness (t_s)	0.1	10000	mm	linear

Figure 0.137 shows the measured test zone pressure record (with reduced data density for clarity) used in the analysis along with the best-fit simulation and parameter values. Figure 0.138 presents the pre-test history, and Figure 0.139 and Figure 0.140 shows the Ramey B normalized best-fit pressure and pressure derivatives for the PI and PW sequences respectively.

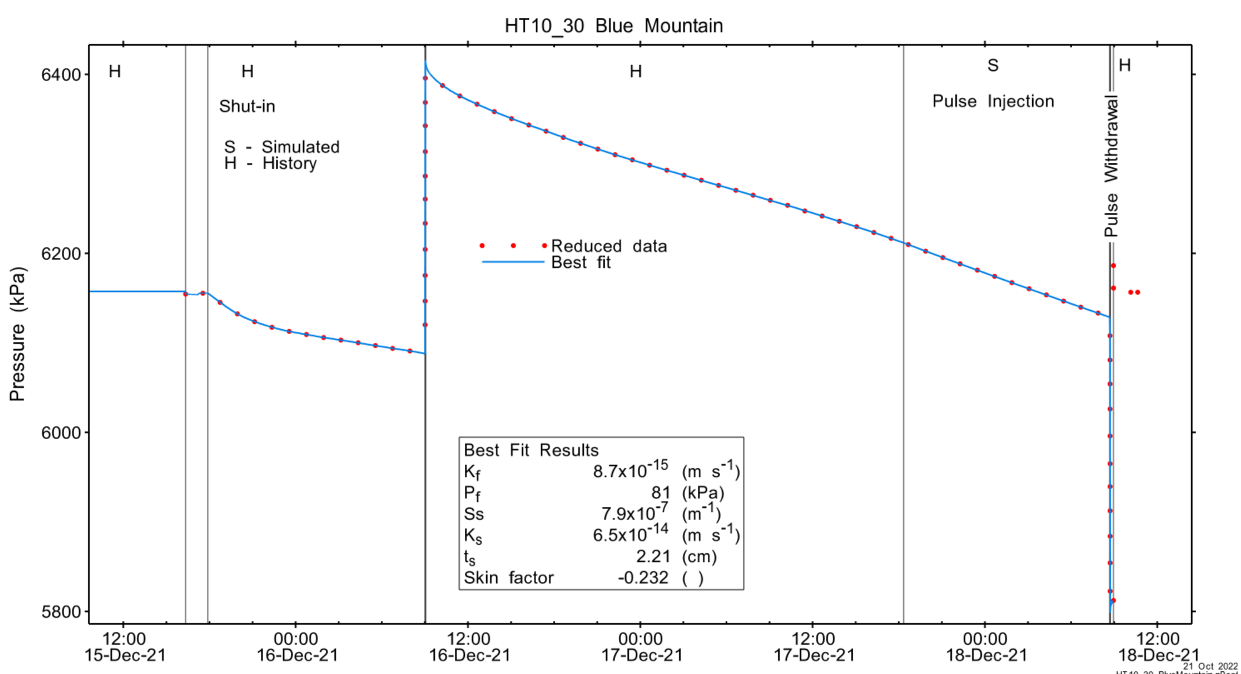

Figure 0.137 Annotated testing sequence showing best-fit simulation and parameter estimates.

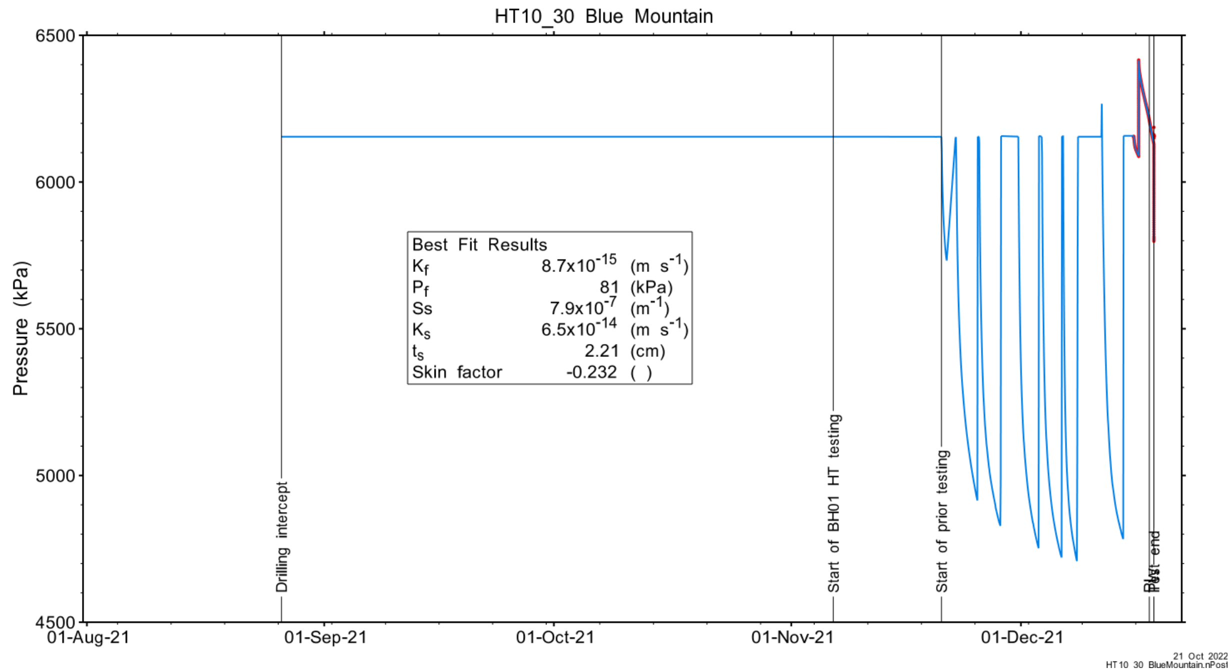

Figure 0.138 Annotated HT10_30 testing sequence showing pre-test history, best-fit simulation and parameter estimates.

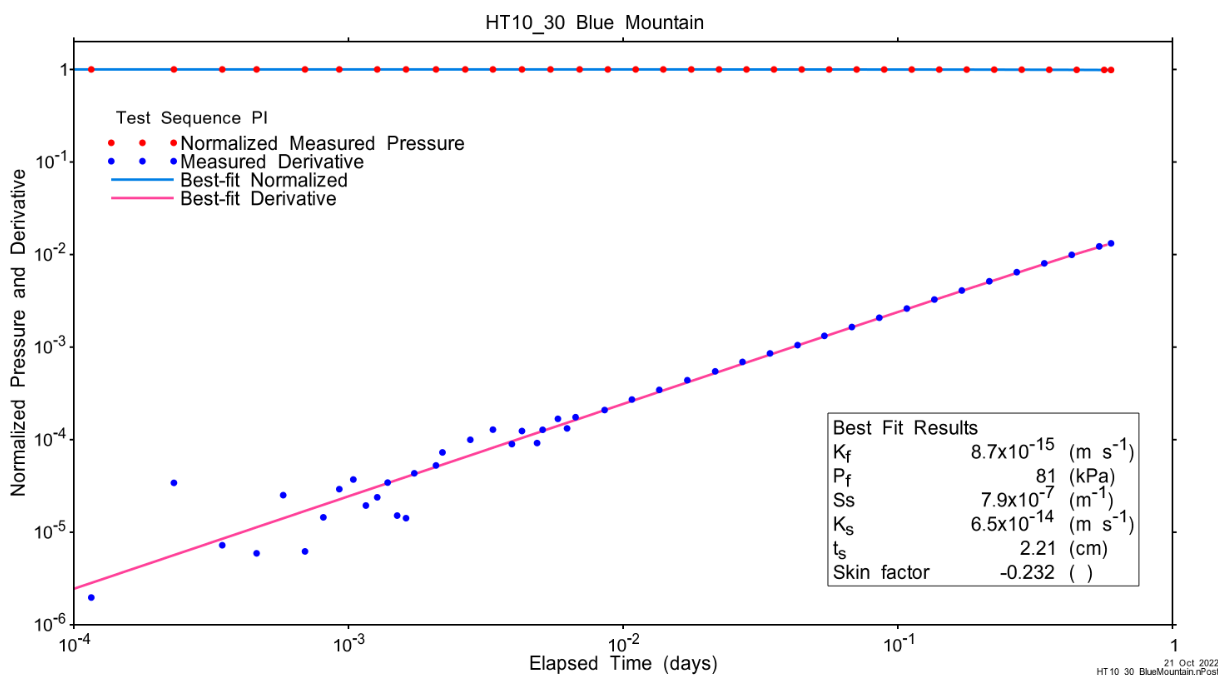

Figure 0.139 Log-log plot showing Ramey B normalized pressure and derivative response for PI best-fit simulation.

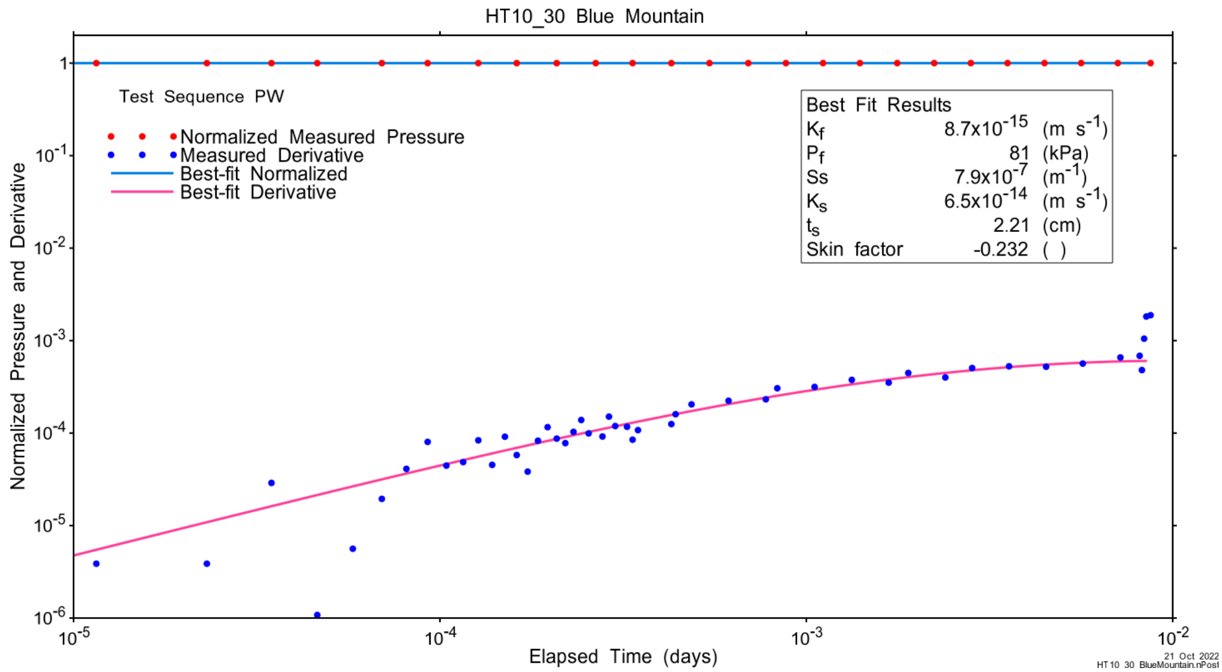

Figure 0.140 Log-log plot showing Ramey B normalized pressure and derivative response for PW best-fit simulation.

Figure 0.141 and Figure 0.142 show the normalized parameter sensitivity response for the PI and PW test sequences at the best fit. Sensitivity to all parameters except for K_s was still increasing at the end of both tests, suggesting increased test duration may have improved the estimates.

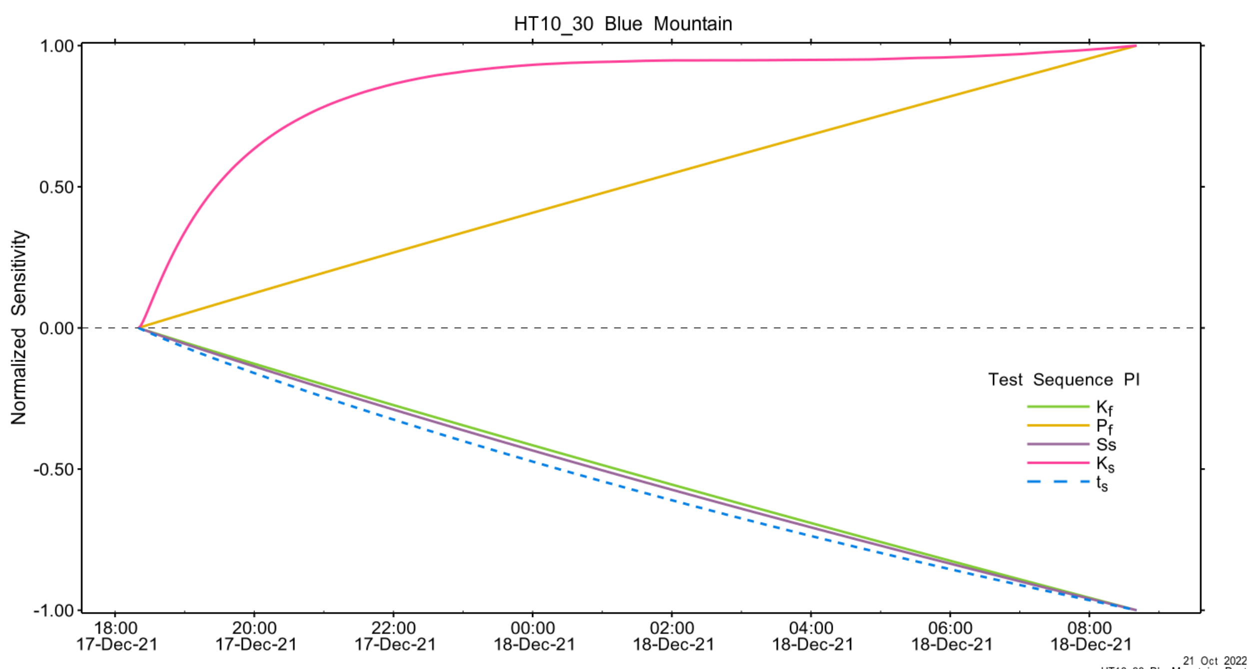

Figure 0.141 Normalized Jacobian for PI test sequence for the best-fit simulation.

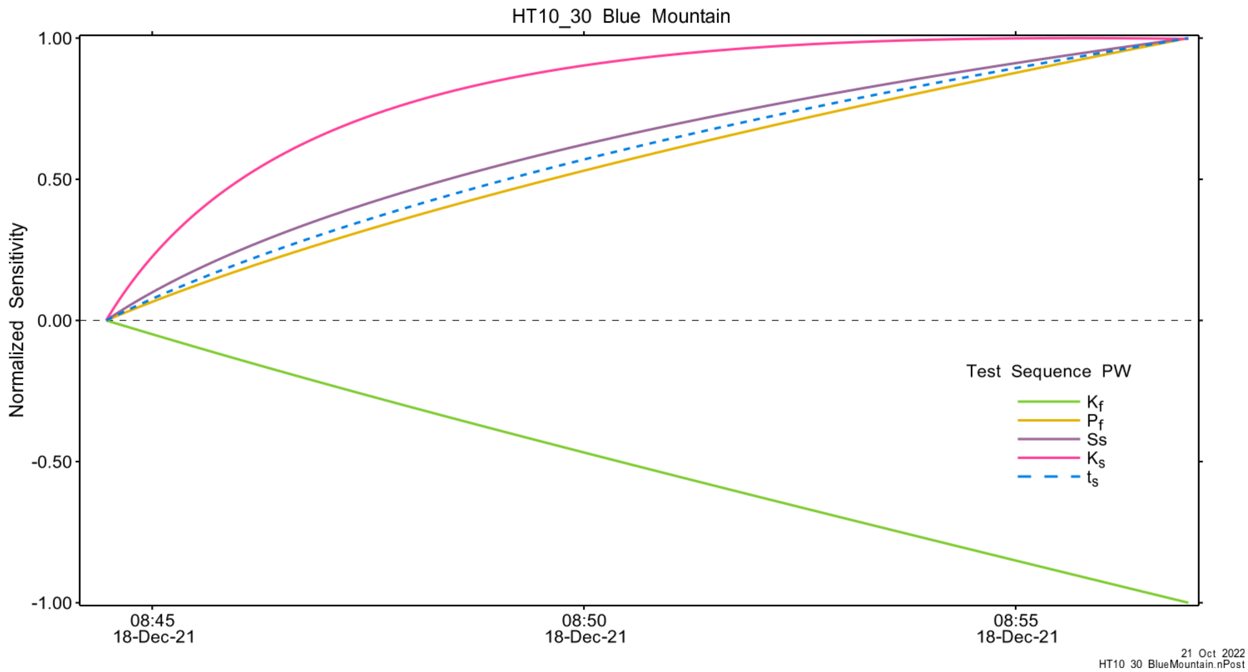

Figure 0.142 Normalized Jacobian for PW test sequence for the best-fit simulation.

A.10.3 Uncertainty Analyses

The CDF of normalized fit values for all converged simulations and the selected fit discriminant are shown in Figure 0.143.

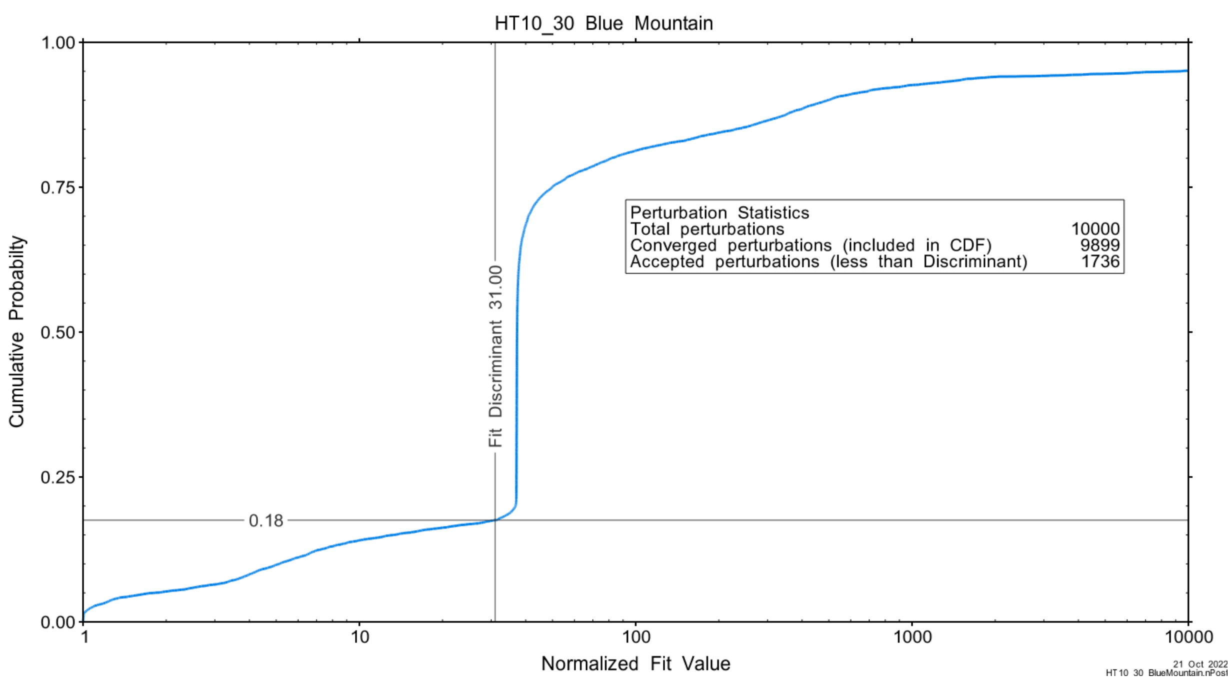

Figure 0.143 Fit value cumulative distribution function.

Summary cross parameter scatter plots for selected formation and skin parameters are given in Figure 0.144 and Figure 0.145. The light pink dots on the figures are the initial parameter estimates, with red dots overlaying those initial parameter values that resulted in accepted optimization results. The grey dots are converged optimizations which did not meet the fit discriminant. Larger varying color symbols represent the fit value of accepted optimizations, with the blue values representing the best fit.

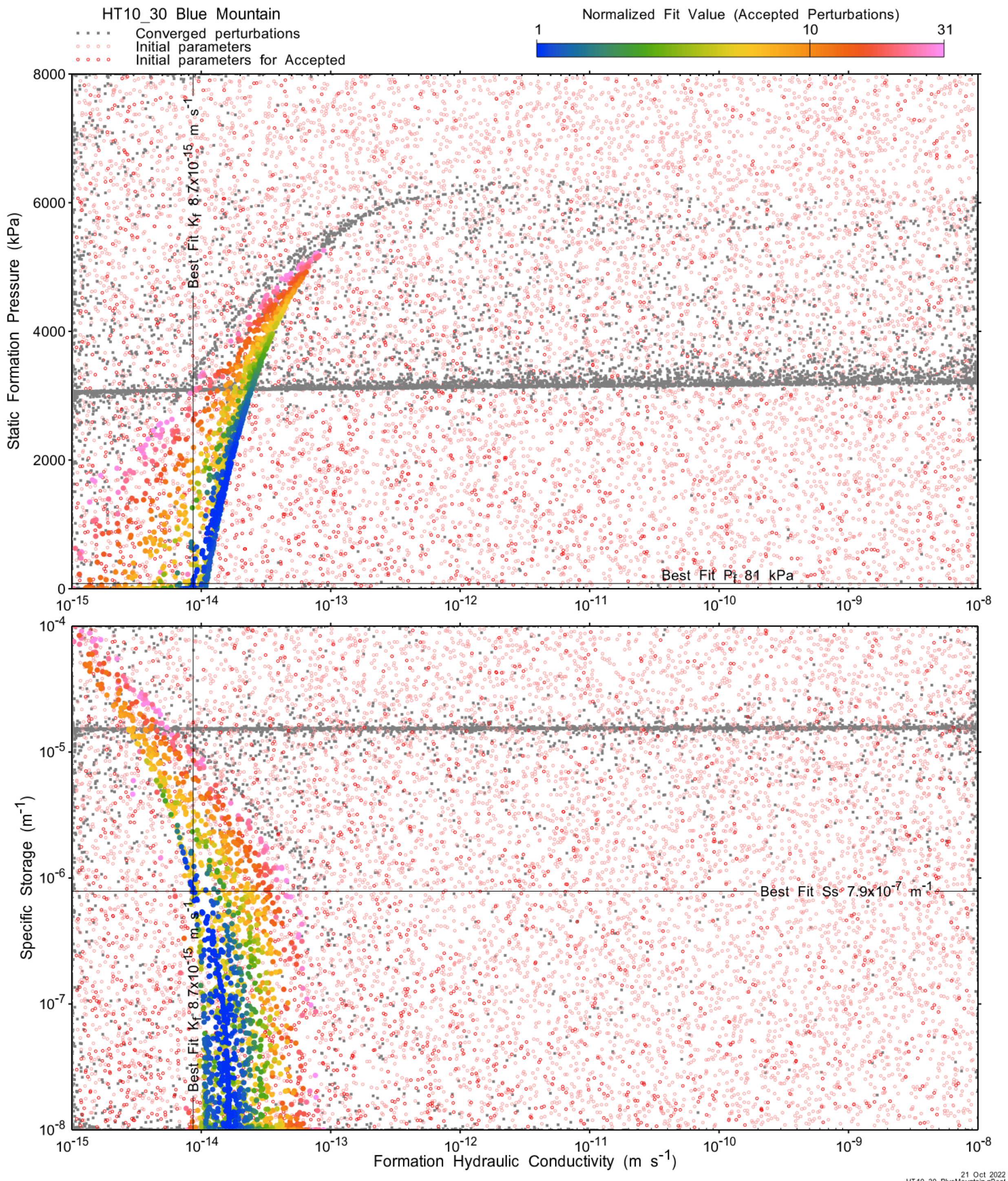

Figure 0.144 XY-scatter plot showing estimates of formation hydraulic conductivity (K_f) vs static formation pressure (P_f) (top panel) and specific storage (Ss) (bottom panel).

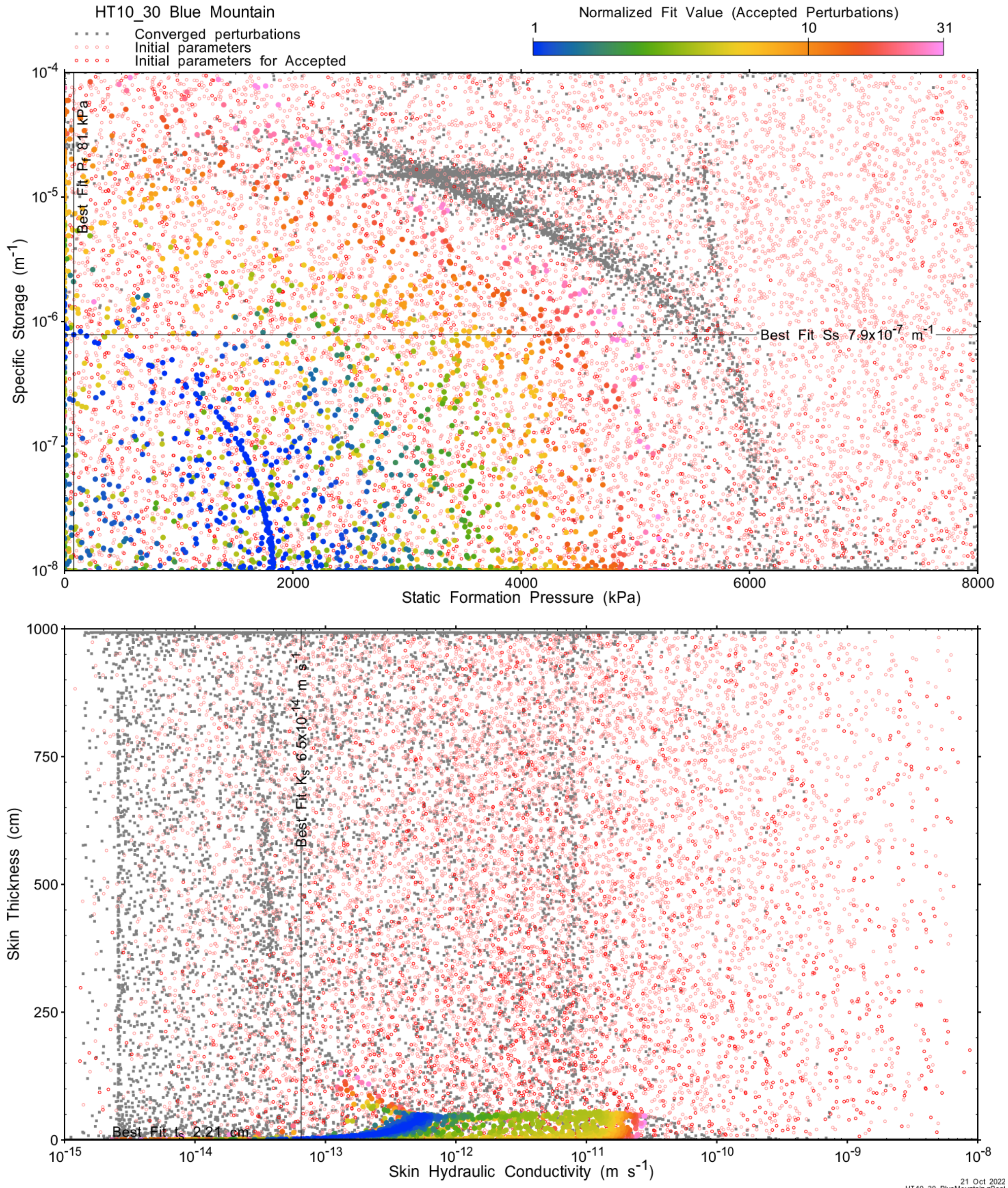

Figure 0.145 XY-scatter plot showing estimates of static formation pressure (P_f) vs specific storage (Ss) (top panel) and skin hydraulic conductivity (K_s) vs skin thickness (t_s) (bottom panel).

Confidence limits and median values are determined from the CDF of accepted optimization results (i.e. the varying color values in the above figures), with best fit value, 5% and 95% confidence indicated on Figure 0.146 and Figure 0.147.

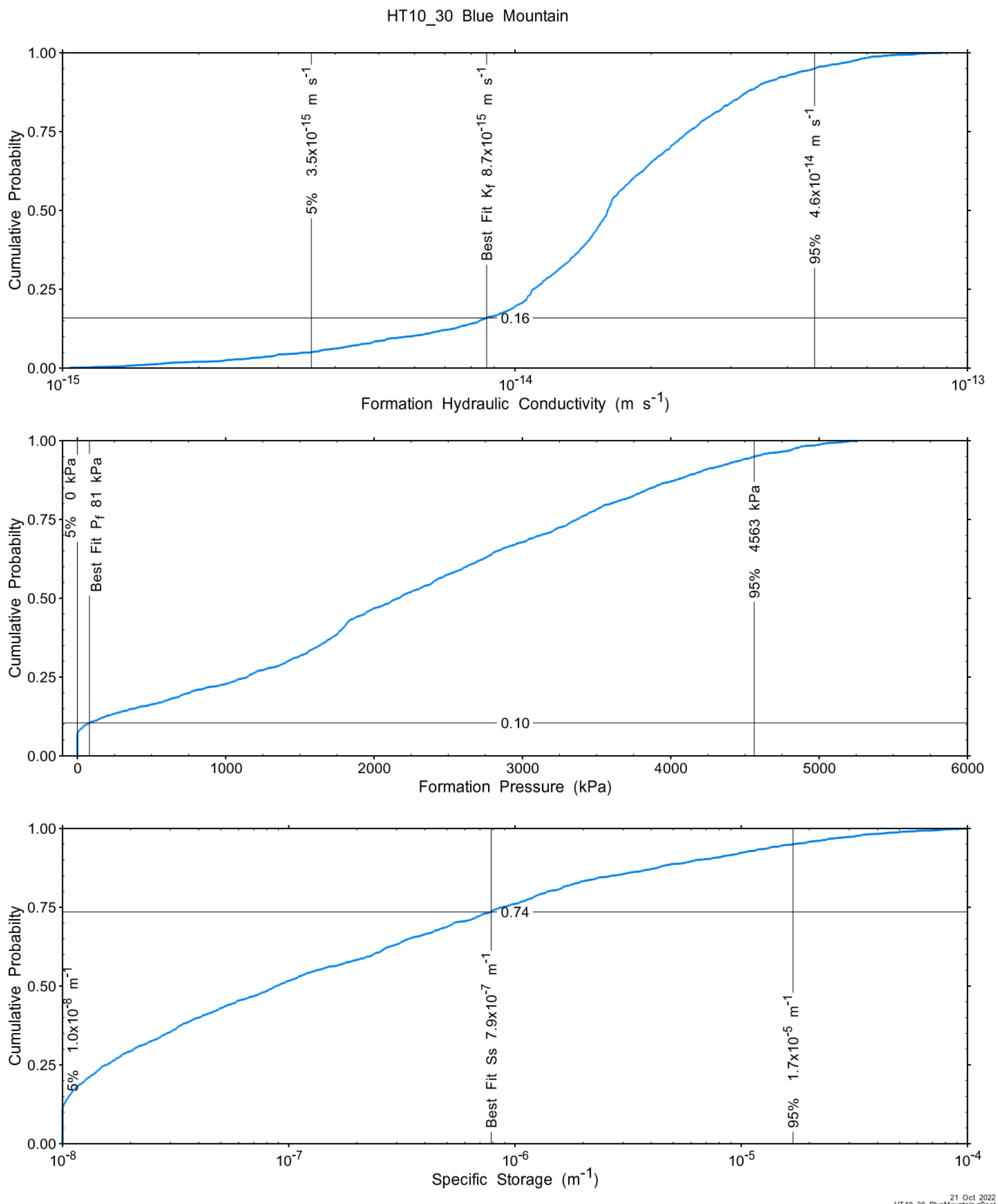

Figure 0.146 Cumulative distribution functions and parameter limits for formation hydraulic conductivity (K_f) (top panel), static formation pressure (P_f) (middle panel) and specific storage (Ss) (bottom panel).

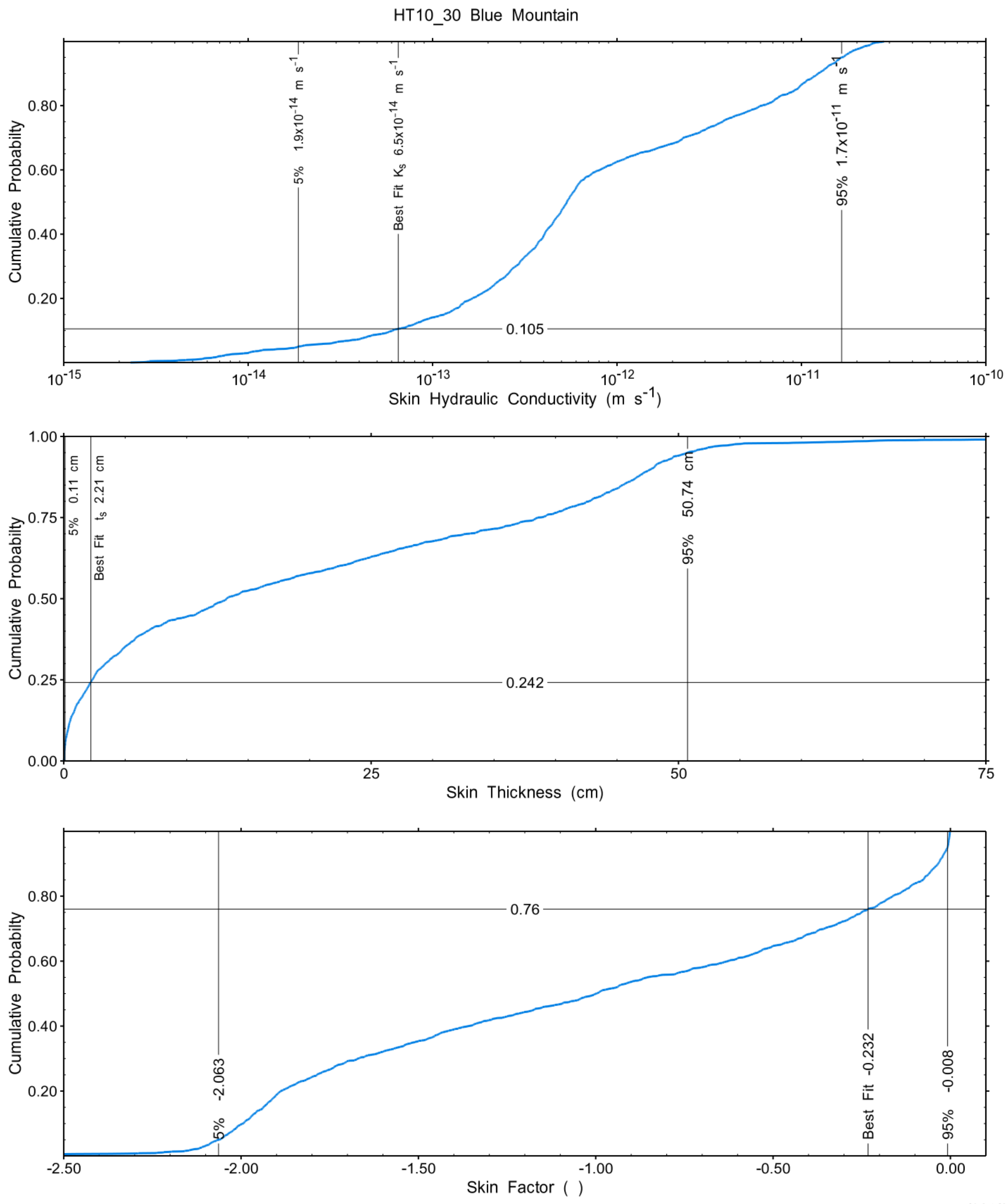

Figure 0.147 Cumulative distribution functions and parameter limits for skin hydraulic conductivity (K_s) (top panel), skin thickness (t_s) (middle panel) and skin factor (s) (bottom panel).

A summary of perturbation results is presented in Figure 0.148, with Ramey-processed perturbations in Figure 0.149. Those perturbations (1263 of 10,000) with all parameters within the 5% and 95% range present a good fit to the measured test zone data.

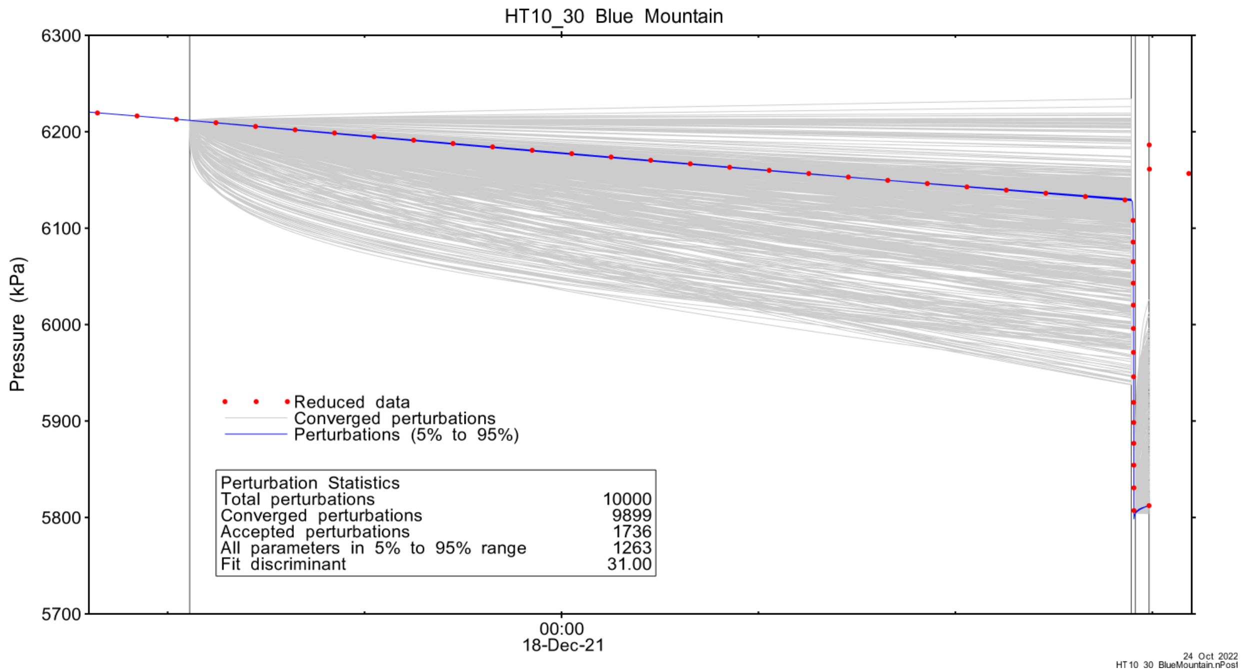

Figure 0.148 Perturbation results – all converged, accepted, and within 5% to 95% for all parameters.

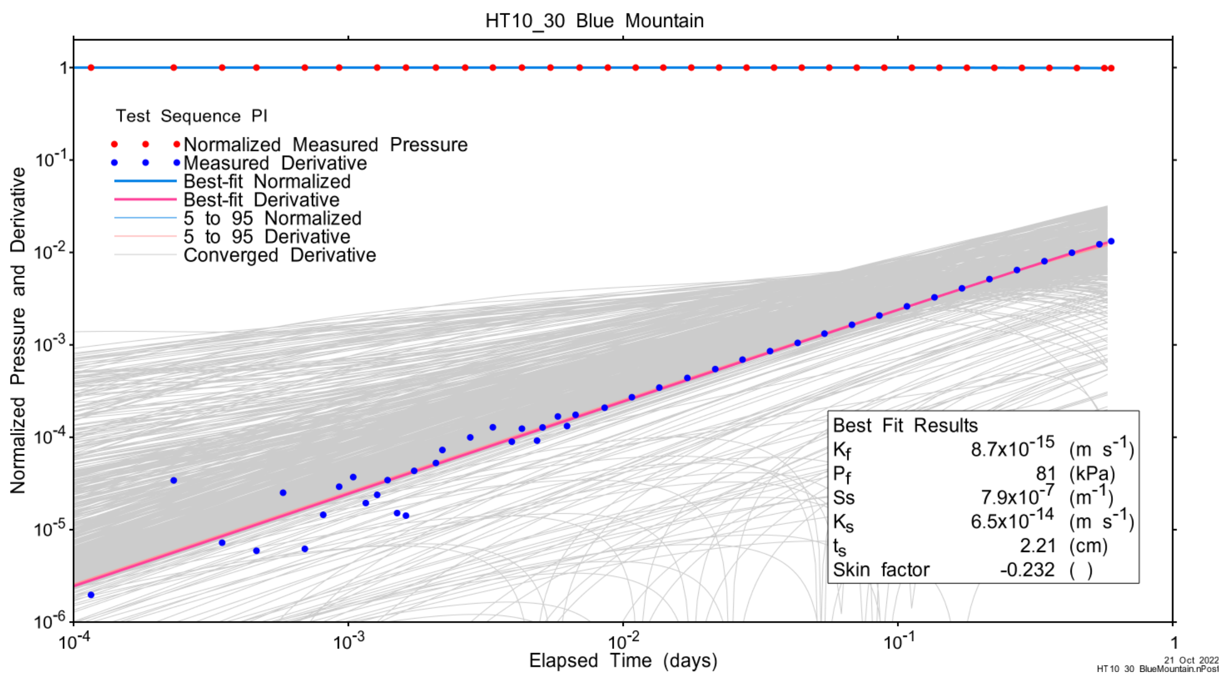

Figure 0.149 Log-log plot showing Ramey B normalized pressure and derivative response for PI sequence for all converged optimizations and those within 5% to 95% for all parameters.

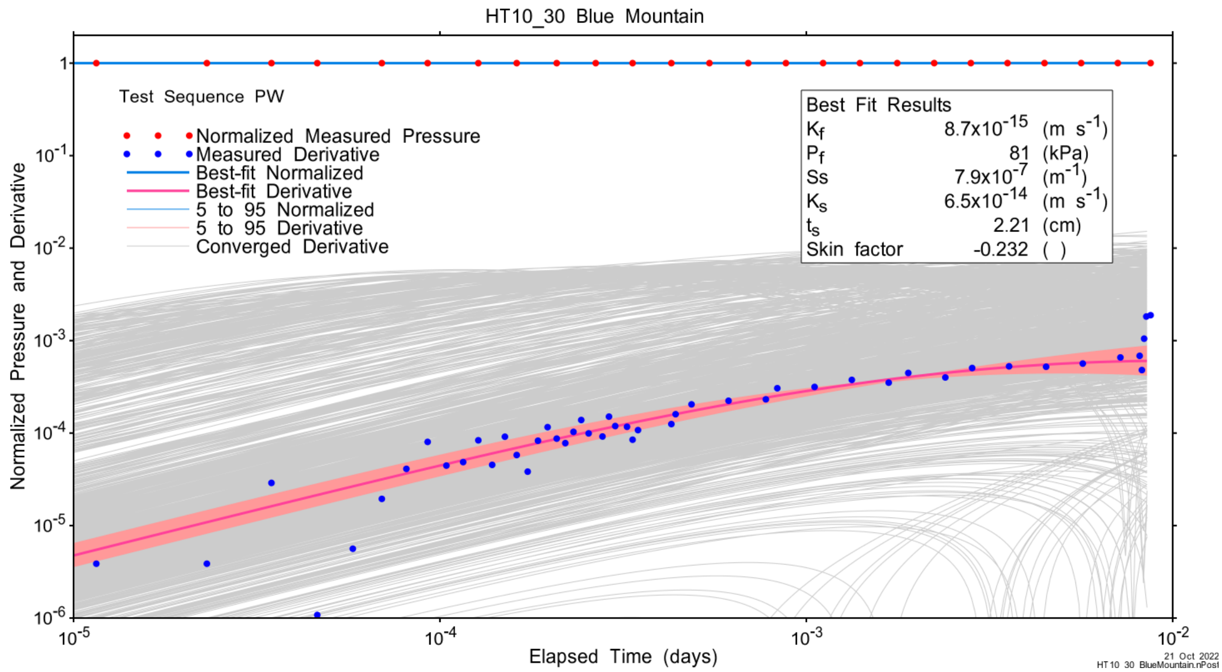

Figure 0.150 Log-log plot showing Ramey B normalized pressure and derivative response for PW sequence for all converged optimizations and those within 5% to 95% for all parameters.

A summary of best-fit parameter estimates and ranges is given in Table 0.49.

Table 0.49 Summary of the HT10_30 parameter estimates.

Parameter	Best Fit	5%	Median	95%
K_f (m/s)	8.7E-15	3.5E-15	1.6E-14	4.6E-14
P_f (kPa)	81	0	2164	4563
Ss (1/m)	7.9E-07	1.0E-08	8.8E-08	1.7E-05
K_s (m/s)	6.5E-14	1.9E-14	5.3E-13	1.7E-11
t_s (cm)	2.21	0.11	13.25	50.74
s (-)	-0.232	-2.063	-0.998	-0.008

Parameter correlations for all perturbations with all parameters within the 5% to 95% limits are given in Table 0.50.

Table 0.50 Pearson cross-correlations of 5% to 95% parameters

	Log(K_f)	P_f	Log(Ss)	Log(K_s)	t_s	s
Log(K_f)	1.000	0.869	-0.460	0.066	0.299	-0.328
P_f	0.869	1.000	-0.060	0.059	0.013	0.012
Log(Ss)	-0.460	-0.060	1.000	-0.170	-0.911	0.966
Log(K_s)	0.066	0.059	-0.170	1.000	0.242	-0.287
t_s	0.299	0.013	-0.911	0.242	1.000	-0.972
s	-0.328	0.012	0.966	-0.287	-0.972	1.000

A.10.4 Additional Figures

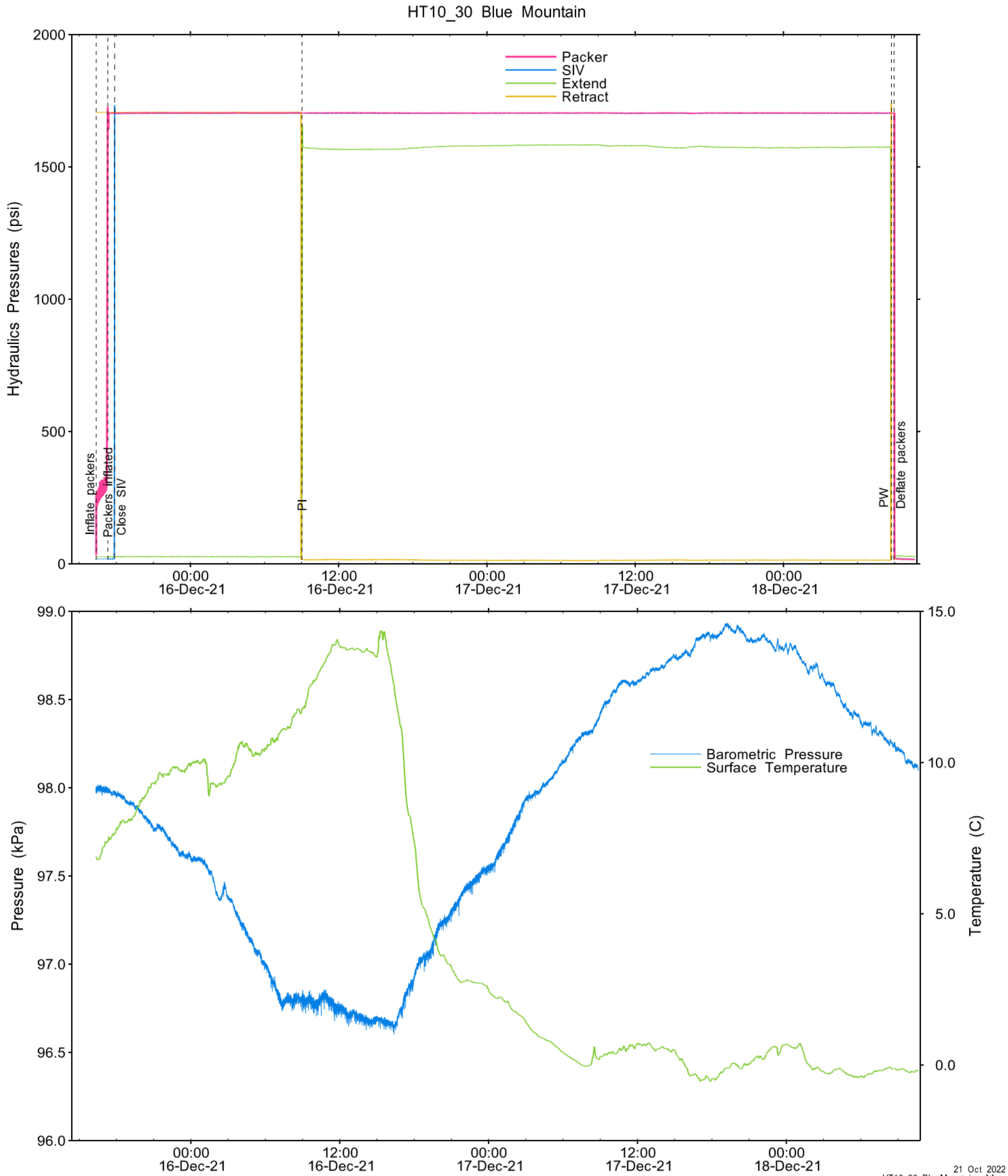

Figure 0.151 Hydraulics pressures and surface temperature/barometric pressure.

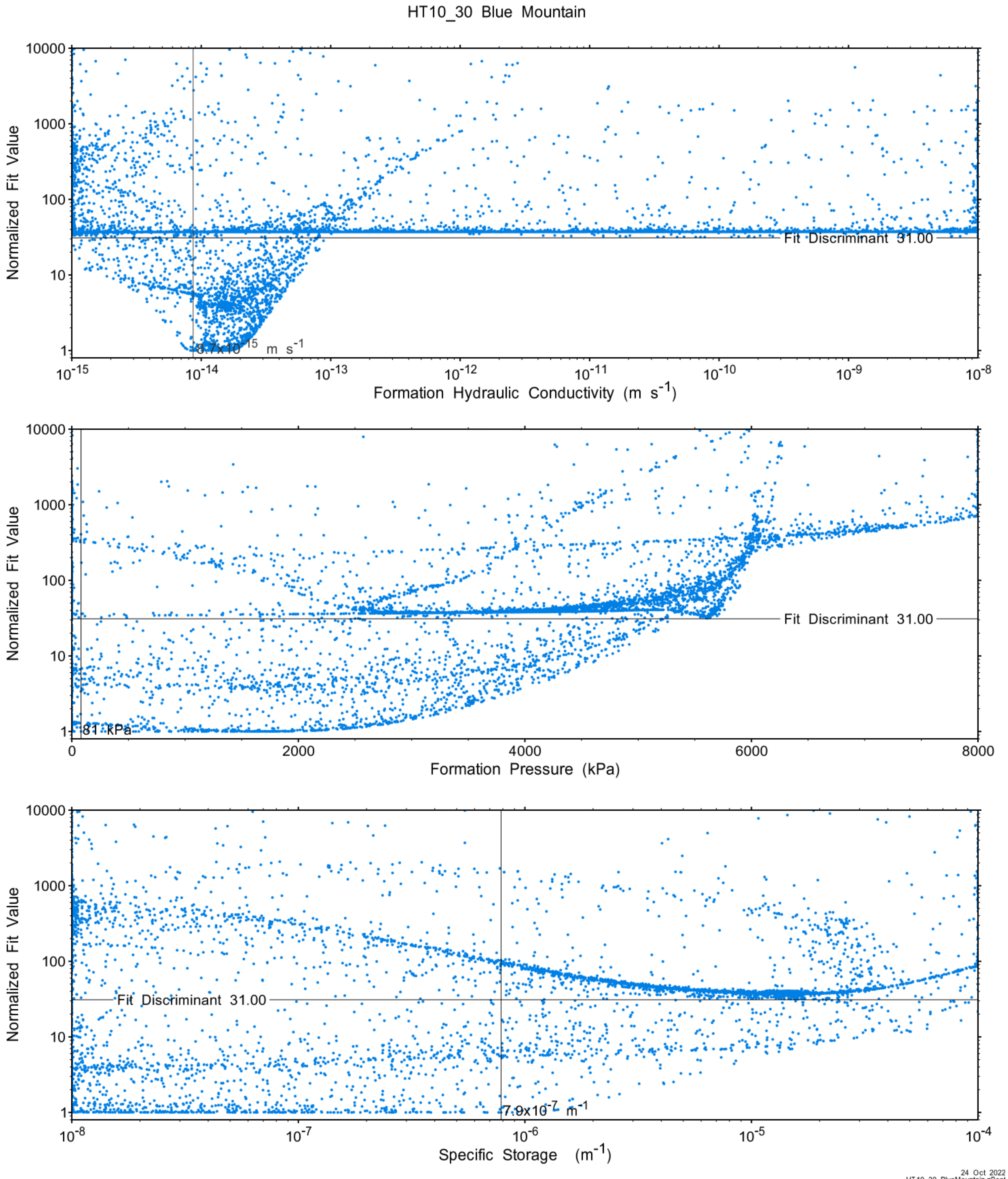

Figure 0.152 XY-scatter plot showing the formation parameter space normalized fit values.

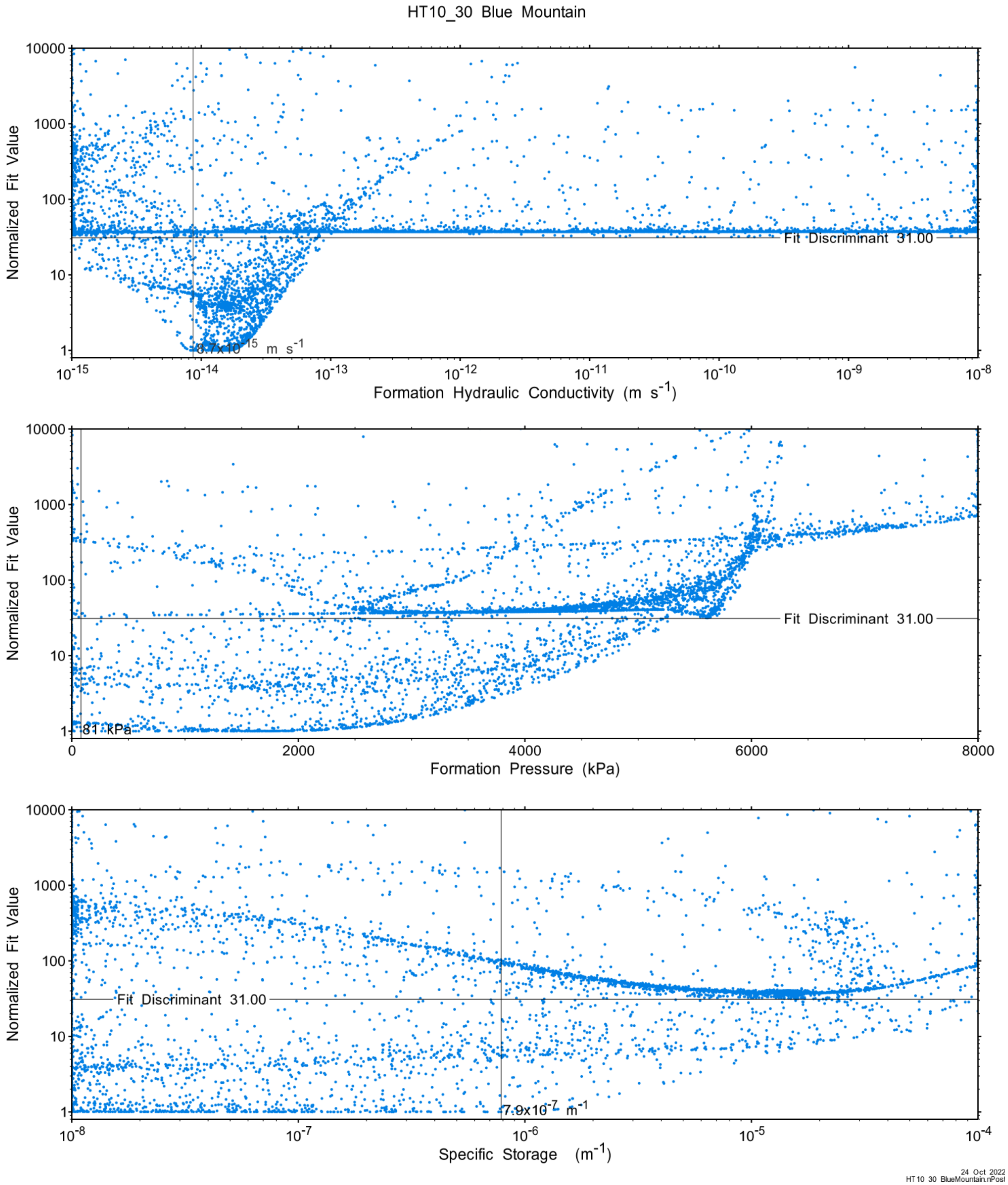

Figure 0.153 XY-scatter plot showing the skin parameter space normalized fit values.

A.11 HT11_30 Upper Cobourg

The SB_BH01 interval from 646.00 to 676.05 mBGS tested in HT11_30 includes the upper part of the Cobourg Formation. A single PI test with a duration of 2 days was conducted.

A.11.1 Test Data Summary

Table 0.51 and Figure 0.154 provide a summary of test events and a plot of pressures measured while testing, respectively.

Table 0.51 HT11_30 Summary of Test Events.

Event	Start Date & Time	Duration (days)	TZ Pressure (kPa)
Drilling intercept	21-08-29 08:30	83.26	6601
Prior testing	21-11-20 14:45	28.04	variable
Shut-in	21-12-18 15:45	0.72	6605
Pulse injection	21-12-19 09:01	2.00	7293
Test end	21-12-21 09:03		7052

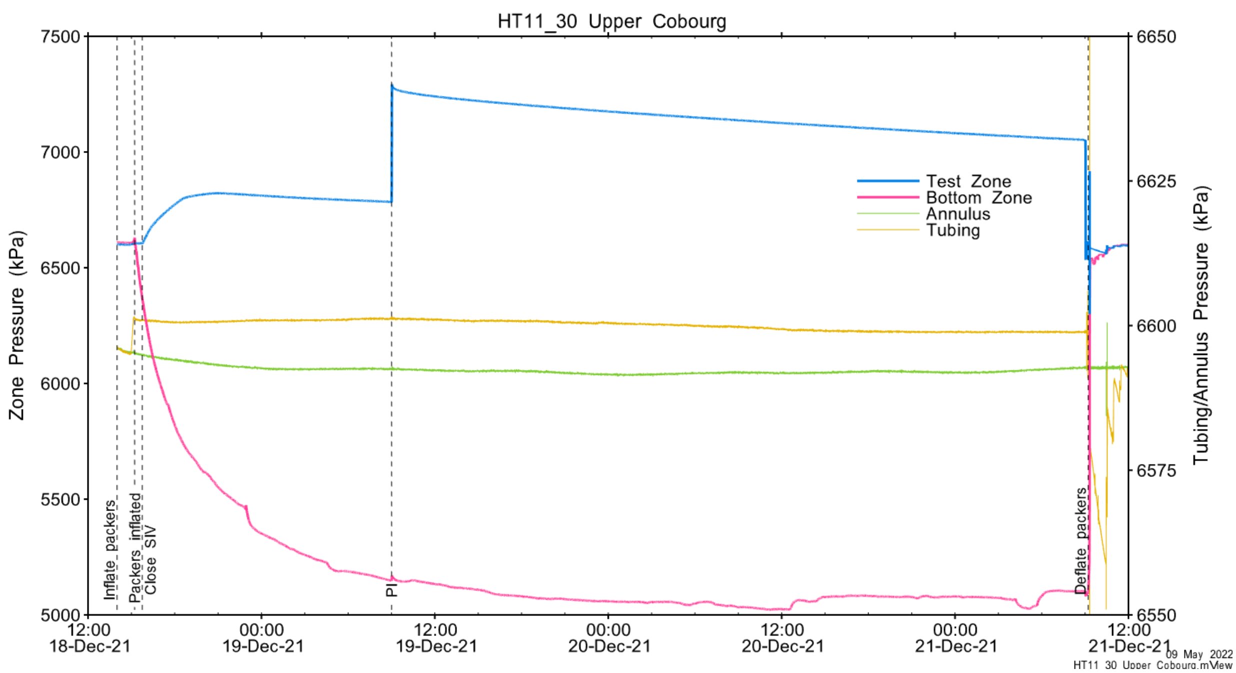

Figure 0.154 HT11_30 test events and pressures.

A.11.2 Test Analyses

Table 0.52 is a summary of test-specific input parameters used in the analyses, while Table 0.53 presents the optimized parameters and allowed ranges.

Table 0.52 nSIGHTS Input Parameters.

Parameter	Value	Units
Test zone radius	6.86	cm
Test zone compressibility	4.54E-10	1/Pa
Test zone fluid density	1046	g/L
Test zone length	30.05	m

Table 0.53 nSIGHTS Parameter Optimization Ranges.

Parameter	Minimum	Maximum	Units	Type
Formation hydraulic conductivity (K_f)	1E-16	1E-10	m/s	log
Formation pressure (P_f)	0	6000	kPa	linear
Specific storage (Ss)	1E-08	1E-04	1/m	log
Skin hydraulic conductivity (K_s)	1E-16	1E-13	m/s	log
Skin thickness (t_s)	0.1	931	mm	linear

Figure 0.155 shows the measured test zone pressure record (with reduced data density for clarity) used in the analysis along with the best-fit simulation and parameter values. Figure 0.156 presents the pre-test history, and Figure 0.157 shows the Ramey B normalized best-fit pressure and pressure derivatives.

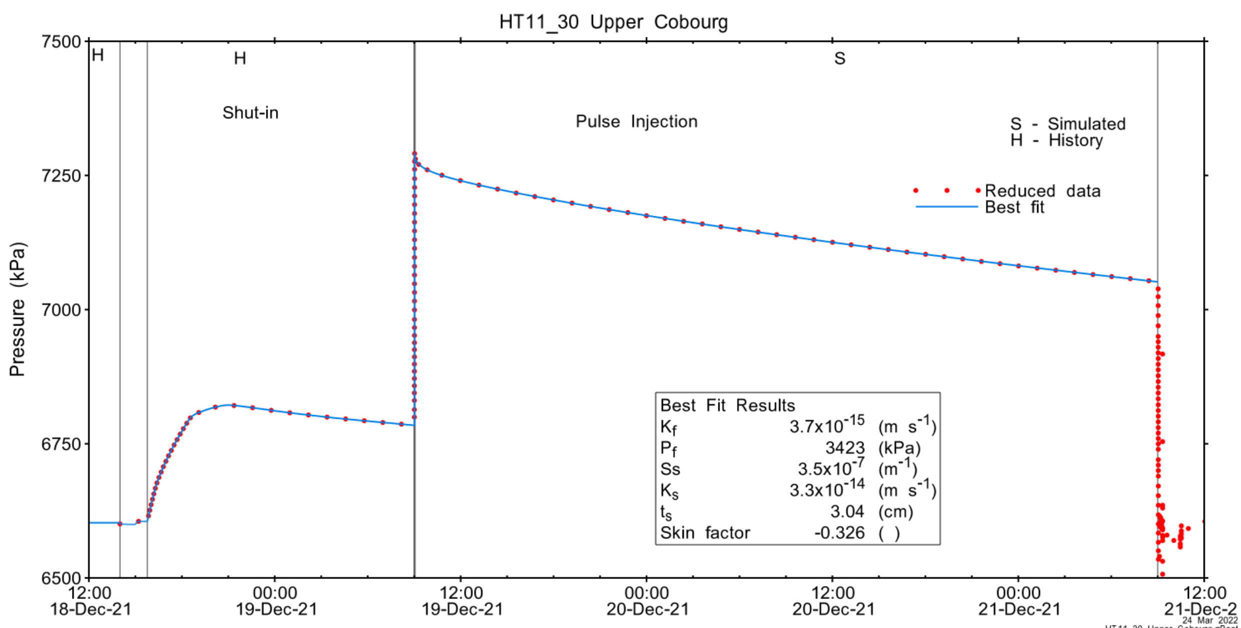

Figure 0.155 Annotated testing sequence showing best-fit simulation and parameter estimates.

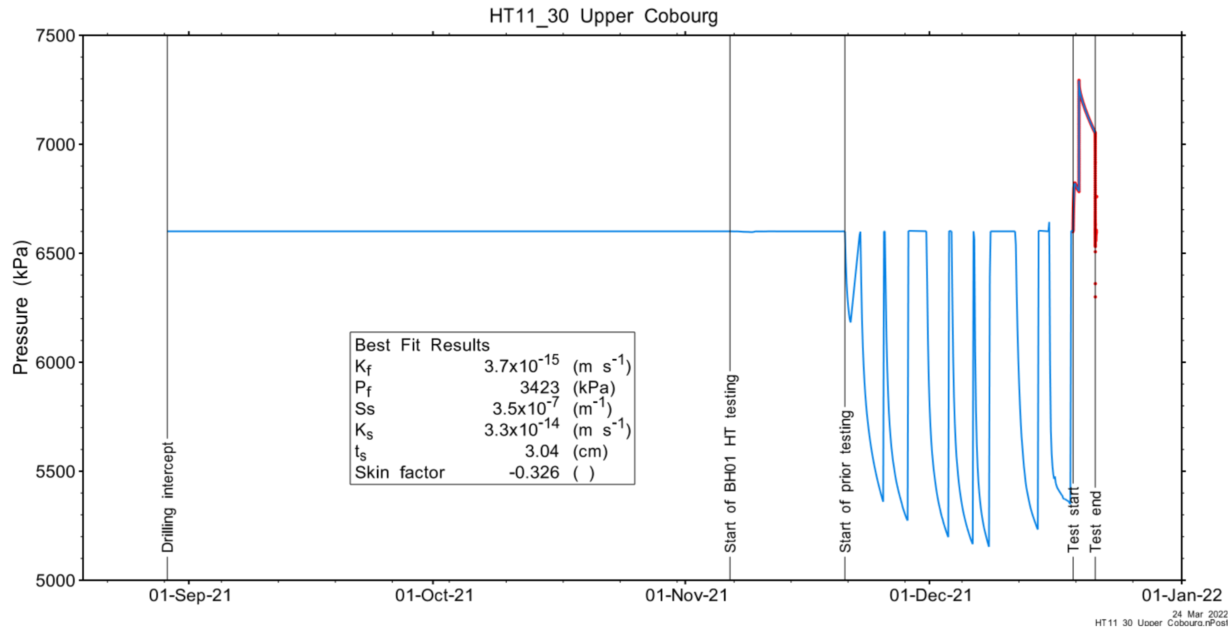

Figure 0.156 Annotated HT11_30 testing sequence showing pre-test history, best-fit simulation and parameter estimates.

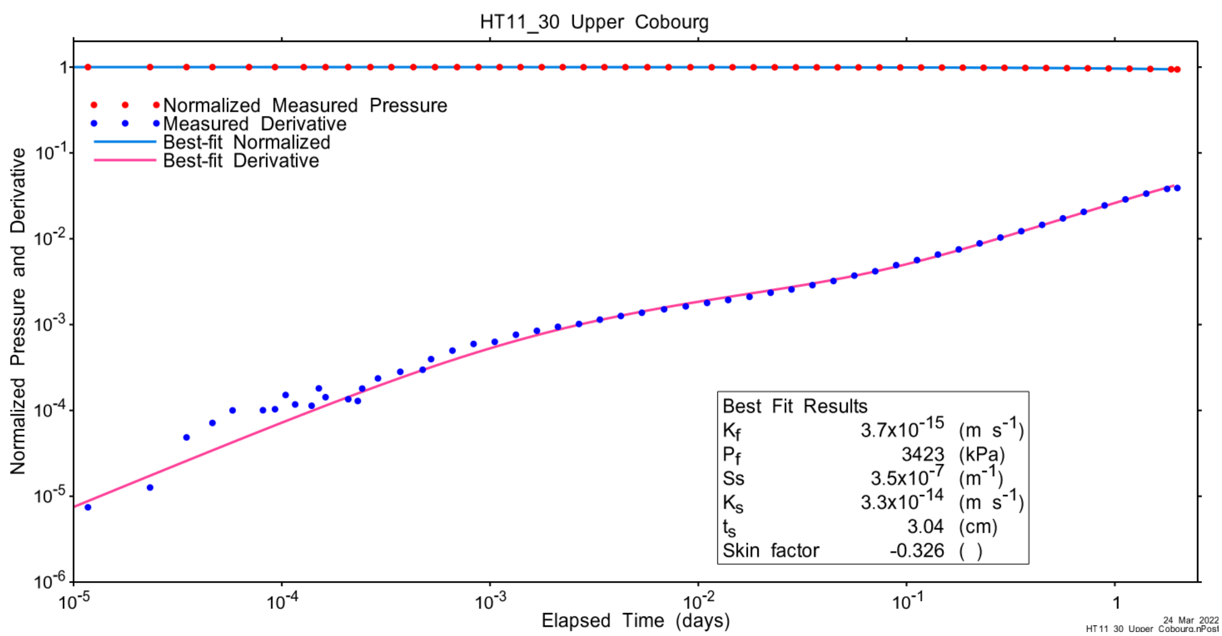

Figure 0.157 Log-log plot showing Ramey B normalized pressure and derivative response for best-fit simulation.

Figure 0.158 shows the normalized parameter sensitivity response for the best fit. Skin-related parameters are most sensitive during the early-time response. Sensitivity for K_f, P_f and Ss continues to rise – additional test time may have improved the estimates.

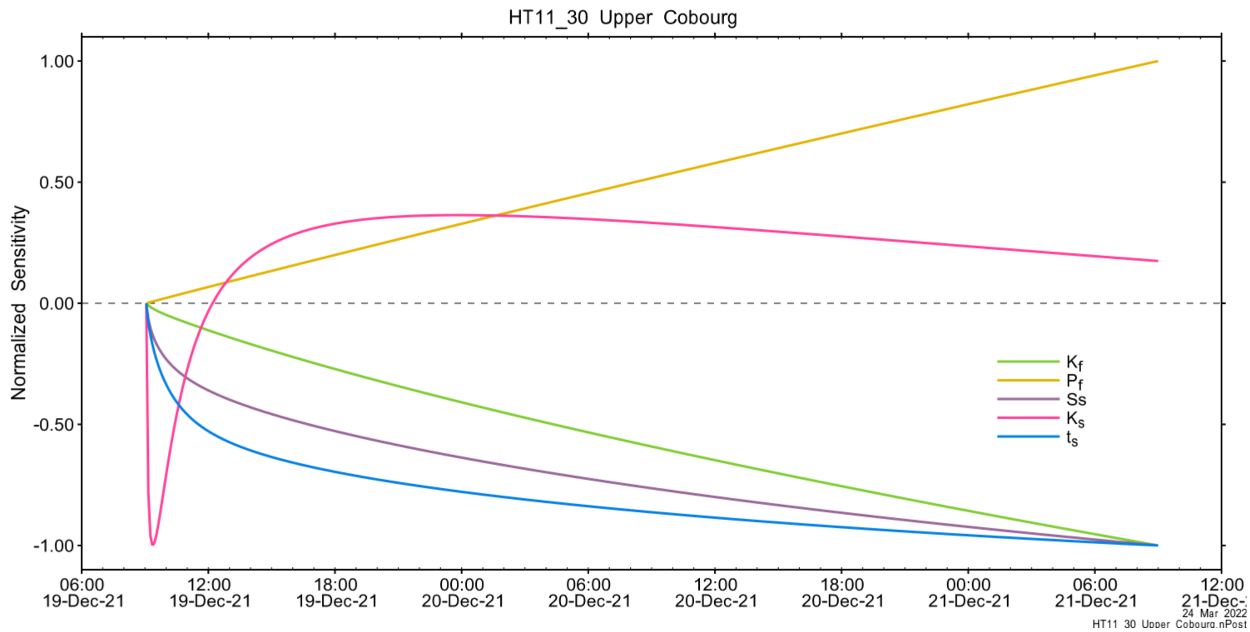

Figure 0.158 Normalized Jacobian for best-fit simulation.

A.11.3 Uncertainty Analyses

The CDF of normalized fit values for all converged simulations and the selected fit discriminant are shown in Figure 0.159.

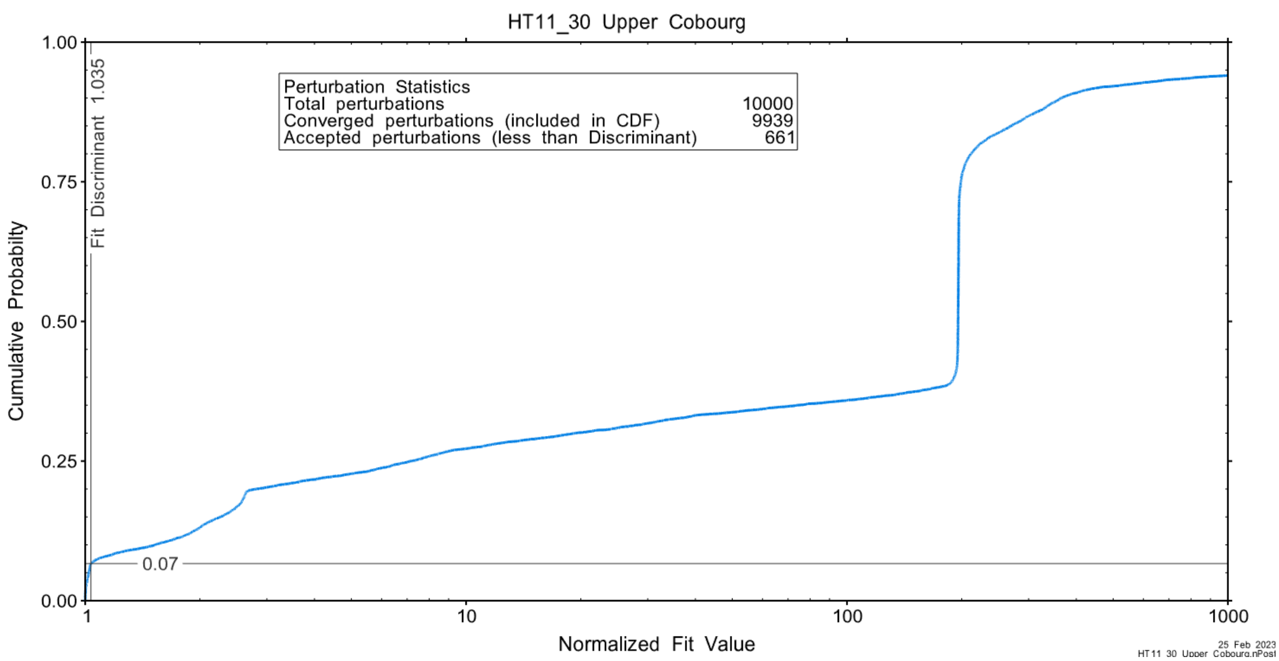

Figure 0.159 Fit value cumulative distribution function.

Summary cross parameter scatter plots for selected formation and skin parameters are given in Figure 0.160 and Figure 0.161. The light pink dots on the figures are the initial parameter estimates, with red dots overlaying those initial parameter values that resulted in accepted optimization results. The grey dots are converged optimizations which did not meet the fit discriminant. Larger varying color symbols represent the fit value of accepted optimizations, with the blue values representing the best fit.

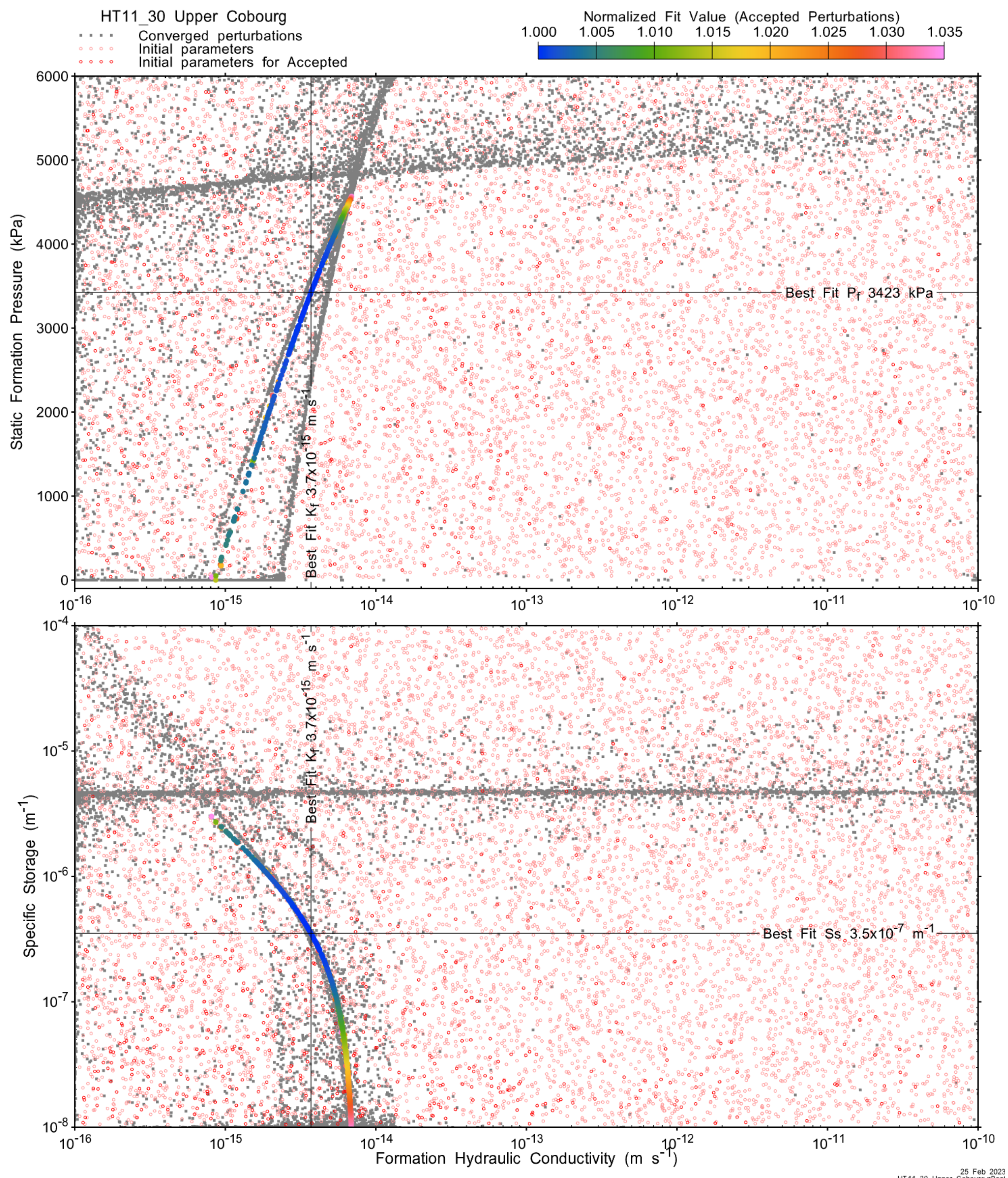

Figure 0.160 XY-scatter plot showing estimates of formation hydraulic conductivity (K_f) vs static formation pressure (P_f) (top panel) and specific storage (Ss) (bottom panel).

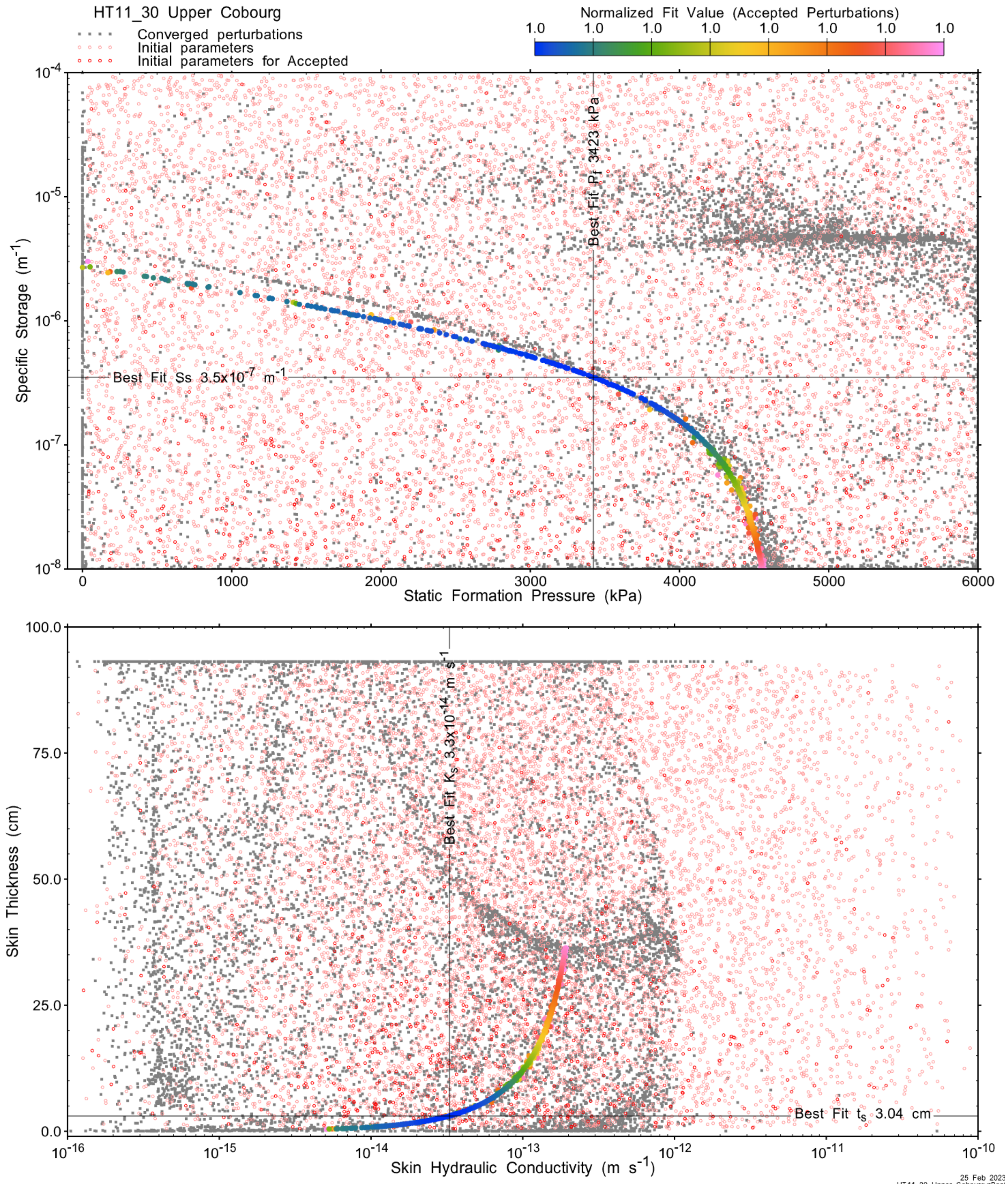

Figure 0.161 XY-scatter plot showing estimates of static formation pressure (P_f) vs specific storage (Ss) (top panel) and skin hydraulic conductivity (K_s) vs skin thickness (t_s) (bottom panel).

Confidence limits and median values are determined from the CDF of accepted optimization results (i.e. the varying color values in the above figures), with best fit value, 5% and 95% confidence indicated on Figure 0.162 and Figure 0.163.

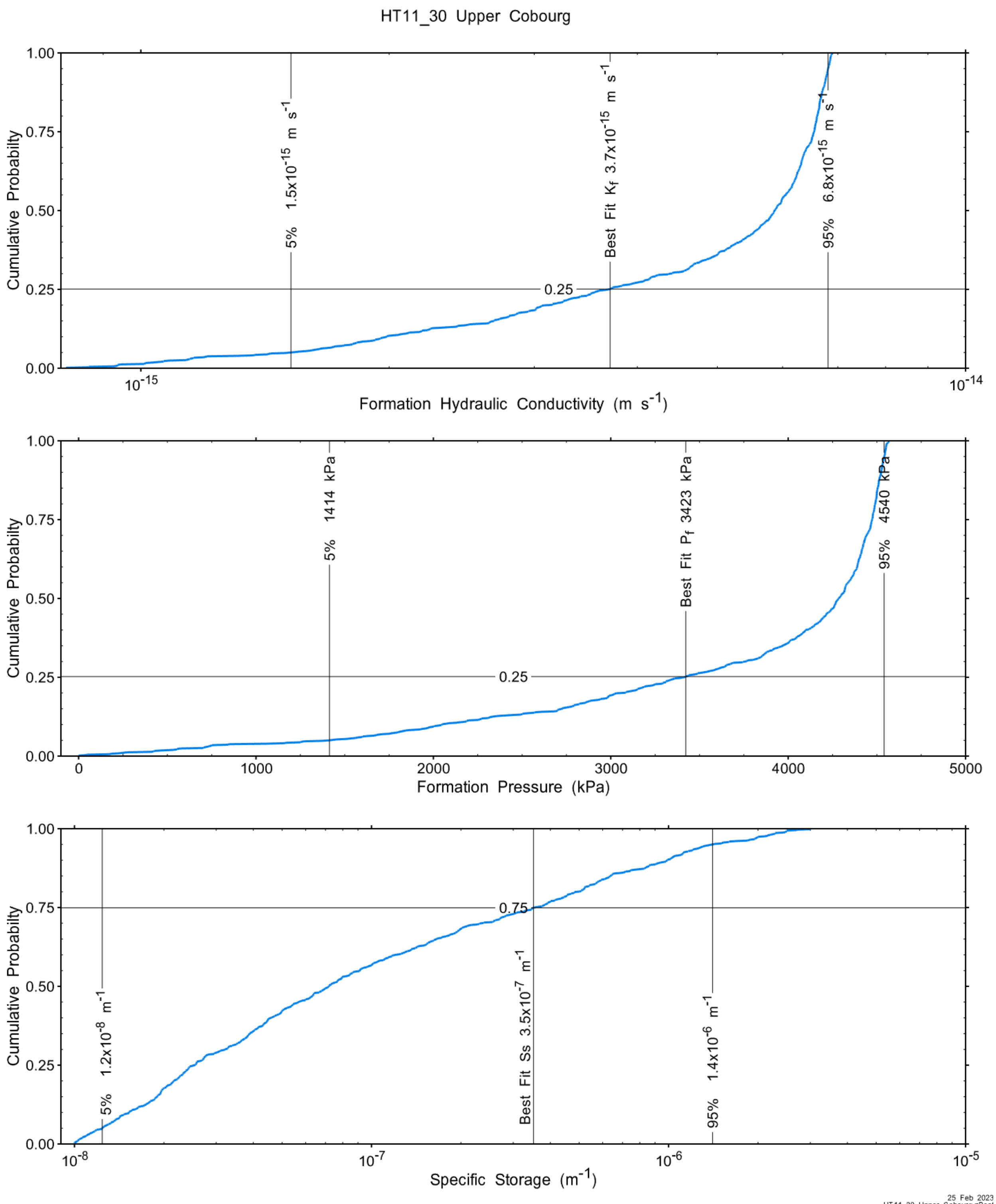

Figure 0.162 Cumulative distribution functions and parameter limits for formation hydraulic conductivity (K_f) (top panel), static formation pressure (P_f) (middle panel) and specific storage (Ss) (bottom panel).

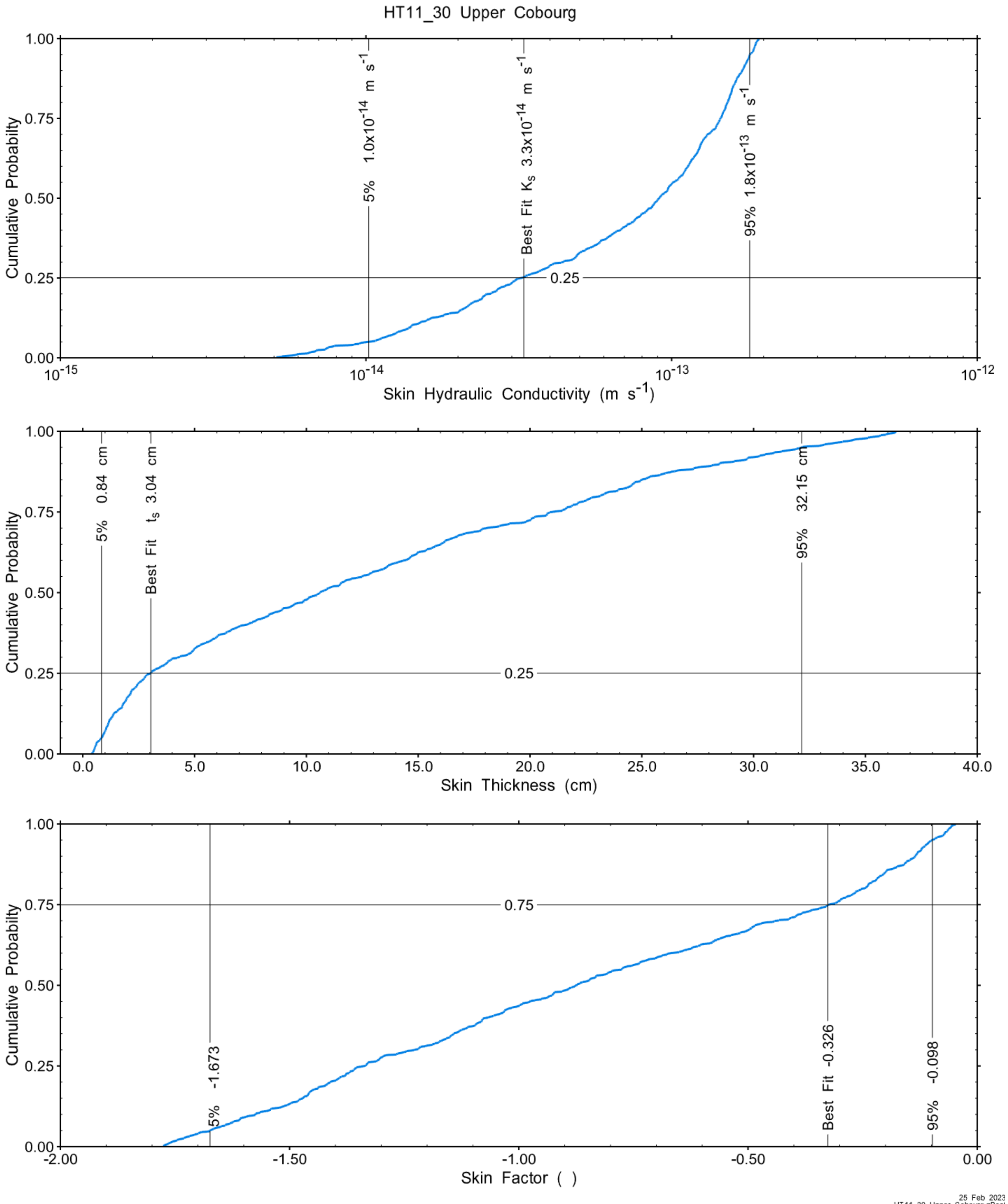

Figure 0.163 Cumulative distribution functions and parameter limits for skin hydraulic conductivity (K_s) (top panel), skin thickness (t_s) (middle panel) and skin factor (s) (bottom panel).

A summary of perturbation results is presented in Figure 0.164, with Ramey-processed perturbations in Figure 0.165. Those perturbations (592 of 10,000) with all parameters within the 5% and 95% range match the measured test zone data well.

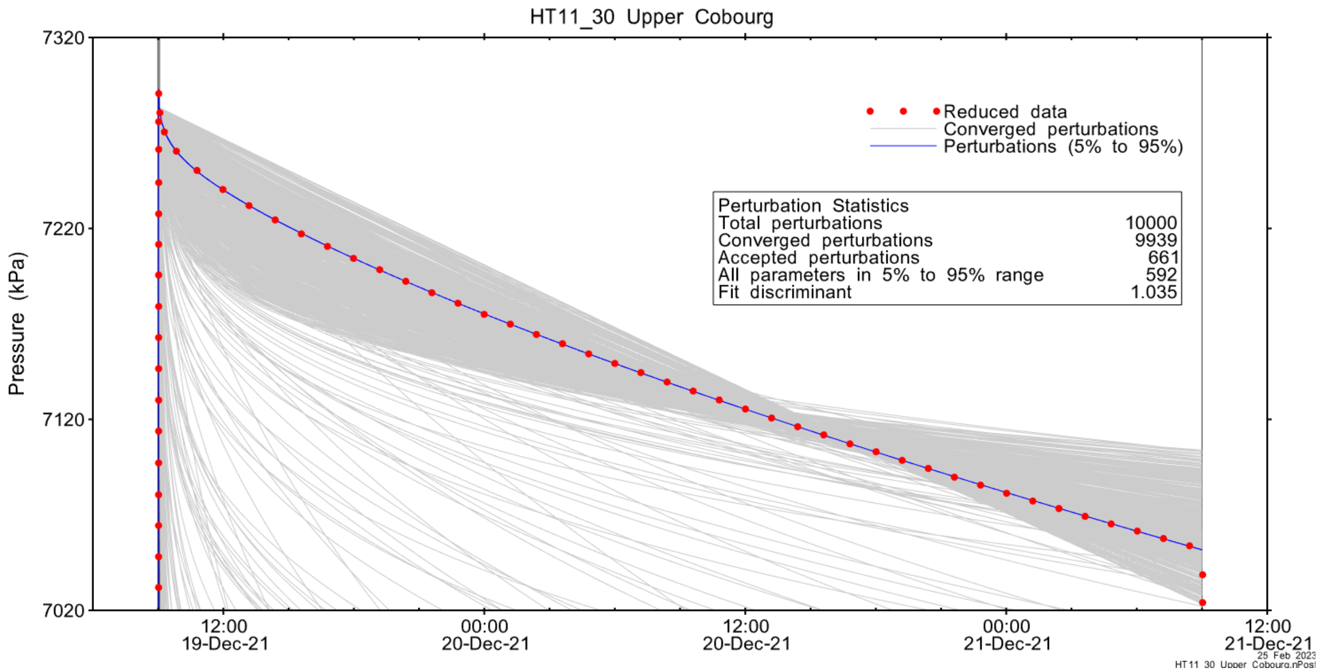

Figure 0.164 Perturbation results – all converged, accepted, and within 5% to 95% for all parameters.

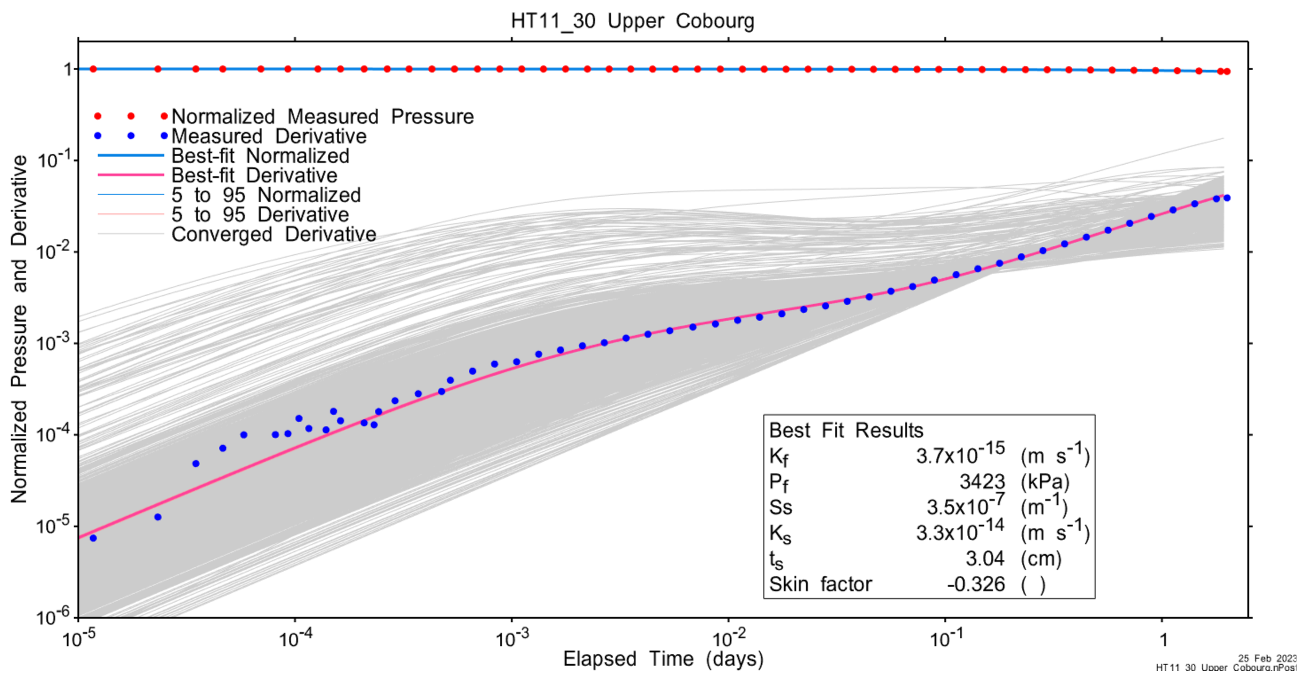

Figure 0.165 Log-log plot showing Ramey B normalized pressure and derivative response for all converged optimizations and those within 5% to 95% for all parameters.

A summary of best-fit parameter estimates and ranges is given in Table 0.54.

Table 0.54 Summary of the HT11_30 parameter estimates.

Parameter	Best Fit	5%	Median	95%
K_f (m/s)	3.7E-15	1.5E-15	5.9E-15	6.8E-15
P_f (kPa)	3423	1414	4284	4540
Ss (1/m)	3.5E-07	1.2E-08	7.2E-08	1.4E-06
K_s (m/s)	3.3E-14	1.0E-14	9.1E-14	1.8E-13
t_s (cm)	3.04	0.84	10.61	32.15
s (-)	-0.326	-1.673	-0.875	-0.098

Parameter correlations for all perturbations with all parameters within the 5% to 95% limits are given in Table 0.55.

Table 0.55 Pearson cross-correlations of 5% to 95% parameters

	Log(K_f)	P_f	Log(Ss)	Log(K_s)	t_s	s
Log(K_f)	1.000	0.999	-0.938	0.977	0.785	-0.876
P_f	0.999	1.000	-0.921	0.965	0.759	-0.853
Log(Ss)	-0.938	-0.921	1.000	-0.990	-0.947	0.989
Log(K_s)	0.977	0.965	-0.990	1.000	0.892	-0.958
t_s	0.785	0.759	-0.947	0.892	1.000	-0.982
s	-0.876	-0.853	0.989	-0.958	-0.982	1.000

A.11.4 Additional Figures

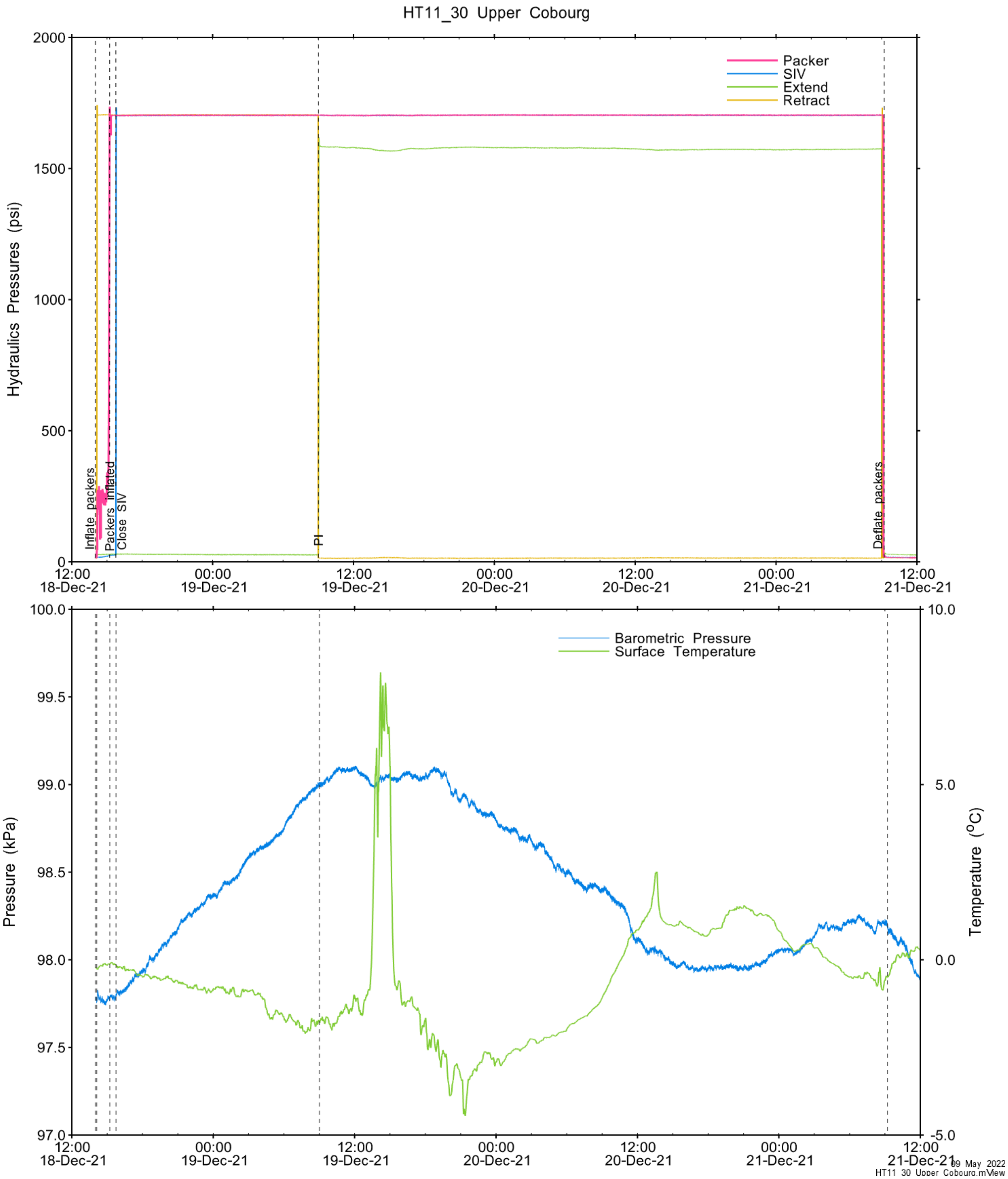

Figure 0.166 Hydraulics pressures and surface temperature/barometric pressure.

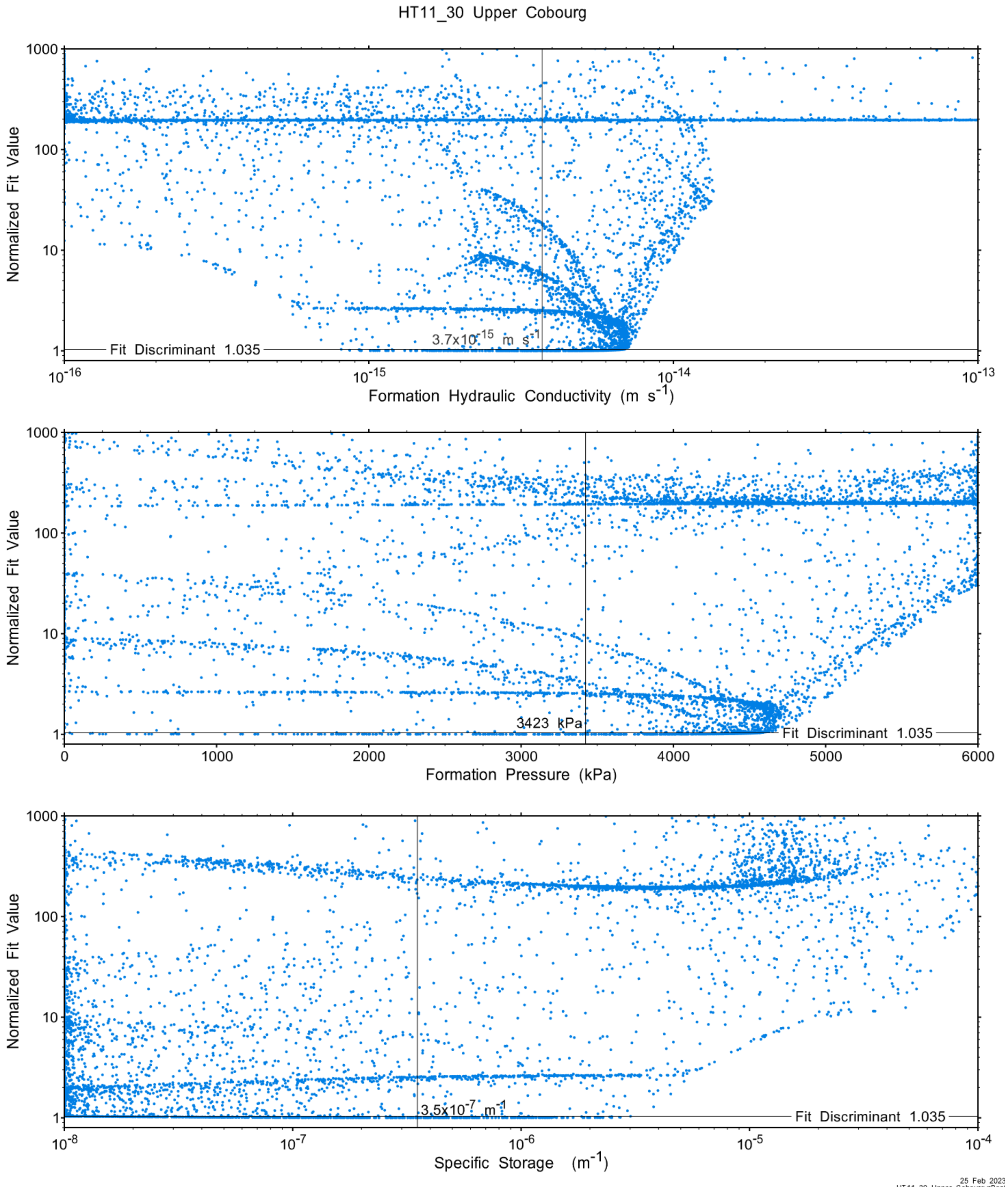

Figure 0.167 XY-scatter plot showing the formation parameter space normalized fit values.

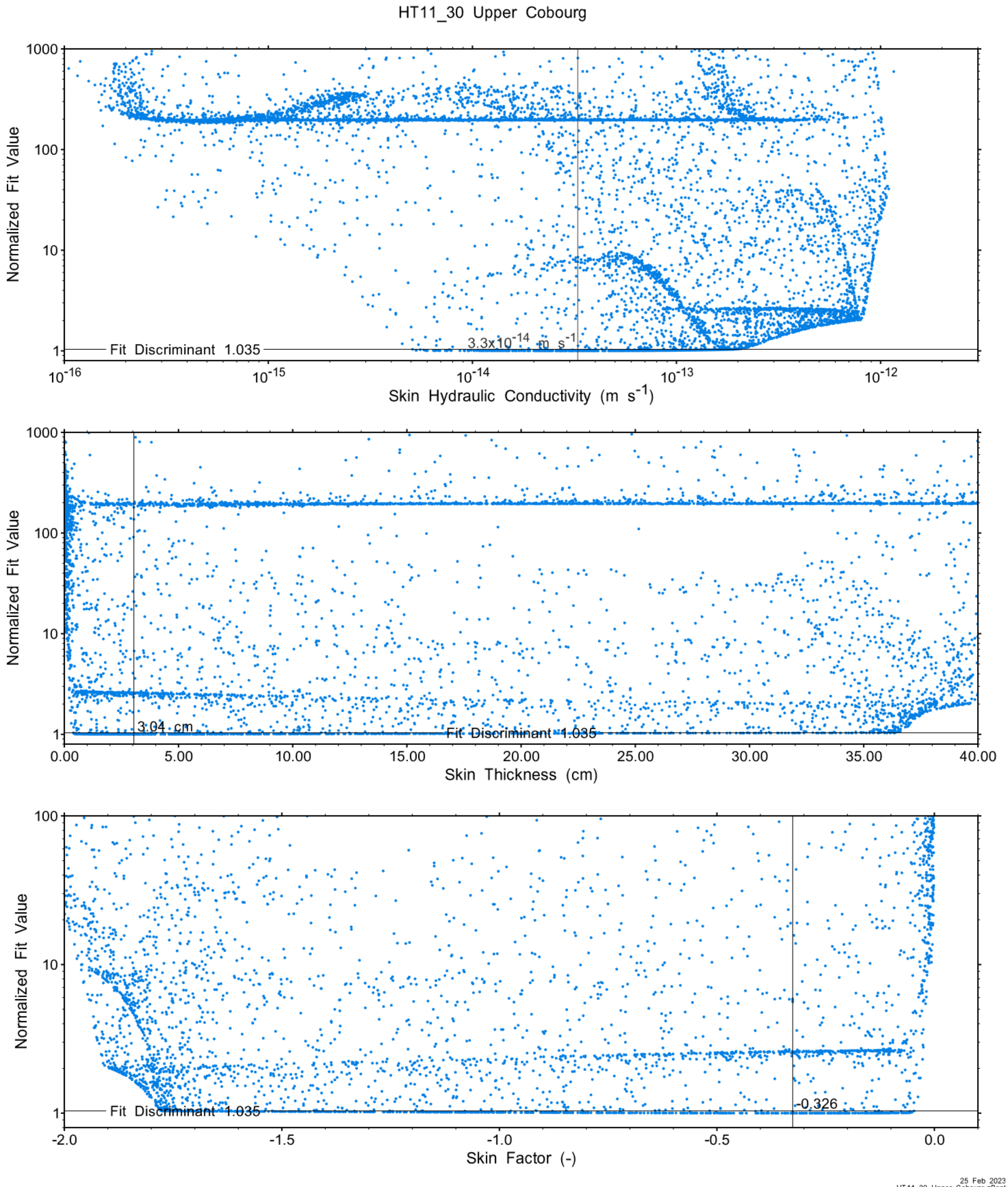

Figure 0.168 XY-scatter plot showing the skin parameter space normalized fit values.

A.12 HT12_30 Lower Cobourg

The SB_BH01 interval from 661.40 to 691.45 mBGS tested in HT12_30 includes the lower part of the Cobourg Formation. A single PI test with a duration of 2 days was conducted.

A.12.1 Test Data Summary

Table 0.56 and Figure 0.169 provide a summary of test events and a plot of pressures measured while testing, respectively.

Table 0.56 HT12_30 Summary of Test Events.

Event	Start Date & Time	Duration (days)	TZ Pressure (kPa)
Drilling intercept	21-08-29 16:40	82.92	6760
Prior testing	21-11-20 14:45	31.00	variable
Shut-in	21-12-21 14:52	0.76	6763
Pulse injection	21-12-22 09:01	2.00	7624
Test end	21-12-24 09:03		7406

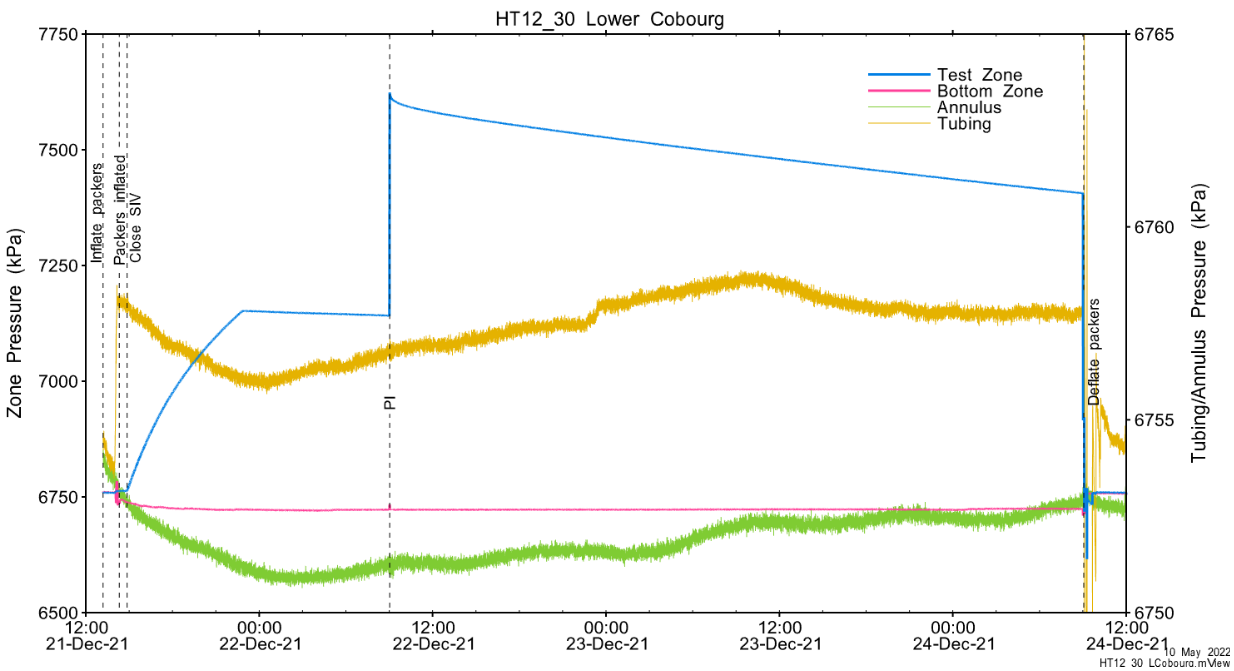

Figure 0.169 HT12_30 test events and pressures.

A.12.2 Test Analyses

Table 0.57 is a summary of test-specific input parameters used in the analyses, while Table 0.58 presents the optimized parameters and allowed ranges.

Table 0.57 nSIGHTS Input Parameters.

Parameter	Value	Units
Test zone radius	6.923	cm
Test zone compressibility	4.69E-10	1/Pa
Test zone fluid density	1046	g/L
Test zone length	30.05	m

Table 0.58 nSIGHTS Parameter Optimization Ranges.

Parameter	Minimum	Maximum	Units	Type
Formation hydraulic conductivity (K_f)	1E-15	1E-10	m/s	log
Formation pressure (P_f)	0	4500	kPa	linear
Specific storage (Ss)	1E-08	1E-04	1/m	log
Skin hydraulic conductivity (K_s)	1E-16	1E-10	m/s	log
Skin thickness (t_s)	0.1	931	mm	linear

Figure 0.170 shows the measured test zone pressure record (with reduced data density for clarity) used in the analysis along with the best-fit simulation and parameter values. Figure 0.171 presents the pre-test history, and Figure 0.172 shows the Ramey B normalized best-fit pressure and pressure derivatives.

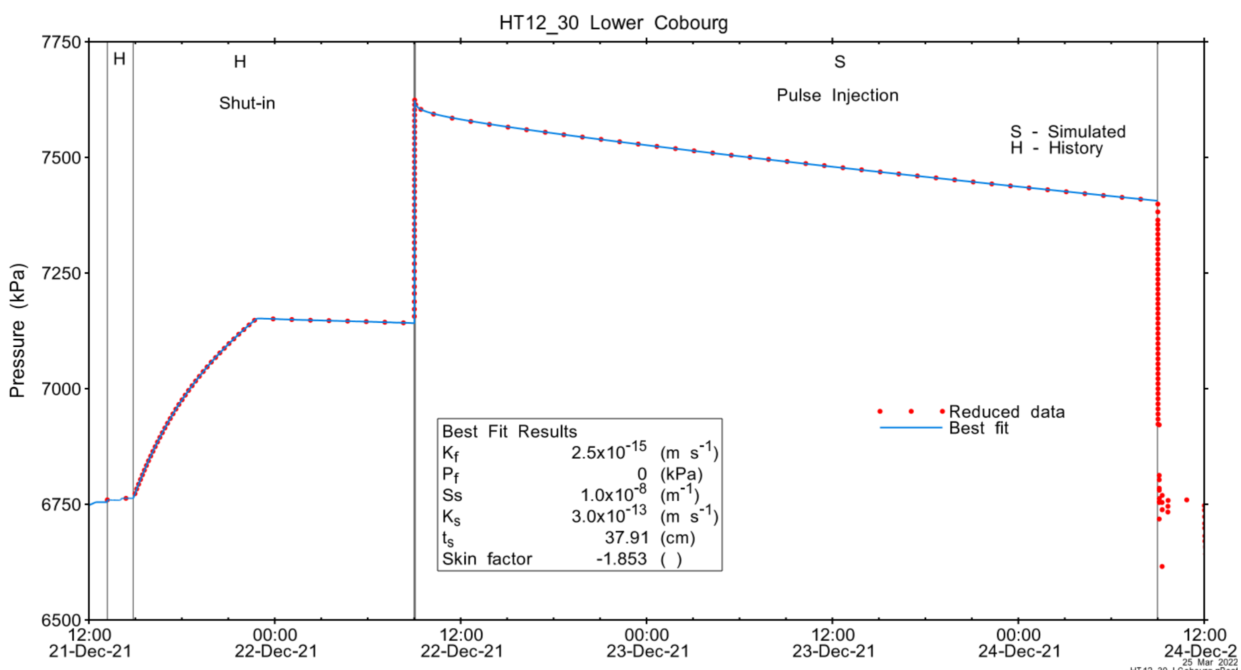

Figure 0.170 Annotated testing sequence showing best-fit simulation and parameter estimates.

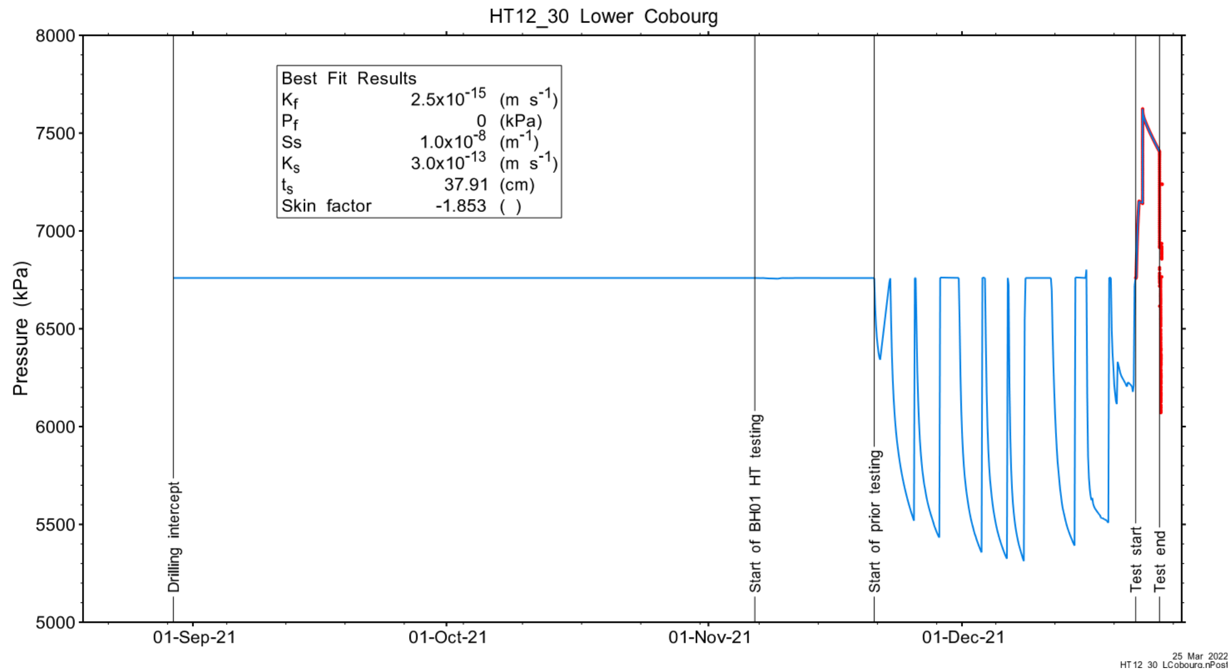

Figure 0.171 Annotated HT12_30 testing sequence showing pre-test history, best-fit simulation and parameter estimates.

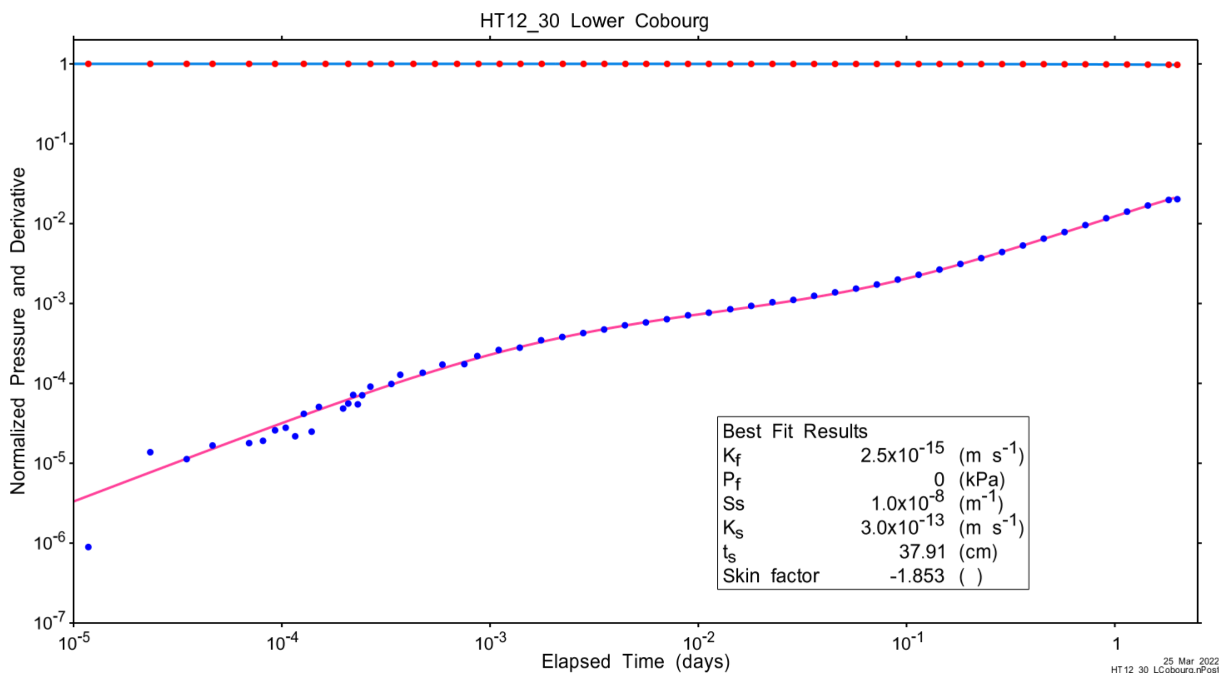

Figure 0.172 Log-log plot showing Ramey B normalized pressure and derivative response for best-fit simulation.

Figure 0.173 shows the normalized parameter sensitivity response for the best fit. K_s is most sensitive during the early-time response. Sensitivity for K_f, P_f, Ss, and t_s continues to rise – additional test time may have improved the estimates.

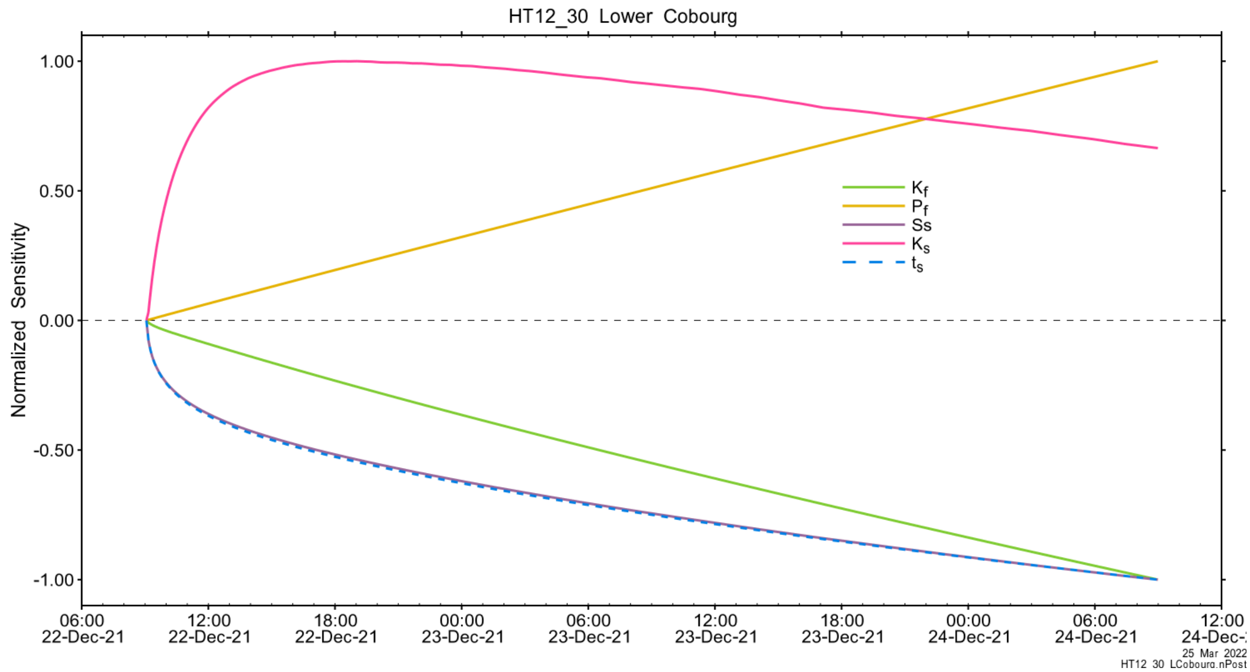

Figure 0.173 Normalized Jacobian for best-fit simulation.

A.12.3 Uncertainty Analyses

The CDF of normalized fit values for all converged simulations and the selected fit discriminant are shown in Figure 0.174.

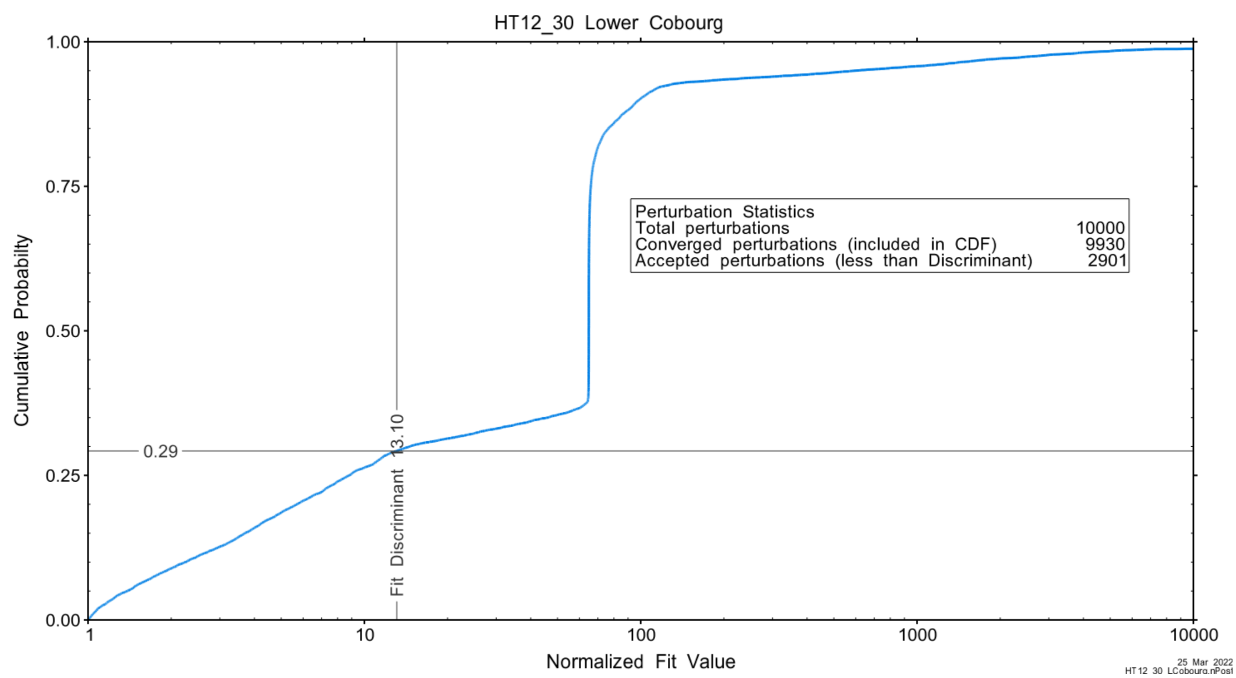

Figure 0.174 Fit value cumulative distribution function.

Summary cross parameter scatter plots for selected formation and skin parameters are given in Figure 0.175 and Figure 0.176. The light pink dots on the figures are the initial parameter estimates, with red dots overlaying those initial parameter values that resulted in accepted optimization results. The grey dots are converged optimizations which did not meet the fit discriminant. Larger varying color symbols represent the fit value of accepted optimizations, with the blue values representing the best fit.

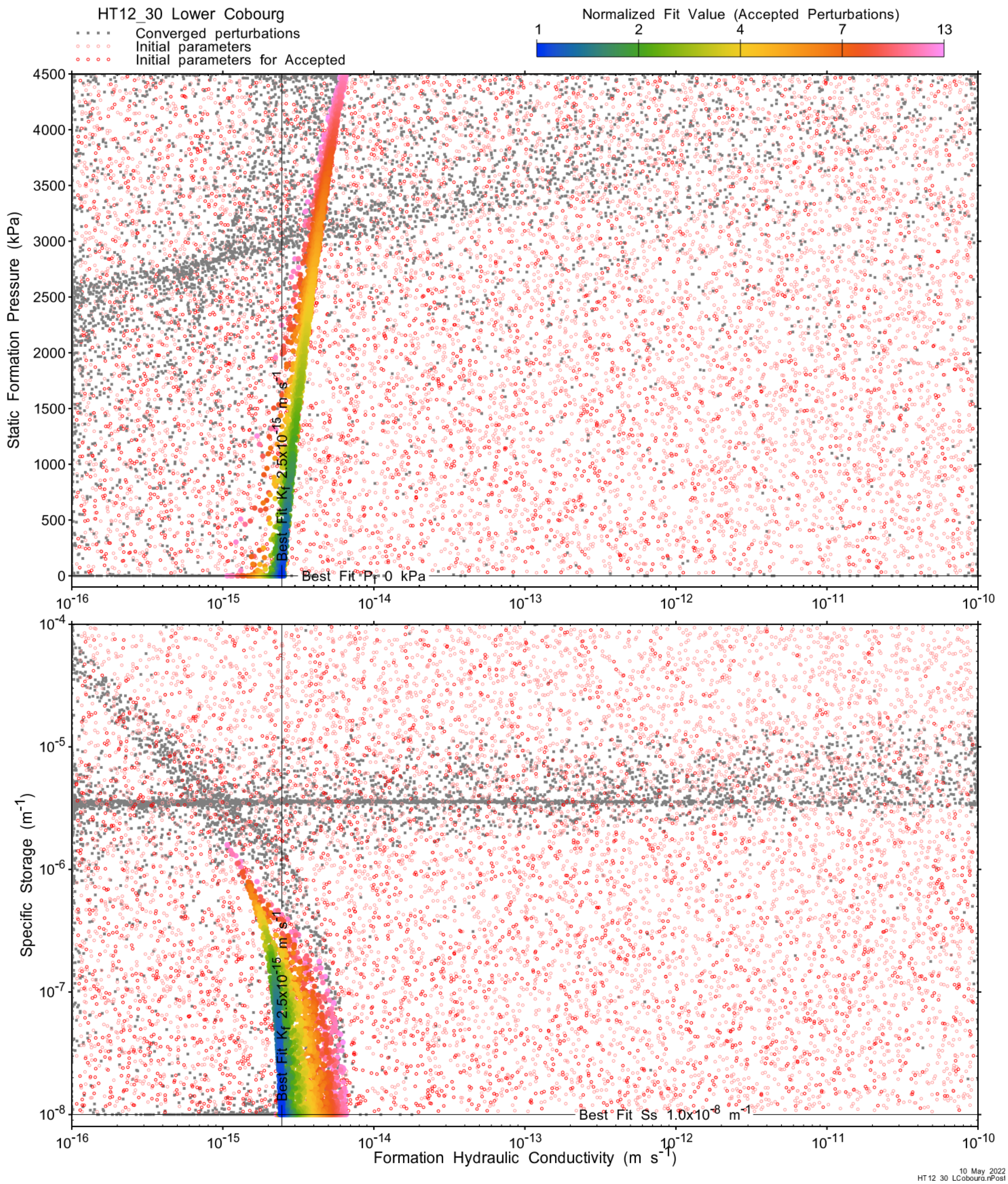

Figure 0.175 XY-scatter plot showing estimates of formation hydraulic conductivity (K_f) vs static formation pressure (P_f) (top panel) and specific storage (Ss) (bottom panel).

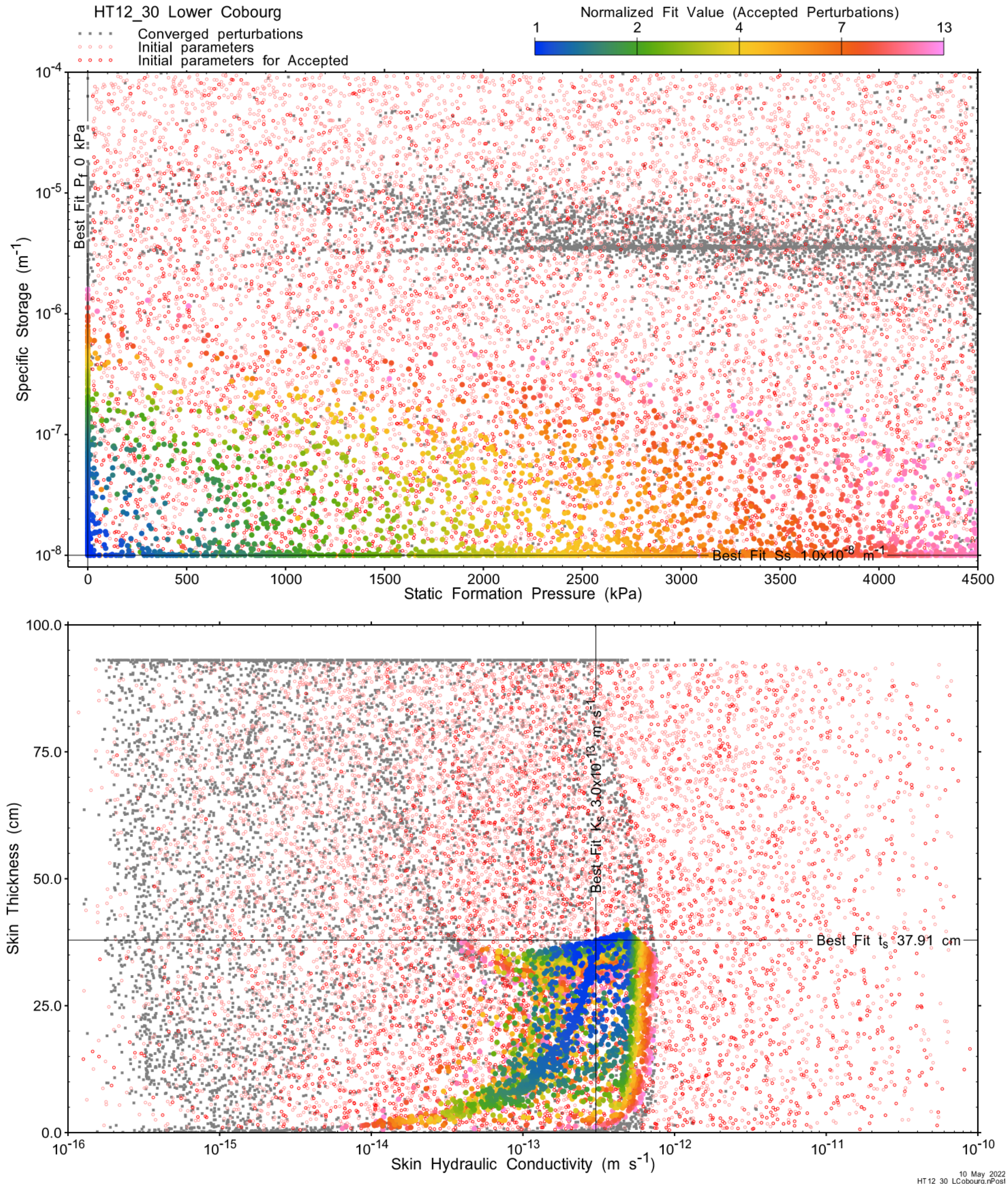

Figure 0.176 XY-scatter plot showing estimates of static formation pressure (P_f) vs specific storage (Ss) (top panel) and skin hydraulic conductivity (K_s) vs skin thickness (t_s) (bottom panel).

Confidence limits and median values are determined from the CDF of accepted optimization results (i.e. the varying color values in the above figures), with best fit value, 5% and 95% confidence indicated on Figure 0.177 and Figure 0.178.

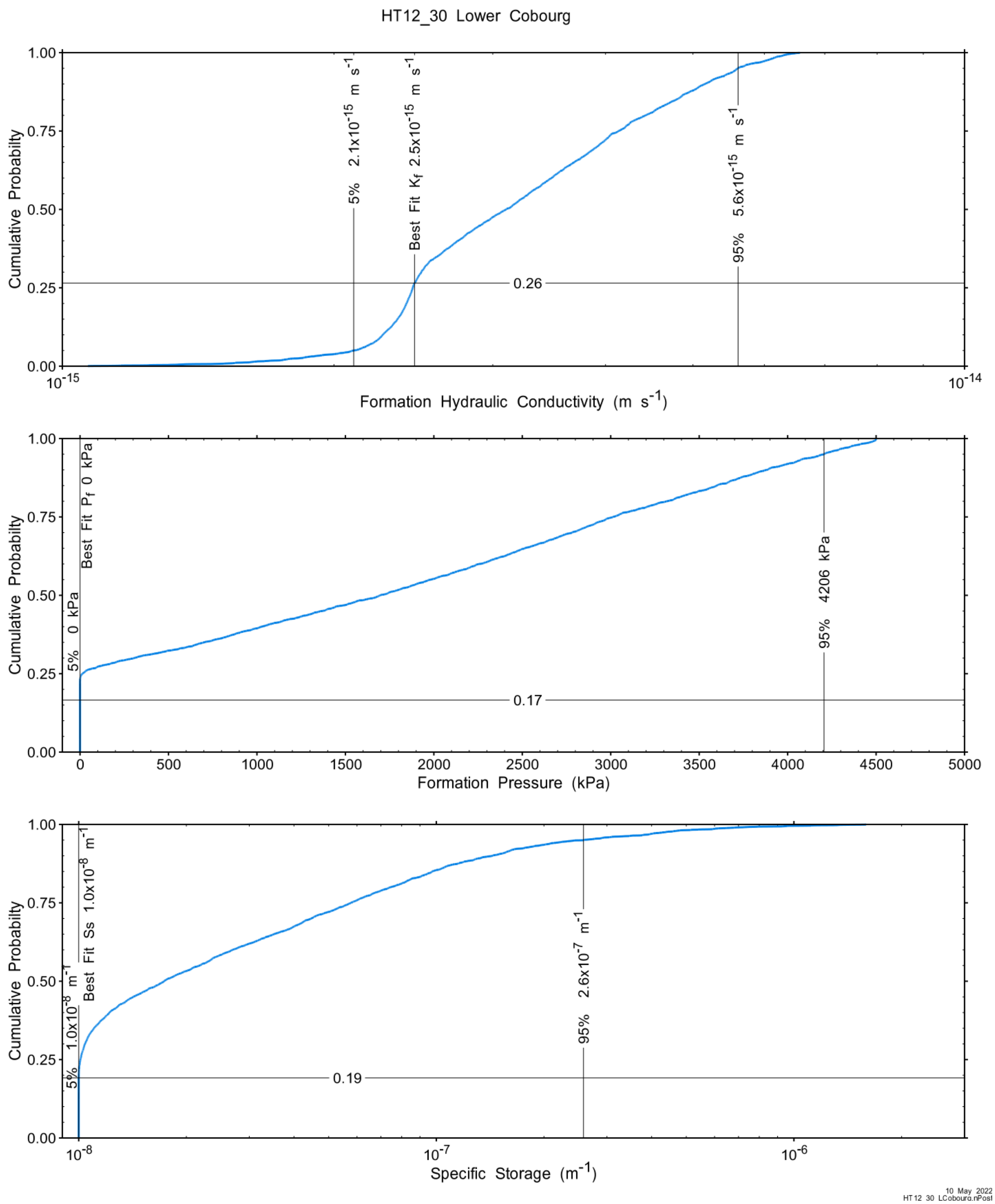

Figure 0.177 Cumulative distribution functions and parameter limits for formation hydraulic conductivity (K_f) (top panel), static formation pressure (P_f) (middle panel) and specific storage (Ss) (bottom panel).

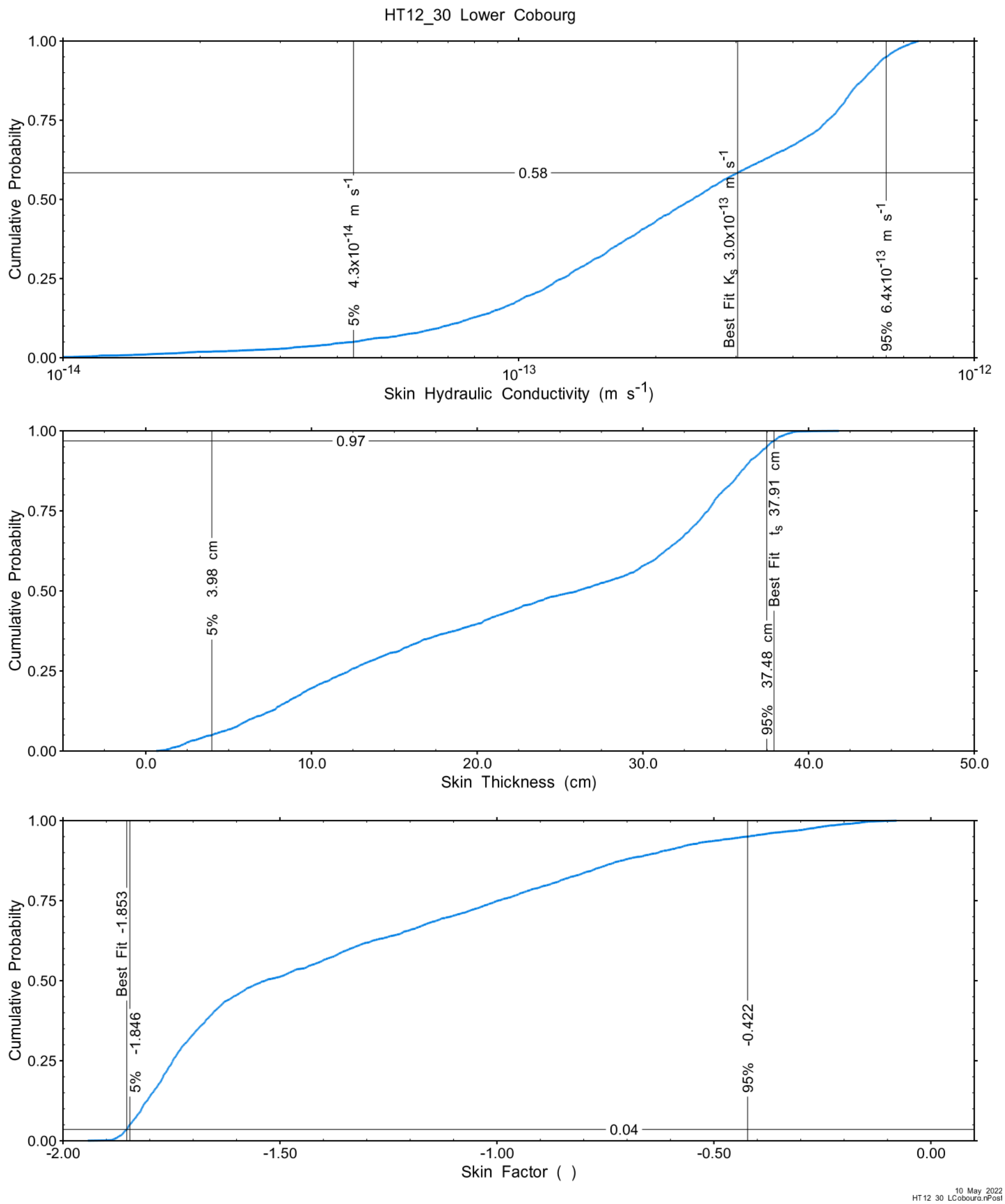

Figure 0.178 Cumulative distribution functions and parameter limits for skin hydraulic conductivity (K_s) (top panel), skin thickness (t_s) (middle panel) and skin factor (s) (bottom panel).

A summary of perturbation results is presented in Figure 0.179, with Ramey-processed perturbations in Figure 0.180. Those perturbations (1991 of 10,000) with all parameters within the 5% and 95% range present a very good fit to the measured test zone data.

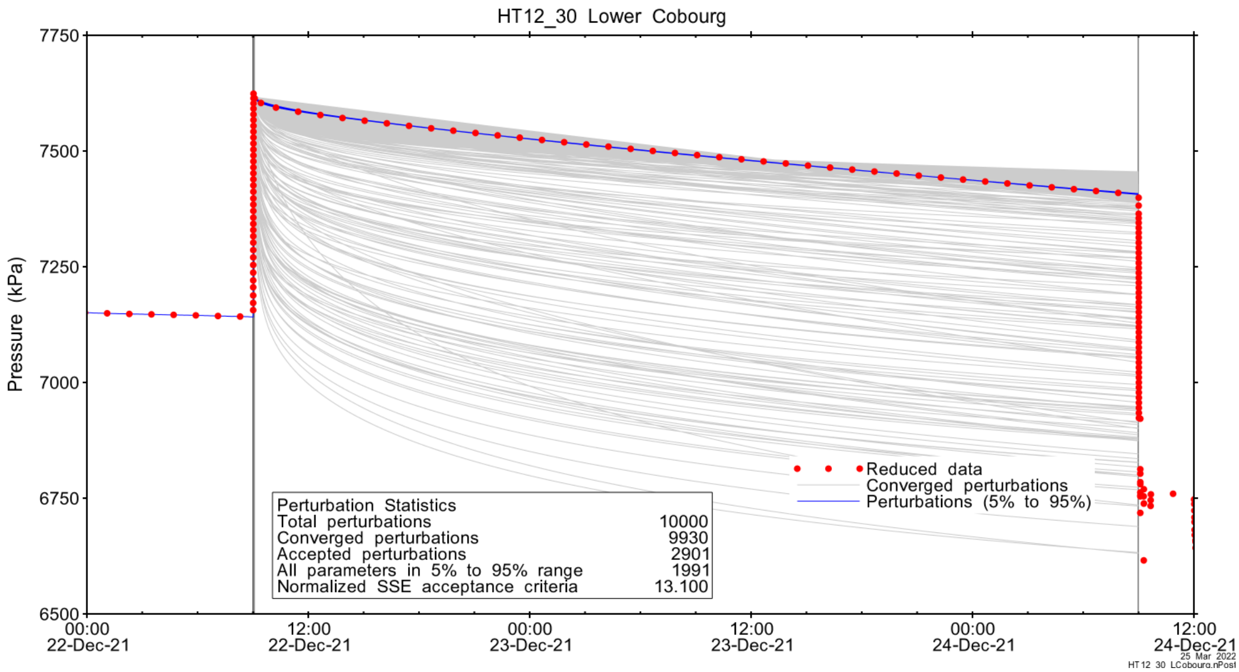

Figure 0.179 Perturbation results – all converged, accepted, and within 5% to 95% for all parameters.

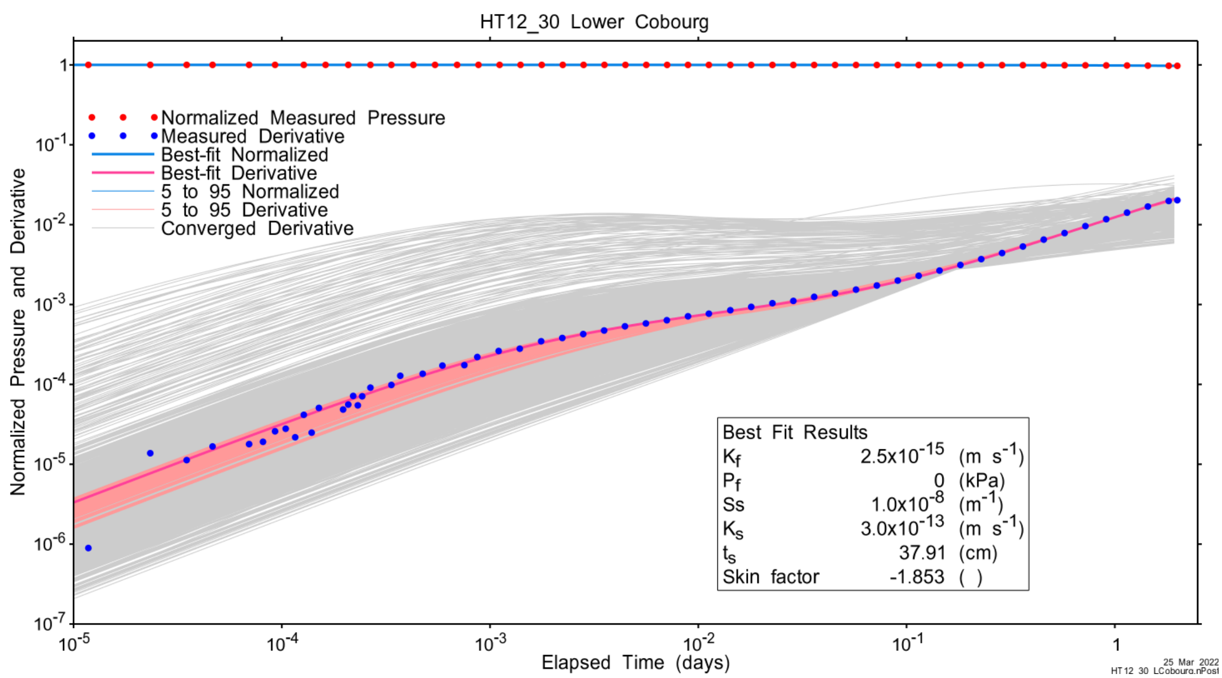

Figure 0.180 Log-log plot showing Ramey B normalized pressure and derivative response for all converged optimizations and those within 5% to 95% for all parameters.

A summary of best-fit parameter estimates and ranges is given in Table 0.59.

Table 0.59 Summary of the HT12_30 parameter estimates.

Parameter	Best Fit	5%	Median	95%
K_f (m/s)	2.5E-15	2.1E-15	3.1E-15	5.6E-15
P_f (kPa)	0	0	1697	4206
Ss (1/m)	1.0E-08	1.0E-08	1.7E-08	2.6E-07
K_s (m/s)	3.0E-13	4.3E-14	2.4E-13	6.4E-13
t_s (cm)	37.91	3.98	26.05	37.48
s (-)	-1.853	-1.846	-1.535	-0.422

Parameter correlations for all perturbations with all parameters within the 5% to 95% limits are given in Table 0.60.

Table 0.60 Pearson cross-correlations of 5% to 95% parameters

	Log(K_f)	P_f	Log(Ss)	Log(K_s)	t_s	s
Log(K_f)	1.000	0.975	-0.408	0.077	0.305	-0.290
P_f	0.975	1.000	-0.261	0.142	0.178	-0.159
Log(Ss)	-0.408	-0.261	1.000	-0.336	-0.976	0.984
Log(K_s)	0.077	0.142	-0.336	1.000	0.404	-0.454
t_s	0.305	0.178	-0.976	0.404	1.000	-0.988
s	-0.290	-0.159	0.984	-0.454	-0.988	1.000

A.12.4 Additional Figures

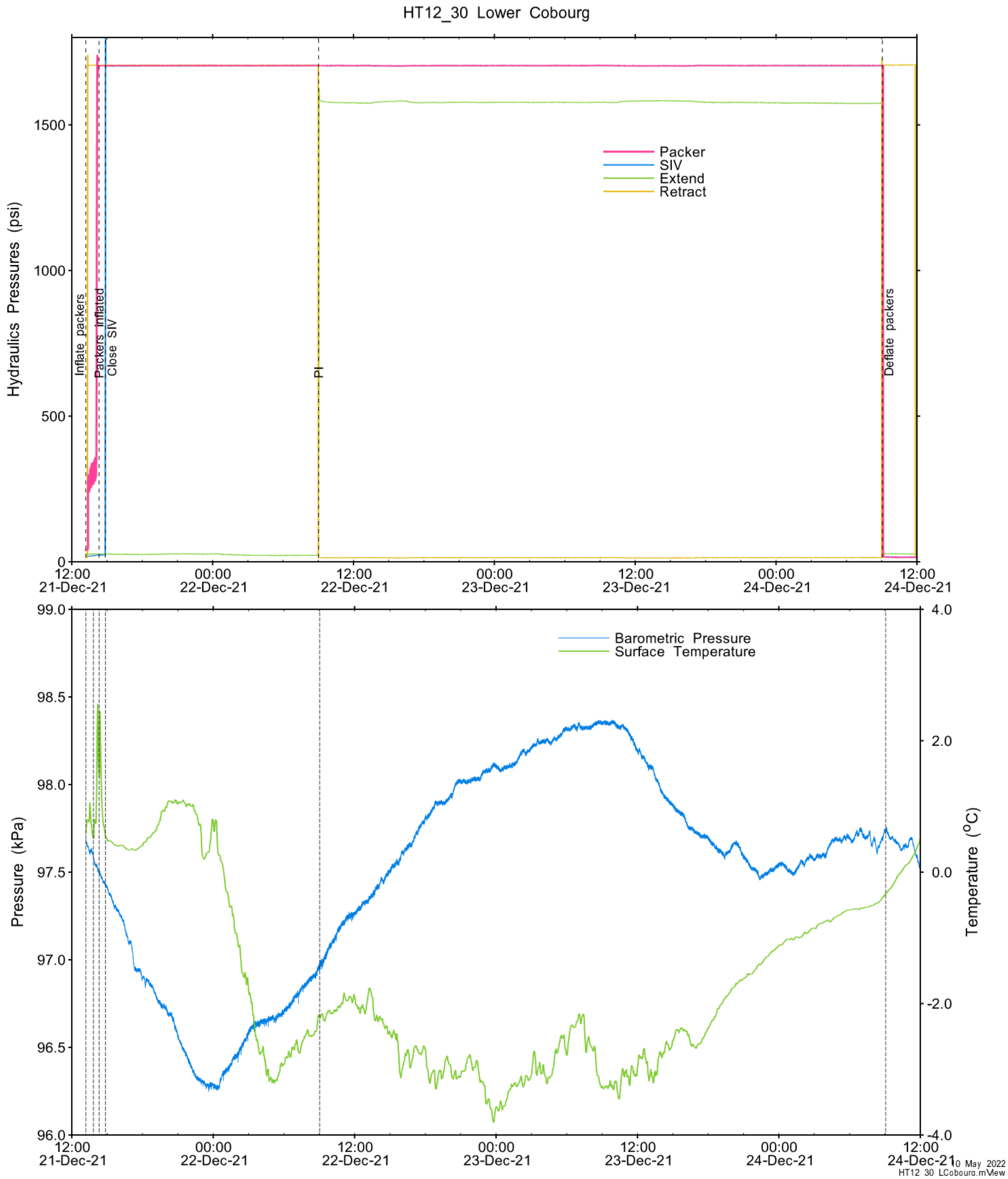

Figure 0.181 Hydraulics pressures and surface temperature/barometric pressure.

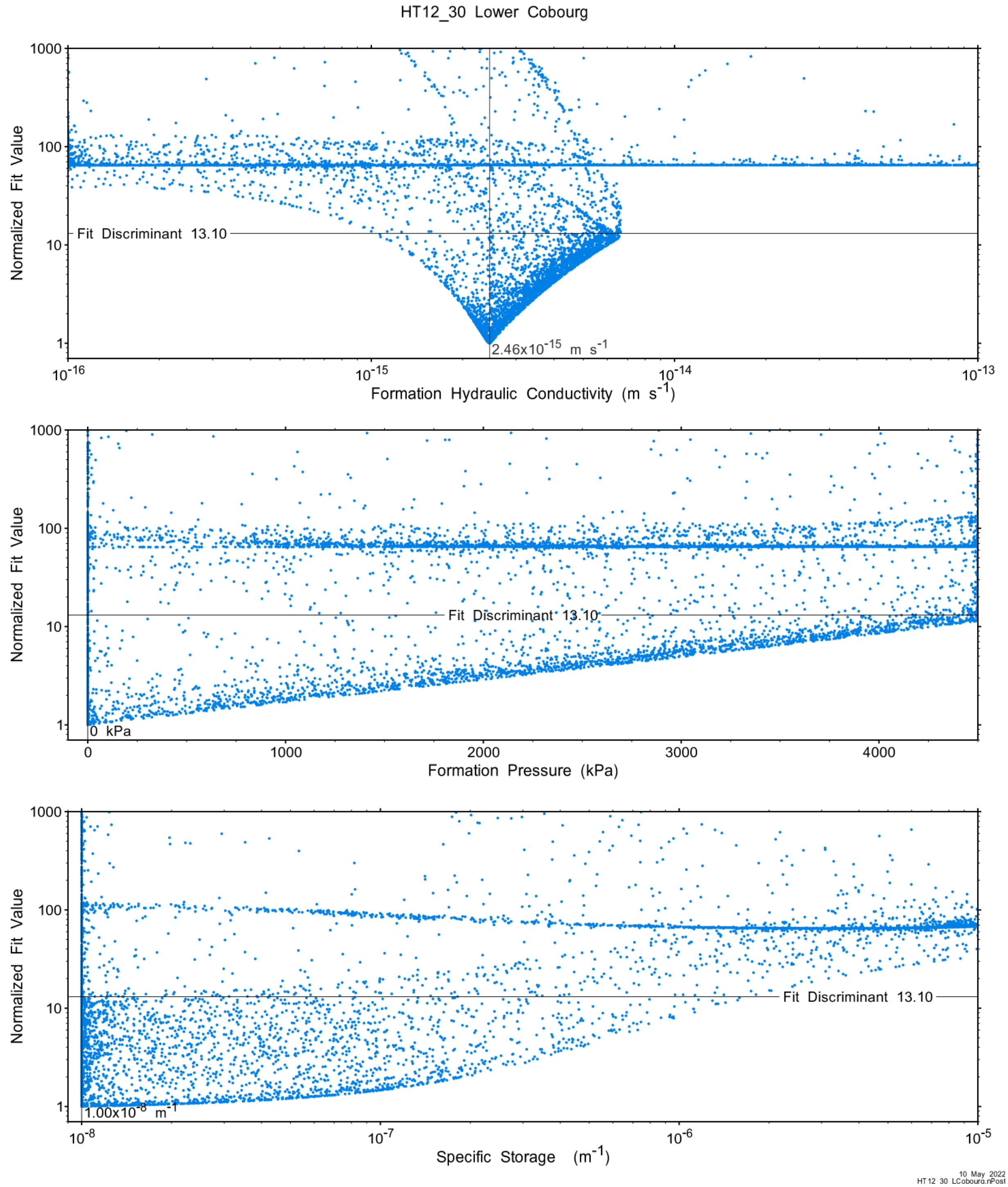

Figure 0.182 XY-scatter plot showing the formation parameter space normalized fit values.

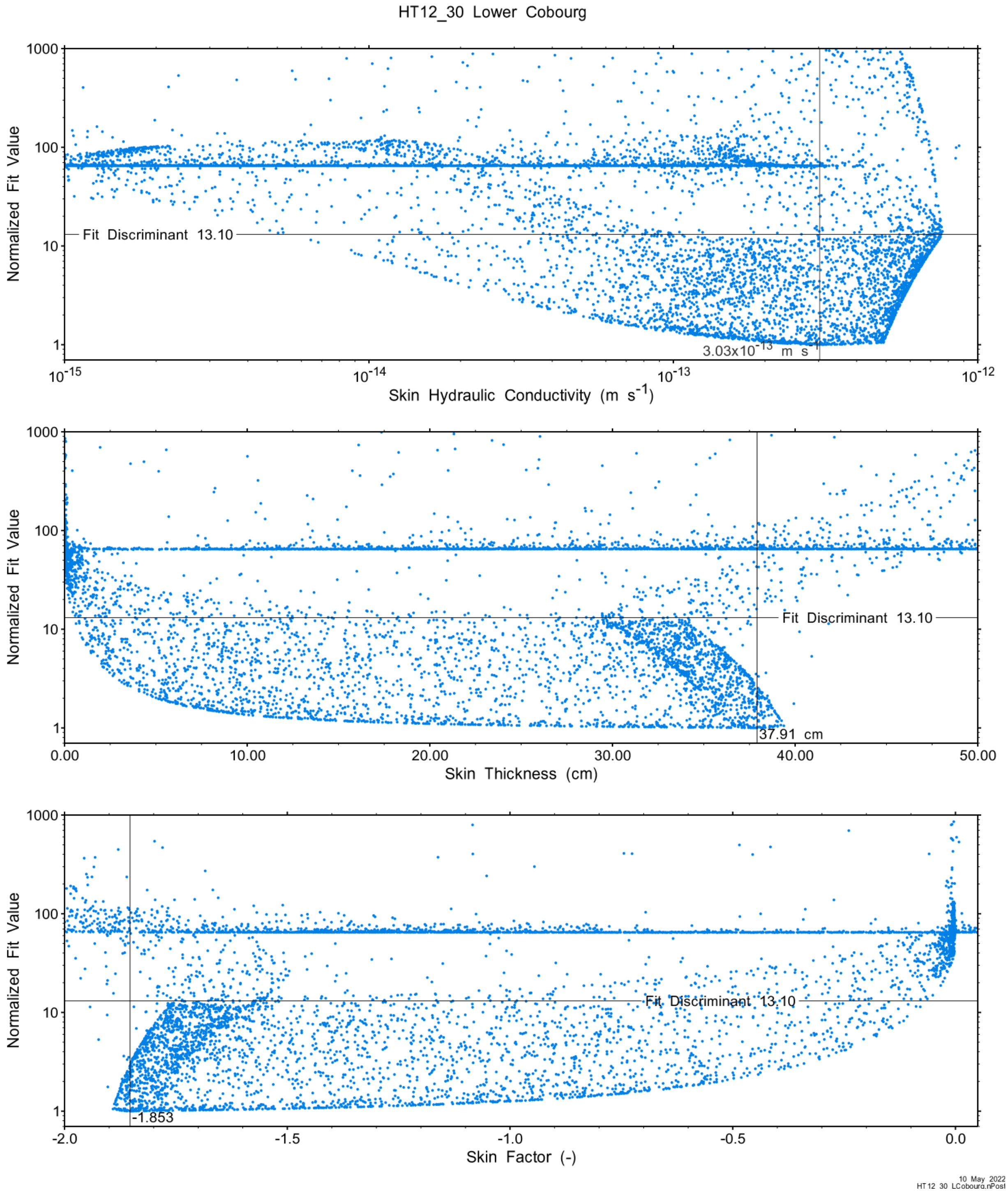

Figure 0.183 XY-scatter plot showing the skin parameter space normalized fit values.

A.13 HT13_30 Sherman Falls

The SB_BH01 interval from 706.75 to 736.80 mBGS tested in HT13_30 includes the majority of the Sherman Falls Formation. A single PI test with a duration of 2 days was conducted.

A.13.1 Test Data Summary

Table 0.61 and Figure 0.184 provide a summary of test events and a plot of pressures measured while testing, respectively.

Table 0.61 HT13_30 Summary of Test Events.

Event	Start Date & Time	Duration (days)	TZ Pressure (kPa)
Drilling intercept	21-09-02 16:52	78.91	7239
Prior testing	21-11-20 14:45	34.16	variable
Shut-in	21-12-24 18:40	0.60	7238
Pulse injection	21-12-25 09:01	2.00	8184
Test end	21-12-27 09:00		7792

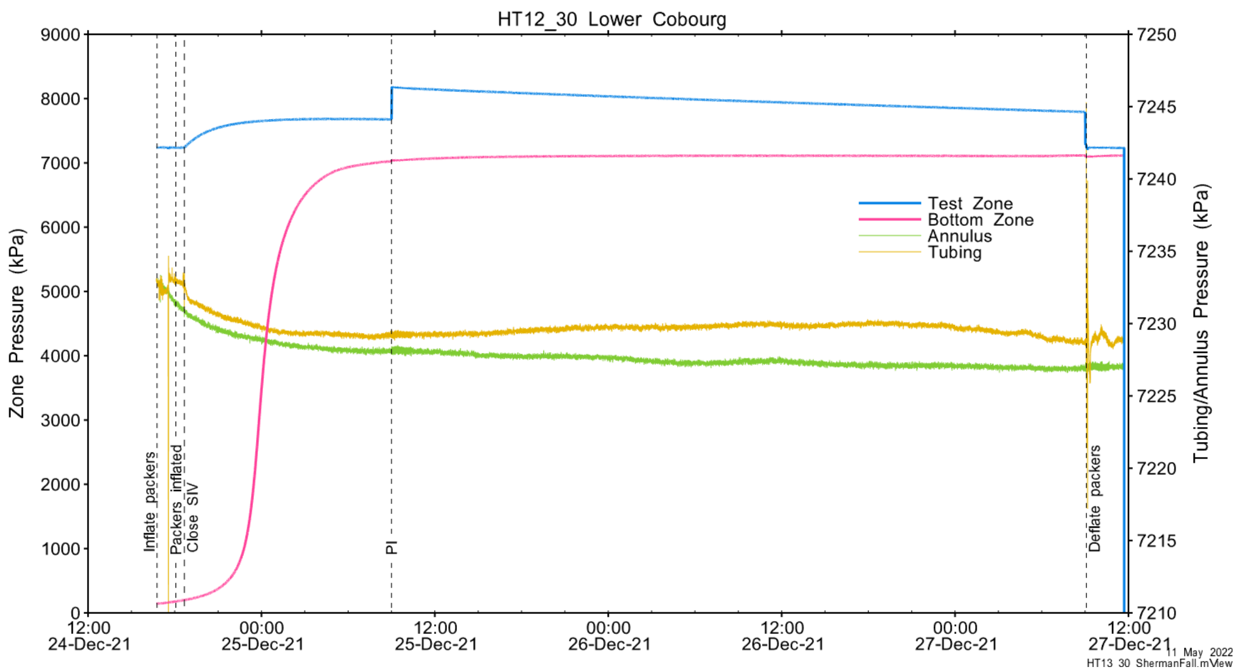

Figure 0.184 HT13_30 test events and pressures.

A.13.2 Test Analyses

Table 0.62 is a summary of test-specific input parameters used in the analyses, while Table 0.63 presents the optimized parameters and allowed ranges.

Table 0.62 nSIGHTS Input Parameters.

Parameter	Value	Units
Test zone radius	6.862	cm
Test zone compressibility	4.54E-10	1/Pa
Test zone fluid density	1047	g/L
Test zone length	30.05	m

Table 0.63 nSIGHTS Parameter Optimization Ranges.

Parameter	Minimum	Maximum	Units	Type
Formation hydraulic conductivity (K_f)	1E-15	1E-10	m/s	log
Formation pressure (P_f)	0	6000	kPa	linear
Specific storage (Ss)	1E-08	1E-04	1/m	log
Skin hydraulic conductivity (K_s)	1E-15	1E-10	m/s	log
Skin thickness (t_s)	0.1	931	mm	linear

Figure 0.185 shows the measured test zone pressure record (with reduced data density for clarity) used in the analysis along with the best-fit simulation and parameter values. Figure 0.186 presents the pre-test history, and Figure 0.187 shows the Ramey B normalized best-fit pressure and pressure derivatives.

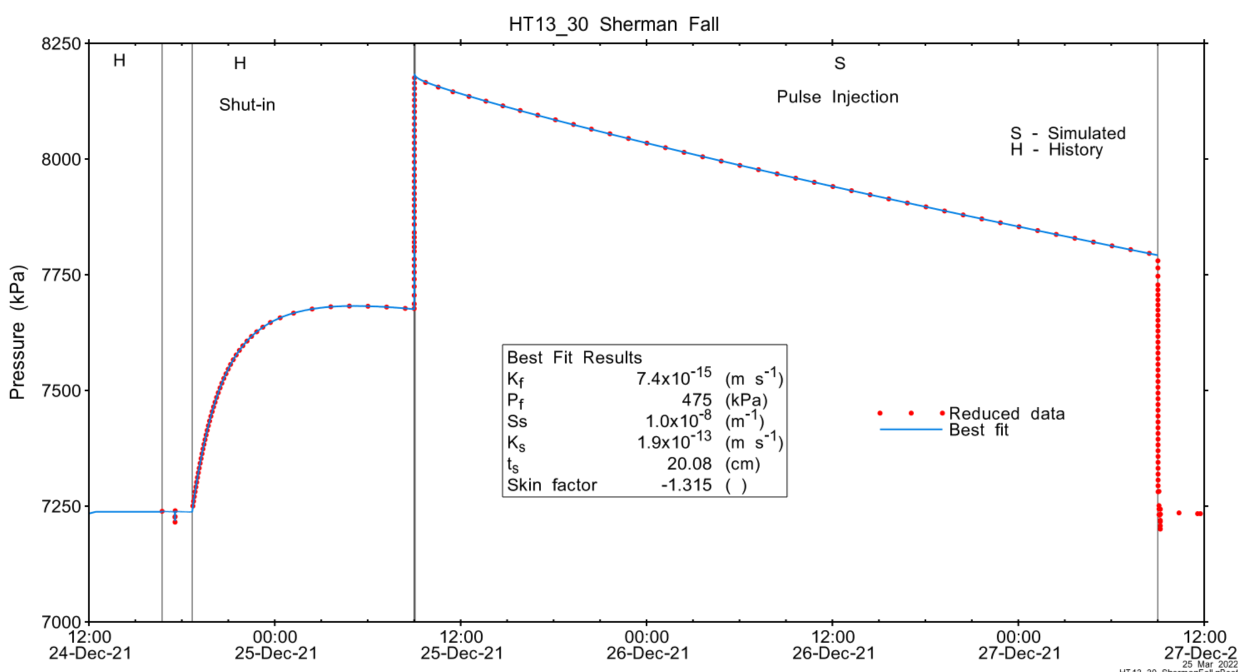

Figure 0.185 Annotated testing sequence showing best-fit simulation and parameter estimates.

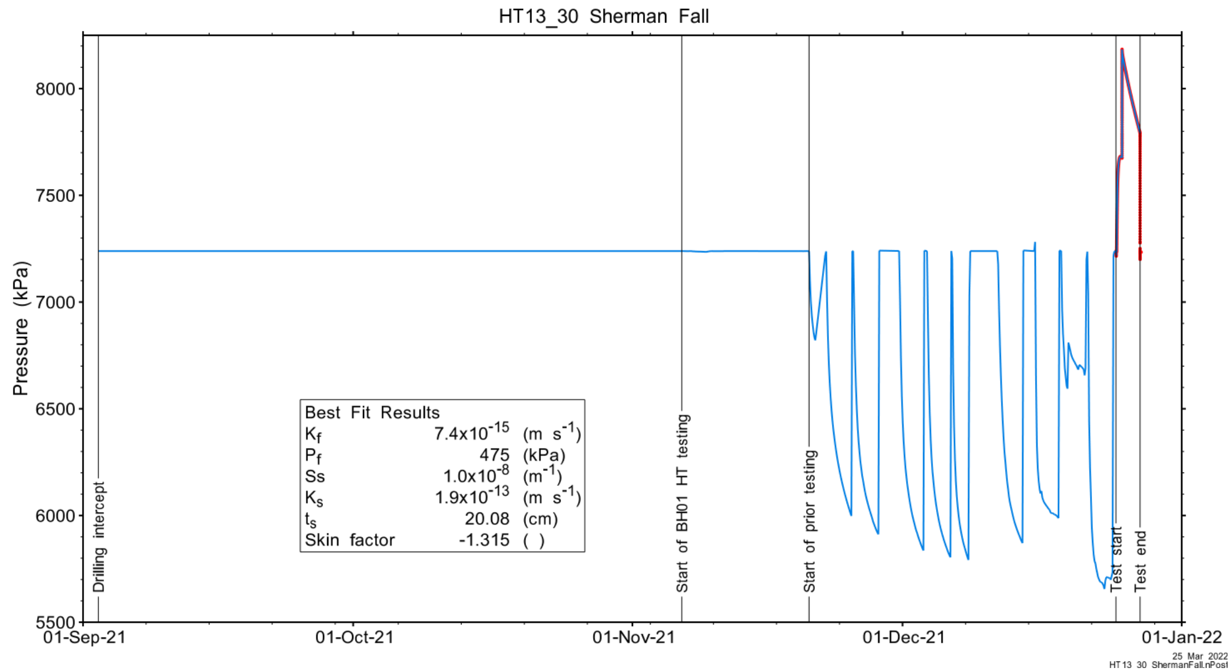

Figure 0.186 Annotated HT13_30 testing sequence showing pre-test history, best-fit simulation and parameter estimates.

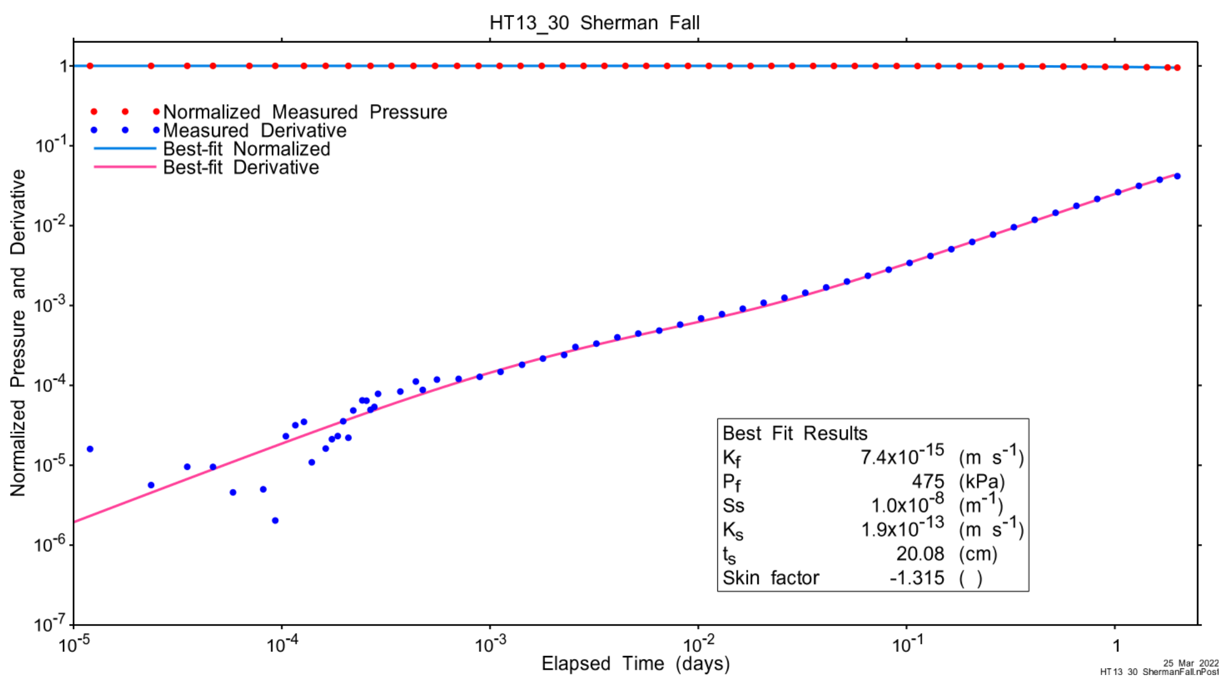

Figure 0.187 Log-log plot showing Ramey B normalized pressure and derivative response for best-fit simulation.

GEOFIRMA ENGINEERING

Figure 0.188 shows the normalized parameter sensitivity response for the best fit. Skin-related parameters are most sensitive during the early-time response. Sensitivity for all fitting parameters continues to rise – additional test time may have improved the estimates.

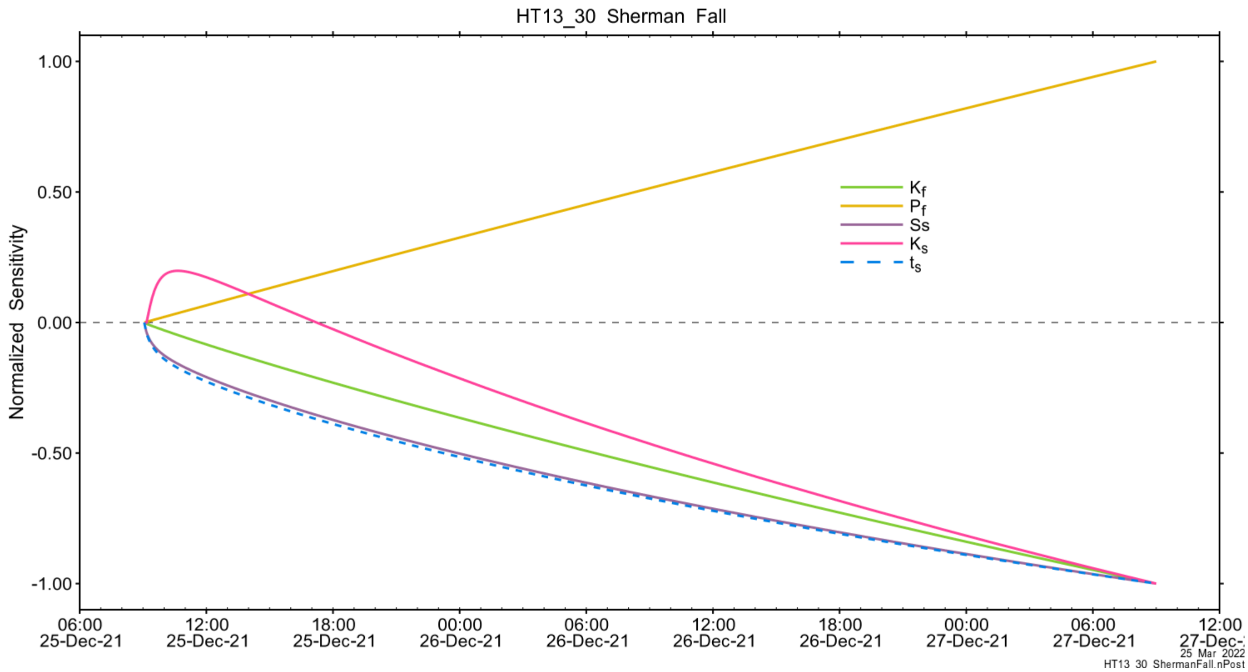

Figure 0.188 Normalized Jacobian for best-fit simulation.

A.13.3 Uncertainty Analyses

The CDF of normalized fit values for all converged simulations and the selected fit discriminant are shown in Figure 0.189.

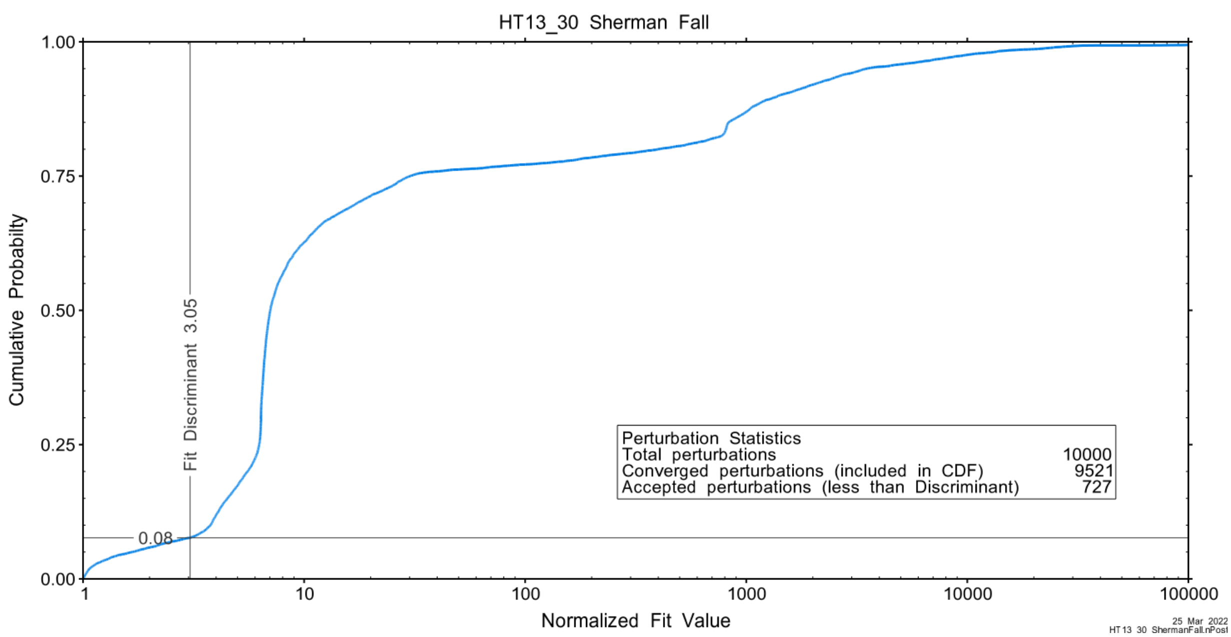

Figure 0.189 Fit value cumulative distribution function.

Summary cross parameter scatter plots for selected formation and skin parameters are given in Figure 0.190 and Figure 0.191. The light pink dots on the figures are the initial parameter estimates, with red dots overlaying those initial parameter values that resulted in accepted optimization results. The grey dots are converged optimizations which did not meet the fit discriminant. Larger varying color symbols represent the fit value of accepted optimizations, with the blue values representing the best fit.

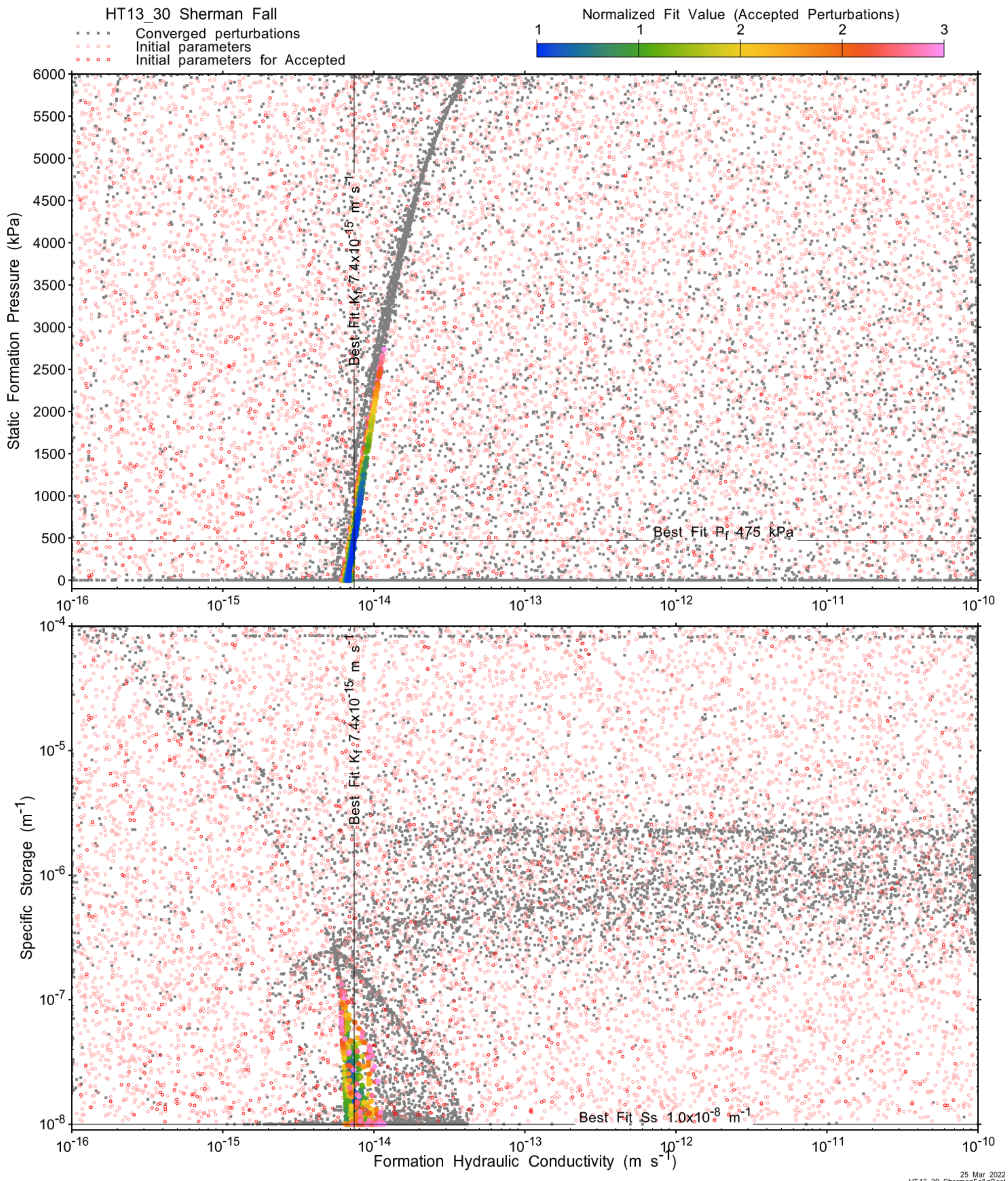

Figure 0.190 XY-scatter plot showing estimates of formation hydraulic conductivity (K_f) vs static formation pressure (P_f) (top panel) and specific storage (Ss) (bottom panel).

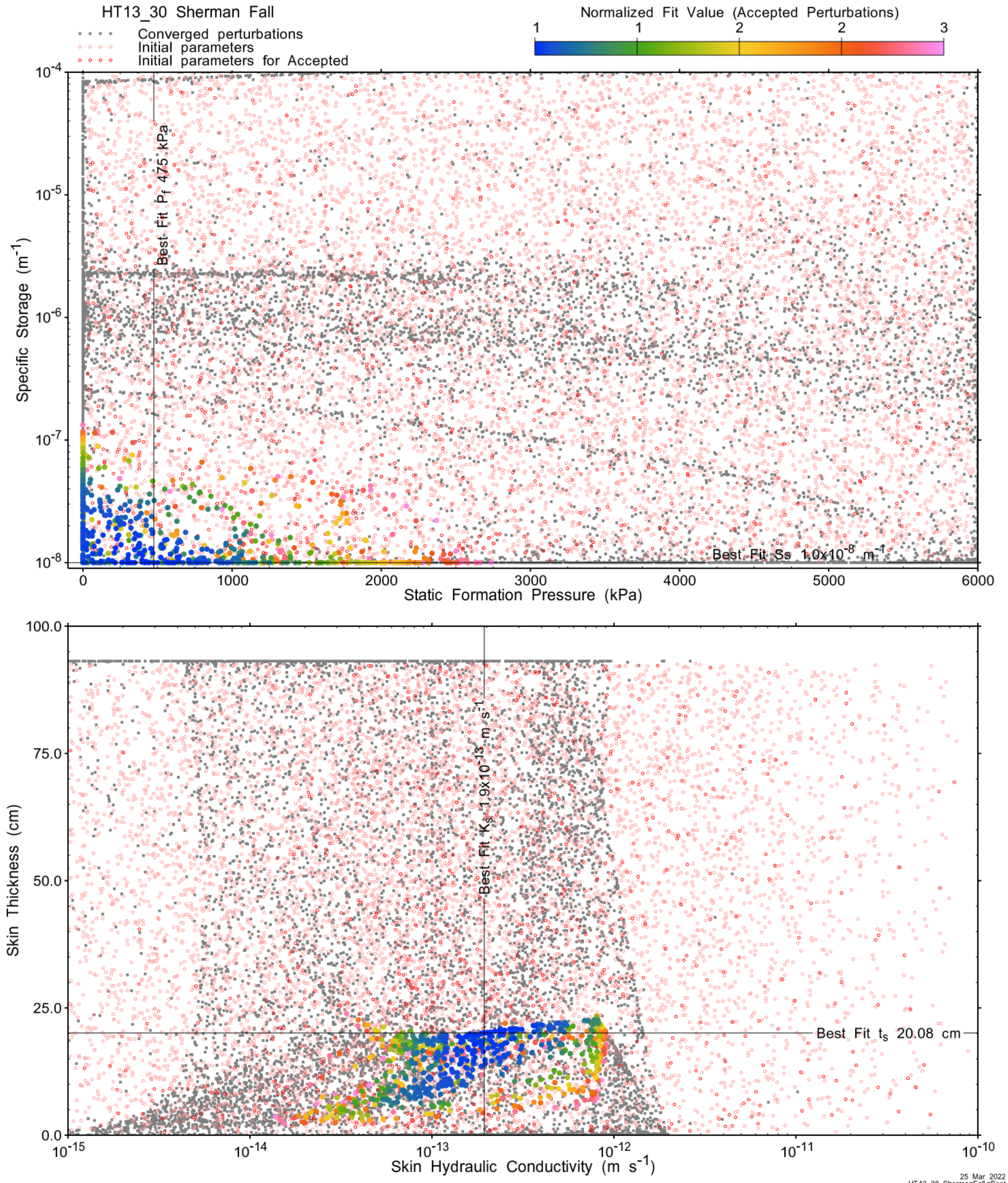

Figure 0.191 XY-scatter plot showing estimates of static formation pressure (P_f) vs specific storage (Ss) (top panel) and skin hydraulic conductivity (K_s) vs skin thickness (t_s) (bottom panel).

Confidence limits and median values are determined from the CDF of accepted optimization results (i.e. the varying color values in the above figures), with best fit value, 5% and 95% confidence indicated on Figure 0.192 and Figure 0.193.

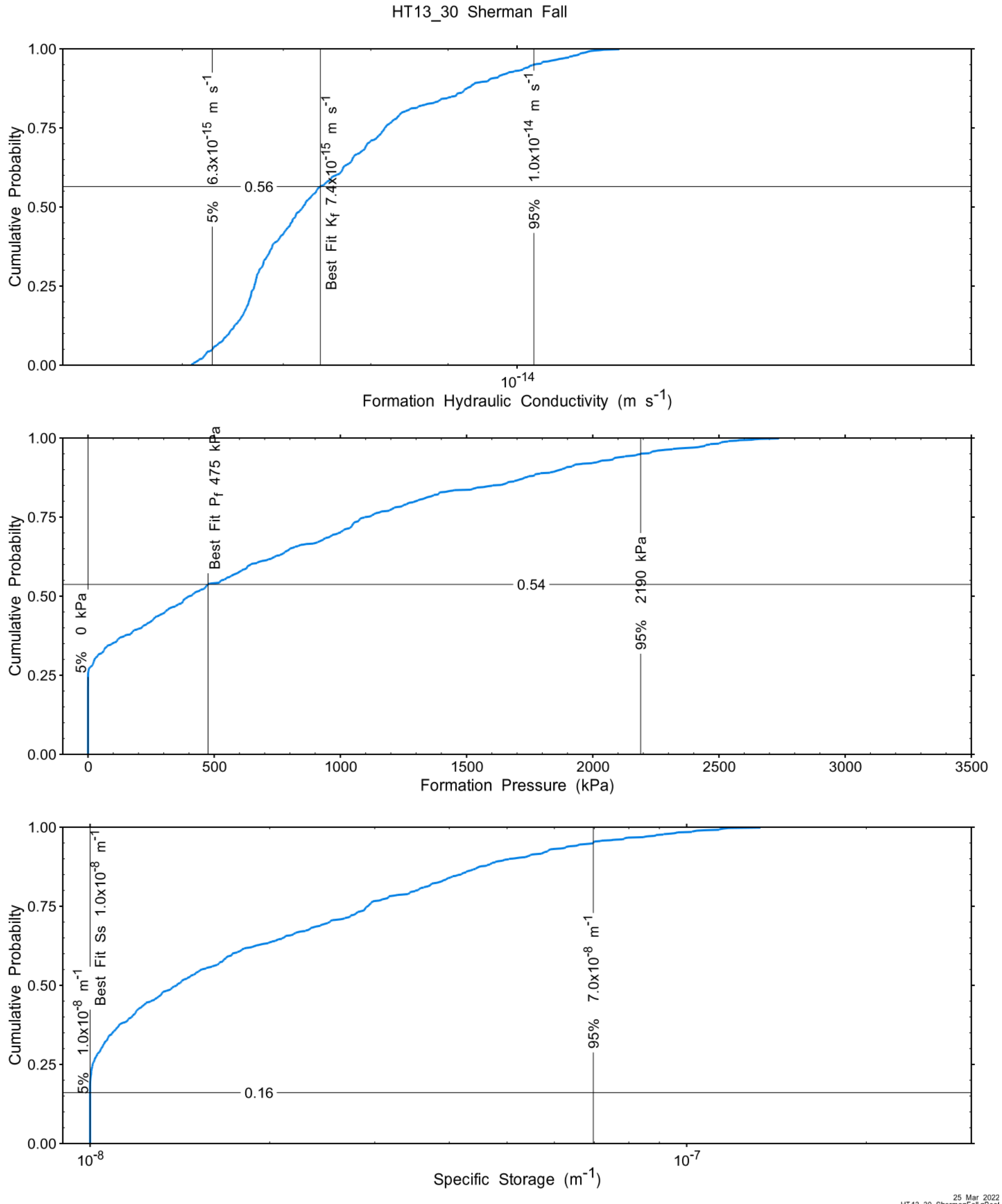

Figure 0.192 Cumulative distribution functions and parameter limits for formation hydraulic conductivity (K_f) (top panel), static formation pressure (P_f) (middle panel) and specific storage (Ss) (bottom panel).

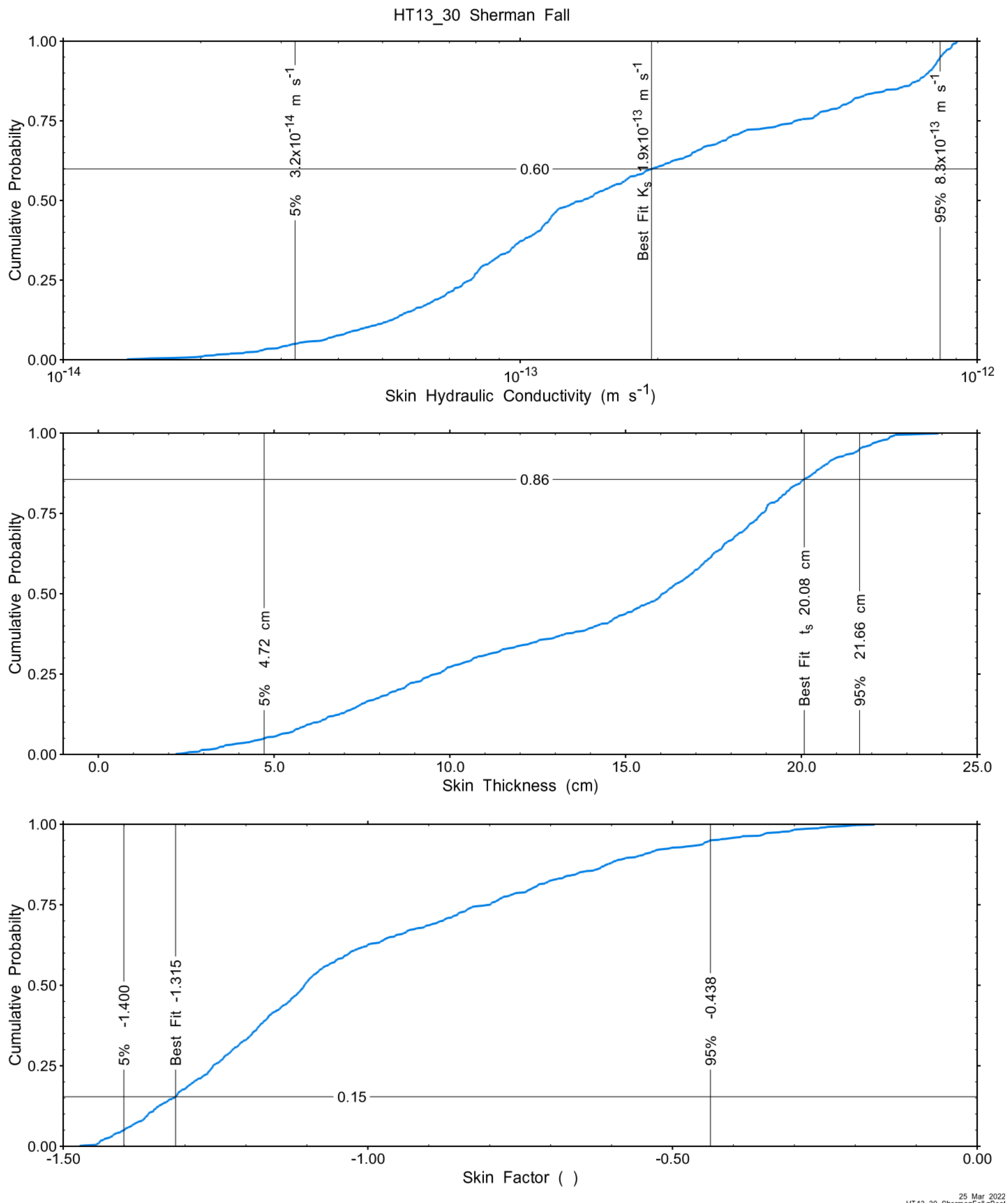

Figure 0.193 Cumulative distribution functions and parameter limits for skin hydraulic conductivity (K_s) (top panel), skin thickness (t_s) (middle panel) and skin factor (s) (bottom panel).

A summary of perturbation results is presented in Figure 0.194, with Ramey-processed perturbations in Figure 0.195. Those perturbations (493 of 10,000) with all parameters within the 5% and 95% range present a very good fit to the measured test zone data.

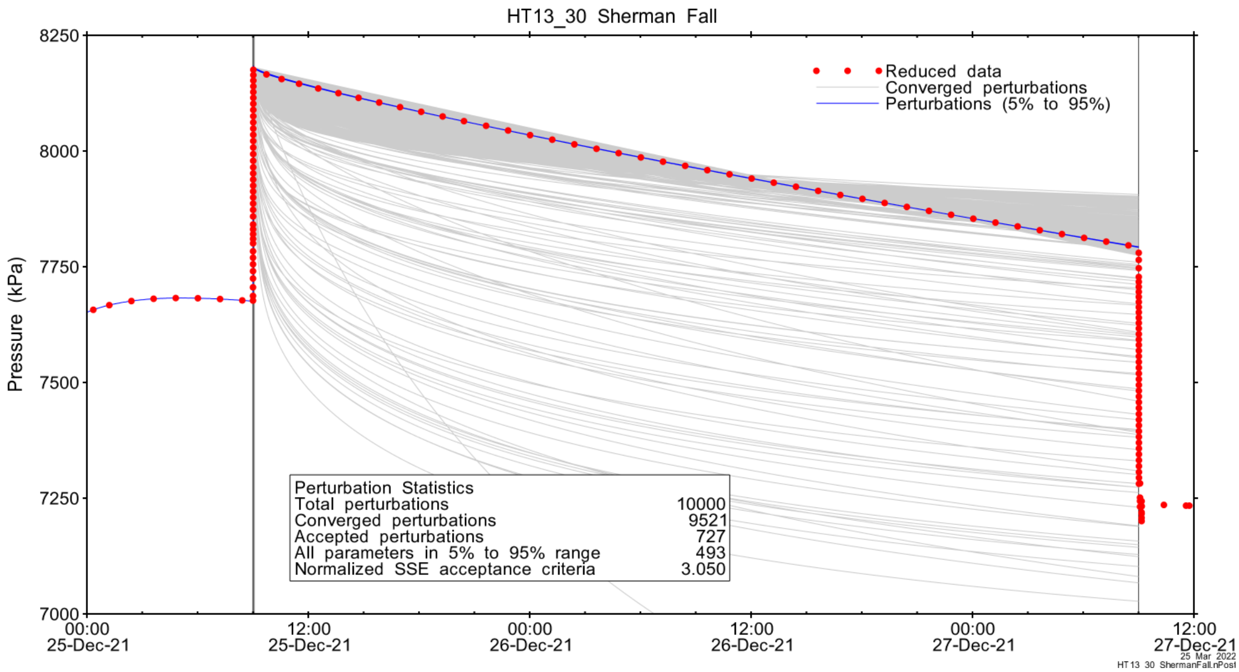

Figure 0.194 Perturbation results – all converged, accepted, and within 5% to 95% for all parameters.

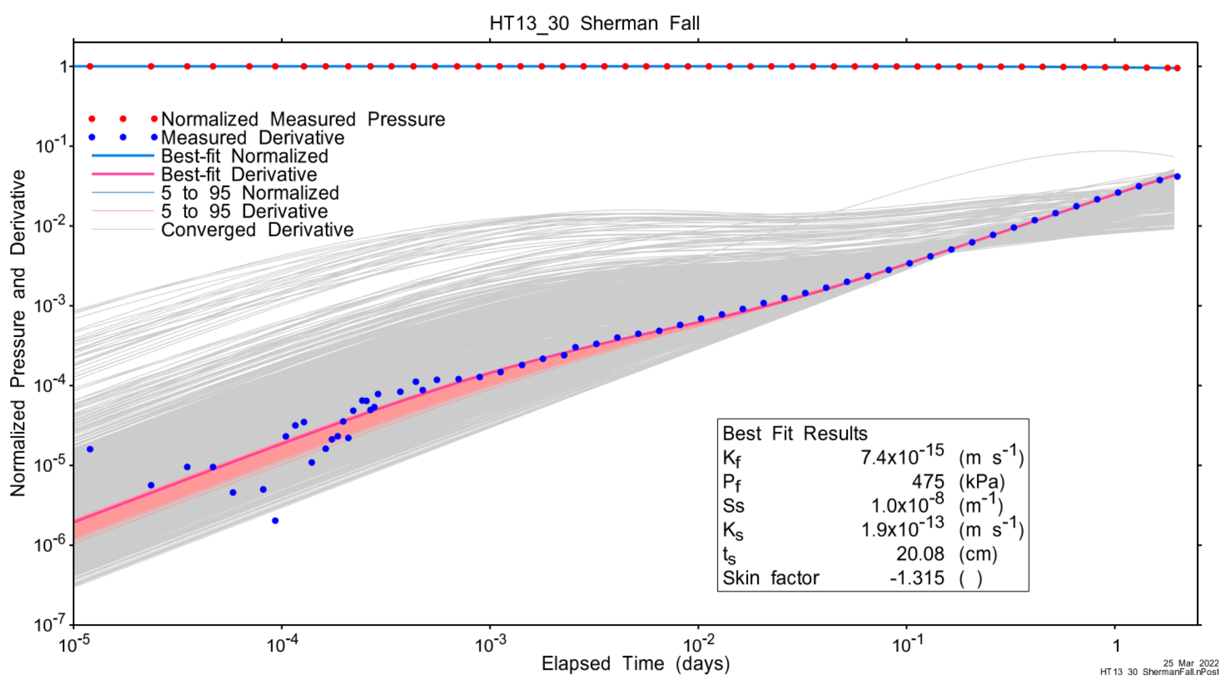

Figure 0.195 Log-log plot showing Ramey B normalized pressure and derivative response for all converged optimizations and those within 5% to 95% for all parameters.

A summary of best-fit parameter estimates and ranges is given in Table 0.64.

Table 0.64 Summary of the HT13_30 parameter estimates.

Parameter	Best Fit	5%	Median	95%
K_f (m/s)	7.4E-15	6.3E-15	7.2E-15	1.0E-14
P_f (kPa)	475	0	400	2190
Ss (1/m)	1.0E-08	1.0E-08	1.4E-08	7.0E-08
K_s (m/s)	1.9E-13	3.2E-14	1.4E-13	8.3E-13
t_s (cm)	20.08	4.72	16.03	21.66
s (-)	-1.315	-1.400	-1.104	-0.438

Parameter correlations for all perturbations with all parameters within the 5% to 95% limits are given in Table 0.65.

Table 0.65 Pearson cross-correlations of 5% to 95% parameters

	Log(K_f)	P_f	Log(Ss)	Log(K_s)	t_s	s
Log(K_f)	1.000	0.980	-0.372	-0.432	0.179	-0.033
P_f	0.980	1.000	-0.300	-0.314	0.118	0.004
Log(Ss)	-0.372	-0.300	1.000	-0.257	-0.971	0.925
Log(K_s)	-0.432	-0.314	-0.257	1.000	0.390	-0.566
t_s	0.179	0.118	-0.971	0.390	1.000	-0.971
s	-0.033	0.004	0.925	-0.566	-0.971	1.000

A.13.4 Additional Figures

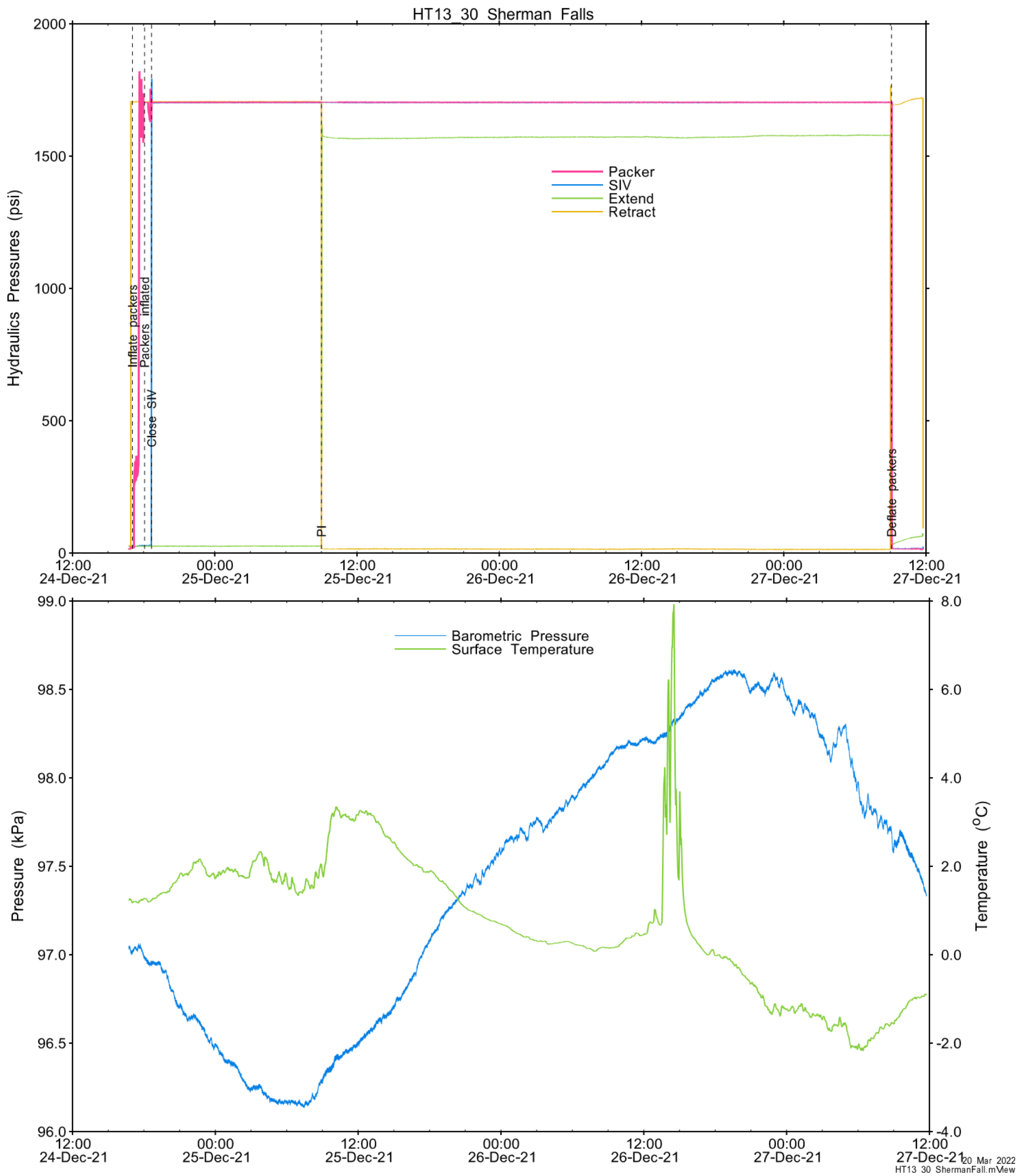

Figure 0.196 Hydraulics pressures and surface temperature/barometric pressure.

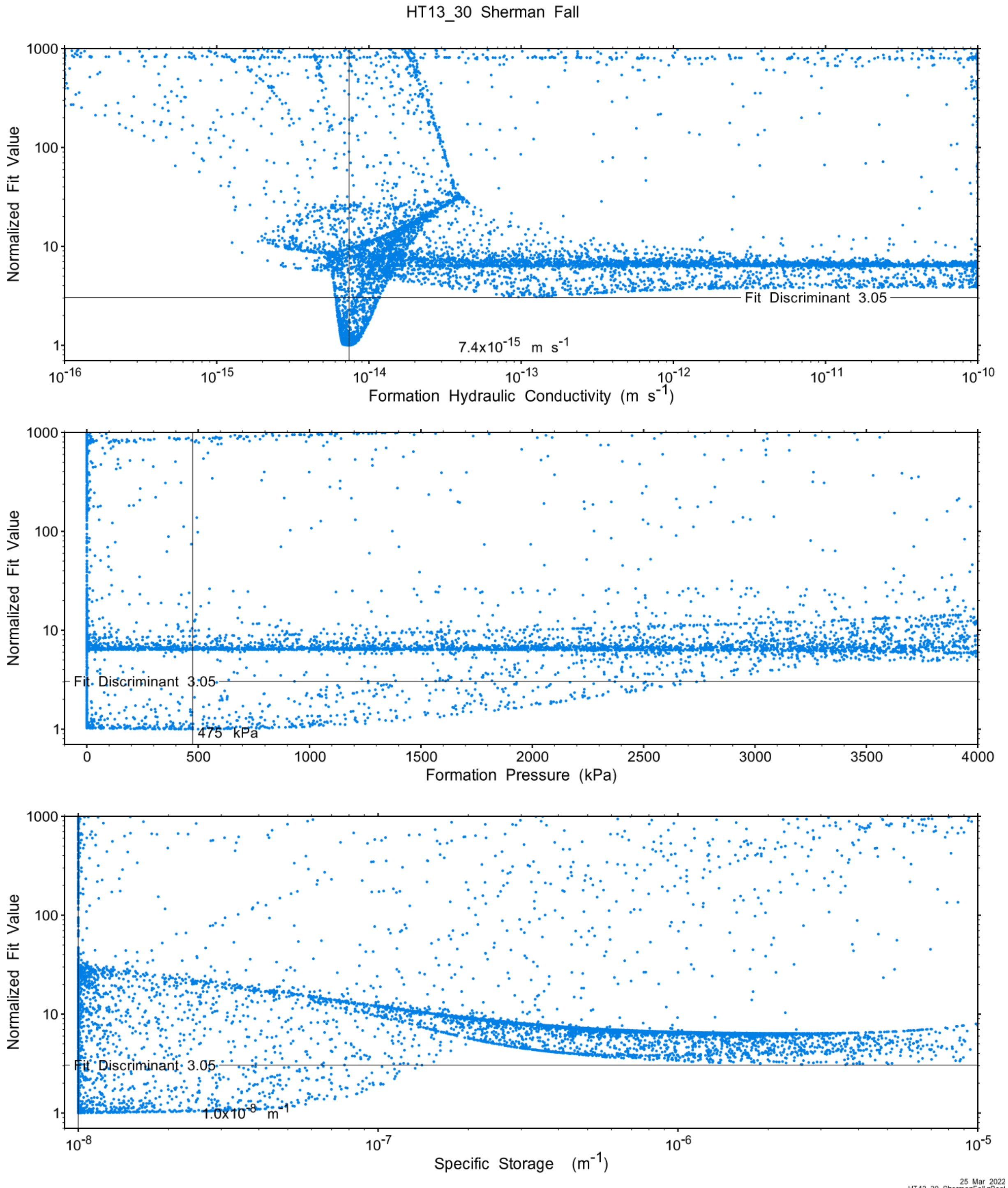

Figure 0.197 XY-scatter plot showing the formation parameter space normalized fit values.

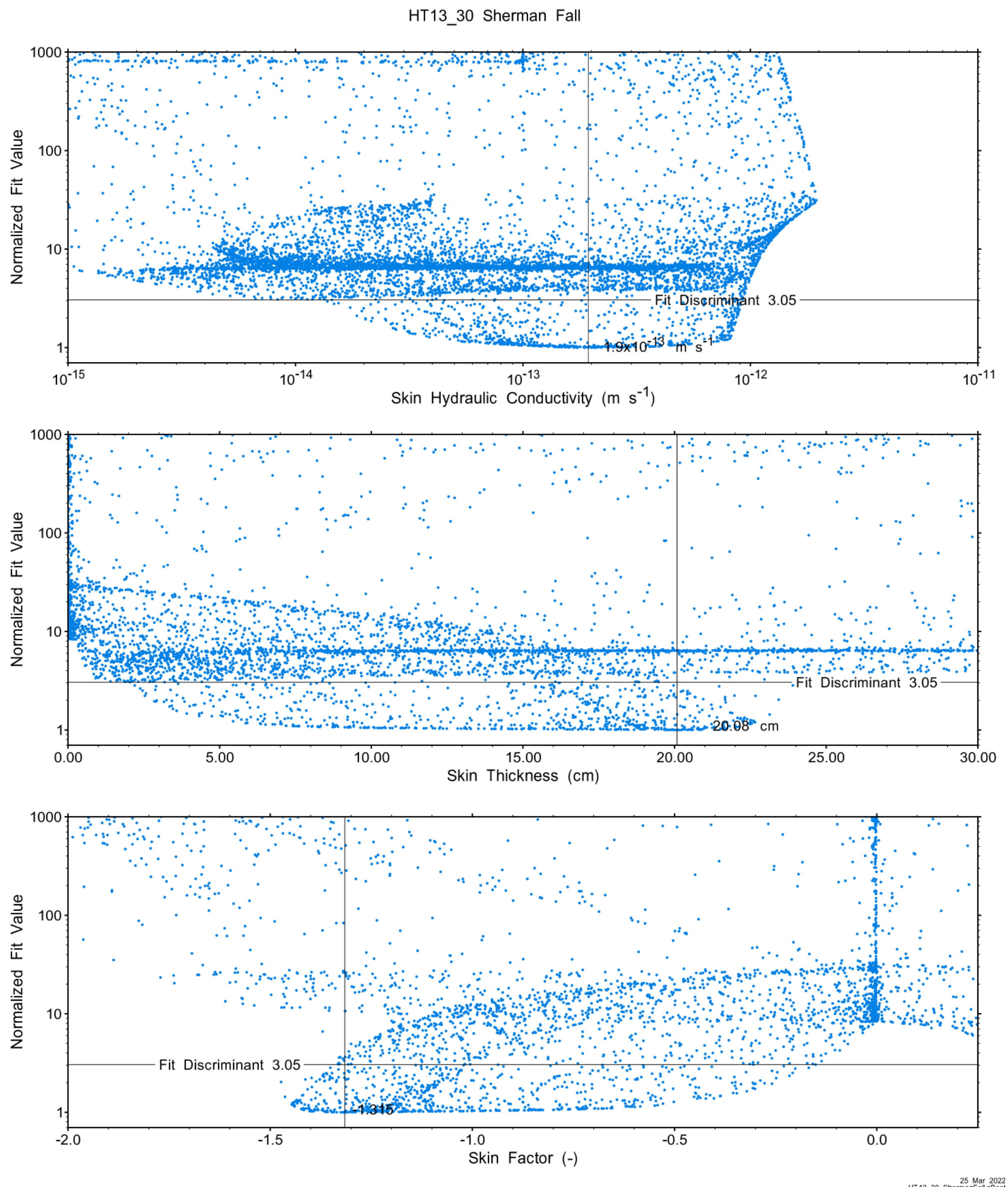

Figure 0.198 XY-scatter plot showing the skin parameter space normalized fit values.

A.14 HT14_30 Kirkfield

The SB_BH01 interval from 750.75 to 780.80 mBGS tested in HT14_30 includes the lower two thirds of the Kirkfield Formation. A PI test with a duration of 2 days and a PW with a duration of 3.375 hours were conducted. The initial PI test was anomalous with a break in slope approximately 30 hours after test commencement. Given the extremely low hydraulic conductivity indicated by analyses of the remaining test, this may have been indicative of a very low high pressure leak, possibly from the upper packer. Notwithstanding the cause, the condition appeared to be eliminated after the inflection. The test-ending confirmatory PW was extended for three hours to provide additional test coverage. Optimization was performed using a combined fit that included both valid test segments.

A.14.1 Test Data Summary

Table 0.66 and Figure 0.199 provide a summary of test events and a plot of pressures measured while testing, respectively.

Table 0.66 HT14_30 Summary of Test Events.

Event	Start Date & Time	Duration (days)	TZ Pressure (kPa)
Drilling intercept	21-09-11 03:30	70.47	7896
Prior testing	21-11-20 14:45	141.02	variable
Shut-in	22-04-10 15:12	0.72	8902
Pulse injection (anomalous)	22-04-11 08:31	1.28	8857
Pulse injection (analyzed)	22-04-12 15:13	0.75	7896
Pulse withdrawal	22-04-13 09:07	0.14	7290
Test end	22-04-13 12:31		7358

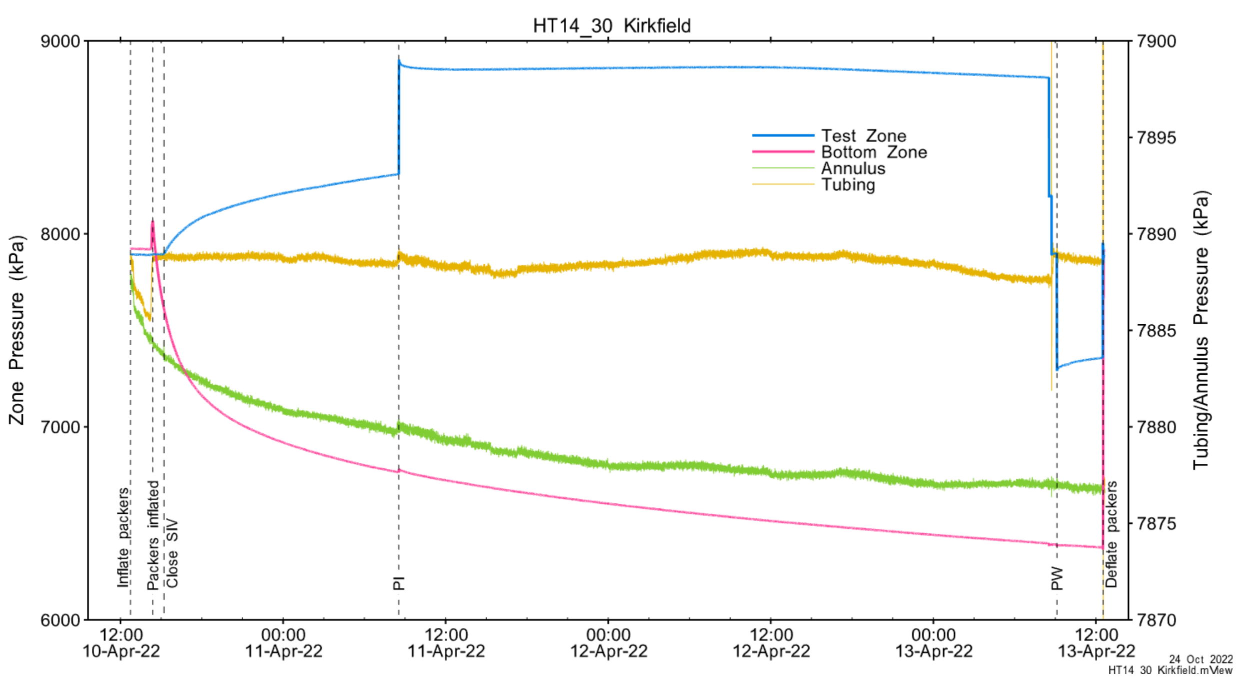

Figure 0.199 HT14_30 test events and pressures.

A.14.2 Test Analyses

Table 0.67 is a summary of test-specific input parameters used in the analyses, while Table 0.68 presents the optimized parameters and allowed ranges.

Table 0.67 nSIGHTS Input Parameters.

Parameter	Value	Units
Test zone radius	6.673	cm
Test zone compressibility	4.12E-10	1/Pa
Test zone fluid density	1092	g/L
Test zone length	30.05	m

Table 0.68 nSIGHTS Parameter Optimization Ranges.

Parameter	Minimum	Maximum	Units	Type
Formation hydraulic conductivity (K_f)	1E-16	1E-12	m/s	log
Formation pressure (P_f)	4000	7500	kPa	linear
Specific storage (Ss)	1E-08	1E-04	1/m	log
Skin hydraulic conductivity (K_s)	1E-16	1E-12	m/s	log
Skin thickness (t_s)	0.1	2000	mm	linear

Figure 0.200 shows the measured test zone pressure record (with reduced data density for clarity) used in the analysis along with the best-fit simulation and parameter values. A second plot details the anomalous response in the first PI test. Figure 0.201 presents the pre-test history.

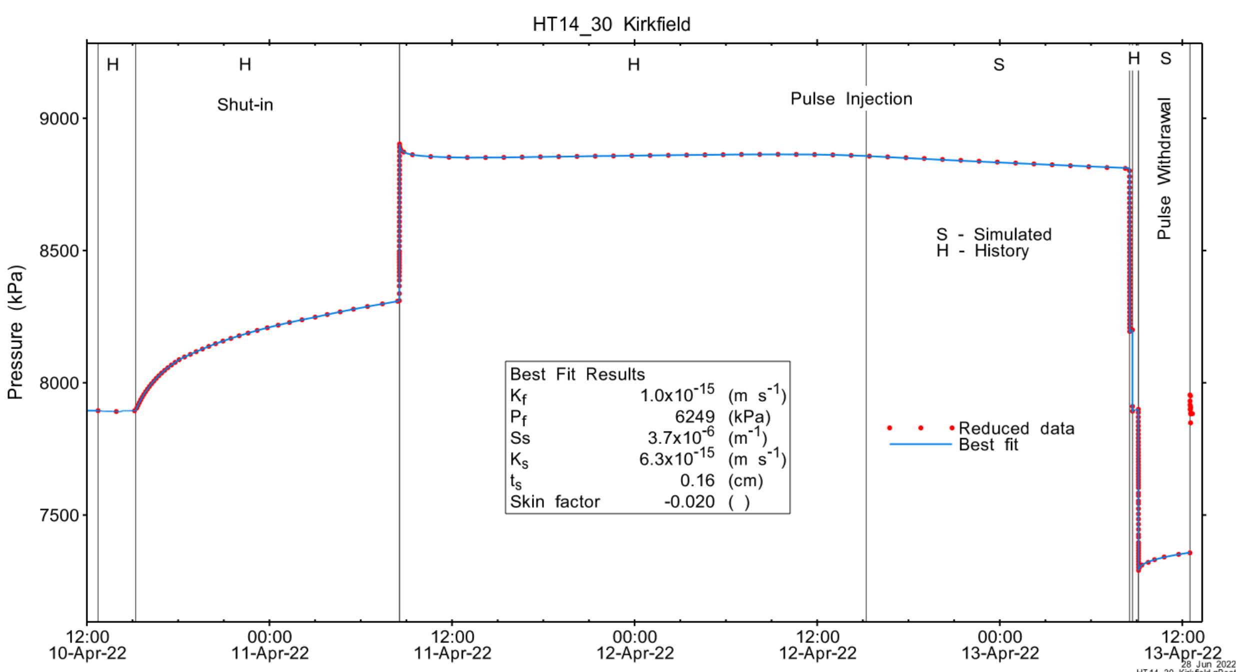

Figure 0.200 Annotated testing sequence showing best-fit simulation and parameter estimates.

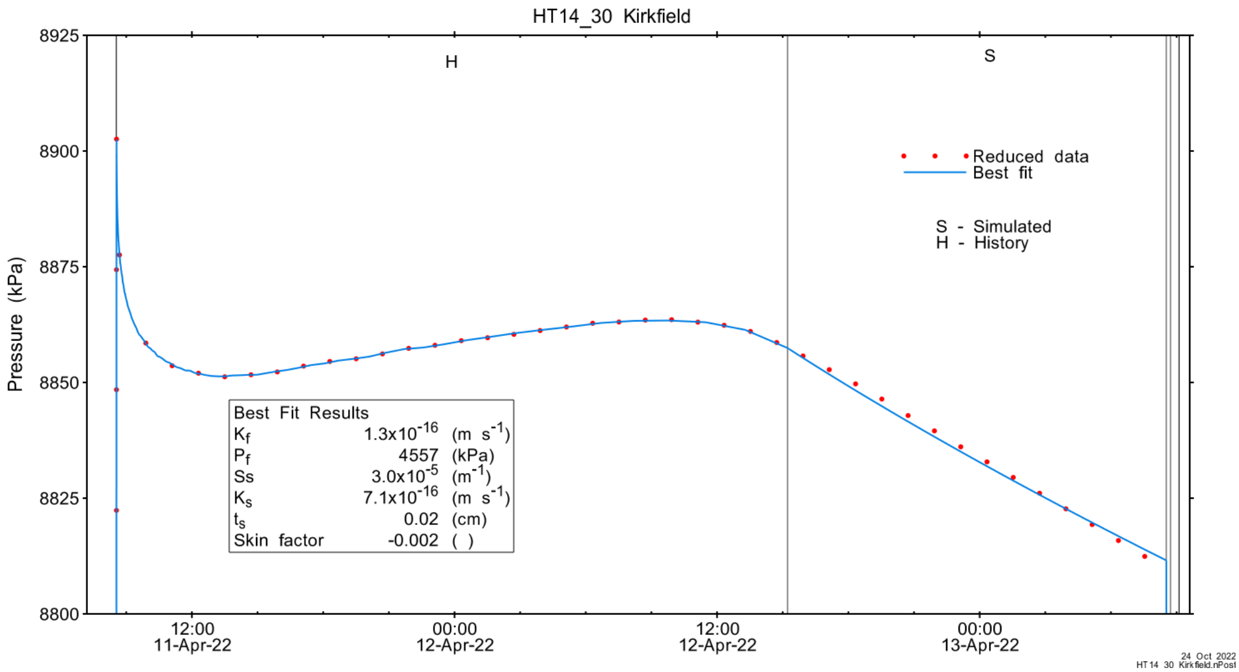

Figure 0.201 Annotated testing sequence showing best-fit simulation and parameter estimates (PI test only).

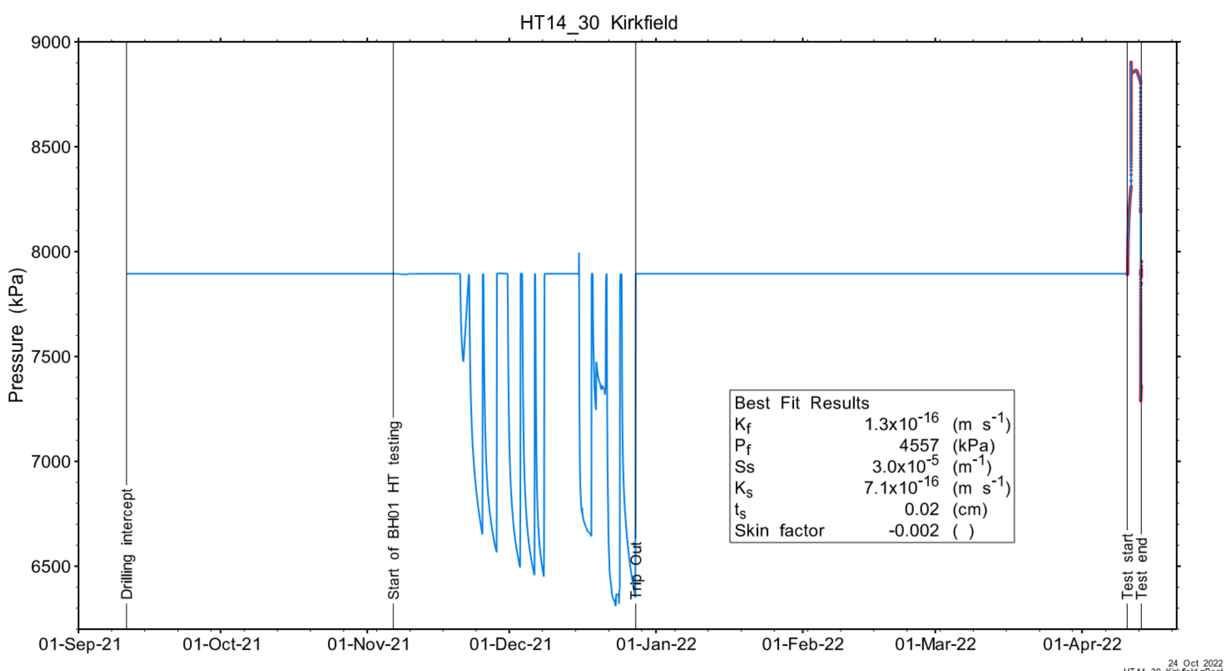

Figure 0.202 Annotated HT14_30 testing sequence showing pre-test history, best-fit simulation and parameter estimates.

Figure 0.203 shows the Ramey B normalized best-fit pressure and derivatives for the PI test, while Figure 0.204 shows the same data for the PW sequence.

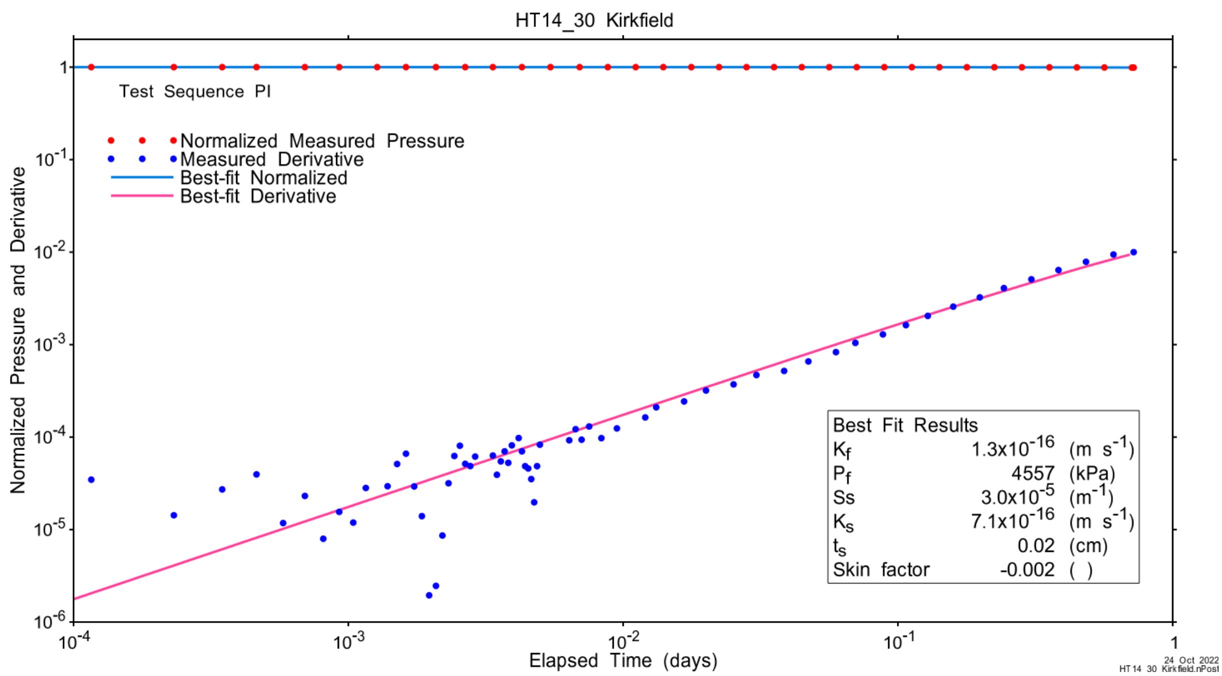

Figure 0.203 Log-log plot showing Ramey B PI normalized pressure and derivative response for best-fit simulation.

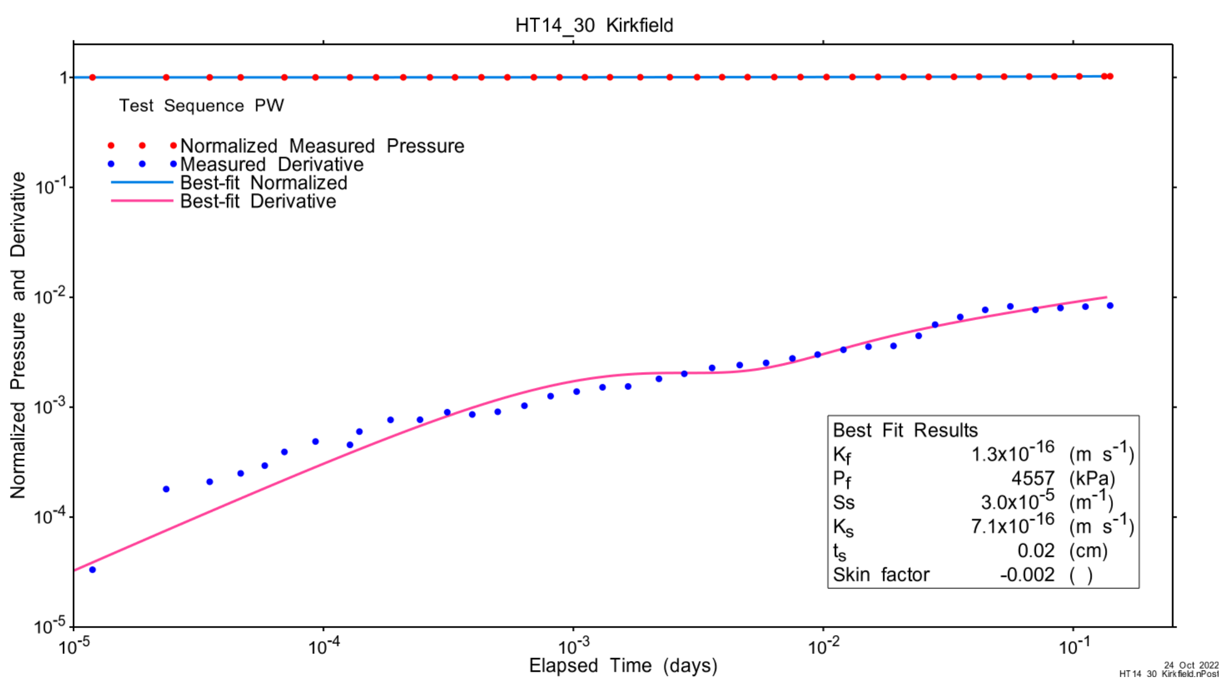

Figure 0.204 Log-log plot showing Ramey B PW normalized pressure and derivative response for best-fit simulation.

Figure 0.205 and Figure 0.206 show the normalized parameter sensitivity response for the best fit for the PI and PW sequences respectively. Skin-related parameters are most sensitive during the early-time response. Sensitivity for all fitting parameters continues to rise – additional test time may have improved the estimates.

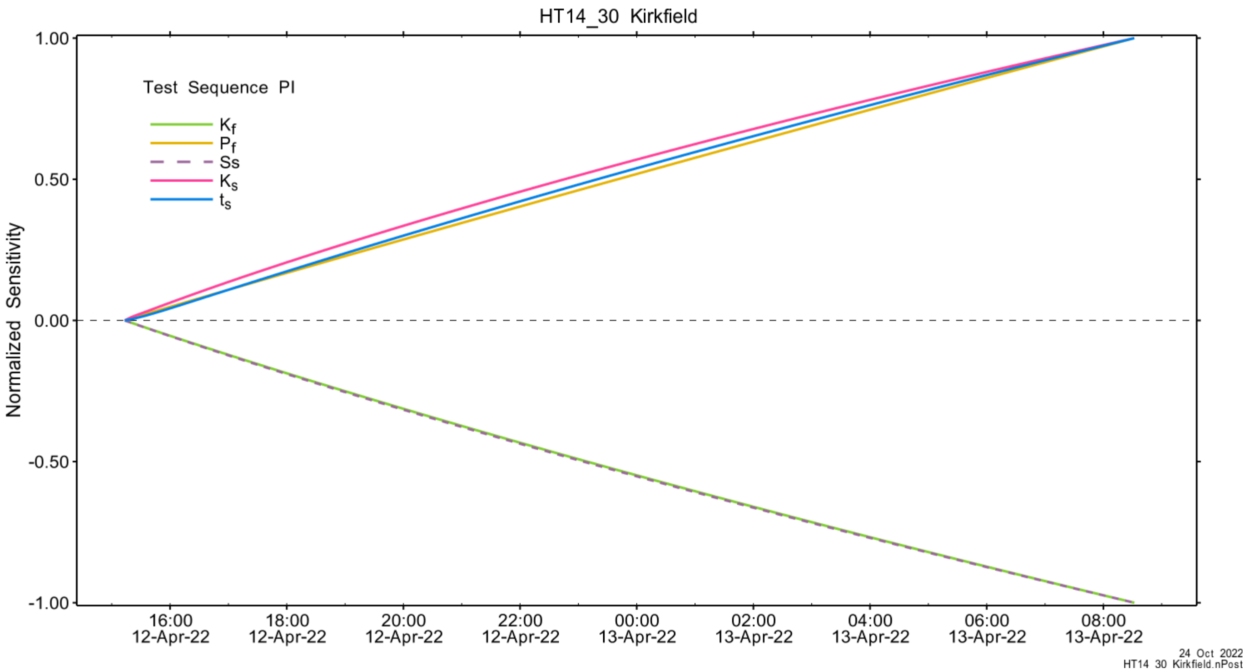

Figure 0.205 Normalized Jacobian for PI sequence for best-fit simulation.

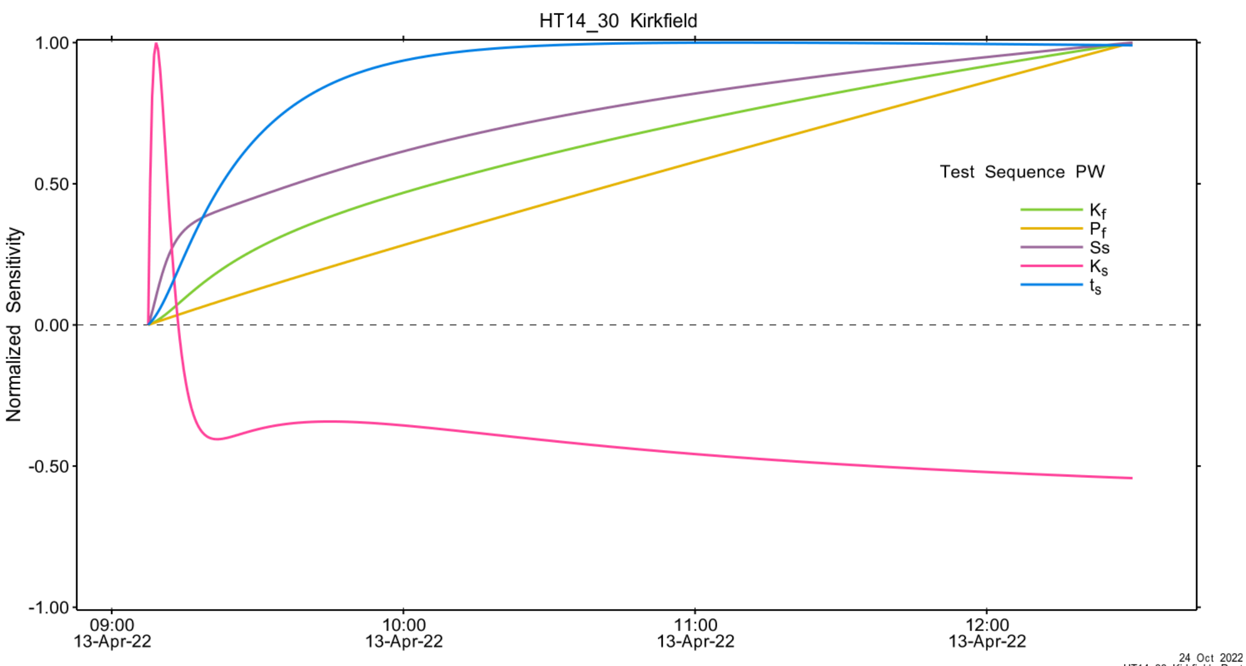

Figure 0.206 Normalized Jacobian for PW sequence for best-fit simulation.

A.14.3 Uncertainty Analyses

The CDF of normalized fit values for all converged simulations and the selected fit discriminant are shown in Figure 0.207.

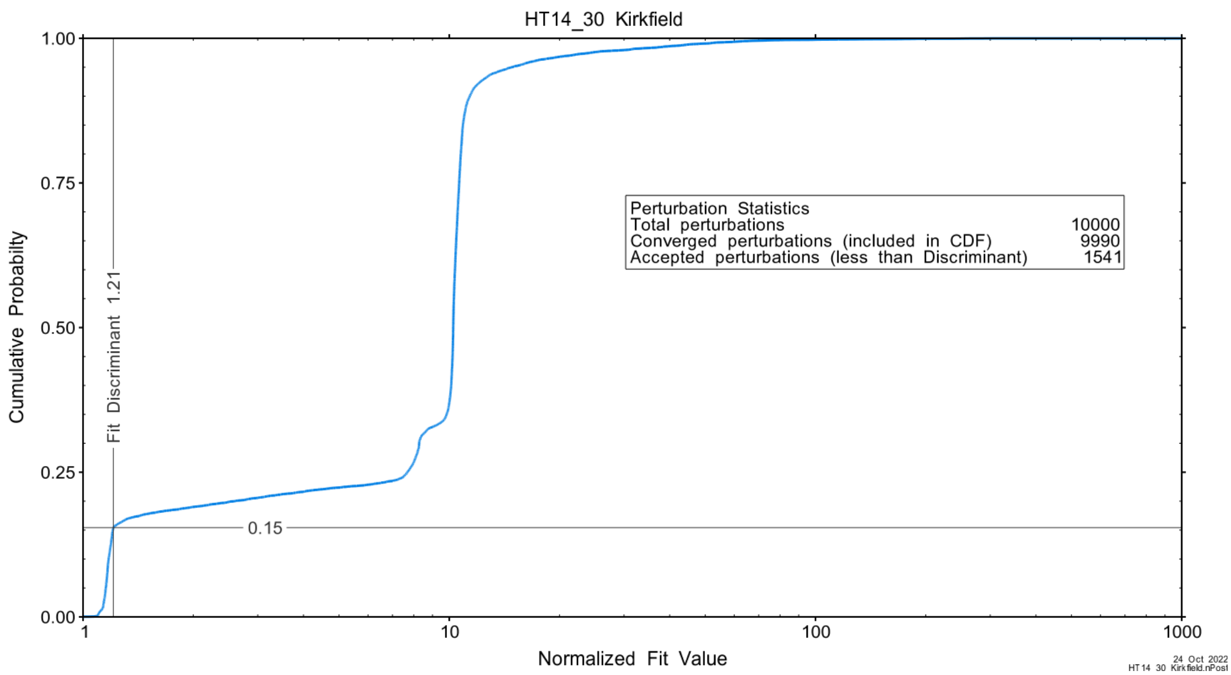

Figure 0.207 Fit value cumulative distribution function.

Summary cross parameter scatter plots for selected formation and skin parameters are given in Figure 0.208 and Figure 0.209. The light pink dots on the figures are the initial parameter estimates, with red dots overlaying those initial parameter values that resulted in accepted optimization results. The grey dots are converged optimizations which did not meet the fit discriminant. Larger varying color symbols represent the fit value of accepted optimizations, with the blue values representing the best fit.

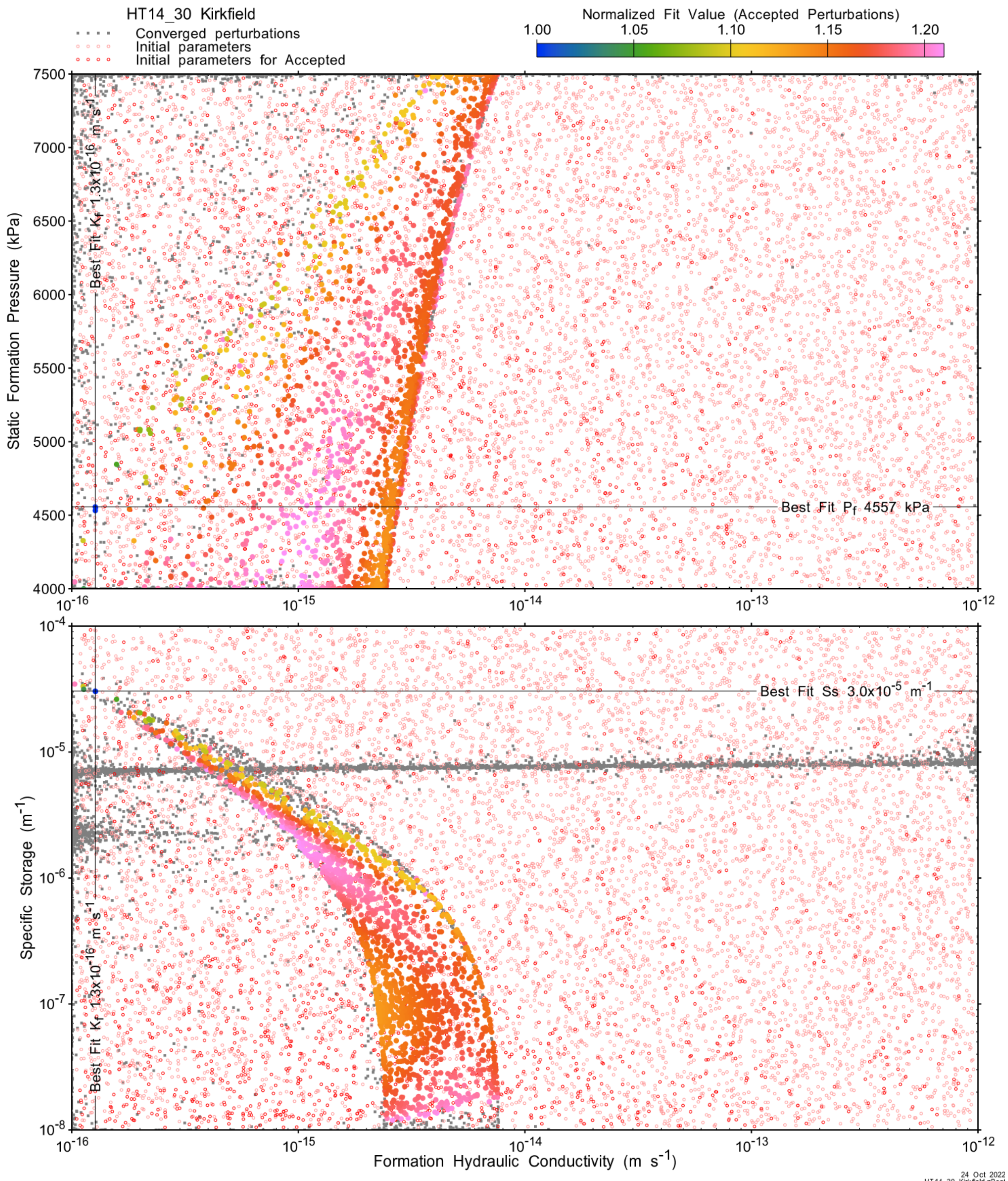

Figure 0.208 XY-scatter plot showing estimates of formation hydraulic conductivity (K_f) vs static formation pressure (P_f) (top panel) and specific storage (Ss) (bottom panel).

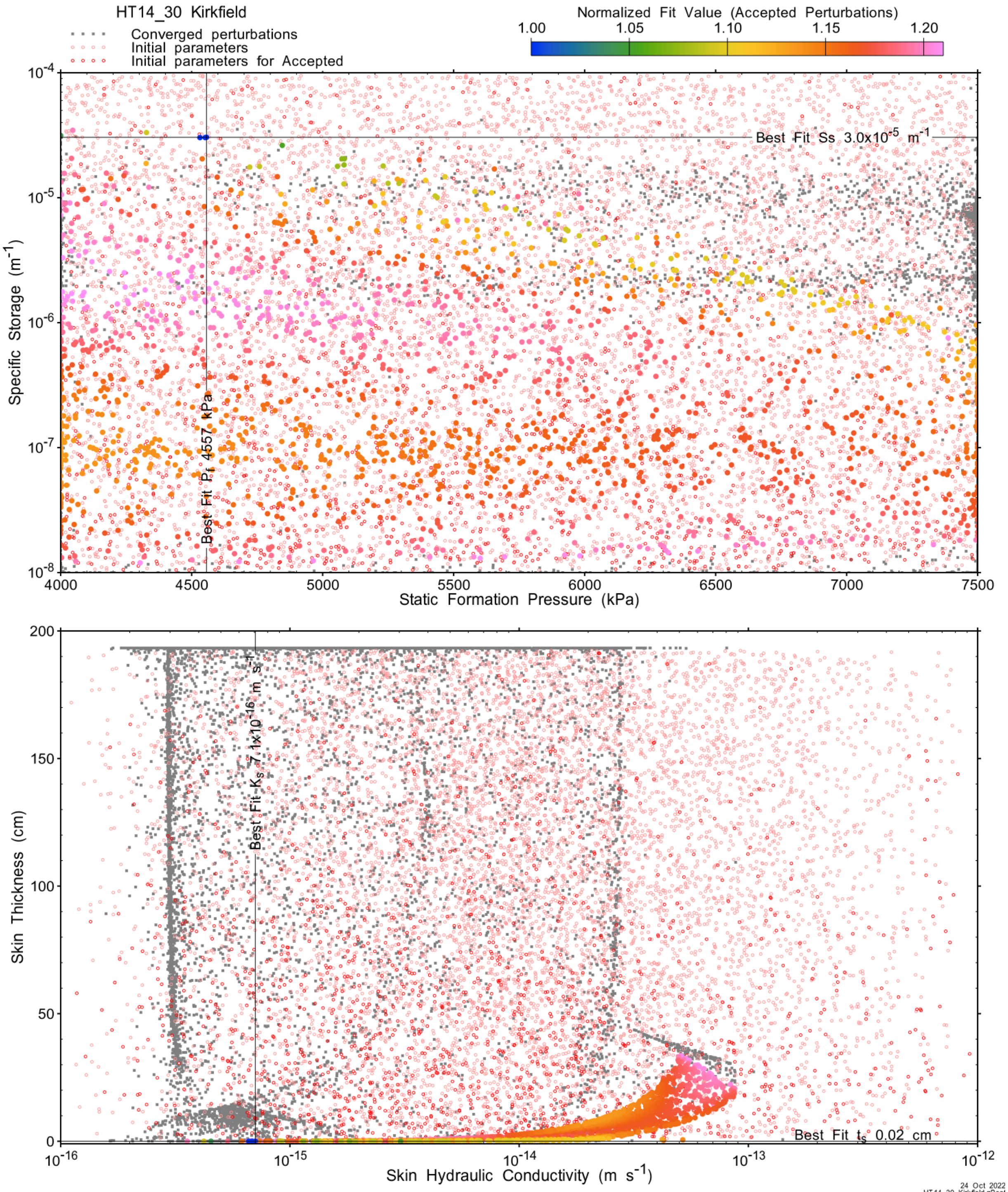

Figure 0.209 XY-scatter plot showing estimates of static formation pressure (P_f) vs specific storage (Ss) (top panel) and skin hydraulic conductivity (K_s) vs skin thickness (t_s) (bottom panel).

Confidence limits and median values are determined from the CDF of accepted optimization results (i.e. the varying color values in the above figures), with best fit value, 5% and 95% confidence indicated on Figure 0.210 and Figure 0.211.

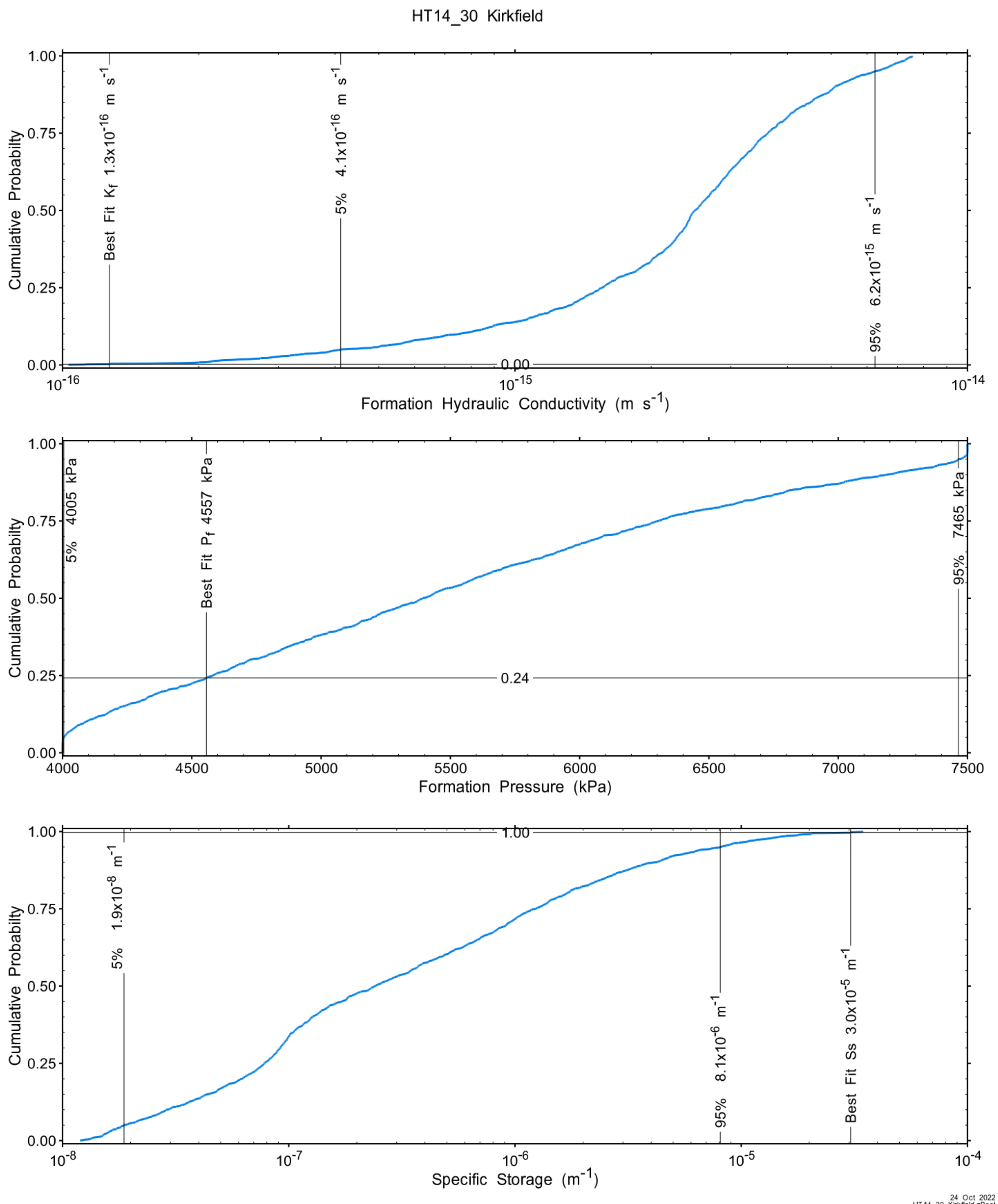

Figure 0.210 Cumulative distribution functions and parameter limits for formation hydraulic conductivity (K_f) (top panel), static formation pressure (P_f) (middle panel) and specific storage (Ss) (bottom panel).

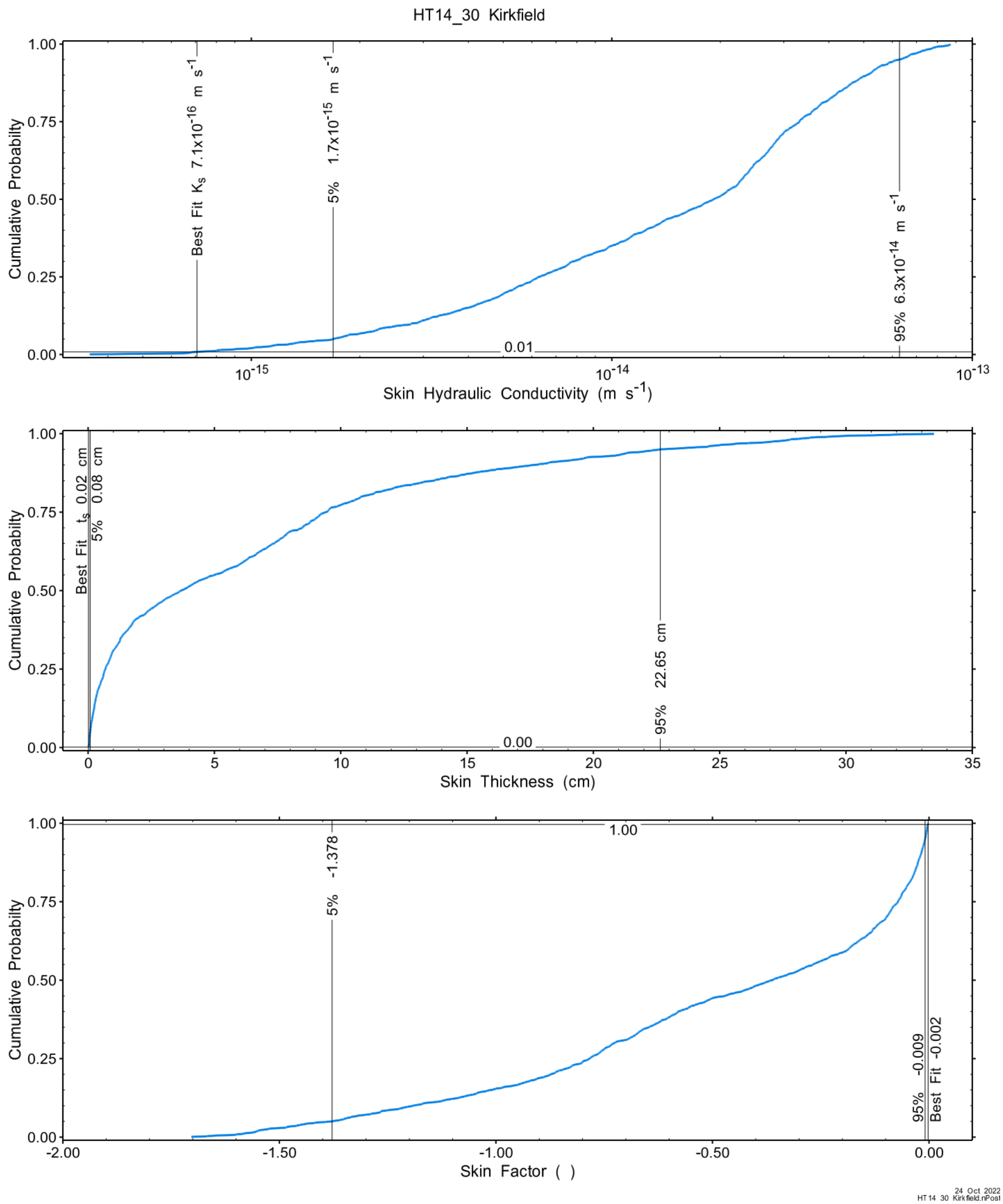

Figure 0.211 Cumulative distribution functions and parameter limits for skin hydraulic conductivity (K_s) (top panel), skin thickness (t_s) (middle panel) and skin factor (s) (bottom panel).

A summary of perturbation results is presented in Figure 0.212 , with Ramey-processed perturbations in Figure 0.213. Those perturbations (1171 of 10,000) with all parameters within the 5% and 95% range present a very good fit to the measured test zone data.

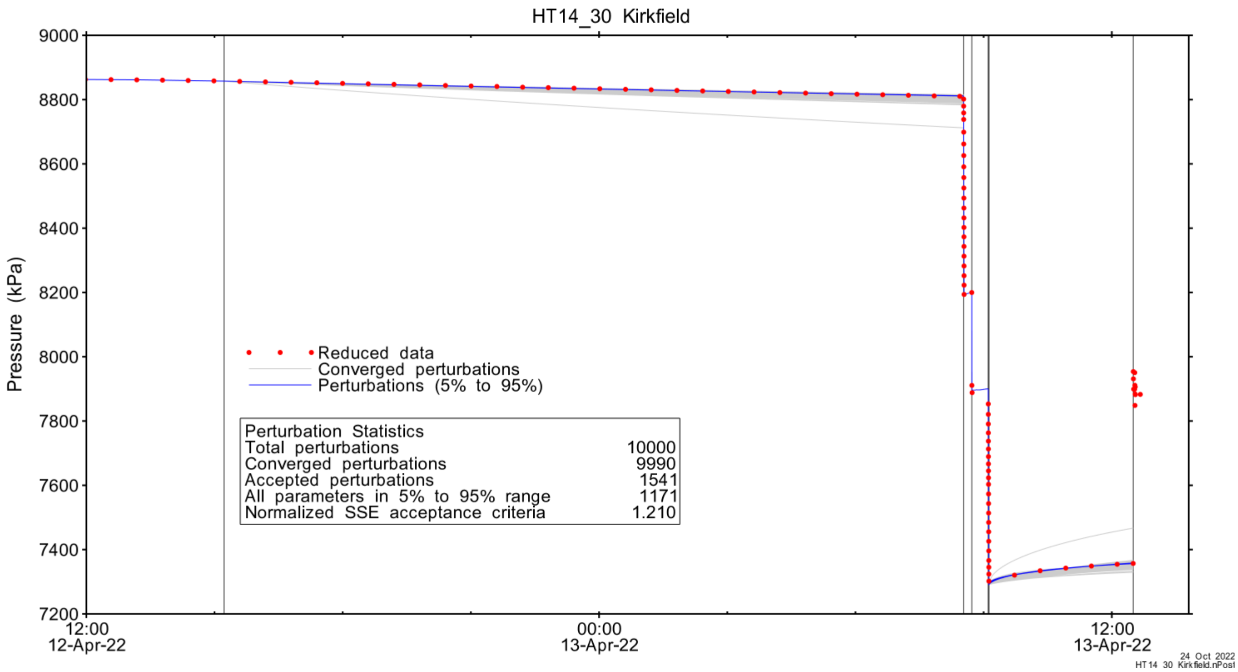

Figure 0.212 Perturbation results – all converged, accepted, and within 5% to 95% for all parameters.

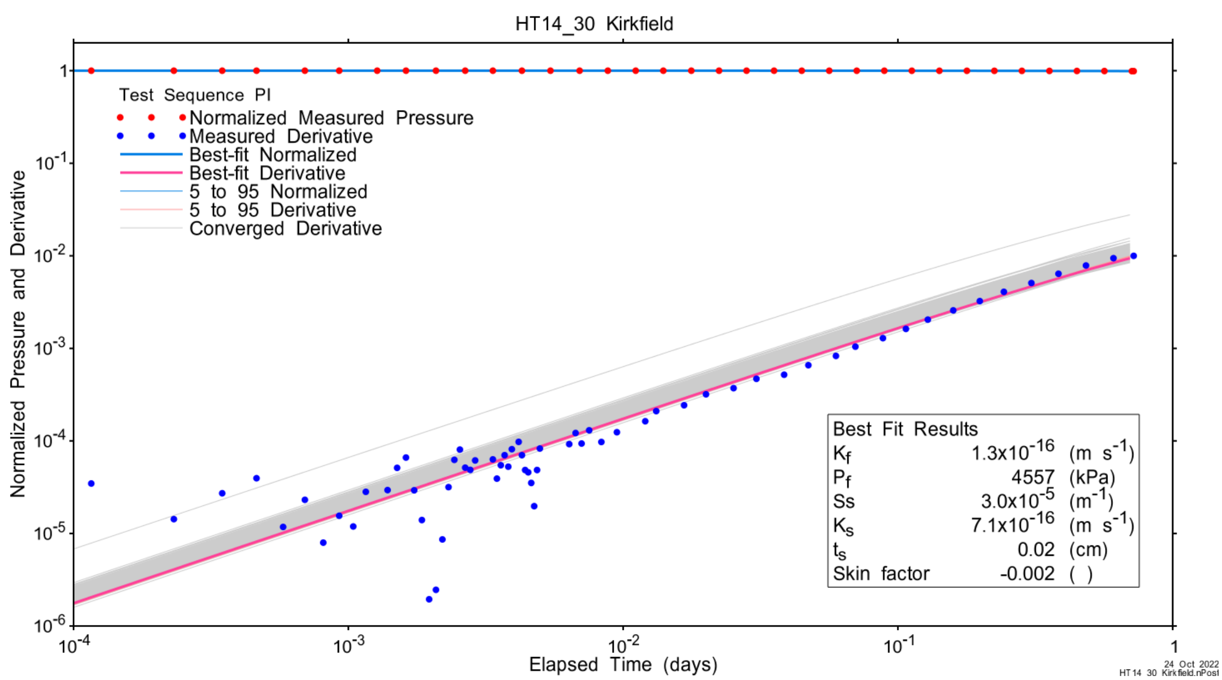

Figure 0.213 Log-log plot showing Ramey B normalized pressure and derivative response for test sequence PI for all converged optimizations and those within 5% to 95% for all parameters.

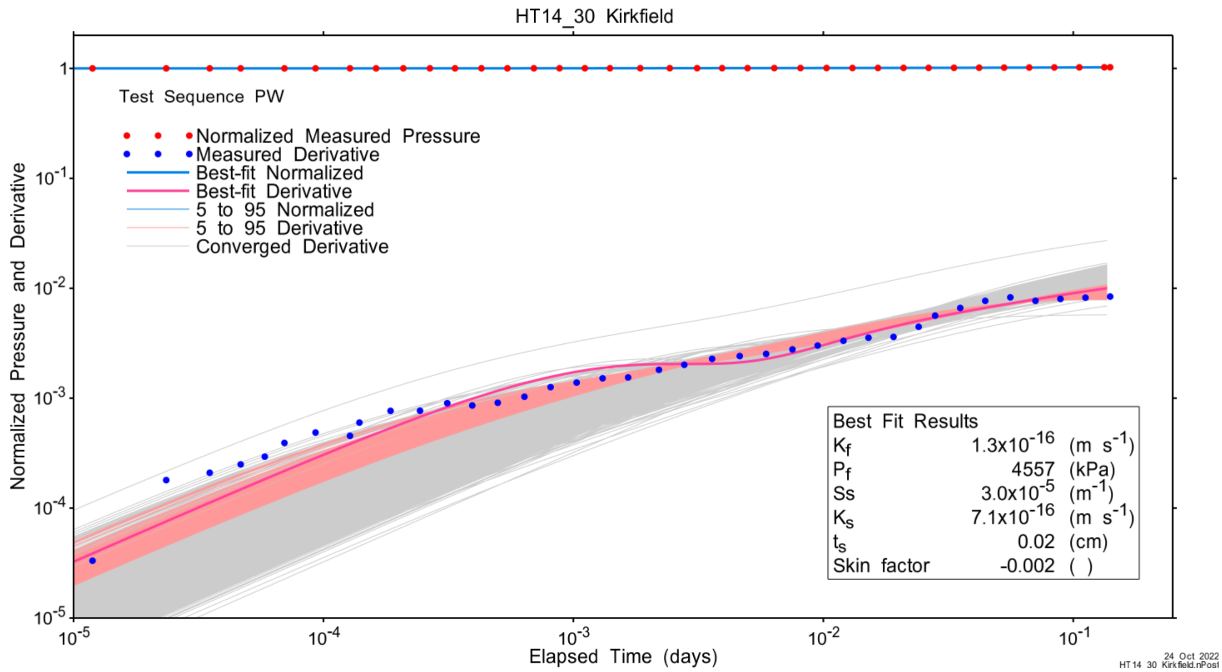

Figure 0.214 Log-log plot showing Ramey B normalized pressure and derivative response for test sequence PW for all converged optimizations and those within 5% to 95% for all parameters.

A summary of best-fit and parameter ranges is given in Table 0.69.

Table 0.69 Summary of the HT14_30 parameter estimates.

Parameter	Best Fit	5%	Median	95%
K_f (m/s)	1.3E-16	4.1E-16	2.5E-15	6.2E-15
P_f (kPa)	4557	4005	5393	7465
Ss (1/m)	3.0E-05	1.9E-08	2.4E-07	8.1E-06
K_s (m/s)	7.1E-16	1.7E-15	1.9E-14	6.3E-14
t_s (cm)	0.02	0.08	3.68	22.65
s (-)	-0.002	-1.378	-0.363	-0.009

Parameter correlations for all perturbations with all parameters within the 5% to 95% limits are given in Table 0.70.

Table 0.70 Pearson cross-correlations of 5% to 95% parameters

	Log(K_f)	P_f	Log(Ss)	Log(K_s)	t_s	s
Log(K_f)	1.000	0.513	-0.833	0.920	0.589	-0.652
P_f	0.513	1.000	-0.061	0.322	-0.037	0.034
Log(Ss)	-0.833	-0.061	1.000	-0.947	-0.899	0.946
Log(K_s)	0.920	0.322	-0.947	1.000	0.813	-0.864
t_s	0.589	-0.037	-0.899	0.813	1.000	-0.987
s	-0.652	0.034	0.946	-0.864	-0.987	1.000

A.14.4 Additional Figures

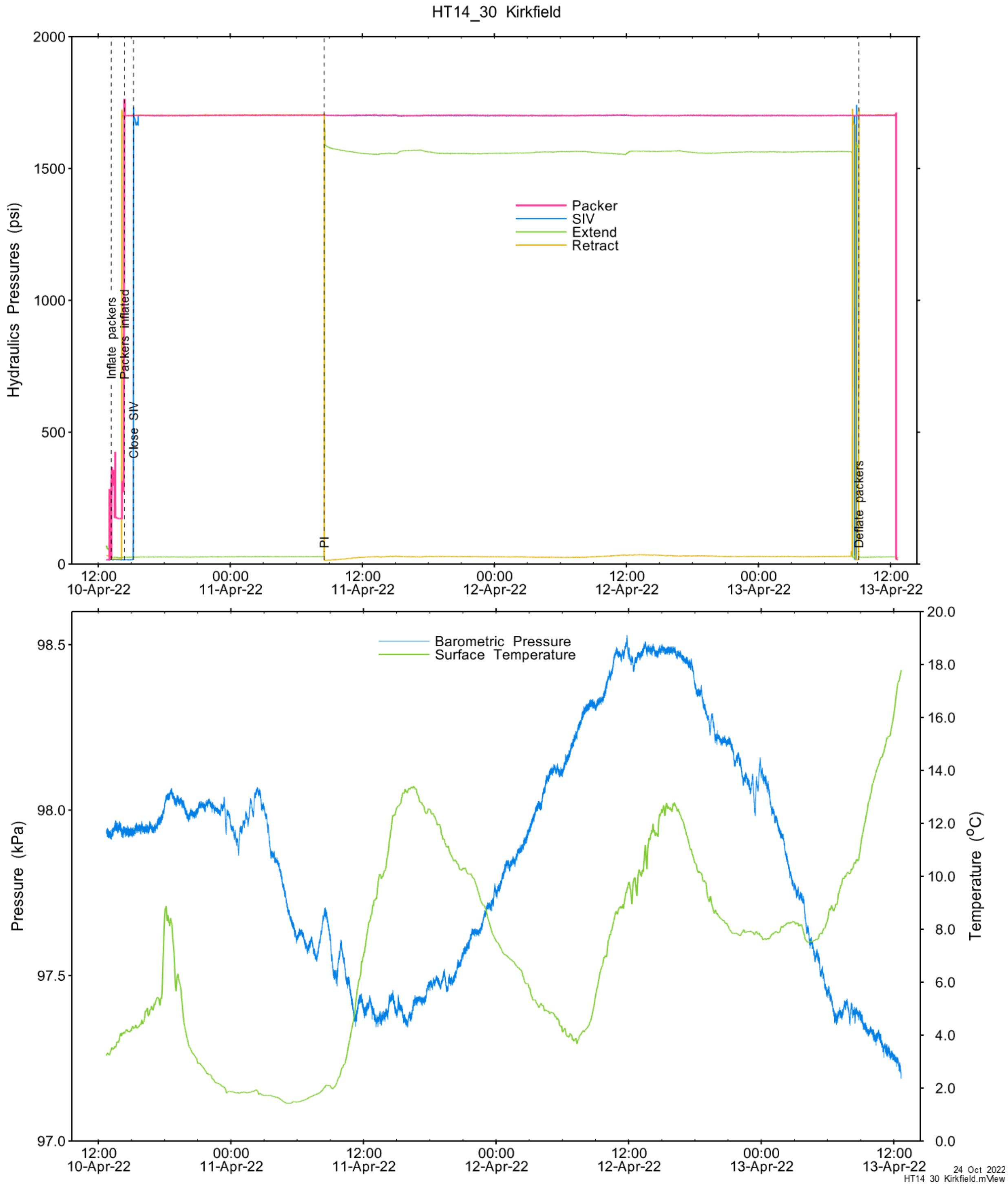

Figure 0.215 Hydraulics pressures and surface temperature/barometric pressure.

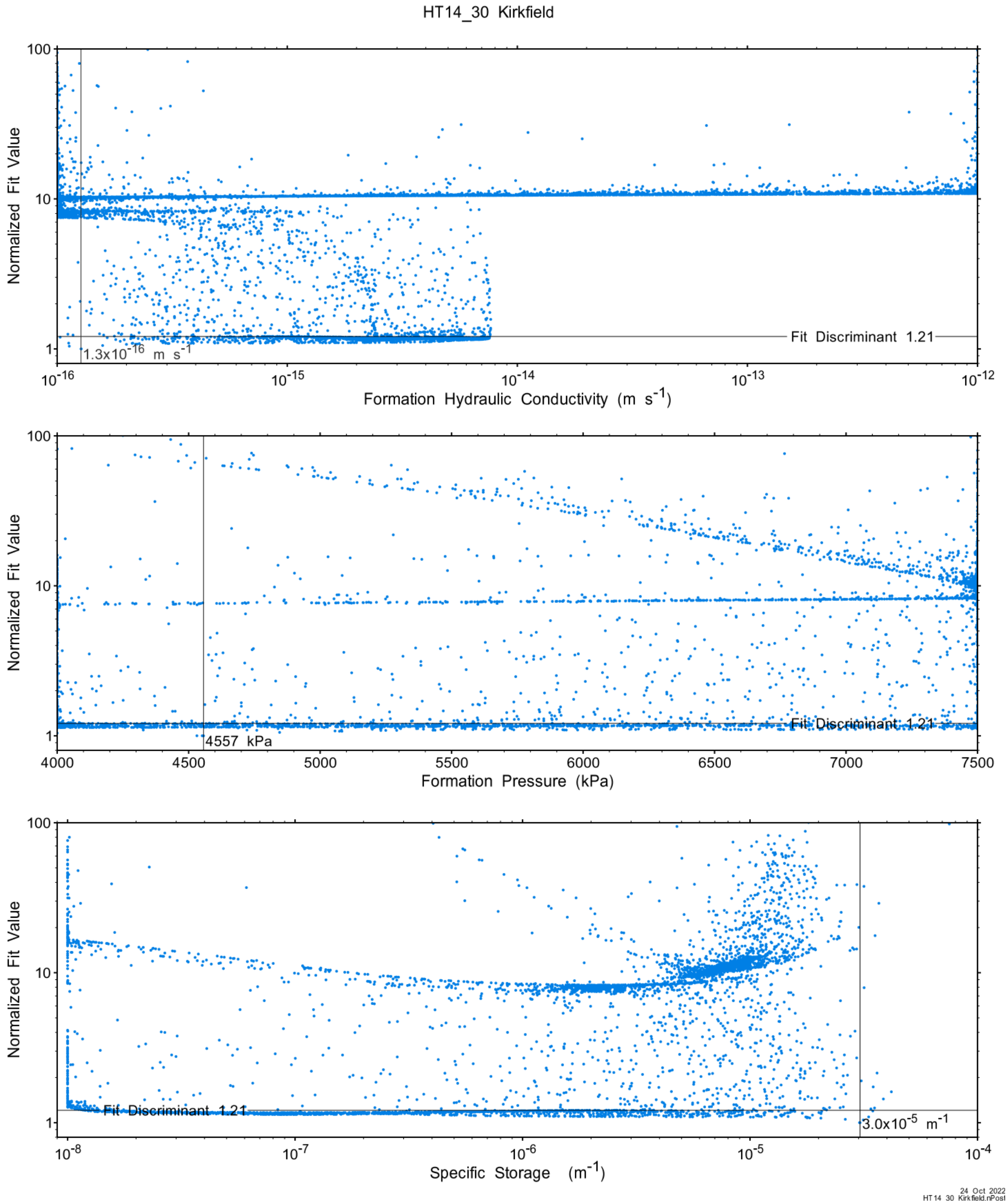

Figure 0.216 XY-scatter plot showing the formation parameter space normalized fit values.

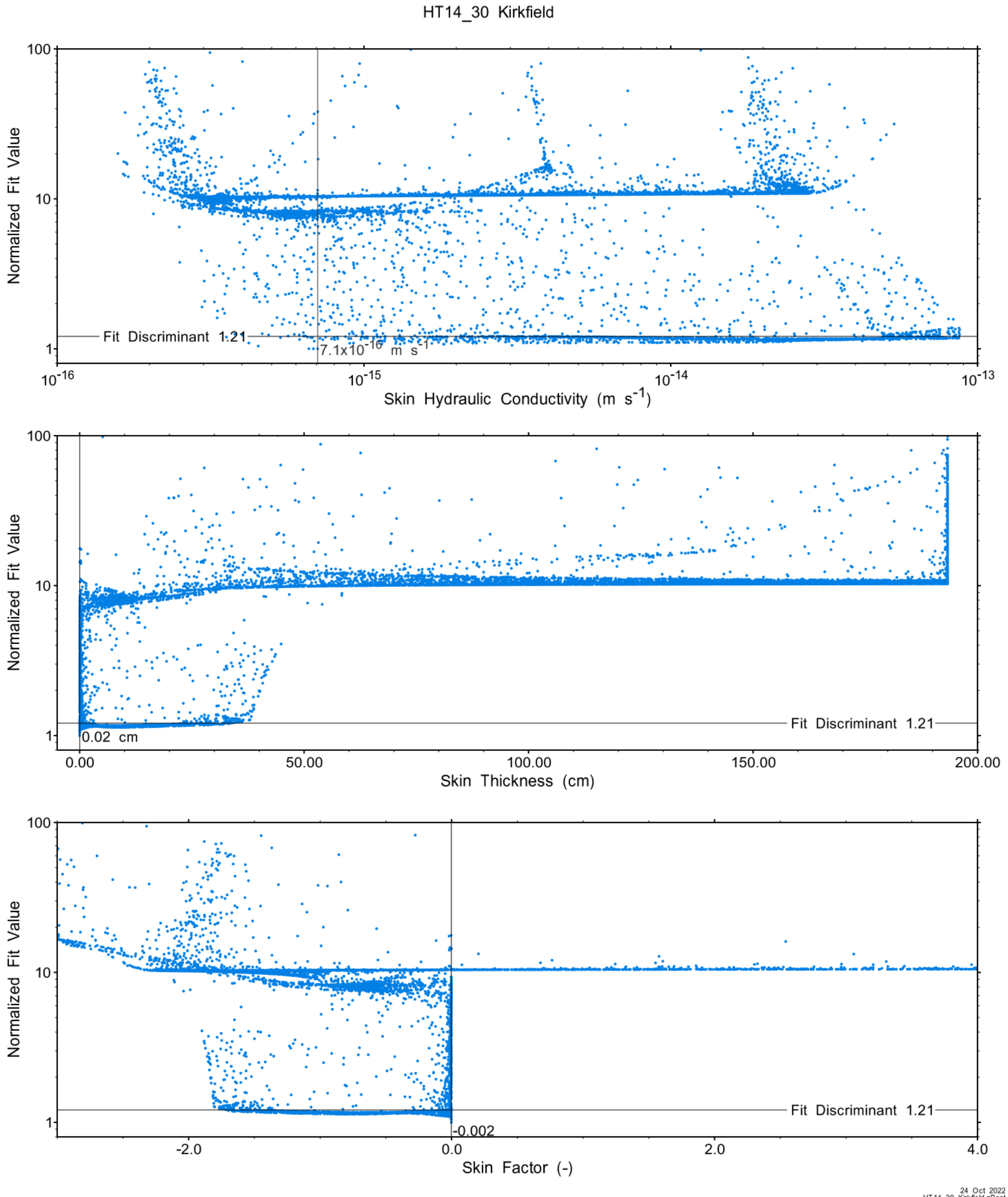

Figure 0.217 XY-scatter plot showing the skin parameter space normalized fit values.

A.15 HT15_30 Gull River

The SB_BH01 interval from 815.00 to 845.05 mBGS tested in HT15_30 includes the central section of the Gull River Formation. A PI test with a duration of 2 days was conducted.

A.15.1 Test Data Summary

Table 0.71 and Figure 0.218 provide a summary of test events and a plot of pressures measured while testing, respectively.

Table 0.71 HT15_30 Summary of Test Events.

Event	Start Date & Time	Duration (days)	TZ Pressure (kPa)
Drilling intercept	21-09-14 05:13	67.40	8572
Prior testing	21-11-20 14:45	144.07	variable
Shut-in	22-04-13 16:31	0.66	8576
Pulse injection	22-04-14 08:20	2.02	7296
Test end	22-04-16 08:43		6374

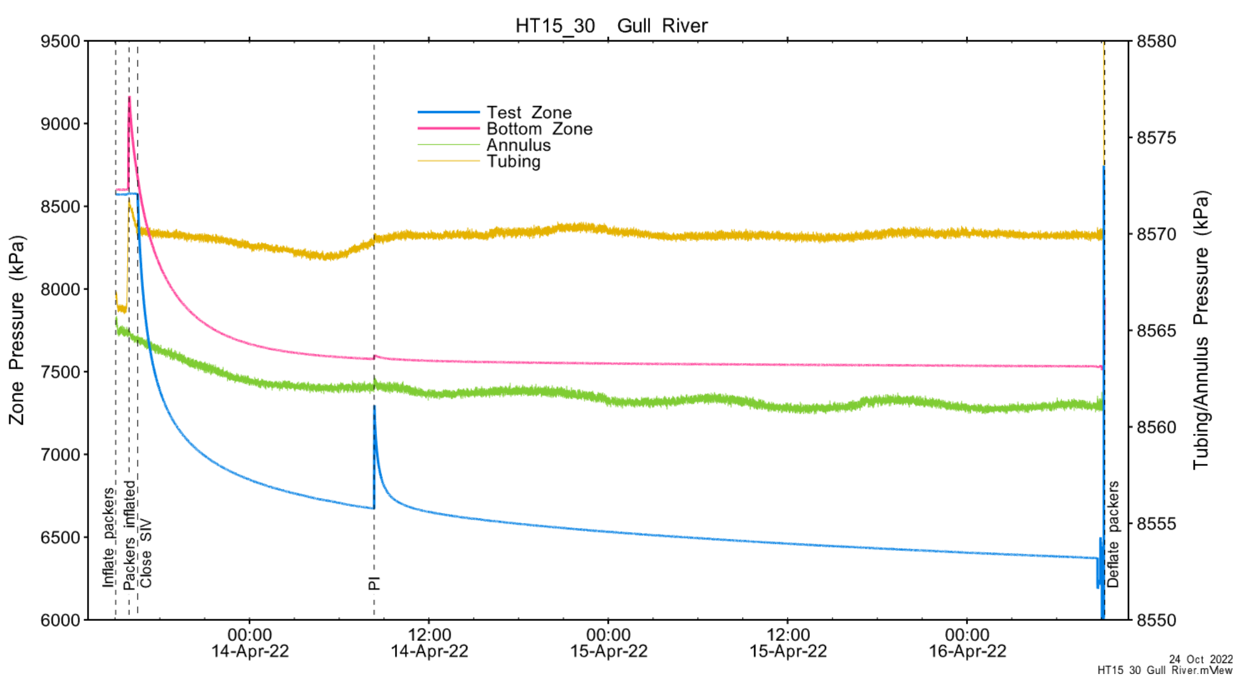

Figure 0.218 HT15_30 test events and pressures.

A.15.2 Test Analyses

Table 0.72 is a summary of test-specific input parameters used in the analyses, while Table 0.73 presents the optimized parameters and allowed ranges.

Table 0.72 nSIGHTS Input Parameters.

Parameter	Value	Units
Test zone radius	6.29	cm
Test zone compressibility	4.43E-10	1/Pa
Test zone fluid density	1092	g/L
Test zone length	30.05	m

Table 0.73 nSIGHTS Parameter Optimization Ranges.

Parameter	Minimum	Maximum	Units	Type
Formation hydraulic conductivity (K_f)	1E-14	1E-09	m/s	log
Formation pressure (P_f)	2000	8000	kPa	linear
Specific storage (Ss)	1E-08	1E-04	1/m	log
Skin hydraulic conductivity (K_s)	1E-14	1E-09	m/s	log
Skin thickness (t_s)	0.013	10000	cm	linear

Figure 0.219 shows the measured test zone pressure record (with reduced data density for clarity) used in the analysis along with the best-fit simulation and parameter values. Figure 0.220 presents the pre-test history, and Figure 0.221 shows the Ramey B normalized best-fit pressure and pressure derivatives.

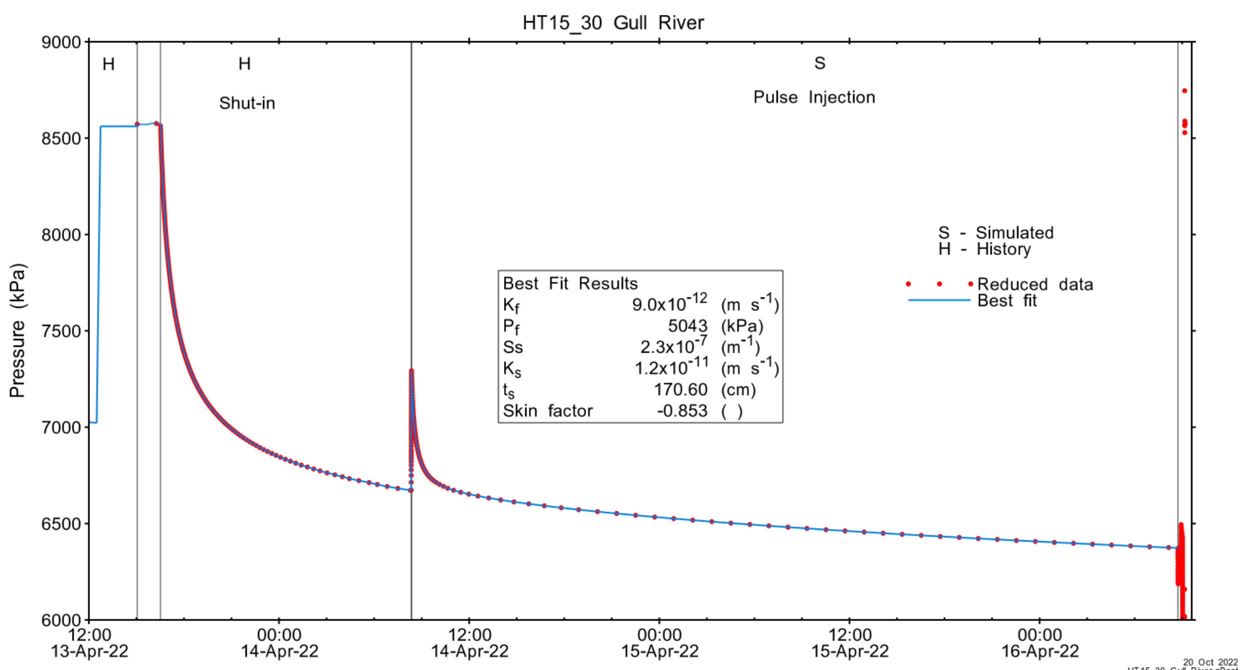

Figure 0.219 Annotated testing sequence showing best-fit simulation and parameter estimates.

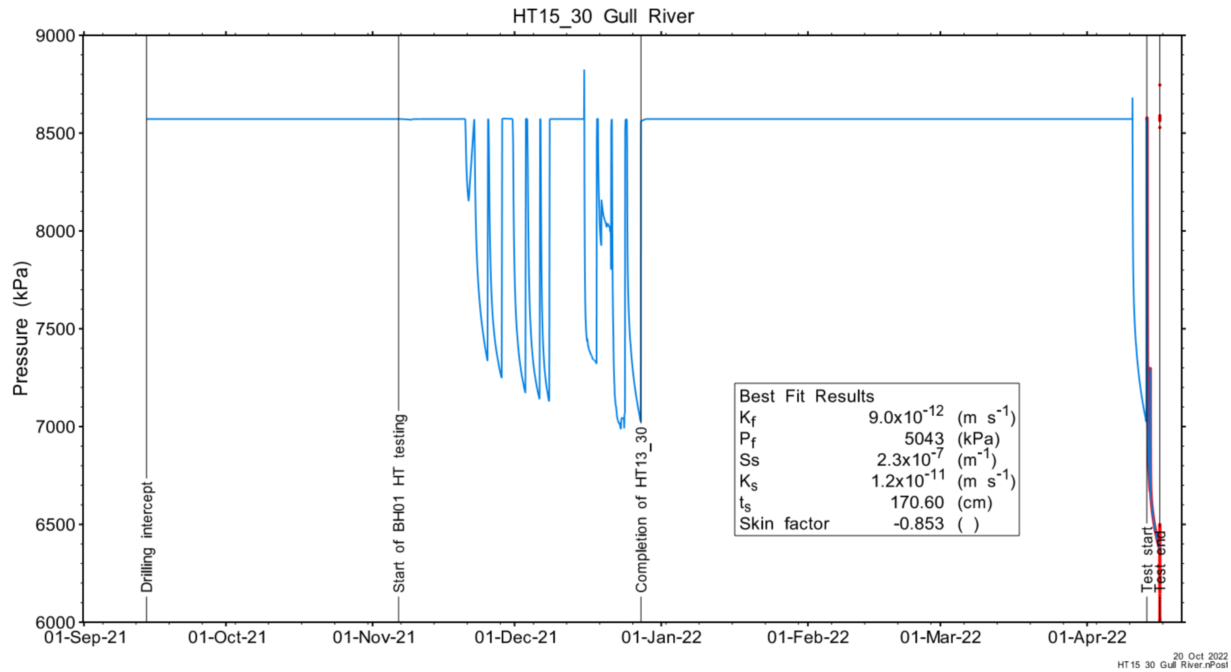

Figure 0.220 Annotated HT15_30 testing sequence showing pre-test history, best-fit simulation and parameter estimates.

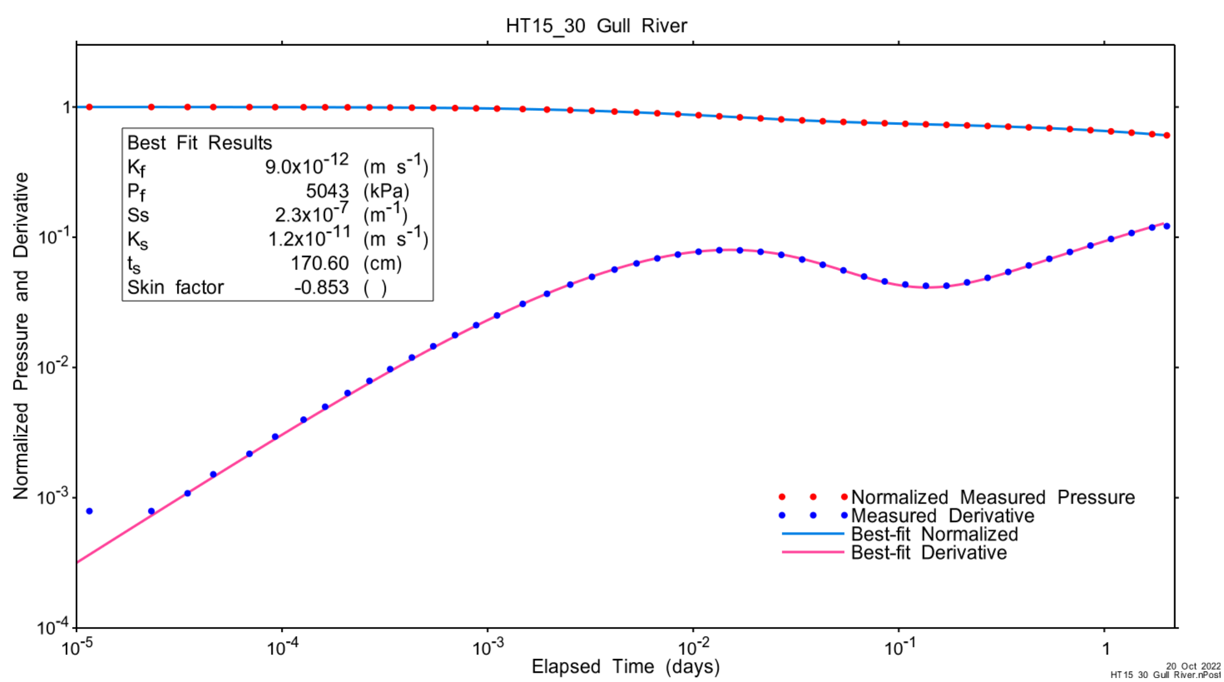

Figure 0.221 Log-log plot showing Ramey B normalized pressure and derivative response for best-fit simulation.

Figure 0.222 shows the normalized parameter sensitivity response for the best fit. Sensitivity for all fitting parameters was relatively constant by the end of the test, indicating that the test duration was sufficient for well-constrained parameter estimation.

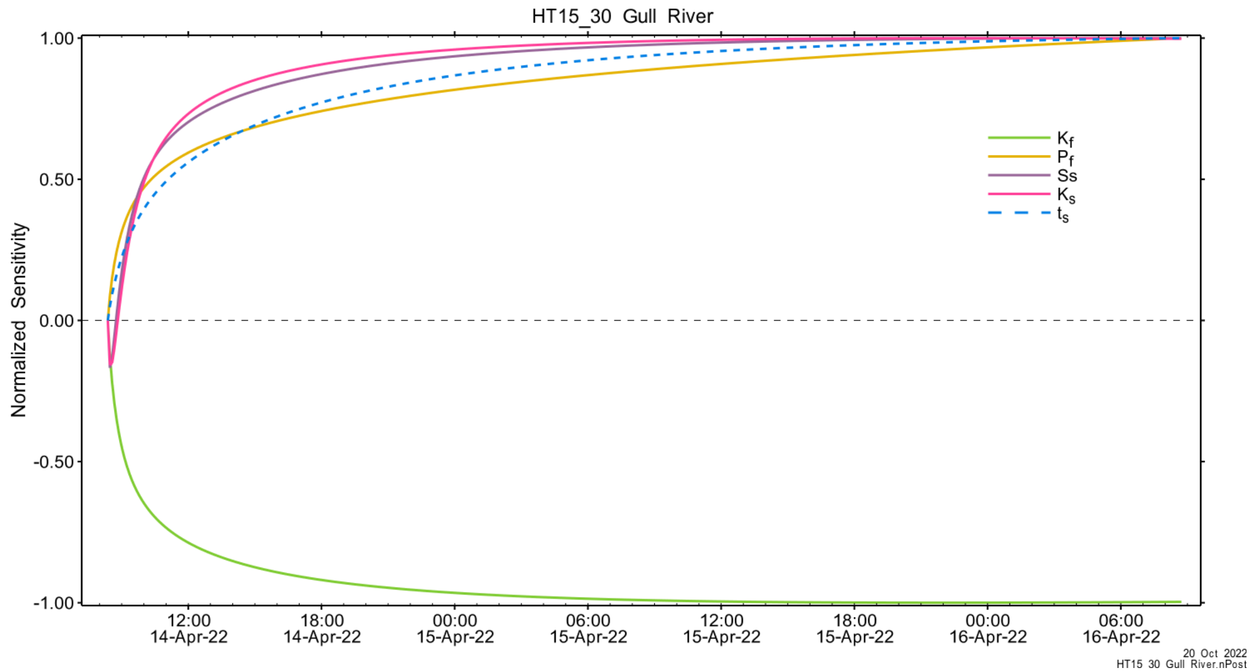

Figure 0.222 Normalized Jacobian for best-fit simulation.

A.15.3 Uncertainty Analyses

The CDF of normalized fit values for all converged simulations and the selected fit discriminant are shown in Figure 0.223.

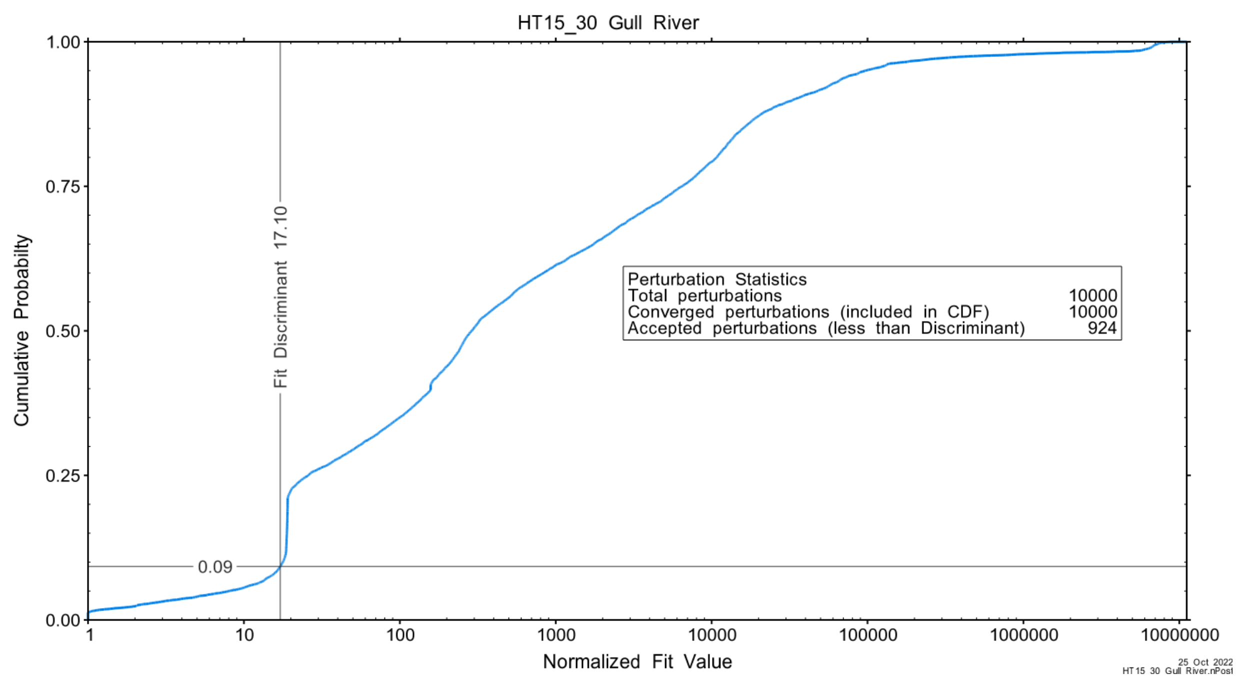

Figure 0.223 Fit value cumulative distribution function.

Summary cross parameter scatter plots for selected formation and skin parameters are given in Figure 0.224 and Figure 0.225. The light pink dots on the figures are the initial parameter estimates, with red dots overlaying those initial parameter values that resulted in accepted optimization results. The grey dots are converged optimizations which did not meet the fit discriminant. Larger varying color symbols represent the fit value of accepted optimizations, with the blue values representing the best fit.

Interestingly, the figures show the presence of a local minimum in addition to the global minimum within the fit discriminant limits. The minima are particularly noticeable in the Ss parameter domain, as indicated by the two discrete sets of colored symbols in the bottom half of Figure 0.224 and the top half of Figure 0.225. The two minima can be seen clearly in the scatter plots of parameter values vs. fit values in Section 6.15.4. The presence of the minima has little impact in the analyses, other than widening the confidence limits for Ss.

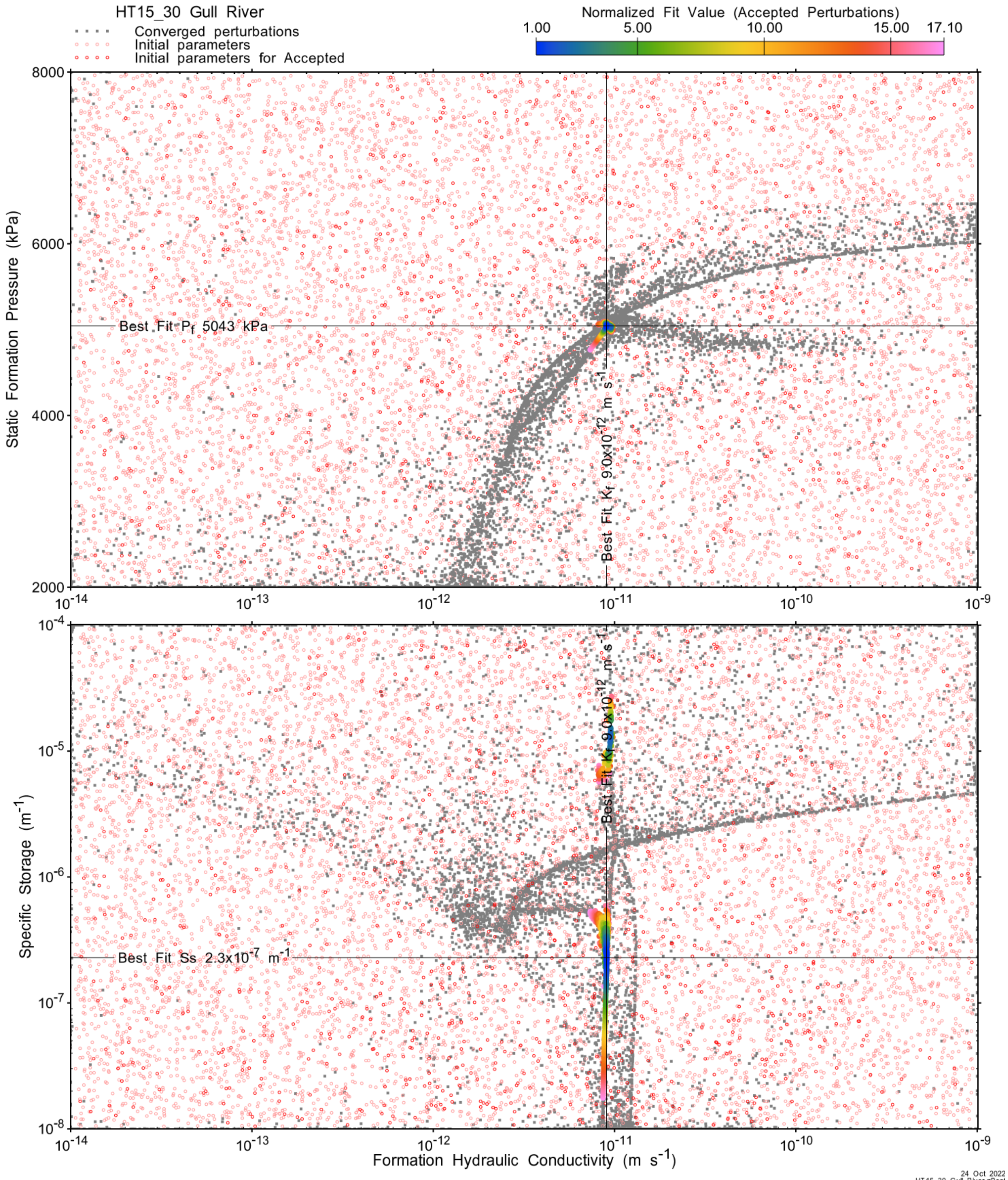

Figure 0.224 XY-scatter plot showing estimates of formation hydraulic conductivity (K_f) vs static formation pressure (P_f) (top panel) and specific storage (Ss) (bottom panel).

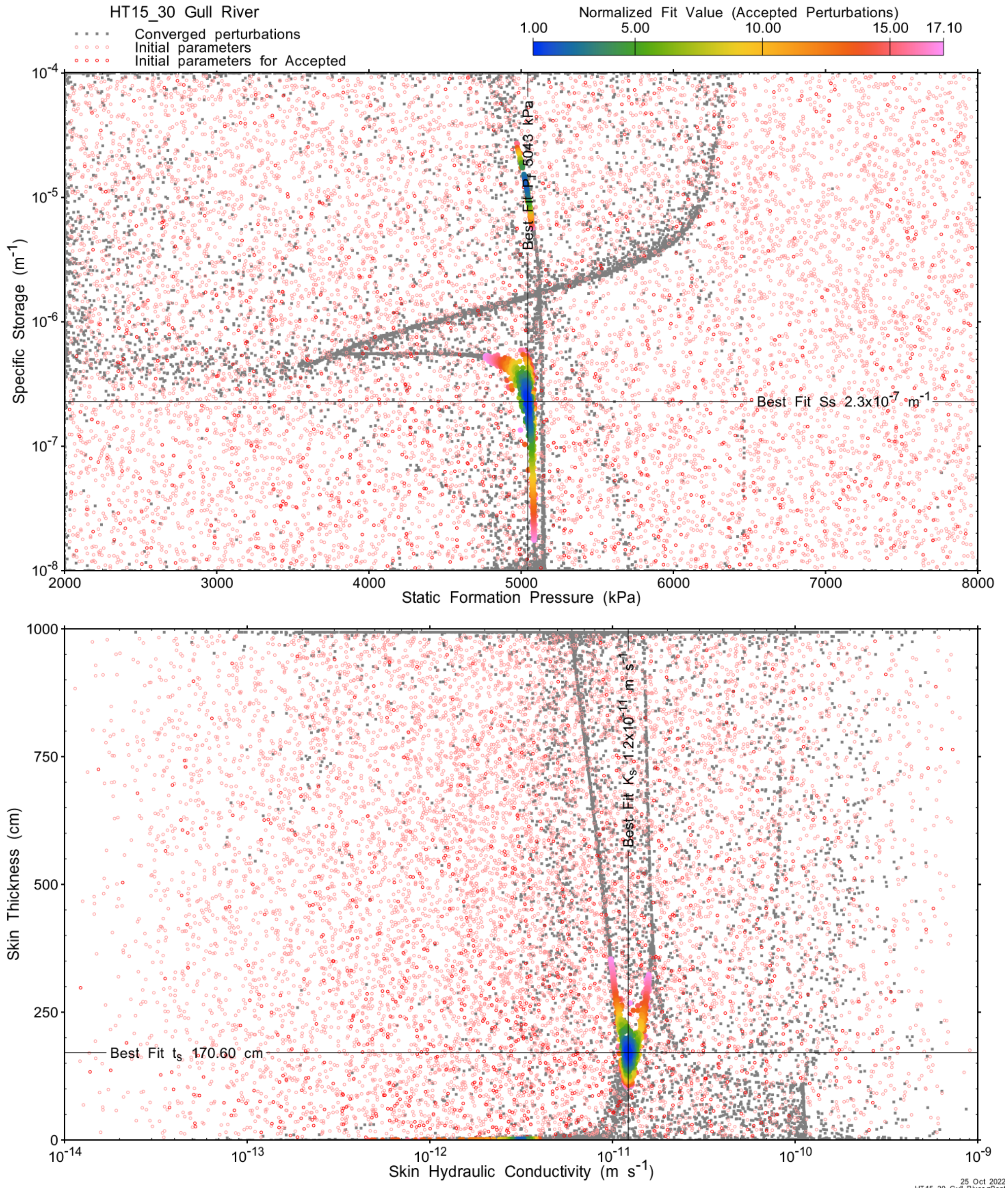

Figure 0.225 XY-scatter plot showing estimates of static formation pressure (P_f) vs specific storage (Ss) (top panel) and skin hydraulic conductivity (K_s) vs skin thickness (t_s) (bottom panel).

Confidence limits and median values are determined from the CDF of accepted optimization results (i.e. the varying color values in the above figures), with best fit value, 5% and 95% confidence indicated on Figure 0.226 and Figure 0.227.

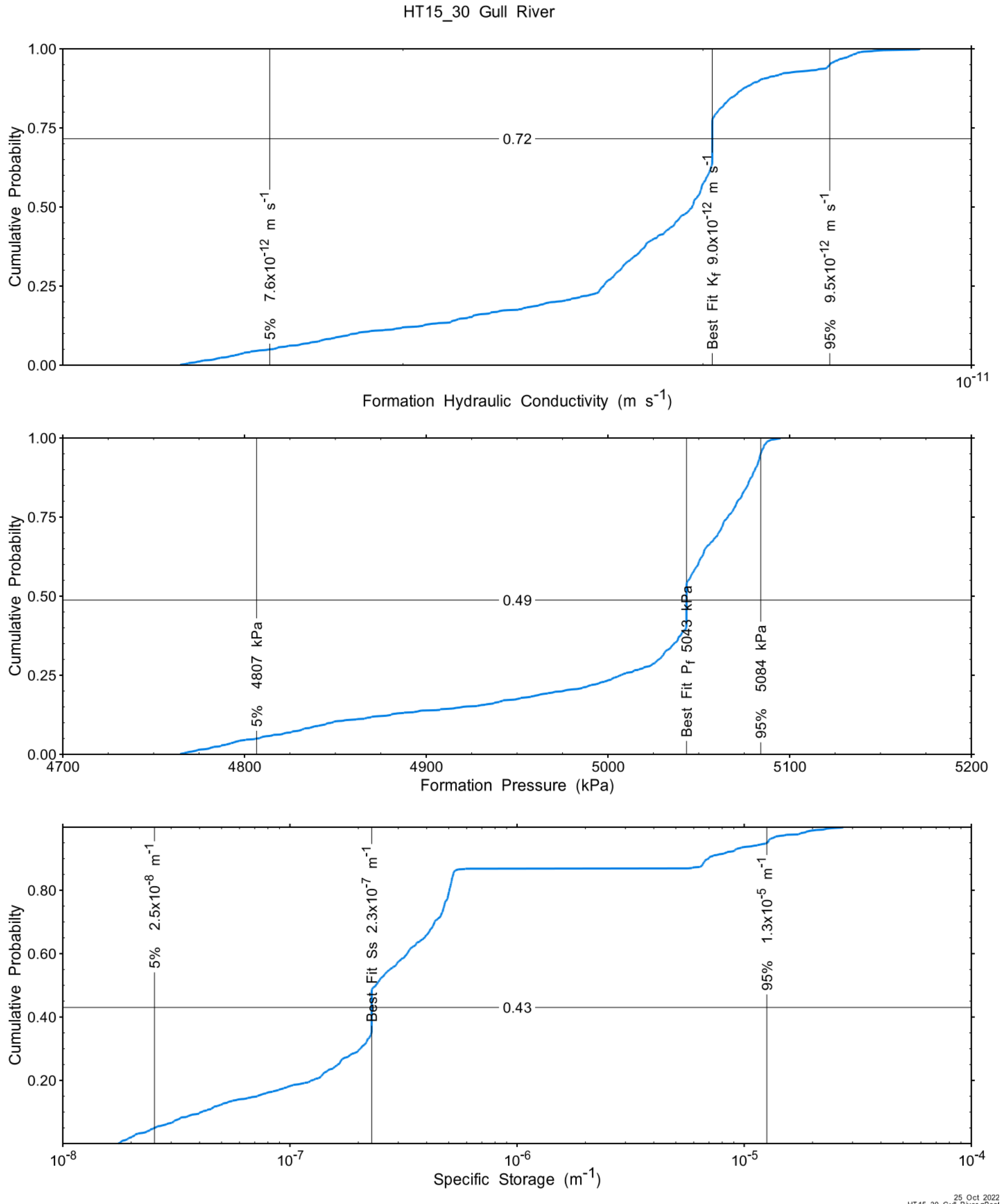

Figure 0.226 Cumulative distribution functions and parameter limits for formation hydraulic conductivity (K_f) (top panel), static formation pressure (P_f) (middle panel) and specific storage (Ss) (bottom panel).

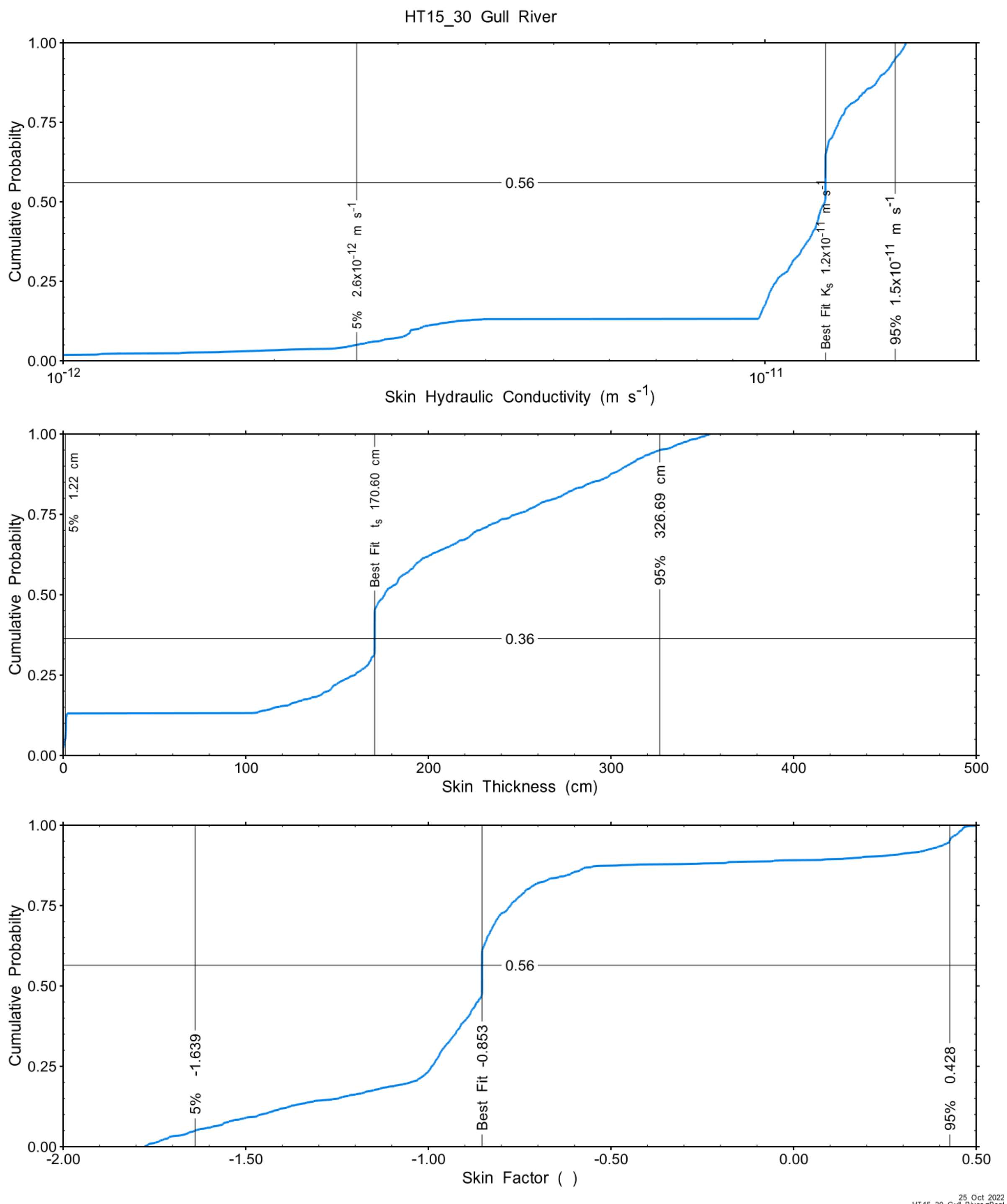

Figure 0.227 Cumulative distribution functions and parameter limits for skin hydraulic conductivity (K_s) (top panel), skin thickness (t_s) (middle panel) and skin factor (s) (bottom panel).

A summary of perturbation results is presented in Figure 0.228, with Ramey-processed perturbations in Figure 0.229. Those perturbations (709 of 10,000) with all parameters within the 5% and 95% range present a very good fit to the measured test zone data.

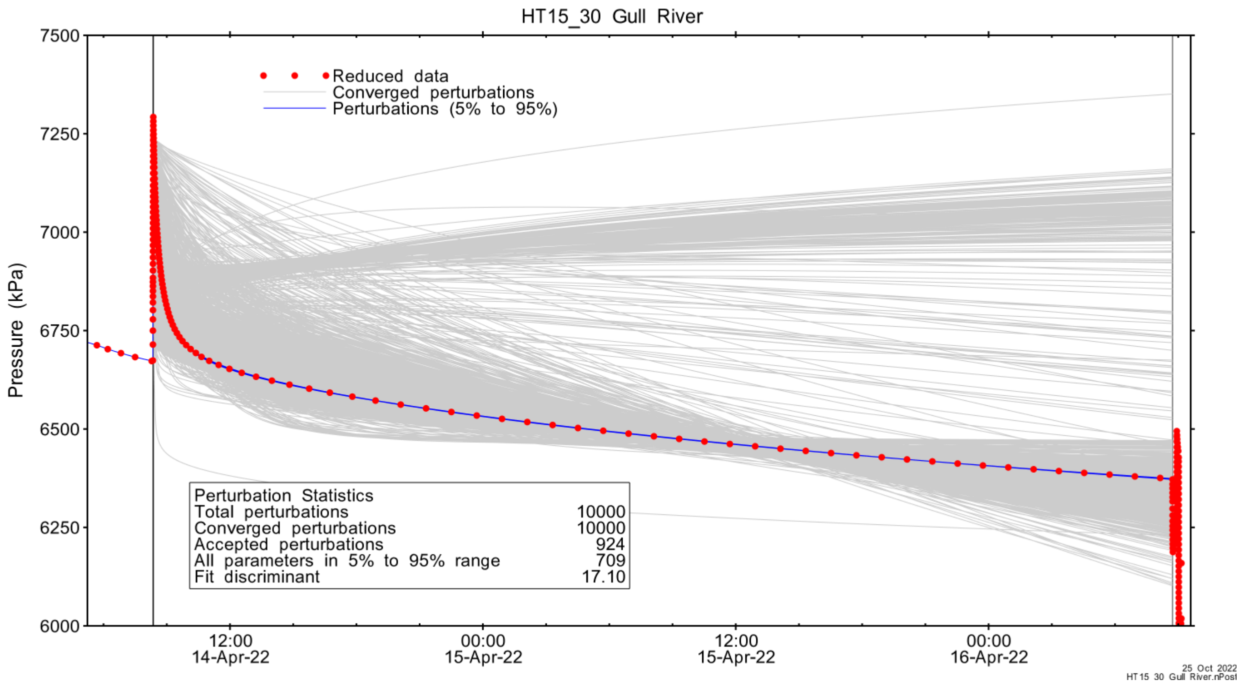

Figure 0.228 Perturbation results – all converged, accepted, and within 5% to 95% for all parameters.

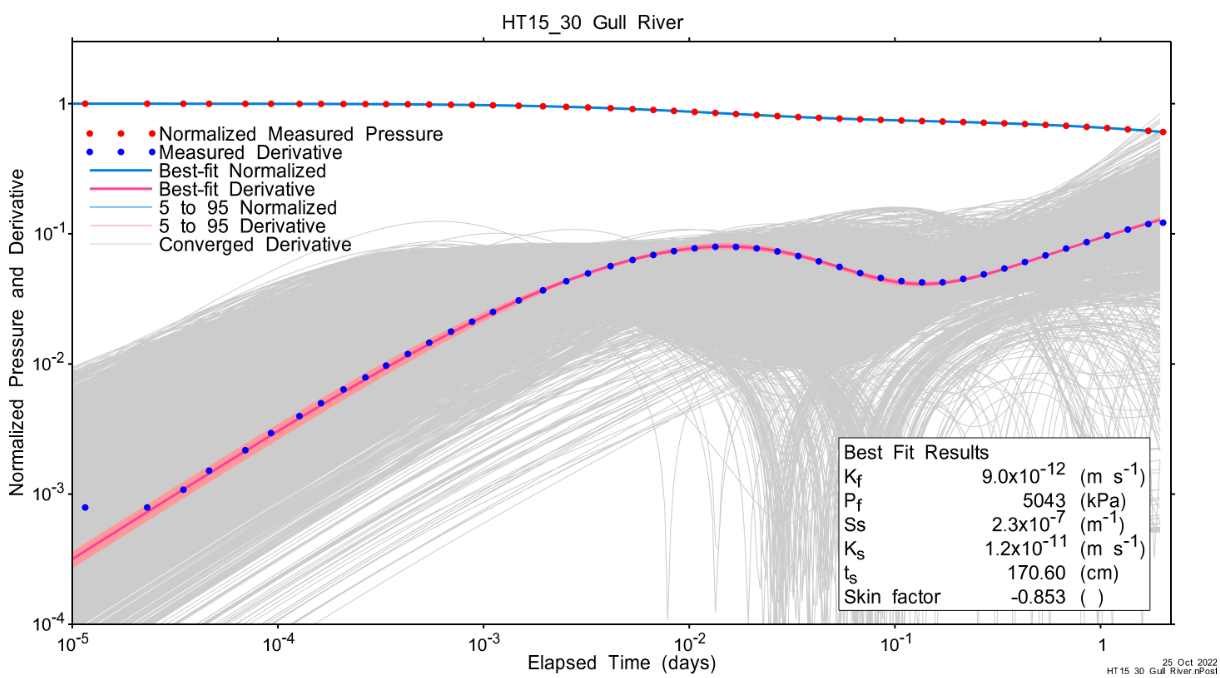

Figure 0.229 Log-log plot showing Ramey B normalized pressure and derivative response for all converged optimizations and those within 5% to 95% for all parameters.

A summary of best-fit parameter estimates and ranges is given in Table 0.74.

Table 0.74 Summary of the HT15_30 parameter estimates.

Parameter	Best Fit	5%	Median	95%
K_f (m/s)	9.0E-12	7.6E-12	9.0E-12	9.5E-12
P_f (kPa)	5043	4807	5043	5084
Ss (1/m)	2.3E-07	2.5E-08	2.4E-07	1.3E-05
K_s (m/s)	1.2E-11	2.6E-12	1.2E-11	1.5E-11
t_s (cm)	170.60	1.22	176.14	326.69
s (-)	-0.853	-1.639	-0.853	0.428

Parameter correlations for all perturbations with all parameters within the 5% to 95% limits are given in Table 0.75.

Table 0.75 Pearson cross-correlations of 5% to 95% parameters

	Log(K_f)	P_f	Log(Ss)	Log(K_s)	t_s	s
Log(K_f)	1.000	0.910	-0.066	0.018	-0.868	0.238
P_f	0.910	1.000	-0.418	0.264	-0.677	-0.128
Log(Ss)	-0.066	-0.418	1.000	-0.902	-0.371	0.953
Log(K_s)	0.018	0.264	-0.902	1.000	0.418	-0.871
t_s	-0.868	-0.677	-0.371	0.418	1.000	-0.629
s	0.238	-0.128	0.953	-0.871	-0.629	1.000

A.15.4 Additional Figures

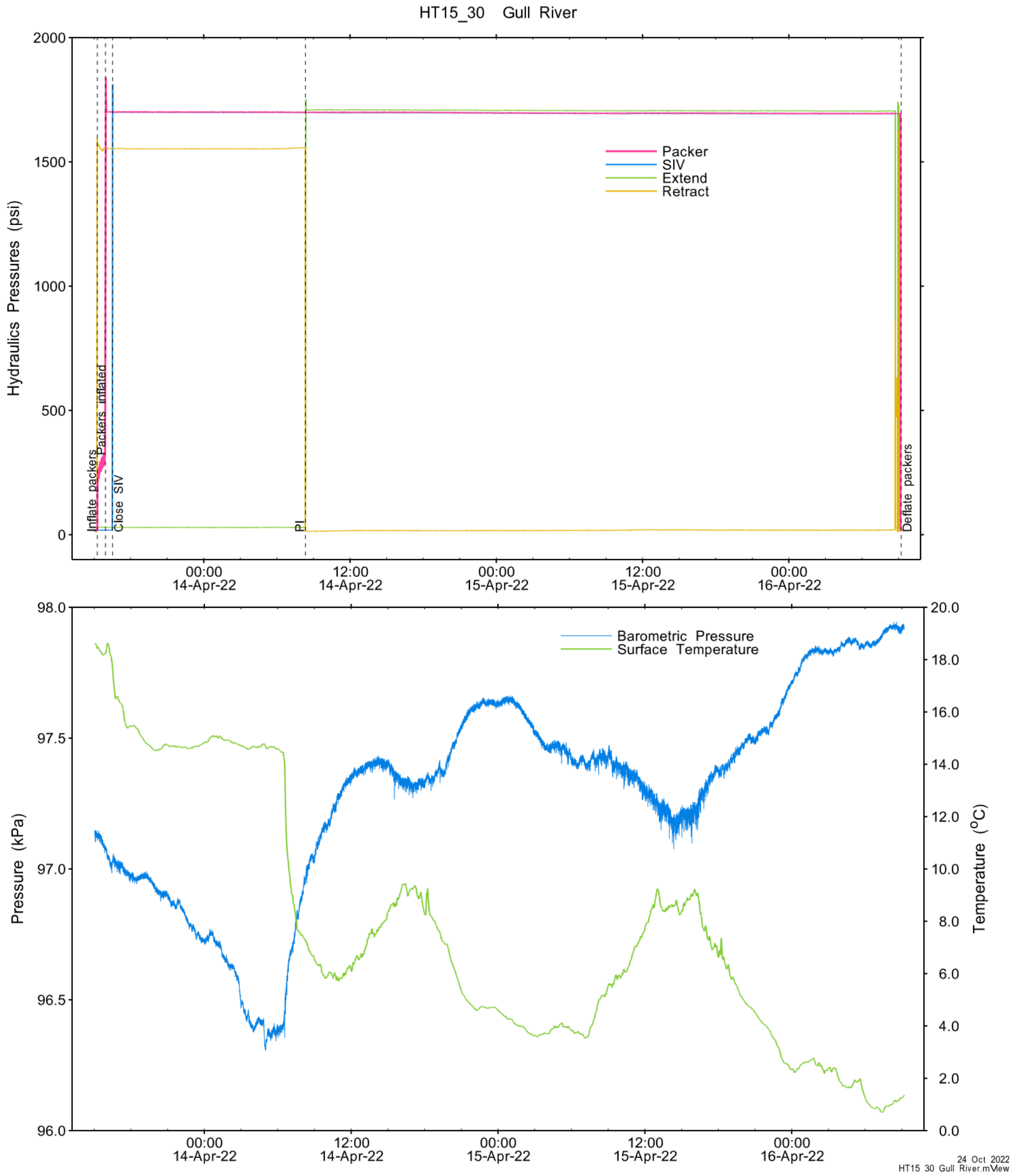

Figure 0.230 Hydraulics pressures and surface temperature/barometric pressure.

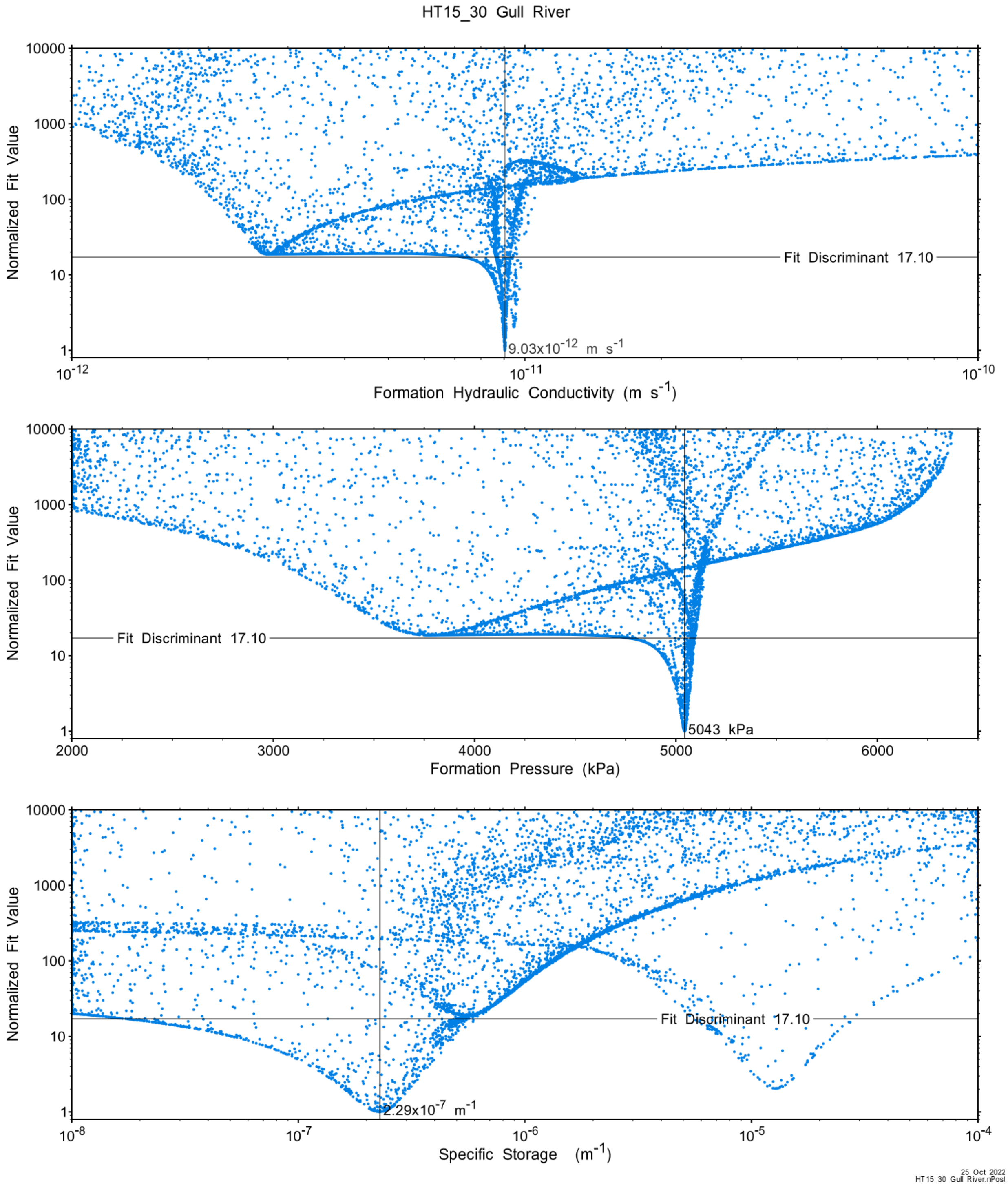

Figure 0.231 XY-scatter plot showing the formation parameter space normalized fit values.

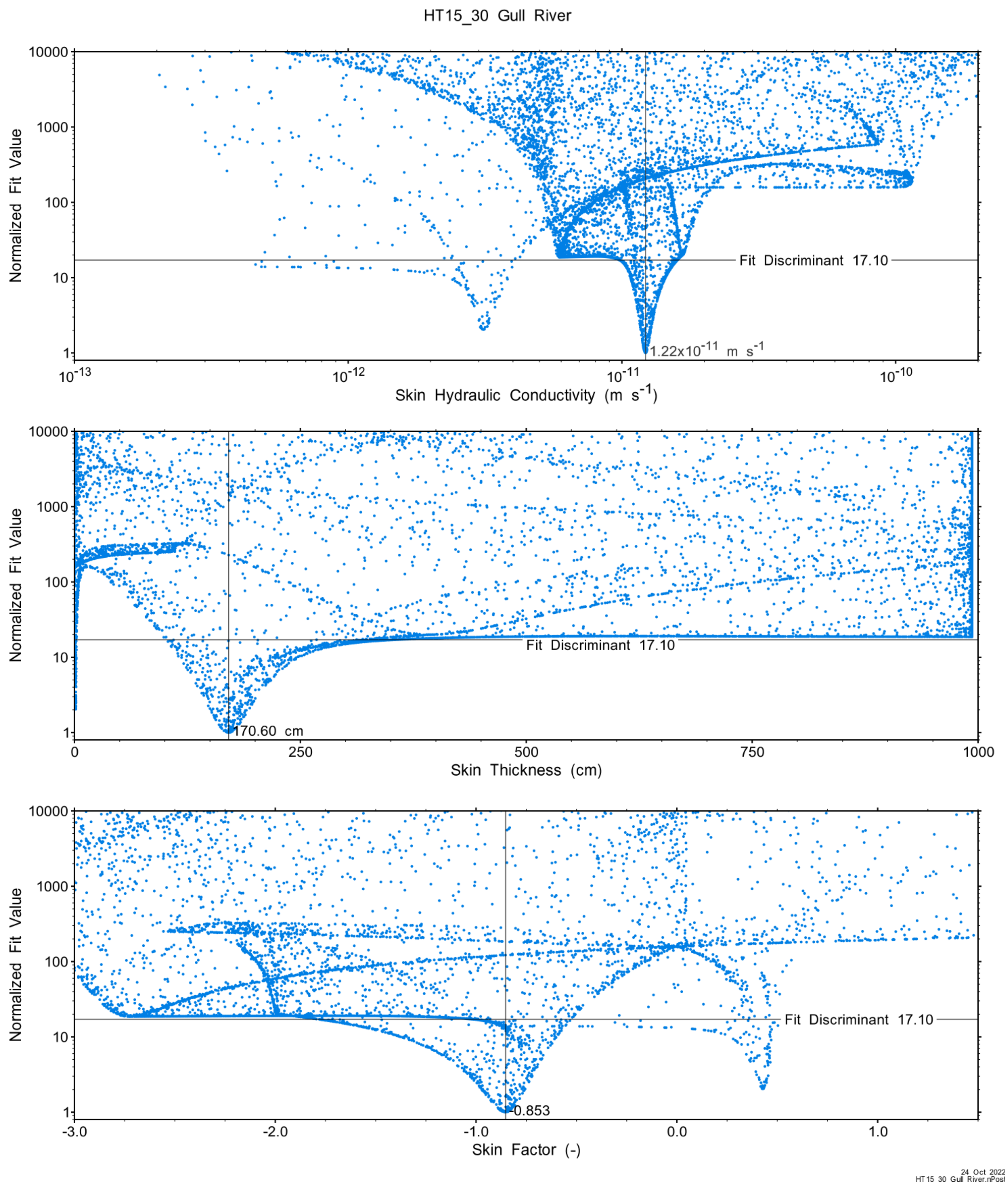

Figure 0.232 XY-scatter plot showing the skin parameter space normalized fit values.

A.16 HT01_05 Lower Salina A2

The SB_BH01 interval from 269.70 to 274.73 mBGS tested in HT01_05 consists of the bottom 5 m of the approximately 20-m-thick A2 Carbonate Unit of the Salina Group. A single SW test was performed which fully recovered within 15 minutes.

A.16.1 Test Data Summary

Table 0.76 and Figure 0.233 provide a summary of test events and a plot of pressures measured while testing, respectively.

Table 0.76 HT01_05 Summary of Test Events.

Event	Start Date & Time	Duration (days)	TZ Pressure (kPa)
Drilling intercept	21-07-20 18:00	122.86	2752
Prior testing	21-11-20 14:45	152.89	variable
Shut-in	22-04-22 11:59	0.86	2752
Slug withdrawal	22-04-23 08:32	0.03	2622
Test end	22-04-23 09:12		2754

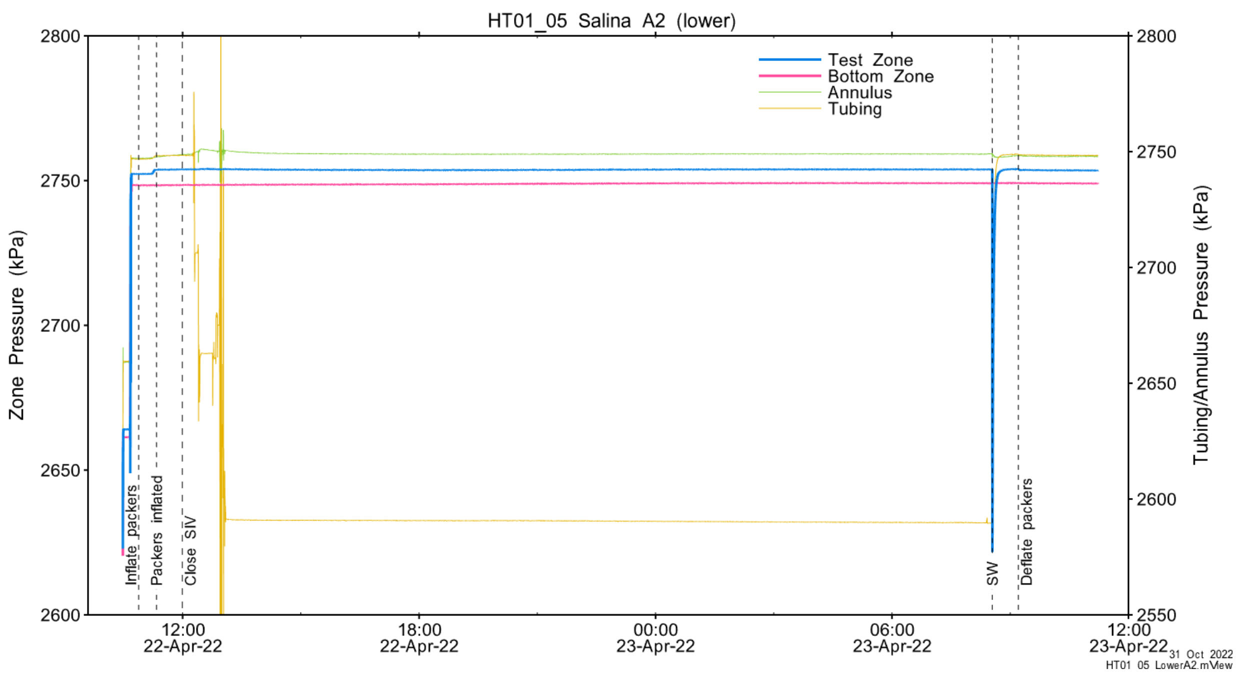

Figure 0.233 HT01_05 test events and pressures.

A.16.2 Test Analyses

Table 0.77 is a summary of test-specific input parameters used in the analyses, while Table 0.78 presents the optimized parameters and allowed ranges.

Table 0.77 nSIGHTS Input Parameters.

Parameter	Value	Units
Test zone radius	6.35	cm
Tubing string radius	2.54	cm
Test zone fluid density	1092	g/L
Test zone length	5.03	m

Table 0.78 nSIGHTS Parameter Optimization Ranges.

Parameter	Minimum	Maximum	Units	Type
Formation hydraulic conductivity (K_f)	1E-09	1E-03	m/s	log
Formation pressure (P_f)	2600	2900	kPa	linear
Specific storage (Ss)	1E-08	1E-04	1/m	log
Skin hydraulic conductivity (K_s)	1E-09	1E-03	m/s	log
Skin thickness (t_s)	0.01	10000	cm	linear

Figure 0.234 shows the measured test zone pressure record (with reduced data density for clarity) used in the analysis along with the best-fit simulation and parameter values, with Figure 0.235 showing the response during the test sequence. Figure 0.236 presents the pre-test history and Figure 0.237 shows the Ramey B normalized best-fit pressure and pressure derivatives.

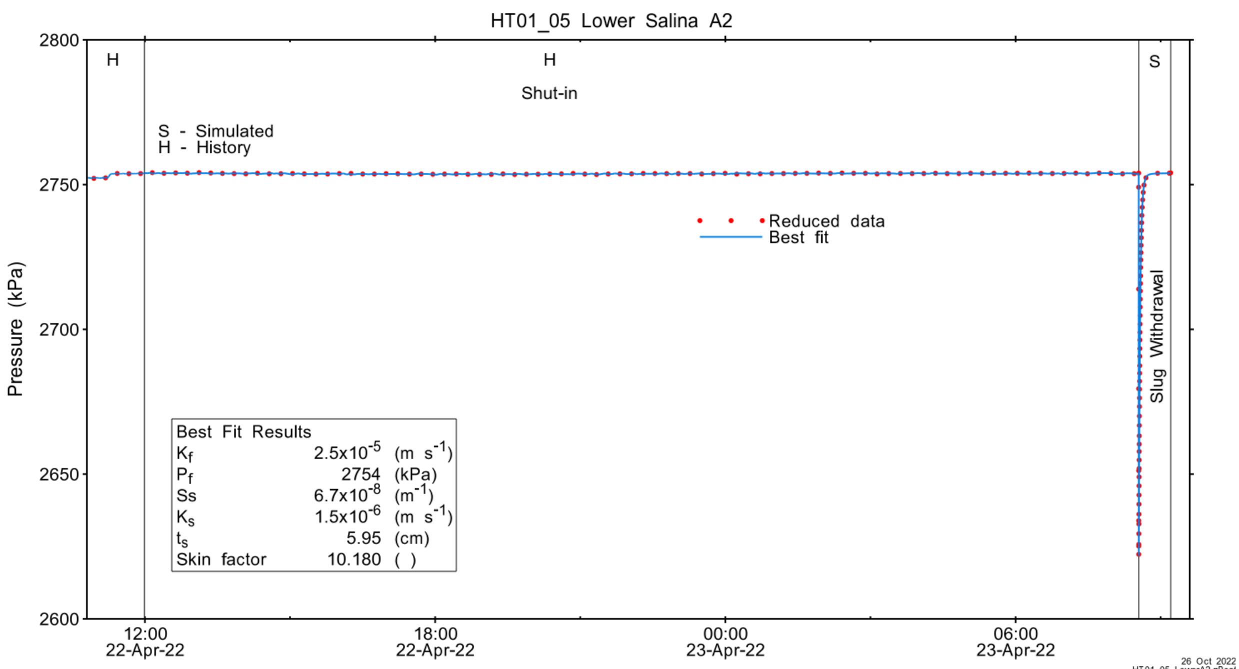

Figure 0.234 Annotated testing sequence showing best-fit simulation and parameter estimates.

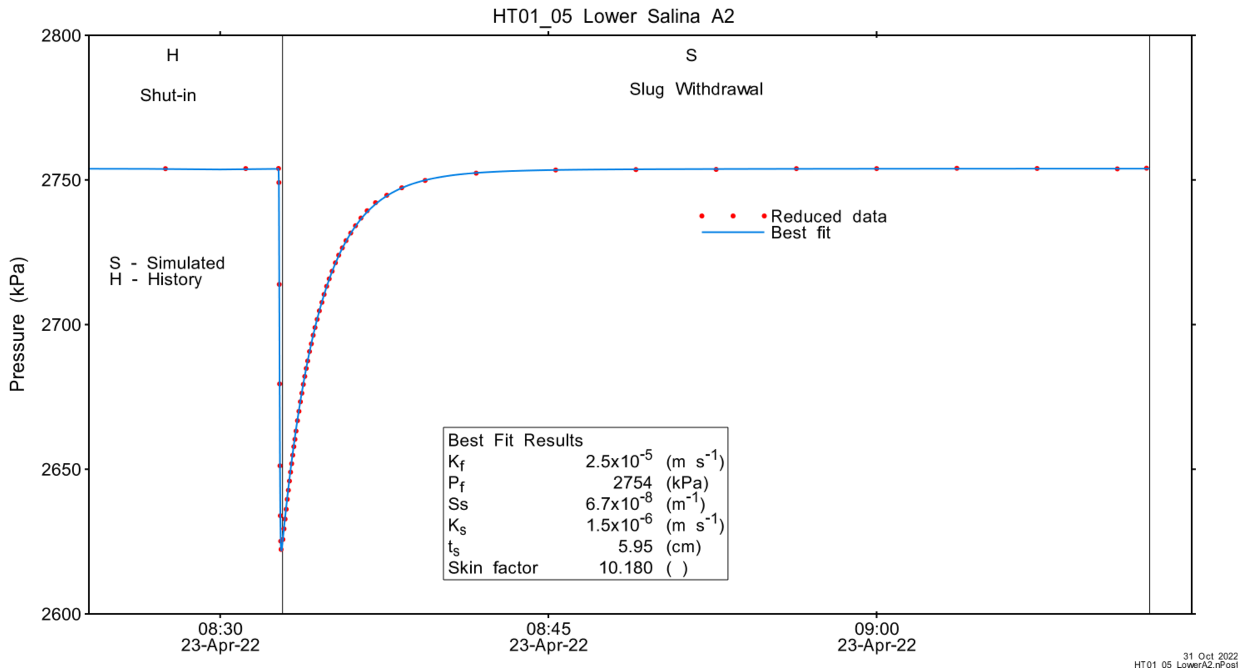

Figure 0.235 Detail of best-fit simulation during SW test sequence.

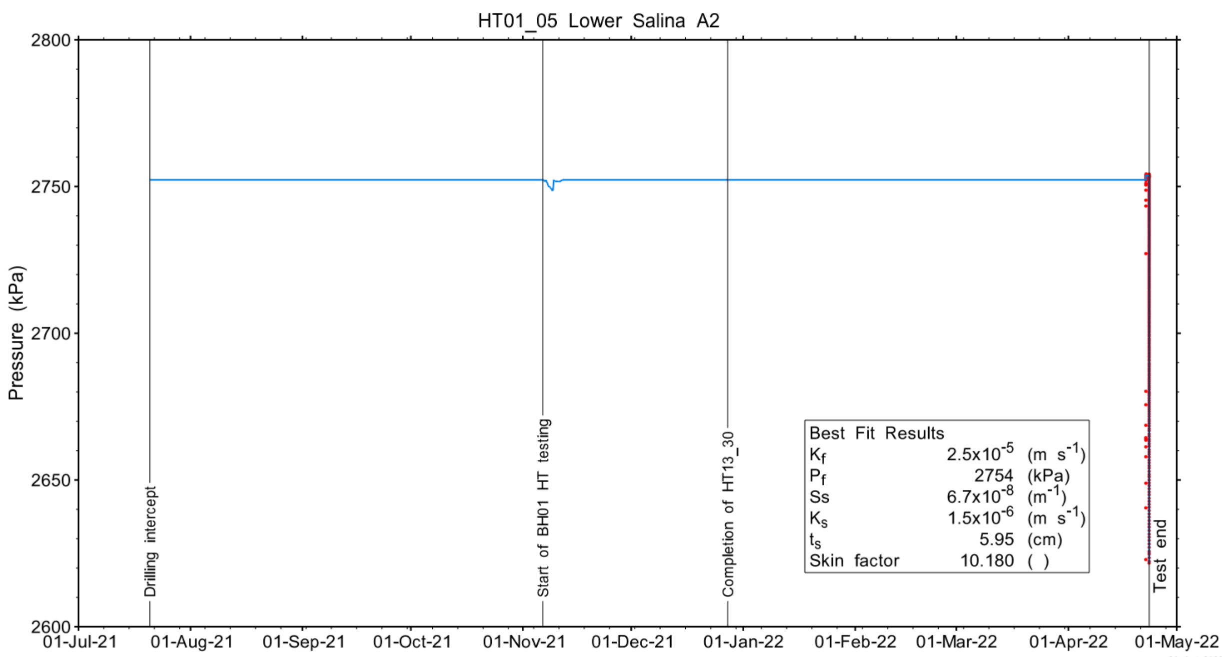

Figure 0.236 Annotated HT01_05 testing sequence showing pre-test history, best-fit simulation and parameter estimates.

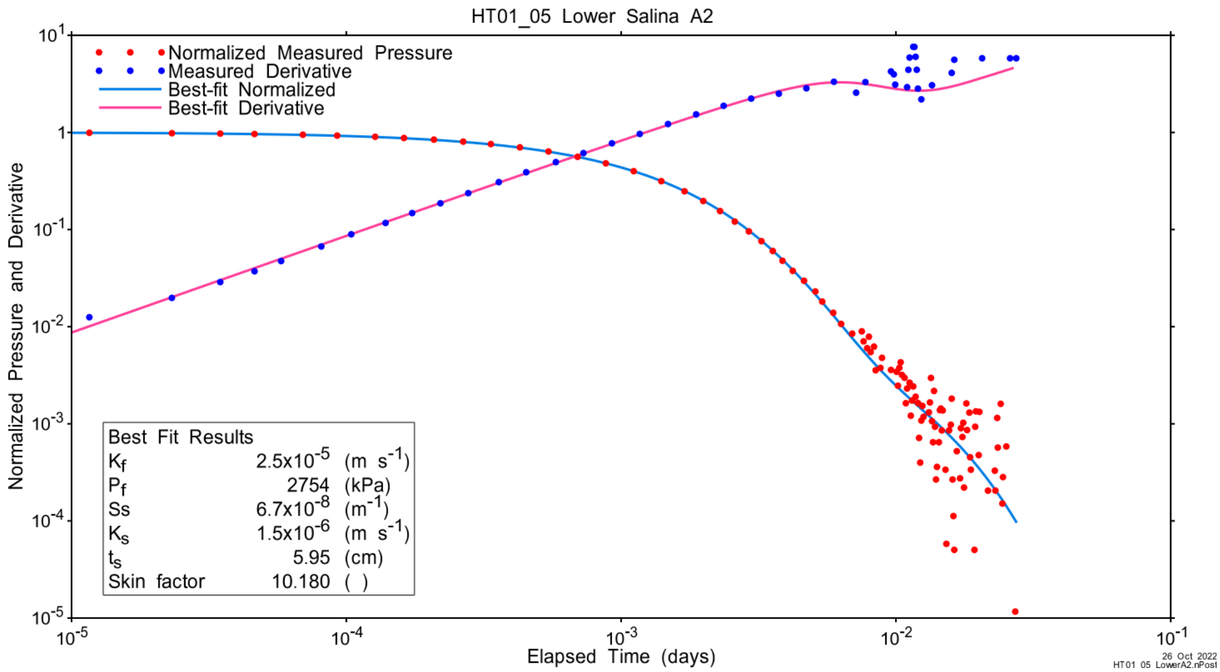

Figure 0.237 Log-log plot showing Ramey B normalized pressure and derivative response for best-fit simulation.

Figure 0.238 shows the normalized parameter sensitivity response for the best fit. Sensitivity for all fitting parameters was constant by 30 minutes after the test commenced, indicating that the test duration was sufficient for well-constrained parameter estimation.

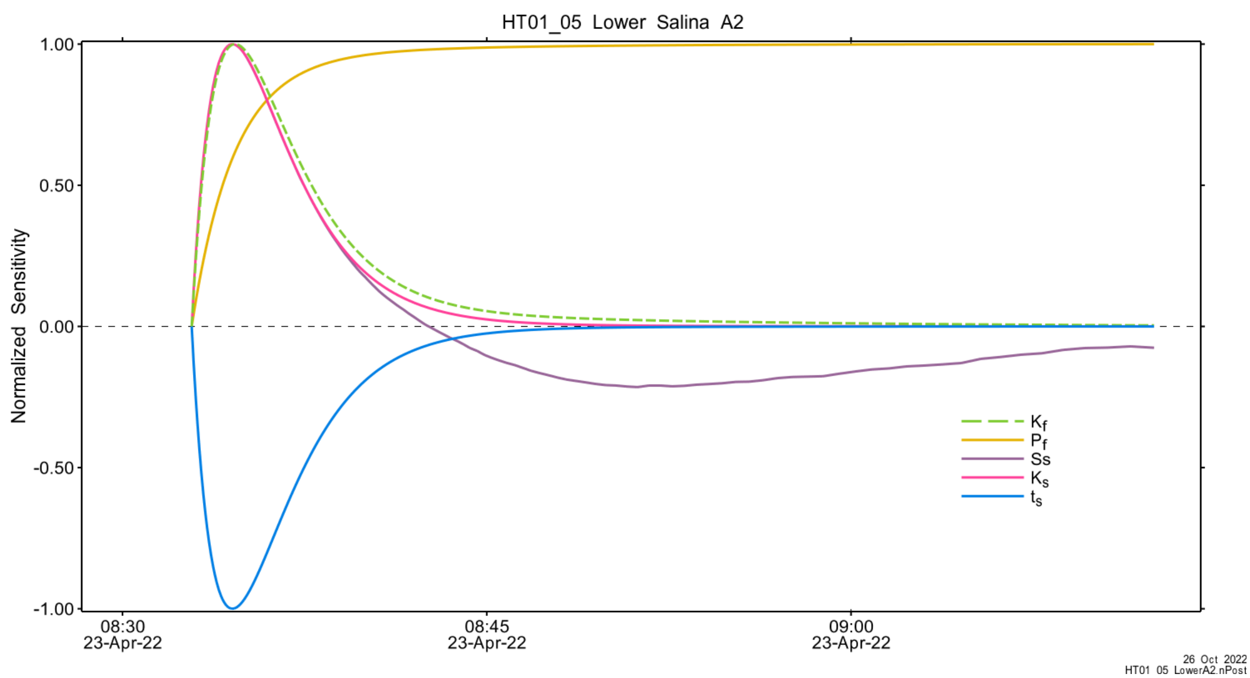

Figure 0.238 Normalized Jacobian for best-fit simulation.

A.16.3 Uncertainty Analyses

The CDF of normalized fit values for all converged simulations and the selected fit discriminant are shown in Figure 0.239.

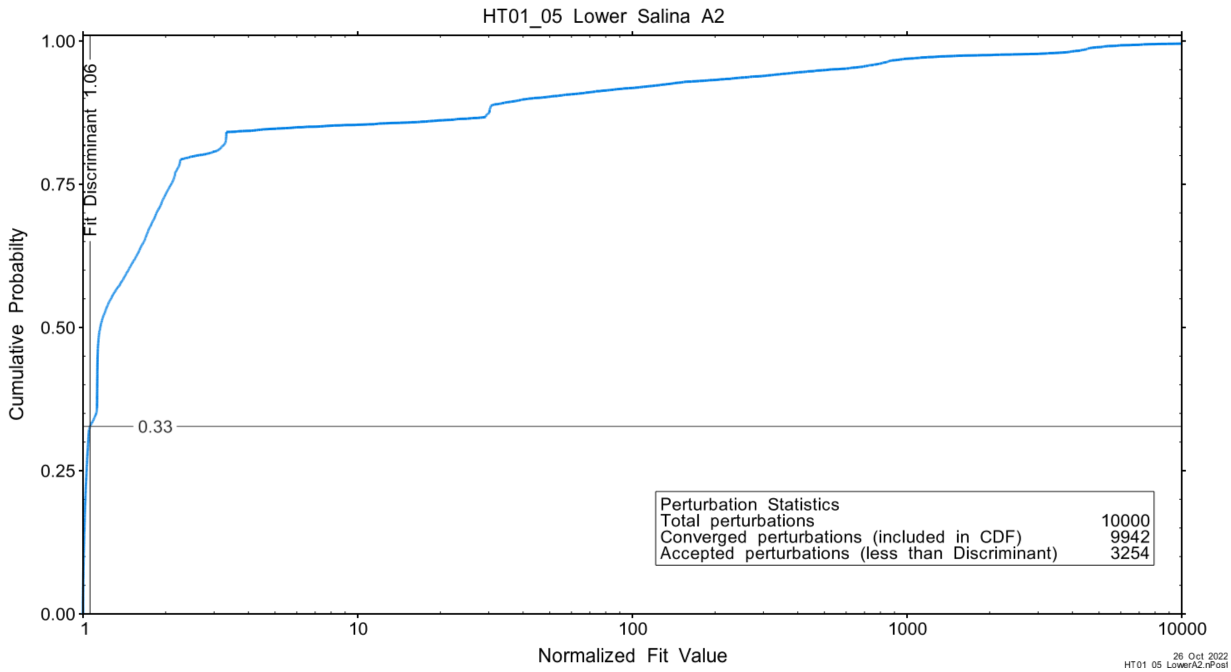

Figure 0.239 Fit value cumulative distribution function.

Summary cross parameter scatter plots for selected formation and skin parameters are given in Figure 0.240 and Figure 0.241. The light pink dots on the figures are the initial parameter estimates, with red dots overlaying those initial parameter values that resulted in accepted optimization results. The grey dots are converged optimizations which did not meet the fit discriminant. Larger varying color symbols represent the fit value of accepted optimizations, with the blue values representing the best fit.

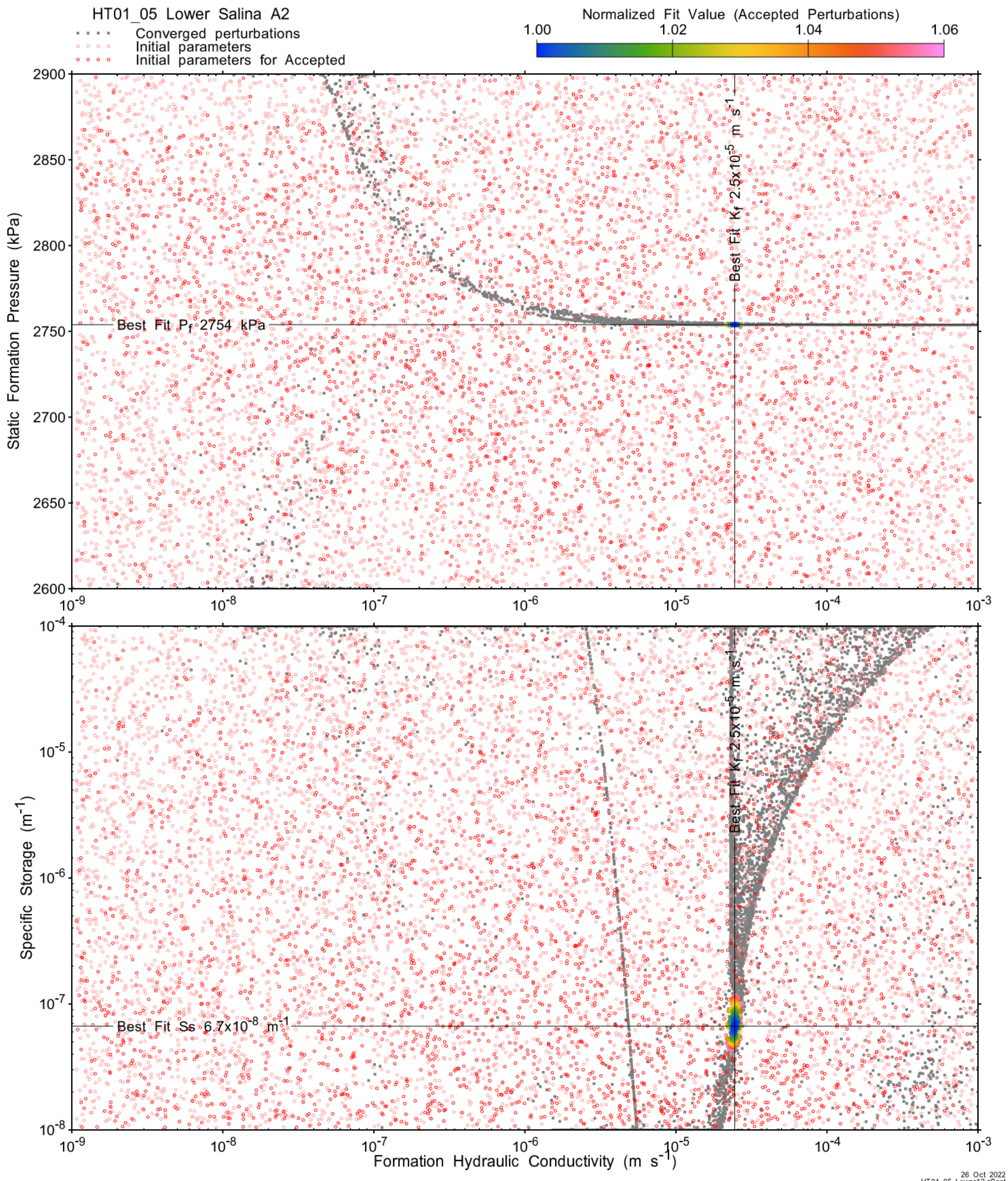

Figure 0.240 XY-scatter plot showing estimates of formation hydraulic conductivity (K_f) vs static formation pressure (P_f) (top panel) and specific storage (Ss) (bottom panel).

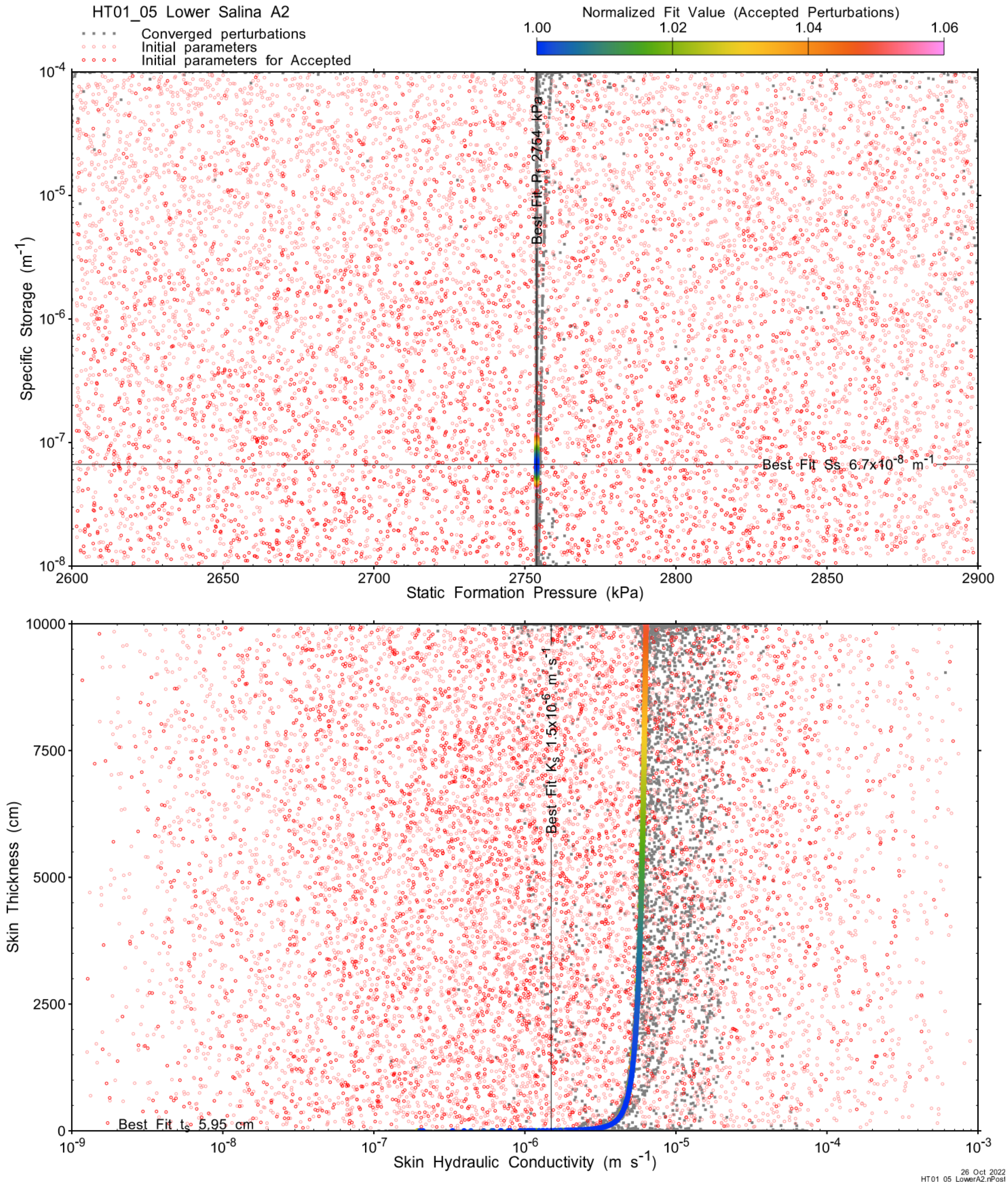

Figure 0.241 XY-scatter plot showing estimates of static formation pressure (P_f) vs specific storage (Ss) (top panel) and skin hydraulic conductivity (K_s) vs skin thickness (t_s) (bottom panel).

Confidence limits and median values are determined from the CDF of accepted optimization results (i.e. the varying color values in the above figures), with best fit value, 5% and 95% confidence indicated on Figure 0.242 and Figure 0.243.

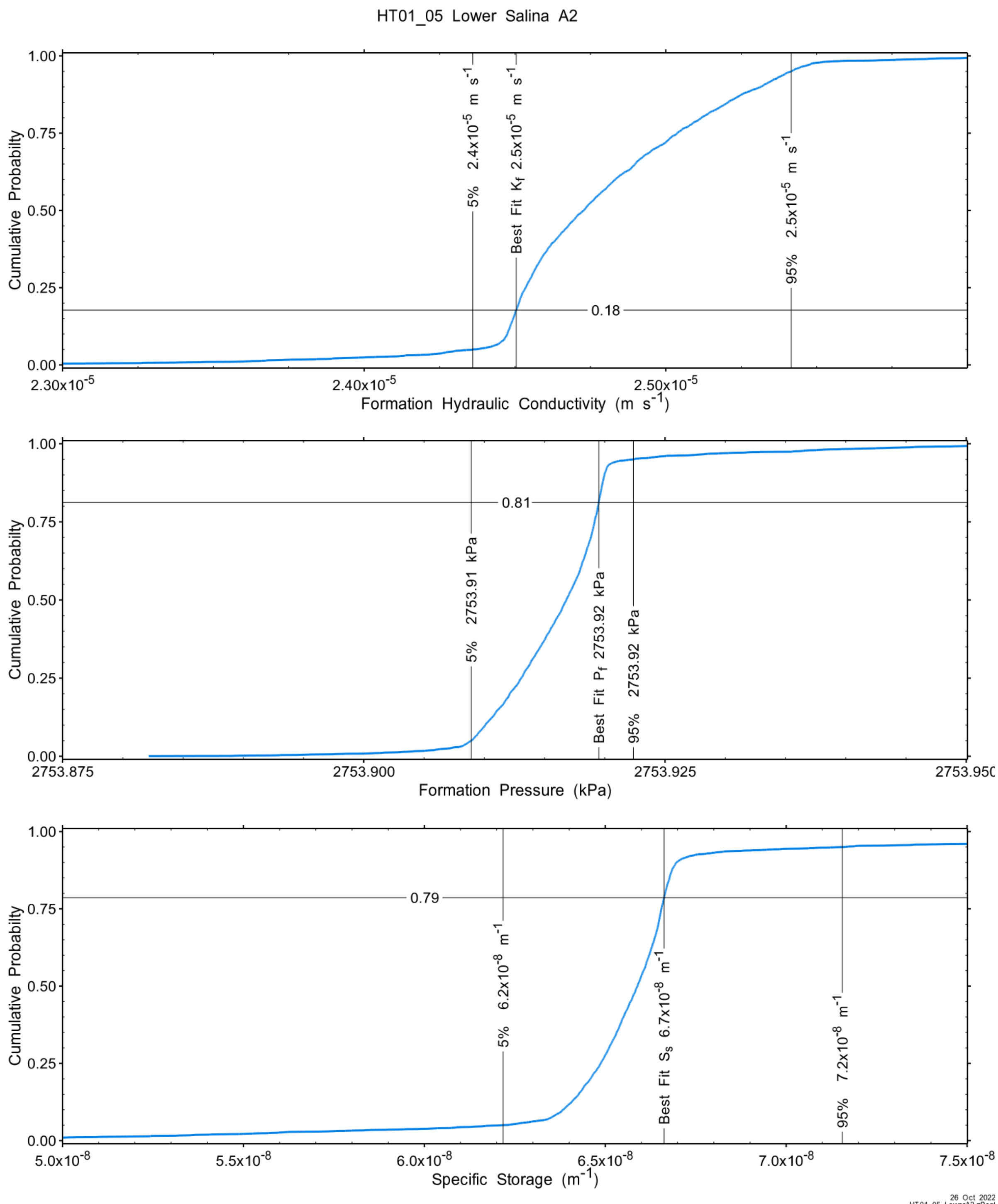

Figure 0.242 Cumulative distribution functions and parameter limits for formation hydraulic conductivity (K_f) (top panel), static formation pressure (P_f) (middle panel) and specific storage (Ss) (bottom panel).

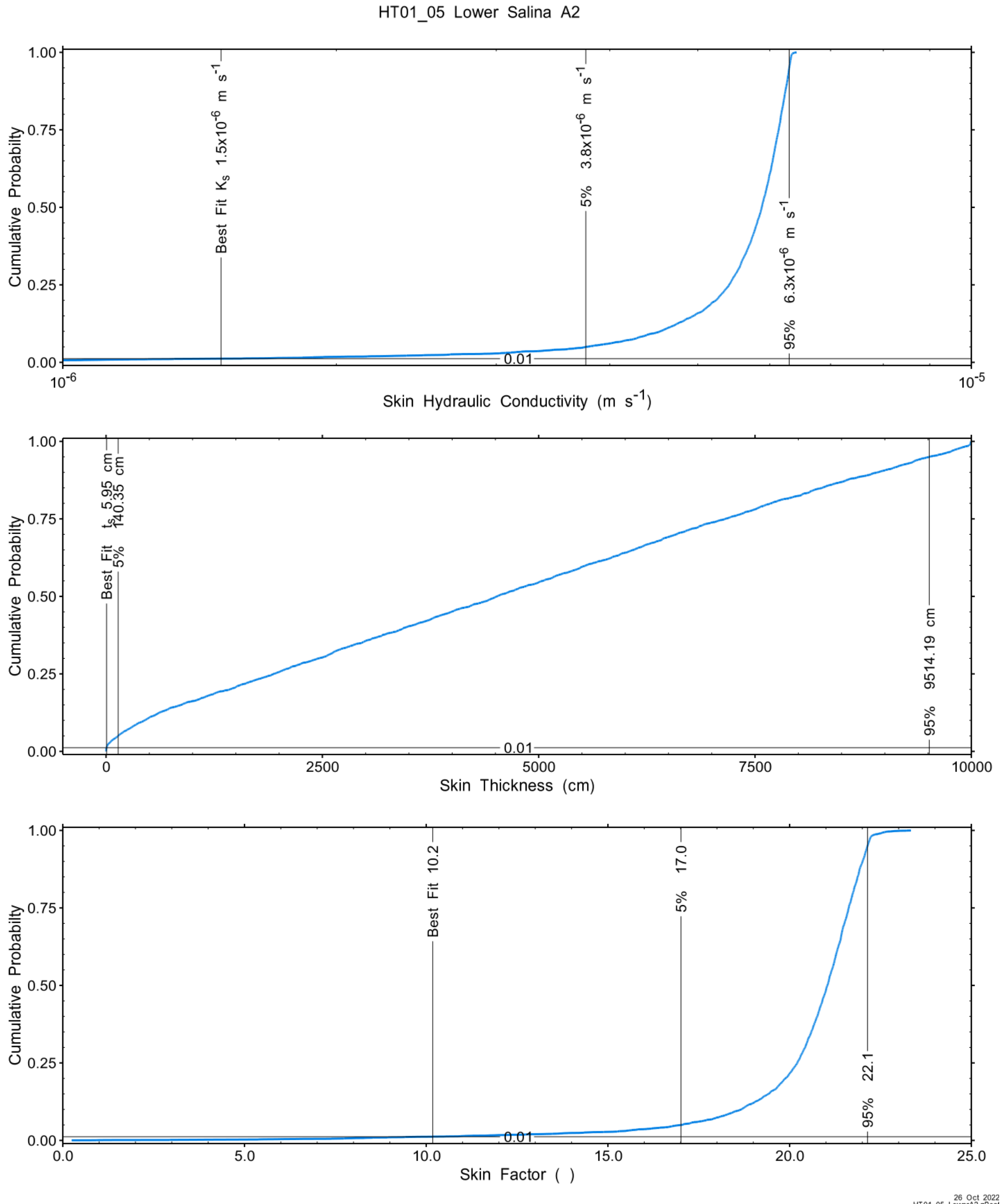

Figure 0.243 Cumulative distribution functions and parameter limits for skin hydraulic conductivity (K_s) (top panel), skin thickness (t_s) (middle panel) and skin factor (s) (bottom panel).

A summary of perturbation results is presented in Figure 0.244, with Ramey-processed perturbations in Figure 0.245. Those perturbations (2619 of 10,000) with all parameters within the 5% and 95% range present a very good fit to the measured test zone data.

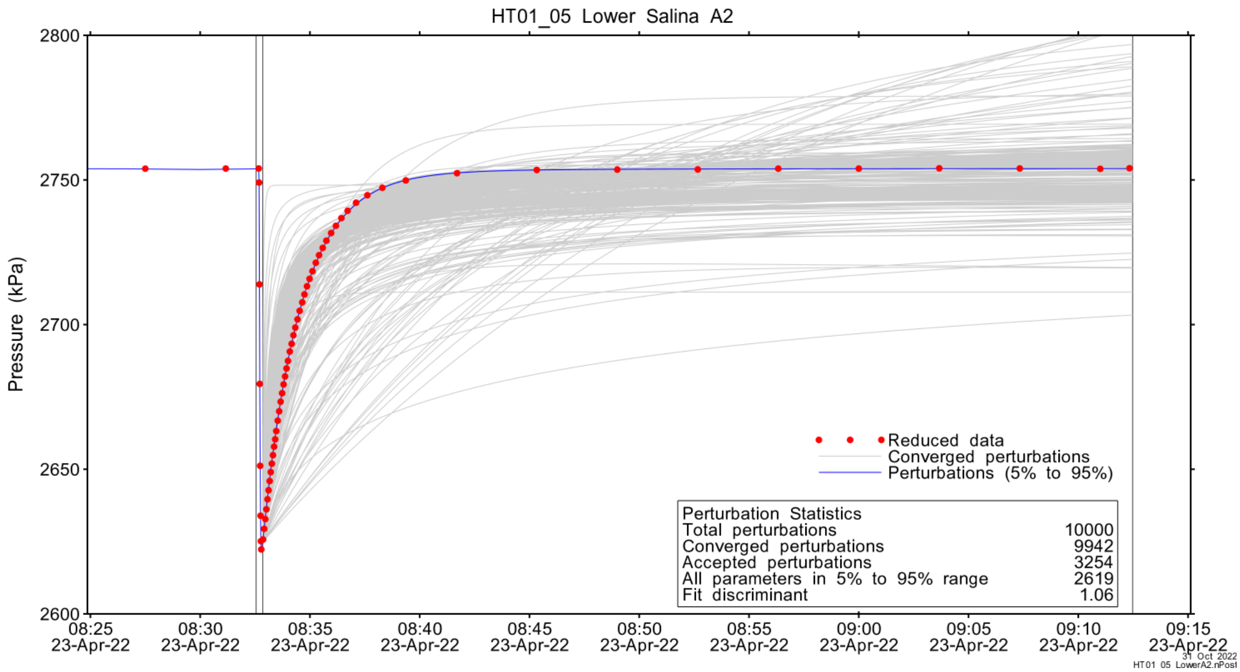

Figure 0.244 Perturbation results – all converged, accepted, and within 5% to 95% for all parameters.

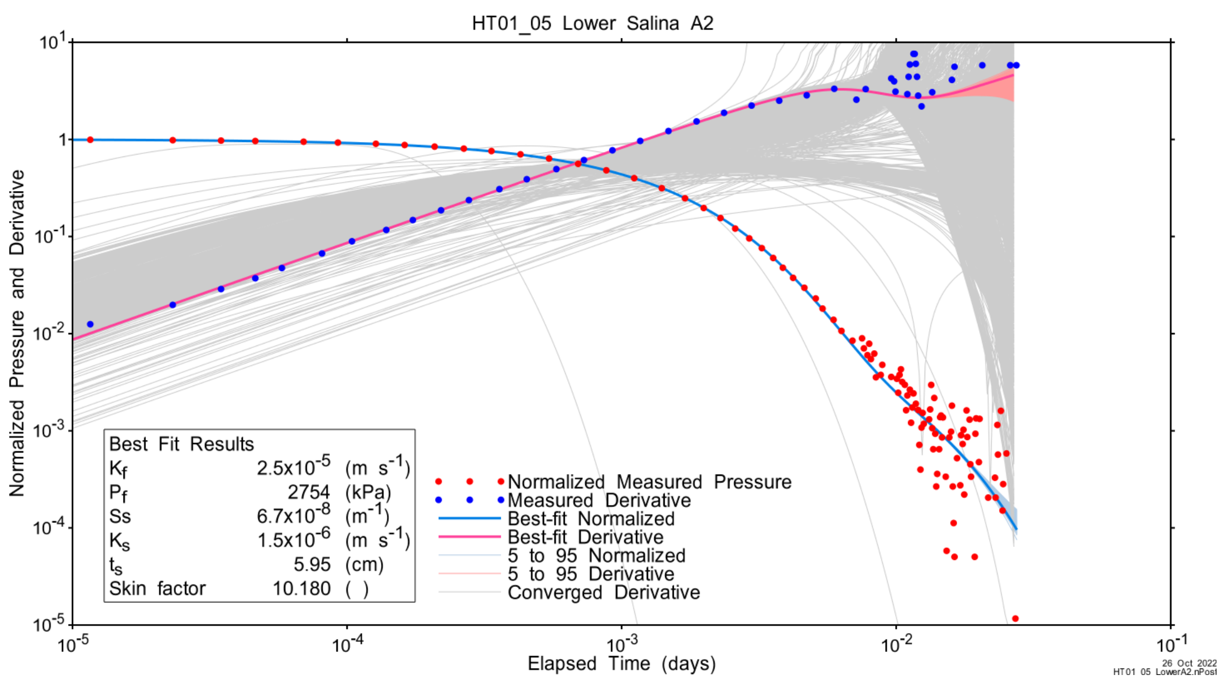

Figure 0.245 Log-log plot showing Ramey B normalized pressure and derivative response for all converged optimizations and those within 5% to 95% for all parameters.

A summary of best-fit and parameter ranges is given in Table 0.79.

Table 0.79 Summary of the HT01_05 parameter estimates.

Parameter	Best Fit	5%	Median	95%
K_f (m/s)	2.5E-05	2.4E-05	2.5E-05	2.5E-05
P_f (kPa)	2754	2754	2754	2754
Ss (1/m)	6.7E-08	6.2E-08	6.6E-08	7.2E-08
K_s (m/s)	1.5E-06	3.8E-06	5.9E-06	6.3E-06
t_s (cm)	5.95	140.35	4517.62	9514.19
s (-)	10.180	17.010	21.039	22.143

Parameter correlations for all perturbations with all parameters within the 5% to 95% limits are given in Table 0.80.

Table 0.80 Pearson cross-correlations of 5% to 95% parameters

	Log(K_f)	P_f	Log(Ss)	Log(K_s)	t_s	s
Log(K_f)	1.000	-0.956	-0.649	0.752	0.953	0.832
P_f	-0.956	1.000	0.832	-0.743	-0.943	-0.815
Log(Ss)	-0.649	0.832	1.000	-0.569	-0.728	-0.605
Log(K_s)	0.752	-0.743	-0.569	1.000	0.872	0.991
t_s	0.953	-0.943	-0.728	0.872	1.000	0.923
s	0.832	-0.815	-0.605	0.991	0.923	1.000

A.16.4 Additional Figures

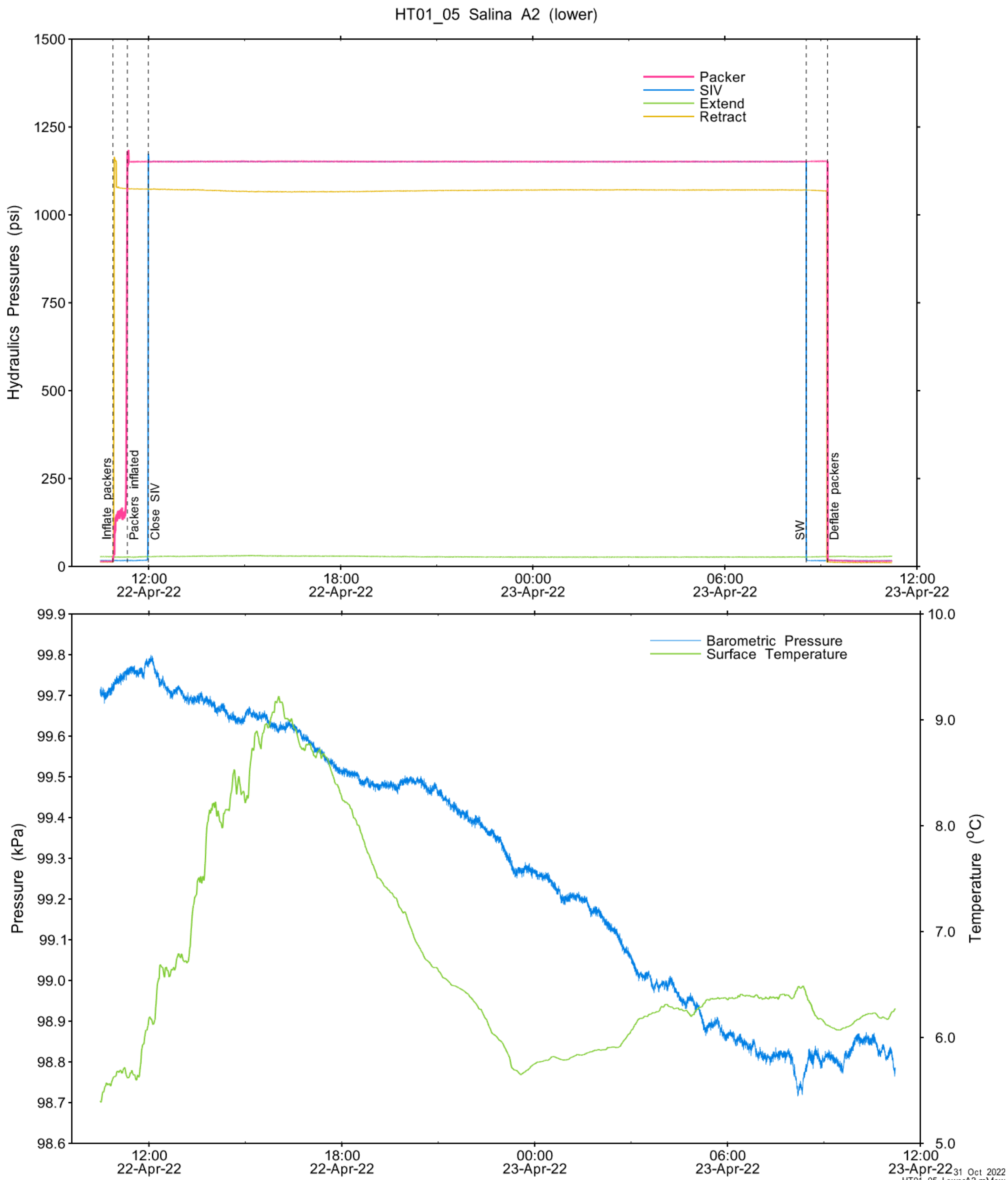

Figure 0.246 Hydraulics pressures and surface temperature/barometric pressure.

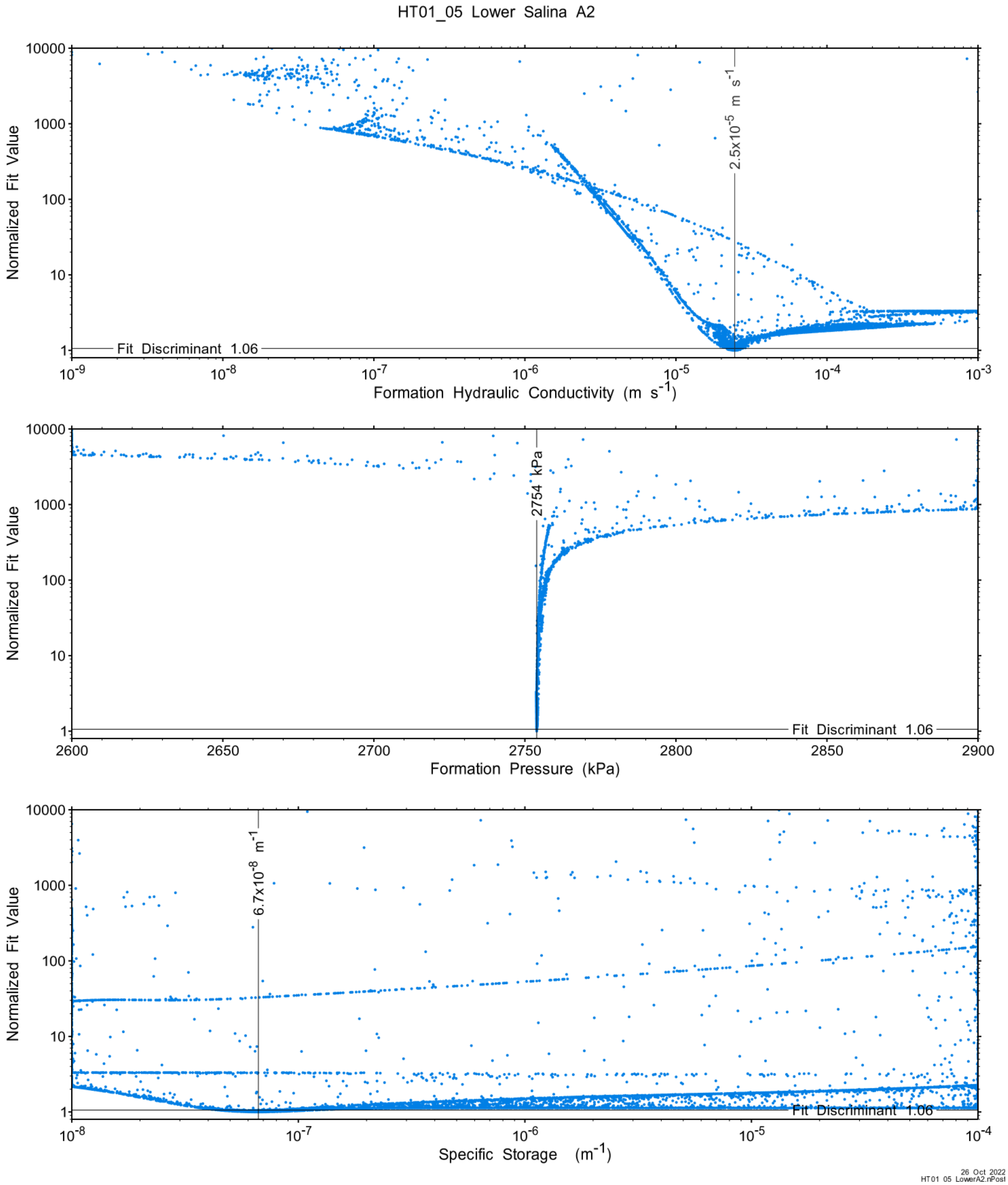

Figure 0.247 XY-scatter plot showing the formation parameter space normalized fit values.

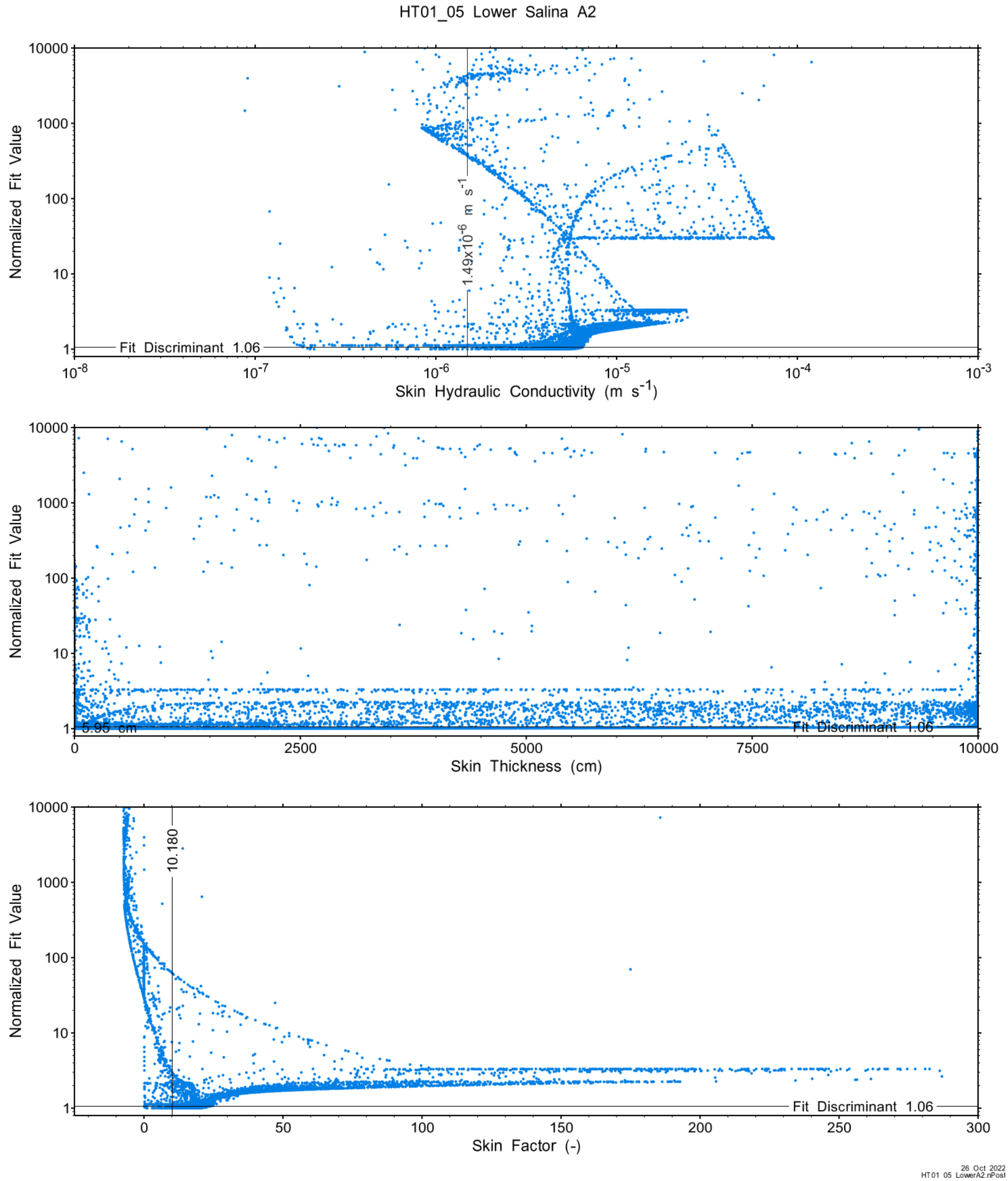

Figure 0.248 XY-scatter plot showing the skin parameter space normalized fit values.

A.17 HT02_05 Blue Mountain/Collingwood

Because of a post-test revision of stratigraphic boundaries (see Section 5), the SB_BH01 interval from 640.20 to 645.23 mBGS tested in HT02_05 covered the lower 4.5 m of the Blue Mountain Formation and only the upper 0.5 m of the Collingwood Member instead of being wholly contained within the Collingwood Member as intended. A single PI test was performed. Rather than the standard two-day test, the PI was extended to three days due to staffing issues.

A.17.1 Test Data Summary

Table 0.81 and Figure 0.249 provide a summary of test events and a plot of pressures measured while testing, respectively. Minor oscillations can be seen in the later stages of the PI test response.

Table 0.81 HT02_05 Summary of Test Events.

Event	Start Date & Time	Duration (days)	TZ Pressure (kPa)
Drilling intercept	21-08-27 15:40	84.96	6638
Prior testing	21-11-20 14:45	172.83	variable
Shut-in	22-05-12 10:37	0.89	6565
Pulse injection	22-05-13 07:58	2.94	6752
Test end	22-05-16 06:36		6558

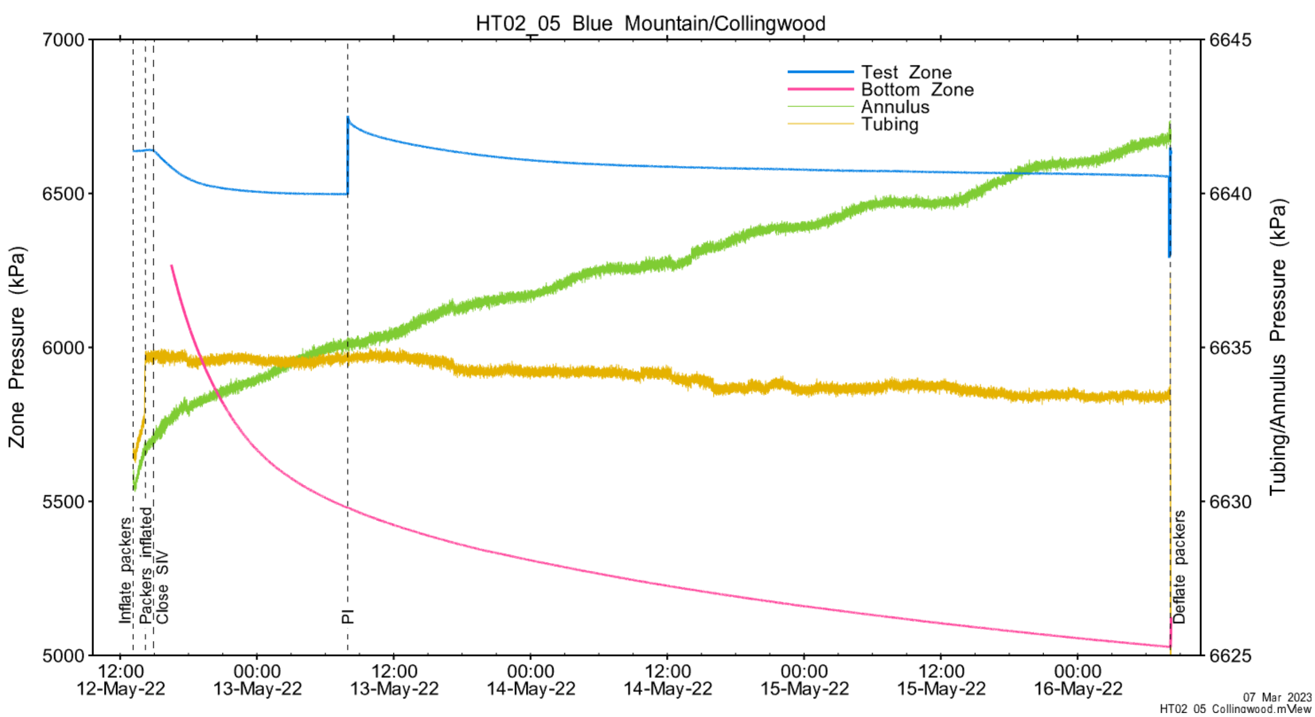

Figure 0.249 HT02_05 test events and pressures.

A.17.2 Test Analyses

Table 0.82 is a summary of test-specific input parameters used in the analyses, while Table 0.83 presents the optimized parameters and allowed ranges.

Table 0.82 nSIGHTS Input Parameters.

Parameter	Value	Units
Test zone radius	6.90	cm
Test zone compressibility	6.87E-10	1/Pa
Test zone fluid density	1096	g/L
Test zone length	5.03	m

Table 0.83 nSIGHTS Parameter Optimization Ranges.

Parameter	Minimum	Maximum	Units	Type
Formation hydraulic conductivity (K_f)	1E-15	1E-08	m/s	log
Formation pressure (P_f)	5000	8000	kPa	linear
Specific storage (Ss)	1E-08	1E-04	1/m	log
Skin hydraulic conductivity (K_s)	1E-15	1E-08	m/s	log
Skin thickness (t_s)	0.01	100	cm	linear

Figure 0.250 shows the measured test zone pressure record (with reduced data density for clarity) used in the analysis along with the best-fit simulation and parameter values. Figure 0.251 presents the pre-test history and Figure 0.252 shows the Ramey B normalized best-fit pressure and pressure derivatives.

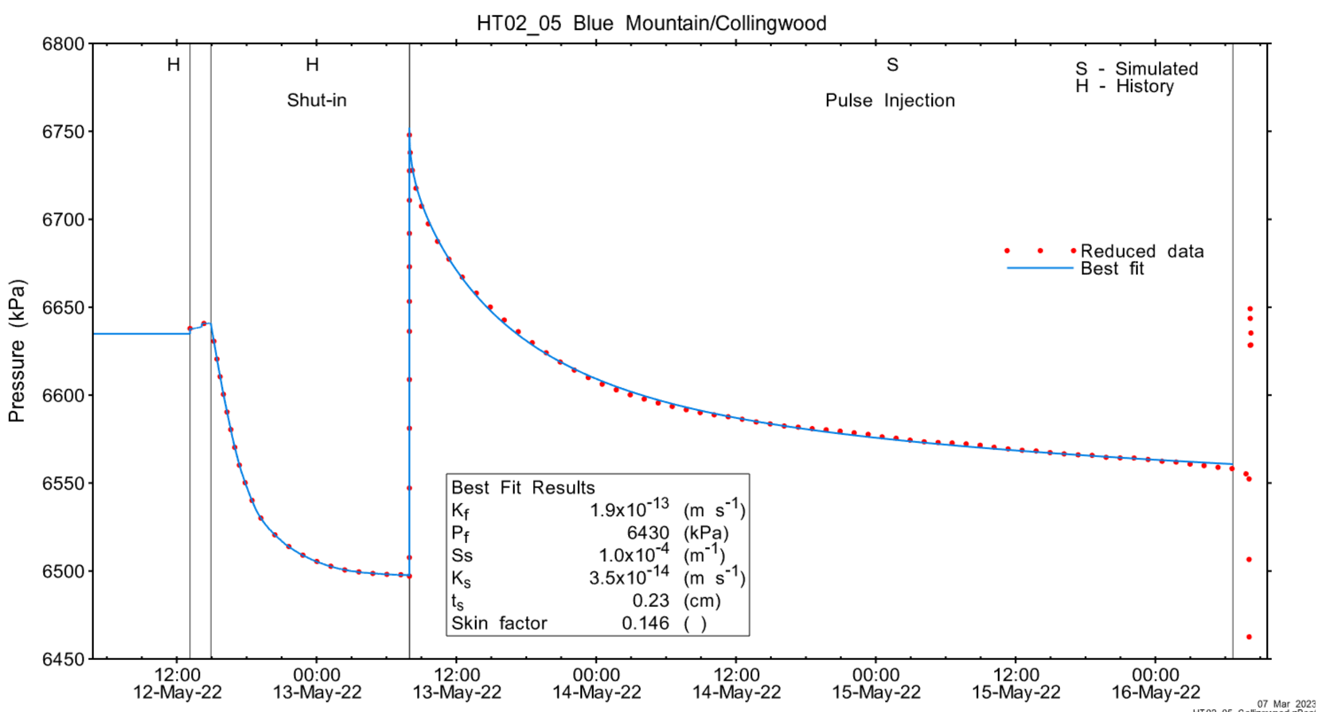

Figure 0.250 Annotated testing sequence showing best-fit simulation and parameter estimates.

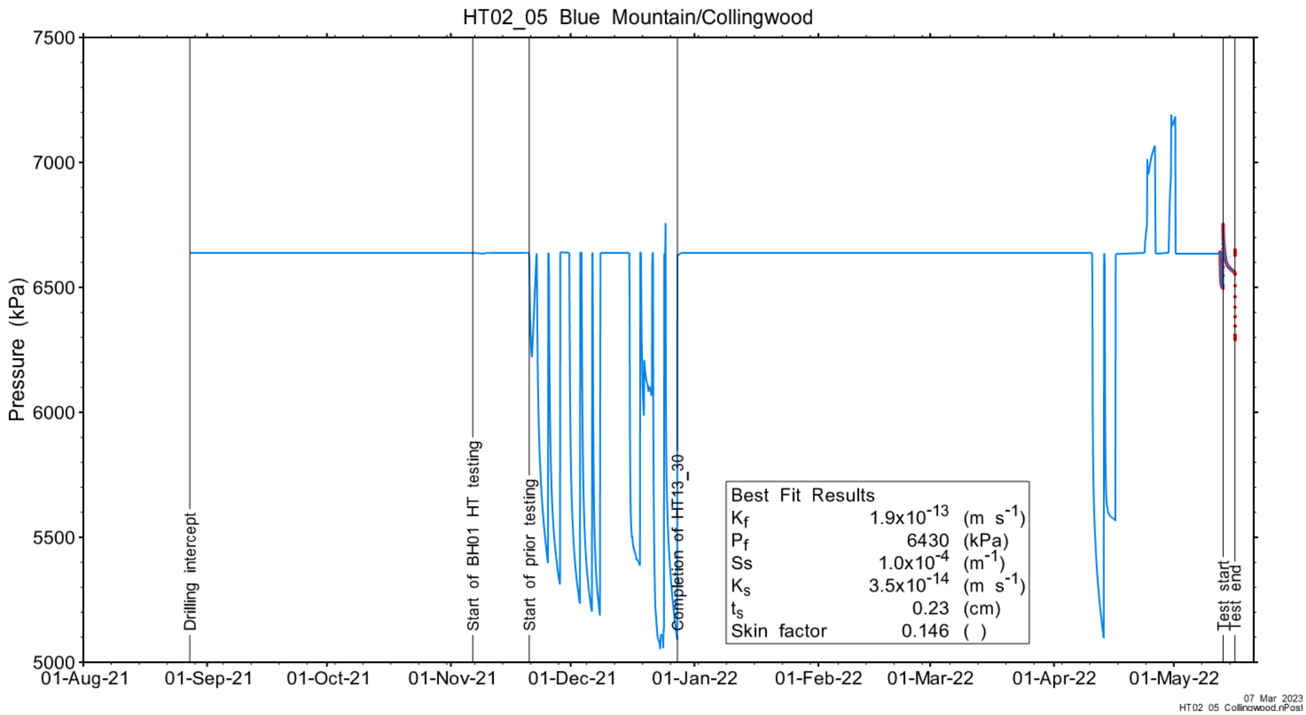

Figure 0.251 Annotated HT02_05 testing sequence showing pre-test history, best-fit simulation and parameter estimates.

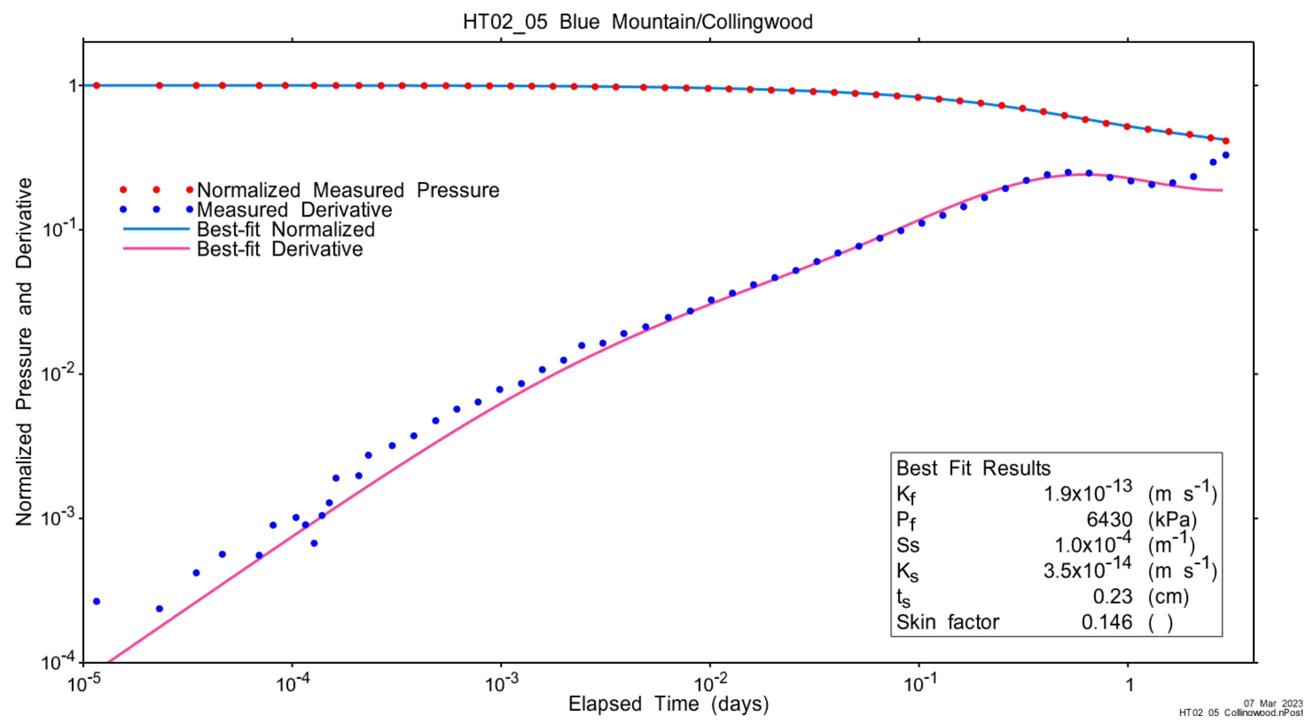

Figure 0.252 Log-log plot showing Ramey B normalized pressure and derivative response for best-fit simulation.

Figure 0.253 shows the normalized parameter sensitivity response for the best fit. Sensitivity for formation pressure was increasing at the end of the test.

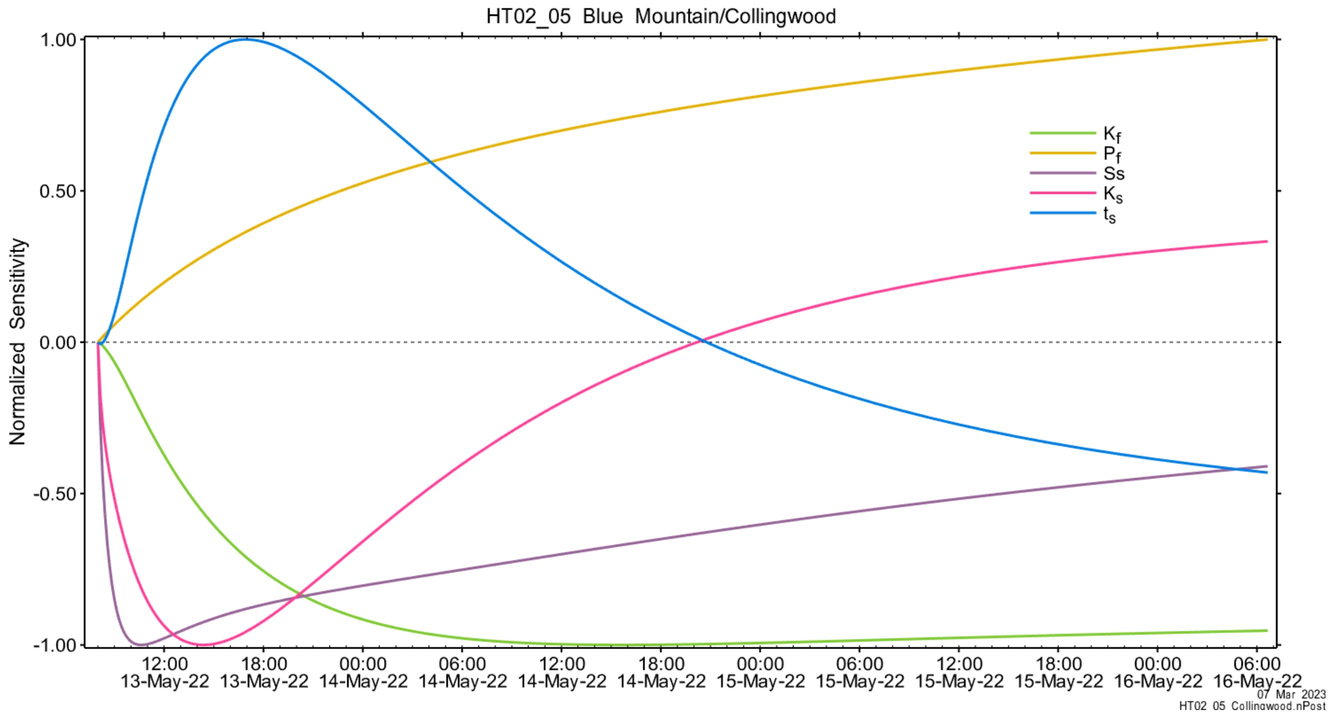

Figure 0.253 Normalized Jacobian for best-fit simulation.

A.17.3 Uncertainty Analyses

The CDF of normalized fit values for all converged simulations and the selected fit discriminant are shown in Figure 0.254.

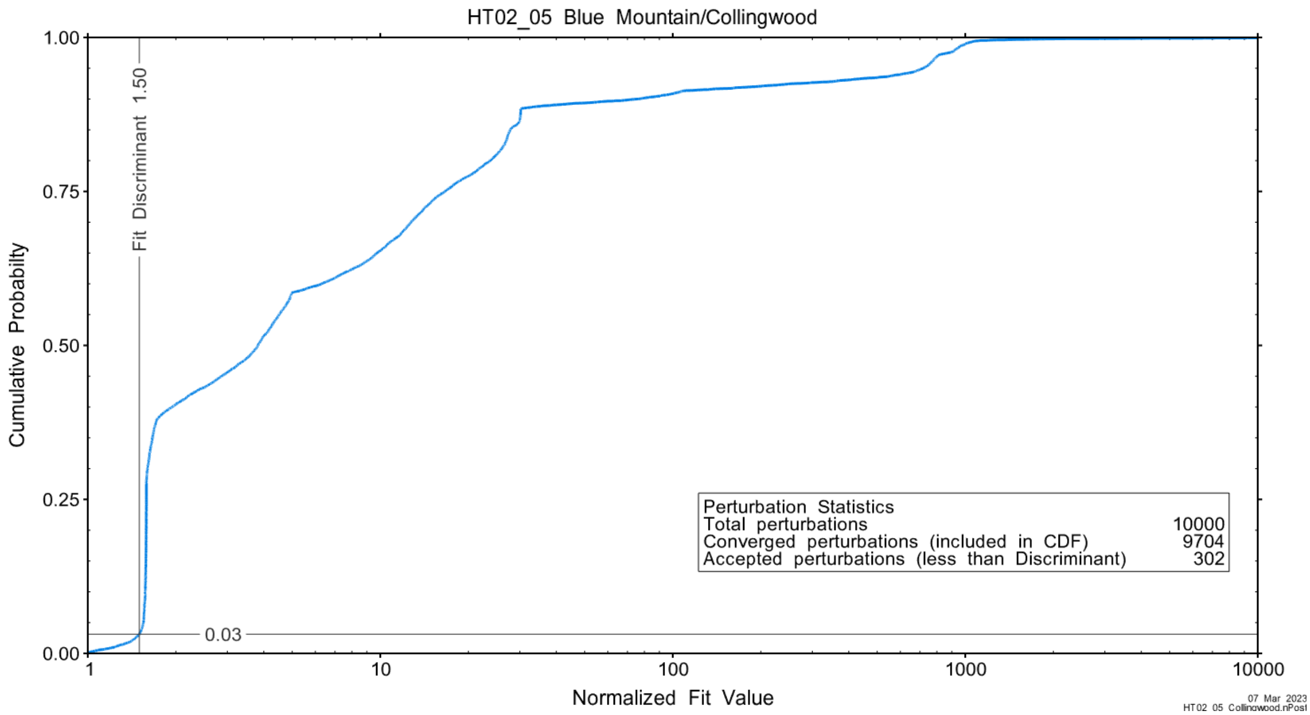

Figure 0.254 Fit value cumulative distribution function.

Summary cross parameter scatter plots for selected formation and skin parameters are given in Figure 0.255 and Figure 0.256. The light pink dots on the figures are the initial parameter estimates, with red dots overlaying those initial parameter values that resulted in accepted optimization results. The grey dots are converged optimizations which did not meet the fit discriminant. Larger varying color symbols represent the fit value of accepted optimizations, with the blue values representing the best fit.

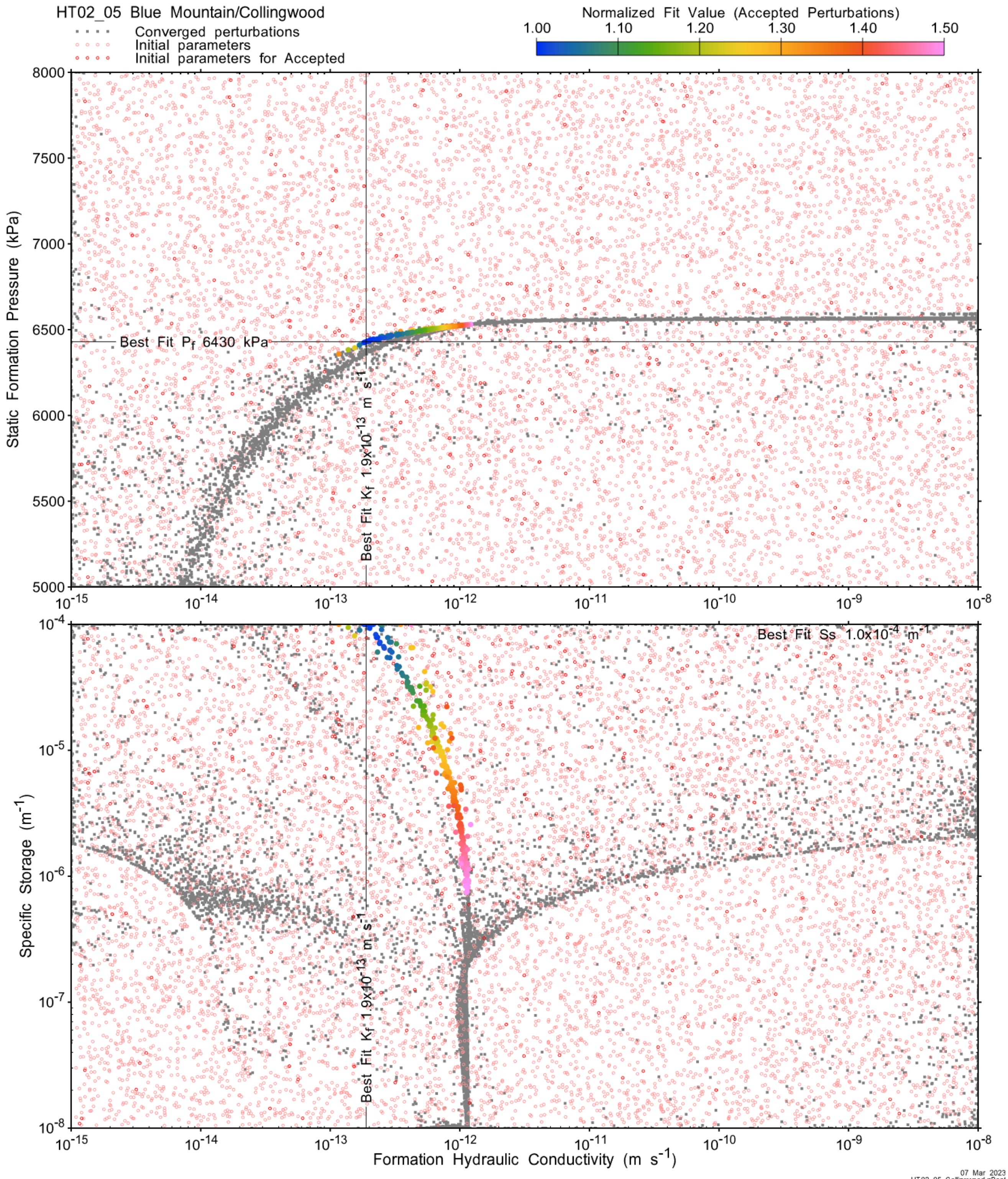

Figure 0.255 XY-scatter plot showing estimates of formation hydraulic conductivity (K_f) vs static formation pressure (P_f) (top panel) and specific storage (Ss) (bottom panel).

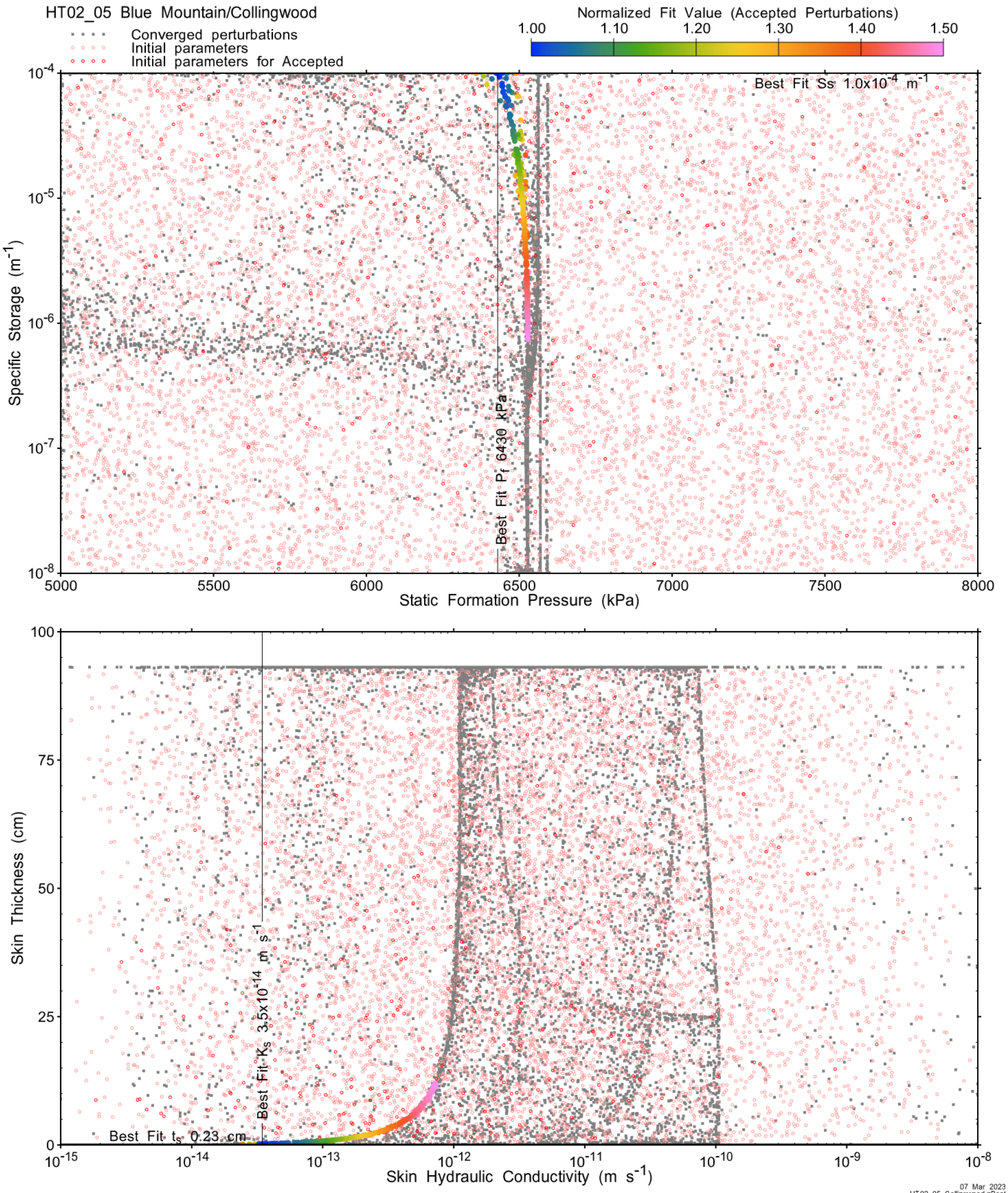

Figure 0.256 XY-scatter plot showing estimates of static formation pressure (P_f) vs specific storage (Ss) (top panel) and skin hydraulic conductivity (K_s) vs skin thickness (t_s) (bottom panel).

Confidence limits and median values are determined from the CDF of accepted optimization results (i.e. the varying color values in the above figures), with best fit value, 5% and 95% confidence indicated on Figure 0.257 and Figure 0.258.

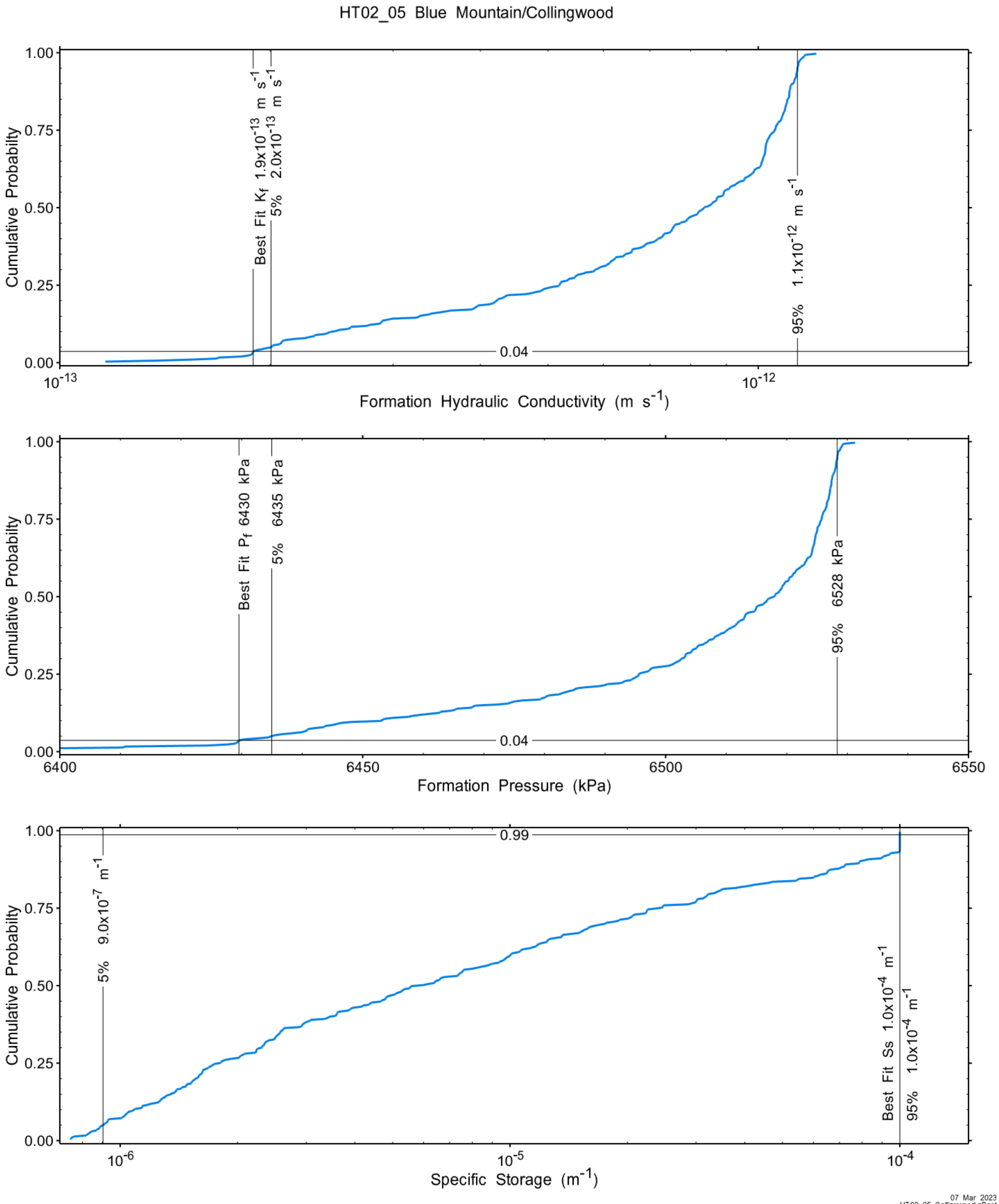

Figure 0.257 Cumulative distribution functions and parameter limits for formation hydraulic conductivity (K_f) (top panel), static formation pressure (P_f) (middle panel) and specific storage (Ss) (bottom panel).

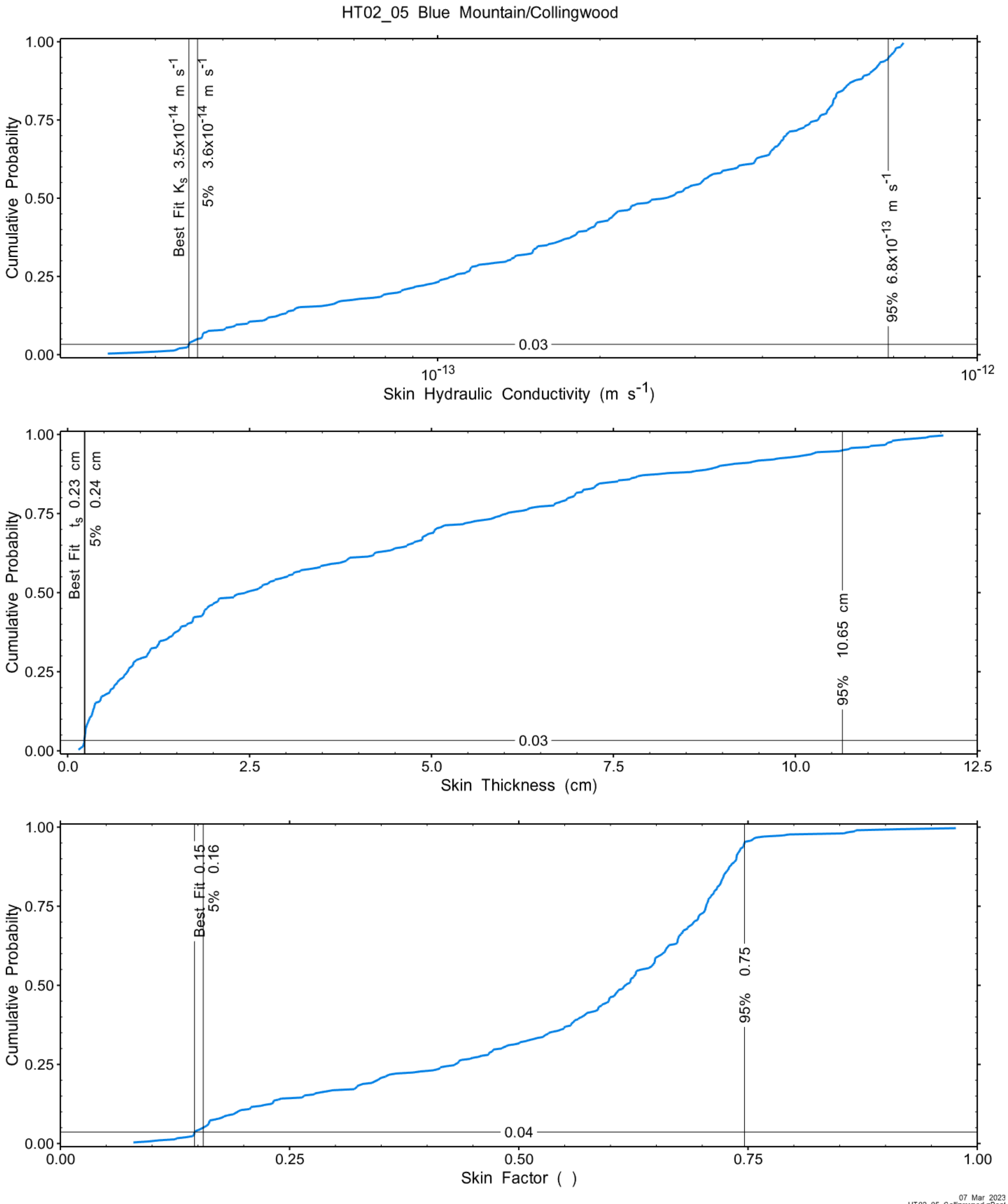

Figure 0.258 Cumulative distribution functions and parameter limits for skin hydraulic conductivity (K_s) (top panel), skin thickness (t_s) (middle panel) and skin factor (s) (bottom panel).

A summary of perturbation results is presented in Figure 0.259, with Ramey-processed perturbations in Figure 0.260. Those perturbations (242 of 10,000) with all parameters within the 5% and 95% range present a very good fit to the measured test zone data.

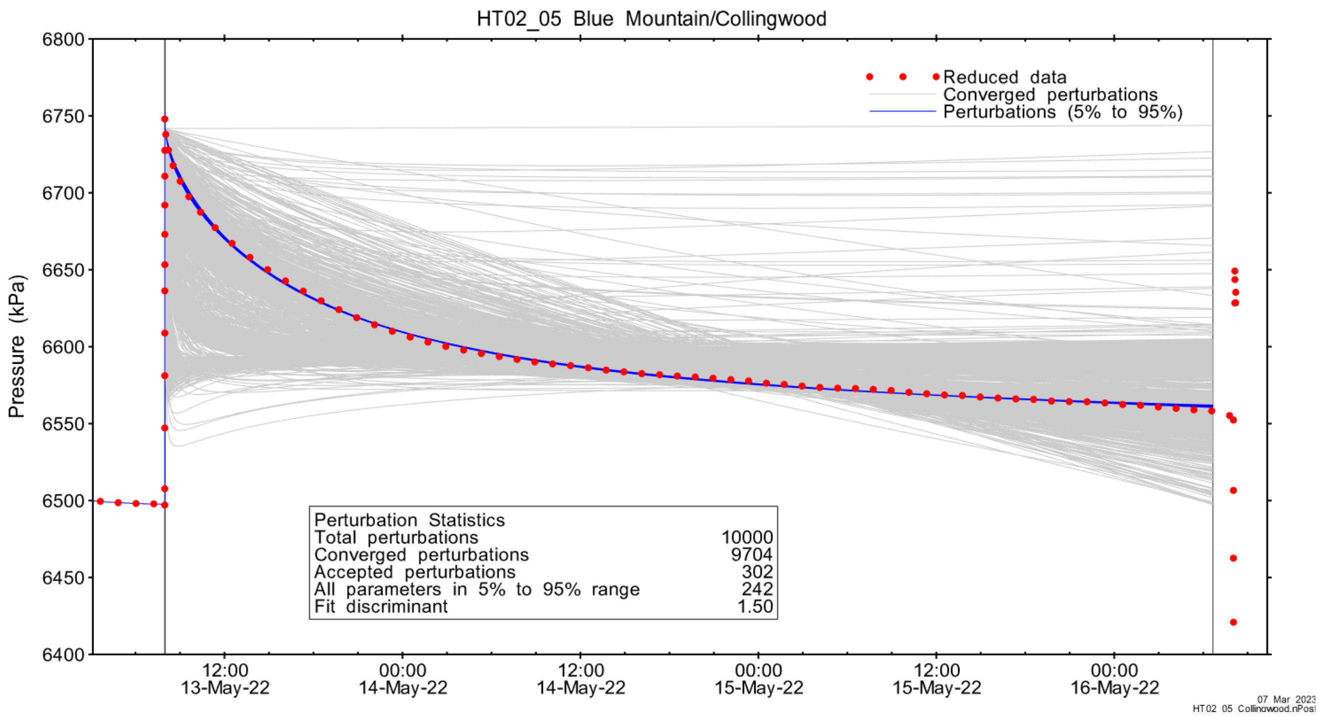

Figure 0.259 Perturbation results – all converged, accepted, and within 5% to 95% for all parameters.

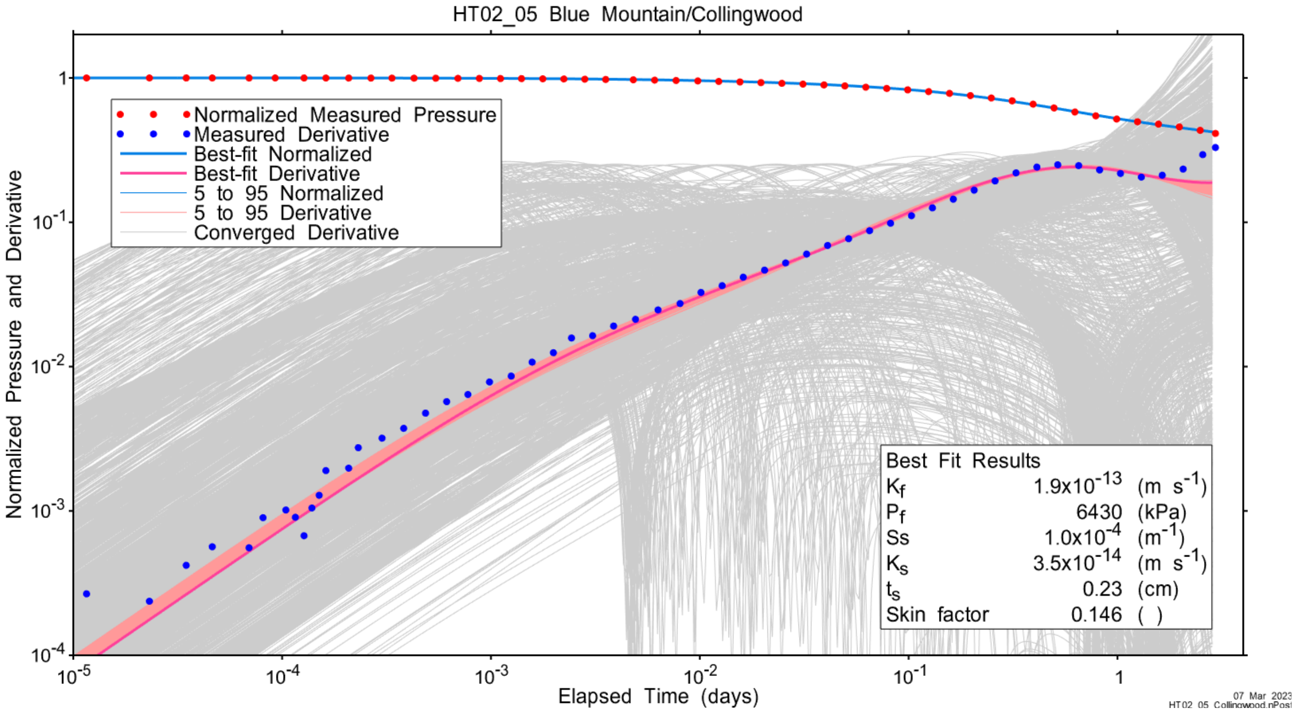

Figure 0.260 Log-log plot showing Ramey B normalized pressure and derivative response for all converged optimizations and those within 5% to 95% for all parameters.

A summary of best-fit parameter estimates and ranges is given in Table 0.84.

Table 0.84 Summary of the HT02_05 parameter estimates.

Parameter	Best Fit	5%	Median	95%
K_f (m/s)	1.9E-13	2.0E-13	8.4E-13	1.1E-12
P_f (kPa)	6430	6435	6518	6528
Ss (1/m)	1.0E-04	9.0E-07	5.8E-06	1.0E-04
K_s (m/s)	3.5E-14	3.6E-14	2.6E-13	6.8E-13
t_s (cm)	0.23	0.24	2.44	10.65
s (-)	0.146	0.156	0.616	0.746

Parameter correlations for all perturbations with all parameters within the 5% to 95% limits are given in Table 0.85.

Table 0.85 Pearson cross-correlations of 5% to 95% parameters

	Log(K_f)	P_f	Log(Ss)	Log(K_s)	t_s	s
Log(K_f)	1.000	0.989	-0.952	0.978	0.795	0.968
P_f	0.989	1.000	-0.902	0.940	0.728	0.962
Log(Ss)	-0.952	-0.902	1.000	-0.994	-0.917	-0.879
Log(K_s)	0.978	0.940	-0.994	1.000	0.891	0.920
t_s	0.795	0.728	-0.917	0.891	1.000	0.677
s	0.968	0.962	-0.879	0.920	0.677	1.000

A.17.4 Additional Figures

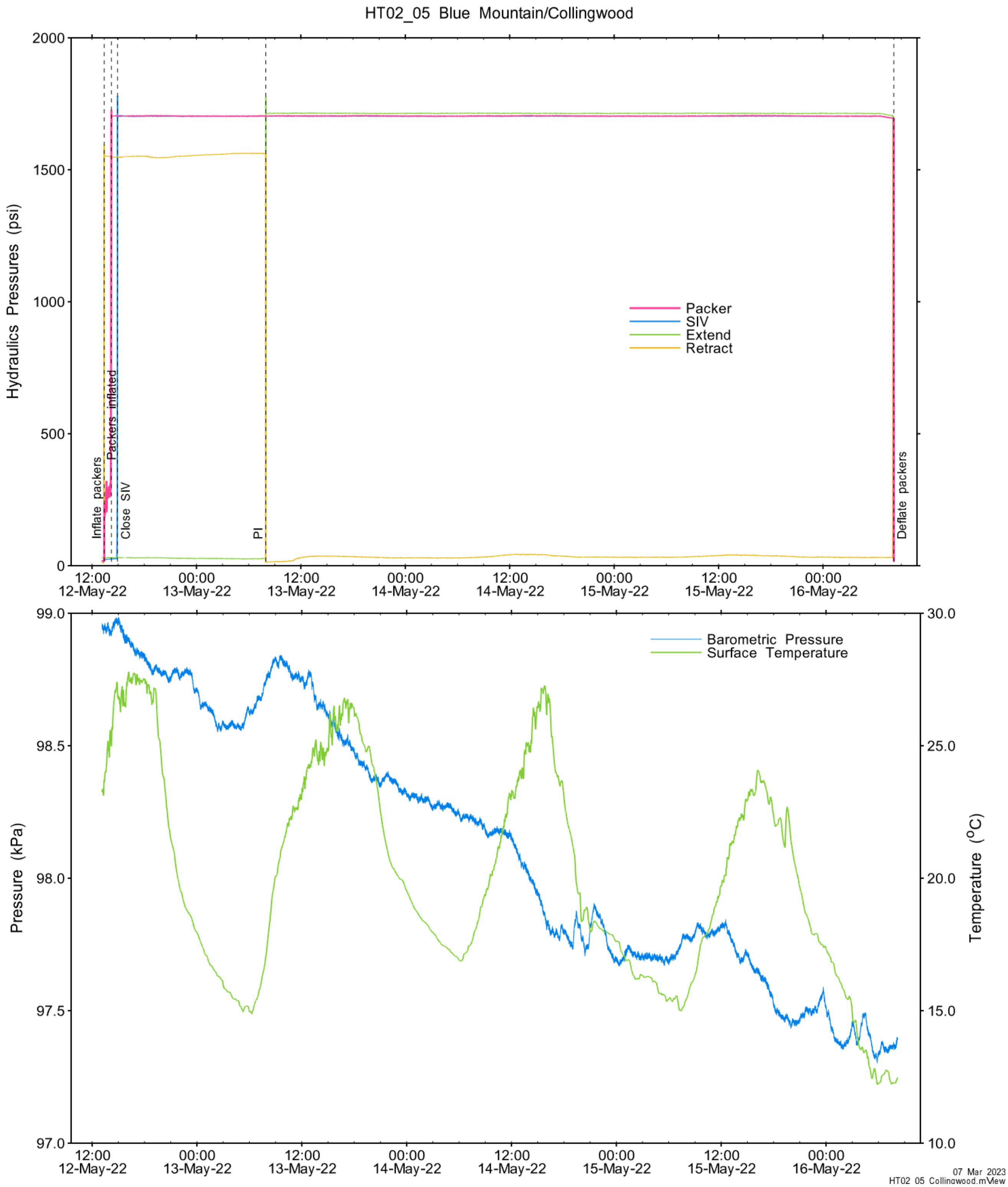

Figure 0.261 Hydraulics pressures and surface temperature/barometric pressure.

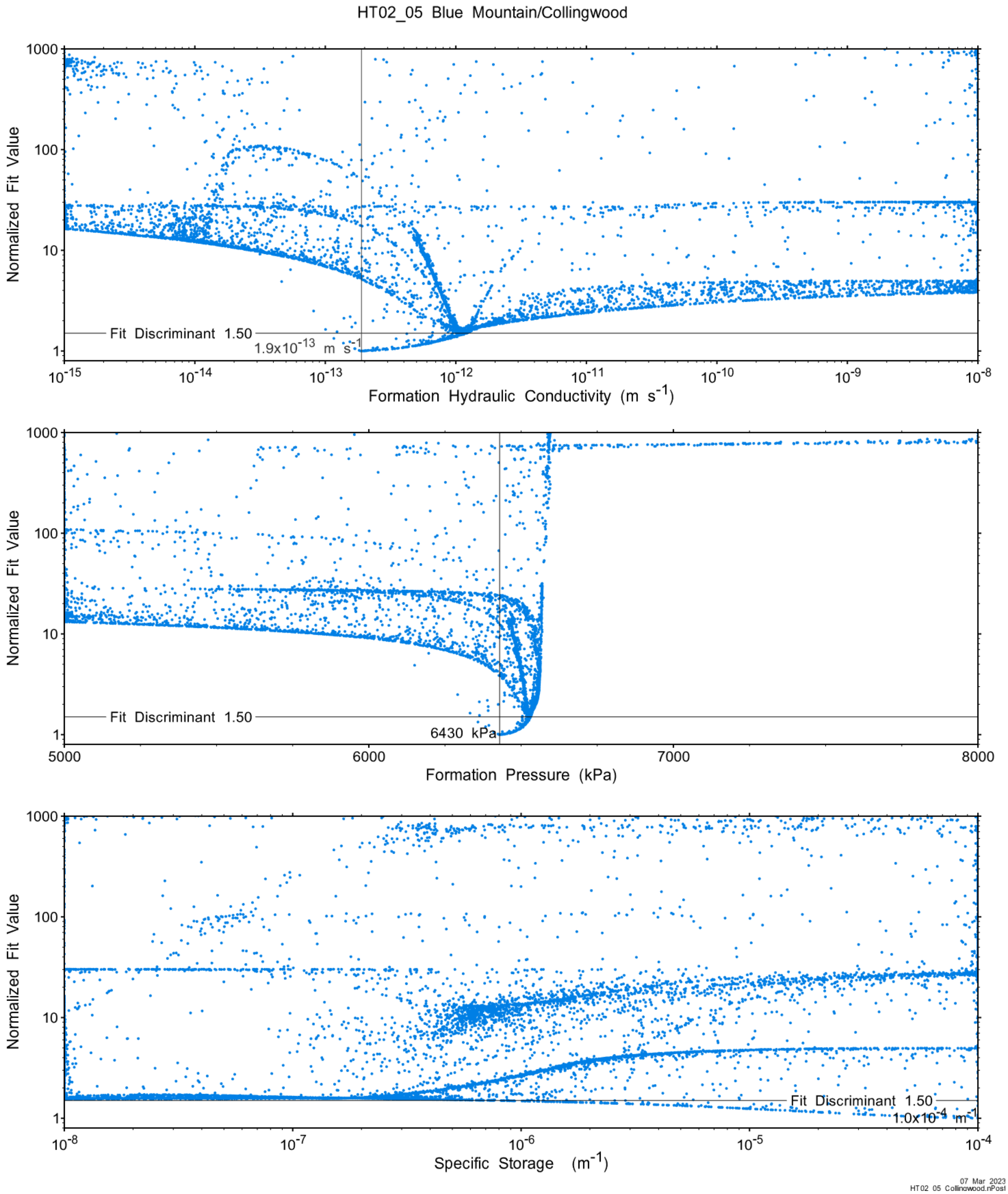

Figure 0.262 XY-scatter plot showing the formation parameter space normalized fit values.

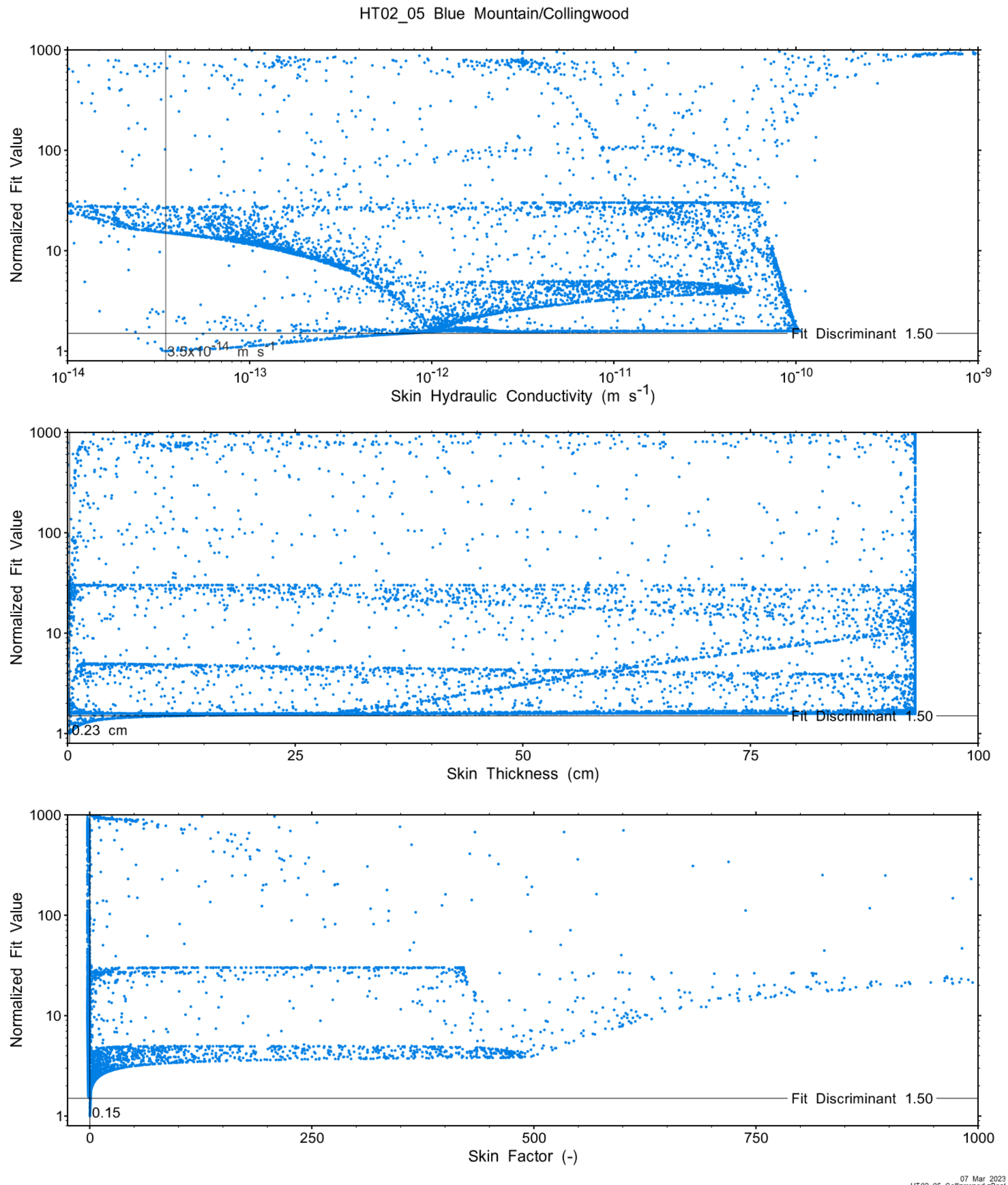

Figure 0.263 XY-scatter plot showing the skin parameter space normalized fit values.

A.18 HT03_05 Cobokonk

The SB_BH01 interval from 788.00 to 793.03 mBGS tested in HT03_05 consists of the middle 5 m of the approximately 20-m-thick Coboconk Formation. A single PI test was performed.

A.18.1 Test Data Summary

Table 0.86 and Figure 0.264 provide a summary of test events and a plot of pressures measured while testing, respectively.

Table 0.86 HT03_05 Summary of Test Events.

Event	Start Date & Time	Duration (days)	TZ Pressure (kPa)
Drilling intercept	21-09-12 14:30	54.88	8296
Prior testing	21-11-06 11:43	177.33	variable
Shut-in	22-05-02 19:34	0.52	8298
Pulse injection	22-05-03 08:02	2.00	8797
Test end	22-05-05 08:04		8302

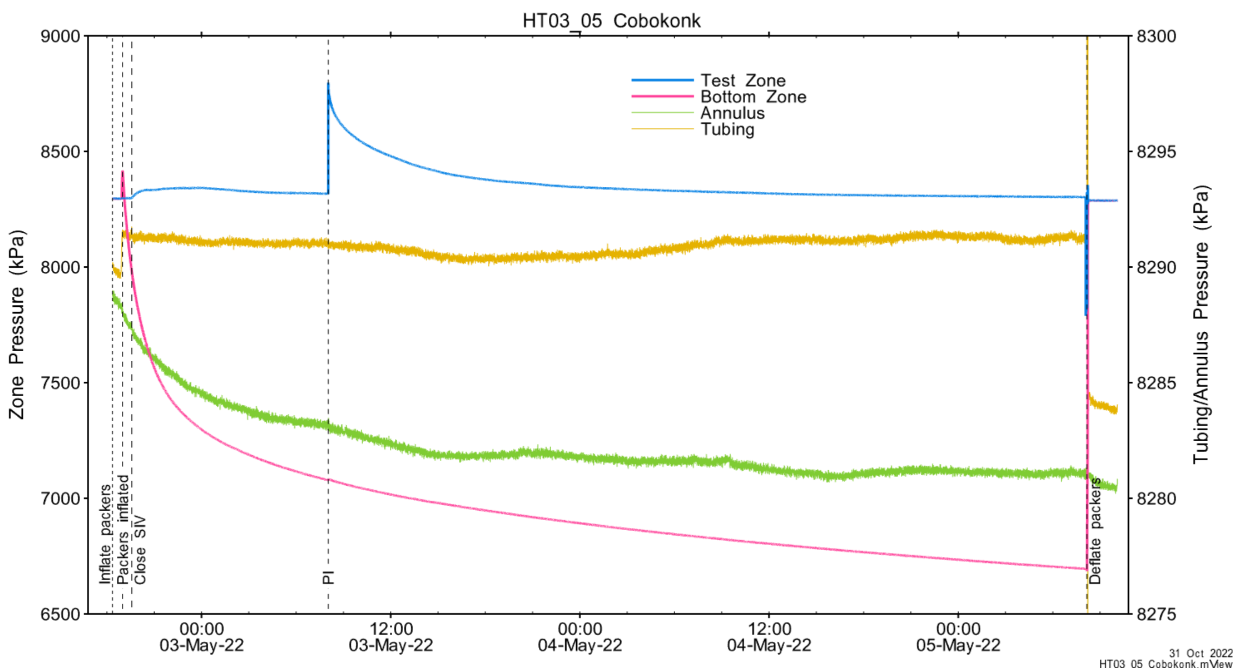

Figure 0.264 HT03_05 test events and pressures.

A.18.2 Test Analyses

Table 0.87 is a summary of test-specific input parameters used in the analyses, while Table 0.88 presents the optimized parameters and allowed ranges.

Table 0.87 nSIGHTS Input Parameters.

Parameter	Value	Units
Test zone radius	6.34	cm
Test zone compressibility	4.23E-10	1/Pa
Test zone fluid density	1084	g/L
Test zone length	5.03	m

Table 0.88 nSIGHTS Parameter Optimization Ranges.

Parameter	Minimum	Maximum	Units	Type
Formation hydraulic conductivity (K_f)	1E-15	1E-09	m/s	log
Formation pressure (P_f)	7000	10000	kPa	linear
Specific storage (Ss)	1E-08	1E-04	1/m	log
Skin hydraulic conductivity (K_s)	1E-15	1E-09	m/s	log
Skin thickness (t_s)	0.01	1000	cm	linear

Figure 0.265 shows the measured test zone pressure record (with reduced data density for clarity) used in the analysis along with the best-fit simulation and parameter values. Figure 0.266 presents the pre-test history and Figure 0.267 shows the Ramey B normalized best-fit pressure and pressure derivatives.

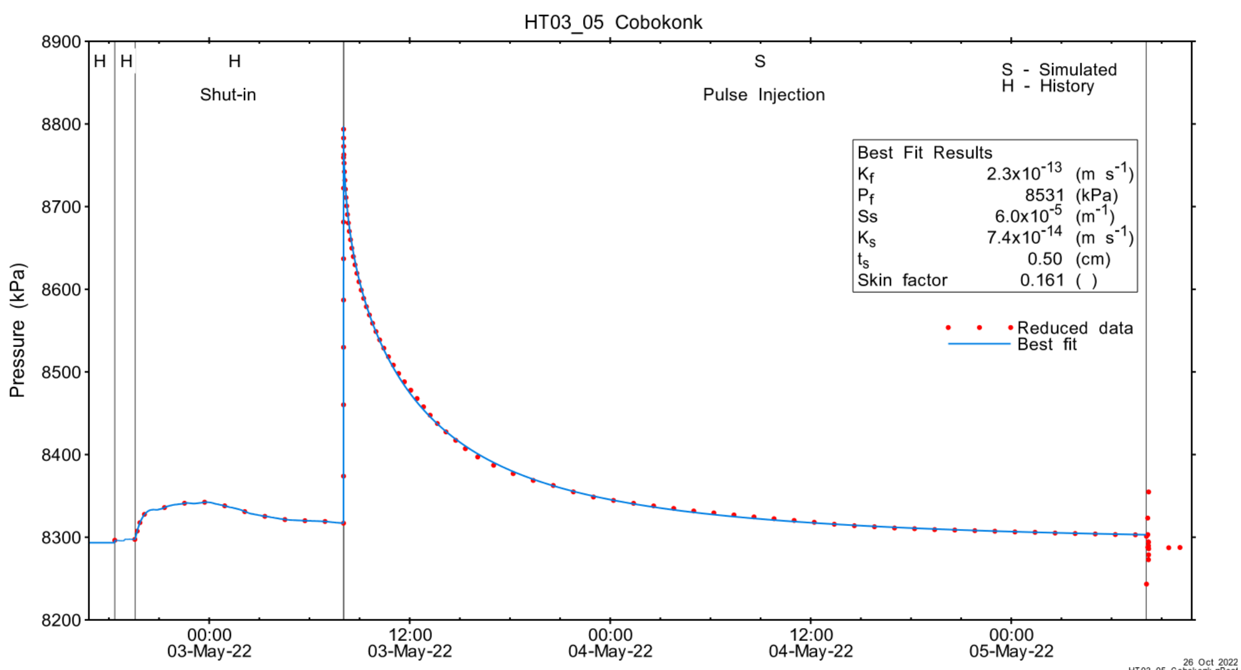

Figure 0.265 Annotated testing sequence showing best-fit simulation and parameter estimates.

GEOFIRMA ENGINEERING

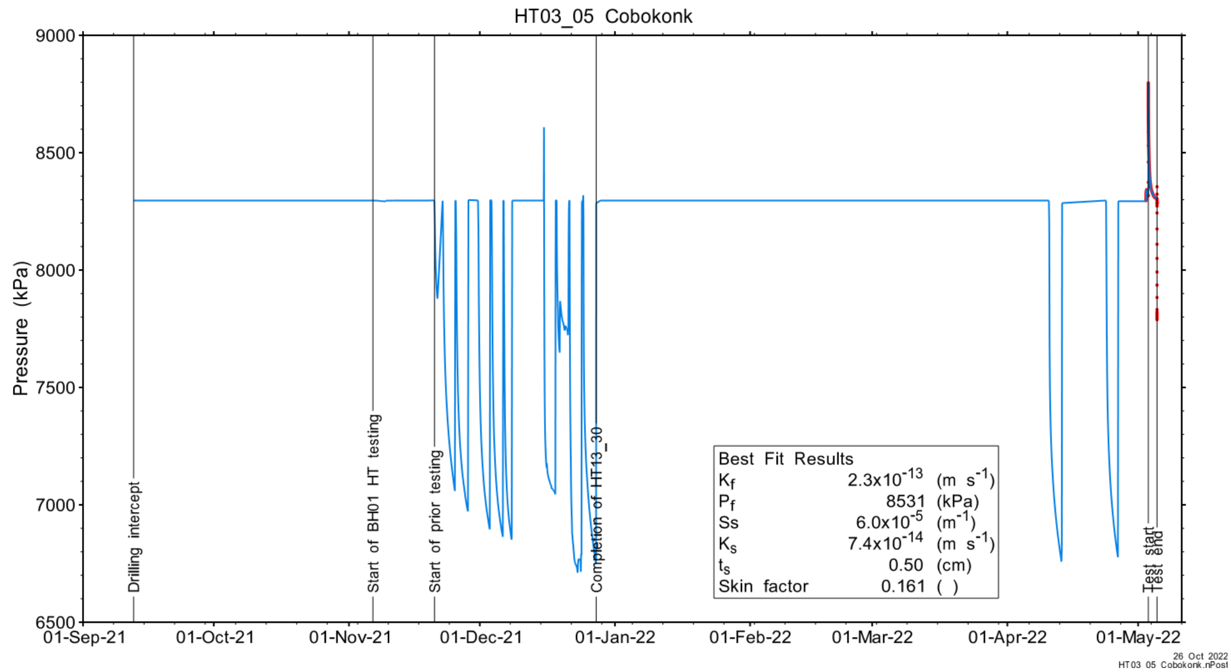

Figure 0.266 Annotated HT03_05 testing sequence showing pre-test history, best-fit simulation and parameter estimates.

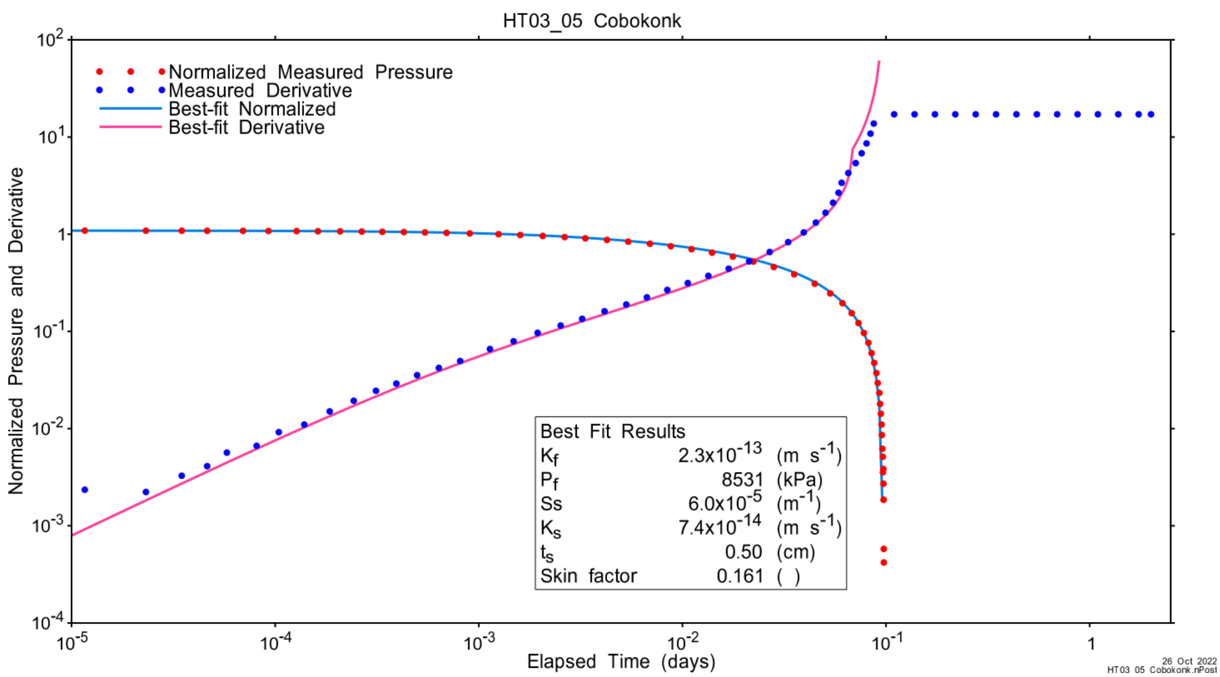

Figure 0.267 Log-log plot showing Ramey B normalized pressure and derivative response for best-fit simulation.

Figure 0.268 shows the normalized parameter sensitivity response for the best fit. Only sensitivity for static formation pressure was increasing at the end of the test.

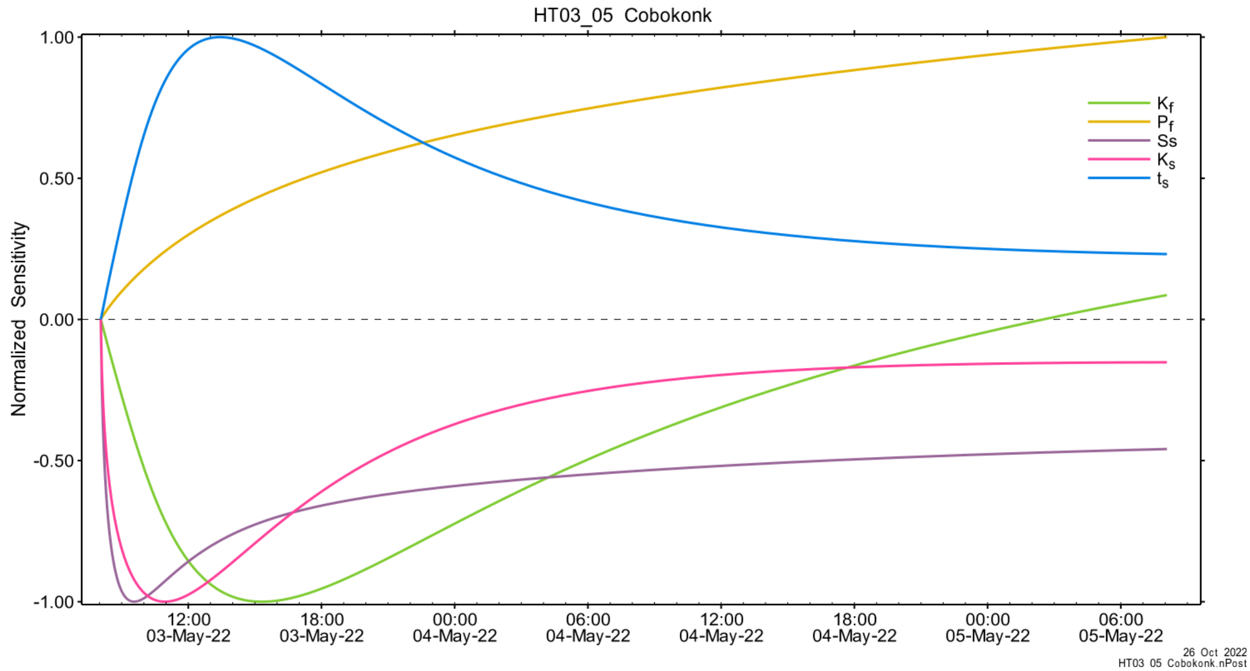

Figure 0.268 Normalized Jacobian for best-fit simulation.

A.18.3 Uncertainty Analyses

The CDF of normalized fit values for all converged simulations and the selected fit discriminant are shown in Figure 0.269.

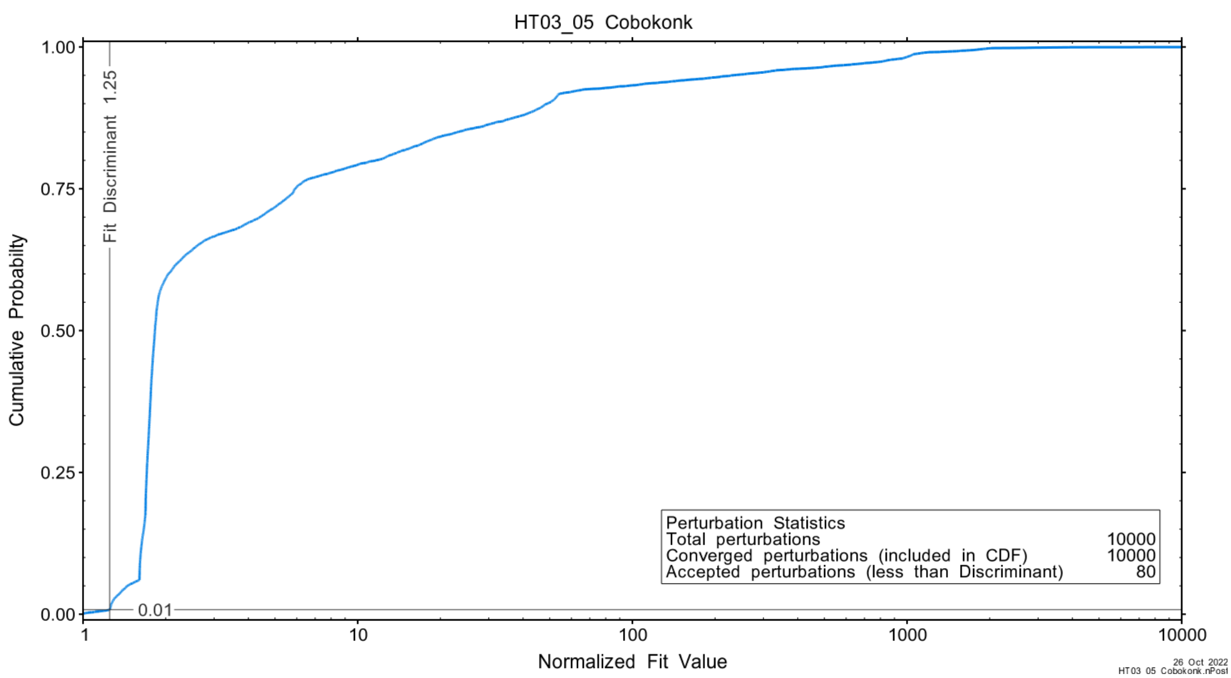

Figure 0.269 Fit value cumulative distribution function.

Summary cross parameter scatter plots for selected formation and skin parameters are given in Figure 0.270 and Figure 0.271. The light pink dots on the figures are the initial parameter estimates, with red dots overlaying those initial parameter values that resulted in accepted optimization results. The grey dots are converged optimizations which did not meet the fit discriminant. Larger varying color symbols represent the fit value of accepted optimizations, with the blue values representing the best fit.

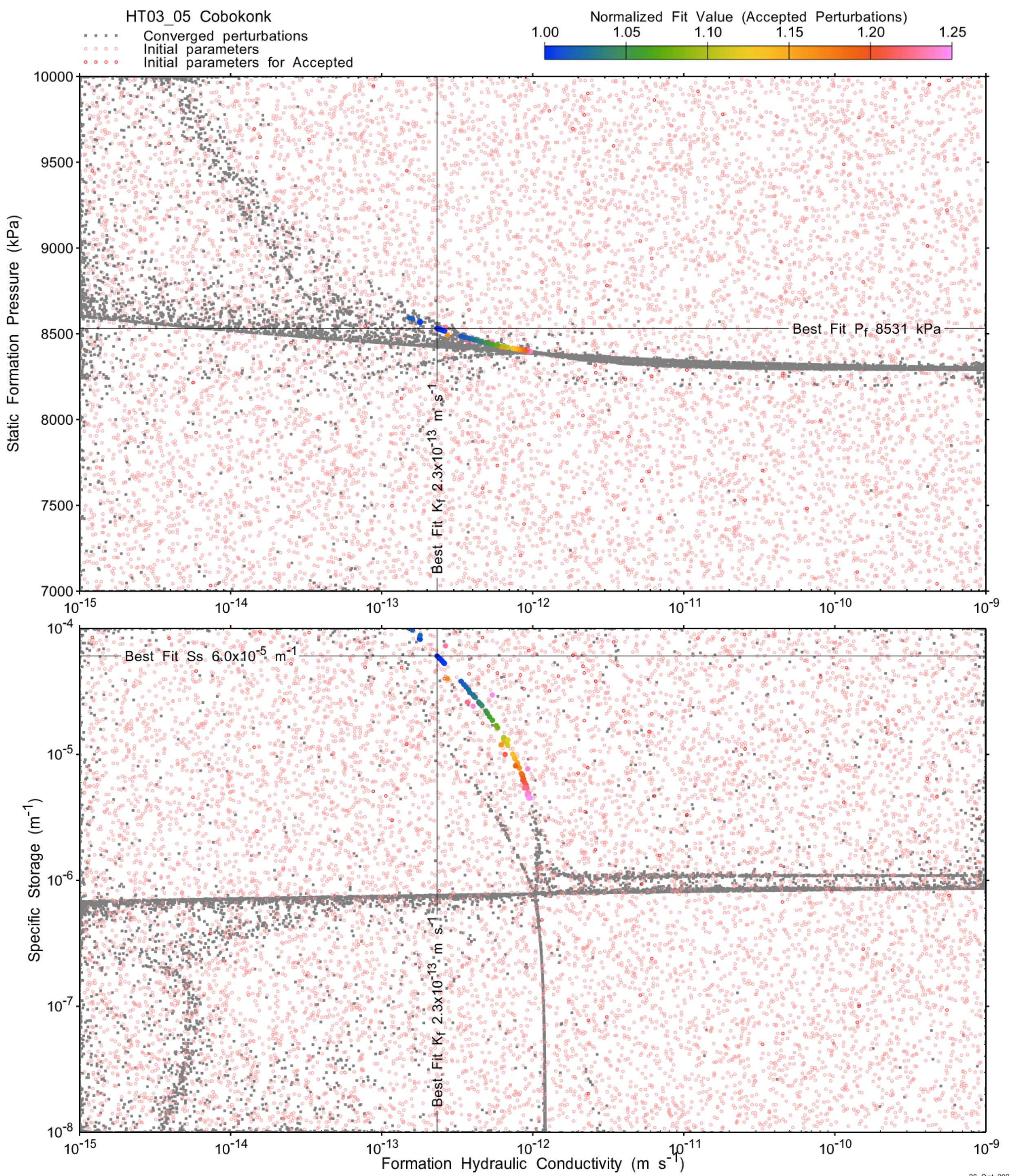

Figure 0.270 XY-scatter plot showing estimates of formation hydraulic conductivity (K_f) vs static formation pressure (P_f) (top panel) and specific storage (Ss) (bottom panel).

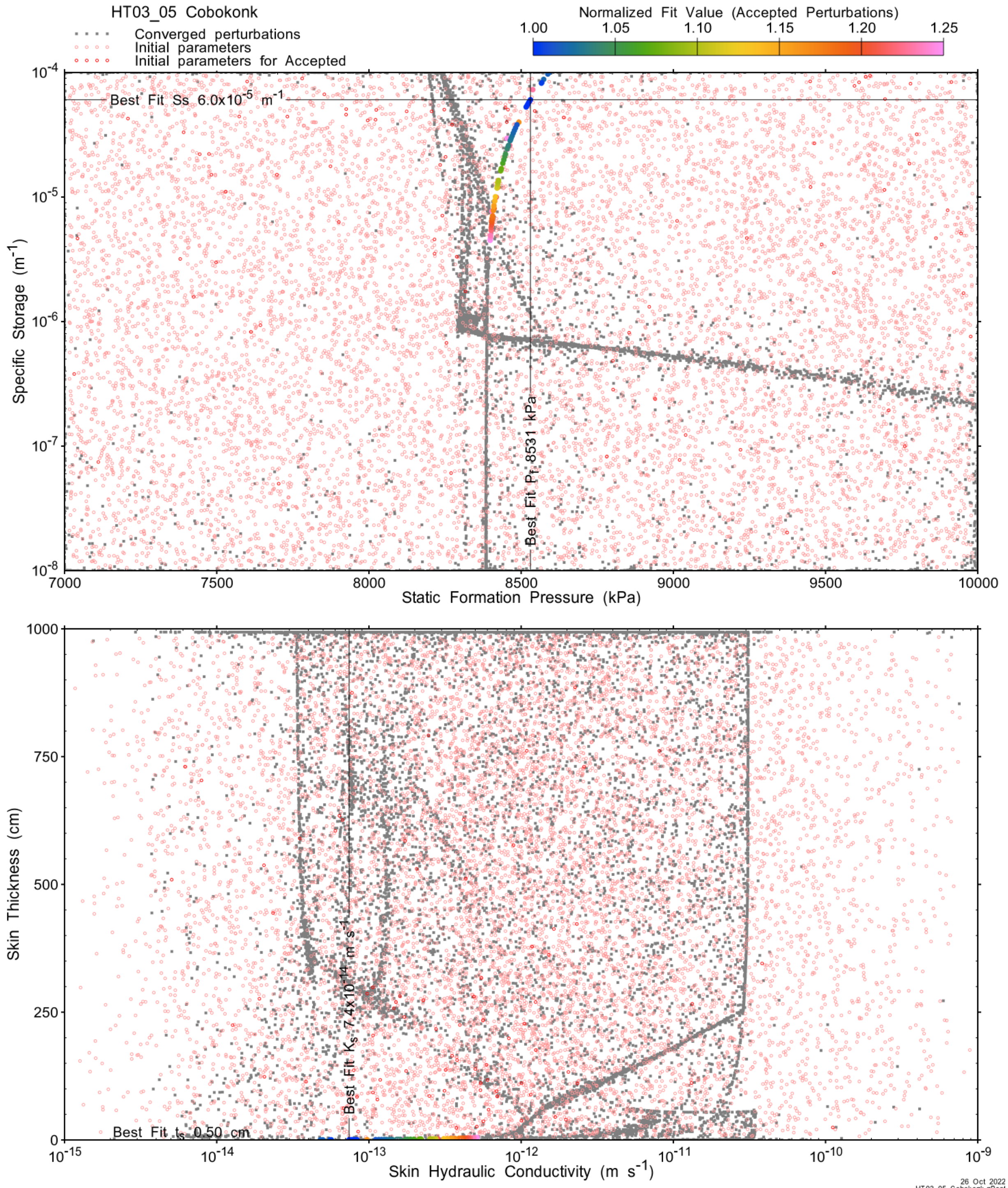

Figure 0.271 XY-scatter plot showing estimates of static formation pressure (P_f) vs specific storage (Ss) (top panel) and skin hydraulic conductivity (K_s) vs skin thickness (t_s) (bottom panel).

Confidence limits and median values are determined from the CDF of accepted optimization results (i.e. the varying color values in the above figures), with best fit value, 5% and 95% confidence indicated on Figure 0.272 and Figure 0.273.

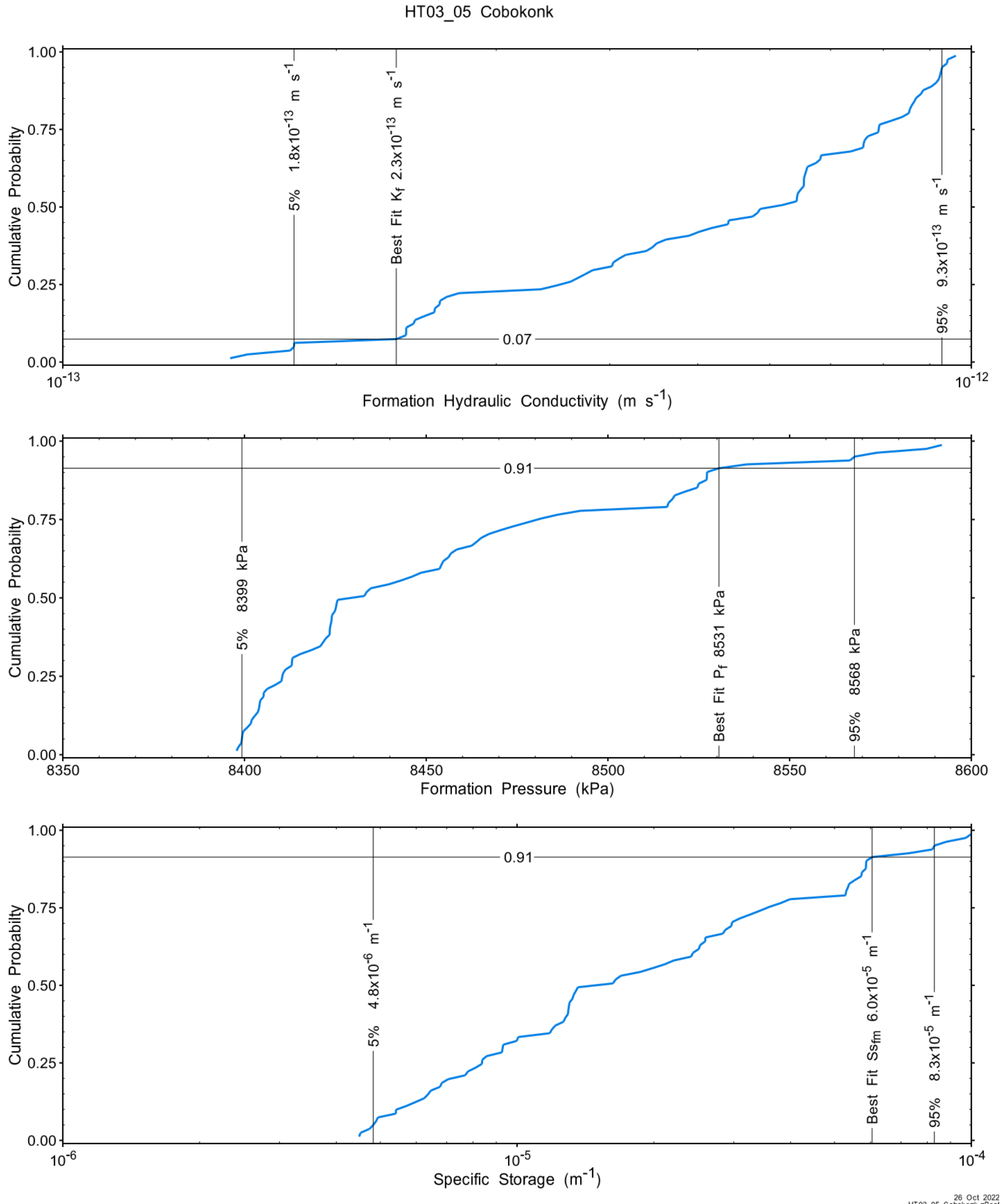

Figure 0.272 Cumulative distribution functions and parameter limits for formation hydraulic conductivity (K_f) (top panel), static formation pressure (P_f) (middle panel) and specific storage (Ss) (bottom panel).

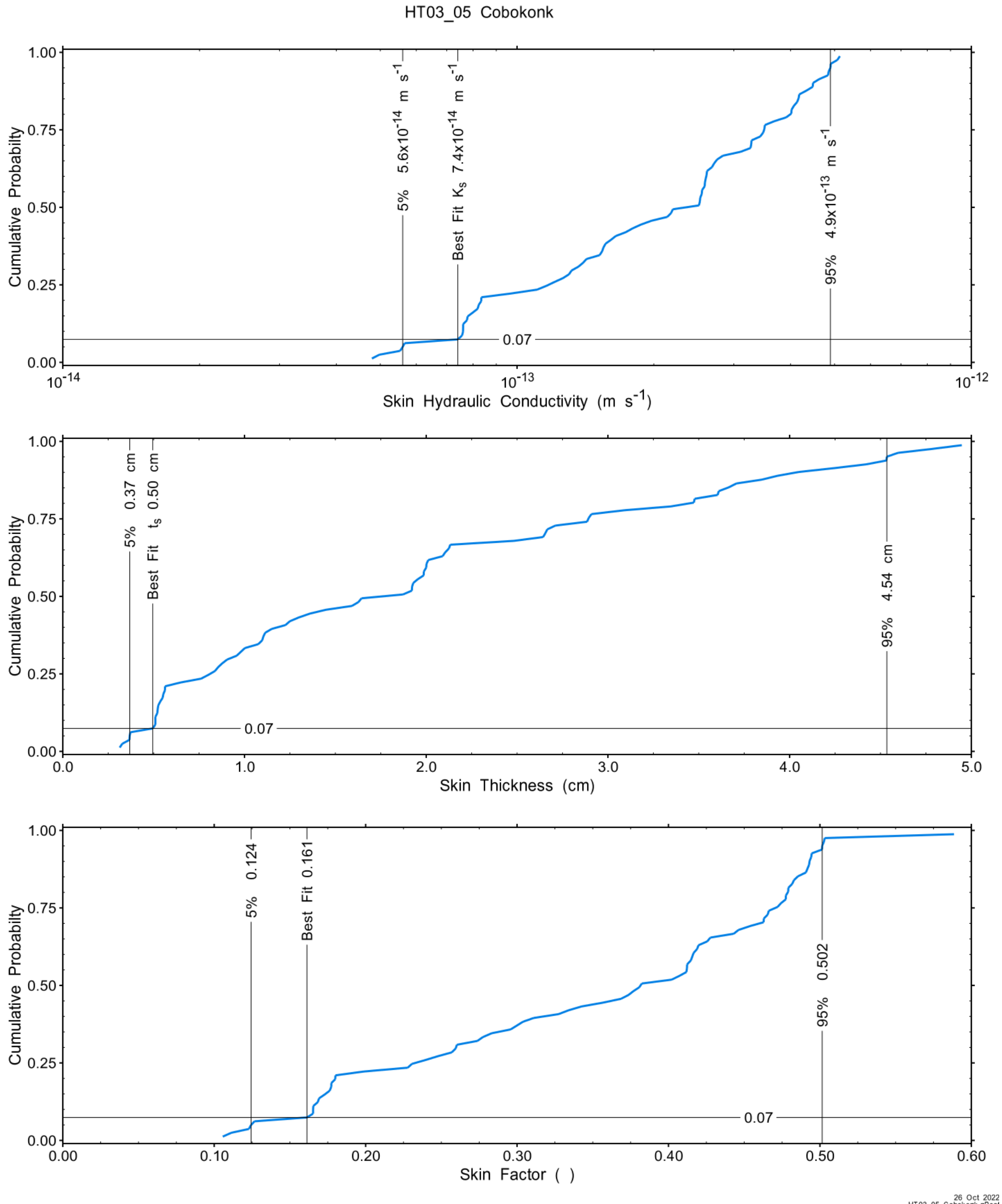

Figure 0.273 Cumulative distribution functions and parameter limits for skin hydraulic conductivity (K_s) (top panel), skin thickness (t_s) (middle panel) and skin factor (s) (bottom panel).

A summary of perturbation results is presented in Figure 0.274, with Ramey-processed perturbations in Figure 0.275. Those perturbations (67 of 10,000) with all parameters within the 5% and 95% range present a very good fit to the measured test zone data.

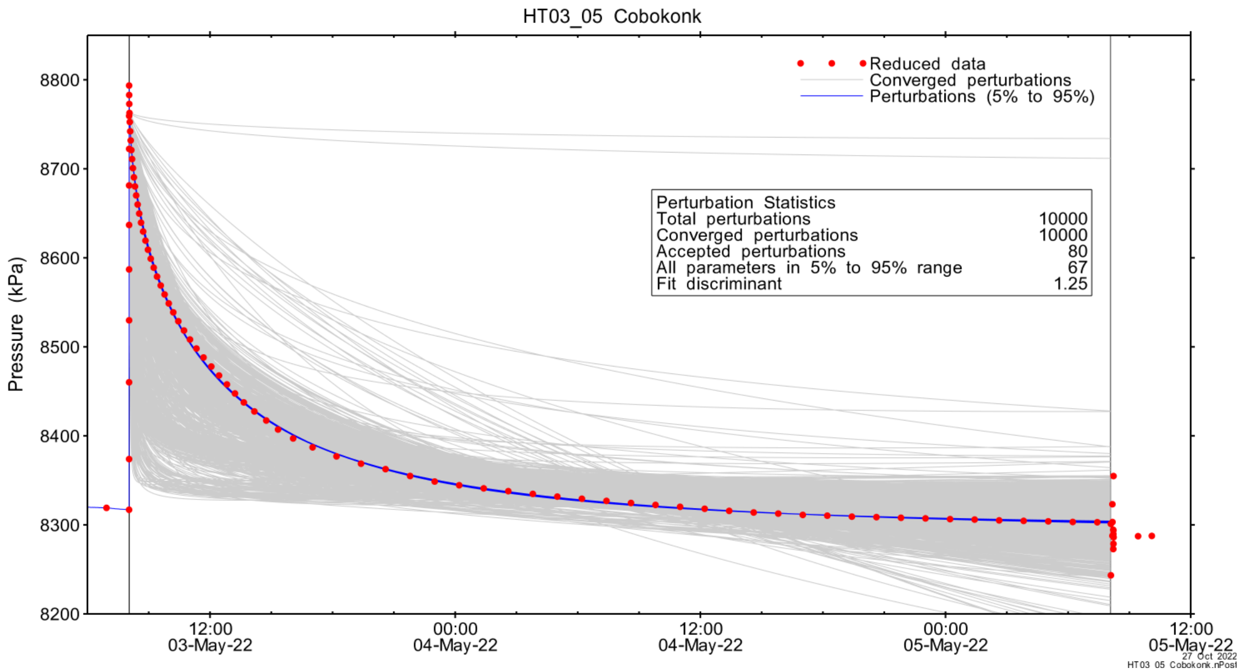

Figure 0.274 Perturbation results – all converged, accepted, and within 5% to 95% for all parameters.

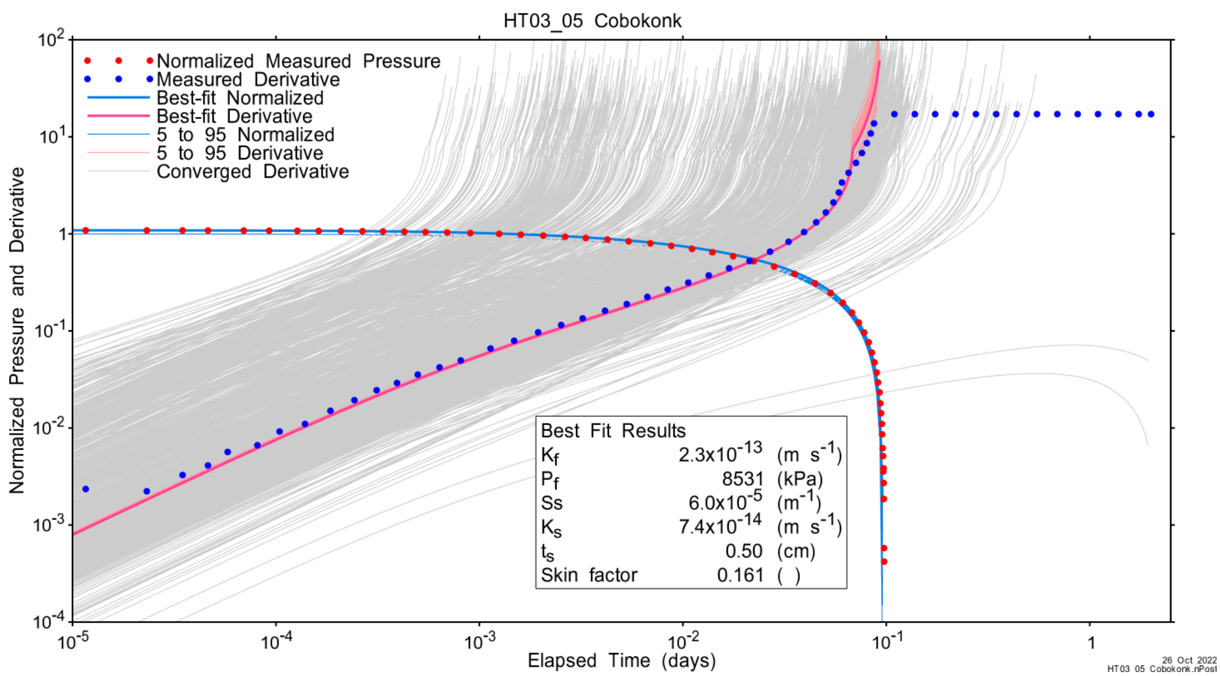

Figure 0.275 Log-log plot showing Ramey B normalized pressure and derivative response for all converged optimizations and those within 5% to 95% for all parameters.

A summary of best-fit parameter estimates and ranges is given in Table 0.89.

Table 0.89 Summary of the HT03_05 parameter estimates.

Parameter	Best Fit	5%	Median	95%
K_f (m/s)	2.3E-13	1.8E-13	6.0E-13	9.3E-13
P_f (kPa)	8531	8399	8429	8568
Ss (1/m)	6.0E-05	4.8E-06	1.5E-05	8.3E-05
K_s (m/s)	7.4E-14	5.6E-14	2.4E-13	4.9E-13
t_s (cm)	0.50	0.37	1.76	4.54
s (-)	0.161	0.124	0.382	0.502

Parameter correlations for all perturbations with all parameters within the 5% to 95% limits are given in Table 0.90.

Table 0.90 Pearson cross-correlations of 5% to 95% parameters

	Log(K_f)	P_f	Log(Ss)	Log(K_s)	t_s	s
Log(K_f)	1.000	-0.956	-0.649	0.752	0.953	0.832
P_f	-0.956	1.000	0.832	-0.743	-0.943	-0.815
Log(Ss)	-0.649	0.832	1.000	-0.569	-0.728	-0.605
Log(K_s)	0.752	-0.743	-0.569	1.000	0.872	0.991
t_s	0.953	-0.943	-0.728	0.872	1.000	0.923
s	0.832	-0.815	-0.605	0.991	0.923	1.000

A.18.4 Additional Figures

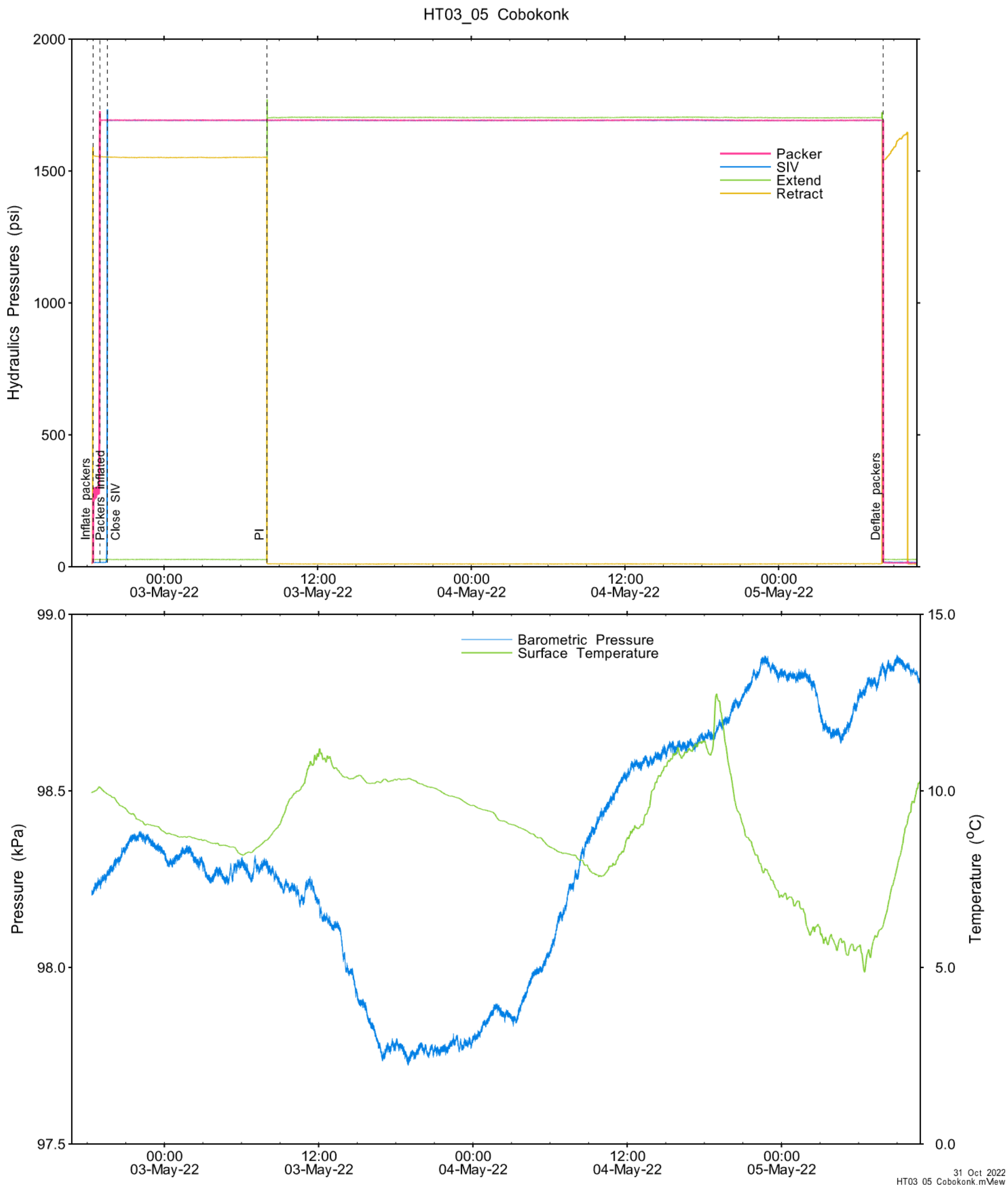

Figure 0.276 Hydraulics pressures and surface temperature/barometric pressure.

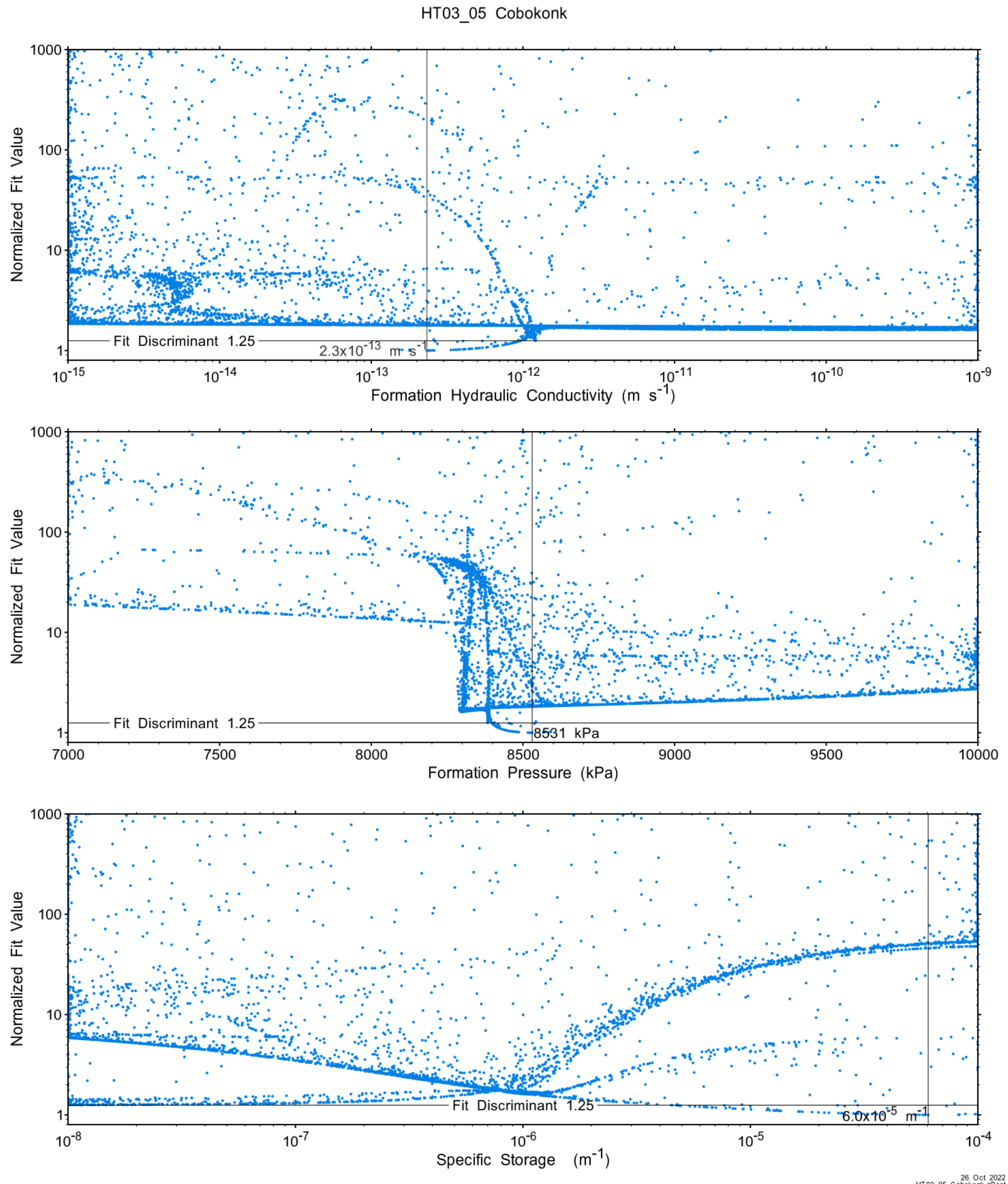

Figure 0.277 XY-scatter plot showing the formation parameter space normalized fit values.

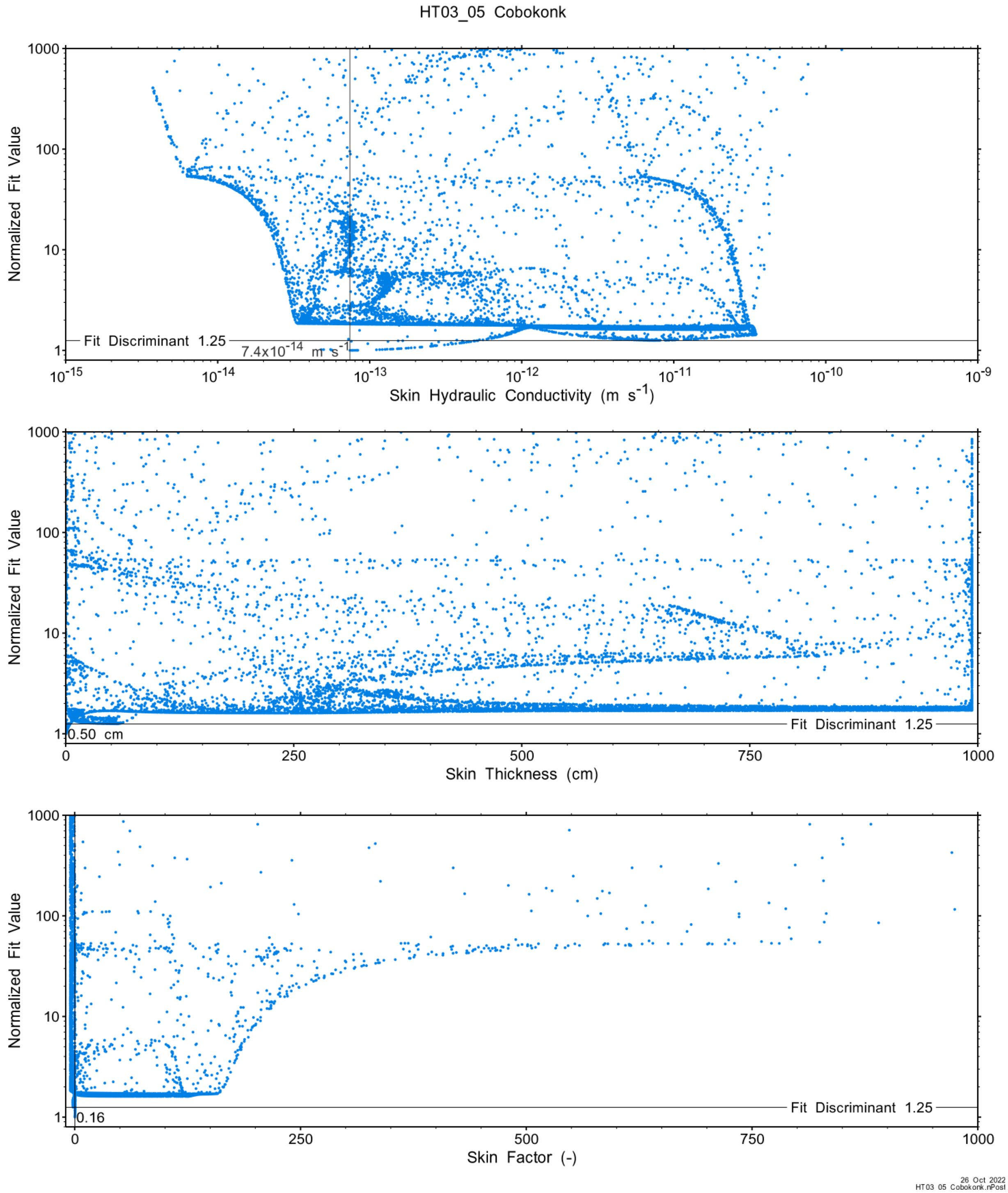

Figure 0.278 XY-scatter plot showing the skin parameter space normalized fit values.

A.19 HT04_05 Shadow Lake

The SB_BH01 interval from 855.00 to 860.53 mBGS tested in HT04_05 consists of the middle 5 m of the approximately 7-m-thick Shadow Lake Formation. A single PI test was performed.

A.19.1 Test Data Summary

Table 0.91 and Figure 0.279 provide a summary of test events and a plot of pressures measured while testing, respectively. The test was terminated by opening the shut-in valve after a two-day duration. However, examination of test data indicated an anomalous change in slope at approximately 04:06 on 8 May 2022. Data beyond that point were not included in the analyses. There was also some difficulty with SIV closure; several open/shut cycles were required before closure was confirmed. The initial attempt at SIV closure was 14:03, closure was verified at 18:15.

Table 0.91 HT04_05 Summary of Test Events.

Event	Start Date & Time	Duration (days)	TZ Pressure (kPa)
Drilling intercept	21-09-15 11:20	66.14	9011
Prior testing	21-11-20 14:45	166.15	variable
Shut-in (final)	22-05-05 18:15	0.57	9011
Pulse injection	22-05-06 07:59	1.84	9363
Test end	22-05-08 04:06		8802

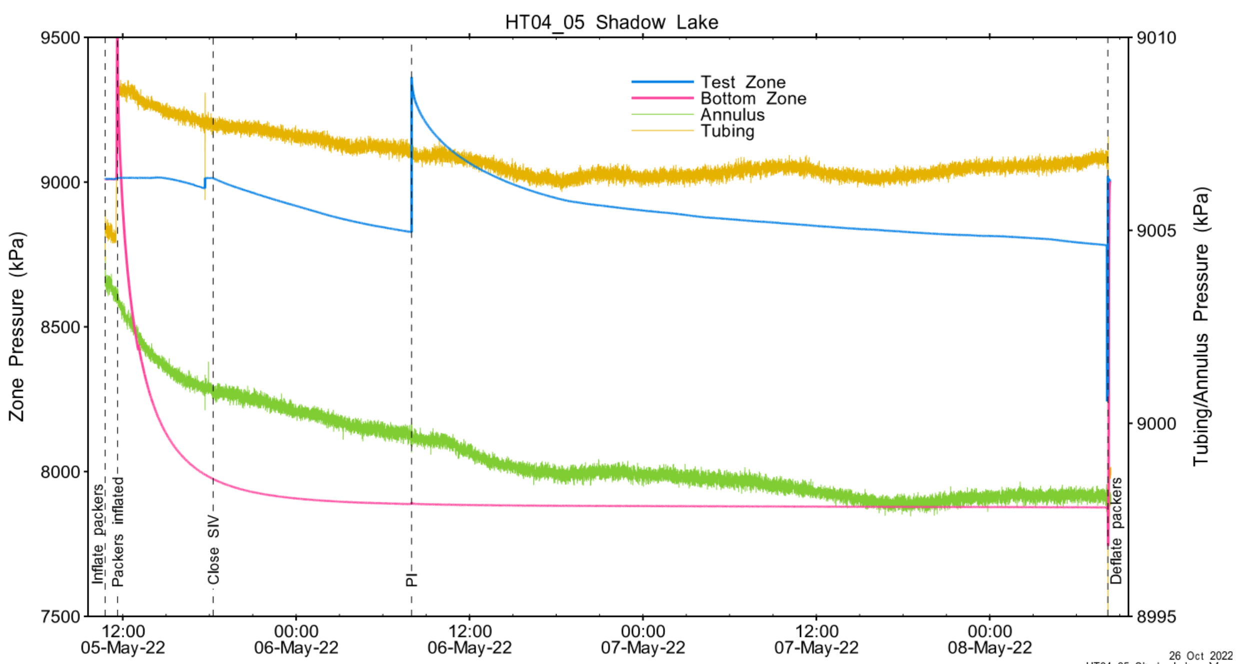

Figure 0.279 HT04_05 test events and pressures.

A.19.2 Test Analyses

Table 0.92 is a summary of test-specific input parameters used in the analyses, while Table 0.93 presents the optimized parameters and allowed ranges.

Table 0.92 nSIGHTS Input Parameters.

Parameter	Value	Units
Test zone radius	6.315	cm
Test zone compressibility	3.82E-10	1/Pa
Test zone fluid density	1085	g/L
Test zone length	5.03	m

Table 0.93 nSIGHTS Parameter Optimization Ranges.

Parameter	Minimum	Maximum	Units	Type
Formation hydraulic conductivity (K_f)	1E-15	1E-10	m/s	log
Formation pressure (P_f)	7000	10000	kPa	linear
Specific storage (Ss)	1E-08	1E-04	1/m	log
Skin hydraulic conductivity (K_s)	1E-15	1E-10	m/s	log
Skin thickness (t_s)	0.01	500	cm	linear

Figure 0.280 shows the measured test zone pressure record (with reduced data density for clarity) used in the analysis along with the best-fit simulation and parameter values. Figure 0.281 presents the pre-test history and Figure 0.282 shows the Ramey B normalized best-fit pressure and pressure derivatives.

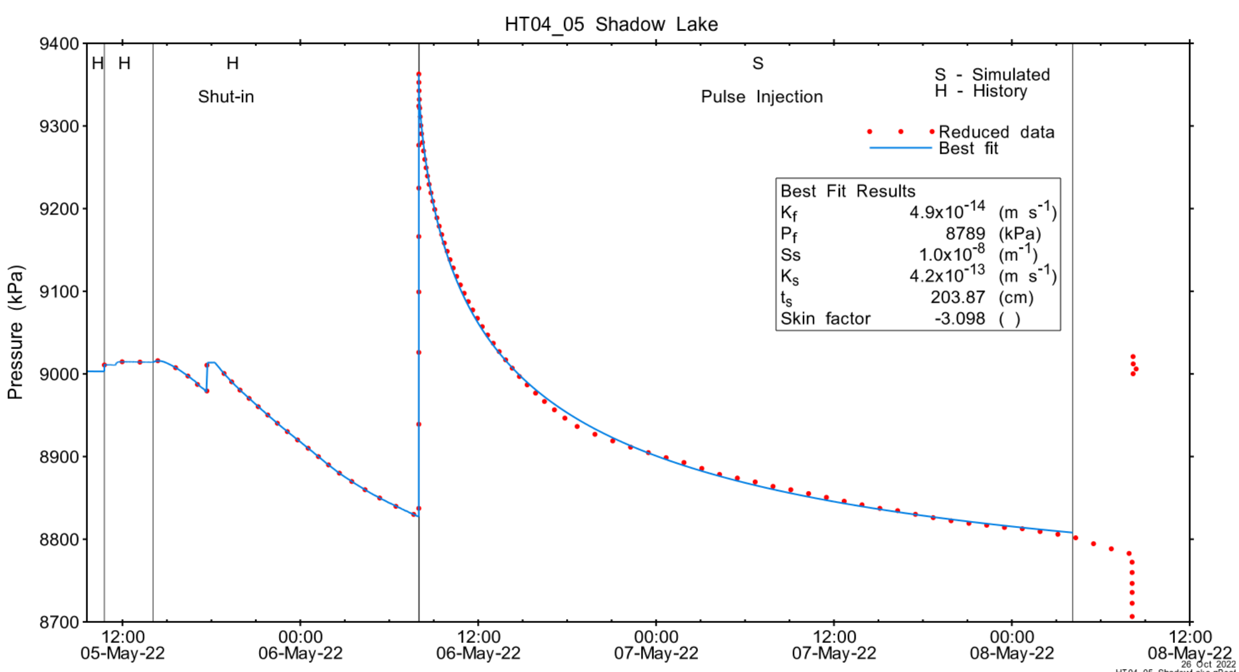

Figure 0.280 Annotated testing sequence showing best-fit simulation and parameter estimates.

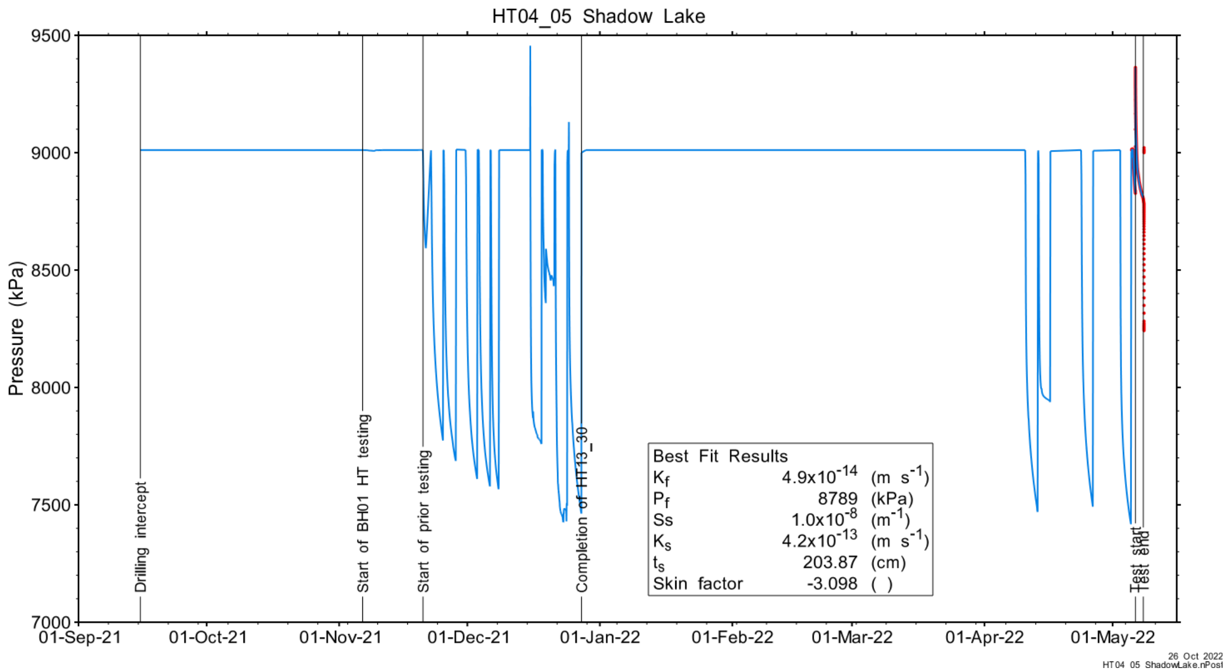

Figure 0.281 Annotated HT04_05 testing sequence showing pre-test history, best-fit simulation and parameter estimates.

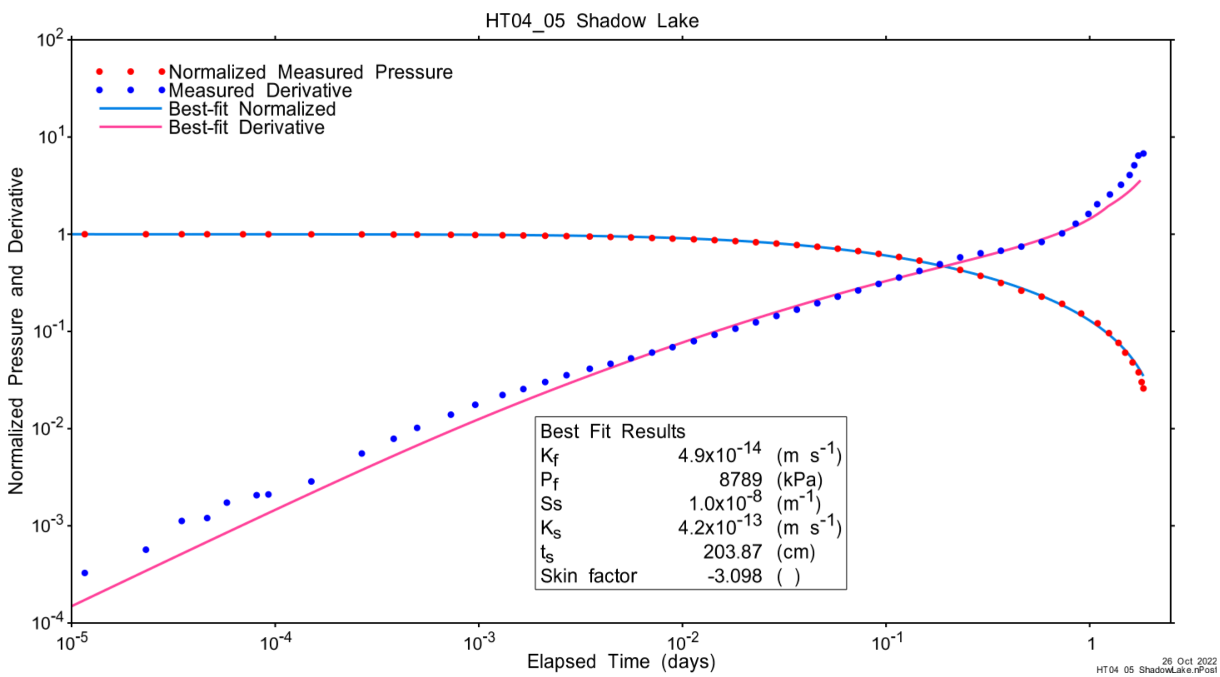

Figure 0.282 Log-log plot showing Ramey B normalized pressure and derivative response for best-fit simulation.

Figure 0.283 shows the normalized parameter sensitivity response for the best fit. Sensitivity for formation pressure was increasing at the end of the test.

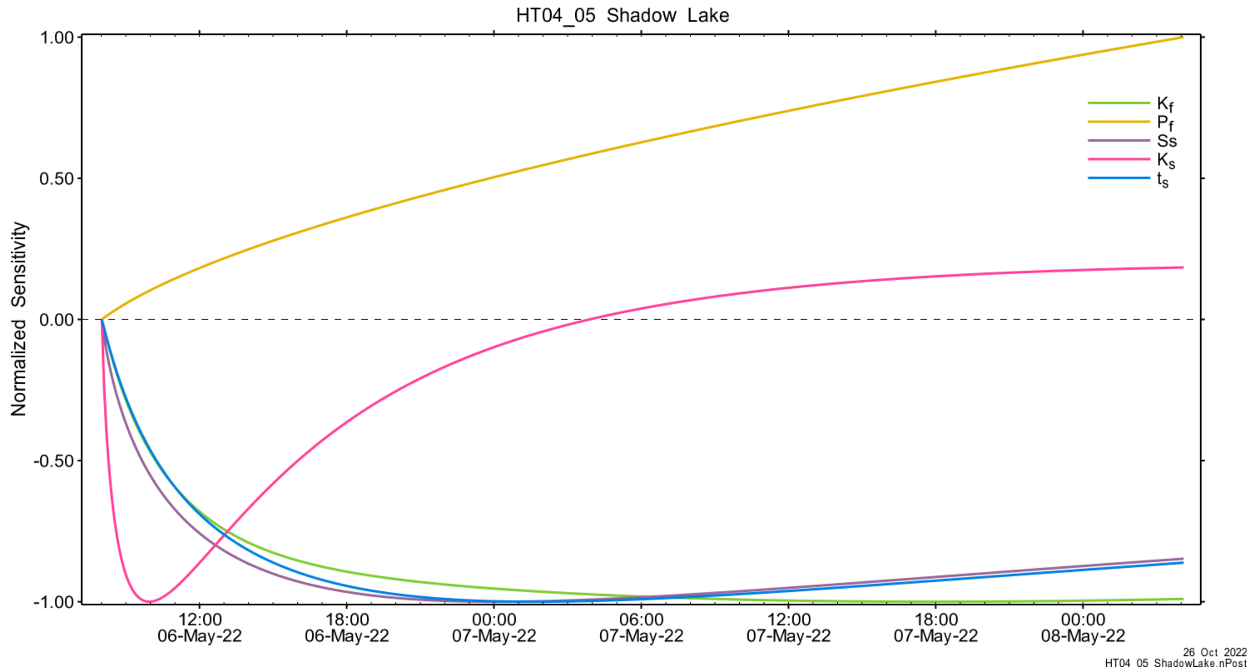

Figure 0.283 Normalized Jacobian for best-fit simulation.

A.19.3 Uncertainty Analyses

The CDF of normalized fit values for all converged simulations and the selected fit discriminant are shown in Figure 0.284.

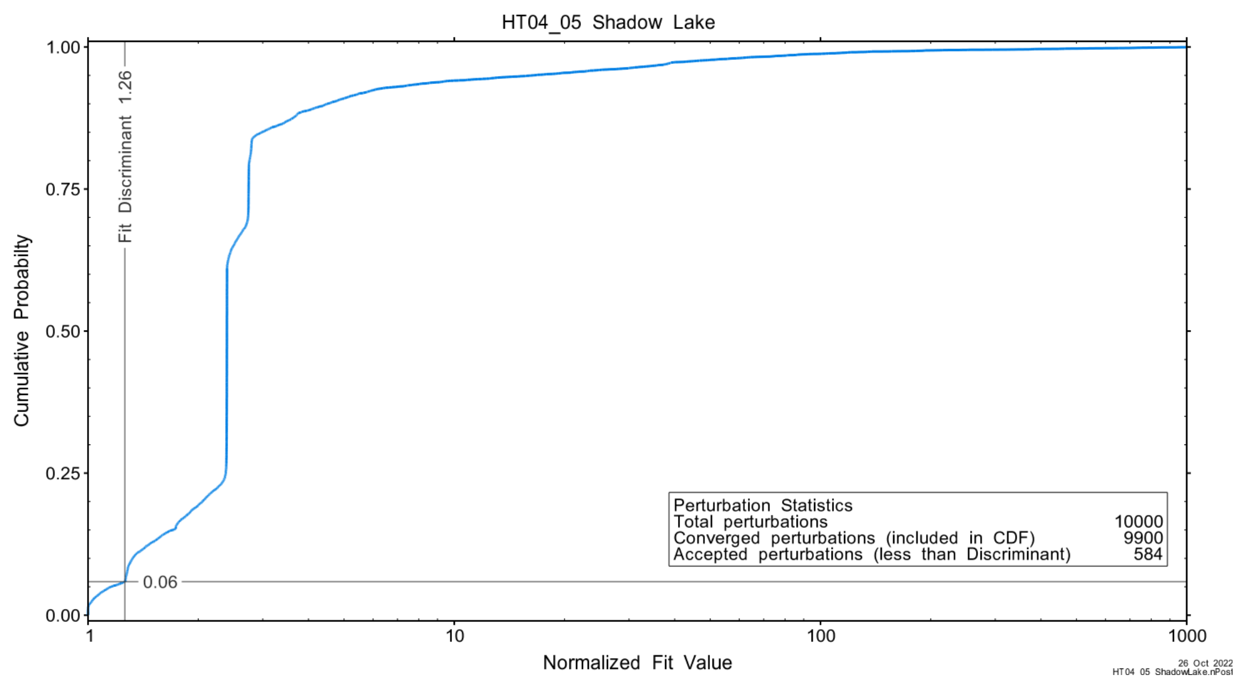

Figure 0.284 Fit value cumulative distribution function.

Summary cross parameter scatter plots for selected formation and skin parameters are given in Figure 0.285 and Figure 0.286. The light pink dots on the figures are the initial parameter estimates, with red dots overlaying those initial parameter values that resulted in accepted optimization results. The grey dots are converged optimizations which did not meet the fit discriminant. Larger varying color symbols represent the fit value of accepted optimizations, with the blue values representing the best fit.

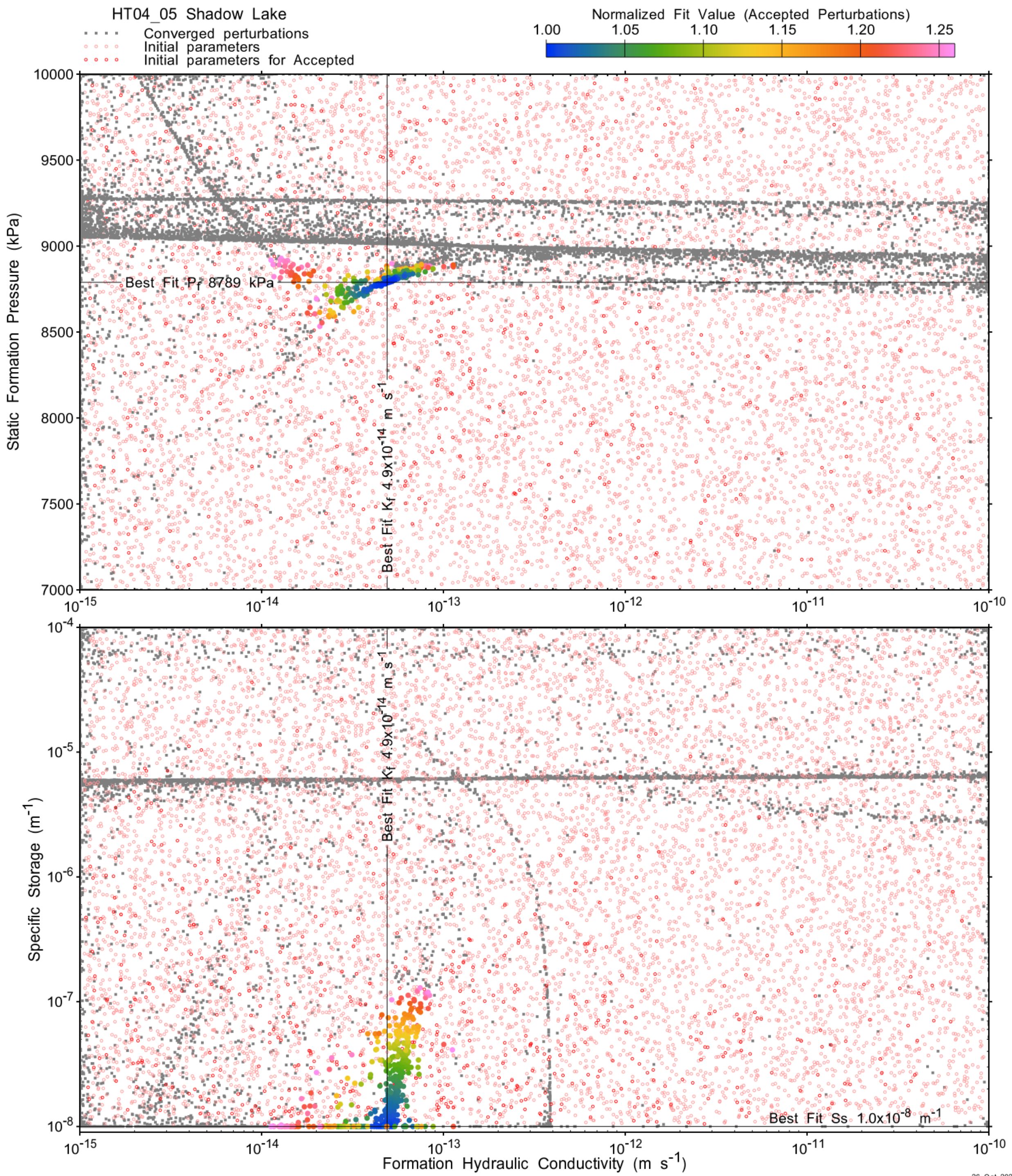

Figure 0.285 XY-scatter plot showing estimates of formation hydraulic conductivity (K_f) vs static formation pressure (P_f) (top panel) and specific storage (Ss) (bottom panel).

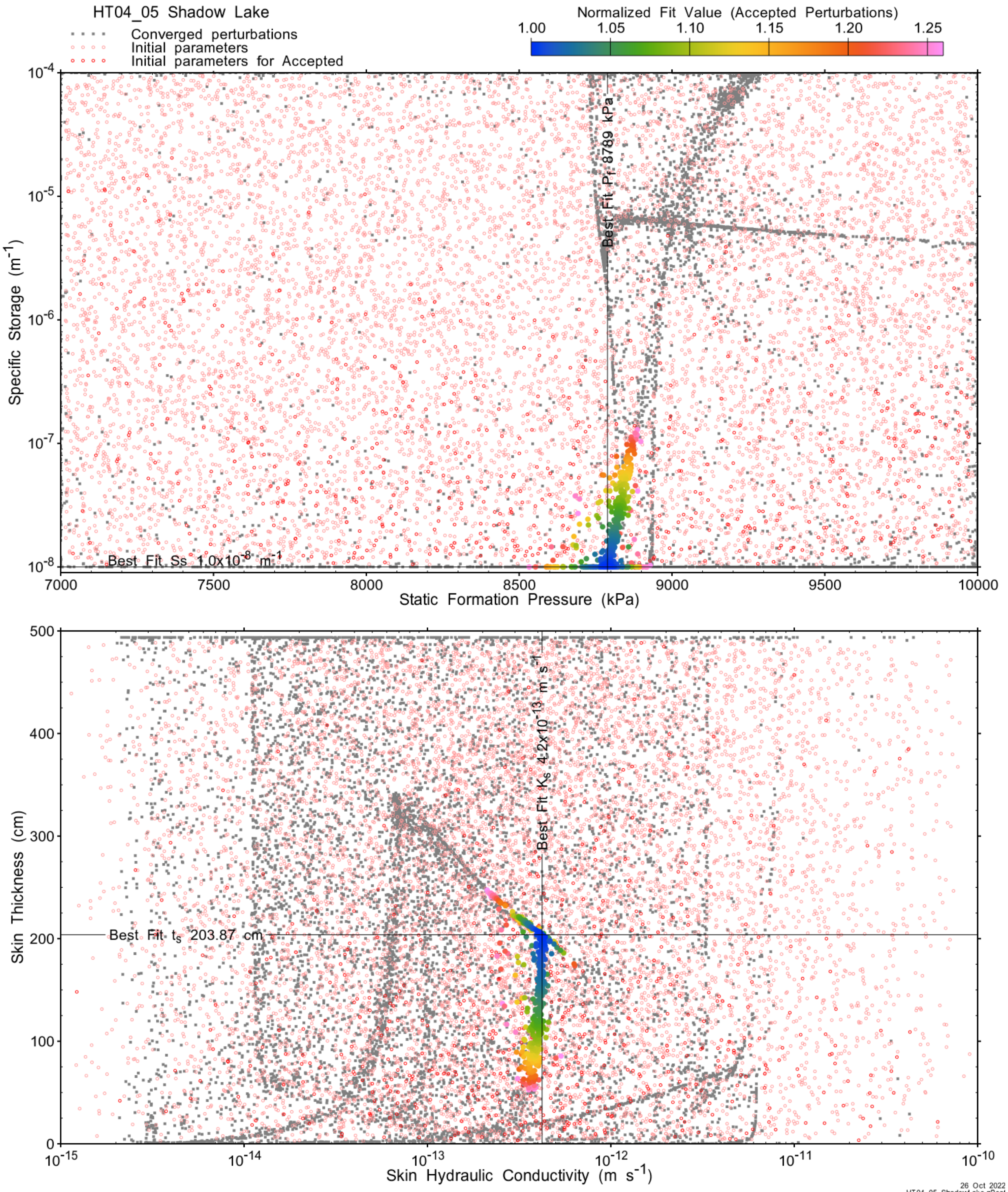

Figure 0.286 XY-scatter plot showing estimates of static formation pressure (P_f) vs specific storage (Ss) (top panel) and skin hydraulic conductivity (K_s) vs skin thickness (t_s) (bottom panel).

Confidence limits and median values are determined from the CDF of accepted optimization results (i.e. the varying color values in the above figures), with best fit value, 5% and 95% confidence indicated on Figure 0.287 and Figure 0.288.

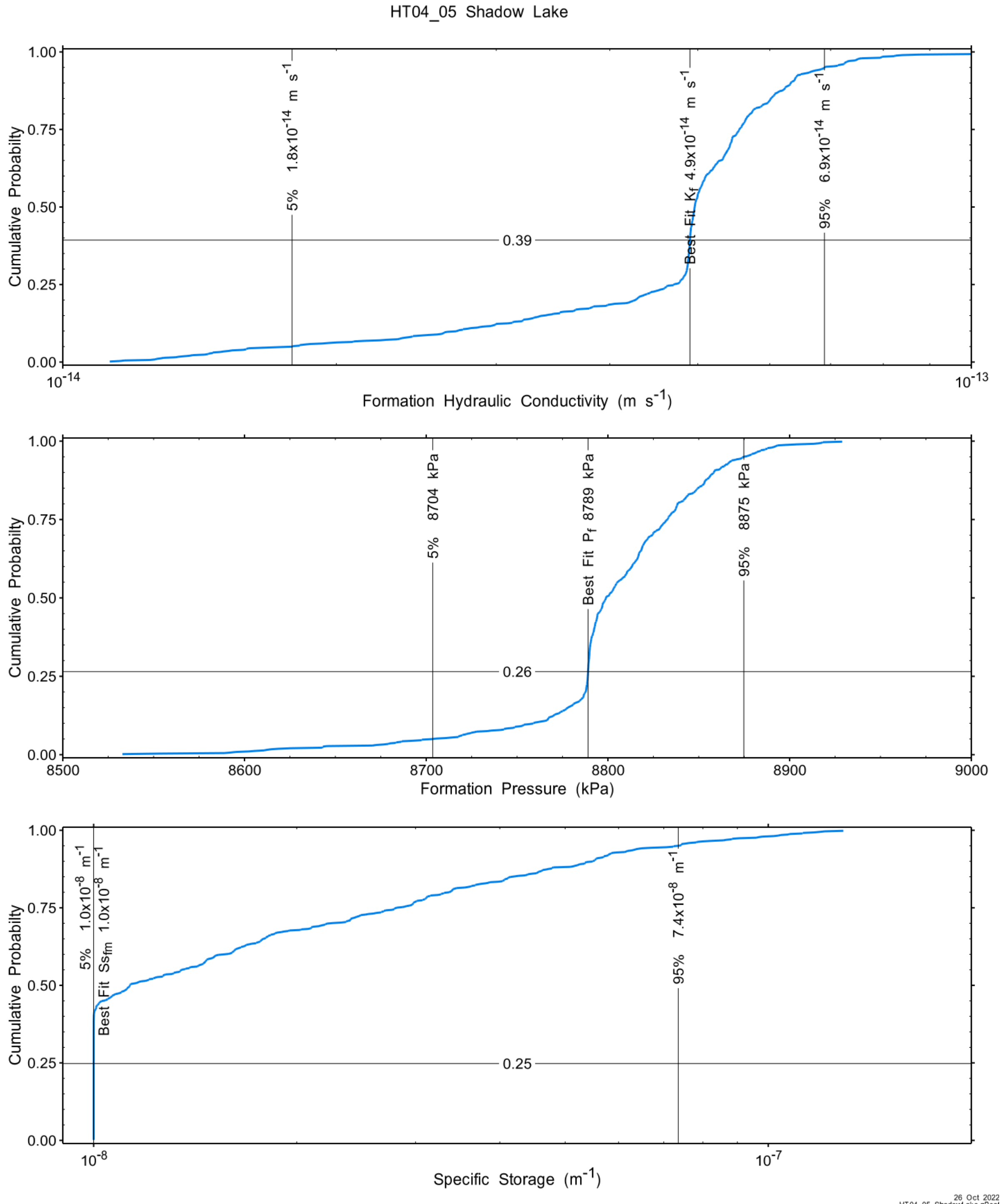

Figure 0.287 Cumulative distribution functions and parameter limits for formation hydraulic conductivity (K_f) (top panel), static formation pressure (P_f) (middle panel) and specific storage (Ss) (bottom panel).

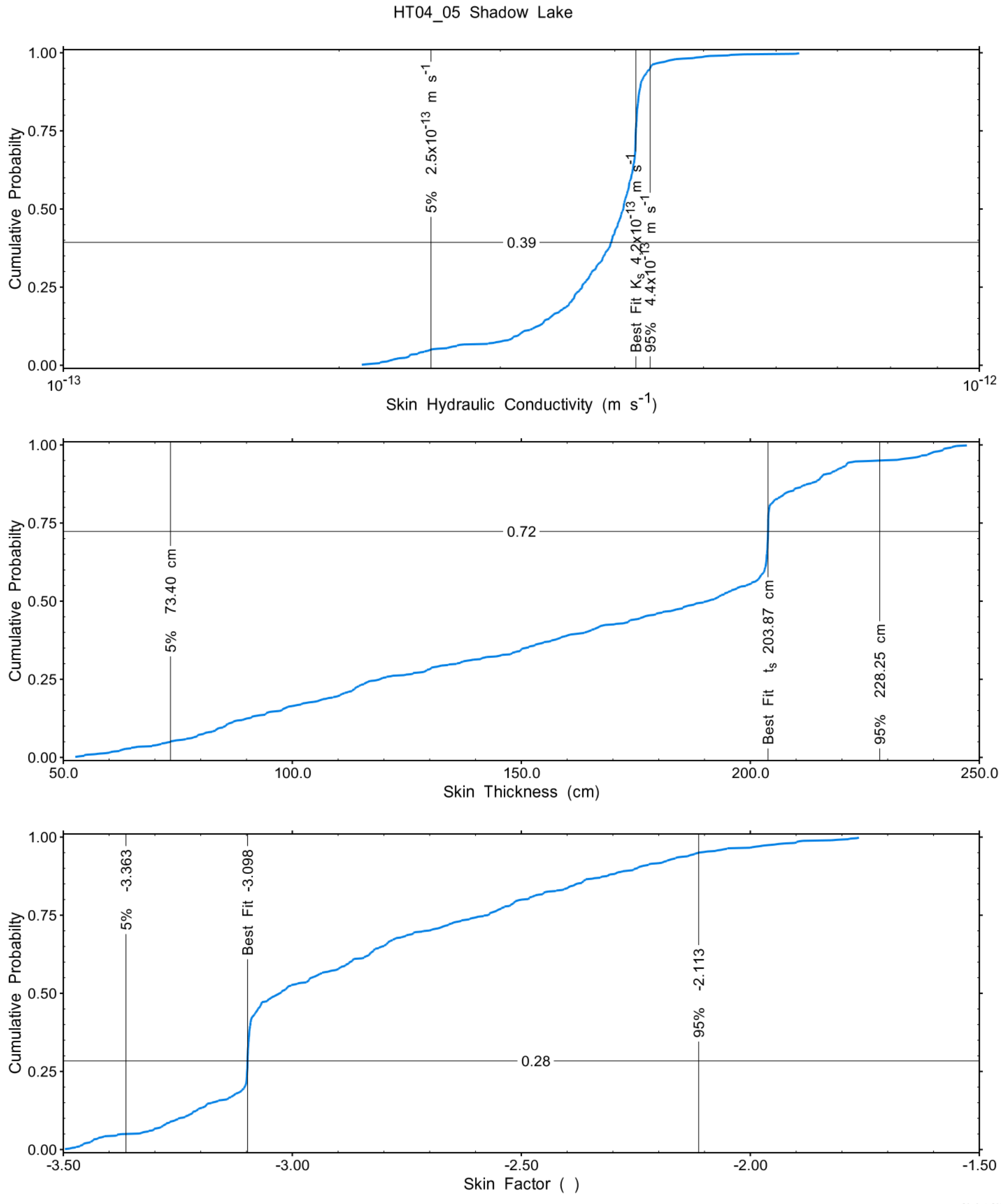

Figure 0.288 Cumulative distribution functions and parameter limits for skin hydraulic conductivity (K_s) (top panel), skin thickness (t_s) (middle panel) and skin factor (s) (bottom panel).

A summary of perturbation results is presented in Figure 0.289, with Ramey-processed perturbations in Figure 0.290. Those perturbations (441 of 10,000) with all parameters within the 5% and 95% range present a very good fit to the measured test zone data.

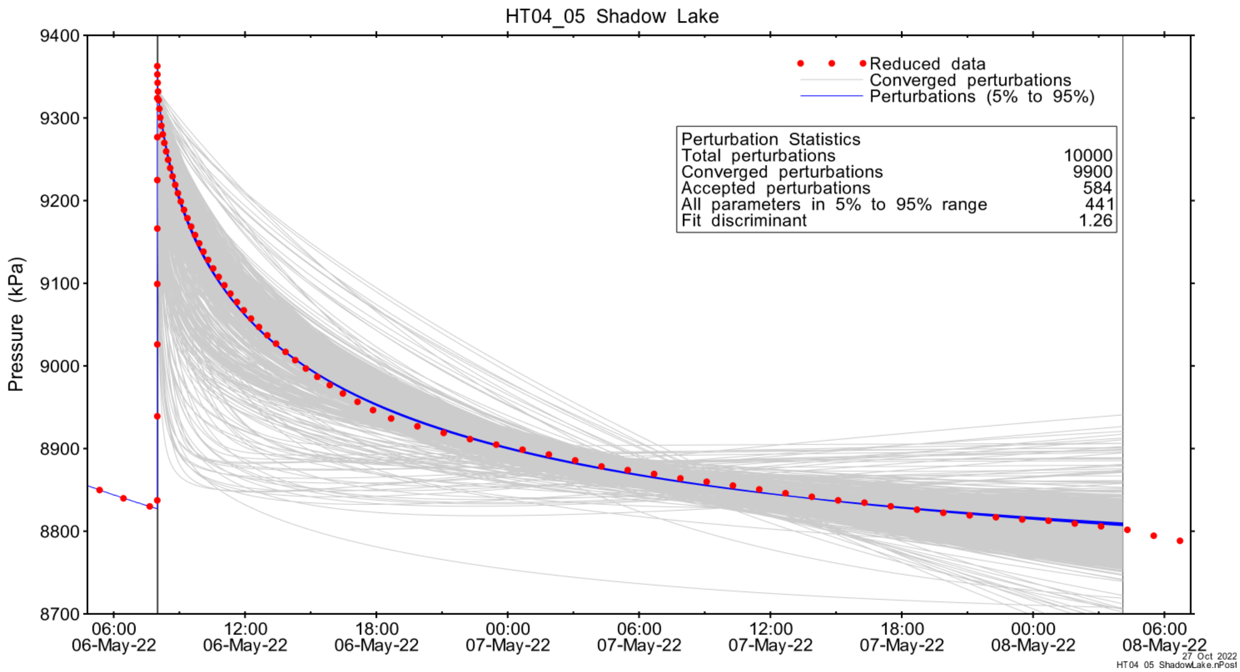

Figure 0.289 Perturbation results – all converged, accepted, and within 5% to 95% for all parameters.

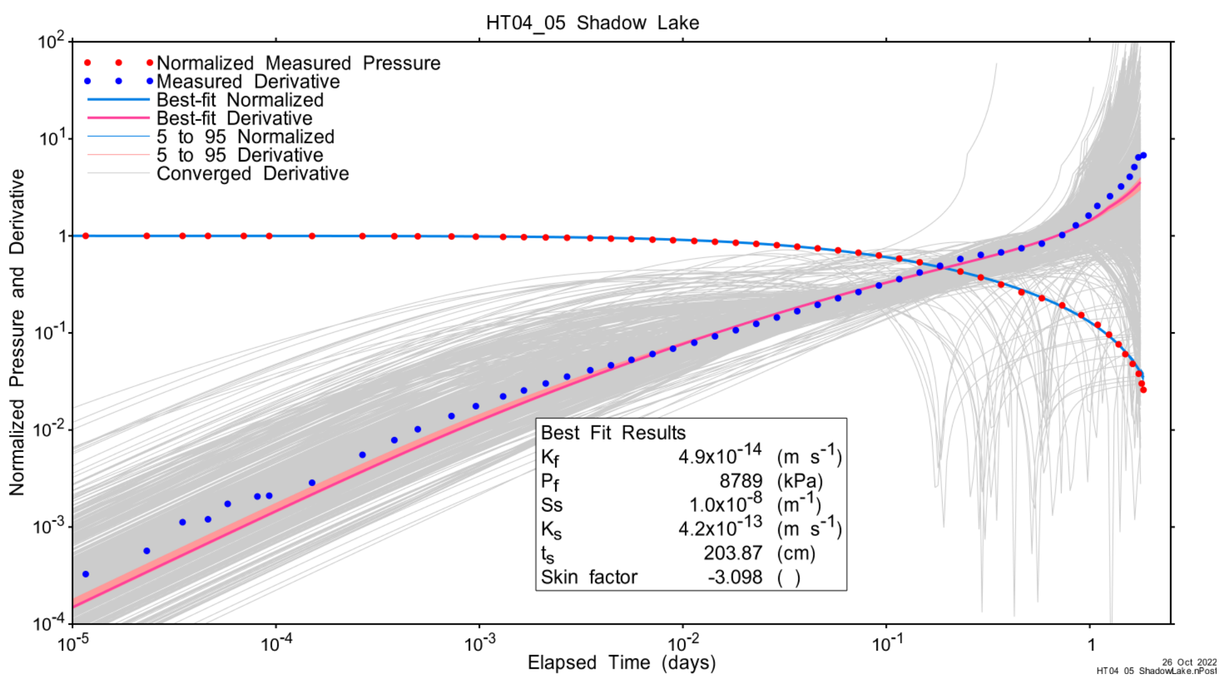

Figure 0.290 Log-log plot showing Ramey B normalized pressure and derivative response for all converged optimizations and those within 5% to 95% for all parameters.

A summary of best-fit parameter estimates and ranges is given in Table 0.94.

Table 0.94 Summary of the HT04_05 parameter estimates.

Parameter	Best Fit	5%	Median	95%
K_f (m/s)	4.9E-14	1.8E-14	5.0E-14	6.9E-14
P_f (kPa)	8789	8704	8799	8875
Ss (1/m)	1.0E-08	1.0E-08	1.1E-08	7.4E-08
K_s (m/s)	4.2E-13	2.5E-13	4.1E-13	4.4E-13
t_s (cm)	203.87	73.40	190.58	228.25
s (-)	-3.098	-3.363	-3.028	-2.113

Parameter correlations for all perturbations with all parameters within the 5% to 95% limits are given in Table 0.95.

Table 0.95 Pearson cross-correlations of 5% to 95% parameters

	Log(K_f)	P_f	Log(Ss)	Log(K_s)	t_s	s
Log(K_f)	1.000	0.773	0.490	0.567	-0.563	0.612
P_f	0.773	1.000	0.729	0.081	-0.755	0.790
Log(Ss)	0.490	0.729	1.000	-0.436	-0.990	0.989
Log(K_s)	0.567	0.081	-0.436	1.000	0.343	-0.300
t_s	-0.563	-0.755	-0.990	0.343	1.000	-0.992
s	0.612	0.790	0.989	-0.300	-0.992	1.000

A.19.4 Additional Figures

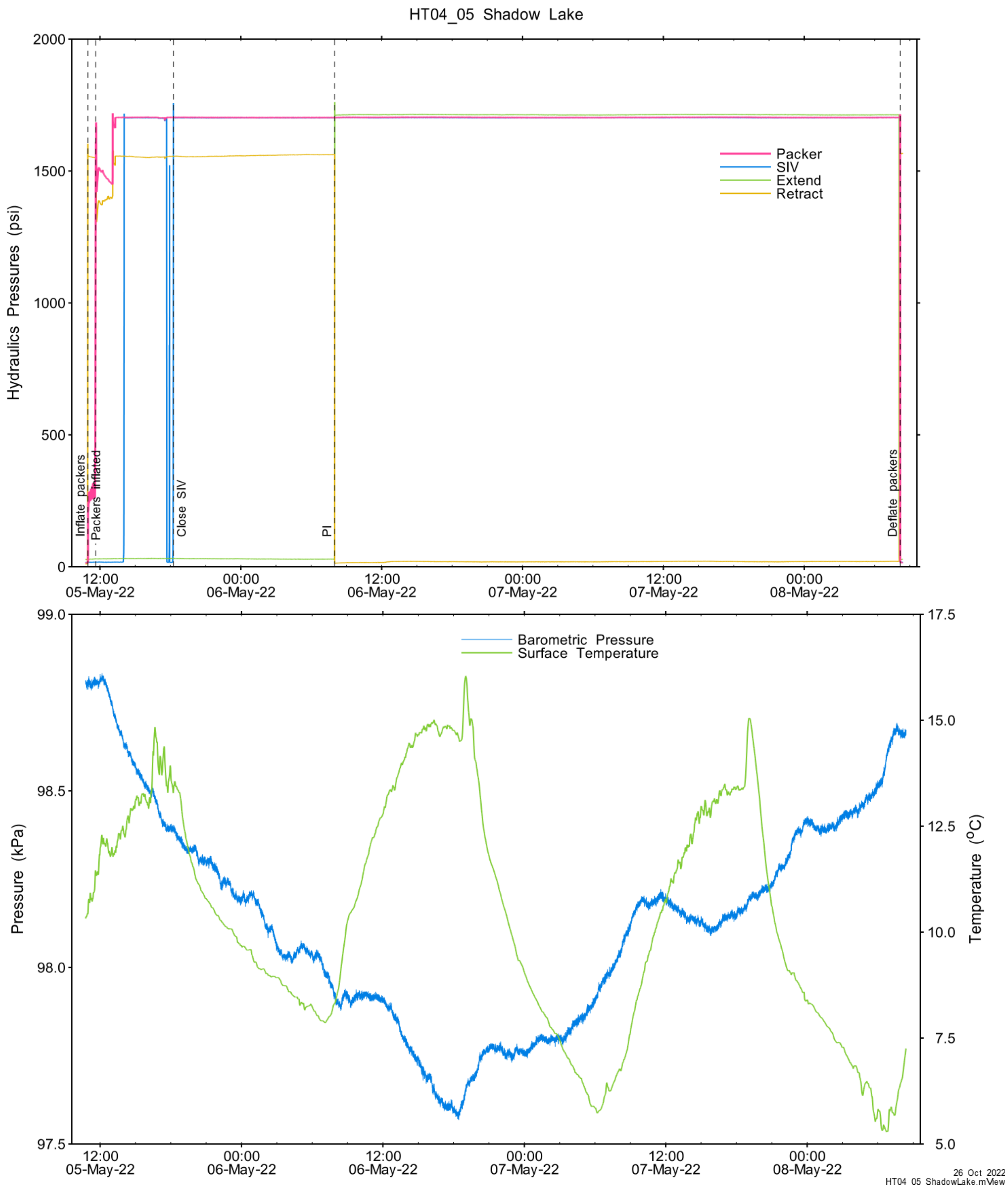

Figure 0.291 Hydraulics pressures and surface temperature/barometric pressure.

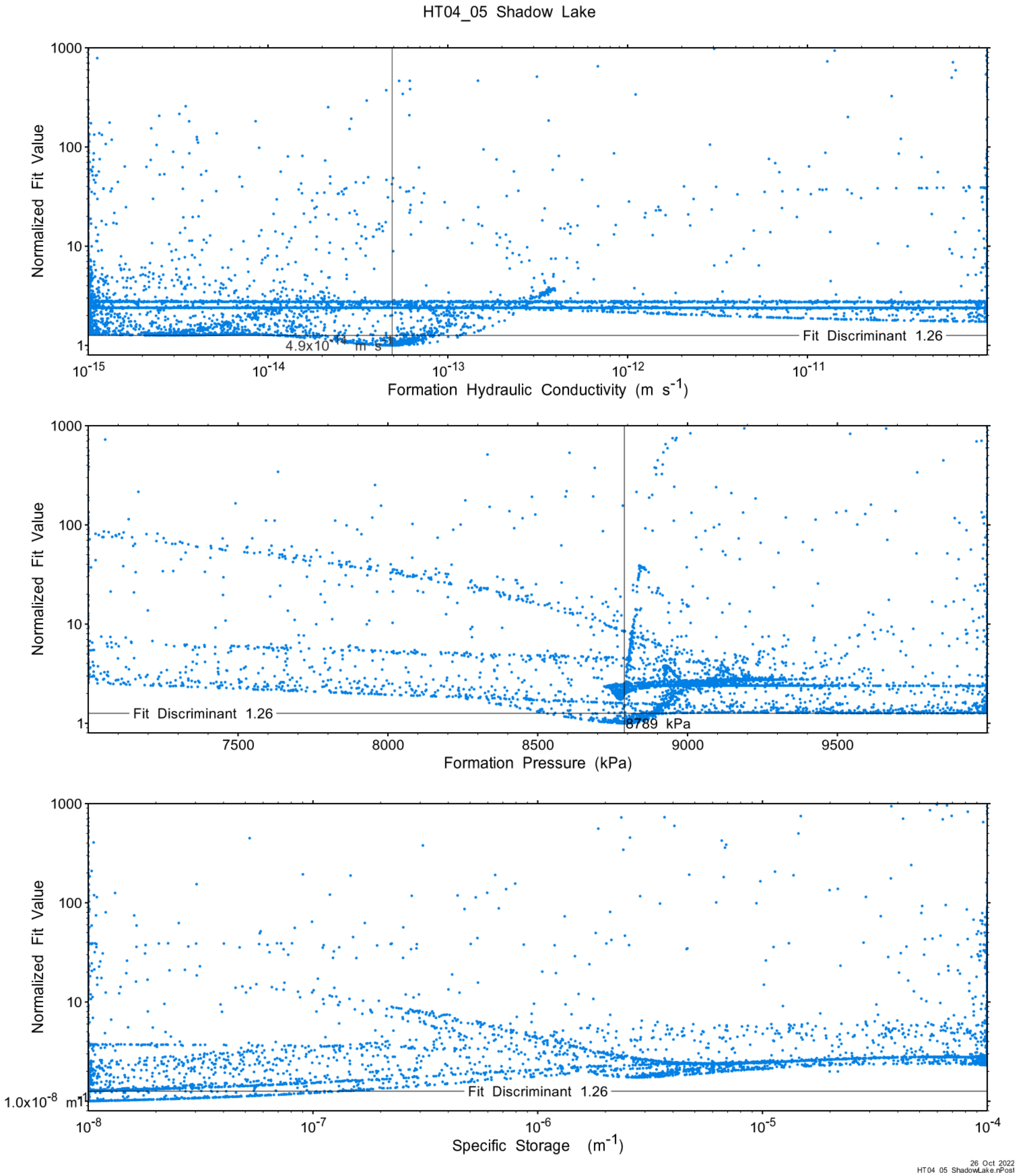

Figure 0.292 XY-scatter plot showing the formation parameter space normalized fit values.

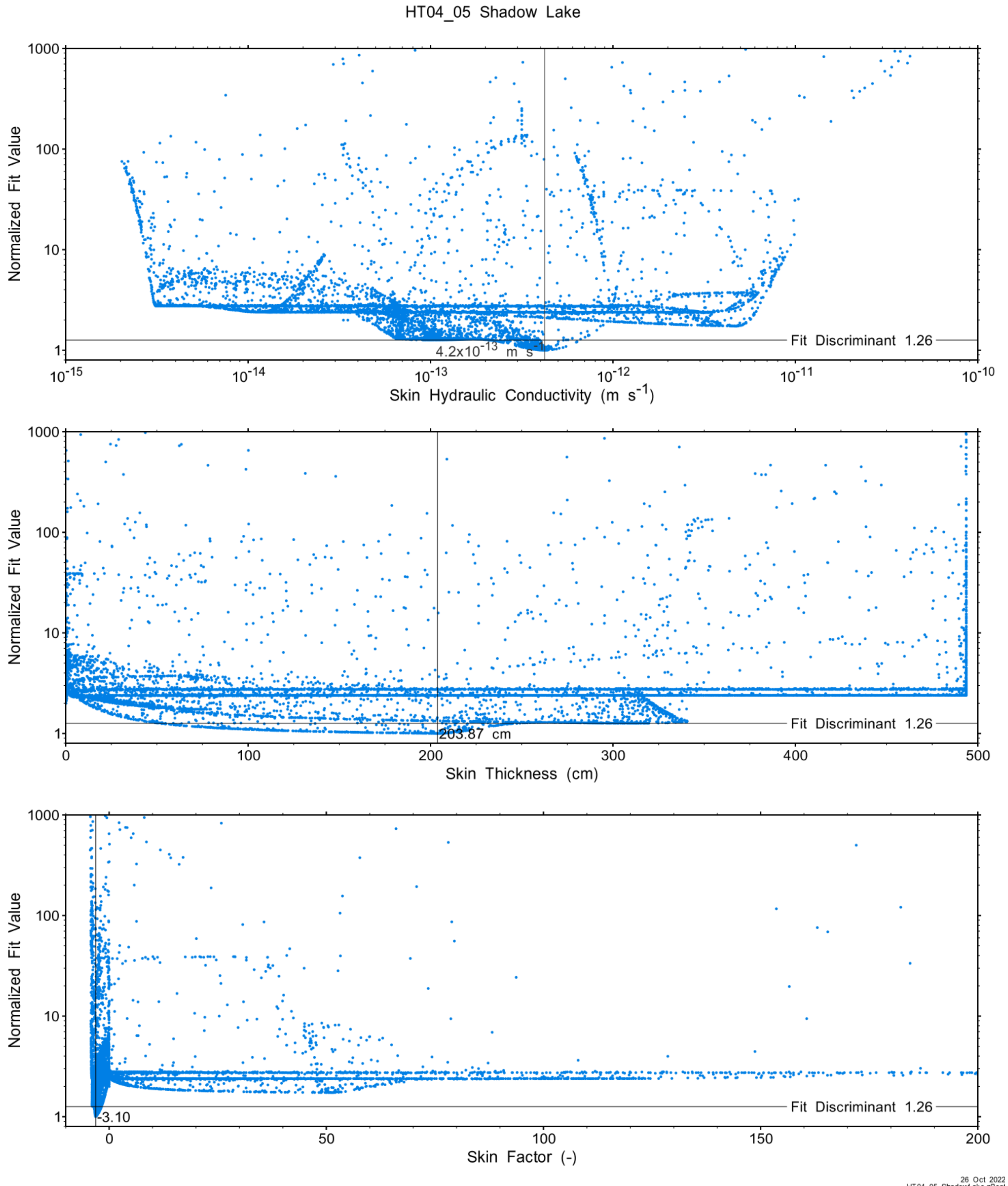

Figure 0.293 XY-scatter plot showing the skin parameter space normalized fit values.

A.20 HT05_05 Precambrian

The SB_BH01 interval from 864.00 to 869.03 mBGS tested in HT05_05 consists of 5 m of the Precambrian Grenville Province, starting approximately 3.65 m below the top of the Precambrian. A single PI test was performed.

A.20.1 Test Data Summary

Table 0.96 and Figure 0.294 provide a summary of test events and a plot of pressures measured while testing, respectively. The test was terminated by opening the shut-in valve after a two-day duration.

Table 0.96 HT05_05 Summary of Test Events.

Event	Start Date & Time	Duration (days)	TZ Pressure (kPa)
Drilling intercept	21-09-15 17:00	65.91	9025
Prior testing	21-11-20 14:45	169.77	variable
Shut-in	22-05-09 09:19	0.95	9028
Pulse injection	22-05-10 08:04	2.00	8965
Test end	22-05-12 08:03		8320

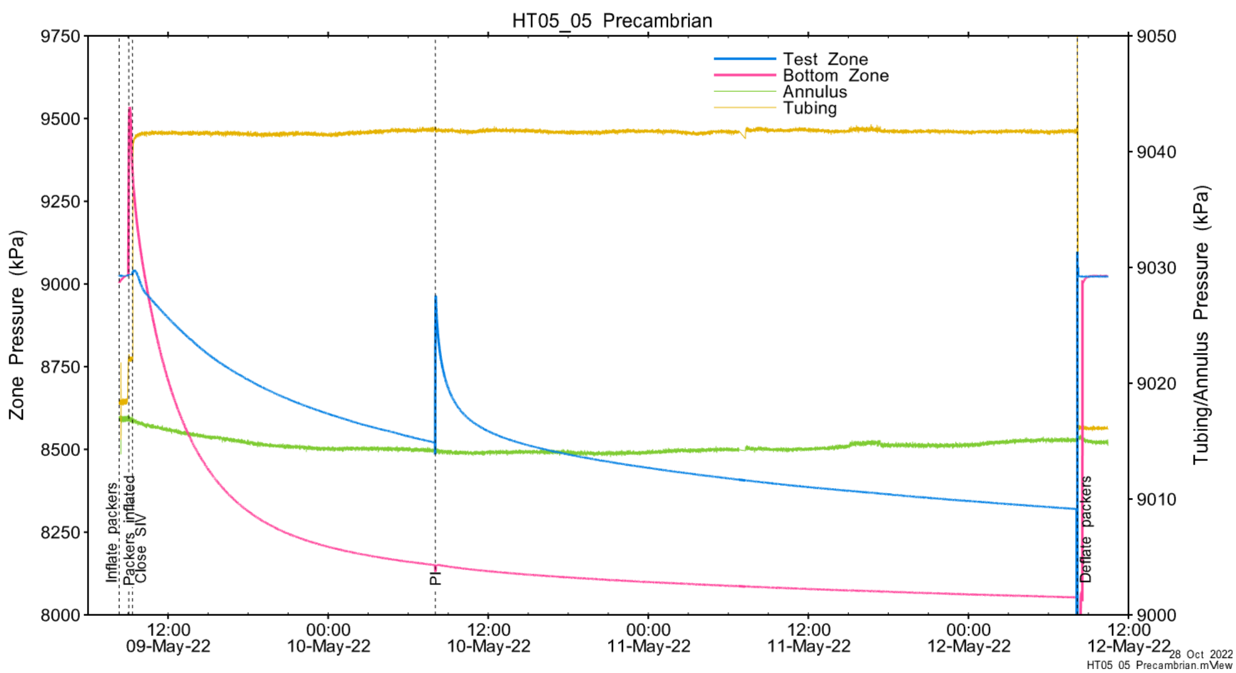

Figure 0.294 HT05_05 test events and pressures.

A.20.2 Test Analyses

Table 0.97 is a summary of test-specific input parameters used in the analyses, while Table 0.98 presents the optimized parameters and allowed ranges.

Table 0.97 nSIGHTS Input Parameters.

Parameter	Value	Units
Test zone radius	6.197	cm
Test zone compressibility	3.93E-10	1/Pa
Test zone fluid density	1086	g/L
Test zone length	5.03	m

Table 0.98 nSIGHTS Parameter Optimization Ranges.

Parameter	Minimum	Maximum	Units	Type
Formation hydraulic conductivity (K_f)	1E-15	1E-10	m/s	log
Formation pressure (P_f)	4000	9000	kPa	linear
Specific storage (Ss)	1E-08	1E-04	1/m	log
Skin hydraulic conductivity (K_s)	1E-15	1E-10	m/s	log
Skin thickness (t_s)	0.01	500	cm	linear

Figure 0.295 shows the measured test zone pressure record (with reduced data density for clarity) used in the analysis along with the best-fit simulation and parameter values. Figure 0.296 presents the pre-test history and Figure 0.297 shows the Ramey B normalized best-fit pressure and pressure derivatives.

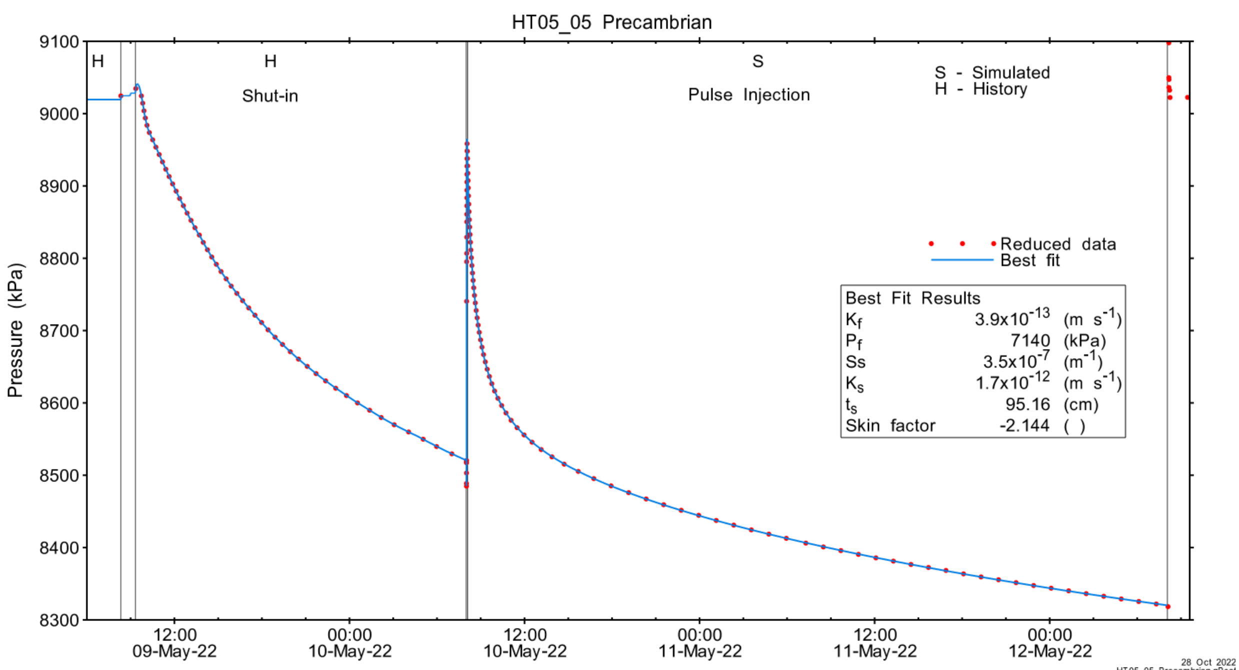

Figure 0.295 Annotated testing sequence showing best-fit simulation and parameter estimates.

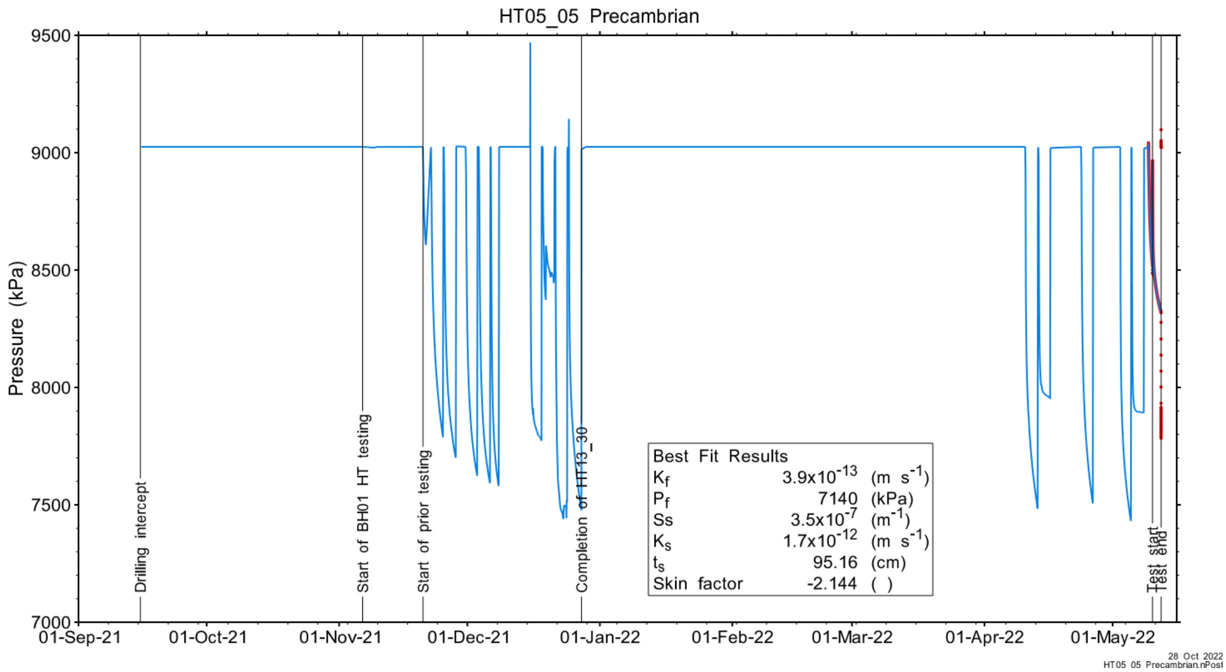

Figure 0.296 Annotated HT05_05 testing sequence showing pre-test history, best-fit simulation and parameter estimates.

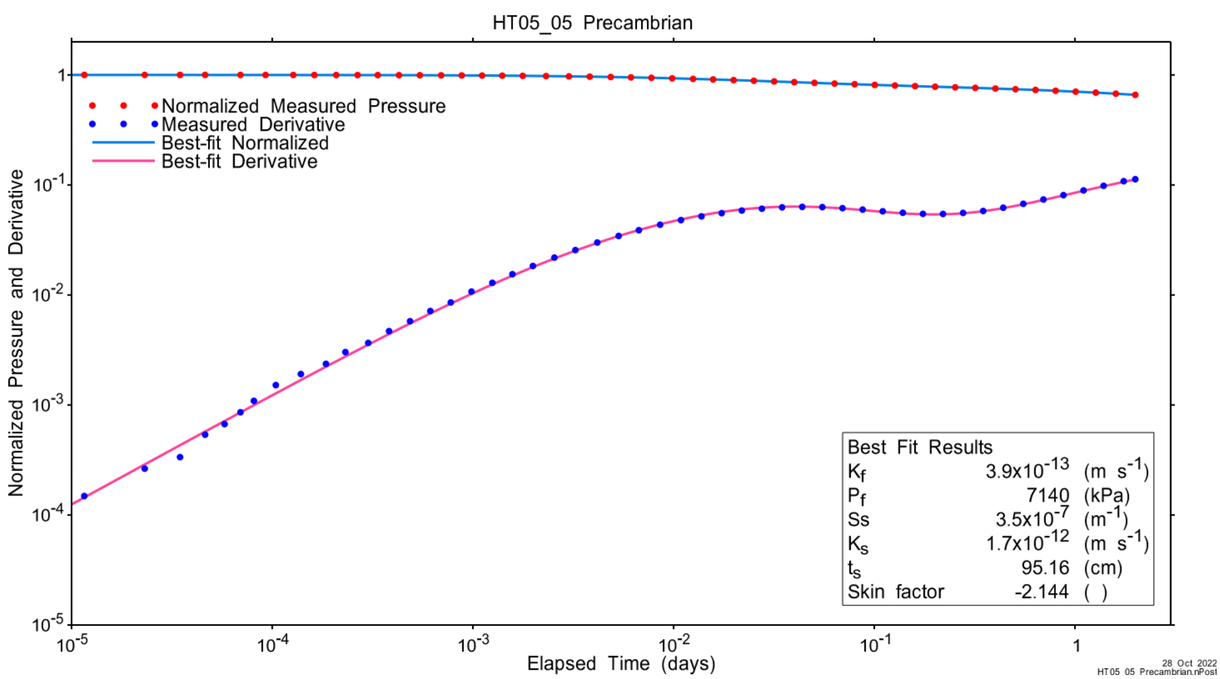

Figure 0.297 Log-log plot showing Ramey B normalized pressure and derivative response for best-fit simulation.

Figure 0.298 shows the normalized parameter sensitivity response for the best fit. Sensitivity for all parameters was increasing at the end of the test.

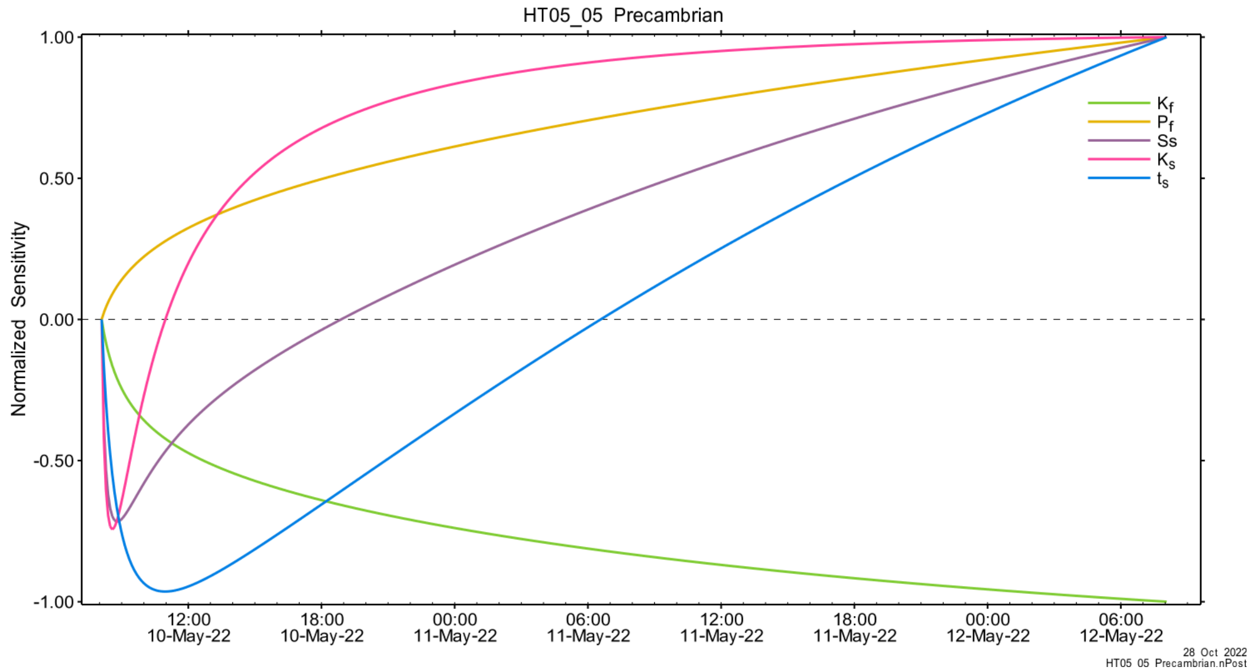

Figure 0.298 Normalized Jacobian for best-fit simulation.

A.20.3 Uncertainty Analyses

The CDF of normalized fit values for all converged simulations and the selected fit discriminant are shown in Figure 0.299.

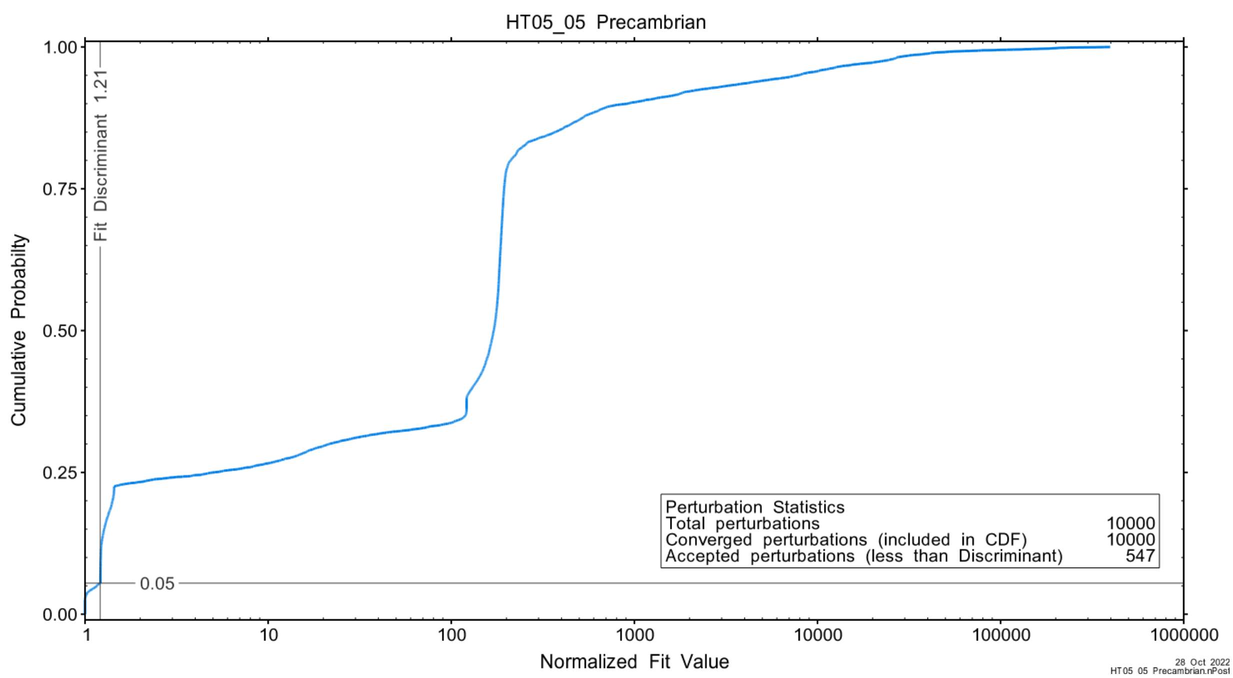

Figure 0.299 Fit value cumulative distribution function.

Summary cross parameter scatter plots for selected formation and skin parameters are given in Figure 0.300 and Figure 0.301. The light pink dots on the figures are the initial parameter estimates, with red dots overlaying those initial parameter values that resulted in accepted optimization results. The grey dots are converged optimizations which did not meet the fit discriminant. Larger varying color symbols represent the fit value of accepted optimizations, with the blue values representing the best fit.

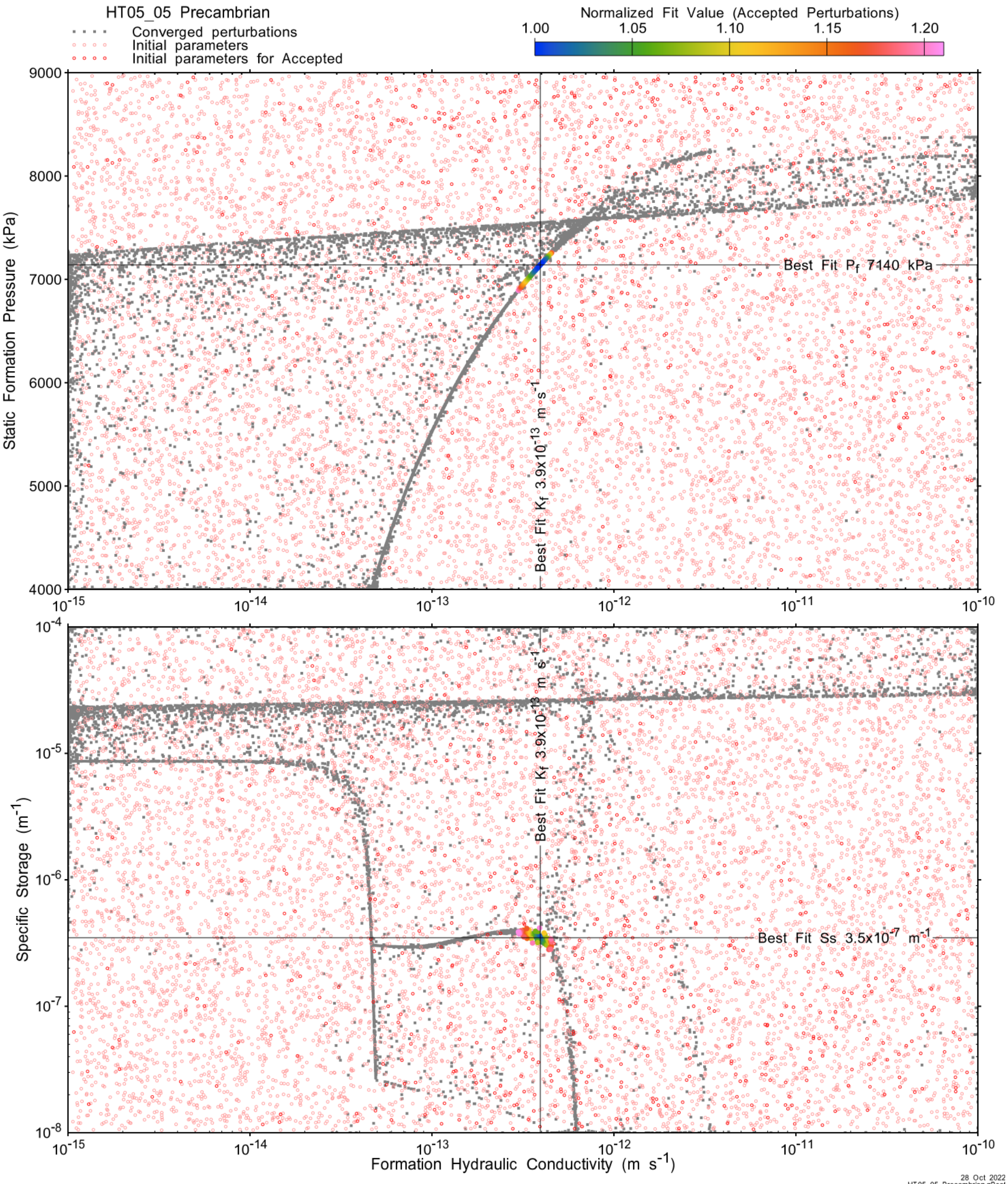

Figure 0.300 XY-scatter plot showing estimates of formation hydraulic conductivity (K_f) vs static formation pressure (P_f) (top panel) and specific storage (Ss) (bottom panel).

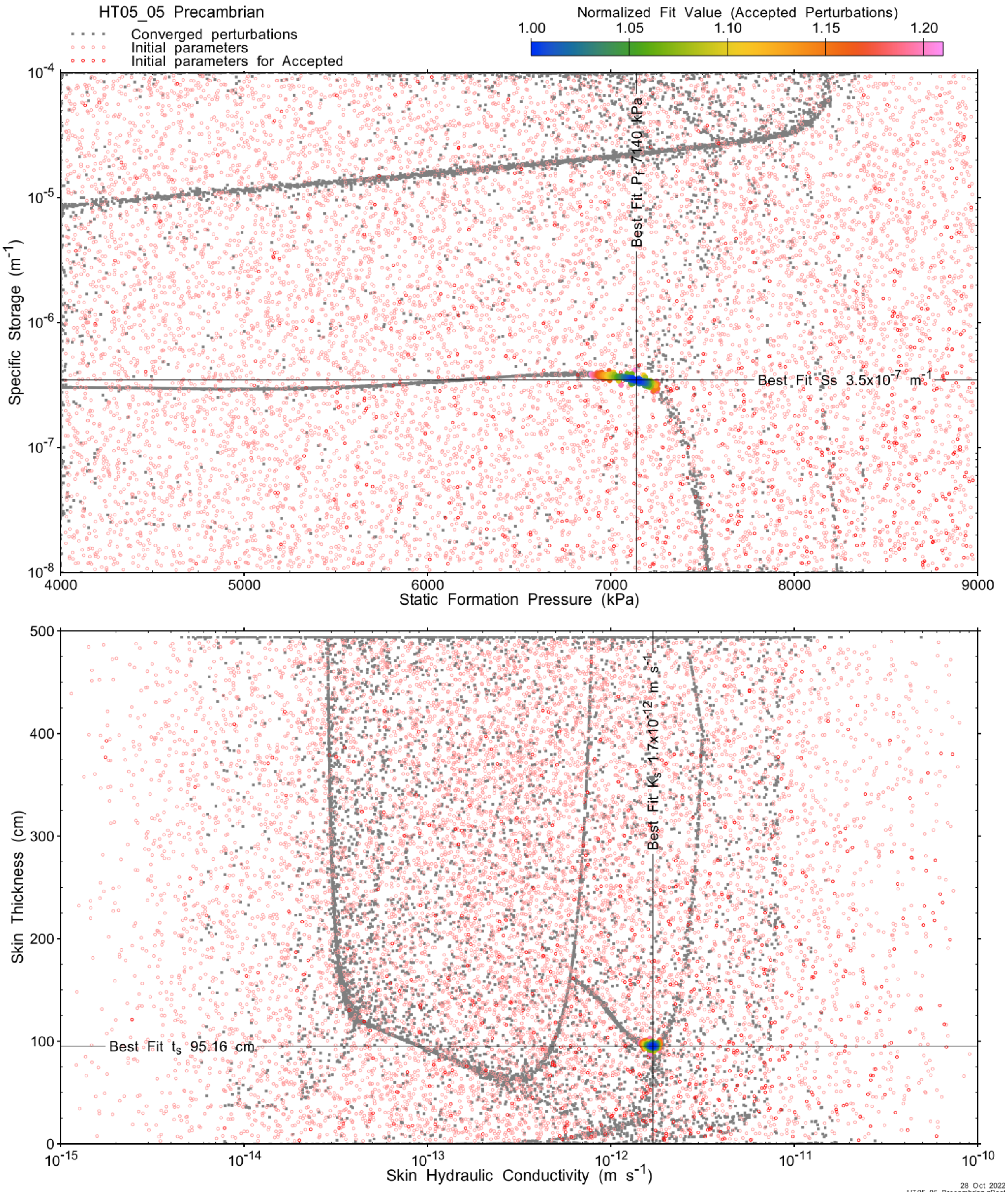

Figure 0.301 XY-scatter plot showing estimates of static formation pressure (P_f) vs specific storage (Ss) (top panel) and skin hydraulic conductivity (K_s) vs skin thickness (t_s) (bottom panel).

Confidence limits and median values are determined from the CDF of accepted optimization results (i.e. the varying color values in the above figures), with best fit value, 5% and 95% confidence indicated on Figure 0.302 and Figure 0.303.

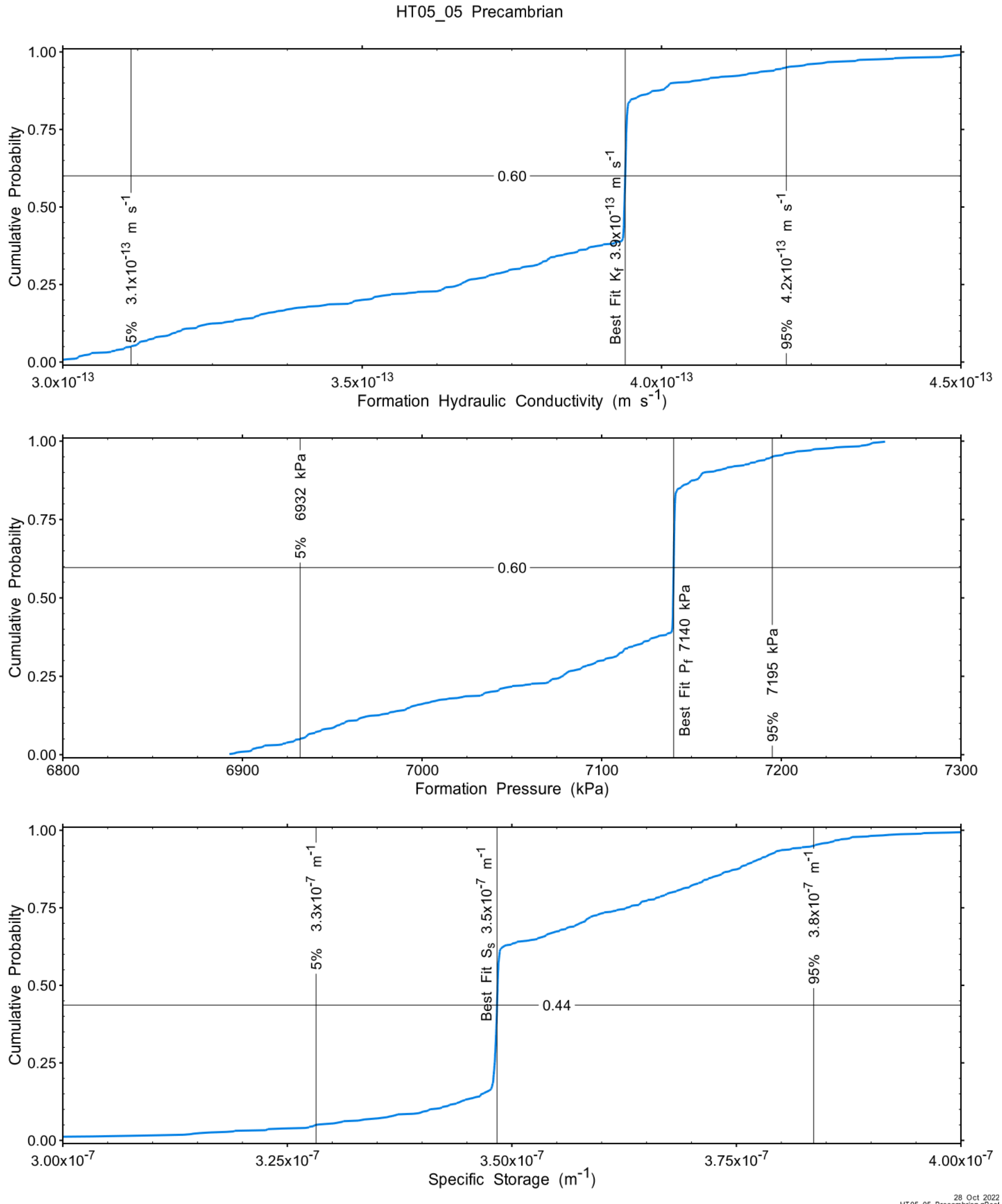

Figure 0.302 Cumulative distribution functions and parameter limits for formation hydraulic conductivity (K_f) (top panel), static formation pressure (P_f) (middle panel) and specific storage (Ss) (bottom panel).

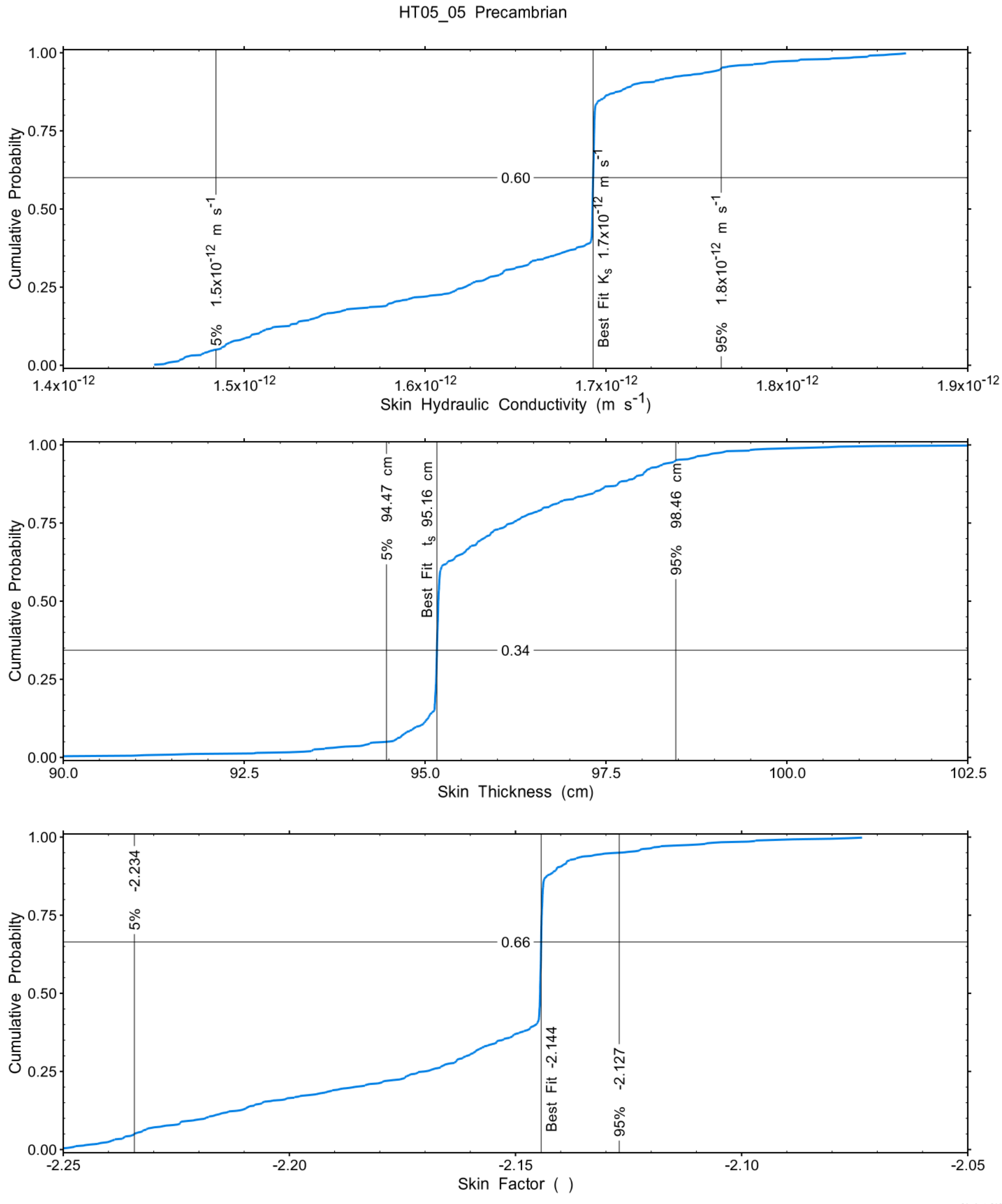

Figure 0.303 Cumulative distribution functions and parameter limits for skin hydraulic conductivity (K_s) (top panel), skin thickness (t_s) (middle panel) and skin factor (s) (bottom panel).

A summary of perturbation results is presented in Figure 0.304, with Ramey-processed perturbations in Figure 0.305. Those perturbations (444 of 10,000) with all parameters within the 5% and 95% range present a very good fit to the measured test zone data.

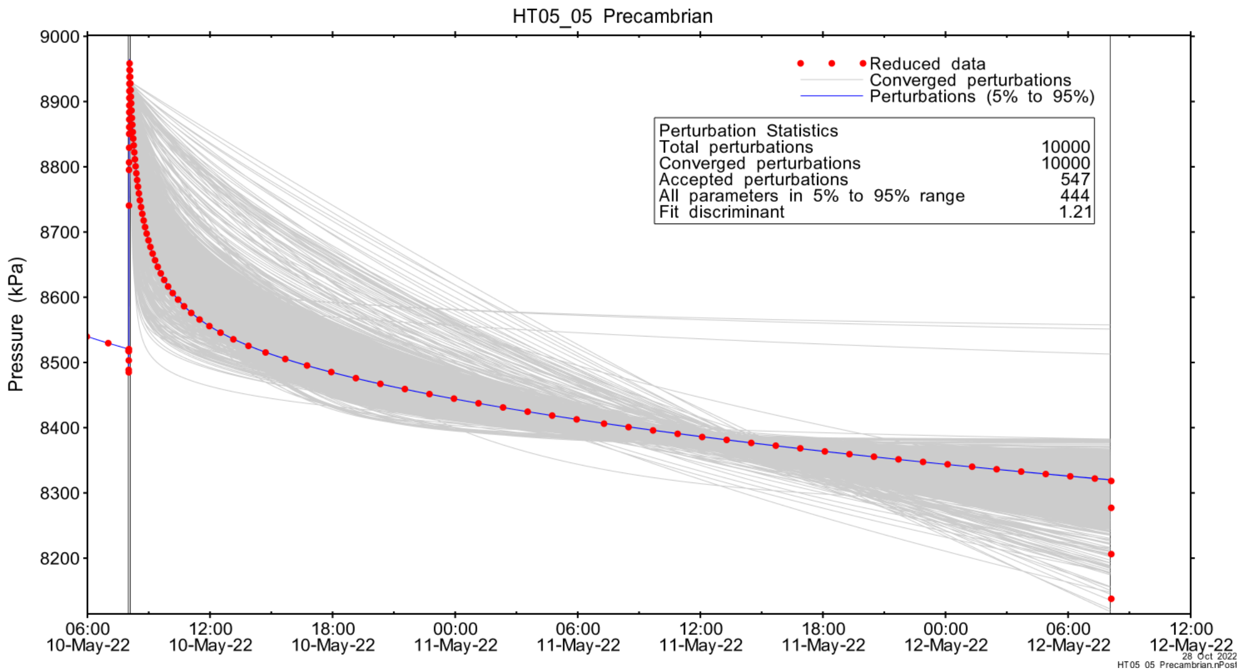

Figure 0.304 Perturbation results – all converged, accepted, and within 5% to 95% for all parameters.

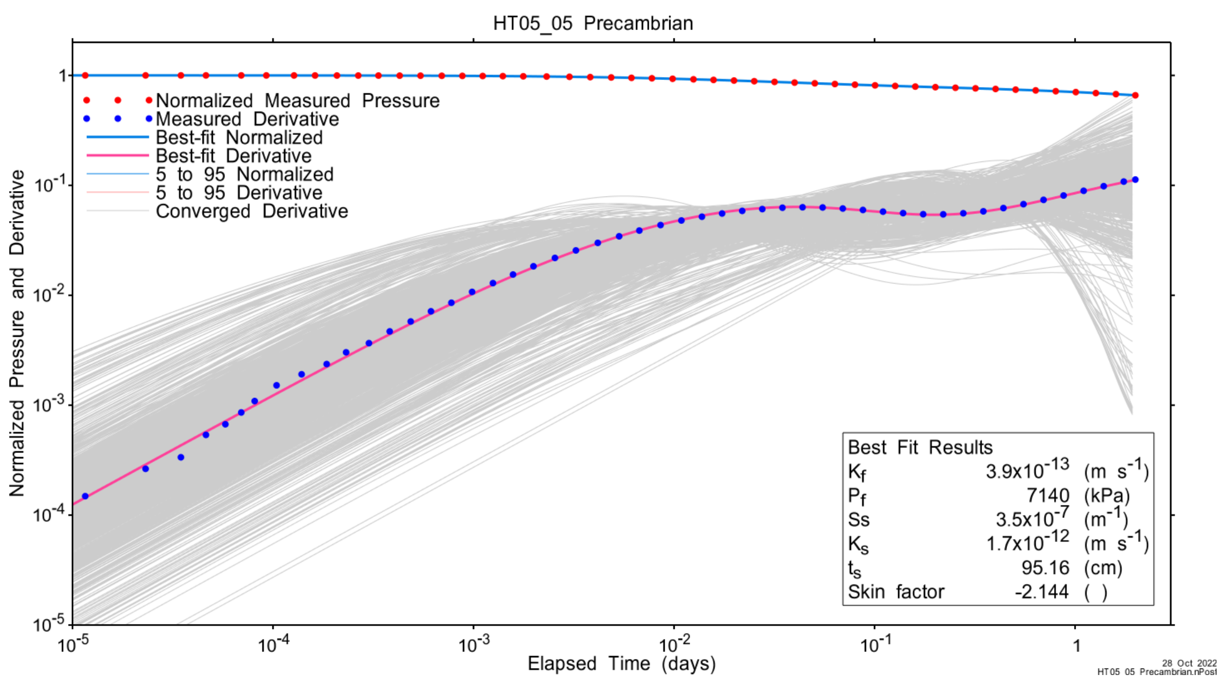

Figure 0.305 Log-log plot showing Ramey B normalized pressure and derivative response for all converged optimizations and those within 5% to 95% for all parameters.

A summary of best-fit and parameter ranges is given in Table 0.99.

Table 0.99 Summary of the HT05_05 parameter estimates.

Parameter	Best Fit	5%	Median	95%
K_f (m/s)	3.9E-13	3.1E-13	3.9E-13	4.2E-13
P_f (kPa)	7140	6932	7140	7195
Ss (1/m)	3.5E-07	3.3E-07	3.5E-07	3.8E-07
K_s (m/s)	1.7E-12	1.5E-12	1.7E-12	1.8E-12
t_s (cm)	95.16	94.47	95.18	98.46
s (-)	-2.144	-2.234	-2.145	-2.127

Parameter correlations for all perturbations with all parameters within the 5% to 95% limits are given in Table 0.100.

Table 0.100 Pearson cross-correlations of 5% to 95% parameters

	Log(K_f)	P_f	Log(Ss)	Log(K_s)	t_s	s
Log(K_f)	1.000	1.000	-0.946	0.999	-0.893	0.989
P_f	1.000	1.000	-0.944	0.999	-0.896	0.990
Log(Ss)	-0.946	-0.944	1.000	-0.957	0.702	-0.888
Log(K_s)	0.999	0.999	-0.957	1.000	-0.877	0.983
t_s	-0.893	-0.896	0.702	-0.877	1.000	-0.950
s	0.989	0.990	-0.888	0.983	-0.950	1.000

A.20.4 Additional Figures

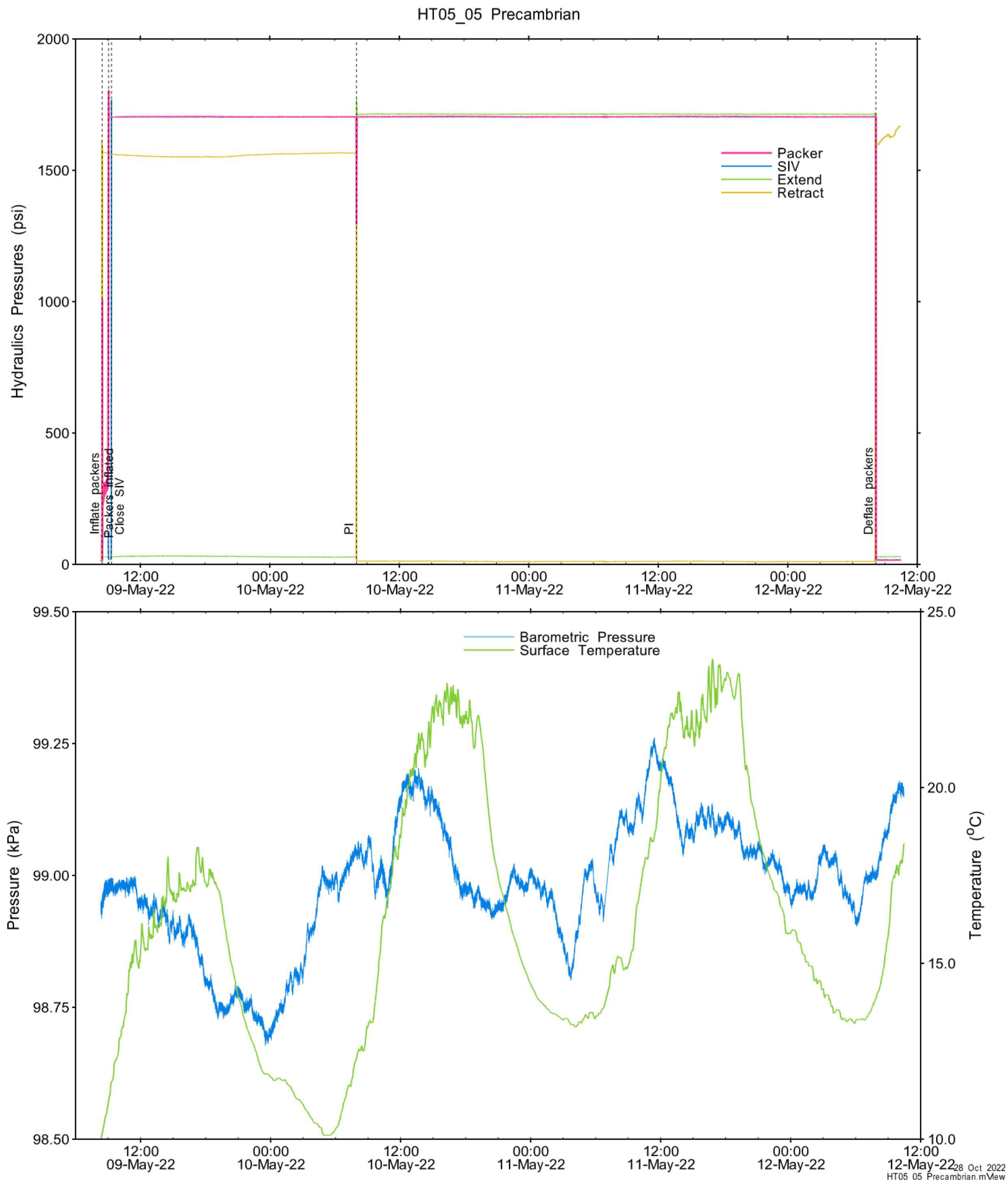

Figure 0.306 Hydraulics pressures and surface temperature/barometric pressure.

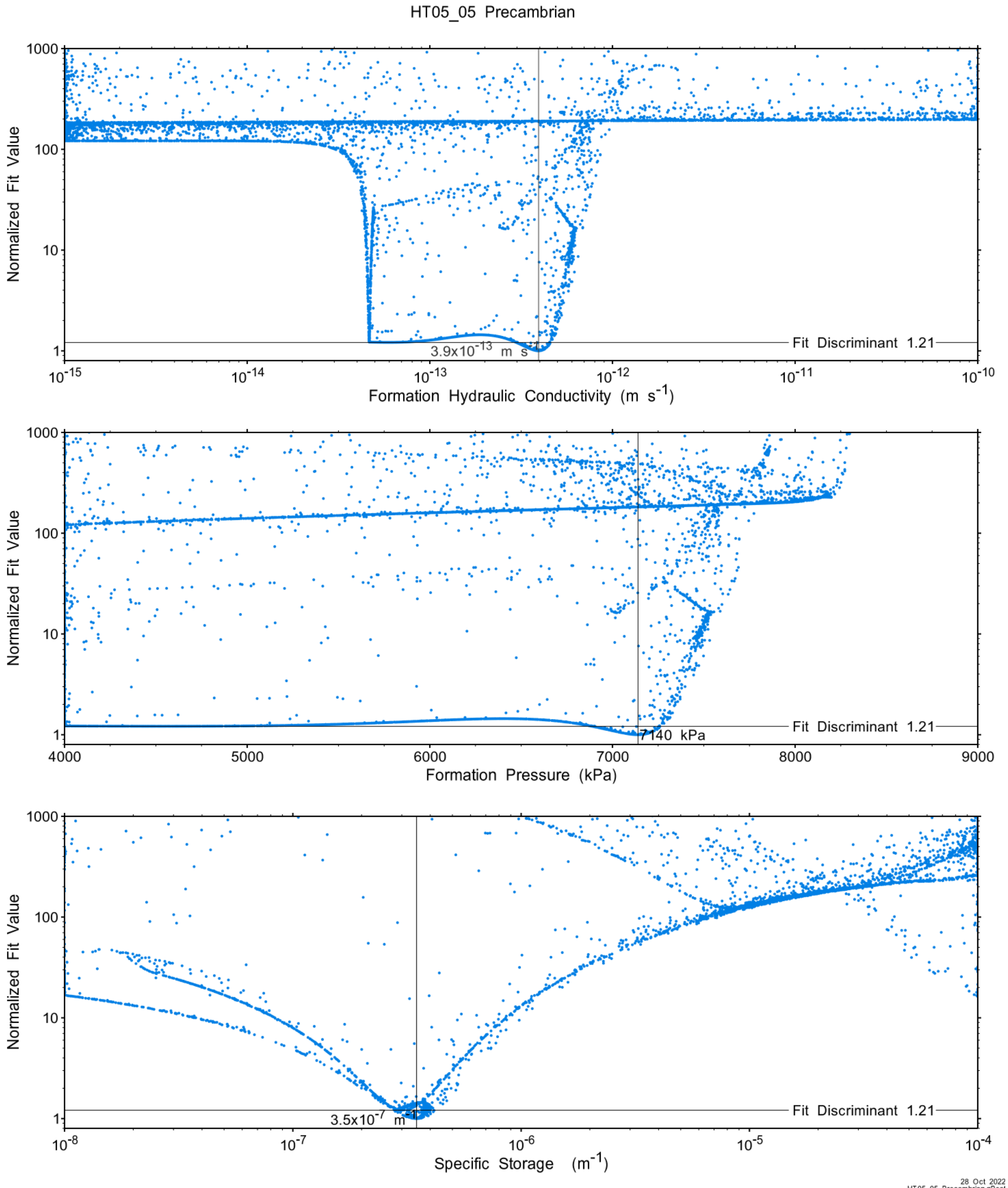

Figure 0.307 XY-scatter plot showing the formation parameter space normalized fit values.

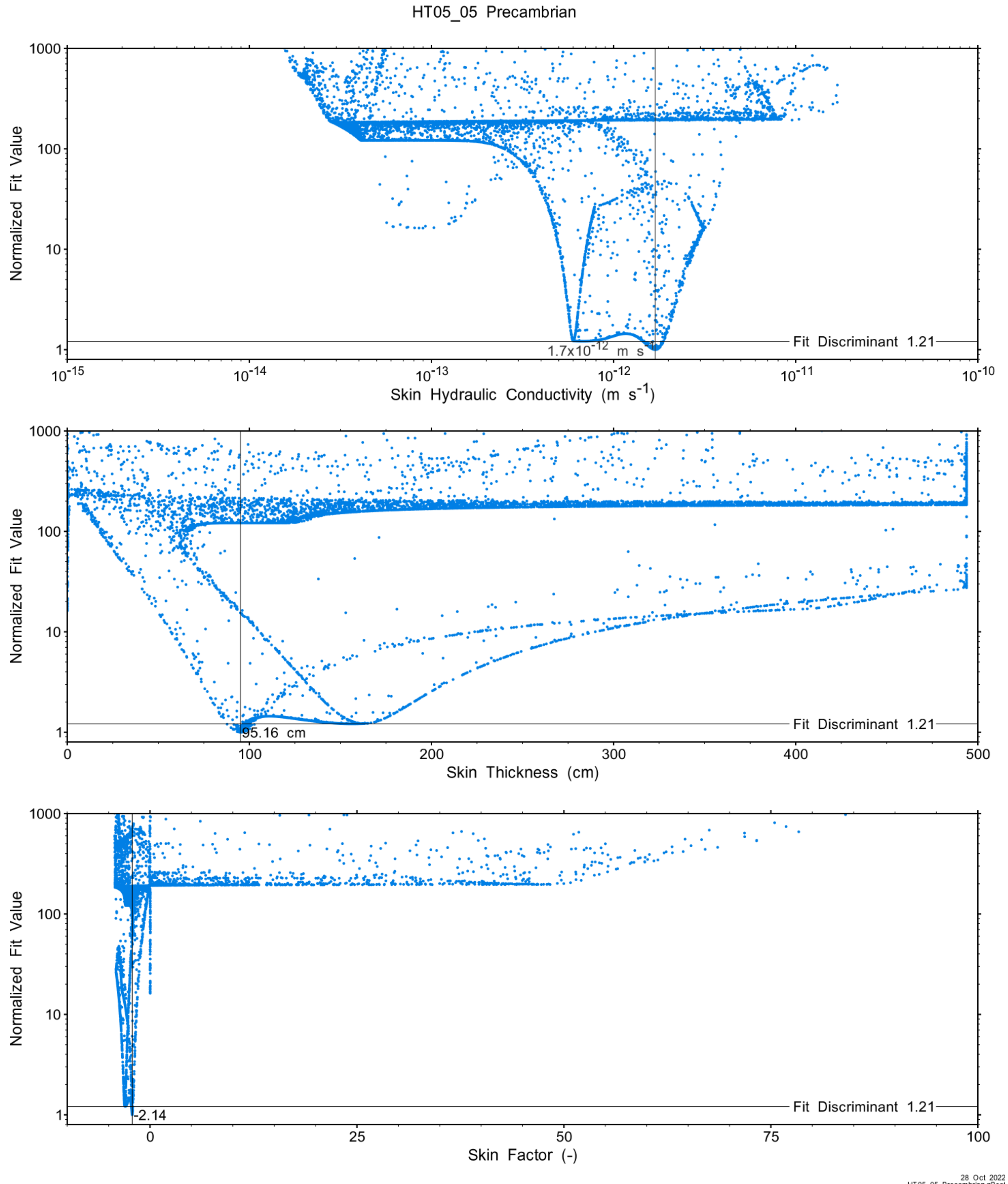

Figure 0.308 XY-scatter plot showing the skin parameter space normalized fit values.